Healing and repair mechanisms in fetal membrane defects after trauma, strain and fetal surgery

Submitted in partial fulfilment of the requirements of the
Degree of Doctor of Philosophy
(Queen Mary University of London)

Presented by

ELENI COSTA

Statement of originality

I, Eleni Costa, confirm that the research included within this thesis is my own work or that where it has been carried out in collaboration with, or supported by others, that this is duly acknowledged below and my contribution indicated. Previously published material is also acknowledged below.

I attest that I have exercised reasonable care to ensure that the work is original, and does not to the best of my knowledge break any UK law, infringe any third party's copyright or other Intellectual Property Right, or contain any confidential material.

I accept that the College has the right to use plagiarism detection software to check the electronic version of the thesis.

I confirm that this thesis has not been previously submitted for the award of a degree by this or any other university. The copyright of this thesis rests with the author and no quotation from it or information derived from it may be published without the prior written consent of the author.
Signature

Eleni Costa

Date: 27/02/2022

Abstract

Iatrogenic preterm premature rupture of the fetal membranes (iPPROM) is a major complication after diagnostic or invasive fetal surgical interventions, often associated with adverse perinatal outcomes. Strategies to seal human FM defects with glues, collagen or fibrin plugs have failed to restore structural function of the FM and promote tissue regeneration and defect repair, and none are in routine clinical use. In this thesis, the mechanisms of human FM healing after iatrogenic rupture were investigated, to translate this to pregnancies affected by spontaneous PPROM. The concentration of the gap-junction protein Connexin 43 (Cx43) has been associated with poor wound healing mechanisms in skin models and its expression was increased in FM defect sites taken from fetoscopic interventions.

The present study examined the healing mechanisms in amniotic membrane (AM) defects after trauma, cyclic tensile strain (CTS) and fetal surgery. There was evidence that Cx43 increased in expression in term AM following *in vitro* trauma concurrent with αSMA-expressing myofibroblast differentiation and collagen polarisation examined by SHG imaging. Both the wound healing marker TGFβ1 and Cx43 gene expression were significantly increased after trauma. To investigate mechanotransduction mechanisms, preterm AM was subjected to 2% CTS for 24 hours. Collagen fibres were polarised in the direction of strain concurrent with differential effects on markers for ECM (collagen, elastin, GAGs), inflammation (PGE_2) and healing (Cx43 and TGFβ1) in a donor and tissue-dependent manner. Morphological changes in AM cell populations in iPPROM defects and spontaneous PPROM showed myofibroblast differentiation, changes in collagen alignment and lack of wound closure.

The results obtained in this study contribute to our knowledge on AM wound healing and repair capabilities, mechanotransduction mechanisms in preterm AM and the influence of fetal surgical interventions on AM cell types and collagen integrity. Establishing how Cx43 regulates AM cell function and healing after trauma and CTS could be an approach to repair defects in FM.

Acknowledgements

I would like to thank my supervisors Dr, Tina Chowdhury, Prof. Anna David and Prof. Jan Deprest for their continued enthusiasm and support throughout this project. My sincere thanks to the Fetal Medicine Unit staff at UCLH who assisted in the collection of placentas and allowed me to observe fetoscopies and open fetal surgery at UCLH. I would like to extend my thanks to Dr. Chris Thrasivoulou for his training on confocal and multiphoton microscopy, and for sharing his expertise on Cx43. I am grateful for the support by the QMUL Principal PhD Studentship (50%, stipend and fees), the Rosetrees Trust (M808) medical research charity, the Prenatal Therapy Fund at UCLH Charity, and the Institute of Bioengineering (QMUL) for funding this project. Finally, I would like to thank Nicole for supporting me through this thesis with her strength and compassion.

Table of Contents

List of Figures

List of Tables

List of abbreviations

ADF = Adult dermal tissue

AECs = Amniotic epithelial cells

AF = Amniotic fluid

AK = Adult keratinocytes

AM = Amniotic membrane

AMCs = Amniotic mesenchymal cells

AP-1 = Activator protein 1

BrdU = Bromodeoxyuridine

CAM = Cervical amniotic membrane

CAPs = Contractile-associated proteins

CBB = Cyclic biaxial burst testing

CCL = Chemokine ligand

CD = Cluster of differentiation

CDH = Congenital diaphragmatic hernia

CM = Chorionic membrane

CMCs = Chorionic mesenchymal cells

CMP = Connexin mimetic peptide

COX-1/2 = Cyclooxygenase 1/2

CS = Chrondroitin sulphate

CSE = Cigarette smoke extract

C-section = Caesarean section

CTFs = Cell traction forces

CTS = Cyclic tensile strain

Cx43 = Connexin 43

Cx43as = Cx43 antisense

Cx43asODN = Cx43 antisense oligonucleotide

D = Dissipated energy ratio

DAM = Decellularized amniotic membrane

DAMPs = Damage-associated molecular patterns molecules

DMEM = Dulbecco′s modified Eagle′s medium

DS = Dermatan sulphate

E = Elastic modulus

E_1 = Low elastic modulus

E_2 = High elastic modulus

ECM = Extracellular matrix

EMT = Epithelial to mesenchymal transition

ERK1/2 = Extracellular signal-regulated protein kinase ½

FBS = Fetal bovine serum

FCS = Fetal calf serum

FGR = Fetal growth restriction

FM = Fetal membrane

Fmax = Maximum force

FOXO = Forkhead box protein O

GA = Gestational age

GAGs = Glycosaminoglycans

GM-CSF = Granulocyte-macrophage-colony-stimulating-factor

HA = Hyaluronic acid

hAMSCs = Human amniotic mesenchymal stromal cells

HMGB1 = High mobility group box 1

HNDF = Human neonatal fibroblasts (HNDF)

HS = Heparan sulphate

IGF = Insulin-like growth factors

ILs = Interleukins

IMF = Immunofluorescence

iPPROM = Iatrogenic Preterm prelabour rupture of the fetal membranes

JFF = Juvenile foreskin fibroblasts

KHLS = Keratoderma-hypotrichosis-leukonychia totalis syndrome

KS = Keratan sulphate

LOX = Lysyl oxidase

LOXL1-4 = LOX like enzymes

LPS = Lipopolysaccharide

MAPKs = Mitogen-activated protein kinases

MET = Mesenchymal-to-epithelial transition

MMPs = Matrix metalloproteinases

MSCs = Mesenchymal stem cells

NAC = N-Acetyl-cysteine

NF-kB = Nuclear factor kappa B

NK cells = Natural killer cells

NO = Nitrous oxide

Oct-4 = Octamer-binding transcription factor 4

ODDD = Oculodentodigital dysplasia

PAM = Placental amniotic membrane

PAMPs = Pathogen-associated molecular patterns

PARPs = Increase in Poly (ADP-ribose) polymerase

PBEF = Pre-B cell colony-enhancing factor

PBS = Phosphate-buffered saline

PDGF = Platelet-derived growth factor

PEG = Polyethylene glycol

PGDH-2 = 5-OH prostaglandin dehydrogenase-2

PGE_2 = Prostaglandin E_2

$PGF_{2\alpha}$ = PGF_2 alpha

PPROM = Preterm prelabour rupture of the fetal membranes

PRA = Progesterone receptor A

PRB = Progesterone receptor B

PTGFR = Prostaglandin F2-alpha receptor

ROM = Rupture of the fetal membranes

ROS = Reactive oxygen species

RT-qPCR = Real time-quantitative polymerase chain reaction

SASPs = Senescence-associated secretory phenotypes

SBA = Spina Bifida Aperta

SEM = Scanning electron microscopy

SGA = Small for gestational age

SHG = Second Harmonic Generation

siRNA = Small interfering RNA

SOX-2 = Sex determining region Y box-2

SP1 = Specificity protein 1

sPPROM = Spontaneous preterm prelabour rupture of the fetal membranes

sPTL = Spontaneous preterm labour

SSEA-4 = Stage-specific embryonic antigen-4

TGFβ = Transforming growth factor β

TIMPs = Tissue inhibitors of metalloproteinases

TLR = Toll-like receptor

TNFα = Tumour necrosis factor-α

TTTS = Twin-to-twin transfusion syndrome

UTS = Ultimate tensile strength

VEGF = Vascular endothelial growth factor

WISH cells = Human amniotic epithelial cell line

ZAM = Zone of altered morphology

ZO-1 = Zona occludens protein-1

αSMA = α smooth muscle actin

Chapter 1

The structure, function and healing mechanisms of human fetal membranes

Chapter 1: The function, structure, and mechanical properties of human fetal membranes

1.1 Introduction

The present thesis explores the architecture and wound healing mechanisms of the fetal membranes (FM). The fetal membranes are a part of the placenta and encapsulate the developing fetus within a uterine sac filled with amniotic fluid (AF) and their integrity throughout gestation is essential in ensuring a successful pregnancy [1-3]. If the fetal membrane becomes compromised or ruptures before normal gestation (defined from 37 to 40 weeks gestational age (GA)) due to infections or preterm prelabour rupture of the fetal membranes (PPROM) this can lead to preterm birth [1-14]. The FM can also rupture following diagnostic fetsocopic interventions (e.g. amniocentesis) or invasive *in utero* fetal surgeries to correct fetal abnormalities (e.g. for spina bifida aperta (SBA) correction) [1-7,15,16]. Throughout this thesis, preterm rupture of the FM that is a consequence of medical interventions will be referred to as iatrogenic preterm prelabour rupture of the fetal membranes (iPPROM). Strategies to repair and promote healing of the fetal membranes following medical interventions have been largely unsuccessful due to poor healing capacity of patches developed, weak tissue adhesion, inadequate prevention of infections with antibiotic material and poor biocompatibility [4,15]. This creates a need for improved understanding of the wound healing properties of the fetal membranes to inform the development of such biomaterials to better repair damaged fetal membranes.

The introductory **Chapters 1** and **2** will explore the inflammatory mechanisms that lead to FM rupture and the wound healing mechanisms of the FM following this event. **Chapter 1** will explore the risk factors leading to PPROM and iPPROM followed by the current biomaterial strategies to seal the FM after rupture. I will then explore the structure and organisation of the human fetal membranes, the different cell types that reside within the FM and amniotic fluid and the composition and structure of extracellular matrix (ECM) components in the FM that play an essential role in maintaining the structural integrity of the tissue. The focus will then shift to discuss the physiological events of parturition leading to fetal membrane rupture in normal pregnancy, followed by the molecular events that lead to the degradation of the FM after trauma, surgery or

spontaneous rupture. The chapter will conclude with a discussion on the mechanical properties and mechanotransduction mechanisms of the FM after stretch. Fetal membranes experience increasing stretch throughout gestation as the fetus grows, an important factor to consider throughout this thesis when examining the wound healing mechanisms of the tissue and its ability to heal after excessive strain and pressure build up from the amniotic fluid.

Chapter 2 will focus on the wound healing mechanisms of the fetal membranes following surgery, trauma or rupture associated with infection and/or PPROM in different animal and human *in vitro* and *in vivo* models. This will include an overview of the gap junction protein connexin-43 (Cx43) which is proposed to play a role in wound healing processes of tissues such as in the skin. Previous evidence in our lab has demonstrated the increased expression of Cx43 at the wound edge of human fetoscopic wounds over 3 mm in diameter and in small artificial wounds (0.8 mm) in an *in vitro* trauma model [17]. The role of Cx43 in wound healing will be discussed in the context of different models (skin, chronic ulcers, corneal endothelium, buccal mucosal tissue and gingival tissues, and in the myometrium and FM) through *in vitro* and *in vivo* gain and loss of function models. Finally, the role of fibroblasts and myofibroblast (MF) differentiation in wound healing during classical wound healing processes such as in the skin will be discussed. These cell types are of interest when exploring the wound healing mechanisms of the FM, as evidence explored throughout both introductory chapters highlights their presence throughout gestation, labour induction, and wound healing as seen in *in vivo* and *in vitro* trauma models. These chapters provide the rationale to the aims and hypothesis of the thesis, which can be found at the end of **Chapter 2** in **Section 2.5.**

1.2 Preterm Prelabour Rupture of the Fetal Membranes

The global burden of preterm birth has remained unchanged in the last decades, with the UK having one of the highest incidence rates in the world [1]. Between 7 to 8% of pregnant women in the UK and 1 in 7 in London deliver before normal gestation time (before 37 weeks) costing the National Health Service (NHS) £3.4 billion pounds annually for delivery and survival of both the mother and the fetus [1]. Worldwide, PPROM leads to an estimated of 16 million cases of preterm births, with a minimal number of fetuses surviving past the ages of 5 [1]. PPROM is defined by the rupture of the fetal membranes before 37 weeks of gestation and the onset of labour [1-3]. 40% of premature labours are a consequence of PPROM and its prevalence is between 3 to 8% of all pregnancies and are estimated to increase the average price of hospitalisation by 40% [1-3]. Spontaneous PPROM (sPPROM) amounts to approximately two thirds of premature birth and its causes are not well defined [1-3].

Rupture of the FM threatens both the life of the child and the mother due to the heightened risk of infection and thus delivery may be recommended to ensue almost immediately if there is evidence of infection [2]. NICE guidelines recommend either management delivery, or expectant management [2]. Expectant management refers to the 'watch and wait' approach and doctors do not perform any medical or surgical treatment, waiting for labour to begin naturally [2]. Before 34^{+0} weeks gestation, NICE guideless recommend not to offer labour induction unless there are additional obstetric indications (including infection or fetal compromise) [2]. Between 34^{+0} and 37^{+0} weeks, healthcare professionals discuss the options and potential outcomes of either expectant management or induction of labour with the patient [2]. After 34^{+0} weeks (but before 37^{+0} weeks), if a woman presents with a positive group B streptococcus test at any time in their current pregnancy, patients are offered immediate induction of labour or caesarean birth [2].

1.2.1 PPROM Risk Factors

Risk factors for PPROM are multifactorial and not well understood [6] **(Figure 1.1).** Maternal risk factors influence the onset of PPROM, including previous preterm pregnancies associated with PPROM, long-term drug and alcohol abuse, smoking, obesity, vascular collagen disorders, maternal age and history of sexually transmitted diseases [6]. Infection is the most common trigger of PPROM, with 13% - 60% of pregnant women experiencing chorioamnionitis, a bacterial infection of the FM [4]. These complications can lead to increase maternal death due to sepsis, unplanned caesarean sections and/or endometriosis [5]. Women with uterine-placental conditions such as cervical shortening or excessive uterine distension as with polyhydramnios (excessive amniotic fluid) experience an increased risk by 10 - 15% for PPROM [6]. Microorganism infections have been shown to promote the secretion of prostaglandins (such as prostaglandin E_2 (PGE_2)) which initiate uterine contractions and matrix metalloproteinases (MMPs) that break down extracellular matrix proteins and rupture the cervical membrane [7].

Cervical trauma from full dilatation caesarean section, cervical surgery for pre-cancer removal and/or cervical weakness, can result in reduced cervical function and loss of the cervical mucus plug [8]. Motile micro-organisms that usually reside in the vagina are enabled to ascend through the cervix leading to the activation of pro-inflammatory factors such as proteolytic enzymes and cytokines to weaken and mechanically stress the FM [9-11]**.** Furthermore, repeated FM overstretching decreases the membrane's elasticity which affects its susceptibility to PPROM [8]. In non-infected membranes an increase in relaxin secretion has been recorded, a protein involved in the upregulation of MMPs and plasminogen, leading to ECM breakdown, membrane failure and eventual rupture [8].

The latency period between the rupture of the membranes and labour initiation is essential in PPROM management [6]. Gestational age and latency to labour have an inverse relationship, with mothers at 24 to 28 weeks having a longer latency period to those closer to term [6]. This is important because these pregnancies are most likely to be managed conservatively, aiming for fetal maturity before delivery is expedited [6]. Regardless, approximately 95% of pregnancies

complicated by PPROM are delivered within 72 hours of rupture [6]. Sustained rupture of the FM further increases the risk of chorioamnionitis [6,7]. Vaginal bleeding has been correlated with PPROM induction due to the increased maternal systemic inflammatory response that activates the extrinsic pathway of coagulation through monocyte release of tissue factor (TF) [12-14]. This results in increased thrombin expression, associated with decidual cell secretion of MMP-1 and MMP-3 that degrade FM extracellular matrix [12-14]. Thrombin further activates myometrial and uterine contractions which may lead to preterm labour with or without rupture of the FM [12-14].

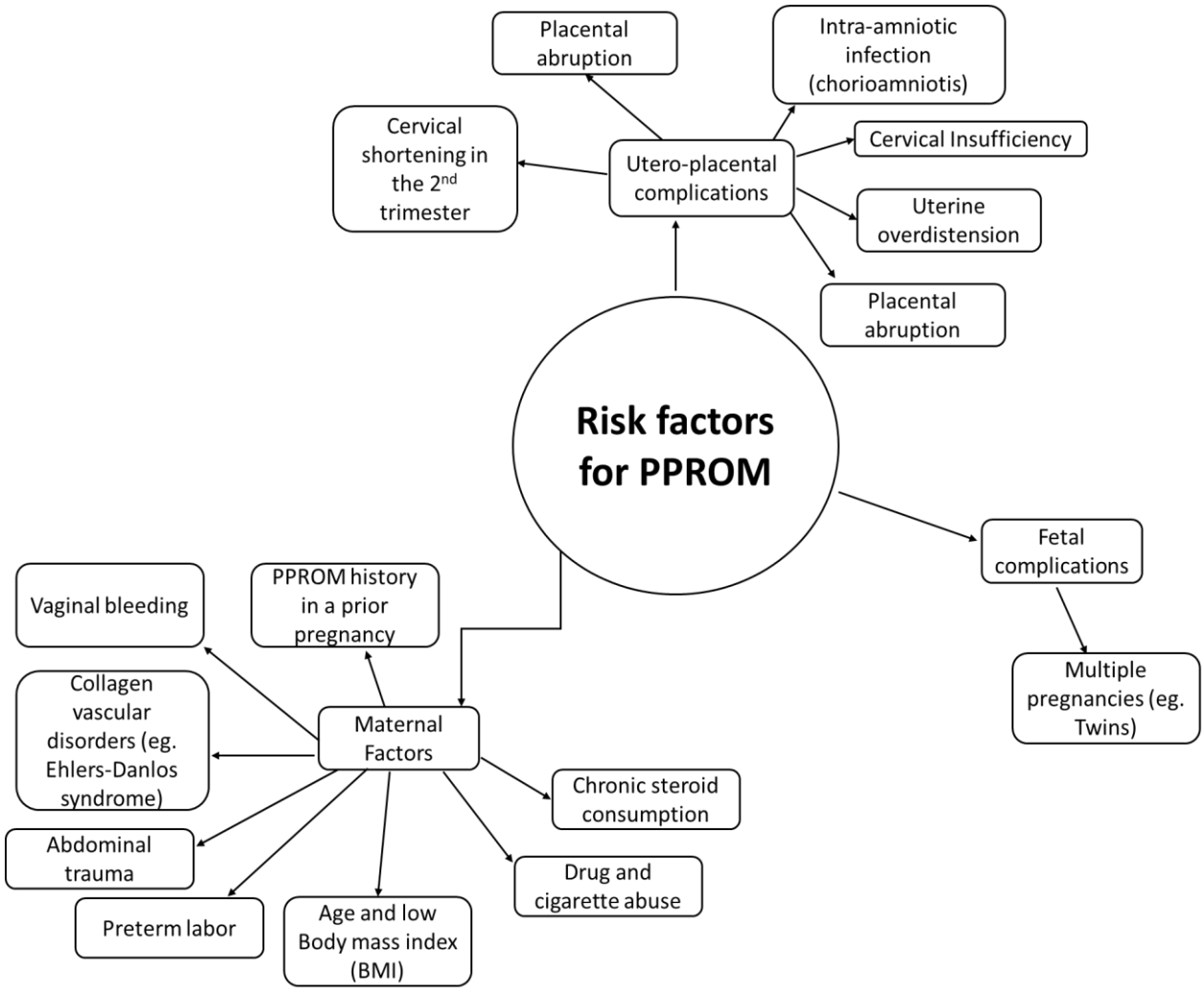

Figure 1.1: *Summary of risk factors that contribute to the onset of preterm prelabour rupture of the fetal membranes (PPROM). Factors include maternal, fetal and utero-placental complications [5-14]. Original Figure.*

1.2.2 Iatrogenic PPROM

iPPROM is a major complication after diagnostic or invasive fetoscopic interventions and is often associated with adverse perinatal outcomes [6]. Owing to extensive research and innovation in recent years, birth defects, structural, genetic, or placental abnormalities can be corrected, decreasing fetal mortality, and increasing the probability of neonates reaching adulthood [6] **(Figure 1.2).** In around 35% of fetal surgeries, the membranes separate leading to loss of tissue strength and AF leakage, undermining the success and reliability of these interventions [8]. Intrauterine infection rates are further increased due to AF leakage, highlighting the inconsistent outcomes in the field [8]. In most cases, there is limited healing potential of the membranes after fetoscopy or open fetal surgery [15-18].

The use of fetoscopy is the most common type of fetal surgery, whereby a trocar is inserted into the uterus penetrating the maternal decidua, myometrium and the amniochorion [19] **(Figure 1.2)**. Examples of these interventions include fetoscopic laser photocoagulation in the treatment of twin-to-twin transfusion syndrome (TTTS) and congenital diaphragmatic hernia correction (CDH) using an endoluminal tracheal occlusion [19]. Both surgeries lead to increased neonatal survival rates (57% and 75% in TTTS and CDH respectively) but pregnancies present with PPROM incidence at 39% for TTTS and up to 33% in CDH [19,20].

Amniocentesis testing utilises a small diameter needle (0.9 to 1. 2 mm) that passes through the FM to collect amniotic fluid to check for genetic or chromosomal related conditions such as Down Syndrome [21]. Conflicting studies have described the incidence rate of PPROM and subsequent miscarriage following amniocentesis [21]. The NHS claims the risk of miscarriage is decreased to 1 in 100 if amniocentesis is carried out after 15 weeks of gestation [1]. Another study determined that perinatal survival in amniocentesis related PPROM pregnancies was 82% higher than those complicated by spontaneous PPROM, suggesting the size of the tear on the membrane may influence fetal mortality outcomes [21].

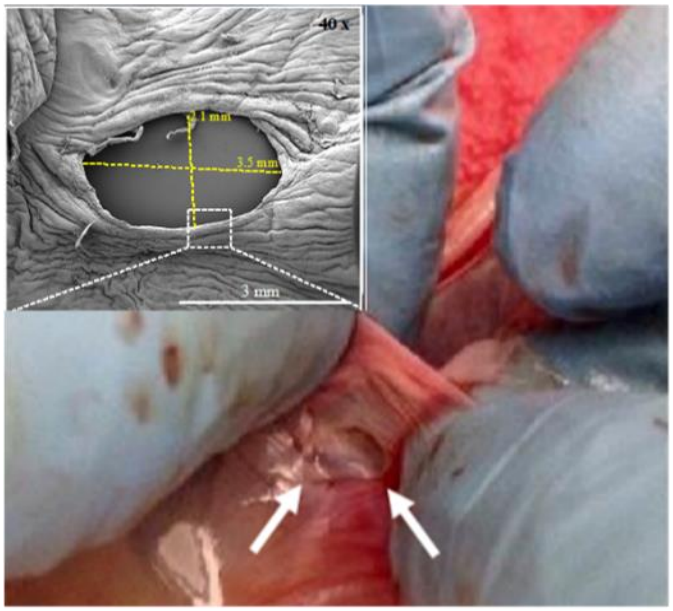

***Figure 1.2**: Fetoscopy for the correction of twin-to-twin transfusion syndrome (TTTS). Wounded amniotic membrane after fetoscopic surgery with diameters of 1 mm x 3 mm. Image adapted from Barrett et al., 2016 [17].*

Spina Bifida Aperta, or myelomeningocele, is a neural tube defect occurring in approximately 4.9/10 000 births [22]. SBA results due to failed closure of the neural tube by the 6th week of gestation, leading to injury of the exposed spinal cord and the brain throughout pregnancy [22,23]. SBA is a chronic disease associated with a high morbidity rate, usually dependent on the severity of the spinal cord defect [23]. Cerebral spinal fluid leakage causes significant damage to the brain and remains the leading cause of death in 17% of SBA cases [23]. *In utero* open fetal SBA repair for the correction of the spinal cord defect has become a gold standard procedure in selected cases of SBA [24]. Fetal clinical outcomes are promising, however preterm birth is recorded to occur in 12.8% of cases with mean gestational ages of 34.1 ± 3.1 weeks, while the incidence rate of PPROM is a staggering 46% [25].

Previous research in developing biomaterial strategies to seal FM defects has revolved around the use of natural polymers (e.g. collagen, fibrin [Tissel], polyethylene glycol [COSEAL] and elastin) to replenish the loss of ECM proteins in the wound and aid the natural healing mechanism [26]. These original strategies have, unfortunately, failed to deliver clinically meaningful outcomes **(Table 1.1)**. They have however sparked a new era of bio-inspired molecule synthesis from nature for wound healing that can be translated to the fetal membrane [26]. Several studies have explored

the use of synthetic and/or bioinspired polymer hydrogel adhesives to obstruct the open wound and hinder any amniotic fluid leakage [27-31]. Others have investigated decellularized amniotic membranes (DAMs) for their low antigenicity and anti-inflammatory properties, however their utility is limited by lack of adhesive properties [30-33]. **Table 1.1** summarizes key studies in FM sealing strategies over the last 2 decades. All this clinical and pre-clinical data suggests poor integration, healing, and biocompatibility of sealants, highlighting the urgent need for clinical solutions to repair FM after trauma, PPROM and surgery [34-37].

Table 1.1: *Summary of key studies in fetal membrane (FM) sealing strategies in the last two decades. Key findings describe whether clinically tested models were used on PPROM or iatrogenic PPROM (iPPROM) patients. AF = amniotic fluid, GA = gestational age, PEG = polyethylene glycol, DAM = decellularized amniotic membrane.*

Sealant	Model	Species	Key findings	Reference
Gelatin sponge plug (Gelfoam)	Clinically tested	Human	No improved outcomes after plugging the fetoscopic port site.	Papanna *et al*., 2010 [38]
Collagen plug combined with fibrinogen and plasma	FM explant	Human	Decrease in AF leakage in 30% of patients. Minimal fibrin synthesis observed.	Engels *et al*., 2013 [39]
Collagen plug	Clinically tested	Human	From 54 patients who received the collagen plug, 48% developed PPROM; and of the 87 who did not receive the collagen plug, 39% went on to develop iPPROM.	Engels *et al*., 2014 [37]
Laser wielding	FM explant	Human	Polytetrafluoroethylene was grafted onto term human fetal membrane explants followed by laser wielding with moderate success.	Mendoza *et al*., 1999 [40]
Amniopatch (intra-amniotic injection of mixtures of maternal platelets and	Clinically tested	Human	AF volume was restored in 2 patients following 7 days, while one patient received a second procedure. All infants delivered were viable.	Pathak *et al*., 2010 [41]

fibrin cryoprecipitate)				
Amniopatch	Clinically tested	Human	11.8% for sPPROM and 36.4% for iPPROM success.	Chmait *et al*., 2017 [42] Sung *et al*., 2017 [36]
Collagen amniograft	Clinically tested	Human	Endoscopic placement of collagen graft over a 2 cm defect sealed with fibrin. AF leakage prominent for 14 days.	Quintero *et al*., 2002 [35]
Peptide amphiphiles with Cx43 antisense	FM explant	Human	Co-culture of plug and Cx43 antisense with FM led to increased collagen levels and fibril expression across the defect, F-actin and nuclear cell contraction after 5 days.	Barrett *et al*., 2021 [43]
Mussel-mimetic adhesive	Inflation device Human FM explant	Human	Term FM sealed with cPEG withstood pressures typical of those reached during uterine contractions. Hydrogels showed strong resistance to degradation by collagenase, plasmin and enzymatic activities in the AF.	Haller *et al*., 2011 [29]
SprayGel	FM explants	Human	The *in situ* formed PEG hydrogel remain adherent to the tissue for five days, after which the hydrogels disintegrated through hydrolysis.	Bilic *et al*., 2010 [28]
Decellularized AM (DAMs)	Fetoscopy model	Rabbit	Compared to synthetic polyester-urethane scaffold (DegraPol), DAMs displayed better sealing capacity and reepithelization of the defects with minimal inflammation.	Ochsenbein-Kölble *et al*., 2007 [33]
Hybridized DAMs with cPEG	Fetoscopy model	Rabbit	cPEG-DAM composite hydrogels tightly adhered to fetal membrane over a period of 1 week. hybrid hydrogel promoted	Mallik *et al*., 2007 [44]

			recruitment of different cell populations to the defect site.	
Tissuepatch	Fetoscopy model	Rabbit	Tissuepatch is biocompatible and achieved complete sealing of rabbit fetal membranes after trauma compared to conventional collagen plugs.	Engels *et al*., 2018 [34]
Collagen plug enriched with AF cells	Fetoscopy model	Rabbit	Collagen plugging occulted at day 23 GA, increased cell proliferation in the defect, poor plugs adhesion.	Liekens *et al*., 2008 [45]
Sandcastle worm mimetic	Fetoscopy model	Yucatan miniature pig	Treated groups had no difference in survival, possibly owing to spontaneous healing in swine.	Papanna *et al*., 2015 [15]
Collagen plug	Fetoscopy model	Sheep	Rapid degradation when administered *in vivo.*	Devlieger *et al*., 2002 [46]

1.3 Structure and organisation of the human fetal membranes

The fetal membranes comprise the innermost avascular amniotic membrane which is in direct contact with the fetus and the amniotic fluid, and the outermost chorionic membrane (CM) that attaches to both the AM and the maternal decidua [47-50] **(Figure 1.3)**. The complicated anatomy of the FM is essential to the maintenance of FM elasticity, tensile strength, and pressure endurance throughout normal pregnancy [47-50]. Examination of the FM by immunofluorescent (IMF) microscopy and second harmonic generation (SHG) imaging demonstrates distinct cell sub-populations embedded within a 3D extracellular matrix network **(Figure 1.3).**

1.3.1 Structure and organisation of the amniotic membrane

The epithelial layer is the innermost layer of the AM and is comprised of a single layer of cuboidal cells termed **amniotic epithelial cells (AECs)** resting on top of the basement membrane which are rich is collagen types III, IV, V, elastin, and glycoproteins (laminin, fibronectin) [47-50] **(Figure 1.3)**. The compact layer, which lies under the basement membrane, is composed by a dense, connective tissue of stromal matrix (made of collagen types I, III, V, VI, fibronectin, elastin and glycosaminoglycans (GAGs) and sustains the mechanical properties (such as stiffness, elasticity, and tensile strength) of the AM throughout the pregnancy [51,52]. Underneath this, macrophages and **amniotic mesenchymal cells (AMCs)** reside within the fibroblast layer of the AM surrounded by a loose network of disordered collagen types I, III and VI interspersed with non-collagenous glycoproteins (laminin and fibronectin) and elastin [48,50,51,53]. The subsequent layer is termed the 'spongy' intermediate layer (or *zona spongiosa*) which acts as a physical barrier and stress absorbent between the AM and the CM rich in collagen, proteoglycans (decorin and biglycan) and GAGs [48,50,51,53]. **Sections 1.4** and **1.5** describe in more detail the cell types within the AM and which cells contribute to the structure of the AM by secreting stromal matrix components.

1.3.2 Structure and organisation of the chorionic membrane

The chorionic membrane is vascularised, adheres to the AM via the spongy layer and is composed of four layers [54-56] **(Figure 1.3)**. The innermost part of the CM that adheres to the spongy layer of the AM is termed the cellular layer and made up of a single thick layer of trophoblasts [54-56]. The density of the cellular layer dramatically decreases (and is frequently completely absent) from the time of labour and birth in spontaneous deliveries [57]. The chorionic reticular layer is rich in collagen types I, III, IV V, and VI arranged in a parallel network, with the presence of proteoglycans (primarily decorin and biglycan) and fibronectin [54]. This is the thickest part of the chorionic membrane and is mostly composed of chorionic mesenchymal cells (CMCs) that have dendritic morphologies and an abundance of macrophages [50,54,56].

A pseudo-basement membrane of collagen IV, laminin and fibronectin forming a dense connective tissue separates the reticular layer with the trophoblast layer, secreted by resident AMCs in the AM and CMCs in the CM [48]. Branching fibres from the pseudo-basement membrane anchor to the following trophoblast layer [48]. This final part of the chorion (also known as cytotrophoblast layer) adheres to the maternal decidua and is made up by two cell populations: vacuolated chorion laeve cells and the chorionic trophoblast cells [50,55,56,58]. This is the deepest chorionic layer (comprised of 2 to 10 trophoblasts deep), whereby cells reside within a matrix of collagen types III, IV, V and VI [50,56,59].

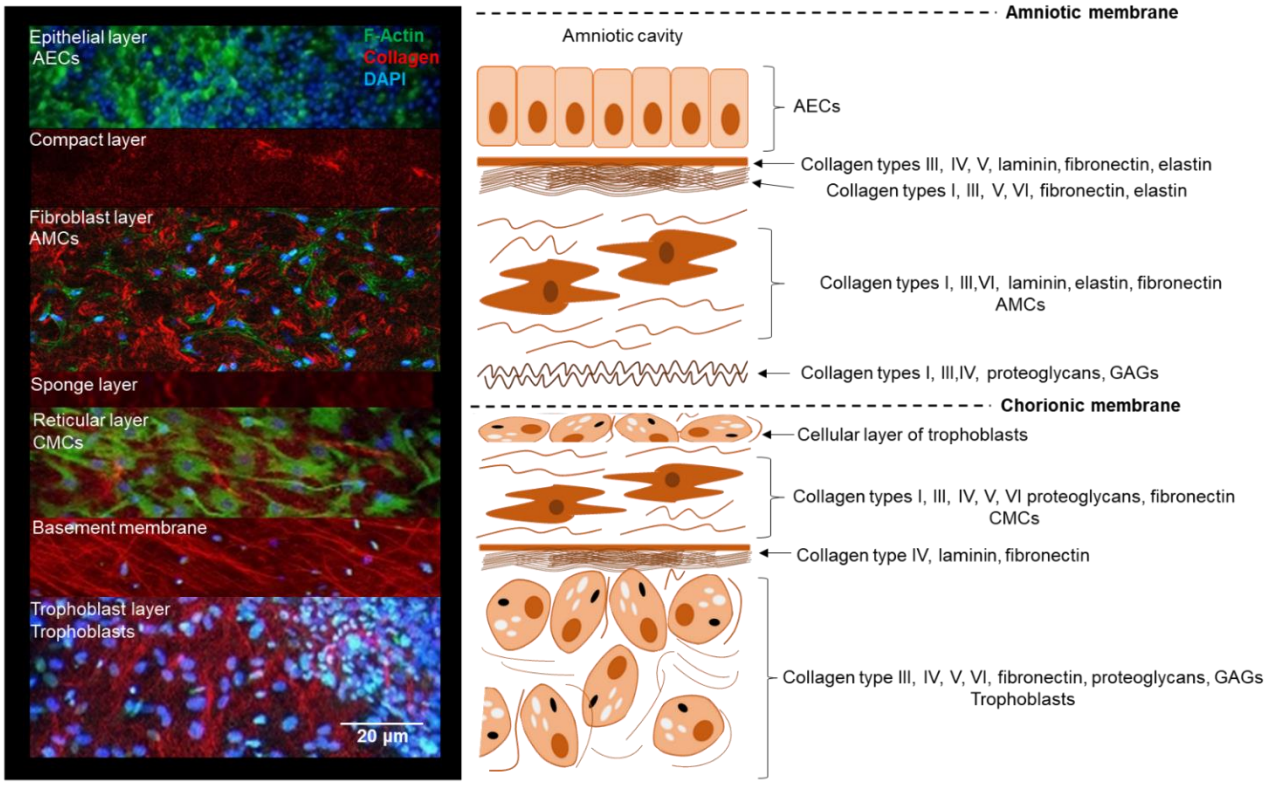

Figure 1.3: *Structure of the fetal membrane. Schematic representation of the different layers that make up the fetal membranes. The amnion is composed of five layers: the epithelial layer comprised of* ***amniotic epithelial cells (AECs)****, followed by basement and compact layers organised by a connective network of interstitial collagens (types I, III, IV, VI, V) non-fibrillar glycoproteins (laminin, fibronectin) and elastin that sustain the mechanical strength of the AM throughout normal gestation. Macrophages and* ***amniotic mesenchymal cells (AMCs)*** *reside within the fibroblast layer of the AM and reticular layers of the CM) surrounded by a loose network of extracellular matrix (ECM) proteins (elastin, collagen types I, III, VI, laminin and fibronectin, GAGs). The CM adheres to the AM via the spongy layer within a dense non-fibrillar mesh of collagen, GAGs and proteoglycans (decorin, biglycan). The CM is made up of four layers called the cellular layer (absent in term CM), reticular layer (comprised of AECs) pseudo-basement layer and the trophoblast layer, all with varying abundance of fibrillar and non-fibrillar glycoproteins and proteoglycans. Second harmonic generation images show the organisation of collagen fibres in the AM and CM (left panel). This is an orininal figure with immonofluorescent images taken by myself. AM = amniotic membrane, CM = chorionic membrane, CMCs = chorionic mesenchymal cells. Scale bar = 20 µm.*

1.4 Cell types in human fetal membranes and human amniotic fluid

The human FM organisation is dependent on several distinct cell populations which affect the ECM composition and subsequent mechanical properties. AECs, AMCs, immune cells (macrophages, neutrophils, natural killer cells (NK)) and trophoblasts all contribute to membrane integrity and function [48] **(Table 1.2)**. The density and functionality of each subpopulation depends on gestational age, species, and tissue layer [48].

In the human AM, AECs form flattened, cuboidal pavement cells. Microvilli project from the apical surfaces of AECs into the amniotic fluid [51,58,60]. Intercellular communication and tight junctions between adjacent AECs are achieved by the presence of vacuoles or desmosomes connected via distinct intracellular canals [51,58,60]. Microvilli further protrude within the vacuoles, confirming the presence of an extensive organisation of membrane channels that interconnect to each other and the ECM [51,58,60]. The bases of AECs have complex, asymmetrical shapes and projections that directly adhere to the basement membrane [51,58,60]. AECs are responsible for the secretion of ECM glycoproteins (laminin, fibronectin, nidogen) and collagen types III, IV and V that comprise the basement membrane [55].

Studies following AECs isolation from human AM demonstrate that this cell population has anti-inflammatory properties and will inhibit macrophage migration by secreting anti-inflammatory factors such as interleukin-10 and 1Ra (IL-10, Ra), transforming growth factor β (TGFβ) and PGE_2 [58,61,62]. Furthermore, AECs have antimicrobial and antifibrotic features, both of which contribute to their ability to promote wound healing in the AM and makes them excellent candidates for regenerative medicine applications [63-65]. Novel studies have shown mouse and human AECs are able to undergo mesenchymal-to-epithelial transition (EMT) in response to trauma or pro-inflammatory factors such as tumour necrosis factor α (TNFα) [66,67]. Human AECs *in vitro* possess key stem cell characteristics such as pluripotency marker octamer-binding transcription factor 4 (Oct-4) and sex determining region Y box-2 (SOX-2), contributing to their differentiation potential and therapeutic use [68]. In clinical trials of cryopreserved placental allografts and dehydrated FM

for the treatment of chronic diabetic ulcers, AECs decreased wound size, enhanced closure, shortened healing time and promoted re-epithelialization [69,70].

Resident AMCs in the AM and CMCs in the CM have fibroblastic morphologies and secrete ECM components (collagen types I, III, V, VI, fibronectin, elastin and GAGs) to the basement and compact layers of the FM. After the first trimester of pregnancy, the density of AMCs declines [51]. Like AECs, AMCs show differentiation potential by expressing pluripotent stem cell markers (Oct-4 and stage-specific embryonic antigen-4 (SSEA-4)) and differentiation markers (eg. CD90 and CD105) [52,71,72]. CMCs also possess stem-cell like characteristics (Nanog, Oct-4), express differentiation markers (such as CD90) and secrete immunomodulatory factors (IL-10, 8, PGE_2) *in vitro* [58,73,74]. In a rhesus monkey, chorionic trophoblasts and CMCs were found to produce 5-OH prostaglandin dehydrogenase-2 (PGDH-2), a prostaglandin inhibitor, with variable abundance throughout gestation and labour initiation [75].

Studies have reported the presence of differentiated myofibroblasts expressing alpha smooth muscle actin (αSMA) with flatted morphologies and elongated lamellipodia in human AM after both term and preterm labour, correlating with increased swelling in the reticular and connective tissue layers of the FM and enhanced MMP-2 and 9 expressions [76,77]. Richardson *et al.,* 2020 determined the ability of AECs to differentiate via EMT to myofibroblasts and consequently MF contractile phenotypes [77]. To do this, they measured the ratio of vimentin/actin and N-cadherin/E-cadherin and EMT-associated growth factor TGFβ and transcription factors SLUG and SNAIL in term in labour (vaginal) and term not in labour (Caesarean-sections (C-sections)) explants [77]. Vimentin was shown to be increased within term in labour membranes, suggesting EMT was occurring during labour [77]. E-cadherin is a marker of epithelial adherent junctions and N-cadherin is a marker of mesenchymal adherent junctions and thus EMT [77]. Using immunohistochemistry and western blotting, the authors found term in labour AM had higher N-cadherin and lower E-cadherin relative to term not in labour explants, indicating EMT was occurring by AECs at the time of labour and vaginal delivery [77]. In term FM labour deliveries, thus vaginal births, tight junction length was also decreased compared to those delivering via C-sections [77]. EMT requires the

loosening of tight junctions between epithelial cells to occur to allow for migration and contraction, thus a decrease in tight junction length concurrent with decrease in collagen concentration further indicate EMT [77]. Studies in cardiac cells have shown MFs secrete ECM-modifying factors such as chemokines (IL-1α, TNFα), cytokines (IL-8), growth factors (TGFβ) and of interest in FM, inflammatory mediator PGE_2 [78,79]. Baum and Duffy., 2011 defined contractile phenotypes in myocytes via αSMA staining and light microscopy observations of microfilament bundles which form adhesion complexes termed the mature local adhesion or fibronexus [78]. The fibronexus allows the internal microfilaments in myofibroblasts to form bridges to extracellular fibronectin domains and enables cells to generate force and thus, a contractile phenotype [78]. These reports highlight the ability of AMCs to differentiate into contractile phenotypes, influence ECM composition throughout gestation and parturition and create a flexible tissue capable of regeneration and repair [76-77].

Within the AM fibroblast layer, the presence of immune macrophages and dendritic cells have been determined [80-82] **(Figure 1.4)**. *In vitro*, AMCs possess immunomodulatory properties and influence the functionality of innate immune cell populations (e.g. monocytes, macrophages, dendritic cells) [83-85]. AMCs have been found to secrete CCL2/3 modulators of the complement pathway that signal peripheral monocytes to initiate differentiation of pro-inflammatory/active M1-macrophages into anti-inflammatory/regulatory M2-macrophages [86,87]. Macrophages have round morphologies with protruding pseudopodia and have phagocytic activity [80] **(Figure 1.4)**. CD45+ immune cells (macrophages, neutrophils, and NK cells) have been identified to be derived from the FM in non-laboured and laboured term tissue [50]. Another immune cell subtype, called placental villous Hoffbauer macrophages, exhibit M2-macrophage characteristics, express vascular endothelial growth factor (VEGF) for placental vasoregulation and are abundant throughout all cell layers of the FM [50,51,88]. Hoffbauer cells emerge after 4 weeks of gestation, increase in numbers throughout the first trimester and decline toward term [89-91].

The AF contains a plethora of multilineage progenitor or stem cells throughout the course of gestation. AF taken from amniocentesis sampling (between 16 to 20 weeks gestation) shows the

presence of mesenchymal stem cells (MSCs) expressing mesenchymal markers (e.g. CD90 and CD73) cytoskeleton markers (desmin, keratin-8 and vimentin) and pluripotency markers (e.g. Oct-4 and Nanog) [92,93]. At term, MSCs retain their ability to differentiate and have enormous potential for regenerative cell therapy [93]. Transcriptomic and proteomic analysis have identified ECM remodelling proteins expressed by MSCs [94]. These include collagen type II, insulin-like growth factor 2 (IGF2), tissue inhibitor of metalloproteinase 1 (TIMP-1) and TGFβ1 [94]. MSCs have also been found to secrete immunomodulatory factors including IL-8 and 10, interferon-gamma (IFNγ) and VEGF [94]. Of interest, in mouse and rat trauma models, MSCs expressing VEGF recruited cytokines (e.g. IL-27) and endothelial cell growth factor (PD-ECGF) to promote angiogenesis and wound healing [95,96]. Furthermore, immune cell populations (B cells, NK cells and T cells) are abundant in AF from 15 to 35 weeks of gestation [97]. Neutrophil and monocyte/macrophage population increases after 20 weeks of gestation and remains constant until term [97]. Immune cells in the AF play an essential role in priming the FM for parturition and rupture, which will be discussed in more detail in **Section 1.6**. Monocytes/macrophages and neutrophils express ECM cytokines (IL-6, 1α, β and 10) and damage-associated molecular patterns (DAMPs) such as alarmins which indicate immune cell activation [98,99]. These factors are particularly elevated in patients with chorioamnionitis and have been used as a marker for severe intrauterine infection [99,100].

A proposed consensus nomenclature for cell sources isolated from AM tissue explants with distinction between AECs and human amniotic mesenchymal stromal cells (hAMSCs) has been presented recently [101]. On further examination, hAMSCs were isolated in the AM after collagenase digestion and this population may be different to differentiating and proliferating AMCs and myofibroblasts found *in situ* and are embedded within a 3D collagen matrix environment [84]. Whilst recognising the differences in the terminology used to identify a variety of cell sources isolated from AM for applications in cell therapy, hAMCs extracted from AM explants as a total population after collagenase digestion are not the same as differentiating AMCs and myofibroblasts detected *in situ* using novel multiphoton confocal and SHG imaging techniques. The present study uses the terminology of AECs, AMCs and myofibroblasts similar to previous studies [66,76,102-106].

***Table 1.2**: Summary of cell populations in human amniotic membrane (AM), chrorionic membrane (CM) and amniotic fluid (AF). ECM = extracellular matrix.*

Tissue	Cell type	Expression of ECM components, matrix-modifying factors and stress fibres	Immunomodulatory factor expression	Cell morpholgy	References
AM	Amniotic epithelial cells (AECs)	Laminin, fibronectin, nidogen Collagen types III, IV and V	IL-10 IL-RA TGFβ PGE_2	Fattened, cuboidal pavement cells with projecting microvilli into the AF and basement membrane	48, 51, 58, 61,62
	Amniotic mesenchymal cells (AMCs)	Collagen types I, III, V, VI, fibronectin Elastin GAGs Cytokeratins 18, 19, 7 Vimentin N-cadherin	IL-6 IL-8 CCL2/3 TGFβ PGE_2	Flat, dendritic, elongated fibroblastic morphologies	48, 58, 83-85
	Myofibroblasts (MFs)	MMP-2, 9 Collagen type 1 αSMA	IL-1α TNFα IL-8 TGFβ PGE_2	Flat, dendritic, elongated lamellipodia	76-79
	M1/M2 macrophages	-	Anti-inflammatory: IL-1α, TNFα, CCL5 Pro-inflammatory: TGFβ, IL-10	Vacuolated. round morphologies with protruding pseudopodia	48, 80,82, 84,86
	Neutrophils	MMP-9	PGE_2 IL-6 IL-8	Multi-lobulated nuclei	48, 97-99
CM	Hoffbauer macrophages	-	VEGF HLA antigens A, B, and C IL-10 TGFβ	Vacuolated. round morphologies with protruding pseudopodia	48, 51, 88-91
	Chorionic mesenchymal cells (CMCs)	Vimentin MMP-1/2/3	IL-10 IL-8 PGE_2 PGDH-2	Flat, dendritic, elongated fibroblastic morphologies	54, 56, 73-75

	Trophoblasts	Cytokeratin-7 Vimentin	PGDH-2	Vacuolated chorion laeve cells and chorionic trophoblast cells	56 75
AF	Mesenchymal stem cells (MSCs)	Desmin Vimentin Keratin-8 Collagen type II IGF2 TIMP-1	TGFβ1 IL-8, 10 and 27 IFNγ VEGF PD-ECGF	Flat, dendritic, elongated fibroblastic morphologies	93-96
	Immune cell populations Neutrophils, monocytes/macrophages	-	IL-1, 6 and 10 DAMPs such as alarmins	Vacuolated. round morphologies with protruding pseudopodia Multi-lobulated nuclei	80, 98-100

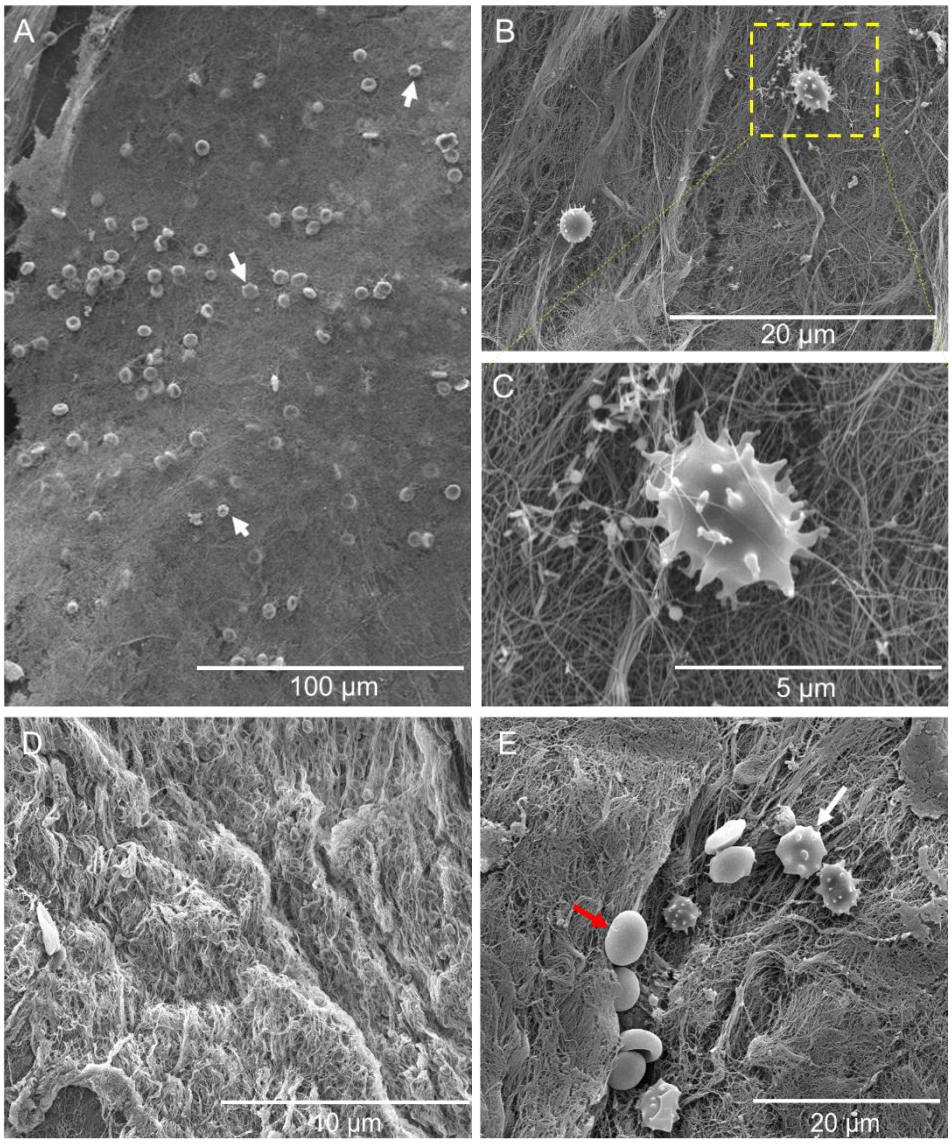

Figure 1.4: *Scanning electron microscopy of the surface of a term AM at the side of CM adhesion. (A) The presence of both erythrocytes and macrophages (white arrows) are seen attached to the AM. (B) Macrophages are trapped within collagen fibres in the AM. (C) Close-up of a macrophage with pseudopodia, interwoven with elongated collagen fibrils. (D) The CM surface at the site where the maternal decidua adheres. Collagen fibrils can be seen to form interwoven structures throughout the tissue. (E) Image showing a cluster of red blood cells (red arrow) and macrophages (white arrow) attached to the exterior of the CM where it was bound to the maternal decidua. Unpublished data, Costa et al., 2020. AM = amniotic membrane, CM = chorionic membrane.*

1.5 Composition and structure of extracellular matrix components in human fetal membranes

The structural integrity of the FM is maintained by an extensive network of ECM fibres whose differential expressions regulate cell movement, adhesion, and differentiation [51,58,60] **(Table 1.3)**. Basement membranes in the AM and CM are essential separators of the different FM cell populations [51,58,60]. The extracellular projections at the apical part of the membrane interact with the base of the AECs in the AM [51,58,60]. The glycoproteins laminin and fibronectin bind to cell membrane integrins in the FM and influence cell morphology, cell adhesion and survival [107,108]. Fibronectin further binds to monomeric collagen and induces collagen fibrillogenesis [109]. Furthermore, fibronectin influences FM tissue inflammation in response to infection and damage via activation of toll-like receptors (TLRs) [109].

Another notable structural protein in the FM is elastin [53]. Elastin is comprised of tropoelastin precursors covalently cross-linked to form insoluble elastic fibres [53]. Some groups have characterised the presence of tropoelastin mRNA in term human FM, while others determined variable degrees of abundance of elastin content in term membranes relative to total weigh (ranging from 0.08 - 36% depending on the technique employed) [53,110,111]. Histological analysis demonstrated the presence of elastin fibres in the basement and compact layers of the AM [48,112]. Elastin plays a role in maintaining the viscoelastic nature of the AM via fibre adhesion to AMCs and AECs through elastin-specific receptors [48,53].

Structural ECM proteins in the compact and spongy layers of the AM are essential in maintaining FM organisation [51,113]. Interstitial collagens type I and III are organised in parallel bundles throughout the compact layer and create interwoven connections between the basal membrane compared to the ECM [51,113]. The layer forms a compact mesh of alternating reticular fibres almost completely lacking any cells [51,113]. During AM inflammation, the compact layer does not thicken and is resistant to oedema and leucocyte infiltration [51,114].

The spongy layer has a hydrated plethora of proteoglycans (decorin and biglycan) and glycoproteins (such as mucin) interwoven within a dense non-fibrillar mesh of mostly collagen types III [113,114]. The presence of heavily glycosylated mucins and proteoglycans which bind to GAGs, create a viscous, water filled environment within the layer [113-115]. GAGs are negatively charged, hydrophilic polysaccharides that attract water molecules into the tissue causing osmotic swelling pressure and influence the FMs' physical properties [113-115]. GAGs bound to a protein core create proteoglycans, while free GAGs and proteoglycans directly bind to collagen, laminin and fibronectin to promote cell-to-cell and cell-to-ECM adhesion [115].

Sulphated GAGs (dermatan sulphate (DS), keratan sulphate (KS), chondroitin sulphate (CS), heparin, and heparan sulphate (HS)) were found to be abundant throughout the whole of the AM, while the non-sulphated hyaluronic acid (HA) was observed in the reticular and trophoblast layers of the chorionic membrane [116-119]. The spongy layer frequently swells and becomes susceptible to oedema, particularly in women undergoing PPROM [47,59]. Oedema has been found to be more prominent near the AM at the cervix, within the area destined to rupture termed the zone of altered morphology (ZAM) in healthy term membranes [47,59].

Table 1.3: *The composition and structure of extracellular matrix components in human fetal membranes relative to key components in the cervix. The list is not comprehensive for ECM elements in cervical cells, but rather used as a reference point. AMCs = amniotic mesenchymal cells. AECs = amniotic epithelial cells, AM =amniotic membrane, CM = chorionic membrane.*

Tissue	Cell layer/type	Collagen type I	Collagen type II	Collagen type III	Collagen type IV	Collagen type V	Collagen type VI	Laminin	Fibronectin	Elastin	Proteoglycans	Free GAGs	References
AM	Basement membrane			x	x	x		x	x	x			48,107,108,112
	Compact layer	x		x		x	x		x	x			19,48,51,112 -114
	Fibroblast layer AMCs	x		x			x	x	x	x			48,50,51,53, 116-119
	Spongy layer	x		x	x						Decorin biglycan	Sulphated GAGs	113,114,11
CM	Reticular layer CMCs	x		x	x	x	x		x		Decorin biglycan	Hyaluronic acid	199
	Basement membrane				x			x	x				51,107-109
	Trophoblast layer Trophoblasts			x	x	x	x		x		Decorin biglycan	Hyaluronic acid	119
Cervix	Cervical fibroblasts, myofibroblasts and epithelial cells	x		x					x	x	Decorin biglycan	Hyaluronic acid	151

1.6 Physiological events of parturition leading to fetal membrane rupture in normal pregnancy

A lot of the knowledge concerning fetal membranes comes from studies of term labour where rupture of the fetal membranes often precedes birth. There is a general decrease in FM thickness due to biochemical changes, repeated stretching and uterine contractions [120-142]. The initiation of spontaneous physiological rupture is controlled by multiple events including the maternal decidua activation, cervical remodelling, myometrium contractions and fetal membrane ripening at the ZAM [120-142].

1.6.1 Uterine inflammation

Activation of pro-inflammatory signalling cascades in the maternal and fetal uterine tissues has been hypothesised to govern the onset of labour [120]. Initiation of parturition is characterised by increased secretion of cytokines and chemokines in the FM, cervix and myometrium [120]. The accumulation of leukocytes within maternal peripheral blood during gestation is documented [121]. During uterine inflammation, an upregulation of TNFα, IL-1β, 6, 8 and 12 were shown to activate peripheral leukocytes, particularly neutrophils and NK cells [120,122-124]. Leukocyte uterine infiltration primes the tissues for parturition as they promote labour mediators, such as MMPs, and the expression of contractile-associated proteins (CAPs) that stimulate the myometrium through uterotonic agonists including PGE_2 and oxytocin [199,126,127].

1.6.2 Decidua activation

The maternal decidua is the innermost layer of the uterus and ensures nutrient and waste exchange during gestation [128]. The decidua's position between the myometrium and the FM allows the decidua to function as a signal transmitter during parturition [128]. The fused amniochorion and maternal decidua starts to disassociate, followed by basement membrane remodelling and degradation [129]. Using mouse models, Shynlova and colleagues induced pre-term labour using E-coli derived lipopolysaccharide (LPS) or the synthetic steroid mifepristone (RU486) and animals were killed during active LPS-induced preterm labour [128]. The authors

determined that myeloid cells (macrophages, neutrophils, monocytes) were increased in mouse decidua during active term and LPS-induced preterm labour, compared to lower concentrations in those before labour induction [128]. Changes in cytokine mRNA levels were measured via qPCR, and increased expressions of TNFα, IL-1β, 6 and 12 were found in both active term and LPS-induced preterm labour decidua [127,128]. In a rat model, researchers found that in decidua taken from both term labour and from preterm labour induced with mifepristone, the concentration of macrophage, neutrophil, and NK cells increased, potentially influencing the release of cytokines and chemokines for further immune cell recruitment to prepare the myometrium for labour [130,131].

Neutrophil recruitment into the decidua is facilitated through CCL5 and CXCL10 chemoattraction found in women after labour, and pre-term birth contributing to the degradation of FM by MMP-1, 9 and 13 [131]. Decidual cells experience senescence at the end of pregnancy, stimulating the expression of senescence-related genes such as placental growth factor (PIGF), VEGF and PGE_2 that propagate signals to induce myometrium contraction [132]. Decidua cells also interact with FMs through expression of MMP-1 and IL-8 which were found to induce neutrophil activity *in vitro*, suggesting their potential ability to remodel FM [133,134] Prostaglandin F2α ($PGF_{2\alpha}$) and the prostaglandin receptor play an essential role in contractility by further increasing the activity of cytokines IL-1β and 6 and MMP-2 and 9 activity which prime the decidua for separation and degradation [133-135].

1.6.3 Myometrium contractions

The myometrium consists of contractile myocytes that generate contractile forces during labour [136,137]. Throughout gestation, the myometrium undergoes structural and functional phenotypic changes in multiple phases: 1) at early gestation, the proliferative phase, 2) the intermediate phase that promotes cellular hypertrophy and ECM remodelling and 3) the contractile phase at the induction of labour [136,137]. Osman *et al.,* 2006 showed that human myometrium increased the expressions of IL-1β, 6 and 8 and marked neutrophil/macrophage infiltration during physiological term labour versus non-labouring women [120]. Interestingly, the presence of anti-inflammatory cytokines (IL-4 and 10) TGFβ and regulate PGE_2 synthesis in the choriodecidua [138]. In a human

term labour study, pro-inflammatory cytokines IL-1β, 8 and TNFα were upregulated in the myometrium, concurrent with increased gene expression of prostaglandin H synthase type-2 (PGHS-2), which codes for COX-2 [137,139]. In animal studies, several indicators have been identified as candidates for myometrial contraction [140-142]. This includes the expression of CAPs, gap junction protein Cx43, receptors for prostaglandin F2-alpha (PTGFR), oxytocin and COX-2 gene expression leading to PGE_2 production and the progression of rupture [140-142]. The expression of the gap junction protein Cx43 significantly increased in myocytes prior to labour, facilitating cell-cell signal transfer to synchronise labour contractions [134,143]. I will explore the role of Cx43 in wound healing and feto-maternal interactions further in **Chapter 2.**

1.6.4 Cervical remodelling

The cervix has remarkable ability to withstand pressure from the growing pregnancy and adapt to changes in tissue weight and stress from the uterine wall [144]. Cervical tissue is comprised of a dense network of extracellular matrix collagens, GAGs (hyaluronic acid in particular), and proteoglycans (e.g. decorin) [145]. During cervical remodelling, GAG expression increases, allowing for rapid tissue hydration, correlating with collagen fibril dispersion and cervix shortening followed by rapid uterine contractions [145]. Several rodent studies have contributed to our understanding of tissue changes at the cervix, including distinct biochemical phases that lead to ripening, softening and dilation of the cervix [146,147]. In a rat study, following the application of uniaxial tensile mechanical tests, the circumference of the cervical canal increased with gestational age [148]. Cervix softening and dilation follows the same pattern to FM activation [148]. During the ripening stage, chemokines attract an influx of neutrophils and macrophages to the tissue, leading to secretion of pro-inflammatory MMPs and cytokines IL-1β and TNFα [149,150]. ECM protein remodelling and structural changes ensue, weakening the cervical tissue to allow for complete dilation [144].

1.6.5 Degradation of fetal membrane ECM components leading to physiological rupture

Physiological rupture of the fetal membranes (ROM) following uterine contractions plays a role in labour induction and development [151]. Researchers have discovered that preterm rupture frequently precedes contractions [151]. Initial studies work performed in rat models determined that the AM undergoes breakdown in collagen type IV (α1 and α2 chains) during natural labour concurrent with increase activities of MMP-2 and 9 [151]. Further apoptosis and remodelling have been observed in rat and human models in both the AM and CM near term, increasing the susceptibility of FM to tearing and rupture [126]. Two separate studies determined high levels of pro-apoptotic caspase-3 and -8 concurrent with Fas and Fas ligand expression and Bcl-2 activation phenotypes in term non-laboured human AM, particularly in the ZAM, which is frequently closest to the cervix [152,153]. All these studies have successfully identified the ZAM, which displays distinct differential biochemical characteristics relative to the rest of the FM [59,126,151-153]. The ECM organisation in the ZAM affects the mechanical properties of the FM through gestation and in preparation for physiological rupture [59,154,155].

1.6.6 Biochemical and structural changes in the zone of altered morphology during parturition

The fetal membrane closest to the cervix at the ZAM undergoes a series of programmed biochemical alterations between 37 and 41 weeks of gestation in preparation for parturition to allow for the eventual rupture of the FM [154,155] **(Figure 1.3)**. The extracellular matrix in the ZAM overlying the cervix is composed primarily of elastin and collagen, which during labour induction, begins to degrade through the consecutive action of proteolytic enzymes [47,132]. *In vitro* and *in vivo* mouse studies have shown the release of a heavily glycosylated fetal fibronectin (onco-fibronectin) binding to AMCs via its extra domain and to Toll-like receptor 4, instigating the activation of MMP-1 and 9 to act on collagen fibrils [156]. Mogami *et al.,* 2013 injected mouse pups with either phosphate-buffered saline (PBS; control) or fetal fibronectin *in utero* on day 17 of gestation, and membranes were harvested on day 19 [156]. In mice treated with fetal fibronectin, MMP-1/9 activation was concurrent with increase in COX-2 mRNA which activated PGE_2 synthesis and nuclear factor kappa-light-chain-enhancer of activated B cells (NF-κB) and ERK1/2

signalling, compared to those treated with PBS [50,156]. High concentrations of fetal fibronectin in the amniotic fluid and cervix of women with either preterm labour or with intact membranes that delivered before 35 weeks GA via C-section was correlated to an increased risk of intra-amniotic infection and inflammation [157]. The mechanism by which this occurs is still unclear [157].

MMP-9 has been shown to be highly overexpressed in the ZAM during parturition [158]. In contrast, the MMP inhibitor TIMP-3 is reportedly decreased in term tissue and in the rest of the FM, further enhancing the breakdown of collagens [126,154,159]. Interestingly, there is a reported decrease of membrane strength (from approximately 14 to 2 N) at the ZAM correlating with the upregulation of MMP-9 and PARP cleavages indicating apoptosis [154]. Lastly, chorionic trophoblasts undergo apoptosis, contributing to the overall thinning of the ZAM [47,132].

The ZAM also contains a plethora of other pro-inflammatory and pro-apoptotic factors and transcriptional activators that translocate during labour and initiate rupture [154,160-163]. These include activation of mitogen-activated protein kinases (MAPKs), increase in Poly (ADP-ribose) polymerase (PARP) cleavage and translocation of transcription factors NF-κB, activator protein 1 (AP-1 and forkhead box proteins O1, O3 and O4 (FOXO-1, 3 and 4), all direct markers of cell apoptosis [154,160-163]. In non-laboured ZAM and primary AECs, MAPK/AP-1 signalling regulated the expression of IL-β-induced MMP-9 expression [161]. FOXO-4 was localised in chorionic trophoblasts, AECs and decidua while FOXO-3 in the syncytiotrophoblasts and chorionic trophoblasts, agreeing with previous reports of cellular layer apoptosis in the ZAM [162]. Lappas and colleagues determined the NF-κB signalling proteins CDP and p300 were upregulated in non-laboured human cervical regions containing the ZAM compared to FM take from near the placenta, concurrent with previous studies showing NF-κB to be a key regulator of IL-6, 8 and TNFα, and presumably enhance collagen remodelling via MMP-9 activation [160,163].

The presence of interleukins (IL-1β, 6 and 8) mRNA has further been described [120,164]. IL-1β was found to influence MMP-9 expression and activity followed by increase in leukocyte concentration and COX-2 expression [120,164]. MMP-2 and 9 was overexpressed in the ZAM of non-laboured human term AM concurrent with swelling of connective tissue and thinning of trophoblast and

decidua layers [126]. MMP-13 expression (which targets collagen type 2) was associated with normal parturition in laboured and pre-laboured term FM, with higher expression seen in PPROM samples with infection [165]. Oxidative stress and the presence of reactive oxygen species (ROS) was determined in non-laboured and laboured term FM and primary AEC cultures followed by a significant decrease in antioxidant enzyme expressions (e.g. glutathione peroxidase) and IL-β-induced increase of MMP-9 expression [164].

Following these changes, the proteoglycans biglycan and decorin, which act to balance collagen fibril assembly and collapse, undergo a 2-fold expression increase and reduction respectively [166]. Interestingly, the expressions of biglycan and decorin have been found to be influenced by inflammation due to microbial infection in preterm animal models and human tissues [167]. Evidence further suggests the compensatory actions of these proteoglycans affect MMP-8 signalling which decreased expression of collagen type IVα1 in mice [167]. In another mouse model, biglycan and decorin signalling depended on TGFβ1 expression in a gestational-dependent manner to control MMP-8, 9 activity and collagen IVα1 degradation [168]. In non-laboured cervical FM, biglycan concentration was found to be 40% lower than mid-zone FM [166]. In spontaneous labour, cervical AM showed a twofold elevation in biglycan concentration, 30% decrease in collagen and 50% decrease in decorin [166]. Interestingly, hyaluronic acid (a non-sulphated GAG) accumulated in between AM and CM in cervical FM concurrent with swelling in intermediate layers [166].

The area covered by the ZAM in different patients is varied (119.4 ± 21.0 cm^2 in one study of term FM) but the existence of the ZAM is evident on all membranes [159]. The AM at the cervical region within the ZAM has been reported to swell relative to membranes closer to the placental disk throughout labour induction [159] **(Figure 1.5)**. Studies have reported marked increase of thickness of connective tissue layers of both the AM and the choriodecidua [159,169,112] **(Figure 1.5C)**. Within the AM, the compact, fibroblasts and reticular layers become thinner, while the spongy (intermediate) layer swells from 14.0 ± 7.3 cm^2 to 25.7 ± 13.2 cm^2 [159,112] **(Figure 1.5C)**.

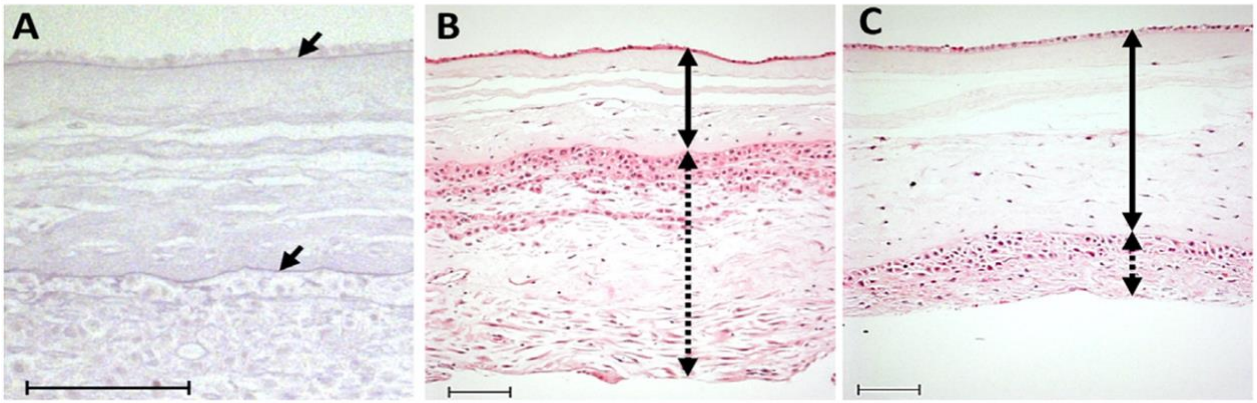

Figure 1.5: *Structural changes in the ZAM. (A) Resorcin fuchsin staining showing elastin fibres (arrow heads). Haematoxylin and eosine (H&E) staining of term human term FM taken near the placental disk (A) and at the ZAM (B). During induction of labour, the ZAM swells at the stromal layers (continuous arrows) relative to FM near the placenta. (C) There is a significant reduction in thickness of the cellular layers (dotted arrows) indicating cells are undergoing programmed apoptosis. Scale bar = 100 µm. Image taken from Mauri et al., 2013 [112]. ZAM = zone of altered morphology, FM = fetal membrane.*

In the chorionic membrane, there is a significant reduction in thickness of the cellular layers (chorionic cytotrophoblasts and maternal decidua) indicating cells are undergoing programmed apoptosis (decidua decreases form 218.8 ± 143 to 19.9 ± 13.1 cm^2) [112] **(Figure 1.5)**. SHG microscopy and histology has further shown collagen deformation and increase in thickness of the spongy layer within the ZAM relative to the rest of the fetal membrane at term [112] **(Figure 1.5)**. The cellular phenotype of the chorionic connective tissue and the reticular layer is altered, with cells differentiating into pro-inflammatory immunoreactive myofibroblasts and expressing αSMA [76,77,170]. The concentration of αSMA-positive myofibroblasts in the chorionic reticular layer correlated with decreased adjacent decidua thickness, however the mechanisms that link myofibroblast differentiation in the CM resulting in decidua thinning remain to be elucidated [159]. Chorionic cells at the ZAM have also been described to express pro-inflammatory glycoproteins tenascin-C and osteonectin, further contributing to ECM remodelling and cellular apoptosis [77,170]. In non-laboured preterm FM, trophoblasts presented pro-inflammatory HLA, B and C surface molecules which activate NK cells and M1-like macrophages to become phagocytic, coupled with overexpression of IL-6, TNFα and IL-8 genes [171]. **Figure 1.6** and **Table 1.4** summarise the changes occurring during ZAM remodelling during labour induction.

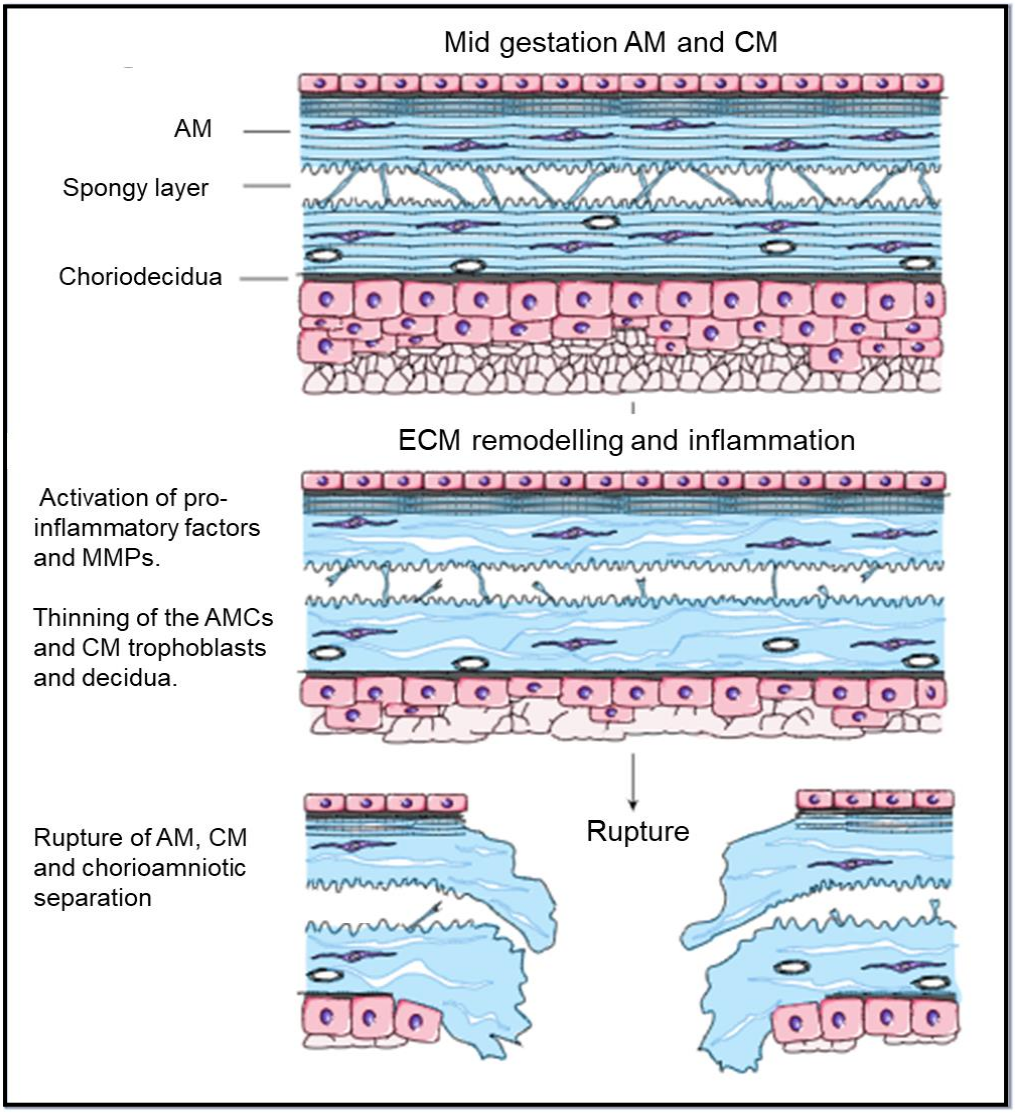

***Figure 1.6**: Simplified schematic representation of physiological fetal membrane (FM) rupture. Biochemical and biomechanical changes in the fetal membrane occur during FM activation. Collagen degradation by matrix metalloproteinases (MMPs) and thinning of chorionic trophoblasts and decidua are a consequence of membrane response to stretching and activation of cyclooxygenase 2 (COX-2) that synthesise the prostaglandin PGE_2, and interleukins 1, 6 and 8 (IL-1, 6, IL-8) and MMP 1, 9 and 13 for extracellular matrix breakdown. Chorioamniotic separation leads to a reduction in FM tensile strength and causes basement membrane degradation. Decreased overall FM thickness initiates AM rupture. Image adapted from Amberg et al., 2021 [172]. AMCs = amniotic mesenchymal cells, AM = amniotic membrane, CM = chorionic membrane. ECM = extracellular matrix.*

Table 1.4: *Pro-inflammatory molecules and their effect on structural integrity of extracellular matrix (ECM) components during fetal membrane activation for labour initiation. AECs = amniotic epithelial cells, AMCs = amniotic mesenchymal cells, AM = amniotic membrane, ZAM = zone of altered morphology.*

Inflammatory biomarkers	Mechanism of ECM degradation	Species	References
MMP-2, 9	Breakdown of collagen type IV α1 and α2 chains during natural labour in rats.	*In vivo* term rats	Lei *et al*., 1999 [151]
IL-1β, 6 and 8	Influence Leukocyte infiltration and COX-2 expression. Influence MMP-9 expression and activity.	Term non-laboured and laboured deliveries AEC primary cell culture of non-laboured AM	Osman *et al*., 2006 [120] Chai *et al*., 2012 [164]
Caspase-3, 8 Fas and Fas ligand	High levels of pro-apoptotic caspase-3 and 8 concurrent with Fas and Fas ligand expression and apoptotic phenotypes in term AM.	Human term AM explants	Kumagai *et al*., 2001 [152]
Caspase-3, 8 Bcl-2	High levels of pro-apoptotic caspase-3 and 8 concurrent with Fas and Fas ligand expression and Bcl-2 activation of the intrinsic pathway.	ZAM of human term non-laboured AM	Reti *et al*., 2007 [153]
NF-κB	NF-κB signalling proteins CDP and p300 were overexpressed in non-laboured human ZAM, concurrent with previous studies showing NF-κB to be a key regulator of IL-6, 8 and TNFα, and presumably enhance collagen remodelling via MMP-9 activation.	ZAM of human term non-laboured AM	Lappas *et al*., 2002 [163] Lappas *et al*., 2008 [160]
Fibronectin	Heavily glycosylated fatal fibronectin binding to AMCs via its extra domain and Toll-like receptor 4, instigating the activation of MMP-1 and 9 to act on collagen fibrils. Increased	*In vitro* mouse AMCs and *in vivo* mice at 19 days of gestation	Mogami *et al*., 2013 [156]

	COX-2 mRNA activated PGE_2 synthesis and NF-κB and ERK1/2 signalling.		
Fibronectin	Increased the expression of insulin growth factor binding protein (IGFBP)-1 or α−1 macroglobulin which directly influence decidua activation.	Human term and preterm cervical sampling and/or amniotic fluid	Oh *et al*., 2019 [157] Lee *et al*., 2011 [173]
Biglycan Decorin	Undergo a 2-fold expression increase and reduction respectively. Their expression is influenced by inflammation due to microbial infection in preterm animal models and human tissues. Evidence suggests the compensatory actions of these proteoglycans affect MMP-8 signalling and TGFβ1 levels. Biglycan and decorin signalling depended on TGFβ1 expression in a gestational-dependent manner to control MMP-8, 9 activity and collagen IV α1 degradation. In non-laboured cervical FM, biglycan concentration was 40% than mid-zone. In spontaneous labour, cervical AM has a twofold increase in biglycan, 30% decrease in collagen and 50% decrease in decorin. Hyaluronic acid accumulated in between AM and CM in cervical FM.	Mouse infection model Mouse model Human FM explants with/without spontaneous labour	De Miranda de Araujo *et al*., 2015 [167] Wu *et al*., 2014[168] Meinert *et al*., 2007 [166]
MMP-9 TIMP-3 PARP cleavage	MMP-9 enhanced collagen breakdown and decreased total FM strength (N) indicating apoptosis.	ZAM of term pre-labour human AM	El Khwad *et al*., 2005 [154] McLaren *et al*., 2000 [126] McParland *et al*., 2003 [159]
FOXO-1, 3 and 4	Pro-apoptotic transcription factor FOXO-4 was localised in chorionic trophoblasts, AECs	ZAM of term pre-labour human AM	Lappas *et al*., 2010 [162]

	and decidua while FOXO3 in the syncytiotrophoblasts and chorionic trophoblasts, agreeing with previous reports of cellular layer apoptosis in the ZAM.		
PARP cleavage MAPK AP-1	MAPK/AP-1 signalling regulated the expression of IL-β induced MMP-9 expression.	ZAM of term pre-labour human AM and primary AECs	Lappas *et al*., 2011 [161]
ROS IL-1β MMP-9	ROS presence was followed by a significant decrease in glutathione peroxidase expression and IL-β-induced increased of MMP-9 expression.	Labor and non-laboured human AM explants AEC primary cell culture of non-laboured AM	Chai *et al*., 2012 [164]
MMP-2, 9	Increase concentration of MMP-2 and 9 in cervical AM concurrent with swelling of connective tissue and thinning of trophoblast and decidua layers.	ZAM of non-laboured term human AM	McParland *et al*., 2000 [76]
MMP-13	MMP-13 identified within both the AM and CM Increase concentration in AF of non-labour, laboured and PPROM patient, higher concentration in PPROM samples with infection.	Non-labour, laboured and PPROM human AM explants	Fortunato *et al*., 2003 [165]

1.7 Degradation of human fetal membranes during preterm spontaneous rupture

1.7.1 Inflammatory mechanisms in the AM and CM that contribute to PPROM

Pathological rupture follows similar biochemical paths to physiological rupture that weaken and ripen the fetal membrane [129]. In the last decade, researchers have identified novel inflammatory pathways that contribute to PPROM. Kumar *et al.*, 2016 have illustrated that the same biochemical alterations and ECM remodelling to physiological rupture occurs when term human FM is incubated *in vitro* with TNFα and/or IL-1β, effectively weakening the membrane and making it more susceptible to tear [129]. Moore's group used primary human AM explants to induce a PPROM phenotype via UV light exposure and freeze/thawing cycles and incubated with thrombin [174]. The author's reported thrombin activated MMP-2 and decreased the mechanical properties of the AM after puncture testing (3.36 ± 0.92 versus 7.64 ± 2.58 N in controls) [174]. In preterm amniotic membranes, thrombin activity was also found to be increased using a fluorescence resonance energy transfer (FRET) protocol [14]. Mogami *et al.,* 2014 compared thrombin activity between ruptured sites and non-ruptured site of AM from term vaginal deliveries and preterm groups via either vaginal or C-section deliveries and did not separate vaginal versus C-sections but distinguished between those with and without PPROM [14]. Thrombin activity was higher in rupture sites of term AM compared to lower activity in preterm AM [14]. The same study showed thrombin increased COX-2 mRNA, PGE_2 synthesis and MMP-1, 2 and 9 concentrations in primary AMCs and in mice after thrombin injections at 17 days of gestation [14]. The authors showed that upregulation of MMP-9 was mediated by protease-activated receptor-1 (PAR-1) by using a selective PAR-1 inhibitor in primary AMCs [14].

Pathological biochemical changes in the ZAM are similar to physiological rupture, with cytokines (e.g. IL-1β and NF-κB) enhancing the secretion of MMP-9 and PGE_2 in the amniotic fluid of patients with chorioamnionitis and PPROM [129,163]. The consecutive actions of these proteins disrupt collagen fibril expression and elastin content in the AM, subsequently leading to tissue ripening and rupture [129]. Using term human FM explants and primary trophoblasts *in vitro* to create a PPROM model, Moore *et al.,* 2021 showed granulocyte-macrophage-colony-stimulating-factor

(GM-CSF) induced the expression of progesterone P4 concurrent with MMP-2 activation to remodel ECM, suggesting if left unchecked, this pathway could promote inflammation and PPROM induction [176]. However, the absence of immune cells in *in vitro* PPROM models that use primary AECs, AMCs and/or trophoblasts such as those used by Mogami *et al*., 2014 [14] and Moore *et al*., 2021 [176] may not best represent the inflammatory molecular mechanisms that occur during fetal membrane rupture. Animal models (mice) and human FM explants have been studied by both groups, but this is something to be aware of when comparing *in vitro* primary cell assays with *in vivo* and *ex vivo* explant assays.

Furthermore, bacterial invasion induces an inflammatory cascade in the FM, causing host immune activation followed by accumulation of macrophages and cytokine expression as the peripheral tissue attempts to fight off the infection, causing permanent damage to the membranes and predispose the FM to PPROM [83,177,178]. Activation of Toll-like receptors by pathogen-associated molecular patterns (PAMPs) activates transcription factor NF-κB by B-cells resulting in p65 translocation and secretion of pro-inflammatory IL-4, 6, 8 and GM-CSF commonly found in bacterial infections [179].

Senescence, a physiological process whereby cells age and stop dividing, has been observed with progressive gestation and in preterm human FM explants through telomere shortening in FM cell populations [178,180-182]. Senescence is thought to be mediated by senescence-associated secretory phenotypes (SASPs) and DAMPs [183]. Richardson *et al.,* 2020 used primary AECs from term not in labour (C-sections) fetal membranes cultured with cigarette smoke extract (CSE) to induce oxidative stress [183]. Using light electron microscopy and western blotting, the authors showed that under oxidative stress, AECs transition to a mesenchymal phenotype, quantified by elongated cell morphologies [183].

Abnormal ROS activation in FM explants has been investigated by Lappas *et al*., 2003, who used term not in labour (C-sections) human FM and AM incubated with and without the presence of the antioxidant N-Acetyl-cysteine (NAC) and LPS to induce inflammation [184]. The authors showed that in LPS-treated membranes, treatment with NAC suppressed PGE_2 release, IL-8, TNFα and

MMP-9 activity concurrent with NF-κB DNA binding activity [184]. Furthermore, lysyl oxidase (LOX) and LOX like enzymes (LOXL1-4) have been shown to remodel the ECM including elastin and induce cellular senescence under oxidative stress [185]. In the same study, FM samples were taken from women with spontaneous preterm birth and intact fetal membranes and from those delivering after PPROM, all of which delivered vaginally and were between 24 to 34 weeks GA [185]. In PPROM samples and an *in vitro* FM explant treated with cigarette smoke extract, the LOX gene was overexpressed relative to term tissues and untreated explants [185]. LOX activity, measured via qPRC (gene expression) and a fluorescent assay (activity) significantly decreased following NAC incubation in PPROM samples compared to controls [185]. Both these studies provide evidence to suggest antioxidant incubation could rescue PPROM-associated phenotypes [184,185]. However, FM explant isolation provides limitations, as there is the absence of strain and amniotic fluid pressure, which plays a role in inflammatory mechanism activation and experiments are done in sterile conditions, thus the absence of infections which further influence FM inflammation.

Moore and colleagues showed p38MAPK activation controls FM senescence via β-galactosidase activity, concurrent with laminin B loss, enlargement of mitochondria and DNA fragmentation [186-188]. Using mouse models, human AECs *in vitro* and FM explants exposed to CSE, the same group released a series of studies showing p32MAPK can be activated via TGFβ1 and is concurrent with p53-mediated senescence [132,186-188]. All effects were inhibited with p38MAPK inhibitors, suggesting its signalling controls FM senescence [186-188].

Researchers have proposed that FM senescence and aging triggers decidua activation through secretion of DAMPs that influence the inflammatory immune response [183,189]. DAMPs represent molecules of cellular injury and tissue damage, including high mobility group box 1 (HMGB1) protein responsible for inflammasome activation [185]. HMGB1 has been found to accumulate in the AF and stimulate oxidative stress, p38MAPK activation and senescence *in vitro* and cause PPROM in mouse models [185,187,190]. Lastly, exosomes carrying inflammatory mediators (PGE_2, MPPs, CAPs) has been shown to cause preterm parturition in mice by reaching the myometrium, cervix and decidua and initiate inflammatory activation [191,192].

The ability of AECs to undergo reversible EMT and mesenchymal-to-epithelial transition (MET) has been proposed to play a role in PPROM and inflammatory phenotype of FMs [77]. Spontaneous labour was associated with AM EMT in both humans and mice relative to non-laboured samples [77]. EMT in AECs was mediated by TGFβ from AF, concentrations of which were higher near term [77]. Exposure to CSE-oxidative stress increased AECs TGFβ release, while antioxidant treatment reduced p38MAPK activation, suggesting TGFβ-mediated signalling via TGFβ-activated kinase binding protein 1 (TAB1) mediated p38MAPK [77]. Progesterone was also found to induce MET via proto-oncogene c-MYC, a known MET activator in cancer [77]. In another study, the same group determined TNFα caused EMT concurrent with decreased E-cadherin, higher vimentin and N-cadherin and MMP-9 activity independent of TGFβ signalling in primary human AECs [67].

Figure 1.7 shows the proposed mechanisms discussed in this section of pathophysiological activation of the FMs leading to PPROM. This figure was developed by Menon *et al.,* 2020 [183] and is not a complete representation of physiological and pathological FM rupture, but rather provides an insight into the mechanisms based on animal, human FM explant and primary FM cell experimentation by that group and others sighted by them within the literature [183]. Menon's work dominates this field, and comparisons between their work and others becomes convoluted as they tend to collaborate with other groups. We will revisit their work in **Chapters 4-7** and discuss whether the work presented in this thesis would fit in their proposed hypothesis.

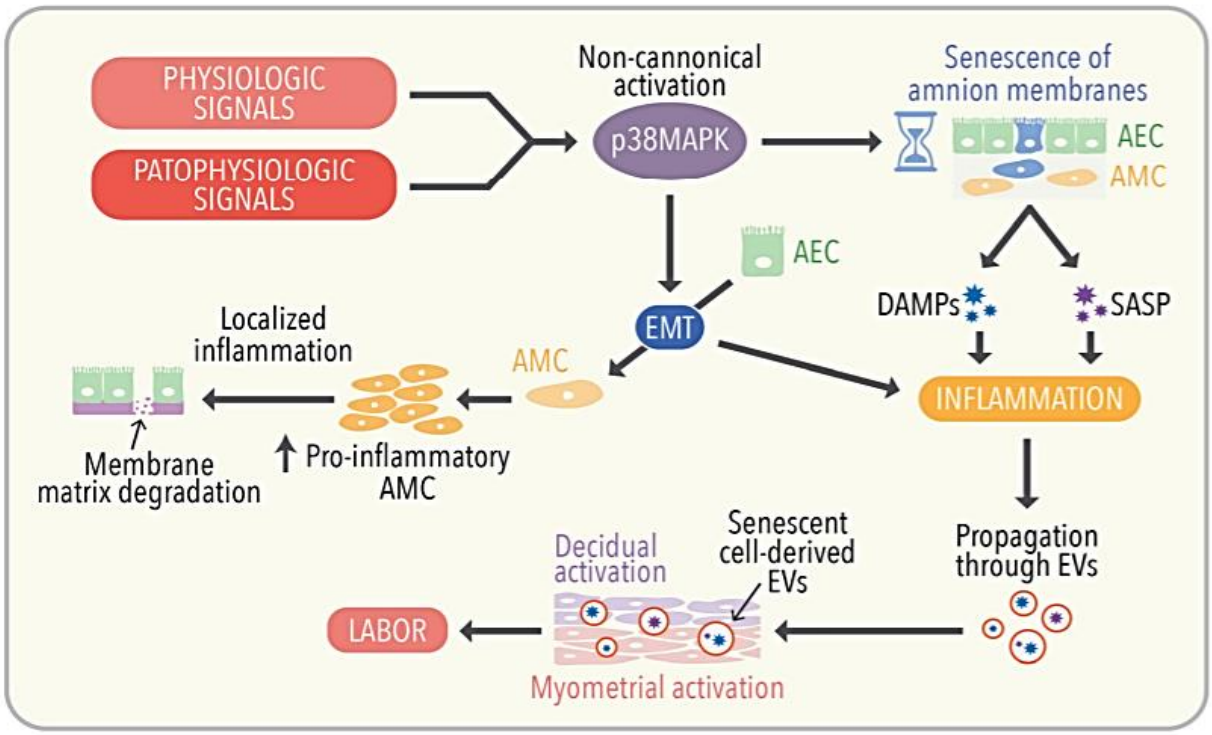

Figure 1.7: *Physiological signals are thought to closely resemble pathophysiological fetal membrane (FM) activation. Non-canonical activation of p38MAPK signalling via increased reactive oxygen species (ROS) concentration can lead to 1) Senescence of amniotic membrane cell populations leading to production of senescence-associated secretory phenotypes (SASPs) and secretion of damage-associated molecular patterns (DAMPs) or 2) the induction of amniotic epithelial cell (AEC) epithelial-to-mesenchymal transition (EMT) leading to amniotic mesenchymal cell (AMC) accumulation which increases localised inflammation and membrane matrix degradation. Extracellular vesicles (EVs) carrying inflammatory mediators have been shown to cause preterm parturition by reaching the myometrium, cervix, and decidua to initiate inflammatory activation and labour. Image taken from Menon et al., 2020* [183] *and hypothesis was formulated by the authors based on experimental evidence.*

1.8 Mechanical properties of the fetal membranes

In the search for optimal PPROM management strategies, the biomechanics of the fetal membrane and how biochemical changes lead to its failure must be better understood. Whole FM thickness at term is between 0.02 to 1.50 mm, while preterm (27-32 weeks GA) FM is thicker at 1.2 to 2.5 mm [193,194]. To determine this, the authors used high-resolution ultrasound imaging [193] and optical coherence tomography [194] on FM from women delivering vaginally and through C-sections at term and preterm [193,194]. Women delivering through C-sections in both term and pre-term gestational ages had higher AM thickness ranges from 0.02 to 0.05 mm compared to the CM at 0.17 to 0.32 mm at term [112,169,195,196]. From approximately 17 to 20 weeks, the FM thickness increases with progression of gestational age, with thickness being greater closer to the placental plate versus the rupture site [196,197]. After the first trimester, the density of FM cellular layers dramatically decreases, followed by a decline of collagen expression in the AM [129]. In a uniaxial testing system, whole FM stiffness was found to decreased from 15 weeks GA (8.84 MPa) to 40 weeks GA (2.29 MPa) [198]. This stable maintenance of strength and stress endurance of the FM possibly develops due to increasing AF pressurisation correlating with advancing gestational age [198]. The following section will describe FM tensile studies, highlighting the difference between FM, AM and CM mechanics **(Table 1.5).**

To characterise mechanical properties of the FM, different approaches to test the tissue have been used [112,203,206] **(Figure 1.8).** Uniaxial tensile testing requires the FM tissue explants to be clamped at both ends and pulled on one axis until failure [112,203,206]. In planar biaxial testing, the FM explant is clamped on four sides and pulled on multiple axis until failure [112,203,206]. Burst testing requires FM explants to be clamped in a ring followed by air or fluid application perpendicular to the tissue plane until failure [112,203,206]. Puncture testing also requires FM explants clamped on a ring, followed by insertion of a spherical metal probe perpendicular to the tissue until failure [112,203,206]. The set-up and design of the mechanical testing device yield stress (σ) versus strain (ε) and load versus displacement (δ) curves, to enable determination of mechanical properties [112,203,206]. Examples include the elastic modulus (E) corresponding to the gradient of the

stress/strain and the maximum force an object can tolerate per unit area called the failure stress (σf) which in turn corresponds to tensile strength, measured in MPa [112,203,206]. Other parameters include rupture strength, work to rupture (J), displacement of rupture or maximum force (Fmax, measured in Newton (N) and stiffness (also measured in MPa). Calculation of mechanical properties is dependent on the method of tissue excision, the shape and size of the explant (e.g. dumbbell vs rectangular) and the thickness of tissue [112,203,206]. Species will also influence the values for mechanical properties [199]. Dumbbell-shaped ovine and porcine FM was found to have higher ultimate tensile stress after uniaxial tensile testing (average 600 and 100 kPA respectively) than human AM (average 250 kPA), owing to their high vascularisation and despite their decreased thickness relative to human AM (average 90 μm for ovine and porcine and 180 μm for human AM) [199].

Using a rounded 3 mm diameter probe to apply force, Pressman and colleagues determined that FM tensile strength increased up to 20 weeks of gestation (average 399 grams to burst until 38 weeks GA), reached a plateau until 39 weeks GA and then significantly dropped before the induction of labour (average 257 grams to burst at 39 to 42 weeks GA) [200]. Another study showed decreasing puncture force correlated with gestational age for whole FM and AM alone, in non-labour caesarean and labour vaginal deliveries [201]. FM, AM and CM alone all decreased in Fmax with increasing GA; at <32 weeks GA, laboured FM Fmax was 4.61 ± 0.10 N and dropped to 3.47 ± 1.57 N by term (>37 weeks GA) while unlaboured FM Fmax was 5.80 ± 1.77 N at <32 weeks and decreased to 4.10 ± 1.62 N by term [201].

Using a uniaxial stress-strain response, Jabareen *et al.,* 2009 used human term FM to analyse stress-strain curves [111]. The authors determined that elastin and collagen content was 2.1% and 1.5% of total dry weigh of the FM [111]. High elastic modulus (E_2, MPa) ranged between 0.42 to 3.61 MPa, while low elastic modulus (E_1; 10^{-2} MPa) ranged between 1.17 and 2.5410^{-2} MPa [111]. Elastin and collagen content had an inversely proportional relationship to the elastic modulus E_1; increasing E_1 correlated with increased elastin content, while increasing E_1 correlated with decreased collagen content [111]. AM and CM thickness also decreased with increasing E_1 [111]. The

authors hypothesised that FM with higher elastin and less collagen could resist deformations with gradual increasing force, whereas FM with more collagen and less elastin has lower resistance to deformation for small strains but can build resistance with larger deformation [111]. Their hypothesis is supported by one 'early delivery' (31 weeks GA) having higher elastin content and lower collagen correlating with the highest value of E_1 ($2.54 \pm 0.61\ 10^{-2}$ MPa, elastin 3.03% w/w, collagen 5.47% d/w) relative to all other term membranes in the study (>38 weeks GA) [111].

Moore's group used a biaxial inflation device to calculate the force require to stretch the FM back to *in vivo* (or *in utero*) surface area as determined by MRI imaging prior to term caesarean delivery [202]. The authors determined that FM taken away from the placenta (reflected) generated a tension of 72.26 N/m corresponding to 15.4 mmHg pressure [202]. Rupture of the FM occurred at 295.08 ± 31.73 N/m corresponding to 34 mmHg pressure, which correlated 70% to physiological surface area [202]. Collagen fibre architecture showed collagen alignment and stretch with increased pressure, while complete rupture and irreversible fibre deformation occurred at 120 mmHg [202]. This is arguably a more accurate representation of the *in utero* environment, in comparison to other models which omit pressure application during fetal membrane stretch. Regardless, the effects of amniotic fluid components and the influence of labour contractions are still lacking in this model, which will further influence the mechanical properties of the FM at rupture.

Despite being thinner in nature, the amniotic membrane has remarkable ability to withstand high pressure and has greater tensile stability and strength due its extensive network of ECM collagens and elastin in its basement membranes, emphasising its role in maintaining FM integrity [203,204]. Ground-breaking work done by Oyen *et al.,* 2004 demonstrated the use of a biaxial puncture loading system, clearly characterising different peak forces in the AM, CM and different regions of the FM [203]. Oyen and colleagues showed that FM taken from vaginal deliveries were significantly weakened by labour and had a slightly lower puncture force at failure (Fmax 4.04 ± 1.52 N) than membrane from unlaboured term deliveries (Fmax 4.26 ± 1.09 N) [203]. Membranes obtained from preterm deliveries had greater average failure force for the whole FM relative to the average of all term membranes and greater Fmax in AM near the placental region (4.3 ± 0.71

vs 2.7 ± 0.76 N) [203]. In contrast, the CM had significantly less integrity and failed at lower loads than intact FM and AM, particularly in preterm samples (Fmax 4.16 ± 1.27 and 5.09 ± 1.30 N in term and preterm respectively [203]. The reduction in strength on all membranes is independent of modes of delivery, emphasising the physiological events undertaken to induce parturition [205].

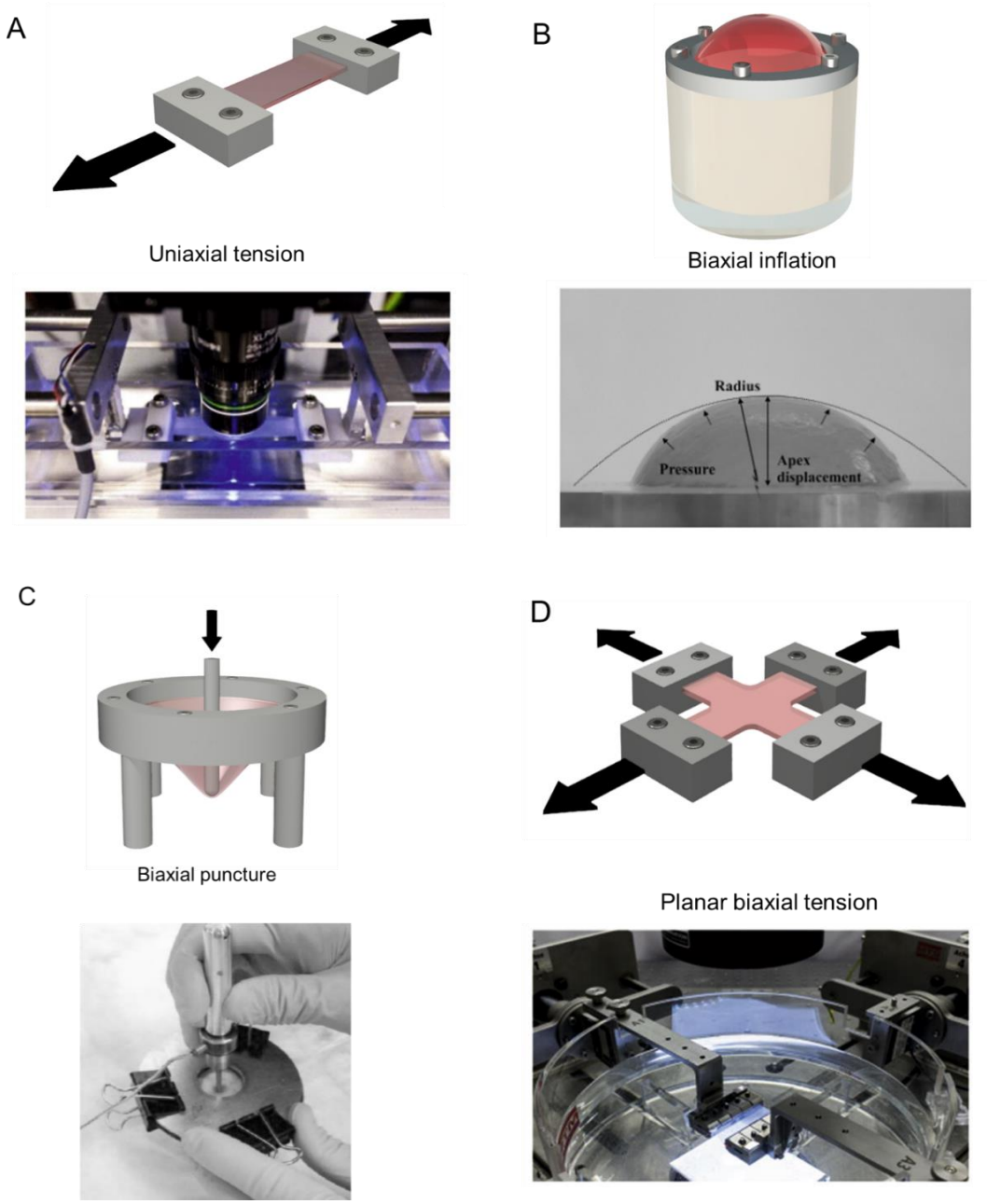

Figure 1.8: *Graphical representations and images of in vitro loading techniques including (A) uniaxial, (B) biaxial inflation (C) puncture testing and (D) planar biaxial tension on human and animal FM explants to determine how stretching influences mechanotransduction signals that lead to membrane failure. Images were taken from Mauri et al., 2015 [206], Oyen et al., 2004 [203] and Mauri et al., 2013 [112].*

1.8.1 Mechanical characterisation and properties of the amniotic membrane

These studies successfully placed the research focus on the amniotic membrane. Generally, research groups split the AM in three regions during experimental work: the **placental amniotic membrane (PAM),** the area closest to the placenta and thus the uterine wall, the midzone area halfway between the placental the cervical region, and the **cervical amniotic membrane (CAM)** approximately 4 inches apart from the placental membrane in term tissue [43,104-106,112,203,206] **(Figure 1.9).** Despite the nomenclature varying slightly between groups, there is a consensus of splitting the membrane in these distinct regions. This is undoubtedly a limitation for mechanical testing of the tissue, as there is no way to know where the placenta has adhered to on the uterine wall and consequently where the membrane overlaying the cervix would be, particularly in C-sections.

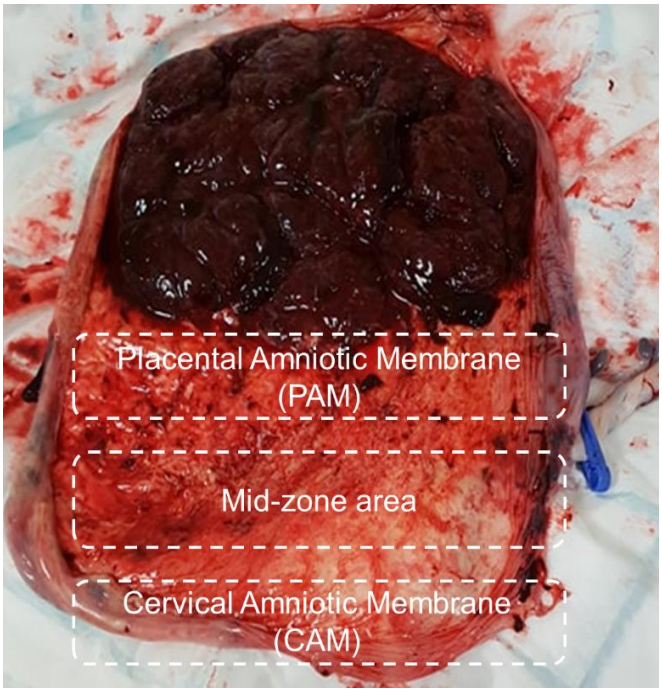

Figure 1.9*: Term placenta and attached fetal membrane taken after informed consent from University College London Hospitals (UCLH). The placental amniotic membrane (PAM), the area closest to the placenta and thus the uterine wall, the midzone area halfway between the placental the cervical region, and the cervical amniotic membrane (CAM) approximately 10 cm apart from the PAM in term tissue. Image taken by myself of a term placenta after C-section.*

This poses an even greater issue when women deliver with intact membranes, whether it be via vaginal or C-section birth. In laboured, vaginal deliveries with ruptured membranes, this might be more obvious, however there is no accepted protocol in the field of fetal membrane mechanics in characterising the cervical tissue following delivery with ruptured FM. During C-sections, surgically cutting and physically manipulating the FM could also alter the position of the 'cervical' and 'placental' regions. Trauma by scalpels and stretching of the FM throughout the C-section would presumably also influence the mechanical properties and consequently mechanotransduction (e.g. PGE_2 release, MMP activities, collagen concentrations etc) mechanisms of that may be detected in FM explants following mechanical stretch [15-20]. These are key points to consider throughout this section, which also contribute to the experimental discrepancies seen in the field of FM mechanics. Nevertheless, this section will highlight studies in mechanical propertied of the AM using the terminologies 'placental' and 'cervical' amniotic membrane.

Using a puncture testing model in term FM, Moore and colleagues supported this notion that AM has higher rupture strength (6.05 ± 2.16 N) than CM (3.96 ± 2.06 N) and required more work to rupture (0.010 ± 0.006 J vs 0.005 ± 0.004 J respectively) [204] **(Figure 3.1)**. This was concurrent with Oyen's work showing Fmax of AM in term laboured and unlaboured was higher than CM (Fmax 2.89 ± 1.08 N and 1.87 ± 0.61 N for laboured AM and CM respectively and Fmax 3.62 ± 1.03 N and 2.18 ± 0.81 N for unlaboured AM and CM respectively) [201]. Oyen and colleagues further determined that AM taken from the placental side was significantly stronger compared to the rest of the AM, with unlaboured groups having higher peak forces than those following physiological rupture (5.62 ± 1.33 N vs 4.01 ± 0.64 N unlaboured term and laboured term respectively) [203]. In a previous study by our lab group using dumbbell-shaped AM uniaxial cyclic tensile strain (CTS), ultimate tensile strength (UTS) was reported to be higher in PAM (4.52 ± 0.6 MPa) than CAM (2.28 ± 0.4 MPa), concurrent with upregulated COX-2, Cx43 and PGE_2 expression and decrease in collagen and elastin content [106].

A recent study characterised the effects of osmolarity and hydration on the tear resistance of term AM using mode I fracture tests [207]. This was to mimic fetoscopic procedures whereby CO_2 dehydration of the AM is expected [207]. Physiological variations in surrounding bath osmolarity did not influence the AM tear resistance, however treatment with physiological saline resulted in higher membrane tearing energy (Γ_a; average 0.032 J/m) than FM treated with distilled water (average 0.014 J/m) [207]. In comparing AM to CM, the same group used data from uniaxial tension and biaxial inflation fracture tests to create a computational model to determine tear resistance of term FM [208]. Tearing energy was found to be higher in AM (average 0.032 J/m) than CM (0.009 J/m) correlating with higher collagen fibril alignment at the AM defect site [208].

Using an *in situ* inflation device with a 1 mm defect in term human AM and SHG imaging, Mazza's group showed that collagen fibrils aligned tangential to the defect with increasing load (J), while unloading led to fibril de-extension back to the original morphologies before application of strain [209]. This indicated collagen fibril deformation is reversible at the edges of a defect, which was comparable to collagen deformation seen in other collagenous tissues such as porcine pericardium [209]. The authors proposed that consecutive actions of collagen and negatively charged proteoglycans respond to uniaxial and equiaxial tension by stretching and remodelling in the direction of strain and thus are responsible the mechanical behaviour of the AM [209].

1.8.2 Comparing and contrasting mechanical testing protocols and how they relate to FM mechanical properties

In a seminal review article, Chua and Oyen., 2009 provided a critical elucidation of studies conducted over a period of five decades on the mechanical properties of whole fetal membranes. According to the authors, the failure strength of the fetal membrane was found consistently to be approximately 0.9 MPa regardless of the biomechanical testing used [210]. Nevertheless, discrepancies between biaxial inflation, puncture and uniaxial tension differed in the range of experimental values [210]. In contrast, the elastic modulus varies significantly between methods with the average value of elastic modulus for uniaxial tensile testing (5.45 MPa) twice the value for biaxial puncture testing (2.35 MPa) [210]. Similarly, Buerzle *et al.,* 2013 and 2012*,* reported that the

average critical deformation or strain at rupture obtained by uniaxial tensile testing (50 -100 %) is about five times more than that from biaxial inflation testing (≤ 20%) [198,211]. Finally, the values of maximum uniaxial membrane tension reported are within the range of 0.15 - 0.98 N/mm [212].

Mazza's group compared critical membrane tension (T_{crit} measured in N/mm) derived from force (in N) versus displacement (in mm) curves in a puncture testing model, to the literature [213]. Values ranged from 0.5 to 0.60 N/mm and 0.46 to 1.33 N/mm and were close their study values (0.46 ± 0.23 N/mm) [213]. In a previous inflation test, the same group observed that maximum membrane tension was 0.23 ± 0.07 N/mm, indicating a discrepancy between tests [198]. Nevertheless, results from both studies were consistent with the notion that during stretch or inflation, the AM generally ruptures first, followed by the CM [213,217]. Regardless, the lack of consensus in mechanical testing apparatus results in inevitable variations in FM and AM mechanical parameters a caution must be applied when comparing studies.

Oyen *et al.,* 2004 further compared biaxial strength (σ_F; defined as the maximum radial stress at failure, converted to MPa) versus uniaxial strength (elastic modulus, E measured in MPa) taken from other studies [203]. The authors determined that average strength values derived from both tests were comparable, but the range of experimental values was significantly smaller in biaxial tests [203]. Following computational modelling, the authors showed that increased AF volume with increasing GA augmented the membrane strength (σ_F; MPa) in laboured term (GA 40, average 1.1 ± 0.4 MPa) versus term unlaboured (GA 39, 1.6 ± 0.4 MPa) and preterm (GA 31, 1.65 ± 0.4 MPa) [203]. In a more recent paper, the same group used a uniaxial fracture test to determine for the first time the fracture toughness of the AM, corresponding to how a membrane with a defect resists fracture [216]. The highest strength (σf) measured was 2.00 ± 1.91 MPa, the elastic modulus was 7.37 ± 1.76 MPa and the highest fracture toughness 1.83 ± 0.18 kJ m^{-2} [208,216].

In another study, Oyen used human term FM to compare cyclic tensile testing using uniaxial and planar equi-biaxial testing [205]. Using cyclic loading and stress relaxation, the authors reported cyclic testing showed dramatic energy dissipation in the first cycle, but hysteresis decreased on subsequent cycles [205]. The load (N) versus time (seconds) and load versus displacement (δ, mm)

response for both testing modes was similar [205]. The dissipated energy ratio (D) versus cycle number was lower in uniaxial relative to biaxial testing, however the response was the same, whereby energy dissipation was highest in the first cycle followed by a constant stead-state dissipation in the rest of the cycles [205]. The authors thus concluded that the AM response is nonlinear and time dependent, concurrent with high collagen fibril content in term FM approximately 50 nm in diameter [205].

Previous research in our group utilised a novel methodology using a bioreactor system to simulate *in utero* AM stretching [105]. The group used a term, unlaboured AM taken from C-sections and CAM and PAM were separately cut into dumbbell shapes of 25 mm x 10 mm [105]. Specimens were clamped on either side by stainless steel screws and inserted within bioreactor chambers and submerged with DMEM + 10% fetal bovine serum (FBS) with inhibitors for Cx43 or AKT [105]. They demonstrated that 2% CTS upregulated Cx43, AKT/PI3K signalling, COX-2, PGE_2 release, and sulphated glycosaminoglycan (sGAG) content, followed by a significant decreased in collagen and elastin [105]. This system will thus be used to investigate mechanotransduction mechanisms in preterm human AM in **Chapter 5**.

1.8.3 Discrepancies between mechanical testing apparatus and FM mechanical properties

In the literature, there is a clear discrepancy between calculated mechanical parameters in the field of FM mechanics due to several factors. These include different apparatus used to apply strain, different measurements by separate groups (as summarised in **Table 1.5**), FM collected at variable gestational ages and whether these donors had undergone labour with ruptured FM (vaginal or C-section) or had intact membranes at delivery. There is no consensus as to which device (as summarised in **Figure 1.8**) best represents the *in utero* environment, including intrauterine amniotic fluid pressure and biological content (growth factors, enzymes etc) and fetal movement, all of which change throughout gestation. Furthermore, labour contractions could also be mimicked *in vitro* and *ex vivo*, however the influence of contractions on FM mechanical integrity varies depending on gestational age (preterm versus term) and other factors such as utero-

placental complications, maternal factors, oligohydramnios, infections and PPROM [1-14]. The same can be said about FM taken from deliveries without contractions and with intact membranes.

To best mimic *in utero* physiological conditions, Sumanovac *et al.,* 2017 compared the use of cyclic biaxial burst testing (CBB) versus standard burst tests [214]. FM was taken from term placentas from both vaginal and C-section deliveries [214]. The authors split the FM into placental and cervical regions and to C-section and vaginal deliveries [214]. They determined that CBB values were higher than standard tests in placental (83.8 ± 19.4 mmHg vs 69.3 ± 17.9 mmHg) and cervical FM (67.9 ± 23.4 mmHg vs 58.1 ± 15.8 mmHg) [214]. In unlaboured term FM, cyclic pressures were higher than laboured FM (80.6 ± 22.4 mmHg versus 73.5 ± 22.7 mmHg respectively) [214]. The authors attributed the differences in measurements taken with standard test bursts and cyclic biaxial burst testing to the heterogeneity of the FM throughout different regions of the membrane and biological differences between patients [214]. We could also argue that one apparatus, in this case CBB, has a higher sensitivity compared to the older standard tests, as also suggested by the authors, however this would need to be more extensively experimentally compared to the literature and using more *n* numbers using different apparatus [214].

The aforementioned paper [214], as well as other inflation tests such as the ones used by Moore's group [202] mentioned throughout **Section 1.8,** provide more appropriate physiological methodologies for investigating the effect of pressure on the FM throughout different regions and gestational age [202,214]. Verbruggen *et al.,* 2017 developed a computational model using previously reported measurements of the uterus and stiffness and thickness of the AM and CM in term and in PPROM samples [215]. This study created a model of the FM using these parameters to predict FM rupture and PPROM [215]. By applying pressure through the software, the authors determined that modelling the mechanics of the AM and CM separately led to different tissue behaviour than when measuring each membrane as a constituent layer of the fetal membrane [215]. Thus, computational models could also pave the road for better understanding of FM mechanics by using data obtained through variable methodologies and experimentation [203.208,215].

Table 1.5: *Summary of different mechanical testing apparatus, values for mechanical properties and their relationship with extracellular matrix components and fetal membrane (FM) strength. AM = amniotic membrane, CM = chorionic membrane, GA = gestational age. PAM = placental amniotic membrane, CAM = cervical amniotic membrane.*

Mechanical testing apparatus	Parameters used to characterise mechanical properties	Reference
Uniaxial tensile testing	Average FM stiffness decreased from 15 weeks GA (8.84 MPa) to 40 weeks GA (2.29 MPa)	Buerzle and Mazza., 2013 [198]
Uniaxial tensile testing	E_2 ranged between 0.42 to 3.61 MPa. E_1 ranged between 1.17 and 2.5410^{-2} MPa. Elastin and collagen content was 2.1% and 1.5% of total dry weigh of the FM. increasing E_1 correlated with increased elastin content, while increasing E_1 corelated with decreased collagen content. A preterm sample had higher elastin content and lower collagen correlating with the highest value of E_1 at $2.54 \pm 0.61\ 10^{-2}$ MPa.	Jabareen *et al*., 2009 [111]
Uniaxial tensile testing (fracture test)	Treatment with physiological saline resulted in higher membrane tearing energy (Γ_a; average 0.032 J/m) than FM treated with distilled water (average 0.014 J/m).	Bircher *et al*., 2019 [208]
Uniaxial tensile testing	Elastic modulus *E* average = 5.45 MPa	Chua and Oyen., 2009 [210]
Uniaxial tensile testing	Maximum uniaxial membrane tension within the range of 0.15 – 0.98 N/mm.	Joyce *et al*., 2009 [212]
Uniaxial tensile testing with CTS	UTS was higher in PAM (4.52 ± 0.6 MPa) than CAM (2.28 ± 0.4 MPa), concurrent with upregulated COX-2 Cx43 and PGE_2 expression and decrease in collagen and elastin content	Chowdhury *et al*., 2014 [102]
Cyclic tensile testing in uniaxial and planar equi-biaxial testing	The dissipated energy ratio (D) versus cycle number was lower in uniaxial relative to biaxial testing, however the response was the same, whereby energy dissipation was highest in the first cycle followed by a constant stead-state dissipation in the rest of the cycles.	Oyen *et al*., 2005 [205]
Uniaxial fracture test	Highest strength (σf) measured was 2.00 ± 1.91 MPa, the elastic modulus was 7.37 ± 1.76 MPa and the highest fracture toughness 1.83 ± 0.18 kJ m-2	Koh *et al*., 2019 [216]
Biaxial puncture testing	AM had higher rupture strength (6.05 ± 2.16 N) than CM (3.96 ± 2.06 N) and required more work to rupture (0.010 ± 0.006 J vs 0.005 ± 0.004 J for AM and CM respectively).	Arikat *et al*., 2006 [204]
Biaxial puncture testing	Laboured FM were weakened by labour and had a slightly higher puncture force at failure (Fmax 4.04 ± 1.52 N) than membrane from unlaboured term	Oyen *et al*., 2004 [203]

	deliveries (Fmax 4.26 ± 1.09 N). Preterm FM had with greater average failure force at Fmax 4.3 ± 0.71 vs 2.7 ± 0.76 N in term FM. CM had significantly failed at lower loads than intact FM and AM, particularly in preterm samples (Fmax 4.16 ± 1.27 and 5.09 ± 1.30 N in term and preterm respectively). Placental AM was stronger compared to the rest of the AM, with unlaboured groups having higher peak forces than those following physiological rupture (5.62 ± 1.33 vs 4.01 ± 0.64 N unlaboured term and laboured term respectively)	
Biaxial puncture testing	Critical membrane tension T_{crit} was 0.46 ± 0.23 N/mm.	Buerzle *et al*., 2014 [213]
Biaxial puncture testing	Elastic modulus E = 2.35 MPa	Chua *et al*., 2009 [210]
Biaxial puncture testing	Fmax of AM in term laboured and unlaboured was higher than CM (Fmax 2.89 ± 1.08 N and 1.87 ± 0.61 N for laboured AM and CM respectively and Fmax 3.62 ± 1.03 N and 2.18 ± 0.81 N for unlaboured AM and CM respectively). At <32 weeks GA, laboured FM had Fmax of 4.61 ± 0.10 N and dropped to 3.47 ± 1.57 N by term (>37 weeks GA) while unlaboured FM had Fmax of 5.80 ± 1.77 N at <32 weeks and decreased to 4.10 ± 1.62 N by term.	Oyen *et al*., 2006 [201]
Biaxial inflation (with 1 mm defect)	Collagen fibrils aligned tangential to the defect with increasing load (J), while unloading led to fibril de-extension back to the original morphologies, indicating collagen fibril deformation is reversible at the edges of a defect.	Ehret *et al*., 2017 [209]
Biaxial inflation	Placental FM generated a tension of 72.26 N/m corresponding to 15.4 mmHg pressure. Rupture of the FM occurred at 295.08 ± 31.73 N/m corresponding to 34 mmHg pressure. Results correlated with collagen deformation and alignment with increased pressure.	Joyce *et al*., 2016 [202]
Biaxial inflation	Critical membrane tension T_{crit} was 0.23 ± 0.07 N/mm.	Buerzle *et al*., 2013 [198]
Biaxial burst testing	CBB values were higher than standard tests in placental (83.8 ± 19.4 vs 69.3 ± 17.9 mmHg) and cervical FM (67.9 ± 23.4 vs 58.1 ± 15.8 mmHg). In unlaboured term FM, cyclic pressures were higher than laboured FM (80.6 ± 22.4 versus 73.5 ± 22.7 mmHg respectively).	Sumanovac *et al*., 2017 [214]
Biaxial burst testing	At 20 - 38 weeks GA, tensile strength was average 399 grams to burst. At 39 - 42 weeks GA, tensile strength decreased to average 257 grams to burst.	Pressman *et al*., 2002 [200]

	ritical membrane tension T_{crit} was 0.46 to 1.33 N/mm.	
Computational modelling using biaxial strength (σ_F) and uniaxial strength (elastic modulus)	Increased AF volume with increasing GA augmented the membranes strength (σ_F; MPa) in laboured term (GA 40, average 1.1 ± 0.4 MPa) versus term unlaboured (GA 39, 1.6 ± 0.4 MPa) and preterm (GA 31, 1.65 ± 0.4 MPa.	Oyen *et al*., 2004 [203]
Computational model using uniaxial tension and biaxial inflation fracture tests to determine tear resistance of term FM.	Tearing energy was found to be higher in AM (average 0.032 J/m) than CM (0.009 J/m) correlating with higher collagen fibril alignment at the AM defect site	Bircher *et al*., 2019 [208]
Computational model using previously reported measurements of the uterus, FM stiffness and thickness of the AM and CM in term and PPROM samples	By applying pressure through the software, the authors determined that modelling the mechanics of the AM and CM separately led to different tissue behaviour than when measuring each membrane as a constituent layer of the fetal membrane	Verbruggen et al., 2017 [215]
Ex vivo bioreactor model	Cyclic tensile strain (2% CTS) using a bioreactor upregulated Cx43, AKT/PI3K signalling, COX-2, PGE_2 release, and sGAG content, followed by a significant decreased in collagen and elastin	Barrett et al., 2019 [105]

1.9 Mechanotransduction mechanisms in fetal membranes after stretch

Multiple studies have been focused on the application of *in vitro* loading techniques including uniaxial, biaxial, inflation and/or puncture testing on human and animal FM explants and cell extracts to determine how repetitive stretching influences mechanotransduction signals that lead to membrane failure [218-221]**.** Importantly, researchers have primarily focused on term human FM, with limited work being done on preterm membranes [218-221]. *In vivo a*nd *in vitro* experiments have shown fetal membranes respond to mechanical stimuli and stretch by activating COX-1/2 enzymes that synthesise PGE_2 isoforms, secrete pro-inflammatory cytokines (e.g. IL-6, IL-8) and collagenases for ECM breakdown that prepare the membrane for rupture [218-221] **Table 1.6** summarises mechanotransduction changes in human fetal membrane explants or cell types relevant to feto-maternal interactions. An early study by El Maradny *et al.,* 1996 utilised human term whole fetal membrane, AM or muscles of the lower uterine segment in an *ex vivo* stretch model to induce a static stretch of 40% to 70% for 2 and 4 hours [218]. Using immunohistochemistry, they showed that stretch induced significantly increased IL-8 concentration in all three tissue types at both time points [218]. This was concurrent with significantly increased collagenase activity, as measured through an enzyme activity assay following stretching for 4 hours [218].

Nemeth *et al.,* 2000 collected fetal membranes delivering at term (38 - 42 weeks of gestation) and preterm (30 - 36 weeks of gestation without evidence of infection) following C-sections [221]. Explants were stretched up to 225% their original size for 4, 18 and 32 hours [221]. Using quantitative Northern blot analysis, it was shown that IL-8 and Pre-B cell colony-enhancing factor (PBEF) expressions were significantly increased in preterm membranes only at 4 hours following distention, and their expression levels did not change in the other time points compared to non-stretched controls [221]. PBEF is an anti-apoptotic cytokine involved in both early- and late-stage apoptosis and correlates with the reduction in caspase 8 and 3 activation [221].

PBEF expression was upregulated during labour in both preterm and term fetal membranes and elevated in those with intrauterine infection [223,224]. In human fetal membranes following infection, PBEF expression has been associated with the pro-inflammatory cytokines TNF-α, IL-1β, and IL-

6 and LPS [223]. In amniotic epithelial cell line (WISH cells), treatment with the aforementioned factors resulted in PBEF upregulation suggesting a direct link between pro-inflammatory factor release and PBEF expression [223]. Kendall CE and colleagues released a series of studies investigating the effect of pro-inflammatory factors treatment and static stretch on the involvement of upstream transcription factors NF-κB and AP-1 on in the expression of PBEF primary human amniotic epithelial cells and WISH cells [222,225]. Following treatment with NF-κB and AP-1 inhibitors and using a combination of immunofluorescence microscopy, western immunoblotting and qPCR, the authors determined that the stimulation of both cell lines with IL-1β and static stretch increased expressions of PBEF and IL-8 [222,225]. These results support the observation that PBEF is up-regulated *in vivo* during labour and provide an insight into the mechanism by which NF-κB, AP-1 and IL-1β control the up-regulation of PBEF [222-225].

Increased COX-2 expression and subsequent prostaglandin synthesis plays an essential role in the onset and progress of labour [226]. The expression and activity of COX-2 in the myometrium has been shown to increase at term and with the onset of labour [226]. Stretch of the sheep uterus was associated with increased COX-2 mRNA expression [227] while inflation of the human uterus with a balloon in postpartum women further resulted in increased prostaglandin synthesis [228].

Sooranna *et al.,* 2004 have thus investigated the effect of stretch on prostaglandin synthesis in primary human uterine myocytes taken from women following non-pregnant (NP) hysterectomies and C-sections from those who were pregnant not in labour (NL) and pregnant in labour (L) [229]. The primary myocytes were subjected to 1 hour or 6 hours of static stretch [229]. Using qPCR and western blot analysis, the authors found that COX-2 expression was similar in samples obtained from NP and L groups, while both had significantly greater than those found in the NL group [229]. Following 16% stretch at both time point, cells from all groups increased their expression of COX-2 mRNA [229]. The authors then focused on the pregnant not in labour group [229]. Application of 16% stretch for 6 hours correlated with increased COX-2 protein levels, prostaglandin I2 metabolite and PGE_2 concentrations in the media [229]. Electrophoretic mobility shift assay using nuclear protein extracts from stretched and upstretched myocytes showed increased nuclear protein DNA

binding activity of AP-1 but not of NF-κB, suggesting that human myocytes stretch results in increased COX-2 activity through activation of the AP-1 mechanism [229]. The same group investigated the effects of uniaxial mechanical stretch of primary AECs taken from term elective C-sections [219]. Using qPCR and western immunoblotting, it was shown that 11% stretch for 1 and 6 hours resulted in increased expression of COX-2 and PGE_2 production [219]. This was concurrent with increased expressions of AP-1 and NF-κB and IL-1β, suggesting the involvement of both transcriptional regulators in AEC mechanotransduction mechanisms [219].As mentioned in **Section 1.8.2,** previous work done by our group utilised human non-laboured term fetal membranes in a bioreactor system [105,106]. Application of 2% CTS on human non-laboured term FM mediated changes in Cx43 expression, COX-2, PGE_2 and collagen and elastin content, highlighting the role of mechanotransduction processed in membrane weakening [105,106]. To avoid repetition, please refer to **Section 1.8.2.**

Biochemical and biomechanical studies of human FM have failed to detect elastin consistently. Some groups have characterised the presence of tropoelastin mRNA in term human FM, while others failed to agree on the percentage of elastin in term membranes relative to total weight (ranging from 0.08% - 36% depending on the technique employed) [53,110,111]. Previous work by our team has determined the presence of elastin in term AM using a fastin-elastin spectrophotometric technique [105]. A comprehensive study by Mazza and colleagues used a uniaxial tensile strain device (0 to 20% strain) on term human FM, correlating stress-strain response to biochemical parameters [111]. Collagen and elastin content were found to decrease and increase respectively after 20% strain. Interestingly, the same authors reported that an 'early delivery' membrane (31 weeks GA) was an outlier in the study, showing significantly higher elastin values, the lowest collagen content and highest stress-strain resistance [111]. This suggests that preterm membranes may behave differently to those collected at term due to differences in structural proteins and proteoglycans throughout gestation [111]. As discussed in **Section 1.2,** the presence of infections, maternal bleeding and other fetal and maternal complications further contribute to the structural anatomy of the fetal membrane throughout different gestational ages, all of which would subsequently affect mechanotransduction mechanisms after stretch.

Table 1.6: *Mechanotransduction changes in human fetal membrane (FM) explants or cell types relevant to feto-maternal interactions. AECs = amniotic epithelial cells.*

Protein/ enzyme	Tissue or cell type	Stretch	Downstream signalling	Reference
Il-1β	Myometrial myocytes	Static 6%-16%		Soorana *et al*., 2005 [230]
IL-6	Human umbilical vein endothelial cells	Cyclic 5, 10%	NF-κB	Sasamoto *et al*., 2004 [220]
	Fetal lung epithelial cells	Cyclic 5, 10, 17%	NF-κB	Copland *et al*., 2007 [231]
IL-8	FM explants	Static 40%-70%		El. Maradny *et al*., 1996 [218]
	FM explants	Static 225%		Nemeth *et al*., 2000 [221]
	Amniotic epithelial-like (WISH)	Static 175%		Nemeth *et al*., 2000 [232]
	Myometrial myocytes	Static 11%		Soorana *et al*., 2005 [230]
	Endometrial stromal cell	Cyclic 25%		Harada *et al*., 2005 [233]
	Cervical fibroblasts	Cyclic 15%	AP-1	Takemura *et al*., 2004 [234]
COX-2	AECs	Static 11%	NF-κB + AP-1	Mohan *et al*., 2007 [219]
	Myometrial myocytes	Static 6%-16%	AP-1	Soorana *et al*., 2004 [229]
	Term FM explants	Cyclic tensile strain 2%		Chowdhury *et al*., 2014 [106]
Cx43	Term FM explants	Cyclic tensile strain 2%	AKT/PI3K	Barrett *et al*., 2019 [105]
MMP	Term FM explants	Cyclic tensile strain 2%		Barrett *et al*., 2019 [105]
Pre-B cell colony-enhancing factor (PBEF)	FM explants	Static 225%		Nemeth *et al*., 2000 [221]
	Amniotic epithelial-like (WISH)	Static 175%		Nemeth *et al*., 2000 [232]
	Amniotic epithelial-like (WISH) and primary AECs	Static 16%	NF-κB + AP-1	Kendal *et al*., 2006 [225]
PGE_2	Term FM explants	Cyclic tensile strain 2%	AKT/PI3K	Chowdhury *et al*., 2014 [106] Barrett *et al.,* 2019 [105]

1.8.1 Mechanotransduction effects on fetal membrane collagen content

Collagen fibre orientation and remodelling have been found to affect the mechanical properties of the AM. Previous work done by lab members have made use of a uniaxial force application in a parallel and perpendicular direction to the collagen fibres [105,106]. Application of a force parallel to collagen orientation led to both a higher tangent modulus and tensile strength relative to force applied perpendicular to the direction of fibres, in both CAM and PAM regions **(Figure 1.10).** Collagen fibres were visualised using SHG imaging, showing fibres aligned to the direction of applied strain [105,106] **(Figure 1.10).**

Mazza and colleagues extensively studied the density, orientation, and cross-linking abilities of the collagen network within term whole FM and AM using uniaxial and multiaxial *ex vivo* models. The authors determined that specimen geometry and direction of strain influenced collagen alignment and content, particularly in the compact and fibroblast layers of the amnion [206]. In another study using term FM, the same group determined that collagen and elastin content had an inversely proportional relationship to strain before failure: with increased strain application, elastin concentrations decreased while collagen increased, probably owing to collagen fibre resistance and reorientation in response to stress loading [111]. Using a membrane inflation device, Moore's team created a comprehensive model to explain the changes in FM fibre alignment after tension application, whereby collagen fibre straightening increased with increased load and stretch [202]. These studies, as well as ones performed by our group showed that at rest, collagen fibres are interwoven in a random fashion throughout both whole FM and AM [111,202,235]. After application of strain, they straighten and distend, presumably affecting the morphology and behaviour of resident cell populations [111,202,235].

Our lab group demonstrated that biaxial repetitive CTS using a bioreactor led to a significant deformation in collagen fibrils with SHG imaging [105] **(Figure 1.10).** Drawing parallels to one non-primate report whereby uterine over distension led to the same biochemical changes observed in our group's study [236], the team concluded that repetitive stretching produced non-recoverable collagen fibre deformation, leading to eventual rupture [105]. Importantly, the group determined that

effects on mechanotransduction processes were strikingly different between PAM and CAM, with the latter having a weakened and less organised collagen orientation and intensity possibly owing to the presence of the ZAM in that area [105].

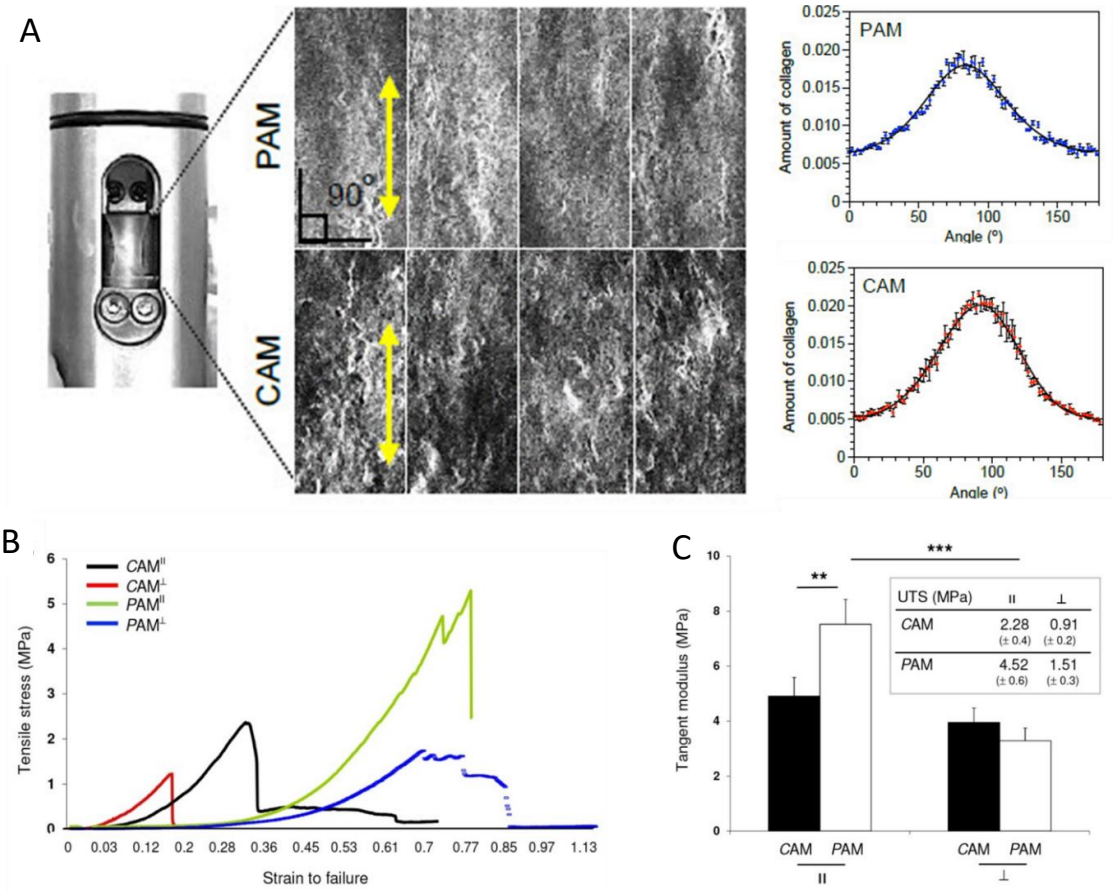

Figure 1.10: *Collagen alignment characterisation and measurement of tensile stress (MPa) and tangent modulus (MPa) after CTS in parallel (ii) or perpendicular (⊥) to collagen fibres. (A) SHG imaging of collagen fibres in PAM and CAM shows fibres aligned tangentially to the application of strain, confirmed using orientation analysis plots (right panel). Force application parallel to collagen orientation led to both higher tensile strength (B) and tangent modulus (C) and relative to force applied perpendicular to the direction of fibres. PAM showed significantly higher strength and resistance to strain than CAM. Images adapted from Barrett et al., 2019 [105] and Chowdhury et al., 2014 [106]. CAM = cervical amniotic membrane, PAM = placental amniotic membrane, UTS = ultimate tensile strength, SHG = second harmonic generation.*

Chapter 2

Wound healing mechanisms of the fetal membrane and the function of Cx43

Chapter 2: Wound healing mechanisms of the fetal membrane and the function of Cx43

2.1 Mechanisms of healing wounds after surgery, trauma or rupture of the fetal membranes

Physiological wound healing is a highly complex process comprised of multiple phases: homeostasis, inflammation, cell proliferation, migration, and extracellular matrix remodelling. To date, there is little evidence suggesting the human FM undergoes a wound healing mechanism when ruptured, with the rate of wound healing dependent on the species (rodents vs rabbits), model system (e.g. tissue region, puncture device, defect size) and time for repair after injury (days vs months) [8,15,18,237] . Due to the principally avascular nature of the FM (the CM contains a limited supply of blood vessels), it does not exhibit the classical wound healing properties that other tissues experience [8,15,18,237]. In the search for better PPROM interventions, a better understanding of the pathophysiology of FM rupture and healing within its individual components is needed.

2.1.1 Mechanisms of healing fetal membrane defects in pre-clinical animal models

Preclinical studies in animal models have yielded conflicting reports on FM wound healing after iatrogenic rupture [8,15,18,237] **(Table 2.1)**. Simulation of iPPROM using variable trocar sizes *in vivo* has been the standard way to measure FM healing. In 1972, Sopher and colleagues used the first animal model to study FM wound healing in rats *in vivo* using a 21 Gauge needle and harvested for up to 5 days [238]. At day 1, there were thickened edges at the AM with no evident healing [238]. By day 5, there was histologically a reduction of the wound size, possibly owing to uterine contractions, but not complete closure [238]. Limited healing after injury was also reported in fetal membrane defects from sheep, rhesus monkeys and rabbits [27,44,240,239]. In an *in vivo* rabbit model, fetoscopic balloon occlusion the trachea was used for treatment of congenital diaphragmatic hernia at mid-gestation (88 - 99 days) [241]. By day 145, histology showed rabbit defects did not heal [241]. Interestingly, in both sheep and rabbit models, the authors showed upregulation of MMP-2 and 9 and their inhibitors, suggesting matrix remodelling was taking place

[46,241]. Using rabbit models is challenging, as their short gestational period of 31 days does not permit for long-term wound healing investigations and experiments must be limited to 7 days [241].

Despite no evidence of healing in human FM, swine and mouse models are the only species that have presented with complete spontaneous closure of wounds [14,66,82]. In mouse FM, the healing rate was dependent on the size of the defect created by the needle (20 or 26 gauge), with 100% closure in small wounds (0.47 mm) relative to 40% in large diameter (0.91 mm) wounds [66]. Of importance, CM wound closure was almost absent relative to the rate of AM healing [66]. In mouse membranes, healing involved differentiation of vimentin-positive AECs to a mesenchymal-like phenotype [66]. M2-macrophage cell recruitment from the amniotic fluid into the defect site was followed by pro-inflammatory factor upregulation (IL-1β and TNFα) [66]. Injection of collagen type-1 into the defect enhanced the migration of amniotic mesenchymal cells through myosin contractions to repopulate the wound [82]. The same group reported thrombin injections in mid-gestational mice delivered preterm, while concentrations of MMP-8, 9, 3 and PGE_2 was markedly increased in FM of treated animals, suggesting a thrombin-mediated regulation of proteases and PGE_2 release [14].

In mice, the mechanism of healing involved proliferating AECs reported to lose cell to cell adhesion, apical-basal polarity and differentiated to AMCs and expressed high levels of vimentin [66,103]. This intermediate protein is an established mediator of cell migration and wound repair, and in mouse membrane defects was reported to accelerate tissue repair mechanisms [66]. The release of growth factors like TGFβ1 by macrophages stimulates fibroblast-like cell differentiation to myofibroblasts and promote repair via αSMA [66,179,242-244]. Of interest, embryonic wound healing involves the formation of an actomyosin ring at the wound margin, which enables purse string contraction of the wound without activation of an inflammatory mechanism [245,246]. The same mechanism could occur in small mouse defects and possibly small human defects, a notion which will be further explored in **Chapter 4.**

Whilst swine and mouse models have spontaneous FM healing properties, they may not be suitable when translated for repairing defects in human FM [66,103]. The differences in the healing

response could be due to the increased vascular supply to swine and mouse FM which will enhance the rate of inflammation that enables granulation tissue formation and scarring [66,103]. The healing mechanism seen in mice was absent in Yucatan miniature pigs despite spontaneous healing of membrane defects up to 4 mm in diameter 44 days post-laparotomy [15]. Biomechanical studies have shown that human FM are significantly weaker than sheep and swine membranes, contributing to their differential healing capabilities [199]. It is hypothesised that the absence of healing in human FM is an evolutionary mechanism to prevent pathogen accumulation during re-sealing [172]. Clinically, this hypothesis is significant, as latency periods between detection of infections and delivery influence neonatal survival and maternal complications [5]. I will revisit this statement in **Chapter 5.**

Table 2.1: *Mechanisms of healing fetal membrane (FM) defects in pre-clinical animal models. AF = amniotic fluid, GA = gestational age, CM = chorionic membrane.*

Species	Key Findings	Reference
Rats	Laparotomy was performed using a 21G needle (0.8 mm defect diameter) and harvested for up to 5 days. By day 5, there was histologically a reduction of the wound size, possibly owing to uterine contractions, but not complete closure.	Sopher *et al*., 1972 [238]
Sheep	Fetoscopic balloon occlusion the trachea was used for treatment of congenital diaphragmatic hernia at mid-gestation (88 - 99 days). By day 145, histology showed defects did not heal. Upregulation of MMP-2, 9 and TIMPs.	Devlieger *et al*., 2000 [241] Devlieger *et al*., 2002 [46]
Rhesus monkey	Induction of a defect after fetoscopy in *n*=1 rhesus monkey. By week 6, there was no evident healing.	Devlieger *et al*., 2006 [8]
Rabbit	Fetoscopy with a 14G needle (2.1 mm defect diameter) was performed at 23 days, samples were harvest 7 days later. FM integrity was maintained in 25% of animals. There was no evident complete restoration.	Mallik *et al*., 2007 [44]
	Fetoscopy occurred at 23 days and samples were harvested 9 days later. 40% of animals showed FM	Devlieger *et al*., 2000 [241]

	healing. Upregulation of MMP-2, 9 and TIMPs in AF post-surgery.	
Swine	Yucatan miniature pigs underwent laparotomy with 12 F trocar (4 mm defect diameter) at 70 days GA. Spontaneous healing of membrane defects up to 4 mm in diameter 44 days post-laparotomy.	Papanna *et al*., 2015 [15]
Mouse	100% closure in small wounds (0.47 mm) relative to 40% in large diameter (0.91 mm) wounds. CM wound closure was almost absent relative to the rate of AM healing. Differentiation of vimentin-positive AECs to a mesenchymal-like phenotype. M2-macrophage cell recruitment from the amniotic fluid into the defect site was followed by proinflammatory factor upregulation (IL-1β and TNFα).	Mogami *et al*., 2017 [66]
	Injection of collagen type-1 into the defect enhanced the migration of amniotic mesenchymal cells through myosin contractions to repopulate the wound.	Mogami *et al*., 2018 [82]
	Thrombin injections in mid-gestational mice delivered preterm, while concentrations of MMP-8, 9, 3 and PGE_2 was markedly increased in FM of treated animals, suggesting a thrombin-mediated regulation of proteases and PGE_2 release.	Mogami *et al*., 2014 [14]

2.1.2 Mechanisms of healing fetal membrane defects in in vitro trauma models

Mechanisms of healing wounds in FM *in vitro* studies have utilised scratch wound assays using AECs and AMCs derived from both human term and preterm tissue [14,66,247,248] **(Table 2.2).** Bilic *et al.,* 2003 isolated AECs and AMCs from unlaboured term (37 to 38 weeks GA) and preterm placentas after C-section (32 to 36 weeks GA) and cells were grown to confluence, followed by a lesion repair (scratch wound) assay for 0, 16 and 40 hours [247]. The authors determined through proliferation assays (BrdU assay) and light microscopy that AECs derived from both term and preterm FM showed complete lesion repair after 40 hours, while AMCs promoted 40% and 80% repair in term and preterm samples respectively [247]. Interestingly, there were no significant

changes in cell viability and haling in neither term not preterm samples after treatment with growth factors platelet-derived growth factor (PDGF), TNFα or fibrinogen [247]. In contrast, the same group shortly thereafter published a report repeating these experiments on term (37 to 41 weeks GA) and preterm (23 to 36 weeks GA) but altered media conditions, including cells cultured in tissue culture polystyrene or collagen type I [248]. They also treated cells with one of one of the following: 1) Dulbecco′s modified Eagle′s medium (DMEM) + EGF, 2) DMEM +10% FBS, and 3) Ham's F-12:DMEM + 10% FBS which contained high concentrations of L-glutamine [248]. Proliferation rates of human primary AECs and AMCs was highest in those treated with Ham's F-12:DMEM + 10% FBS compared to other three media, emphasising that different mediums and growth factors such as FBS influence cell viability and potentially their ability for differentiation, healing and repair [248]. Preterm AECs and AMCs further showed higher proliferation capacity than term cells [248]. Using these two studies, we can re-iterate the hypothesis that at term, cell populations, have a decreased capability for migration and repair [247, 248]

Using primary human AECs in a scratch wound assay, researchers showed AECs migrated after 72 hours to replenish the artificial wound, with samples treated with TNF and IL-1β exhibiting higher migration capacity concurrent with vimentin and E-cadherin expression compared to untreated control samples [66]. Mogami and colleagues showed that incubation of human primary AMCs, but not AECs, with thrombin resulted in MMP-1 and 9 gene expression and activity, concurrent with COX-2 expression and PGE_2 release [14]. Localization of PAR-1 in AMCs, but not AECs, and decidual cells, suggested PAR-1 induced thrombin-mediated regulation of MMP-9, while TLR4 induced thrombin-mediated regulation of MMP-1 and COX-2 [14]. In comparison, thrombin injections in mid-gestational mice led to preterm deliveries, concurrent with upregulation of MMP-8, 9, 3 and PGE_2 in FM of treated animals, suggesting a thrombin-mediated regulation of proteases and PGE_2 release in the mouse [14].

These studies support the notion that both AECs and AMCs can undergo differentiation to a migratory phenotype, however the experimentation setup (cell medium, stretch application,

primary cell extraction protocols and gestational age differences) influence the wound healing capabilities of either cell type, leading to contrasting findings within the literature [14,66,82,247,248].

Another suggested mechanism of tissue remodelling associated with normal gestation and PPROM is the discovery of FM microfractures [181]. These gaps in the FM caused by cellular shedding exhibit degradation of basement membrane and matrix collagen, generating localised inflammation and cellular migration [181]. The authors determined that microfractures in spontaneous laboured FM were deeper in depth and width than non-laboured FM, whilst microfractures in PPROM samples were larger with more collagen degradation than all other cohorts [181]. Treatment of a term FM explant culture model with CSE resulted in increased number of, width and depth of microfractures as quantified by SHG imaging [181]. Using scratch wound assays of primary AECs, Richardson *et al.,* 2020 have proposed this is mediated via EMT by quantifying differential cytoskeletal protein expression (e.g. vimentin, cytokeratin 8), which increase AEC migratory capacity to replenish AM layers where microfractures have occurred [77]. Cells then transition back to AEC phenotype via MET, mediated by the presence of amniotic fluid and blocked by oxidative stress from CSE [77,181,186].

Nevertheless, studies in primary cells isolated from FMs pose with limitations, including lack of physiological conditions such as amniotic fluid pressure, resident immune cell and stem cell populations in the AF, changes in ECM components and uterine stretching, all of which can influence cellular differentiation *in vivo*. Another consideration is the classification of FM based on gestational age, labour induction and contractions, whether membranes have ruptured before delivery, or whether delivery occurred with intact membranes. Added to that, there are potential molecular and mechanical differences between FM taken from women delivering vaginally or via C-sections due to the activation of the maternal systemic inflammatory response, leading to increased thrombin expression and decidual cell secretion of MMP-1 and MMP-3 that degrade FM ECM [12]. Myometrial and uterine contractions are further activated by thrombin which may lead to preterm labour with or without rupture of the FM [12].

As mentioned in **Section 1.2,** human primary FM cell populations isolated with collagenase digestion may be different to differentiating and proliferating AMCs and myofibroblasts found *in situ* and are embedded within a 3D ECM environment [84]. These cell populations extracted from AM explants as a total population after collagenase digestion presumably to do not produce the same mesenchymal markers thus would not behave the same as differentiating AMCs and myofibroblasts detected *in situ* in FM explants [84.] It would be worth comparing populations of cells extracted with different protocols and those seen *in situ* in FM explants via a variety of techniques to compare mesenchymal and myofibroblast markers, as well proliferation and migration capabilities via light microscopy or IMF-confocal microscopy via scratch wound assays and *in situ* healing.

We have previously developed an artificial *in vitro* trauma model using human term AM submerged in AF derived from TTTS fetoscopies [104]. In small AM defects (0.8 mm diameter), cells migrated at the wound edge to form dense populations, concurrent with polarisation of collagen fibres tangential to the wound [104]. The gap-junction protein Cx43 was preferentially overexpressed in AMCs, with an absence of cell migration across the defect [104]. We and others have shown that Cx43 channel function and activity is involved in all stages of wound healing, including induction of inflammation, cell-cell communication and migration, wound contraction and formation of granulation tissue and scar remodelling [104,105,249-251]. The role of C43 in different tissue healing will be further explored in **Section 2.2.**

Table 2.2: *Mechanisms of healing fetal membrane defects in in vitro trauma models. AM = amniotic membrane, AECs = amniotic epithelial cells, AMCs = amniotic mesenchymal cells, CSE = cigarette smoke extract, EMT = epithelial-to-mesenchymal transition, MET = mesenchymal-to-epithelial transition, SHG = second harmonic generation.*

Model	Key findings	Reference
Scratch wound assay, Primary AECs and AMCs from term and preterm AM	AECs showed complete lesion repair after 40 hours, while AMCs promoted 40% and 80% repair in term and preterm samples respectively.	Bilic *et al*., 2004 [247] Ochsenbein-Kölble *et al*., 2003 [248]
Scratch wound assay and Primary AECs	AECs migrated after 72 hours to replenish the artificial wound, with samples treated with TNF and IL-1β exhibiting even higher migration capacity concurrent with vimentin and E-cadherin expression.	Mogami *et al*., 2017 [66]
Primary human AECs and AMCs	Incubation of human primary AMCs, but not AECs, with thrombin resulted in MMP-1 and MMP-9 gene expression and activity, concurrent with COX-2 expression and PGE_2 release. Localization of PAR-1 in AMCs and decidual cells suggested PAR-1 induced thrombin-mediated regulation of MMP-9, while TLR4 induced thrombin-mediated regulation of MMP-1 and COX-2.	Mogami *et al*., 2014 [14]
FM explants and Term labour samples exposed to CSE	Microfractures in spontaneous laboured FM were deeper in depth and width than non-laboured FM, PPROM samples showed more collagen degradation than all other cohorts. CSE exposure in an FM explant culture model resulted in increased number of, width and depth of microfractures as quantified by SHG imaging.	Richardson *et al*., 2017 [181]
Scratch wound assay Primary human AECs with/without CSE	Proposed healing is mediated via EMT through changes in differential cytoskeletal expression (eg. Vimentin, cytokeratin 8), which increases AEC migratory capacity to replenish AM layers where microfractures have occurred. Cells then transition back to AEC phenotype via MET, mediated by AF and blocked by oxidative stress from CSE.	Richardson *et al*., 2018 [186]
In vitro trauma model	AMCs migrated to the wound edge to form dense populations around the wound. Collagen fibres	Barrett *et al*., 2017 [104]

Human AM explants	were highly polarised in the fibroblast layer in a failed attempt to close the edges of the wound. Cx43 was overexpressed by AMCs and formed plaques between cell-to-cell contacts which prevented migration. There was no healing across the defect site after 92 hours of culture.	

2.1.3 Mechanisms of iPPROM and healing after fetoscopic interventions

The mechanisms that contribute to iPPROM following fetoscopy and open fetal surgery are multifactorial [214]. Postoperative choriomembrane separation has been recorded in 20 - 40% of fetoscopic procedures, leading to collagen disruption and initiating rupture [252,253]. This results in AF accumulation in the myometrium, formation of amniotic bands, umbilical cord strangulation and increased fetal morbidity [237]. At the point of fetoscopic port insertion, cell apoptosis and damage in both the amniotic and chorionic cellular layers has been recorded [17,254]. Fetoscopic practises frequently require the use of liquid or gaseous distention of the FM (e.g., humidified CO_2) leading to increase insufflation pressures in membranes with iPPROM [24,253]. Using dry CO_2 insufflation during fetoscopic interventions improves visualization of the uterine environment and facilitates complex procedures [24]. Studies *in vitro* and in animal models have determined that prolonged exposure to CO_2 increases the likelihood of FM dehydration [172,207]. Collagen within the stromal layers of the FM becomes brittle while damage to the amniotic epithelium triggers the release of MMPs and promotes rupture [172,207,254]. Lastly, the gradual replacement of amniotic fluid with Ringer's lactate, a sodium lactate solution commonly used as IV fluid in dehydrated patients, after fetoscopy has been found to initiate apoptosis in the amniotic epithelium, further enhancing pathological mechanisms and increases the risk of iPPROM [207,254].

In a report published in 2006 using 19 patient samples, Gratacos *et al.,* 2006 did not determine any healing of the FM after fetoscopic surgeries [102]. In the same study, AM defects were larger than those on the CM (14.4 and 11.1 mm^2 respectively) [102]. The study further determined that the defect did not change in size between the time of surgery and delivery [102]. In addition, our group

has shown using a live/dead assay that there was no cell proliferation present in fetal membranes following surgical trauma for TTTS correction [17]. In some surgical interventions, there is evidence of the amnion sliding over the chorionic membrane, preventing amnionic fluid leakage and the creating the illusion of a healed membrane [102,255]. Membrane-decidua adherence has been further attributed to amniotic fluid retention after fetoscopy [256-258]. The same authors reported no evidence of spontaneous healing in FMs following intra-uterine fetoscopy, except for thickened wound edges suggesting an attempt to matrix remodelling [254].

We have previously shown that overexpression of Cx43 and gap junction plaque formation interferes with cell mobility leading to collagen alignment tangential to the defect site and the absence of wound closure in fetoscopic AM defects of over 3 mm in diameter [17]. Using IMF confocal microscopy, our group showed that AECs migrate to the defect site and accumulate to form clusters at the edges of the wound, presumably preventing wound healing mechanism from being activated [17].

Recently, Carvalho and colleagues showed FMs undergo collagen re-deposition at suture sites following SBA open fetal surgery, in contrast to non-suture sites [18,259]. The authors reported an increase in collagen concentration at the defect site concurrent with site-dependent gene expression alterations of MMP-1, 9 and TIMP-1 and 2 in surgical areas, suggesting a complex membrane remodelling process is undertaking in response to trauma [18,259]. Regardless, there is no complete wound closure observed in any human study independent of the procedure used or the size of the defect **(Table 2.3).** The inability of defects to heal highlights the urgency in understand the wound healing mechanisms in human FM, paving the road to develop better therapeutic interventions for PPROM.

Table 2.3: *Mechanisms of iPPROM and healing after fetoscopic interventions*. *AECs = amniotic epithelial cells, SBA = spina bifida aperta, AM = amniotic membrane, AF = amniotic fluid, CM = chorionic membrane.*

Surgery type	Key findings	Reference
Fetoscopy	Using 19 patient samples, the authors did not determine any healing of the amniochorion after fetoscopic surgeries. FM separated from the myometrium at the point of trauma to release AF, with AM defects being larger (14.4 $mm^{2)}$ than those on the CM (11.1 mm^2). The defect did not change in size between the time of surgery and delivery.	Gratacos *et al*., 2006 [102]
Fetoscopy	No cell proliferation present after fetoscopy.	McLaren *et al*., 1999 [47]
Fetoscopy	In some surgical interventions, there is evidence of the amnion sliding over the CM, preventing amnionic fluid leakage and the creating the illusion of a healed membrane.	Johnson *et al*., 1990 [256] Behzad *et al*., 1994 [255]
Fetoscopy	No evidence of spontaneous healing in fetal membranes following intra-uterine fetoscopy, except for thickened wound edges suggesting an attempt to matrix remodelling. Cellular apoptosis at point of fetoscope insertion.	Papanna *et al*., 2013 [258] Papanna *et al*., 2015 [254]
Fetoscopy	Overexpression of Cx43 and gap junction plaque formation interferes with cell mobility leading to collagen alignment tangential to the defect site and the absence of wound closure in fetoscopic defects. AECs migrate to the defect site and accumulate to form clusters at the edges of the wound, presumably preventing wound healing mechanism.	Barrett *et al*., 2016 [17]
Fetoscopy	Postoperative chorioamniotic separation has been recorded in 20 - 40% of fetoscopic procedures, leading to collagen disruption and initiating rupture.	Sanz Cortes *et al*., 2019 [252] Belfort *et al*., 2017 [253]
Fetoscopy	FM separation caused AF accumulation in the myometrium, formation of amniotic bands,	Sydorak., 2002 [237]

	umbilical cord strangulation and increased fetal morbidity.	
Open fetal surgery for spina bifida correction	FMs undergo collagen re-deposition at suture sites following SBA open fetal surgery, in contrast to non-suture sites. There was increase in collagen concentration at the defect site concurrent with site-dependent gene expression alterations of MMP-1/9 and TIMP-1/2 in surgical area. No complete closure was observed.	Carvalho *et al*., 2017 [18] Carvalho *et al*., 2020 [259]

2.2 The structure and function of gap-junction Connexins and Connexin 43

Previous work performed by our group focused on the inhibitory effects of the gap junction protein Cx43 on AM and FM wound healing [17,43,104,105]. Connexins are highly conserved transmembrane proteins that act as subunits to make up gap junction hemichannels with diameters of 1 to 1.5 nm [260] **(Figure 2.1).** Hydrophobic gap junction channels enable intracellular cell communications by allowing the passive diffusion of ions and metabolites (e.g. Ca^{2+}, ATP, cAMP and siRNAs) between adjacent cells [260]. The structure of connexins differ moderately in their cytoplasmic domains which control their different roles in adhesion, signalling and molecular cascades [260]. Different methodologies have been employed to determine the presence and quantity of connexin hemichannels on the cell membrane in cell and animal models of wild type and functional knockouts [261]. These include electrophysiological measurements, biochemical assays (e.g. Western blot, w), immunohistochemistry and IMF confocal microscopy [261]. In this section, I will explore the heterogeneity of connexin hemichannels, particularly Cx43, and their proposed functions depending on tissue region, species and experimental procedures.

Cx43 (*GJA1* gene) is the most ubiquitously expressed connexin with a short half-life (1 - 3 hours), and plays a role in physiological cellular functions, homeostasis, and apoptosis [261]. Six Cx43 proteins associate to form a homomeric gap junction and attach to an adjacent hemichannel [261] **(Figure 2.1).** This resulting 12-Cx43 protein cluster can then translocate to the membrane to form a gap junction [261]. These clusters of gap junctions can be seen using immunostaining and they appear as plaques of approximately 0.1 to 1 μm on the interface between adjacent cells [104]. The protein sequences of connexins are most conserved in the transmembrane and extracellular domains, while the key functional differences between them are due to amino-acid differences in these domains [261]. In different *in vitro* and *in vivo* models, connexins have been found to interact with each other and form partner channels adjacent to each other [261]. The possibility of heteromeric channels made of hemichannels comprised of different connexin isotypes has also been observed [261]. Valiunas *et al.,* 2005 used a multipotent

human mesenchymal stem cell line to investigate gap junction formation between the cells, and between human MSCs (hMSCs) and HeLa cells transfected with rat Cx40, Cx43 and Cx45 [260]. The authors took electrophysiological measurements to determine whether a gap junction activity was present between the cells by recording the junctional currents (I_j) generated after a fixed voltage was applied [260]. Several studies had previously showed that homotypic gap junction channels (comprised of a 6 subunits of a single isotype) typically generated symmetrical currents, indicating that is the dominant functional channel, while heteromeric channels (multiple isotypes) gave rise to asymmetric currents [260]. Detecting specific connexin isotopes becomes more complicated when connexins are co-expressed within a cell junction, in addition to the sizing of channels and the interactions between them [243]. These factors display further variability in terms of current symmetry [260]. Despite the limitations, the authors showed that hMSC-HeLa/Cx43 and hMSC-HeLa/Cx40 cell pairs exhibited both symmetrical and asymmetrical voltage dependence, while hMSC-HeLa/Cx45 pairs always produced asymmetrical I_j, potentially owing to Cx45 channel heterogeneity [260].

This work and other studies highlight the challenges in identifying individual connexin isotypes, thus using multiple methodologies such as immunofluorescent confocal microscopy, immunoprecipitation, electrophysiological measurements and/or protein isolation through western blotting would ensure experimental evidence is valid. The co-localisation of connexins and particularly Cx43 with other connexins, varies between cell types, species, and culture conditions. In one study, Altevogt and Paul., 2004 used adult mouse spinal cord sections to investigate astrocyte-astrocyte and astrocyte-oligodendrocytes gap junction co-localisation via double- and triple-immunofluorescence microscopy [262]. They determined that astrocytes form gap junctions composed of Cx26 only, or gap junctions comprised of co-localised Cx43 and Cx30. Furthermore, astrocytes established heterotypic Cx26-Cx32 channels and heterotypic Cx30/Cx43-Cx47 channels that may also be heteromeric with oligodendrocytes [262]. In contrast, Cx29 does not co-localize with any of the other five connexins investigated, which was confirmed by comparing wild-type mice to a Cx29 mouse knockout model, achieved by replacing the Cx29 coding sequence in frame with a nuclear-localized β-galactosidase [262]. Distribution of connexins

in the mouse spinal cord also varied depending on the region: Immunostaining for all three connexins was quantifiably more evident in grey matter than in white, while there were more Cx43 (1.7 ± 0.6/μm^2) and Cx30 (1.3 ± 0.6/μm^2) immunofluorescent puncta than Cx26 (0.6 ± 0.3/μm^2) [262].

Connexins have also been found to associate with other cell membrane junction proteins. Using a functional knockout of Cx43 in the mouse embryo fibroblast NIH3T3 cell line, Cx43, N-cadherin and N-cadherin-associated proteins zona occludens protein-1 (ZO-1) and β-catenin were found to be co-localized and co-immunoprecipitated within the cell junctions [263]. Using siRNA knockdown of Cx43 and double immunostaining, the authors showed that cell surface expression of Cx43 required N-cadherin localisation, while N-cadherin cell surface expression required Cx43 cell membrane presence, suggesting that Cx43 and N-cadherin are co-assembled in a multiprotein complex containing various N-cadherin-associated proteins [263]. In addition, Cx43 has been found to localise with the tip of actin filaments in embryonic rat astrocytes via a combination of atomic force microscopy and immunocytochemistry [264]. The association of Cx43 localisation with cytoskeletal proteins has also been investigated by others [264]. Butkevich *et al.,* 2004 used mouse brain homogenates to further identify the F-actin binding protein Drebrin (Developmentally regulated brain protein) as a binding partner of the C-tail of Cx43 [265].

Cx43 has also been shown to act as a direct transcriptional regulator of N-cadherin by translocating to the nucleus and binding to the N-cadherin promoter [266]. In this study, the authors examined the role of Cx43 in neural crest development via Cx43 antisense knockdown in Xenopus cephalic embryos [266]. They split the experiments into three distinct models: 1) Fluorescently labelled embryos were dissected from the antisense-treated embryos and grafted into unlabelled host embryo, 2) Neural crest explants were plated on fibronectin following dissection and 3) Single cell assays following dissociation in Ca^{2+}/$Mg2^{+}$-free Danilchick medium [266]. N-cadherin induces cell polarity and is essential for neural crest migration [266]. In all three models, Cx43 knockdown led to a reduction in N-cadherin protein, whereas the levels of E-

cadherin another junctional protein, remained unchanged [266]. Analysis by qPCR and *in situ* hybridization showed that Cx43 knockdown decreased N-cadherin mRNA but did not affect the rate of mRNA degradation [266]. The effects of Cx43 knockdown on decreased neural crest migration, cell polarity, protrusions and cell dispersion were rescued was reversed following co-expression of n-cadherin mRNA [266]. The Cx43 isoform Cx43-20k comprised of a small carboxy-terminal fragment, was found to co-localise in the nucleus of neural crest cells and HeLA cells with N-cadherin, but the full length Cx43 did not [266]. To investigate whether Cx43 was essential in the regulation of N-cadherin expression, they fused the binding domain of the human glucocorticoid receptor with green fluorescent protein (GFP)-tagged Cx43-20k [266]. The construct translocated to the nucleus of neural crest and HeLa cells after dexamethasone treatment [266]. In addition, injection of the construct in embryos rescued the inhibition of N-cadherin expression and cell migration induced by Cx43 knockdown [266]. This evidence suggest that Cx43-20k nuclear localization is essential for N-cadherin regulation, which is conserved across different cell types and subsequently species [266].

Taking together the studies described above, Cx43 is able to co-localise with other connexins, form heteromeric gap junctions with multiple isoforms, translocate to the nucleus to act as a transcriptional activation and form associations with other cell membrane proteins to influence migration, morphology and hemichannel function [260-266]. In the context of wound healing, cytoskeletal associations with Cx43 (N-cadherin, β-catenin, F-actin etc) could potentially influence cell contraction and migration, a notion that will be further discussed below.

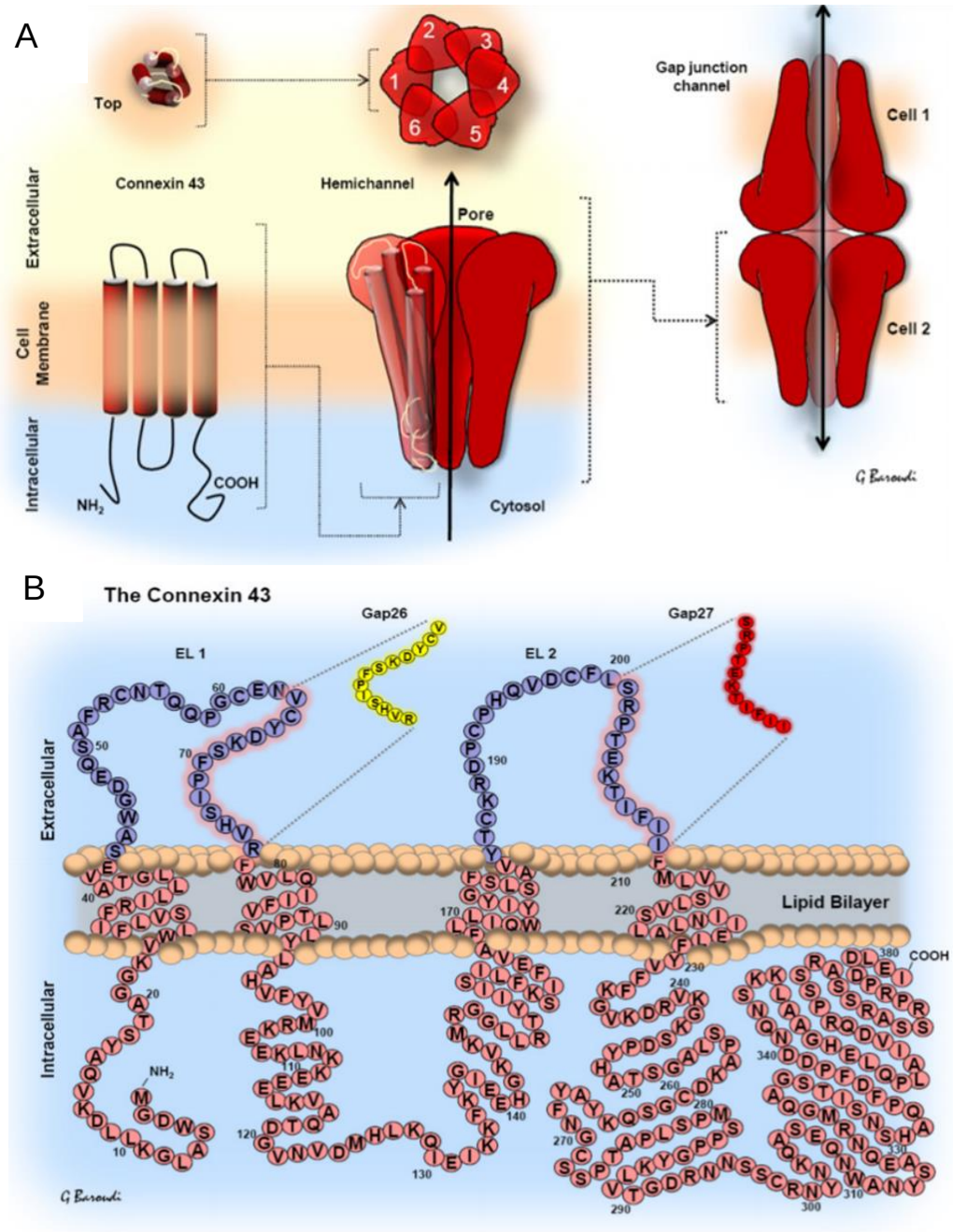

Figure 2.1: *Schematic representation of the formation of gap junctions from Cx43 protein units. (A) Six connexin proteins associate to form a homomeric gap junction and doc to an adjacent hemichannel. The 12 protein cluster translocate to the membrane to form a gap junction. (B) Individual connexin proteins are made up of four transmembrane domains, two extracellular loops, one intracellular cytoplasmic loop, and an N- and C-terminus. Images adapted from Hawat and Baroudi 2012* [267]*.*

2.3 Connexin 43 and inhibition of the wound healing mechanism in *in vitro* and *in vivo* loss and gain of function models

2.3.1 Cx43 expression in skin wounds and vascular endothelial cell healing

During conventional skin wound healing, skin tissue undergoes several healing stages: homeostasis, inflammation, proliferation/migration, and remodelling [244]. Cx43 channel function and activity is involved in multiple stages of skin wound healing, including initiation of inflammation, cell-cell communication and migration, wound contraction and formation of granulation tissue and scar remodelling [268-271] **(Table 1.4).** Several studies have observed molecular differences between the healing of epidermal and deep dermal wounds [280,281]. In this section, I will explore the role of Cx43 in skin wound healing and compared the differences observed in Cx43 and other connexins distribution during epidermal, dermal, and deep wounds.

Becker and colleagues have extensively investigated the role of connexins after trauma, determining that multiple connexin types (including Cx43, 26 and 30) have differential expression patterns throughout the wound healing process [272]. Using 2-day old ICR neonatal mice with 3 mm incisional wounds, Coutinho *et al.,* 2003 showed that Cx26, Cx30, Cx30.1 and Cx43 were expressed at different time points (6 hours and 1, 2, 4 7 and 12 days post wounding) and at variable concentrations [272]. In the epidermis Cx43 was localized in the basal and lower spinous cell layers, whereas Cx26, Cx30, and Cx31.1 were expressed in the upper, differentiating epidermal layers [272]. In the dermis, Cx43 was the most ubiquitously expressed connexin, found in dermal fibroblasts [272]. All four connexins investigated decreased at the wound edge by 6 hours, while by day 1 both Cx31.1 and Cx43 were both downregulated compared to controls (non-wounded tissue) [272]. However, in areas away from the wound, Cx43 continued to be downregulated, while Cx31.1 remained at normal levels in the granular layer [272]. By day 4, Cx43 levels significantly increased and through many epidermal layers and in adjacent regions where cells are proliferating, in contrast to decreased Cx31.1 expression [272]. In the epidermis, Cx43 co-localised with the proliferation marker Ki67 in the epidermal cell layer in controls, however in the wound edge, Cx43 expression was decreased until day 2 and increased again

at day 4 onwards, with evident Cx43-Ki67 co-localisation [272]. Interestingly, Cx43 in the dermis was upregulated in blood vessels at the injury site within 6 hours of injury, but its expression decreases to normal levels compared to controls by day 2 [272].

These experiments showed that Cx43 expression is markedly decreased within 24-48 hours in cutaneous skin injuries in the epidermis, followed by the initiation of keratinocyte migration and fibroblast migration across the wound [272]. The authors concluded that Cx43 upregulation hindered cell migration and fibroblast differentiation during the granulation stage of wound healing [272]. As this paper served more as an observational study, functional knockout, knockdown and gain of function studies were needed for this hypothesis to be accepted, as the presence of other connexins could be influencing wound healing mechanisms.

a) In vitro and in vivo Cx43 pharmacological knockdown studies in skin models

Using this evidence, Becker's group hypothesised that Cx43 functional downregulation via antisense technology would significantly accelerate the wound healing of epidermal mouse injuries [250,273]. Cx43 concentrations have been found to increase in blood vessels smooth muscle cells and endothelial cells of around the wound site within 6 hours following injury [250]. This influx of Cx43 expression has been hypothesised to enhance cell-cell communication, increasing vasodilation, and allowing for leukocyte infiltration into the site of injury [274]. Following Cx43 knockdown using 1 μM antisense (Cx43asODN), wound healing of incisional and excisional mouse epidermal wounds was accelerated as measured over 12 days post injury [273]. This was concurrent with a decrease in neutrophil infiltration which correlated with a reduction in inflammation [273]. Inflammation was quantified using haematoxylin and eosin staining and was directly related to the reduction in granulation area and increase re-epithelisation [273].

Mori *et al.,* 2006 utilised an *in vivo* 8-week-old mouse model with and without the selective downregulation of Cx43 using 1 μM antisense in 30% Pluronic F-127 gel [250]. Application of Cx43asODN within 2 hours on 6 mm sized skin wounds resulted in significant knockdown of Cx43 at the delivery site [250]. Through IMF confocal microscopy, it was determined that there was increased number of BrdU-positive cells in the dermal wound edge following Cx43asODN

incubation, with significantly more proliferating cells accumulating within granulation tissue at days 1 and 2 [250].

TGFβ1 has been proposed to act as both pro- and anti-inflammatory, dependent highly on the species, cell, and tissue type as well as experimental procedures. In the context of skin healing, TGFβ1 has been previously demonstrated to promote fibroblast migration and proliferation [275], enhance wound contraction [276], re-epithelialisation [277] granulation tissue formation through αSMA in myofibroblasts [278] and collagen synthesis and deposition [279]. In Cx43asODN-treated mouse wounds, TGFβ1 mRNA was elevated on day 2 within elongated fibroblast-like cells at the wound edge compared to controls, concurrent with increased collagen type 1α deposition (quantified via hydroxyproline assay) [250]. The expression of TGFβ1 was lowest at days 1 and 7 after injury, suggesting a time-depended activation of TGFβ1 in relation to Cx43, however other factors are potentially also enhancing the wound healing process [250]. The relationship between TGFβ1 and Cx43 in wound healing warrants further investigation, something that will be touched upon further in **Chapters 3** and **4** of this thesis.

The same paper used scratch wound assays using Swiss 3T3 fibroblast cell line, followed by *in vitro* knockdown of Cx43 with Cx43asODN [250]. Cx43asODN treatment resulted in increase of fibroblast migration following 4 hours of initial injury [250]. This was concurrent with significantly higher fibroblast cell density and percentage of wound closure in Cx43asODN-treated fibroblasts relative to untreated controls [250]. In the wound site of mouse wound, collagen expression was also significantly higher at day 2 and 7 of injury, compared to wild type untreated mice [250]. The authors investigated whether these fibroblast-like cells observed throughout the granulation site have myofibroblast characteristics by αSMA antibody immunostaining [250]. At day 7, αSMA staining was significantly higher in Cx43asODN-treated wounds, while by day 10, controls exhibited significantly higher αSMA than those exposed to Cx43asODN [250]. The hypothesis here is that Cx43 is essential in activating myofibroblast differentiation at the first stages of wound healing, but following the granulation stage, Cx43 loss of function hinders myofibroblast

differentiation [250]. Nevertheless, the authors showed that Cx43 knockdown led to accelerated wound healing at the proliferation stage of wound healing [250].

As shown by Becker's group, the expression of Cx43 is rapidly downregulated within hours of Cx43asODN treatment [250,273]. Despite the protein turn-over of Cx43 being 1-2 hours and working in favour of rapid downregulation, only a single application of the antisense was placed and no re-application was performed during the duration of the injury [250,273]. This could allow for Cx43 mRNA to be transcribed and thus translated as the tissue is adapting to other molecular mechanisms during injury and wound healing and results in a limitation to these studies [250,273].

Others have compared the use of Cx43 mimetic peptides to siRNA-mediated knockdown of Cx43 [251]. Connexin mimetic peptides have been designed to mimic small sequences of connexin proteins without altering gene expression [251]. The connexin mimetic peptide (CMP) Gap27 is designed to be targeted to amino acids 204 - 214 (SRPTEKTIFFI sequence) on the second extracellular loop of Cx43 **(Figure 2.1)** and acts to attenuate hemichannel activity and inhibits connexin-mediated communication, rather than knocking down the expression of Cx43 [251]. In contrast, siRNA duplex sequences targeted to Cx43 via Lipofectamine 3000 transfection reagent was used to knockdown Cx43 expression [251]. The authors used four primary cell types: human adult keratinocytes (AK), fibroblasts sourced from juvenile foreskin (JFF), human neonatal fibroblasts (HNDF) and adult dermal tissue (ADF) [251]. In AK and JFF cells, Gap27 improved scrape wound closure rates by over 50%, but did not influence the migration potential of HNDF and ADF cells [251]. In contrast, Cx43-siRNA significantly increased scrape wound closure in all the cell types, concurrent with enhanced TGF-β1 expression (quantified via qPCR) and in JFFs and ADFs [251]. This study highlights the limitations of using peptide mimetics, as despite being effective in hemichannel activity attenuation, it targets only the extracellular loop of Cx43 [251]. Cx43 has other non-gap junction protein functions that may play a role in cell adhesion, migration, and wound healing that can be best targeted and studied using knockdown and knockout techniques [251,280,281].

During the proliferation stage of wound healing in skin injuries, angiogenesis is essential as new blood vessels release growth factors (fibroblast growth factors, VEGF, TGFβ1) to the wound as well as providing structural support. In vascular endothelial cells, Cx43 expression rapidly increased, leading to a cascade of pro-inflammatory pathways to be activated [272]. In the first few hours of trauma, this allows for increase in vasodilation and neutrophil infiltration, promoting the transformation of resident cells (e.g. fibroblasts) to a contractile phenotype to initiate migration and re-epithelialisation at the wound [272]. However, sustained overexpression of Cx43 leads to increased inflammation and damage caused by neutrophil and macrophage action [250,272]. Using IMF microscopy, Mori *et al.,* 2006 showed that Cx43 knockdown with Cx43asODN in mouse lesions led to the formation of blood vessels at day 5 within the granulation tissue, compared to no blood vessel staining in untreated controls [250]. By day 14, the blood vessel density was comparable in both antisense and sense-treated samples, however it was evident that angiogenesis occurred at earlier points in Cx43asODN wounds [250].

b) In vitro and in vivo Cx43 knockout studies in skin models

Other researchers have used transgenic mice to knockout the Cx43 gene completely, instead of just decreasing its expression with knockdown techniques. Cogliati *et al.,* 2015 used a heterozygous Cx43 knockout ($Cx43^{+/-}$) generated by replacing exon 2 of the Cx43 gene with the neomycin resistance gene [280]. Using macroscopic evaluation of wounds and measuring the wound epithelium thickness in $Cx43^{+/-}$ mice, it was shown that Cx43 deficiency accelerated the re-epithelialization of the wound by day 7, a time point associated with the remodelling phase of healing [280]. In addition, greater epithelial projections of the epithelium over wounds were observed at day 3, further highlighting enhance re-epithelialisation is occurring [280]. This was correlated to no changes in newly formed blood vessels compared to wild type mice, which is a contrast to that seen in wounds of wild type mice after Cx43asODN treatment [250]. Another contrast to that study [250] is that collagen protein deposition remained unchanged between wild type and $Cx43^{+/-}$ mice, despite increased mRNA expression of collagen types I and III [280]. However, Cx43 deficiency enhanced the expression of ECM remodelling mediators MMP-2 and

TGFβ1, suggesting potentially enhanced remodelling in $Cx43^{+/-}$ mice relative to wild type [280]. Evidence within this knockout study suggests that in the epidermis, downregulation of Cx43 around wound edges allows successful cell communication, adhesion and subsequently migration to repopulate the wound [280].

In contrast to the epidermal findings, Cx43 was found to be upregulated in fibroblasts in deep dermis immediately after trauma, promoting granulation and scar formation [281]. Wan *et al.,* 2021 investigated whether Cx43 influenced the mobilization of fibroblasts expressing the Engrailed-1 gene (termed the EPFs) and the extracellular matrix of the fascia in deep dermal wounds [281]. The authors used a combination of models to study this, including a whole skin-fascia explant model to observe skin contraction and scar formation *ex vivo* (outside the animal) and an *in vivo* wound healing model in mice for comparison [281]. Double transgenic mice were used, whereby EPFs expressing Engrailed-1 were labelled with a reporter gene to allow for immunofluorescent analysis of that specific cell population [281]. In both models, Cx43 protein expression was upregulated compared to controls (non-wounded tissue) in fascia EPFs within the wound and at the wound margin, peaking at 5 days post-injury [281]. Inhibition of Cx43 activity in whole skin-fascia explants using a small-molecule inhibitor 2-APB and peptide mimetic GAP127 led to significantly reduced scar area and collagen content [281]. The authors then wanted to determine if Cx43 inhibition influenced gap junction intracellular passage of small molecules in cultured NIH 3T3 mouse fibroblasts [281]. Fibroblasts were treated with the membrane permeable fluorescent dye calcein acetoxy-methyl ester to visualise calcein transfer via IMF microscopy between cells. Cx43 inhibitor by 2-APB substantially suppressed calcein transfer into unlabelled 3T3 fibroblasts, while GAP 27 completely abolished calcein transfer to the unlabelled 3T3 fibroblasts [281]. In addition, Cx43 inhibitors further disrupted calcium oscillations (as quantified by calcium indicator dye, Fluo-4 calcein acetoxy-methyl and time-lapse live imaging) and fascia fibroblast migration which normally synthesise ECM proteins in skin-fascia explants, emphasising the role of Cx43 in extracellular communication during skin wound healing [281] **(Figure 2.2)**.

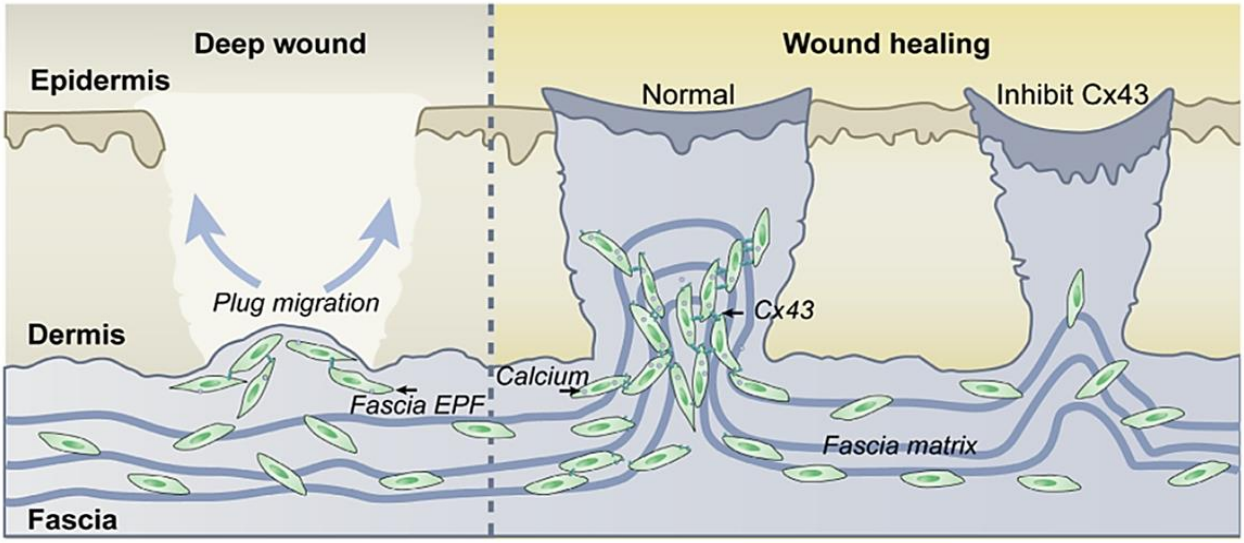

Figure 2.2: *Schematic representation of effects of Cx43 knockdown in deep wounds during scar formation and repair. In deep dermis, fascia fibroblasts migrate towards the centre of the wound and promote extracellular matrix movement to follow. Inhibition of Cx43 disrupts calcium oscillations and migratory potential of fascia fibroblasts leading to incomplete scar formation at the epidermis. Epidermal overexpression of Cx43 has opposite effects on wound repair, however Cx43 gap junction-dependent fascia fibroblasts communication plays an essential role in matrix repopulation and scar formation in deeper wounds. Image taken from Wan et al., 2021 [281]. Cx43 = connexin 43, EPF = Engrailed-1-expressing fibroblasts.*

c) In vitro and in vivo Cx43 gain-of-function mutation studies in skin models

Post-transcriptional modifications of Cx43, such as phosphorylation of S^{364}/S^{365} residues controls trafficking of the hemichannel to the cell membrane and can cause gain-of-function phenotypes associated with skin diseases [282,283,286]. Li *et al.,* 2019 showed that following injury, C57BL/6 female mice treated with an ERK1/2 inhibitor resulted in increased Cx43 expression [284]. Cx43 overexpression antagonised the phosphorylation of ERK1/2, directly affecting MMP-1 synthesis, leading to the promotion of collagen III production and upregulation followed by scar formation [284]. Others have shown that direct phosphorylation of residues S^{279}/S^{282} via Erk1/2 led further influence gap junction permeability [285]. Cottrell *et al.,* 2002 used electrophysiology experiments utilizing mutant S^{279}/S^{282} (via residue substitutions) in a Cx43 knockout mouse cell line to demonstrate that phosphorylation at these sites affected gap junction open probability [285].

These studies highlight how mutations in Cx43 can affect gap junction activity and translocation to the cell membrane. Cx43 mutations have been associated with one syndromic and three non-syndromic skin conditions [286]. Mutations in the *GJA1* gene encoding Cx43 result in a syndromic, autosomal-dominant disorder known as Oculodentodigital dysplasia (ODDD), whereby patients suffer from congenital deformities and complications of the face, eyes, teeth, and limbs [286]. A total of 73 mutations in Cx43 have been associated to ODDD, of which 64 are autosomal dominant missense mutations [286]. Interestingly, phenotypic differences between patients have been attributed to specific mutations [286]. Cx43-G138R mutation resulted in the loss of gap junction channel function [287] while the Cx43-G21R mutation promoted improper oligomerization during plasma membrane translocation, compromising hemichannel docking and resulting in non-functioning [288].

Srinivas *et al.,* 2019 investigated three gain-of-function mutations in the Cx43 gene (Cx43-G8V, Cx43-A44V and Cx43-E227D) via site directed mutagenesis using wild type Cx43 as a template in HeLa cells and Xenopus oocytes [289]. These mutations were chosen as they have been previously associated to non-syndromic skin diseases Palmoplantar keratoderma, congenital Alopecia-1, Erythrokeratodermia variabilis et progressiva, and Inflammatory linear verrucous epidermal nevus respectively [289]. Using electrophysiology experiments, they showed Xenopus oocyte cells with mutant Cx43 significantly increased membrane current flow with large conductance through formation of active hemichannels compared to by wild-type Cx43 cells which were unable to form these hemichannels with increased functionality, while this enhanced membrane current was inhibited by either calcium, or gadolinium [289].

Wang *et al.,* 2015 also characterised a heterozygous mutation in *GJA1* (c.23G>T [p.Gly8Val]) linked to the rare skin disorder Keratoderma-hypotrichosis-leukonychia totalis syndrome (KHLS) [290]. HEK293 cells were transfected with mutant-expressing Cx43(Gly8Val) plasmids, resulting in increased expression of Cx43(Gly8Val) [290]. The authors observed a gain-of-function phenotype, whereby mutant hemichannels had significantly more openings than wild type Cx43 cells through patch-clamp experiments [290]. Using a Ca^{2+} imaging method, the mutant cells were also

found to facilitate increased Ca^{2+} influx at resting potential [290]. Correlating this to an exome analysis linking Cx43(Gly8Val) to KHLS, it was suggested that this gain-of-function effect may result in cytoplasmic Ca^{2+} overload, accelerated apoptosis of keratinocytes and subsequent skin hyperkeratosis associated with the disease [290].

The work highlighted throughout **Section 2.1** indicates an increasing amount of evidence that gap junctional communication between cells coordinates precise molecular mechanisms during the wound healing process [250-290]. Limitations in our understanding of Cx43 activity in human skin wound healing are due to differences in experimental procedures and species heterogeneity, as well as whether the *GJA1* gene has been completely knocked out or decreased in expression via pharmacological knockouts. The next subsections will highlight how changes in expression of Cx43 influence wound healing in other tissue types.

2.3.2 Cx43 expression in chronic ulcers

In chronic ulcers, including diabetic ulcers, pressure ulcers and venus leg ulcers, the overexpression of Cx43 has been correlated with poor wound healing closure, sustained inflammation and phenotypic changes in fibroblasts and keratinocytes [291]. Using IMF microscopy, Brandner *et al.,* 2004 demonstrated that Cx43, 36 and 30 have altered expression patterns at the wound edge of healed human cutaneous wounds compared to chronic leg ulcers taken from venous leg ulcers and diabetic ulcers [292]. Using an *ex vivo* wound healing model, the authors induced wounds in human cutaneous skin taken from biopsies and observed an initial loss of Cx43 expression at the wound edge during the first stages of wound healing at 24 hours post injury, concurrent with Cx26 and Cx30 induction [292]. This expression pattern was repeated even after keratinocyte transplantation. Cx43 was downregulated until 48 hours post injury, and its expression peaked during the epidermal regeneration stage day 5, although it was not as high as in control non-wounded skin [292]. In contrast, all three connexins remained in high concentrations at the wound margins of chronic ulcers, suggesting Cx43 overexpression correlates with wound healing inhibition [292].

Becker's group identified Cx43 overexpression in human venous leg ulcers taken from biopsies throughout both the edges of the epidermis and in the deep epidermis [293,294]. With disease progression marked according to the Clinical Etiologic Anatomic Pathophysiologic classification, pathological skin sections showed epithelial hyper thickening, increased inflammation, and loss of dermal architecture, concurrent with increased Cx26, Cx30 and C43 absolute connexin expression and mean connexin expression per cell [293,294]. The increased expression of Cx43 was most prominent compared to controls of all connexins investigated [293,294].

To experimentally confirm these observational studies, Becker's group induced diabetes with streptozotocin (which generates hyperglycaemia) in rats [294]. Using immunohistochemistry and immunofluorescent microscopy, the authors found that in the intact epidermis, Cx43 and Cx26 protein concentrations decreased, while Cx43 was increased in the dermis, compared to normal rats [294]. Concurrent with altered Cx43 protein expression, cell-to-cell communication using the gap junction permeant dye Lucifer Yellow decreased in the epidermis but was enhanced in the dermis of diabetic rats [294]. Following 24 hours post injury in the diabetic rats, Cx43 expression was increased within a thickened site of keratinocytes at the wound margin, compared to controls which had low levels of Cx43 correlated with migratory cells at the wound edge [294]. This correlated with increased re-epithelialisation by day 5 post injury in normal rats, as measured by 15.7% closure of wounds in control rats, and 6.1% closure in diabetic wounds [294]. Inhibition of Cx43 via Cx43asODN antisense in diabetic rat wounds led to a decrease in Cx43 protein, induced epidermal regrowth to match that of controls, doubled the wound-healing rates and influenced keratinocyte morphology to a thinner phenotype [294].

The same research group demonstrated that Cx43, N-cadherin and the N-cadherin-associated protein ZO-1 were upregulated in skin punch biopsies in the dermis of human venous leg ulcers [295]. As discussed in **Section 2.2,** Cx43 has been found to interact with both N-cadherin and ZO-1. Using a mouse model of wound healing where full thickness skin excision wounds were treated with Cx43 antisense, the authors found that Cx43 and ZO-1 frequently co-localised in untreated wounds, but in Cx43asODN-treated injuries both protein expressions were

significantly decreased [295]. Using Cx43 antisense, it was shown that Cx43 expression in fibroblasts was concurrent with upregulation of N-cadherin and changes in β-catenin cellular localisation, both of which influence cell migration at the wound edge [295].

Due to the ability of N-cadherin and ZO-1 to promote cell adhesion and migration, the same paper asked whether Cx43 knockdown influenced N-cadherin/ZO-1-associated migration rate of 3T3 fibroblasts following scratch wound assays [295]. Using ZO-1 antisense, Cx43 shRNA and N-cadherin shRNA to effectively downregulate the respective proteins in individual experiments, it was shown that the velocity of fibroblast migration was highest in fibroblasts where Cx43 and N-cadherin expression was decreased [295]. This evidence suggests that Cx43 inhibition in fibroblasts may additionally contribute to cell migration by reducing N-cadherin, but with no influence on ZO-1 protein levels [295]. Using hanging drop assays, they further showed that inhibitions of Cx43 and N-cadherin increased the polarisation of the Golgi apparatus protein GM130 towards to wound edge 3 hours post-injury [295]. The Golgi apparatus influences the polarisation of fibroblasts and is thus a marker for cell polarisation. In scratch wound assays [295]. Cx43 inhibition resulted in fibroblasts with significantly larger F-actin-rich lamellipodia protrusions, concurrent with increased Rac1 and Rho-A GTPase activities, which are essential regulators of actin and microtubule dynamics and control cell motility and chemotactic responses through multiple actin-based structures [295].

2.3.3 *Cx43 expression in corneal endothelial wound healing*

The role of Cx43 in corneal endothelial wound healing has also been explored. Upregulation of Cx43 has been found to inhibit corneal endothelial wound healing using an *in vivo* rat injury model, while the application of Cx43 antisense rescued the wound healing mechanism [296]. Using rat models, Nakano *et al.,* 2008 created corneal endothelial injuries by gently scraping cells within the anterior chamber of the eye [296]. The eyes of animals were then treated with siRNA targeting Cx43 to knock down Cx43 expression [296]. Following Cx43 inhibition, five out of six corneas exhibited complete wound closures examined by immunolabelling and propidium iodine staining, compared to incomplete wound healing of controls [296]. This was concurrent with

accelerate wound closure rates and increased number of Ki67-positive proliferating cells in the corneal epithelium by day 1 post injury [296]. Importantly, like seen in skin wounds, ZO-1 and Cx43 proteins were co-localised in the plasma membrane of the endothelium, while Cx43 decreased after 12 hours, accompanied by elongated cells at the wound edge that were not producing αSMA [296]. Cx43 expression resurfaced at day 5 post injury specifically within elongated endothelial cells [296]. During injury, corneal endothelial cells form the retrocorneal fibrous membrane via EMT to contractile myofibroblasts [296]. Using immunofluorescent staining for αSMA, the authors observed an increased in αSMA-expressing myofibroblasts by day 3 post injury in antisense-treated eyes, compared to controls [296]. The distribution of myofibroblasts decreased by day 5, indicating that Cx43 inhibition reduced the formation of the retrocorneal fibrous membrane [296].

Another study utilised streptozocin-induced diabetes in albino rat to investigate potential targeting of Cx43 to enhance corneal wound healing [297]. Rats were split into non-diabetic (controls) and diabetic groups and were subjected to cornea injury. This was followed by treatment with the Cx43 peptide inhibitor Gap27 in as an eyedrop solution in PBS for up to 3 days of injury [297]. Using fluorescein penetration test to study wound closure rate, it was shown that Gap27-inhibition of Cx43 accelerated corneal wound injury closure rate in both diabetic and non-diabetic rats by day 1 post-injury compared to untreated corneas [297]. Using histology, the authors showed that Gap27 treatment reduced the infiltration mononuclear inflammatory cells in both diabetic and non-diabetic corneal epithelium [297]. This was concurrent with increased expression of keratin 12, an epithelial marker, following Gap27 treatment in diabetic and non-diabetic wounds compared to controls, suggesting higher rate of epithelial regeneration [297]. Cx43 immunostaining showed Cx43 expression was higher in diabetic rate corneas in the cytoplasm and nuclei of epithelial cells and keratinocytes [297]. As injury time progressed over 3 days, Cx43 expression decreased in both groups, however remained significantly higher in diabetic corneas to time-matched intact controls [297].

The influence of Cx43 expression on corneal injuries represents a significant deviation from acute and chronic skin wounds, as rat corneal endothelial cells are arrested in the G1 phase of the cell cycle and are maintained in a non-proliferative state, to be activated only after injury [296]. This difference in proliferation states between corneal endothelial cells and keratinocytes of the skin which are constantly replenishing the dead cells at the top of the epidermis highlights the challenges associated with investigating Cx43-induced wound healing inhibition in different tissue types and species.

2.3.4 Cx43 expression in buccal mucosal and gingival tissues

Cx43 expression has also been investigated of oral and gum wound healing, called buccal mucosal tissue and gingival tissues respectively [298,299]. Davis *et al.,* 2013 used 6-week-old male mice with a full thickness incision (3 mm width) through the skin and buccal mucosa to study Cx26, 30 and 43 dynamics during wound healing [299]. Distinct morphological differences between the skin wound and epithelial cells of the buccal mucosa migrated were observed [299]. At 24 hours, buccal mucosal cells formed in a thick lip or "wedge" at the edge of the wounds, while keratinocytes formed a thin tongue of cells with elongated migratory morphologies, which was previously observed by the same team in epidermal wounds [299]. Buccal mucosa cells largely their thickness and shape, and rapidly repopulated the wound, concurrent with more rapid re-epithelialisation compared to the epidermis by 6 hours post-injury [299]. All three connexins investigated were significantly more expressed in the buccal mucosa than the cheek epidermis (26-fold more Cx26, 490-fold more Cx30, and 24-fold more Cx43) with Cx43 being the most ubiquitously expressed through all layers [299]. All three connexins were rapidly downregulated in the buccal mucosa layers by 6 hours of injury, compared to increased expression in the skin as also seen by previous reports [299]. By 48 hours, buccal mucosa wounds had completed re-epithelialisation and Cx43 expression was returning to more normal (intact tissue) levels [299].

Tarzemany *et al.,* 2015 took into consideration that oral mucosal gingiva tissue has higher wound closure rates than then epidermis and hypothesized that Cx43 function is down regulated during human gingival wound healing, promoting the expression of fibroblast genes responsible

for quick and scarless wound healing [298]. Using IMF microscopy and western blot analysis, the authors showed that C×43 was abundantly present in the epithelium of unwounded human gingiva forming large C×43 plaques in connective tissue fibroblasts and in cultured human fibroblasts [298]. As in buccal mucosal tissues [299], Cx43 was significantly downregulated at the early stages of wound healing (3 to 14 days post injury) in epithelial cells and fibroblasts, returning to normal levels at day 60 [298].

In scratch wound assays of human gingival fibroblasts, Gap27 treatment inhibited Cx43 function and decreased cannel-mediated Lucifer Yellow dye transfer and promoted migration [298]. This was concurrent to significant increase in the expression of wound healing-associated genes MMP-1, 3 and 10, TGFβ1 and angiogenesis marker VEGFA in gingival fibroblasts [298]. In contrast, pro-fibrotic ECM genes such as collagen type I, and cell contractility-related genes including αSMA and decorin, which regulates wound healing fibrosis, were significantly downregulated [298]. This provides further evidence of reduced scar formation in human gingival tissue compared to skin models [298]. The authors used selective inhibitors for TGFβ, MEK1/2, p38, GSK3α/β, and the transcription factors AP1 and specificity protein 1 (SP1) to investigate Cx43-mediated signalling via the MAPK (ERK1/2 and p38), GSK3α/β and β-Catenin pathway via western immunoblotting [298]. Following 1 hour of treatment with Gap27, robust phosphorylation of p38, ERK1/2 and GSK3α/β was determined, lasting for 6 hours, before returning to the levels of untreated cells by 24 hours [298]. The authors concluded that in human gingival fibroblasts, inhibition of C×43 by Gap27 induced activation of MAPK and GSK3α/β signalling pathways, which may contribute to the fast wound healing mechanism observed in human gingival tissue [298].

2.3.5 Cx43 expression in the myometrium and fetal membranes

In fetal membranes, limited work has been done to link Cx43 with wound healing inhibition [300,301]. Work performed in rodent models showed Cx43 expression is controlled by transcriptional activators such as oestrogen and influences cell-to-cell exchange of CAPs [300,301]. Throughout gestation, molecular alterations in the myometrium are mediated by both ovarian hormones and

mechanical stretch by inducing CAP genes to prepare the uterus for the onset of labour [136,137,302]. One of these changes includes the upregulation of Cx43, resulting in accumulation of gap junctions to establish ionic coupling among myometrial smooth muscle cells for synchronization of their contractions [136,137, 302]. It has been shown that oestrogen, through is oestrogen receptor activation, controls rodent *GJA1* gene encoding Cx43, which correlated to increased oestrogen levels observed in the myometrium of humans during labour [302]. Others have shown that upregulation of prostaglandin isoforms promotes the expression of labour-associated proteins, including Cx43. Cook *et al*., 2000 and 2003 released a series of papers using mouse labour models to show that PGF_2 alpha ($PGF_{2\alpha}$) induced preterm labour by increasing Cx43, oxytocin receptor, prostaglandin receptor and PTGS-2 [303,304]. Xu *et al.,* 2013 inhibited $PGF_{2\alpha}$ with indomethacin in human myometrial cells and observed that increased of $PGF_{2\alpha}$ acts directly on CX43 expression levels [305].

Early work by Ou *et al.,* 1997 showed that expression of Cx43 and Cx26 was differentially regulated in the rat myometrium during pregnancy and labour [306]. Using pregnant rats compared to non-pregnant rats, the authors induced uterine stretch by either sham operation or placement of a tube in the nongravid uterine horns with and without progesterone treatment [306]. Using immunofluorescence microscopy, punctate Cx43 levels were found to increase in the myometrium after uterine stretch during labour, compared to unlaboured rats, indicative of enhanced gap junction formation [306]. In contrast to Cx43, Cx26 gene expression levels dropped between day 20 and 23, and its expression was not influenced further by stretch. Progesterone administration in the myometrium suppressed CX43 gene and protein expression and decreased myometrial contractility, perhaps to maintain pregnancy and avoid preterm labour [306].

Progesterone acts via its receptors progesterone receptor A (PRA) and progesterone receptor-B (PRB) to regulate Cx43 transport to the cell membrane during pregnancy and labour [307]. Nadeem *et al.,* 2017 used immunofluorescence microscopy and western immunoblotting to determine that progesterone P4 via PRA and PRB differentially regulate Cx43 cellular localisation in human myometrial cell lines expressing either PRA or PRB [307]. Following

treatment with P4, PRA-expressing myocytes formed gap junctions, whereas PRB-expressing cells inhibited junction formation through inhibition of Cx43 transport from the endoplasmic reticulum to the Golgi apparatus [307]. Exogenous expression of the Cx43 isoform Cx43-20K restored Cx43 trafficking to the plasma membrane in PRB-expressing cells, suggesting P4 via PRB controls Cx43 translation to generate the Cx43-20K isoform specifically, facilitating the transport of full length Cx43 to plasma membrane [307]. In contrast, inhibitions of the Cx43-20K isoform via loss-of-function mutagenesis in PRA cells prevented the trafficking of full length Cx43 [307]. Inhibition of the mTOR pathway using the mTOR inhibitor PP242 restored Cx43 translocation to the plasma membrane in PRB-expressing cells, suggesting P4 mediates Cx43 regulation mTOR signalling [307].

Barnett *et al.,* 2020 hypothesised that Cx43 expression, acting as a contractile-associated protein is altered in the spontaneous preterm labour (sPTL) myometrium relative to non-pregnant myometrium [308]. The authors used a guinea pig pregnancy model, which is preferred to other rodent models as they do not experience progesterone withdrawal prior to the onset of labour, mimicking the same even in humans [308]. Cx43 was found to increase in early gestation and remain steady throughout pregnancy in both human myometrial tissues taken from term labour and sPTL, and in the guinea pig compared to non-pregnant animals [308]. As previously mentioned, Cx43's phosphorylation at S^{368} on the C terminus, is essential for gap junction function [308]. Furthermore, Cx43 S-nitrosylation is post-translational modification that acts as a critical mediator of protein function in the myometrium, which was previously found to affect contractile dynamics by the same group [309]. To investigate Cx43 modifications, the authors used an *ex vivo* organ bath by attaching human myometrial tissue strips to a force transducer in a physiologic buffer and then exposed the tissue to either oxytocin followed by nitrous oxide (NO) [308]. Using a combination of immunofluorescence and qPCR analysis, it was shown that Cx43 was S-nitrosylated by NO, correlating to increased Cx43 phosphorylation at S^{368} and promoted hemichannel open states [308]. Cx43 was pharmacologically inhibited using 18b-glycyrrhetinic acid (18b-GA) or the peptide mimetic TAT-Gap19, resulting in decreased myometrial contractions as measured through tension generated by human myometrial tissue in a dose-

dependent manner [308]. These findings highlight the essential role of Cx43 gap junction function in regulating myometrial contractions and how interruption of Cx43 dynamics can influence preterm labour [308].

Previous research in our lab showed increased Cx43 gene and protein correlated with poor cell migration from both the epithelial and fibroblast layers as well as collagen alignment at the wound edge in defects over 3 mm wide after fetoscopic intervention and in small diameter (0.8 mm) wounds [17,104]. Increased Cx43 protein and gene expression at the wound edge was quantified via IMF-confocal microscopy and qPCR, concurrent with increased AEC and AMC death and collagen intensity and polarisation [104]. The authors used an *ex vivo* trauma model to induce 0.8 mm wounds in term human AM submerged human amniotic fluid taken from amnio drainage during TTTS [104]. In both fetoscopic injuries and *ex vivo* small diameter wounds in term AM, AECs formed clusters of cells at the edges of the wound and were unable to migrate to repopulate the wound [17,104]. AMC morphology and differentiation capacity was not investigated in these studies [17,104]. In Chapter 4, I use term fetal membranes taken from C-sections and subject them to the same *ex vivo* trauma model [104] with patient-matched amniotic fluid to investigate Cx43 expression and myofibroblast differentiation within both epithelial and fibroblast layers of the AM. I also examine the gene expression of pro-inflammatory factor TGFβ1 via qPCR at day 1 and 4 post-injury.

2.4 The role of fibroblasts and myofibroblast differentiation in wound healing

Due to the largely avascular nature of the AM, its healing mechanisms do not resemble classical wound healing processes briefly discussed in **Section 2.3**. As explored in **Chapter 1 Section 1.2**, the amniotic and chorionic membranes both contain populations of mesenchymal cells (AMCs, CMCs) which express fibroblastic markers and have fibroblast-like morphologies [47-57]. Throughout the body, fibroblasts are of mesenchymal cell origin and preserve tissue homeostasis by controlling the balance between the synthesis and breakdown of ECM components [244]. They are resident in almost all tissues and in higher concentrations in connective tissues [244]. During injury, fibroblasts become activate and differentiate into highly contractile myofibroblasts that move through the wound to reduce its size [244]. Fibroblasts express vimentin but not αSMA, while MFs express both vimentin and desmin but also myosin and αSMA [244]. Myofibroblasts are classified as an intermediate cell type between smooth muscle cells and fibroblasts [244]. The presence of extensive cell-matrix adhesions, gap junctions and contractile stress fibres made up of cytoplasmic microfilaments such as myosin, allow for MFs to contract and move to heal an open wound [244].

Myofibroblasts accumulate during the proliferation phase of wound healing and their origins tend to be tissue specific [244]. For example, in vascular wound healing, they are thought to be differentiated from pericytes and vascular smooth muscle cells [244]. In the amniotic membrane, they are derived from the resident AMCs in the fibroblast layer [76]. Some studies have shown myofibroblasts are derived through EMT [66,76]. In small mouse amniotic membrane defects, AEC to AMC transition has been shown to occur, as explored in **Chapter 1 Sections 1.6 and 1.7,** and this population was found to migrate from the epithelial layer across the defect site while the fibroblast layer remained compromised [66]. The reversible transition of AECs and AMCs during pregnancy and labour was further investigated in human FM explants, highlighting the capabilities of amniotic cell populations under stress [76-78]. A study using patients whose membranes have ruptured before the end of term determined that AMCs differentiated from vimentin-expressing fibroblasts to αSMA expressing myofibroblasts correlating with increase

swelling in the reticular and connective tissue layers of the FM, highlighting that cell differentiation influences rupture [76]. Although there were no differences in expression of αSMA to term membranes, there were clear morphological changes in myofibroblast populations including the presence of elongated cytoplasmic extensions, something that will be further investigated in **Chapter 4** [76]. To avoid repetition, please refer to **Chapter 1 Sections 1.6.6** and **Section 1.7** for information regarding the role of myofibroblasts in the fetal membranes.

The role of myofibroblasts in the synthesis and secretion of ECM proteins (collagen Types I, VI, XVIII), glycoproteins and proteoglycans for wound healing make them excellent candidates for investigation in the context of FM healing [244]. Interestingly, the number of myofibroblasts were found to be directly correlated with the concentration of subepithelial collagens [244]. Changes in the number of MFs over time further correlate with the rate of wound contraction in skin models [244]. Myofibroblasts express a plethora of other matrix proteins, including MMPs and TIMPs [244]. In terms of FM repair, MMPs, especially MMP-9 and 13 have been reported to be overexpressed in preterm fetal membranes [154,165]. MMP-9 is a collagen type IV collagenase and its abnormal expressions in preterm tissue correlates with other programmed biochemical events leading to labour [154]. The signalling pathways leading to the upregulation of MMP-9 are not very well defined, but the pro-inflammatory cytokines IL-1β and TNFα acting as paracrine or autocrine modulators have been found to influence MMP-9 deregulation in premature membranes [310]. Cytokine (IL-6, TNFα) overexpression is also influenced by intra-uterine infections in the FM, further highlighting the complications associated with bacterial membrane infiltration and PPROM [311].

Another important factor to consider is the ability of myofibroblasts to generate mechanical forces that pull wound edges together. Cell traction forces (CTFs) are generated through actin-myosin filament sliding mediated by ATP [244]. Tension builds up, causing cells to move through the ECM through focal adhesions present at both ends of stress fibres, producing CTF movements [244] **(Figure 2.3).** The ECM thus becomes deformed and remodelled to allow for MFs to penetrate the thick matrix and initiate wound closure [244]. Furthermore, actin polymerisation

enhances traction forces, causing cytoplasmic protrusions to extend from migrating cells [244]. Of importance, αSMA has been found to increase contractility of myofibroblasts by modifying myosin stress fibres, particularly when treated with TGFβ1, a common marker in tissue inflammation and wound healing [312,311].

Locomotive fibroblast cells can also generate traction forces [244]. Some studies suggest that MFs are present toward the end of the proliferation stage of wound healing, contributing to, rather than initiating, the cell contraction process [314,315]. A model introduced by Tomasek *et al.,* 2002 proposed that contractile cells are present in three differentiation levels during the process of wound healing: fibroblasts, proto-myofibroblasts and myofibroblasts [316] **(Figure 2.3).** During each phase, contractile cells undergo morphological changes allowing them to remodel the ECM and generate the appropriate tensile forces needed for wound closure [316] **(Figure 2.3).** It is important to note that in embryonic wound healing, wounds heal following a 'purse-string' contraction model with the absence of inflammation, suggesting a similar mechanism could be happening in FMs [245,246]. Taking this information into consideration, both the role of AMCs and myofibroblasts will be investigated in the context of AM wound healing.

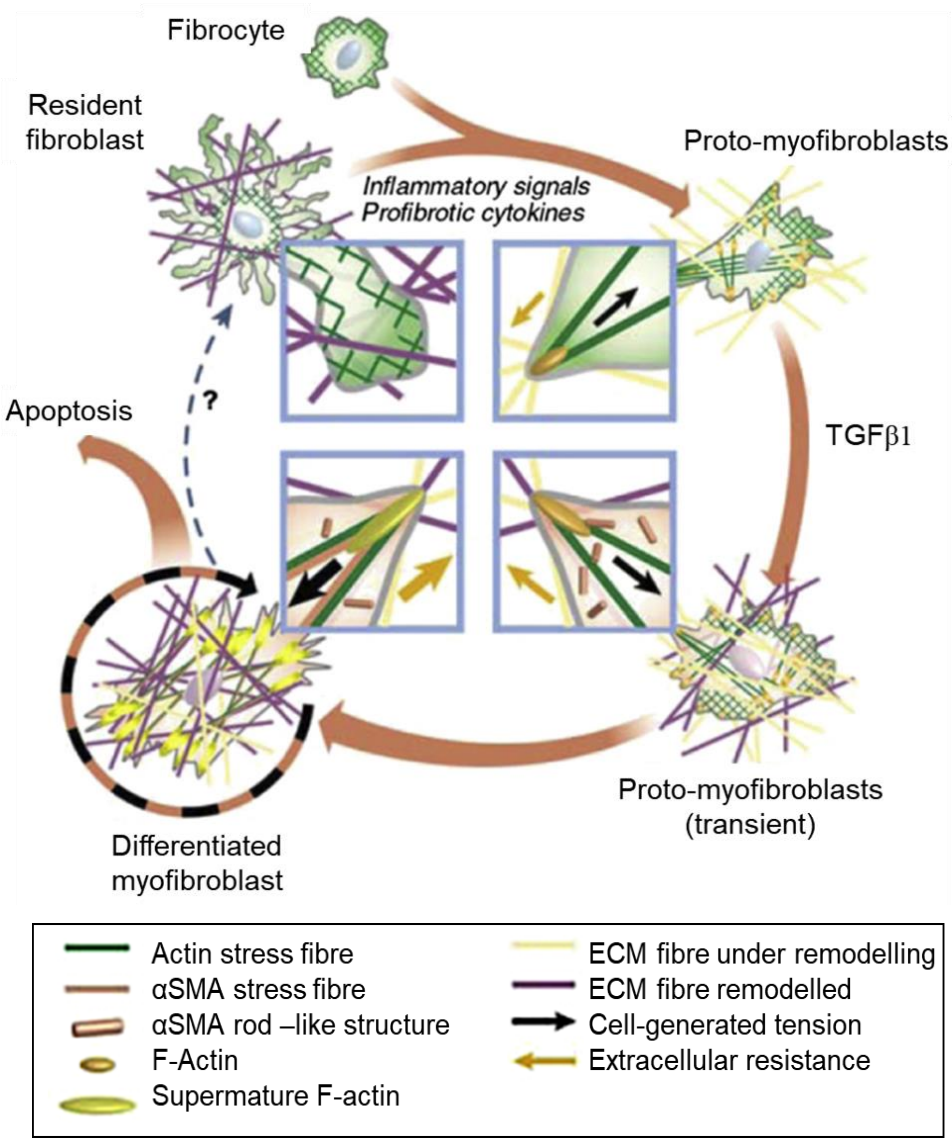

Figure 2.3: *The transformation of fibroblasts to myofibroblasts during canonical wound healing mechanism. Resident fibroblasts become activated to proto-myofibroblasts after the release of pro-inflammatory signals and profibrotic cytokines. The release of TGFβ1 causes differentiation of pro-myofibroblasts to highly contractile myofibroblasts. Cell traction forces are generated through action-myosin filament sliding mediated by ATP. αSMA has been found to increase contractility of myofibroblasts by modifying myosin stress fibres. After successful wound healing, differentiated myofibroblasts either undergo apoptosis or transdifferentiate back to fibroblasts to repopulate the tissue. Image adapted from Li and Wang., 2011* [244]*. ECM = extracellular matrix, TGFβ1 = transforming growth factor β1, αSMA = alpha smooth muscle actin.*

2.5 Aims and Hypothesis

Thesis overview: The present study examines the effects of trauma (**Chapter 4**), cyclic tensile strain (**Chapter 5**) and fetal surgery (**Chapter 6**) on cell types (AMCs, MFs, AECs), structural integrity (collagen/elastin), inflammation (PGE_2) and healing (TGFβ1, Cx43) in term and preterm AM and explored whether Cx43 is a potential target for inflammation and repair. The mechanisms to heal human FM after iatrogenic rupture were examined with a long-term view to translate this to pregnancies affected by spontaneous PPROM. Establishing how Cx43 regulates AM cell function could be an approach to repair defects in FM after trauma.

Chapter 4: Investigating the effects of trauma on the expression of Cx43 and wound healing of term human amniotic membranes

Aim 1: To examine how trauma influences the expressions of Cx43, TGFβ1 and the morphologies of resident cell populations along with collagen content in term fetal membranes.

Hypothesis: Cx43 and TGFβ1 expression will increase following fetal membrane trauma, while resident cell populations will change morphologies to αSMA-expressing myofibroblasts and collagen alignment and concentration will be altered at the wound edge.

Chapter 5: Mechanotransduction mechanisms in human preterm AM defects

Aim 2: To examine the effect of cyclic tensile strain on the activity and concentration of mediators involved in mechanotransduction (Cx43), tissue remodelling (sGAGs, elastin, collagen, TGFβ1) and inflammation (PGE_2) in a gestational-age and tissue-dependent manner.

Hypothesis: Application of CTS and/or trauma in preterm AM will have differential effects on the morphologies of different cell populations, tissue structural integrity, inflammation, and healing in a tissue-dependent manner. Treatment with Cx43 antisense will decrease the weakening mechanotransduction mechanisms induced by CTS and/or trauma.

Chapter 6: Cell morphology and collagen structural changes in large diameter FM defects

Aim 3: To examine Cx43 protein expression by myofibroblasts and AECs and collagen alignment in human FM defects taken from open fetal surgeries for spinal bifida correction or after spontaneous PPROM.

Hypothesis: There is an absence of healing in human AM defects after iatrogenic PPROM (iPPROM) following open fetal surgery and spontaneous PPROM (sPPROM) due to the size of the large diameter wound. This is associated with increased expression of Cx43 and collagen alignment at the wound edge.

Chapter 3

Methods of human tissue *in vitro* culture, optimisation, and analysis

Chapter 3: Methods of human tissue *in vitro* culture, optimisation, and analysis

All methods were performed according to the relevant guidelines and regulations at University College London Hospital and the School of Engineering and Materials Science, Queen Mary University of London (QMUL). Ethical approval for collection of amniotic fluid and fetal membrane samples was granted by the Joint University College London and University College London Hospital Committees, the National Research Ethics Service Committee London, Bloomsbury and the Ethics of Human Research Central Office (REC reference 14/LO/0863). All patients gave written informed consent to provide samples before procedures were performed. The methods are well established and have been described previously.[58-60,120]

3.1 Fetal membrane tissue isolation and collection of human amniotic fluid

Term and preterm human FM were collected from patients following elective caesarean section deliveries, with written informed consent, from University College London Hospital (UCLH) NHS Foundation Trust**.** Term FM was collected from 7 participants and mean maternal age was 35 years (range 33 to 40 years) and mean GA was 38 weeks of gestation (range 37^{+0} to 39^{+1} weeks). Preterm fetal membranes were collected from 17 participants and average maternal age was 35 years (range 25 to 42 years) and mean GA was 32 weeks of gestation (range 27^{+0} to 35^{+6} weeks). AF was taken during elective C-section delivery of term patients (37 to 39 weeks GA). Before the incision into the uterus, some AF was sampled using sterile syringe and blunt quill (5 - 50 ml).

To provide a landmark of the cervical region, a sterile Babcock tissue clip was positioned at the lower part of the FM before placental delivery at caesarean section. Separation of placenta and fetal membranes was performed by gentle traction with a sterile surgical scalpel, followed by a 3-minute washing step with Earl's Balanced Salt Solution (EBSS; E7510, Merck) to remove excess maternal blood. The AM was detached from the CM via gentle traction with sterile forceps. Cervical amniotic membrane was dissected distal form the placenta. Placental

amniotic membrane was cut adjacent to the placenta and around the whole perimeter of the placental disc at a region of at least 10 cm from the identified cervical AM. The AM was then placed in a 50 ml falcon tube filled with Gibco Dulbecco's modified Eagle's medium (DMEM; 12491, ThermoFisher Scientific) supplemented with 5 µg/ml penicillin, 5 µg/ml streptomycin (Merck, P4333) 15 µg/ml ascorbate (Merck, A763) and 20% Fetal Calf Serum (FCS; Merck, F9665) for FM transfer to the laboratory. Fetal membranes and amniotic fluid were transferred from UCLH to QMUL immediately after delivery (the journey was about 1 hour) for term deliveries. For preterm deliveries, FM was sometimes transferred immediately after delivery or if a patient was delivering overnight and I had no access to the labour ward, it was placed in a fridge and collected the day after (up to 8 hours after delivery). The timing between transfer and delivery was attempted to be minimised, however some procedures were out of my control, including mothers delivering outside my access hours to the hospital, whether they consented before or after delivery and other issues such as delayed underground journeys etc.

3.2 Effects of *in vitro* culture of term AM explants with AF fluid samples after trauma

To investigate term fetal membrane wound healing mechanisms in **Chapter 4,** I utilised a well-established *in vitro* AM defect model to examine the effects of trauma [43,104]. Prior to use, the CellCrown™ Insert (Scaffdex Oy, Tampere, Finland) was sterilised in an autoclave up to 140^{o} for 15 minutes, as per manufacturer guidance. After collection from UCLH, term FM was dissected into PAM and CAM regions and the AM and CM were separated via gentle traction. Following separation of AM and CM, AM was cut into 3 cm x 3 cm explants. The CellCrown™ Insert has a pore size diameter of 5 mm, thus the tissue was cut with excess to ensure damage caused prior to placing in the insert did not affect the structural integrity and biochemistry of the 5 mm tissue used during analysis. AM explants were placed onto the crown body and clamped in place by twisting the top ring until the membrane was fully stretched. Excess AM was cut from the sides of the crown insert. A 21 Gauge needle with a wall thickness of 0.15 mm was inserted for 2 minutes at a 90° angle to create a 0.8 mm defect in the AM equivalent to that created by an amniocentesis intervention in CAM and PAM specimens. Control CAM

and PAM specimens taken from the same donor were cultured without the presence of the wound. The trauma model was then transferred into a 12-well plate, fully submerged in human term AF (2 ml) and cultured for 1 and 4 days. Human AF was taken from the same donor as the tissue specimen. Per donor, *n*=6 separate pieces of tissue were cultured for controls and wounded specimens respectively, for both PAM and CAM regions. At the end of the culture period, control and wounded CAM and PAM specimens were either fixed in 4% paraformaldehyde (PFA) for 2 hours or stored in 0.5 ml RNA Later (Invitrogen, AM7020) at -20°C prior to analysis. Following 2 hours of PFA exposure, samples were then fully submerged in EBSS and stored at 4°C awaiting analysis. **Figure 3.1** illustrates the setup in preparing tissue specimens for culture *in vitro*, as previously described [43,104].

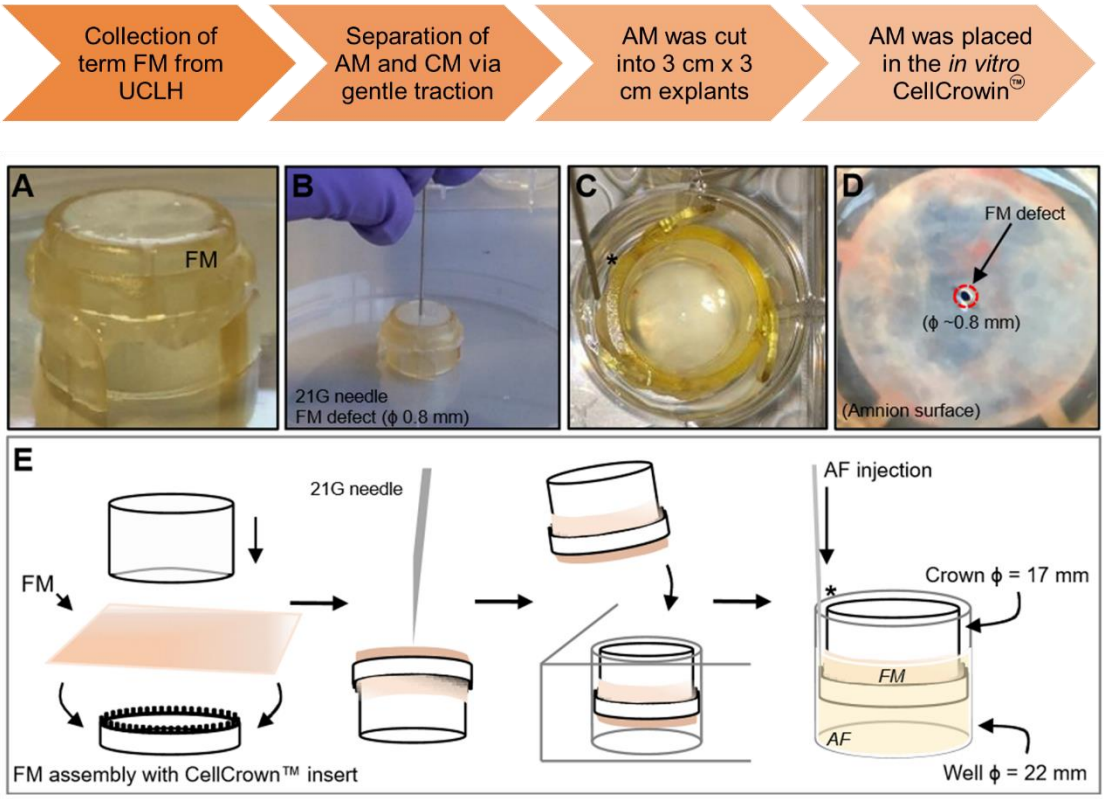

Figure 3.1: *Artificial trauma model using term amniotic membrane as previously described [43]. Top panel: Flow chart of methodology. After collection from UCLH, term FM was dissected into PAM and CAM regions and the AM and CM were separated via gentle traction. (A) AM explants were placed onto the crown body and clamped in place by twisting the top ring until the membrane was fully stretched. Excess AM was cut from the sides of the crown. (B) A 21G needle was inserted for 2 minutes at a 90° angle to create a 0.8 mm defect in the AM. (C) The trauma model was transferred into a 12-well plate, fully submerged in human term AF (2 ml) and cultured for 1 and 4 days. Controls taken from the same donor were cultured identically without the presence of the wound. (D) Close-up of the 0.8 mm defect. Per donor, n=6 separate pieces of tissue were cultured for controls and wounded specimens respectively, for both PAM and CAM regions. Image adapted from Barrett et al., 2020 [43]. CAM = cervical amniotic membrane, PAM = placental amniotic membrane, AM = amniotic membrane, CM = chorionic membrane, AF = amniotic fluid, FM = fetal membrane.*

3.3 Effects of *in vitro* culture of preterm AM explants and application of cyclic tensile strain

3.3.1 Tissue preparation for mechanotransduction experiments

Preterm fetal membranes (*n*=17) were exposed to cyclic tensile strain to investigate mechanotransduction mechanisms over 4 and 24 hours of strain in **Chapter 5**. During C-section before delivery of the placenta, a sterile Babcock tissue clip was placed on the lower edge of the FM within the uterine incision to provide a landmark of the region close to the cervix. The placenta was separated from the uterus and the FM by gentle traction and rinsed with sterile EBSS, as described [43,104,105]. The AM was separated from the CM and the specimens dissected into explants from CAM or PAM tissue regions **(Figure 3.2).** Preterm AM was further dissected using a stainless-steel cutter with fixed dimensions (25 mm x 10 mm). Dumbbell-shaped AM was placed into the mechanical testing chamber in the same orientation to ensure fibre alignment was parallel to the strain.

All specimens were cultured *in vitro* with 2 ml DMEM supplemented with 5 µg/ml penicillin, 5 µg/ml streptomycin, 15 µg/ml ascorbate and 20% FCS in either 12-well plates labelled **free swelling controls**, or inside the BOSE mechanical loading apparatus **(Figure 3.3)**. PAM and CAM specimens were subjected to 2% CTS applied in an intermittent manner using a well-described bioreactor system [105]. Cx43 inhibition was achieved using a well characterised Cx43asODNs short hairpin antisense oligonucleotide in 2 ml media [105]. Untreated samples were used as controls. In samples used for qPCR analysis, Cx43sODNs sense oligonucleotide was added in some samples as a control. After the completion of each experiment, extracted media was placed into labelled falcon tubes while tissue was either snap frozen, fixed in 4% PFA or submerged in RNALater depending on the next experiment.

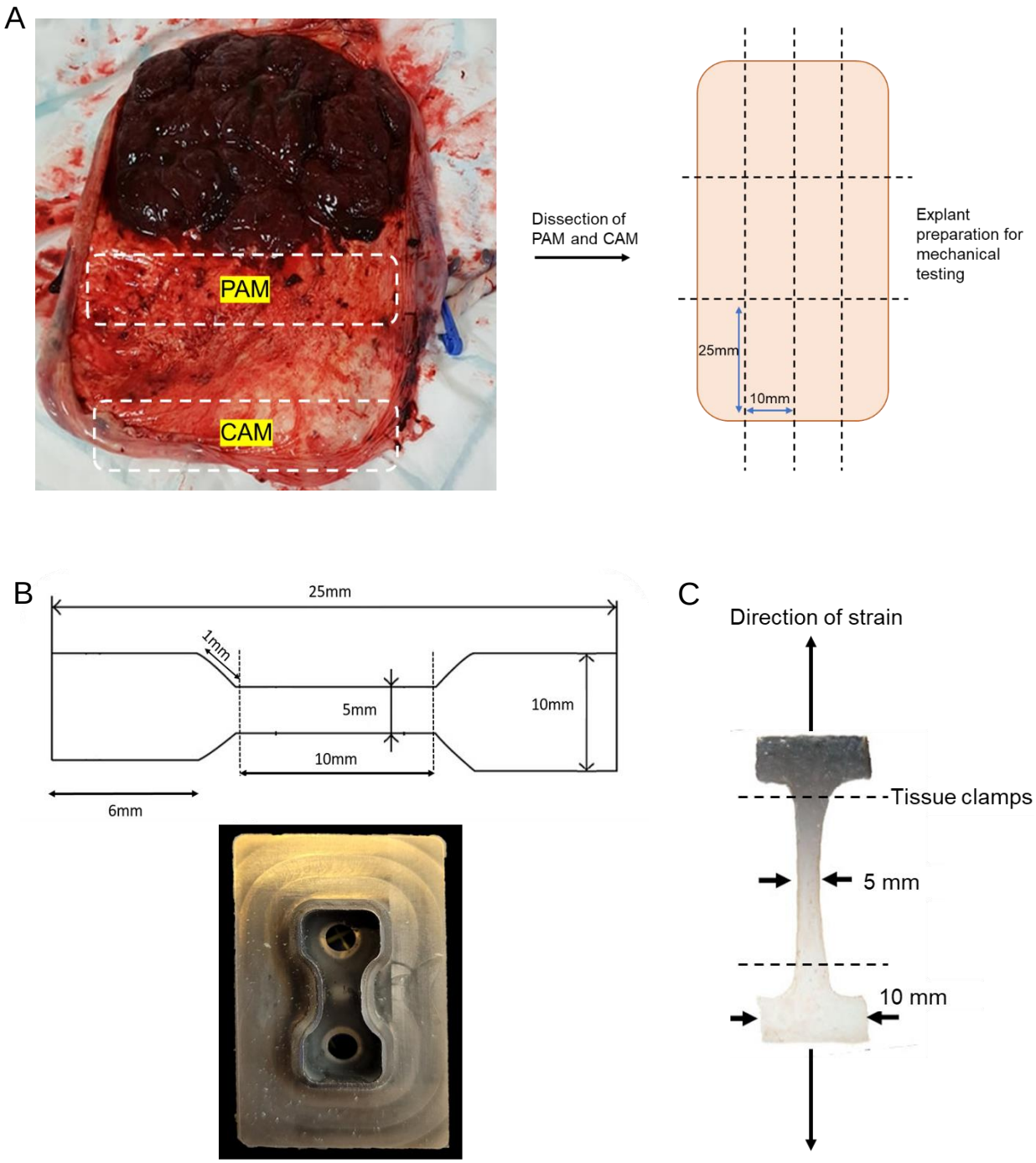

Figure 3.2: *AM dissection in preparation for BOSE chamber assembly and mechanical testing. (A) Preterm AM were dissected into two regions: PAM and CAM. Explants were then dissected into 25 mm x 10 mm samples using a stainless-steel cutter. (B) Schematic showing dimensions for the design of the stainless-steel cutter followed by cutter after completion. (C) Image of an explant in a dumbbell shape dissected using the stainless-steel cutter. After dehydration, specimen weight was between 2 and 25 mg. AM = amniotic membrane. CAM = cervical amniotic membrane, PAM = placental amniotic membrane.*

Specimens were placed on the bottom part of the upper grip and held together by the 1 mm thick plate with clasp screws to hold both the plate and the membrane in place, as seen in **Figure 3.3**. The polyethylene pin was then inserted into the top part of the upper grip to prevent tissue rotation during stretch. The membrane attached to the upper grip was placed inside the BOSE chamber, followed by the insertion of the bottom grip. Two larger screws were inserted into the bottom grip to hold the bottom grip and membrane in place. Some preterm AM within the chamber were subjected to trauma using a 21G needle to create a 0.8 mm defect. Tissue specimens were incubated with 10 µM Cx43 antisense (Cx43asODNs) or sense (Cx43sODNs) oligodeoxynucleotides (stock 50 µM) submerged with 2 ml culture media as extensively optimised in previous studies [105,250] **(Figure 3.4)**.

Previous work in our laboratory has optimised the *ex vivo* BOSE bioreactor system (BOSE Corporation, Eden, Prairie, Minnesota, USA) [105,106]. A full experimental set-up used all 12 loading chambers connected to an actuator arm and fixed within the BOSE loading frame. The whole bioreactor apparatus is contained within a humidified incubator (5% CO_2, 37^{o}C). The CTS set up was designed to best mimic uterine contractions during the onset of labour, with each chamber holding up to 2 ml of culture media (DMEM and 20% FCS). Tensile strain was performed at a frequency of 1 Hz for 4 and 24 hours on dumbbell-shaped preterm AM. The tissue was subjected to 1 minute strain in sinusoidal waveform followed by 9 minutes rest repeated for 24 hours. After 24 hours intermittent CTS, the total number of cycles were 8,640 and total dwell cycles were 12,960. After 4 hours intermittent CTS, the total number of cycles were 1140 and total dwell cycles were 2143. After 4 or 24 hours of CTS, each chamber was carefully dismantled, and the media was pipetted out with a 1000 µl pipette. The dumbbell shaped parts of the samples that were subjected to strain were removed from the chambers while the tissues attached to each grip was cut off.

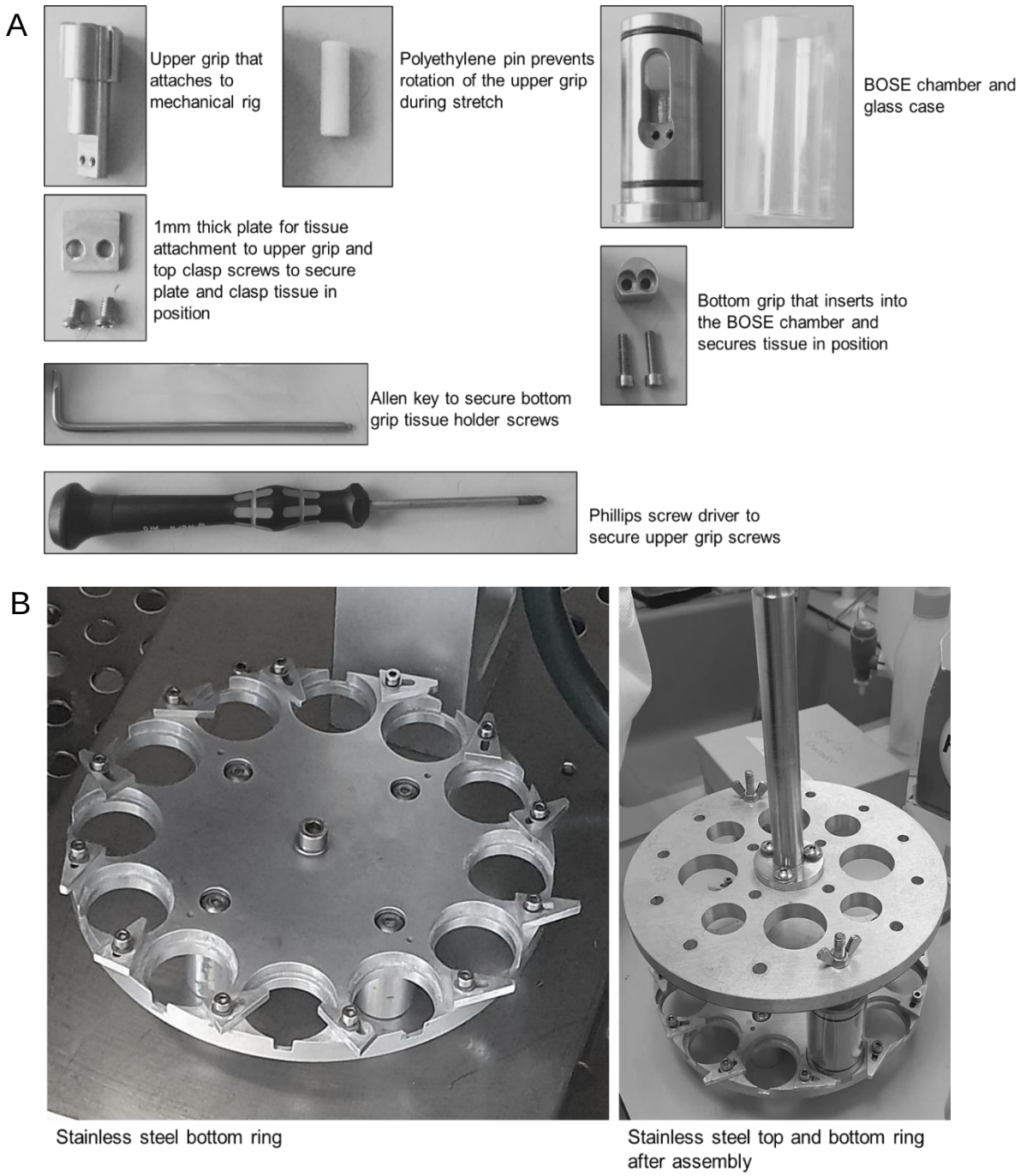

Figure 3.3: *Apparatus used for BOSE chamber assembly and assembly of top and bottom stainless-steel rings. (A) After explant dissection, the AM was placed on the bottom part of the upper grip and held together by the 1 mm thick plate with clasp screws to hold both the plate and the membrane in place. The polyethylene pin was then inserted into the top part of the upper grip to prevent tissue rotation during stretch. The AM attached to the upper grip was placed inside the BOSE chamber, followed by the insertion of the bottom grip. Two larger screws were inserted into the bottom grip to hold the bottom grip and membrane in place. (B) Assembly of the top and bottom stainless-steel rings using 'butterfly' screws attached to the upper grip. AM = amniotic membrane.*

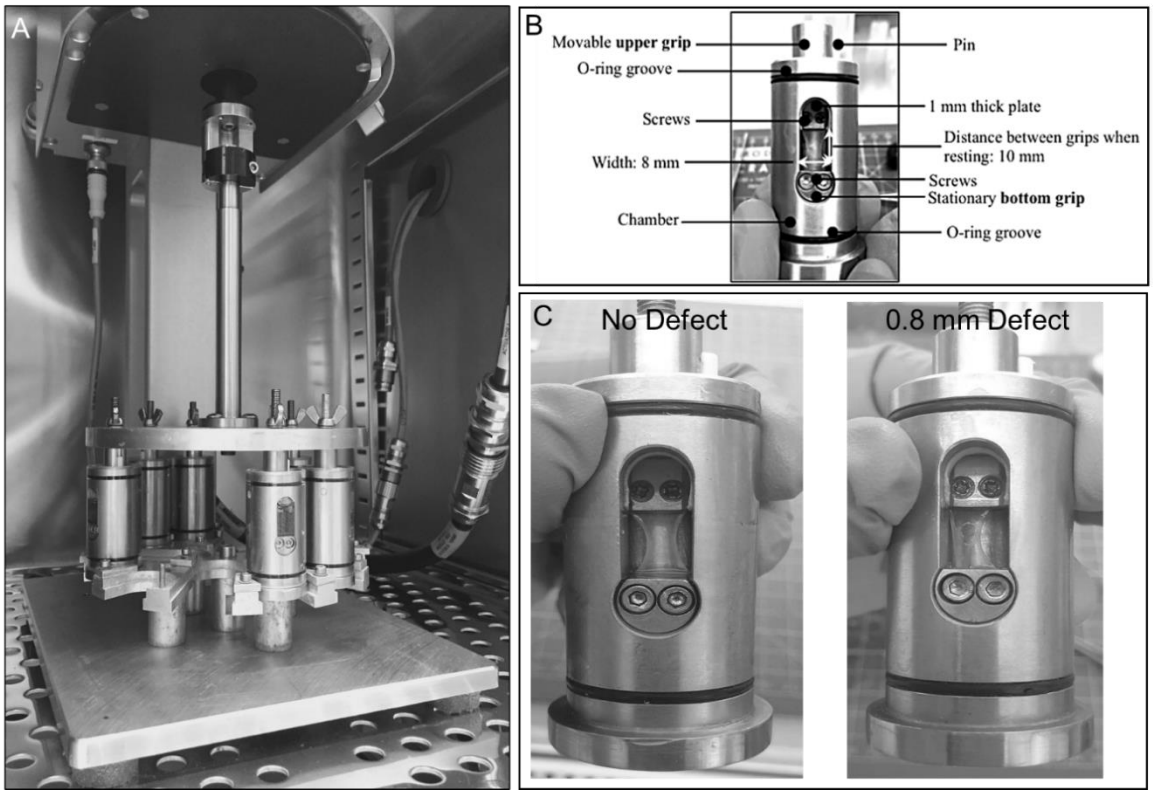

Figure 3.4: *Bose bioreactor system with individual chambers inserted. (B) Complete assembled chamber with human preterm AM explants. The AM was placed on the bottom part of the upper grip and held together by the 1 mm thick plate with clasp screws to hold both the plate and the membrane in place. The membrane attached to the upper grip was placed inside the BOSE chamber, followed by securing the membrane on the bottom grip. (C) Preterm AM sample secured in a dumbbell shape within the chamber with and without a 0.8 mm defect. AM tissue then underwent 2% CTS. Frequency was held at 1 Hz while 24 hours with cycles of 1 minute strain and 9 minutes rest. AM = amniotic membrane. CTS = cyclic tensile strain.*

3.4 Methods of analysis of protein and gene quantification

3.4.1 Immunostaining of Cx43, αSMA and vimentin

For immunostaining, samples were washed twice with PBS for 5 minutes on a shaker, followed by a 5-minute wash with PBS Triton X-100 and lysine (0.1%). This solution allows for cell membrane permeabilisation for primary and secondary antibodies to enter cells and bind to target proteins. AM samples were then submerged in 1% rabbit serum in PBS + Triton X-100 (0.1%) on a shaker at RT for 1 hour.

Control and wounded PAM and CAM specimens were incubated with primary antibodies for Cx43 (diluted 1:100, ThermoFisher Scientific, CX-1B1) and vimentin (1:500, Abcam, ab137321) or anti-alpha smooth muscle actin antibody (1:100, Abcam, ab5694) at 4° in a cold room overnight (16-18 hours) **(Table 3.1).** Following 3x washing steps with PBS, explants were incubated with Alexa-Fluor 568 anti-mouse and/or 488 anti-rabbit secondary antibodies at RT for 2 hours (1:1000, Life Technologies). During the last wash, tissues were counterstained with 1 µg/ml DAPI nuclear stain for 20 minutes. Samples were then washed 3 times in PBS for 5 minutes on a shaker at room temperature (RT).

AM samples were carefully placed onto Superfrost/Plus microscope slides (Fisher, 12-550-15). Using forceps, tissue folds were flattened, and the location of the defect was identified. On the tissue, 3 drops of viscus anti-fade mountant (Fisher, CitiFluor 1797025) was added, followed by covering with clear coverslip (22 x 30-1.5, Fisher, 12-544-D) and gently pressed with the back of the forceps to ensure no air bubbles were present. To seal the coverslip, clear varnish was added onto the edges, and slides were stored at 4^{o}C in the dark until imaging.

Microscope slides were placed into the slide holder on the mechanical stage and could be manipulated using the IPC2U microscope controls in X, Y and Z directions. Before imaging, the Leica STP6000 monitor was switched on and the optical parameter oscillator and remote was connected. Prior to imaging, the condenser was always reset to ensure the light was focused on the correct distance from the sample.

Table 3.1: *Detailed descriptions of primary and secondary antibodies used in immunofluorescence studies. RT = room temperature.*

Antibody	Source	Host animal	Working concentration	Incubation time	Excitation/ Emission	Storage conditions
Connexin 43	ThermoFisher Scientific, CX-1B1	Mouse	1:100	Overnight (18 hours) at 4°	-	Fridge at 4°
Vimentin	Abcam, ab137321	Rabbit	1:500	Overnight (18 hours) at 4°	-	-20°
Alpha smooth muscle Actin	Abcam, ab5694	Rabbit	1:100	Overnight (18 hours) at 4°	-	-20°
Rho/Phalloidin	Invitrogen, R415	-	1:1000	20 minutes at RT	540/565 nm	-20°
Alexa-Fluor 488 (secondary)	Life Technologies	Anti-Rabbit	1:1000	2 hours at RT	493/519 nm	-20°
Alexa-Fluor 568 (secondary)	Life Technologies	Anti-mouse	1:1000	2 hours at RT	579/603 nm	-20°

After immunostaining, control and wounded PAM and CAM regions were imaged using two photon imaging on a Leica TCS SP8 acousto-optic beam splitter (AOBS) multiphoton confocal laser scanning microscope (Leica, Milton Keynes, UK) with a Coherent Chameleon Ultra, Ti Sapphire modelocked IR laser (Coherent UK Ltd, Cambridge UK). Samples were imaged with a 25x, 0.95 NA water-immersion objective. Cx43 signal was imaged with an external HyD detector through an FITC emission filter (500 - 550 nm barrier filter). αSMA and/or vimentin signals were collected at an emission signal between 560 and 600 nm. The DAPI signal was collected through a separate sequence between 400 and 490 nm to avoid bleed through to the other channels. A step size (Z-section interval) of 1.5 μm was used as a constant across all Z-stack images collected. All parameters including detector gain, offset and laser power were

kept constant across all samples and donors to allow for corrected quantification of 8-bit images.

3.4.2 Optimisation of antibody concentrations

All primary and secondary antibodies were appropriately tested via serial dilutions and compared to non-stained negative controls using three separate term donors and three separate samples from each donor from the mid-zone of the FM (*n*=9 separate pieces of tissue). Images were taken using a using a Leica multiphoton laser scanning confocal microscope. Both the epithelial and fibroblast layers of the AM were characterised by going through the Z-stacks (step size 1.5 µm) and determined by morphological differences and the presence of SHG (collagen) signal in the fibroblast layer. Three antibody concentrations were tested in accordance to each product recommended dilutions; 1:10, 1:100 and 1:1000 for αSMA **(Figure 3.5).** For αSMA tests, negative controls (stained with either primary or secondary antibodies only) exhibited green nuclei autofluorescence, while the most concentrated dilutions led to an intensely concentrated signal. The dilutions αSMA were established at 1:100 which produced the clearest fluorescent staining, showing the clearest cell morphology of cells **(Figure 3.5).** Vimentin and Cx43 antibodies have been previously optimised in the lab and the dilutions used were 1:500 and 1:100 respectively. Primary and secondary antibody incubations alone showed no specific staining, while positive staining with both antibodies revealed expected staining of Cx43 plaques and/or vimentin **(Figure 3.6).** No other positive controls were used for αSMA nor Cx43, which poses a limitation in the interpretation of results and will be discussed further in the discussion sections of **Chapters 4-6**.

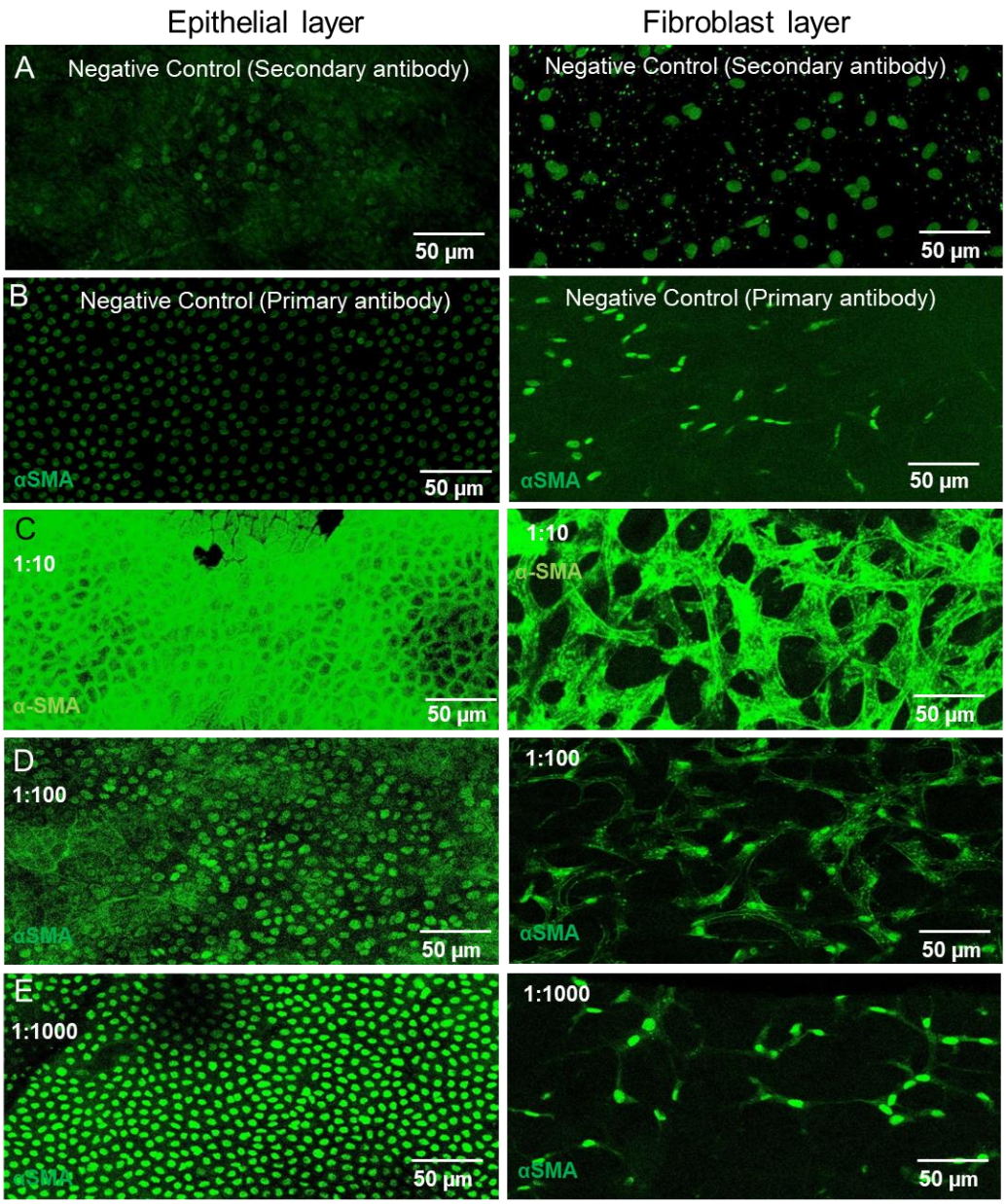

Figure 3.5: *Optimisation of αSMA antibody immunofluorescent staining using IMF confocal laser scanning microscopy on a term PAM sample. Both the epithelial and fibroblast layers of the AM were characterised by going through the Z-stacks (Step size: 1.5) and determined by morphological differences and the presence of SHG (collagen) signal in the fibroblast layer. Three antibody concentrations were tested: (C) 1:10, (D) 1:100 and (E) 1:1000. Negative control tissue (A & B) exhibited green nuclei autofluorescence, while the 1:10 dilution led to an intensely concentrated signal. The 1:100 dilution produced the clearest fluorescent staining in the epithelial and fibroblast layers of the AM, showing the clearest cell morphology of AMCs. Images were taken using a using a Leica multiphoton laser scanning confocal microscope using n=3 donors and n=3 separate pieces of tissue for each donor. Scale bar = 50 µm. αSMA = alpha smooth muscle actin.*

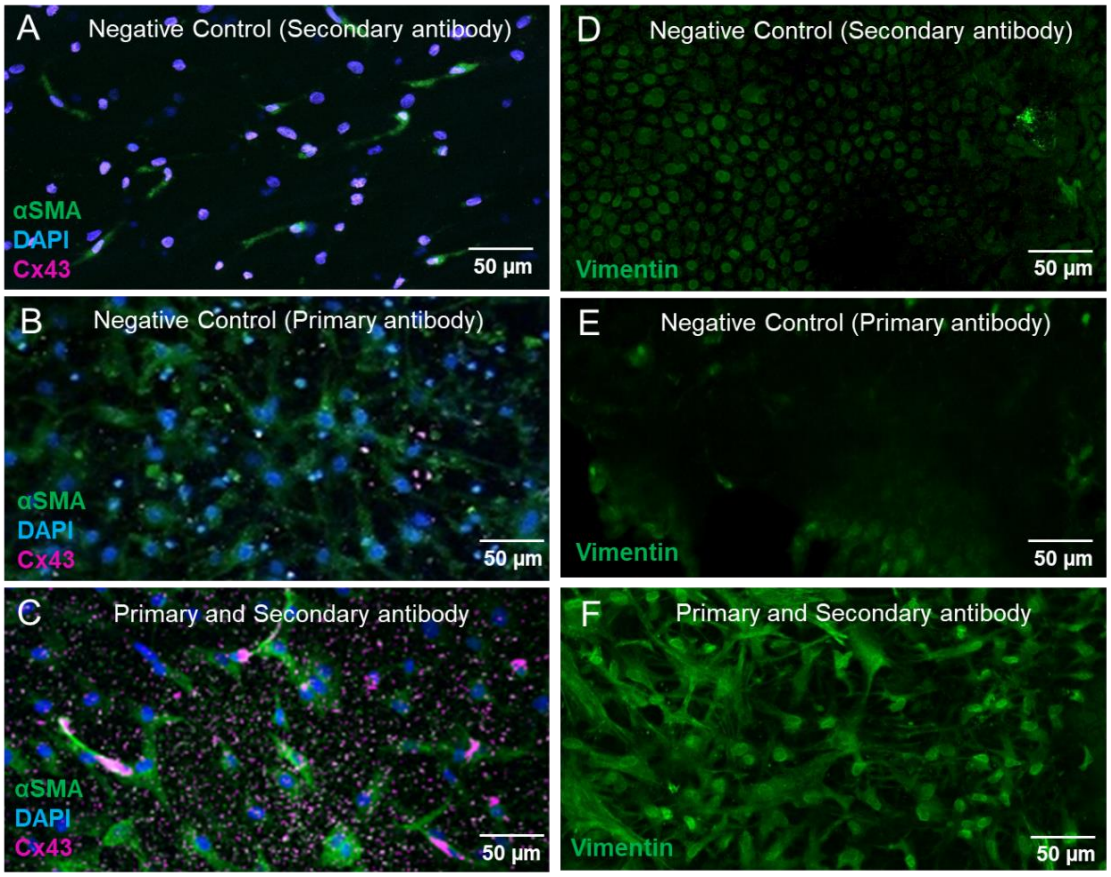

Figure 3.6: *Optimisation of Cx43 and vimentin antibody specificity using IMF confocal laser scanning microscopy on a term PAM samples. For Cx43, the optimised used was 1:100, while for vimentin it was 1:500. (A) Negative control secondary antibody at 1:1000 dilution and (B) Negative control primary antibody at 1:100 dilution alone showed no specific staining for Cx43. Autofluorescence of AMC nuclei is present in negative controls. (C) Positive staining with both antibodies revealed expected staining of Cx43 plaques (magenta staining). (D) Negative control secondary antibody at 1:1000 dilution and (E) Negative control primary antibody at 1:500 dilution alone showed no specific staining for vimentin. (F) Positive staining with both antibodies revealed expected vimentin staining. Images were taken using a using a Leica multiphoton laser scanning confocal microscope using n=3 donors and n=3 separate pieces of tissue for each donor. Scale bar = 50 µm. Cx43 = connexin 43.*

3.4.3 Confocal microscopy and SHG imaging of collagen organisation

Second Harmonic imaging was performed with the same microscope as described in **Section 3.4.1**. A transmission detector was used for the collection of collagen SHG signal with a 430–450 nm barrier filter with a pump wavelength of 880 nm at 80 fs pulse width. To obtain SHG signals the 460/20 nm SHG filter (half 920 nm wavelength) was inserted. The pinhole was set to maximum throughout imaging. The SHG signal was collected sequentially with Cx43 and DAPI signals.

3.3.4 Optimisation of SHG imaging and nuclei autofluorescence

Three separate term donors and three separate samples from each donor from the mid-zone of the FM (*n*=9 separate pieces of tissue) were used in this optimisation. These were the same samples used in **Section 3.4.2**. When initially capturing images of the wound edge, the loss of SHG signal integrity was evident, with blurry fibres or intense signals obscuring the aligned collagen fibres at the wound **(Figure 3.7A).** After the adjustment of the laser scanning power and the changing of the barrier filter to a new one, the collagen fibres could be seen aligning clearly at the wound edge **(Figure 3.7B).** To decrease nuclei autofluorescence, the DAPI 405 nm signal was minimised to a range of 400 - 430 nm to prevent interaction with the 480 nm signal emitted by F-actin and αSMA expressing cells. The 488 nm signal was further adjusted to 460 - 549 nm to ensure maximum exposure was achieved without the excitation levels of the two dyes interacting to produce false negatives **(Figure 3.7).**

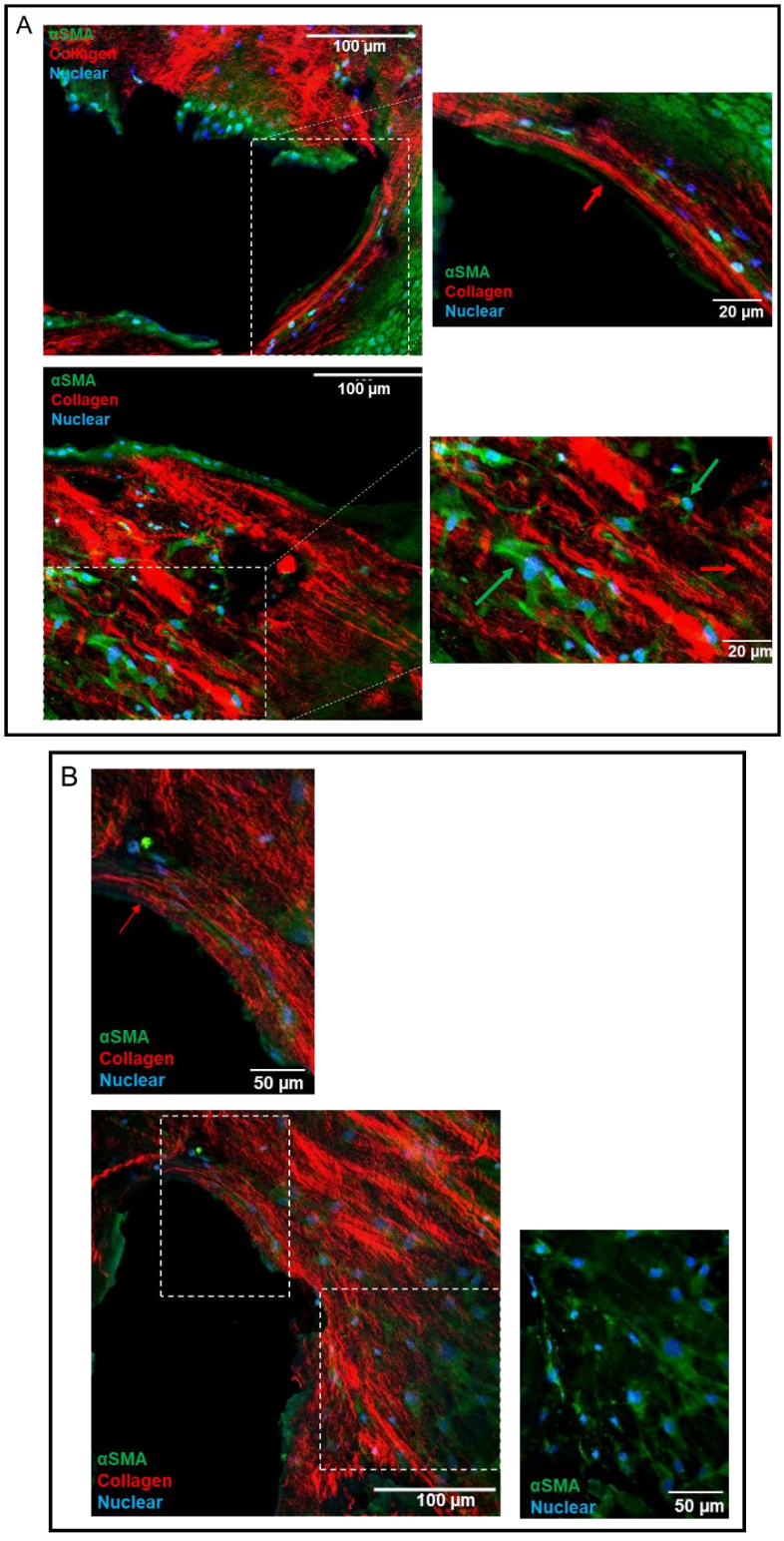

***Figure 3.7**: Optimisation of SHG signalling and nuclei autofluorescence using IMF confocal laser scanning microscopy on a term AM sample. (A) Initial imaging of the fibroblast layer at wound edges with a loss of SGH signal clarity (red arrow) and green nuclei autofluorescence (green arrow). (B) The same sample after laser power and excitation signals were readjusted, with clear collagen fibres seen aligned at the wound edge with significantly less nuclei autofluorescence. Images were taken using a using a Leica multiphoton laser scanning confocal microscope using n=3 donors and n=3 separate pieces of tissue for each donor. Scale bars = 20 µm, 50 µm and 100 µm. SHG = second harmonic generation, AM = amniotic membrane.*

3.5 Confocal image quantification of Cx43, αSMA and collagen

3.5.1 FM cell layer characterisation

The method of collecting immunofluorescent images was extensively optimised by previous researchers in our lab [17,104,105], however the FM cell layer characterisation described in this section was a novel technique developed by myself with the guidance of Prof Chris Thrasivoulou (UCL). Three separate term donors and three separate samples from each donor from the mid-zone of the FM (*n*=9 separate pieces of tissue) were used in this section. Images were acquired using the Leica LAS X software data acquisition system and the different cell layers in the AM were characterised by going through the full thickness of the AM (full volume, Z-step size intervals 1.5 μm) and correlating SHG signal, cell morphology and αSMA expression changes **(Figure 3.8)**. Using previous detailed research on the structure of the FM and expanding on **Figure 1.3** seen in **Chapter 1 Section 1.3**, I characterised each layer by going through the full thickness of the AM and correlating SHG signal, cell morphology and αSMA expression changes. The AM is composed of a layer of AECs at the innermost part of the amniotic cavity, followed by basement and compact layers organised by a connective network of interstitial collagens that sustains the mechanical strength of the AM throughout normal gestation. AMCs and CMCs reside within the fibroblast (AM), sponge (amniochorion interface) and reticular layers (CM) surrounded by a loose network of collagens (shown by SHG). Data was collected at a resolution of 1024 x 1024 and a speed of 600 Hz with bidirectional mode enabled to allow scanning in both directions. A line average of 3 was used to reduce background noise. Raw lif images were processed using either ImageJ software (64bit) or Imaris for Neuroscientists (Oxford Instruments, v9.2).

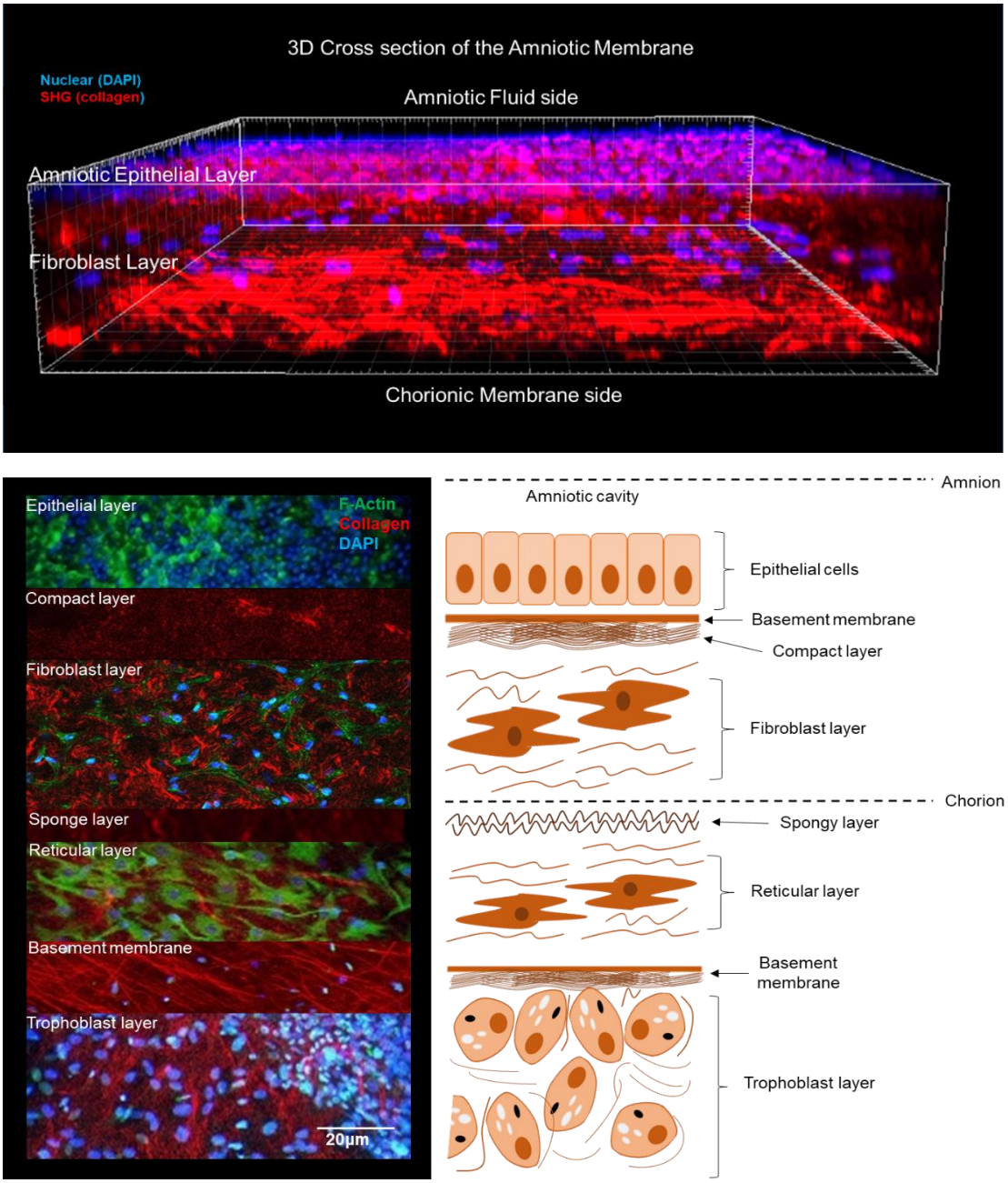

Figure 3.8: *Structure of the fetal membrane. (Top panel) Each layer was characterised by going through the full thickness of the AM and correlating SHG signal, cell morphology and αSMA expression changes. (Bottom panel). The AM is composed of a layer of AECs at the innermost part of the amniotic cavity, followed by basement and compact layers organised by a connective network of interstitial collagens that sustains the mechanical strength of the AM throughout normal gestation. AMCs and CMCs reside within the fibroblast (AM), spongy (amniochorion interface) and reticular layers (CM) surrounded by a loose network of collagens. Images were taken using a using a Leica multiphoton laser scanning confocal microscope using n=3 donors and n=3 seperate pieces of tissue for each donor. Scale bars = 20 μm and 50 μm. αSMA = alpha smooth muscle actin. AECs = amniotic epithelial cells, AMCs = amniotic mesenchymal cells, SHG = second harmonic generation.*

3.5.2 Cx43 protein quantification

Cx43 protein levels were quantitatively measured in ImageJ (Fiji) per cell nuclei and tissue area in control and wounded AM using a well-established pixel-counting method, as optimised by previous researchers in our lab [17,104]. The number of donors and sample size for each analysis varied between **Chapters 4-6**, and this will be indicated appropriately in figure legends throughout the results chapters. After identifying the different layers, maximum projections of the fibroblast and epithelial layers were used for quantification for both AEC and AMC populations **(Figure 3.9)**. During Cx43 pixel counting, images were converted to 8-bit black and white using identical threshold values. Images were then transformed to binary (light background) with a limit of 2 pixels-Infinity to identify Cx43 positive pixels and to ensure any background noise of 2-pixel units and lower was removed. The 'Analyse particle' measurement was then applied, yielding results in pixels. Nuclei counting was performed by the same technique, but instead of pixels the results were obtained as number of particles **(Figure 3.10)**. Smaller background particles were further excluded by using 100-Infinity and the 'fill-hole' feature. To ensure nuclei overlap was not miscounted, the 'watershed' parameter was also applied. Detailed flow charts of both Cx43 and nuclei quantification are presented in **Figures 3.9** and **3.10**.

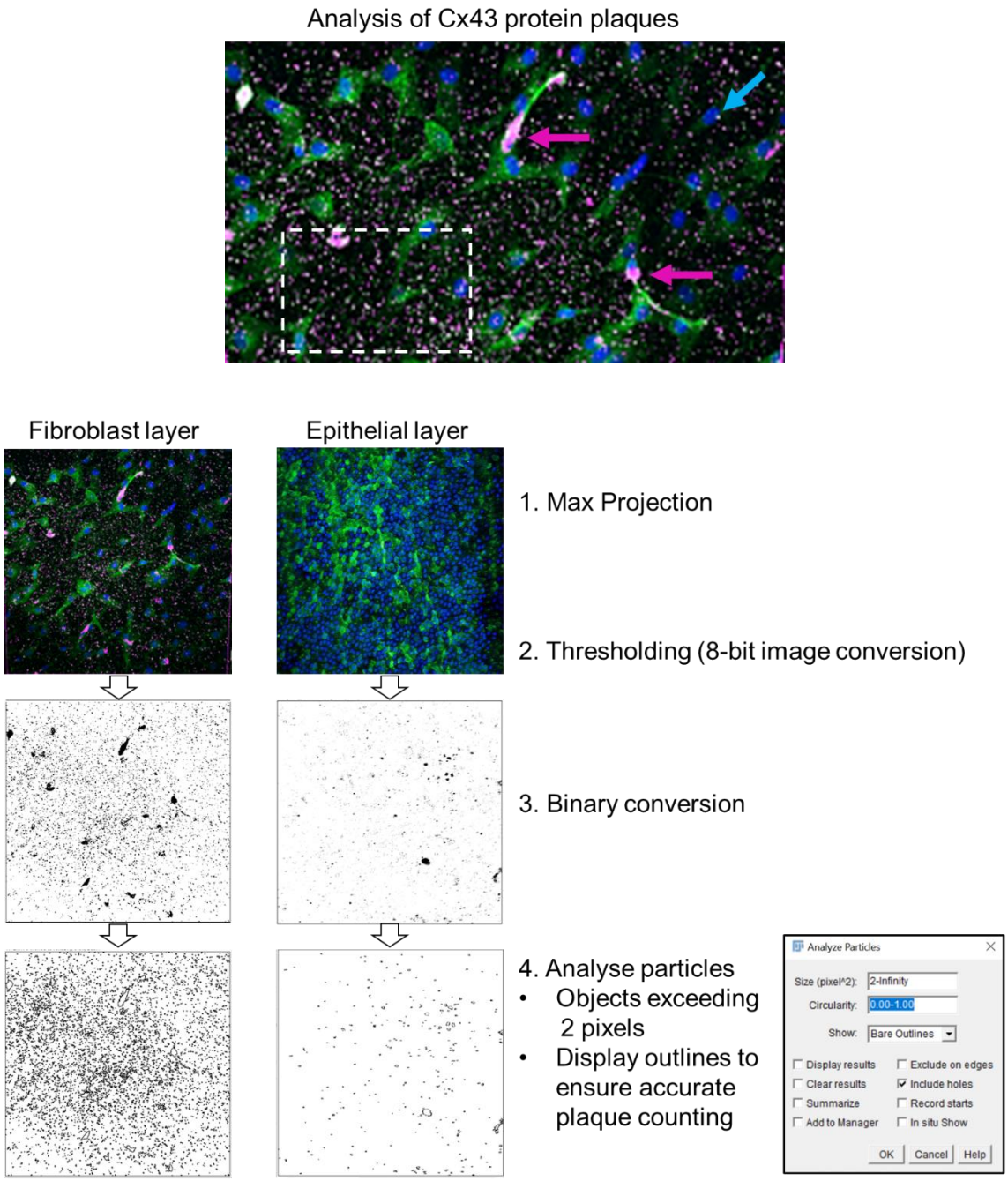

Figure 3.9: *Cx43 pixel counting method in ImageJ (Fiji) Software. Cx43 is present as 0.1-1 µm plaques with varying sizes and shapes within cell nuclei and bodies. Maximum projections of the fibroblast and epithelial layers were used for identification of cell populations. White dotted rectangle indicates Cx43 particles outside MF cytoplasm and were excluded during counting. During Cx43 pixel counting, images were converted to 8-bit black and white using identical threshold values. Images were then transformed to binary (light background) with a limit of 2 pixels-Infinity to identify Cx43 positive pixels and to ensure any background noise of 2-pixel units and lower was removed. The 'Analyse particle' measurement was then applied, yielding results in pixels.*

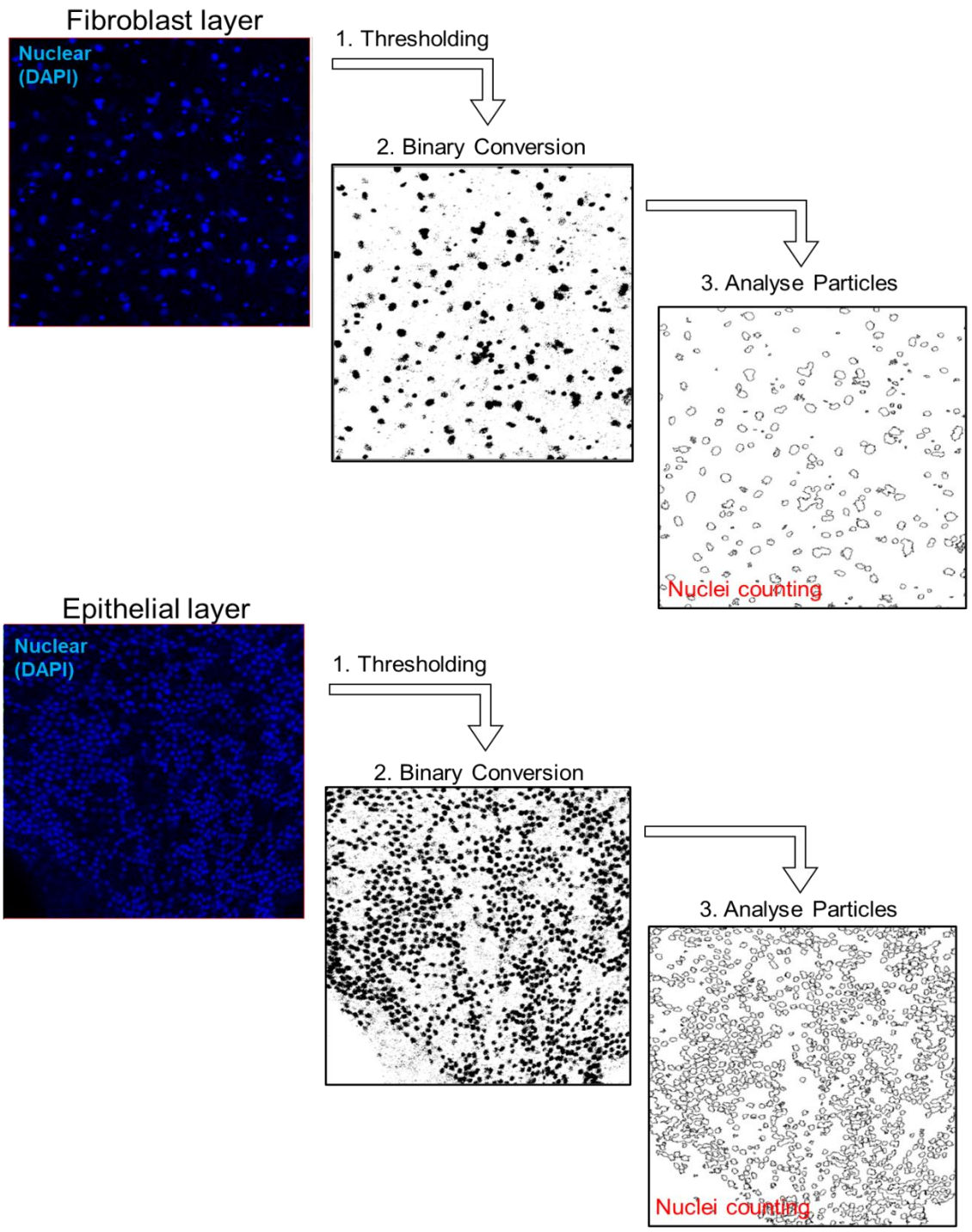

Figure 3.10: *Nuclei counting method in ImageJ (Fiji) Software. Maximum projections of the fibroblast and epithelial layers were used for identification of cell populations. During nuclei counting, images were converted to 8-bit black and white images using identical threshold values. Images were then transformed to binary (light background). Smaller background particles were further excluded by using 100-Infinity and the 'fill-hole' feature. To ensure nuclei overlap was not miscounted, the 'watershed' parameter was also applied. The 'Analyse particle' measurement was then applied, yielding results as number of particles.*

3.5.3 Quantification of nuclei deformation

AEC and AMC nuclei were tangentially aligned at the edges of the wound and had deformed shapes relative to controls. Nuclei deformation was quantified by measuring the circularity of each nuclei in ImageJ Software **(Figure 3.11)**. This method was developed by myself, after consulting Prof Chris Thrasivoulou who has experience in using different quantification software like ImageJ. A maximum RGB projection was converted to binary and a size filter of more than 5 microns was set to ensure background noise was not included in the measurements. The 'Analyse particle' measurement then calculated nuclei circularity. Circularity is defined by 4π*area/perimeter^2 and represents the following: A value of 1.0 indicates a perfect circle. As the value approaches 0.0, it indicates an increasingly elongated shape.

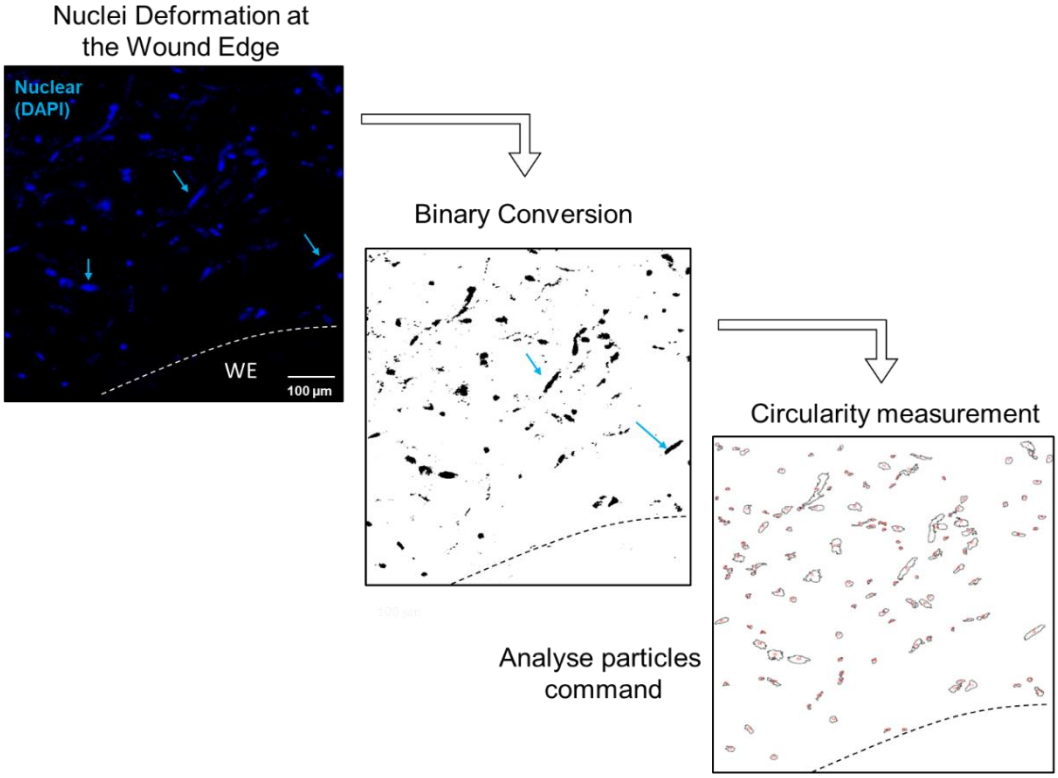

Figure 3.11: *Quantification of nuclei deformation. Nuclei deformation was quantified by measuring the circularity of each nuclei using ImageJ. At the wound edge, nuclei had elongated shapes due to changes in cell morphology and contraction. A maximum RGB projection was converted to binary and a size filter of more than 5 microns was set to ensure background noise was not included in the measurements. The 'Analyse' particle measurement then calculated nuclei circularity.*

3.5.4 SHG quantification of collagen organisation and alignment

To calculate average integrated SHG intensity, I used the same methodology previously used in our lab [17,104,105]. A Z-projection was first chosen depending on the AM layer of interest (epithelial or fibroblast layer). The image was then converted into an 8-bit black and white image followed by thresholding and conversion to binary. A random area was selected for analysis **(Figure 3.12)**. The size of the selected area was maintained for the rest of the samples for direct comparison to be made per donor. Average integrated densities (in pixels) for control and wound edge samples were then plotted on a bar chart. A 3D surface plot was then created for the whole width of the tissue to show SHG intensity distribution across all AM layers. Results from the surface plot were extracted and re-plotted as line graphs for control and wound edge samples.

To determine collagen fibre alignment an orientation distribution analysis using the Directionality ImageJ plug-in (v2) was performed **(Figure 3.12)**. After binary conversion, SHG images were subjected to 2D orientation analysis using the local gradient orientation method. [234] The plug-in calculated the amount of objects that distribute between either 0° and 180° or -90° and 90° depending on the direction of collagen fibres with a bin size of 1° **(Figure 3.12)**.

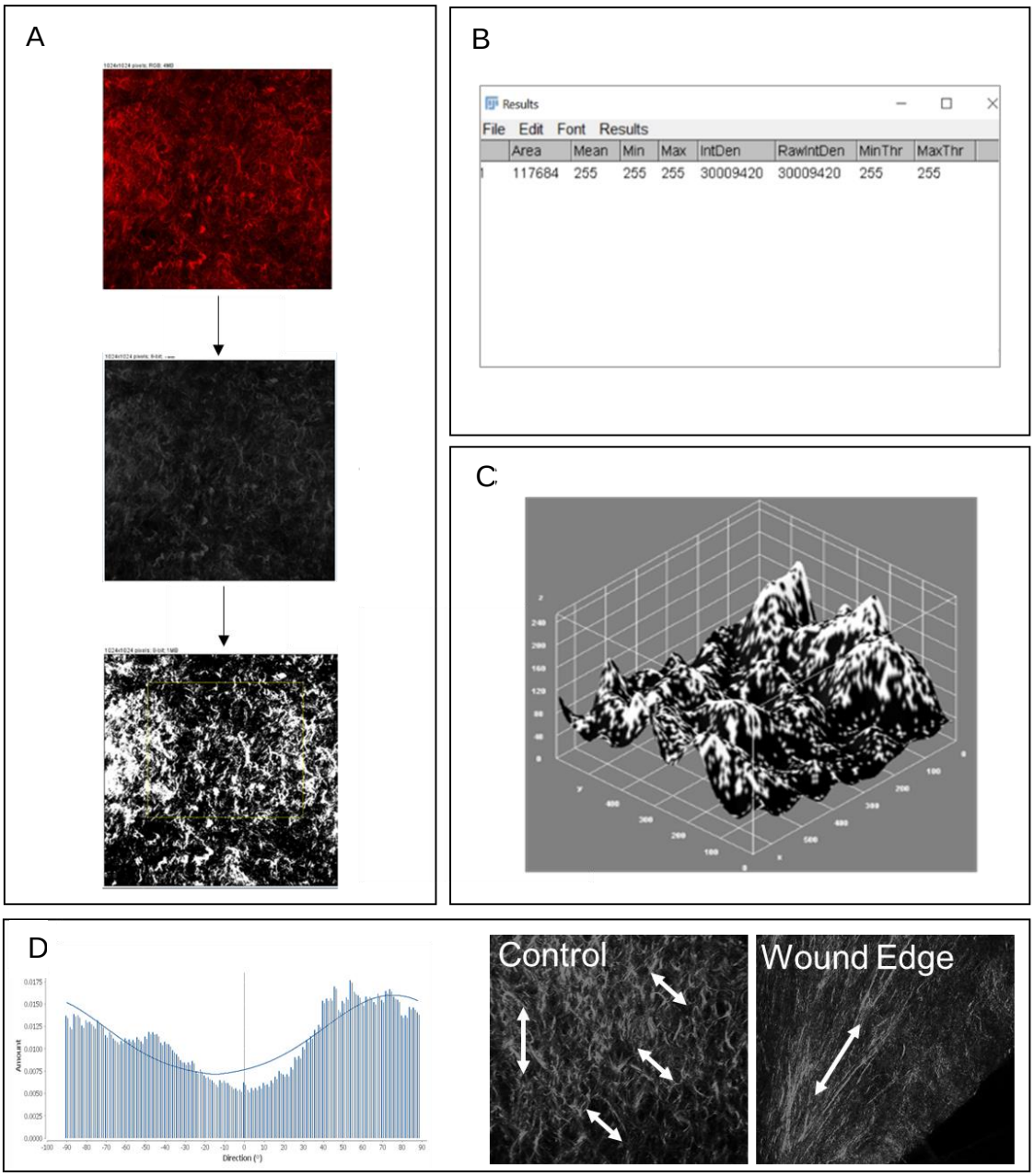

Figure 3.12: *SHG intensity and collagen fibre orientation analysis using ImageJ software. (A) To calculate average integrated SHG intensity, a Z-projection was first chosen depending on the AM layer of interest. The image was converted into an 8-bit image followed by thresholding and conversion to a binary image. A random area of was selected for analysis. (B) Total intensity was measured for the whole Z-stack. (C) A 3D surface plot was then plotted for the whole width of the tissue to show SHG intensity distribution across all AM layers. (D) To calculate directionality of collagen fibres, the directionality plugin in ImageJ was used to calculate the amount of objects that distribute across -90° and 90° or 0 to 120 depending on image direction. All this data was then averaged for each group of interest (e.g. controls and wound edges) and plotted on a bar chart for direct comparison.*

3.5.5 Quantification of cell morphology changes by confocal imaging

To investigate cell morphology alterations, 3D images of the whole AM were loaded onto Imaris 9.5 Software. This method was developed by myself, after consulting Prof Chris Thrasivoulou who has extensive experience using the Imaris software. Using the 'Volume' and 'Surface' commands, individual cells were identified and segmented within the 3D structure **(Figure 3.13)**. Using three random images for both controls and wound edges to avoid bias, I set up a batch process using cell area, nuclei intensity and cell intensity filters for the fibroblast layer of the AM. This process assumes that cells are uniform in shape and in αSMA intensity throughout separate experiments and patients. Data exported represent αSMA intensity (pixels) covered per nuclei and the volume of αSMA-positive AMCs (μm^3) through the whole 3D structure.

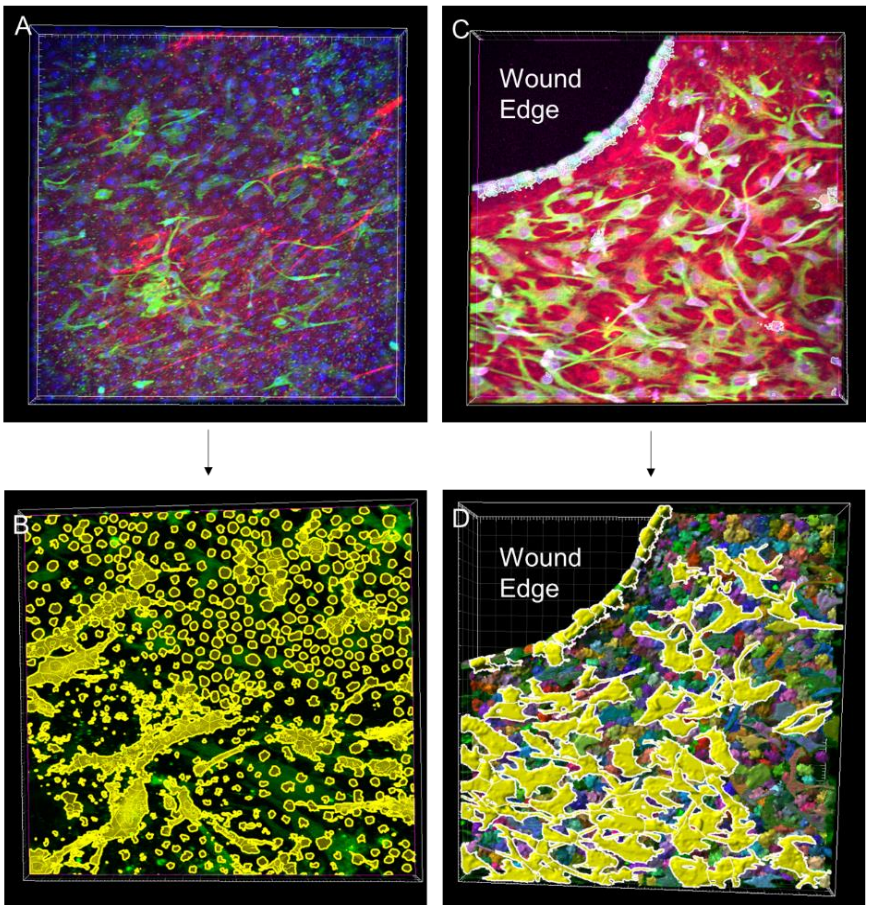

Figure 3.13: *Measurement of αSMA intensity and αSMA-positive cell volume in Imaris 9.5. (A) To count individual nuclei of αSMA-positive cells, the Area filters were used. (B) The filter was manually programmed to calculate maximum and minimum nuclei area limits, and a batch process was set up. (C) Using the Surfaces filter, the software determined αSMA intensity (in pixels) per nuclei within all positive cells in the fibroblast layer throughout the whole of the tissue. (D) The Volume filter was used to calculate the volume of individual AMCs. Cells were coloured by a yellow tint and measured in 3D (μm³) throughout the whole structure. αSMA = alpha smooth muscle actin, AMCs = amniotic mesenchymal cells,.*

3.5.6 SEM analysis of cell types in the AM and CM

The macrostructure and surface topography of whole FM tissues (AM and CM) and defects was evaluated by Scanning Electron Microscopy. SEM works by scanning an accelerated focused electron beam over a sample surface. The magnification used ranged between 20x and 40000x with a resolution of 3 mm and an acceleration voltage of 5kV. SEM permits the visualisation of surface areas up to 50 μm^2 and the imaging of single cells on the surface of the membrane, including AECs, macrophages, and resident red blood cells. By examining nanofibrillar microstructures, collagen and other fibrillar extracellular matrix proteins can be further studied within traumatised membranes.

Following culture, human FM specimens were fixed in 4% paraformaldehyde for 2 hours at room temperature and washed with Milli-Q® water. Samples were passed through a graded ethanol series (20%, 50%, 70%, 90%, 96%, and 100%. v/v for 10 minutes each) to achieve complete dehydration. FM were then dried to critical point (K850, Quorum Technologies, UK). Specimens were mounted on 10 mm SEM mounting blocks and sputter coated with 10 nm gold particles prior to SEM using an FEI Inspect™- F50 (FEI Comp, The Netherlands). This methodology was developed and optimised by a previous member in the laboratory (Dr David Barrett) and I followed the protocol prepared by him and my supervisor [104].

3.6 RNA extraction, cDNA synthesis, optimisation of primers and gene expression by quantitative PCR

3.6.1 Tissue Homogenisation and RNA extraction

The following methodology was developed and optimised by a previous member in the laboratory (Dr David Barrett) and I followed the protocol prepared by him and my supervisor [105]. FM or isolated AM were snap frozen and stored in Eppendorf tubes containing 20 µl RNALater for RNA preservation at -20^{o}C. To achieve whole-tissue homogenisation, the Mikro Dismembranator U (Sartorius) homogenising machine was used. To prevent RNAase contamination, the grinding chamber, steel metal balls, forceps and workbench were all cleaned with RNAse Away (Sigma-Aldrich, 83931). The grinding chamber and sample were placed into a large metal spoon and lowered into liquid nitrogen for 5 minutes to allow the sample to snap-freeze. After liquid draining, the grinding chamber and sample were then removed, assembled with three stainless-steel metal balls and assembled within the dismembranator at 2000 rpm for 1 minute.

Inside a fume hood, 500 µl of TRI-reagent (Sigma-Aldrich, T9424) was added between both chambers ensuring all the sample was covered and left to thaw for 5 minutes at RT. The homogenised sample was pipetted out of the chambers and transferred to an RNase-free microfuge tube, followed by labelling with patient number and sample type. TRI reagent is used to denature proteins and solubilise biological material and is composed of a monophasic solution of phenol and guanidinium isothiocyanate. Samples were then sored at -80^{o}C until RNA isolation was performed.

3.6.2 RNA isolation and purification

On ice, 200 µl chloroform (Sigma-Aldrich, C2432) was added in each RNase-free tube containing the solubilised tissue and vortexed. Chloroform sank to the bottom of the tube. The samples were centrifuged for 5 minutes at 12 000 x g. This step leads to the separation of the solution into 3 phases: A) at the bottom retaining the TRI-reagent colour is the organic phase

comprised of proteins and lipids; B) the middle interphase including DNA and C) the upper aqueous phase containing RNA **(Figure 3.14)**. Using a 200 µl pipette, the aqueous phase was withdrawn without contamination with the interphase and transferred to a fresh RNase-free tube. 500 µl of molecular grade isopropanol was pipetted into the tube, vortexed and allowed to completely precipitate the RNA for 10 minutes at RT **(Figure 3.14)**. This is followed by centrifuging the tube for 10 minutes at 12 000 x g. After supernatant removal, the RNA pellet was washed with 1 ml 75% ethanol that was kept in -20^{o}C and gently mixed by inversion. The sample was centrifuged for 5 minutes at 7500 x g, the supernatant (ethanol) was discarded and the tube was inverted for 10 minutes to ensure all ethanol was evaporated. 100 µl RNase-free water was added into the tube to re-suspend the pellet, followed by gentle vortex to ensure full RNA rehydration **(Figure 3.14)**.

Total RNA purification was achieved using the RNase Mini Kit (Qiagen, 74004) with the recommended protocol by the manufacturer. In the tube, 350 µl lysis buffer RLT and 250 µl 100% ethanol was pipetted, mixed gently and transferred to an RNAeasy column to be placed in the centrifuge at 8 000 x g for 1 minute **(Figure 3.14)**. After the flow through was discarded, 700 µl of wash buffer RW1 was added, followed by 1 minute centrifuge at 8 000 x g. To eliminate DNA contamination, the Ambion® DNA-free™ DNase Treatment Kit was used at this step (Ambion Applied Biosystems, Warrington, UK). DNA concentrations of up to 50 µg DNA/ml can be removed from RNA samples to ensure levels are not detectable during real-time RT PCR. DNase treatment occurred within the spin column. 10X DNase I buffer (0.1 volume) and 1 µl rDNase I was added to the RNA and gently mixed. Reagents and samples were incubated for 30 minutes at 37^{o}C. 0.1 volume of DNase inactivation solution was added to the solution, mixed thoroughly and incubated for 2 minutes at RT. The purification steps were continued by washing the solution with wash buffer RW1 and centrifuged for 1 min @ 8,000 x g. 500 µl of elution buffer PRE was pipetted to the spin column, incubated for 5 minutes at room temperature, and centrifuged for 1 min @ 8,000 x g. The flow through was discarded and cold 75% ethanol was added to the spin column and centrifuged for 2 min @ 8,000 x g. The

RNAeasy spin column was allowed to dry for 5 minutes and the sample was centrifuged for 5 min @ 8,000 x g to remove all traces of ethanol. The spin column containing the purified RNA was transferred to a fresh 1.5 ml collection tube. 50 µl of RNase-free water was added, and the new column was centrifuged for 1 min @ 10,000 x g to elute RNA. The RNA was collected in the flow through. The quality, yield and purity of the RNA preparations and subsequent cDNA was measured using the Nanodrop ND-1000 spectrophotometer **(Figure 3.15)**.

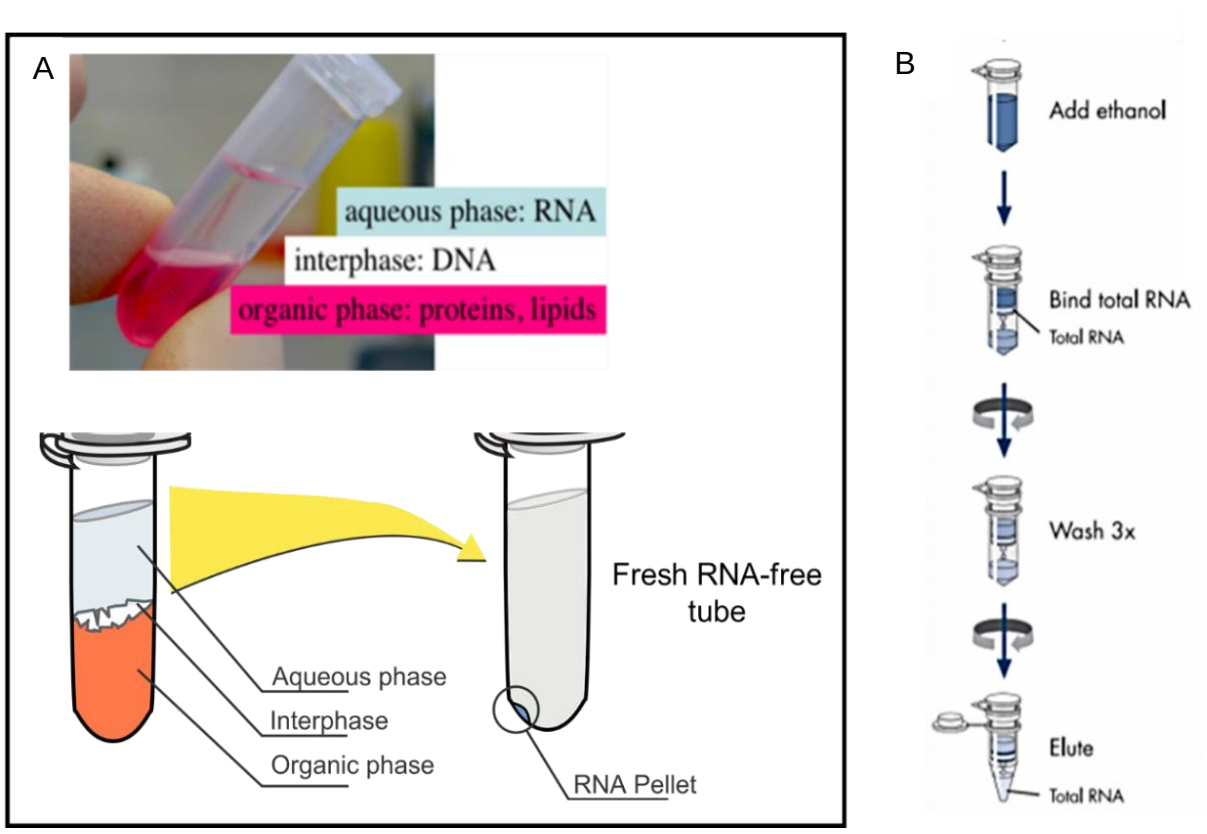

Figure 3.14: *RNA isolation and purification. (A) After addition of chloroform and subsequent centrifugation, the solution separates in 3 phases: a) at the bottom retaining the TRI-reagent colour is the organic phase comprised of proteins and lipids; b) the middle interphase including DNA and c) the upper aqueous phase containing RNA. The aqueous phase was withdrawn without contamination with the interphase and transferred to a fresh RNase-free tube. (B) Total RNA purification was achieved using the RNase Mini Kit (Qiagen) and image was taken from the protocol provided by the manufacturer.*

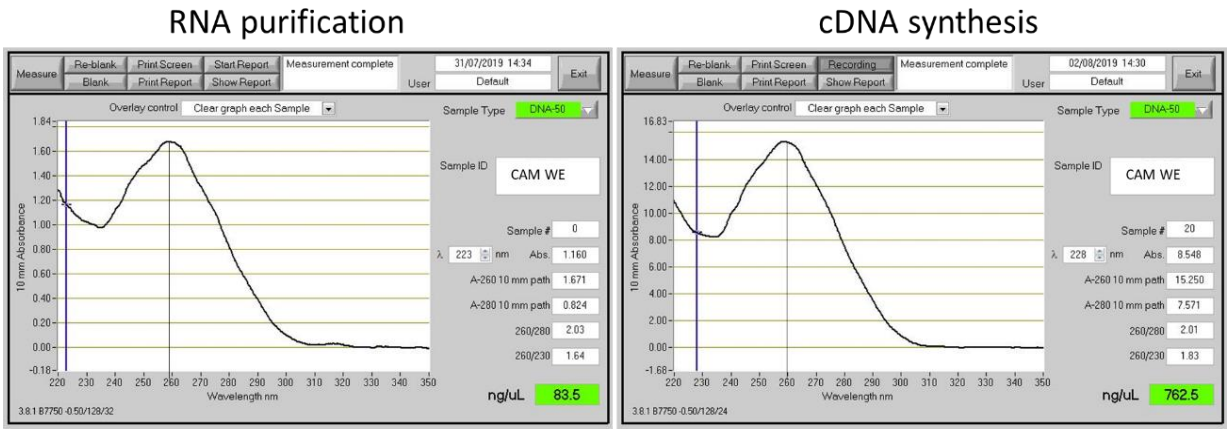

Figure 3.15: *RNA purification and cDNA synthesis. (A) The absorption peak of a purified RNA CAM sample (83 ng/µl). (B) The absorption peak of the subsequent cDNA synthesised (762.5 ng/µl). Both plots have a peak at 260 nm with no other peaks present, indicating there are no impurities in the samples. All measurements were made using the NanoDrop UV Visible Spectrophotometer.*

3.6.3 Reverse transcription for first strand cDNA synthesis

Following RNA isolation and purification, a total of 200 ng RNA was reverse transcribed to full length double stranded cDNA using Enhanced Avian RT First Strand cDNA synthesis kit with oligo(dT) 23 primer (Sigma, STR1). The concentration of RNA was measured using the Nanodrop and the amount of RNA required to yield 20 µl of DNA was calculated to a final reaction volume of 10 µl. Oligo (dT)23 primer (1 µl) and the RNA solution was added to a 500 µl thin-walled PCR microcentrifuge tube and placed on ice **(Figure 3.14)**. Nuclease-free water was used to make up the final volume to 10 ml. To achieve RNA denaturation, the tube was placed in a thermal cycler (Mx3000P Stratagene) for 5 minutes at 70ºC. After denaturation, samples were placed on ice to prevent RNA aggregation. A mastermix was prepared for DNA synthesis using the following:

- 10X buffer for eAMV-RT (1X final concentration)
- Enhanced avian RT enzyme (1 unit/µl)
- RNase inhibitor (1 unit/µl)
- Deoxynucleotide mix (500 µM each dNTP)
- Nuclease-free water

10 µl of mastermix was added to each microcentrifuge tube containing the denatured RNA and mixed gently. Tubes were placed into the thermal cycler at 42ºC for 1 hour. 20 µl of first-strand cDNA was stored at -80ºC until RT-qPCR.

3.6.4 Real-time quantitative PCR (RT-qPCR)

During RT-qPCR, samples were run in triplicate on a on a 96 well plate using the StepOnePlus™ Real-Time PCR System (Applied Biosystems PCR machine, ThermoFisher Scientific) for detection of PCR products using a quantitative SYBR green dye (Promega, A60001). Each well contained 5 µl SYBR green mastermix, 2.5 µl cDNA and 2.5 µl primer pairs. A dissociation/melt curve was also selected to analyse the PCR specificity and check for the formation of primer-dimers in the sample during the final analysis.

The 3-step thermocycling conditions used were the following:

Segment 1:

- 1 cycle:
  - 95ºC for 3 mins

Segment 2:

- 40 cycles:
  - 95ºC for 30 seconds (denature)
  - 55ºC for 1 minute (annealing)
  - 72ºC for 1 minute (extension)

Segment 3:

- 1 cycle:
  - 95ºC for 1 minute
  - 55ºC for 30 seconds
  - 95ºC for 30 seconds

Estimated run time: 2 h 44 min

3.6.5 Assay optimisation

Amplification plots were generated automatically for each reaction with fluorescence (dRn) against cycle number using the StepOnePlus 2.3 Software (Applied Biosystems). Threshold cycle (Ct) values were kept constant for each primer pair throughout all experiments and set

within the lower third of the linear phase of the amplification plot. To standardise the fluorescent reporter signal, ROX reference dye (Promega) was used as an internal reference and normalise for pipetting errors and machine background noise unrelated to PCR products. To calculate relative quantification of candidate genes, the comparative Ct (ΔΔCT) Michael-Pfaffl method was used **(Figure 3.16)**. Ct values were normalised to the target reference gene (GADPH) and the calibrator sample and expressed on a logarithmic scale.

$$Ratio = \frac{(1 + E_{Target})^{\Delta C_T}_{Target}(MEANCalibrator - Sample)}{(1 + E_{Reference})^{\Delta C_T}_{Reference}(MEANCalibrator - Sample)}$$

***Figure 3.16**: The Michael-Pfaffl method. E represents the PCR efficiency for each primer pair.*

3.6.6 Calculating PCR efficiencies and relative gene expressions

Primer PCR efficiencies were optimised to ensure amplification reaction efficiencies ranged between 95 and 110% **(Figures 3.17 and 3.18)**. Reaction efficiency of 100% means the template will double after every PCR cycle at the exponential phase of amplification. The efficiency of reaction can be influenced by the RNA purity used for cDNA synthesis, the primer oligonucleotide length, structure, and GC content as well as non-optimal reagent concentrations. Reaction efficiencies between 90% and 110% are considered acceptable which corresponds to a slope of -3.58 to -3.10 and relate to PCR assay reproducibility. Mean Ct values obtained for each primer pair for known concentrations in the dilution series were plotted against the CT value for the corresponding concentration (y-axis).

The specific primer sequences used for Cx43 and GADPH have been previously described [59], while the TGFβ1 sequences were designed using Primer 3 software. **Table 3.2** shows the forward and reverse gene sequences used along with optimal concentration and reaction efficiency values per primer pair.

To further determine primer specificity and optimisation, a primer titration of concentrations 100 nM, 200 nM and 300 nM for all primer pairs was performed. To calculate PCR efficiencies for the optimal concentration of each primer pair, a ten-fold serial cDNA dilution profile was performed using a known control cDNA template in triplicate and plotted to yield standard curves **(Figure 3.17)**. The reaction efficiency to examine the quality of the overall PCR assay was performed by drawing a linear regression line (R^2 value > 0.99) for the chosen cDNA dilution. Efficiency values calculated for all primer pairs are 2.1 (110%).

PCR efficiencies were defined for Cx43, GADPH and TGFβ1 using the equation:

Amplification efficiency (E) = 10(-1/slope).

Where the linear standard curve produces the correlation coefficient (R2), slope, and the y-intercept.

Table 3.2: *Primer pair sequences for Cx43, GAPDH and TGFβ1.*

Gene	Primer sequence	Concentration (nM)	Reaction Efficiency
Cx43	Forward: 5'CTCGCCTATGTCTCCTCCTG-3', Reverse: 5'-TTGCTCACTTGCTTGCTTGT-3'	300	110%
GAPDH	Forward: 5'-TCTCTGCTCCTCCTGTTC-3', Reverse: 5'-CGCCCAATACGACCAAAT-3'	200	110%
TGFβ1	Forward: 5'-CCCAGCATCTGCAAAGCTC-3', Reverse: 5'-GTCAATGTACAGCTGCCGCA-3'.	200	110%

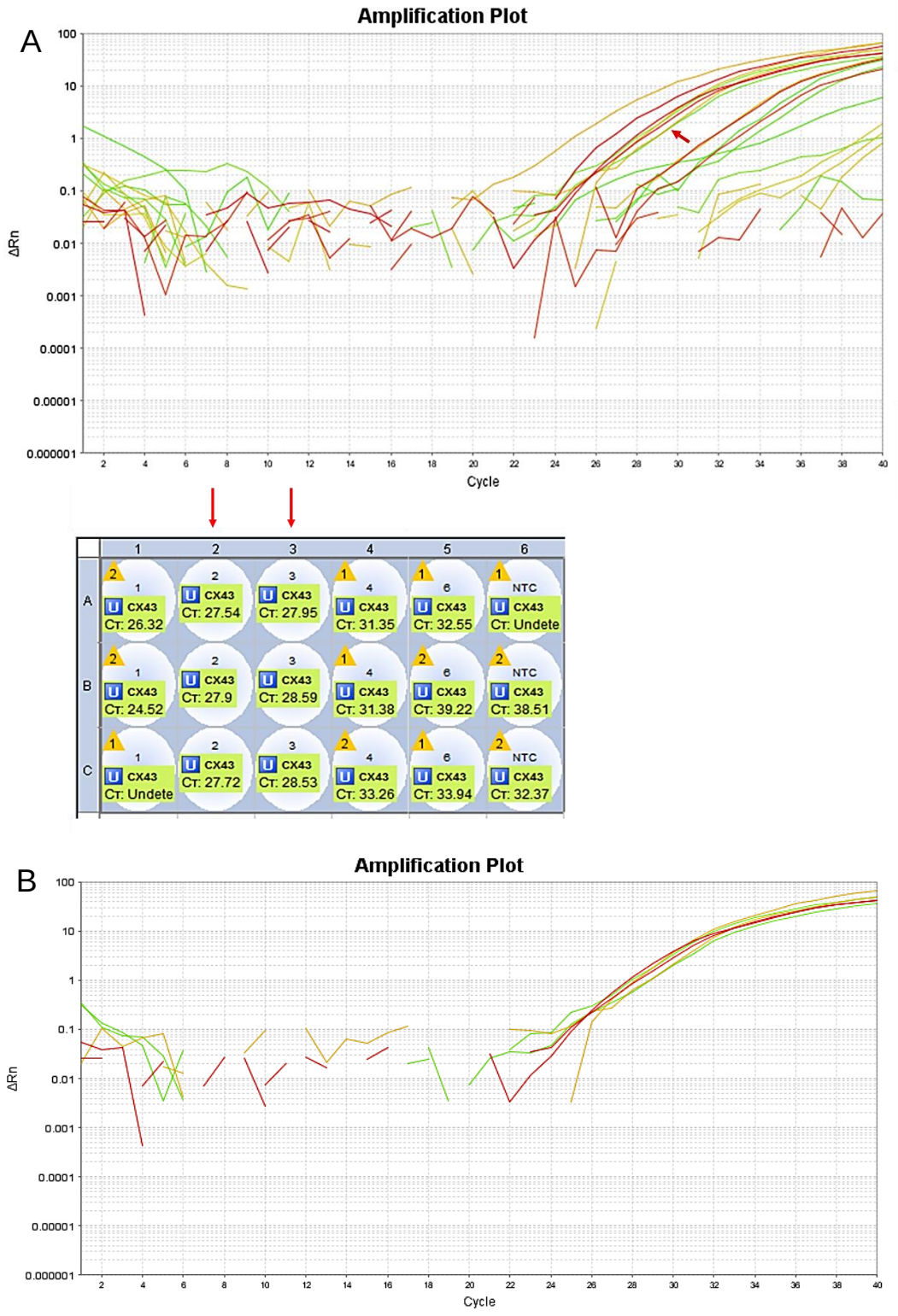

Figure 3.17: *cDNA dilution for primer efficiency calculations. (A) A ten-fold serial cDNA dilution profile was performed using a control cDNA sample in triplicate. (B) The table indicates the 10-fold cDNA dilution series in triplicates vertically, whereby 1 is a non-diluted sample, 5 is the most diluted sample and 6 is NTC. Red arrows indicate the best repeats for Cx43 primers. (C) After identification of the best CT values with no amplification errors, the amplification curves of those triplicates were examined. The triplicates with the lowest CT values were then chosen based on amplification plots with negligible noise indicating removal of DNA contamination.*

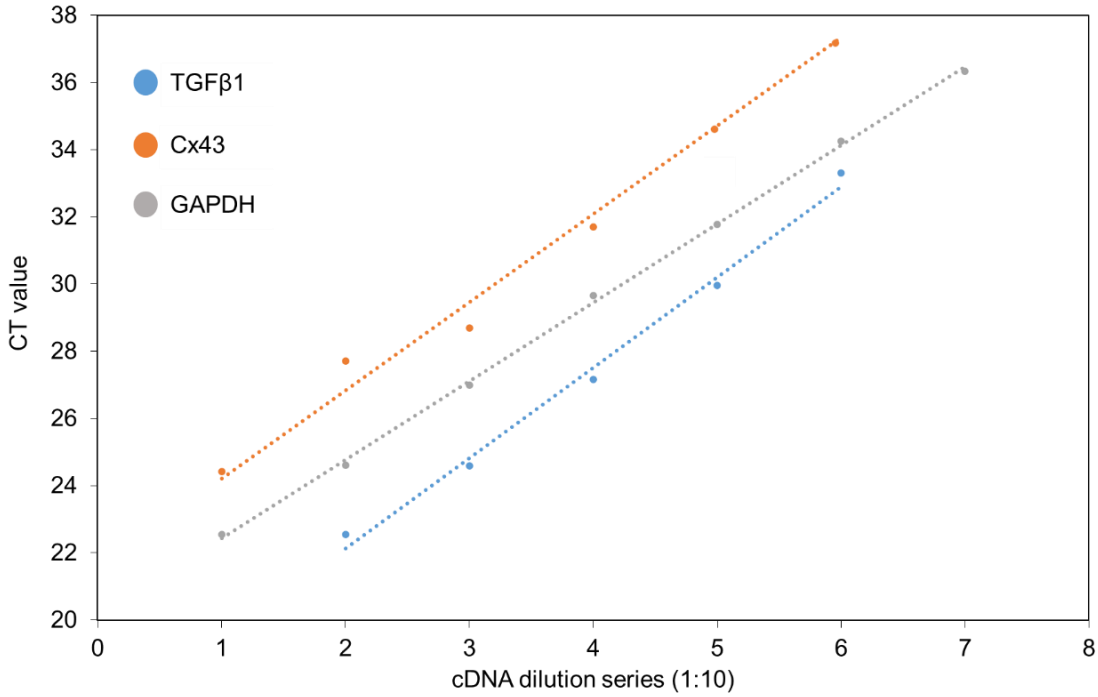

Primer Pair	Linear line equation	R^2	Concentration	Amplification Efficiency
TGFβ1	y = 2.6922x + 16.748	R^2 = 0.9921	300 nM	2.1
Cx43	y = 2.6235x + 21.593	R^2 = 0.9892	200 nM	2.1
GADPH	y = 2.3387x + 20.098	R^2 = 0.9991	200 nM	2.1

Figure 3.18: *Calculating PCR efficiencies. To calculate PCR efficiencies, Threshold CT results were plotted against a 10-fold dilution series of a control human amniotic membrane cDNA to yield standard curves and a linear regression line (equations shown on the graph; R^2 value > 0.99). Reactions were carried out using the StepOnePlus™ Real-Time PCR System (Applied Biosystems PCR machine, TermoFisher Scientific) PCR efficiencies were defined using the equation: Amplification efficiency (E) = 10(-1/slope). Efficiency values calculated for TGFβ1 primer pairs are 2.1 (110%).*

3.7 Biochemical Assay Protocols

All methodologies presented throughout this section were developed and optimised by a previous member in the laboratory (Dr David Barrett) and I followed the protocol prepared by him and my supervisor [105].

3.7.1 Determination of DNA concentration

To calculate DNA concentration and sulphated glycosaminoglycan (sGAG) content, fetal membranes were digested using activated papain enzyme. AM specimens were freeze dried (-106^{o}C, 0.03 mbar) for 24 hours and weighed to measure dry tissue weight. Dry weights for preterm AM were between 2 to 25 mg. Activated papain enzyme digestion solution was prepared at 6.5 pH with 100 mM sodium phosphate buffer (Sigma-Aldrich), 5 mM Na_2EDTA (Sigma-Aldrich), 10 mM L-cysteine (Sigma-Aldrich) and 4U/ml papain (Sigma-Aldrich) in a sterile tube. Samples were then incubated at 60^{o}C on a heat block for 18 hours (overnight). Tubes were then vortexed to ensure full digestion and stored at -80^{o}C until either DNA or GAG assay was performed.

DNA content was determined in whole fetal membrane or amniotic membrane samples using the DNA-specific fluorometric dye, Hoechst 33258 (Sigma-Aldrich, 94403). Hoechst 33258 emits fluorescence at a wavelength of 460 nm and binds to adjacent adenine-thymine base pairs of DNA. To create the standard curve, the following solutions were first prepared (all taken from Sigma-Aldrich): To prepare digest buffer, cysteine hydrochloride (0.788 g) and EDTA (0.403 g) was dissolved in 0.5 L of PBS, ensuring a pH of 6.0 by adjusting with 1M sodium hydroxide (NaOH) of concentrated HCL. 20X SSC buffer stock was prepared dissolving sodium chloride (87.65 g) and trisodium citrate (44.1 g) in 0.5 L deionised H_2O and ensuring a pH of 7.0 deoxyribonucleic acid sodium salt from calf thymus (Sigma-Aldrich, D1501) used as a standard was diluted to 20 µg/ml using digest buffer and 2X saline sodium citrate (SCC) buffer mixed in a 1:1 ratio. To generate the standard curve, the standard was further serially diluted from 1 µl /ml to 17.5 µl /ml. Samples and standards were subsequently plated (100 µl/well) in

triplicate using a white polystyrene 96-well Nunc™ microplate. Hoechst 33258 working concentration was prepared at 1:1000 with SSC/digest buffer (1:1) and added to each well (100 µl/well). Fluorescence was measured at 460 nm using the BMG FLUOstar OPTIMA microplate reader **(Figure 3.19).**

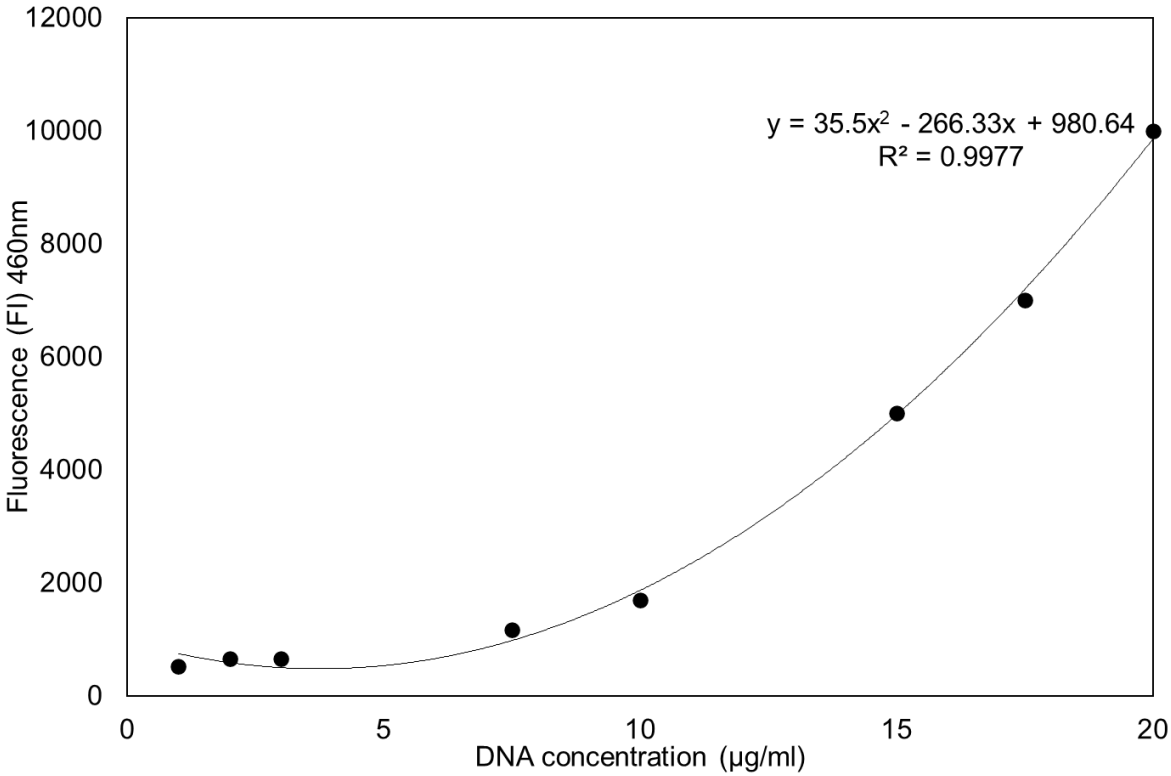

Figure 3.19: *DNA standard curve using serial dilutions of the fluorometric dye Hoechst 33258. There is an inverse relationship of fluorescent intensity at 460 nm to DNA concentration. The polynomial line equation was subsequently used for calculation of sample concentrations.*

3.7.2 Determination of sulphated glycosaminoglycan content

To calculate the total sGAG content in dry tissue and release into the media, the dimethyl methylene blue (DMMB; Sigma-Aldrich, 341088) reagent was used. DMMB is a cationic dye that specifically binds to sulphated glycosaminoglycans (sGAG) with an absorbance at ~525 nm. DMMB (0.016 g) was prepared in a fume hood by adding to 5 ml of ethanol. Sodium formate (2.0 g) was then added to deionised H_2O (850 ml), the two reagents were mixed until

they dissolved and made up to 1 L with deionised H_2O. The pH was adjusted to 3 accordingly with a pH meter and the final reagent was stored in the dark due to light sensitivity.

To generate the standard curve, chondroitin sulphate (Sigma-Aldrich, C6737) was used. The standard (1 mg/ml) was first diluted by 1:10 with digest buffer, followed by a dilution series from 0 to 50 µg/ml. Samples and standard were thoroughly vortexed and plated in triplicate (40 µl/well) in a white polystyrene 96-well Nunc™ microplate. DMMB reagent was then added to each well (250 µl/well) followed by shaking at 360 rpm for 10 seconds and measurement of absorbance at 595 nm in the SpectroNano Star **(Figure 3.20)**.

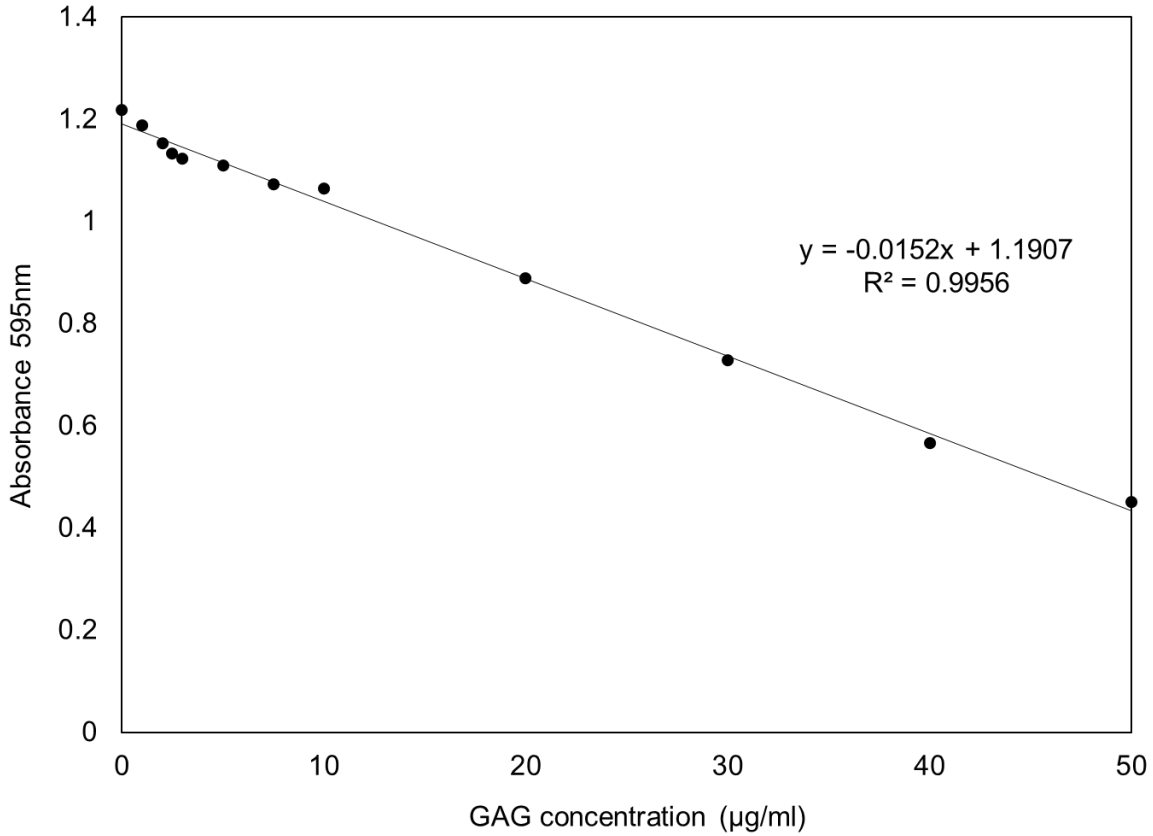

Figure 3.20: *GAG standard curve using DMMB reagent. There is a linear relationship between absorbance at 595 and the concentration of chondroitin sulphate. The equation of the line was used for calculation of sample concentrations.*

3.7.3 Hydroxyproline assay for the quantification of collagen content

In contrast to the previous biochemical assays, to perform the hydroxyproline assay, amniotic membrane samples were digested with pepsin to preserve the triple helix structure of collage. Pepsin (1 mg/ml, Sigma, 10108057001) was dissolved in 0.5 M acetic acid and added to freeze dried tissue samples in micro-centrifuge tubes for 48 hours at 4^{o}C on a rocker. After this incubation, samples were centrifuged at 15000 x g for 1 hour. The supernatant was discarded and 1 ml of 6 M HCl was added to each sample and vortexed. The resuspended pellet was heated to 115^{o}C for 24 hours and then samples were stored at -80^{o}C.

To perform the hydrolysation and neutralization procedure, samples were mixed with 100 µl concentrated HCl (38%) in a 1:1 ratio and vortexed. Tubes were then incubated at 110^{o}C for 18 hours on a heating block. Samples were cooled to room temperature and centrifuged at 5000 x g for 5 minutes, followed by drying in a fume hood for approximately 48 hours in a heating block at 50^{o}C with the tube lids removed. To dissolve the resulting pellet, each sample was gently mixed with pure H_2O until complete resuspension. Samples were stored at 4^{o}C until the hydroxyproline assay was performed. Prior to starting each hydroxyproline assay, solutions were prepared fresh as indicated in **Table 3.3.**

To generate the standard curve, hydroxyproline standards (0 - 1600 ng/ml) were prepared from the 50 µg/ml solution. In a clear 96-well plate, 60 µl of samples and standards were added in triplicate. To each well, 20 µl assay buffer and 40 µl chloramine-T reagent (Sigma-Aldrich, 402869) was pipetted and the plate was incubated for 20 minutes at RT in the dark to allow for hydroxyproline oxidation. DMBA reagent (80 µl; Sigma-Aldrich, D3254) was further added to each well ensuring solution is well mixed. The plate was sealed with an opaque adhesive paper and incubated for 20 minutes at 60^{o}C on a heat block and then cooled to room temperature. After removal of the seal, the absorbance was read at 570 nm with the SpectroNano Star plate reader **(Figure 3.21).**

Table 3.3: *Hydroxyproline Assay solutions. The following solutions were prepared fresh prior to each assay.*

Reagent	Solutions added	Final solution	Storage
Hydroxyproline stock solution	1 mg/ml trans-4-Hydroxy-L-proline (56250 Fluka).	Dissolved in PBE buffer	Stored at 4^{o}C
Hydroxyproline standard working solution	50 µg/ml hydroxyproline solution from 1 mg/ml	Dissolved in PBE buffer	Use fresh
Citrate stock buffer	• 5.04 g citric acid monohydrate (Sigma, C1909) • 11.98 g sodium acetate trihydrate (Sigma S7670) • 7.22 g anhydrous sodium acetate (Sigma, S2889) • 3.4 g sodium hydroxide (Sigma, 655104)	• Dissolved in 80 ml ultra-pure H_2O • 1.26 ml glacial acetic acid was added and pH adjust to 6.1. • Ultra-pure water was added to a total volume of 100 ml and solution filtered using Whatman paper.	Use fresh
Assay buffer	1.5 ml n-propanol (Sigma, 402893)	Added to 1 ml ultrapure H_2O and made up to 7.5 ml using citrate stock buffer.	Use fresh
Chloramine T Reagent	141 mg chloramine T (Sigma, 857319)	• Added to 0.5 ml ultra-pure H_2O and heated to 60^{o}C for 10 minutes to dissolve. • 5 ml n-propanol and 4 ml citrate stock buffer were added.	Solution wrapped in tinfoil until use.
DMBA reagent	4.5 g 4-(Dimethylamino)benzaldehyde (Sigma, 39070)	Dissolved in 6 ml n-propanol and 3 ml 70% perchloric acid (Sigma, 244252)	Solution wrapped in tin-foil until use.

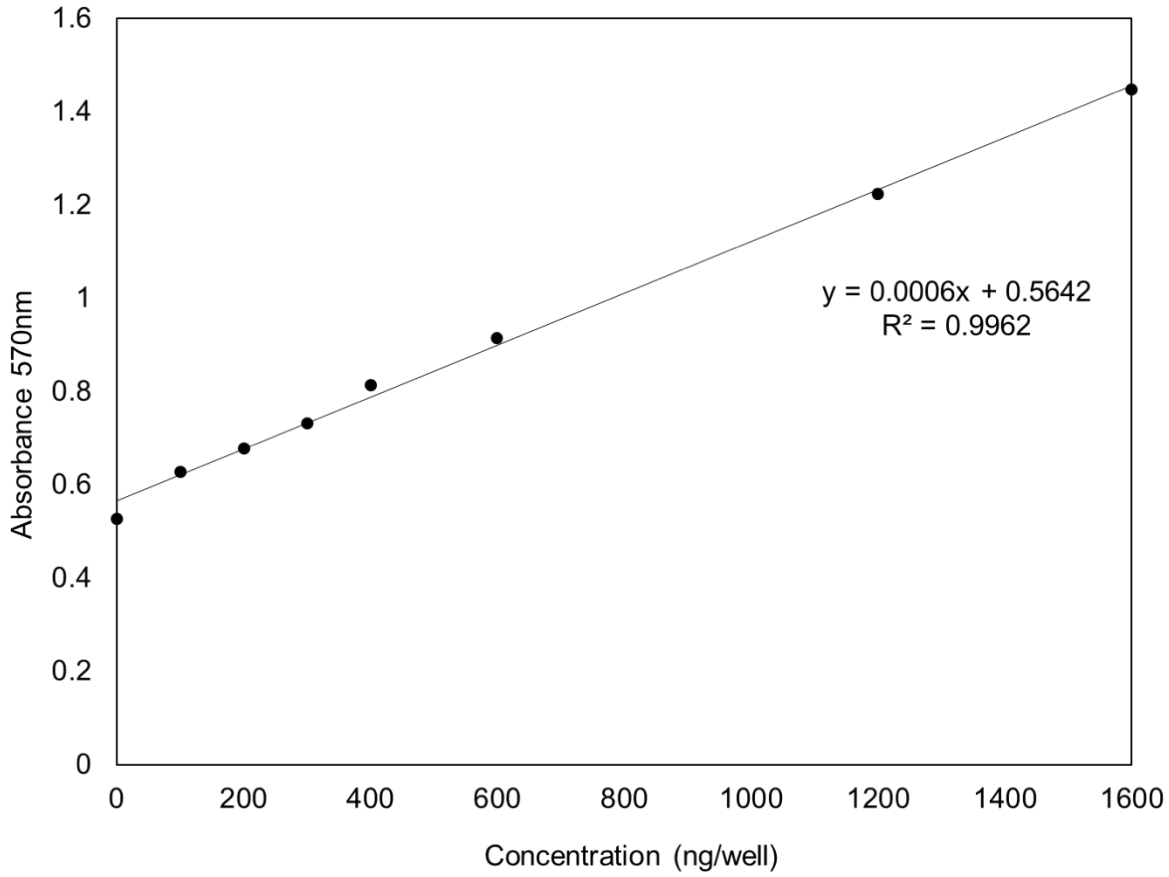

Figure 3.21: *Hydroxyproline standard curve. There is a linear relationship between absorbance at 570 nm and the concentration of trans-4-Hydroxy-L-proline dye. The equation of the line was used for calculation of sample concentrations. Image represents a typical standard curve as seen on a clear 96-well plate.*

3.7.4 Determination of prostaglandin E_2 release

The concentration of prostaglandin E_2 was performed through the Parameter PGE_2 immunoassay (R&D Systems, KGE004B) using a standard protocol included by the provider. All samples underwent a 3-fold dilution with a calibrator diluent. PGE_2 within media samples competes with horseradish peroxidase (HRP)-labelled PGE_2 for a limited number of binding sites on a mouse monoclonal primary antibody through a 1-hour incubation period. The PGE_2-HRP conjugate then competed with the remaining antibody binding sites for 2 hours before the plate was washed to remove unbound material. To determine enzyme activity, a PGE_2 substrate was added for 30 minutes at RT. The reaction was terminated using a stop solution.

The final pigmentation within wells with active PGE_2 activity were yellow. The optical density (absorbance) of each well was measured within 30 minutes using the SpectroNano Star microplate reader set to 450 nm. The standard curve was prepared using diluted PGE_2 standards (stock 25000 pg/vial) **(Figure 3.22).**

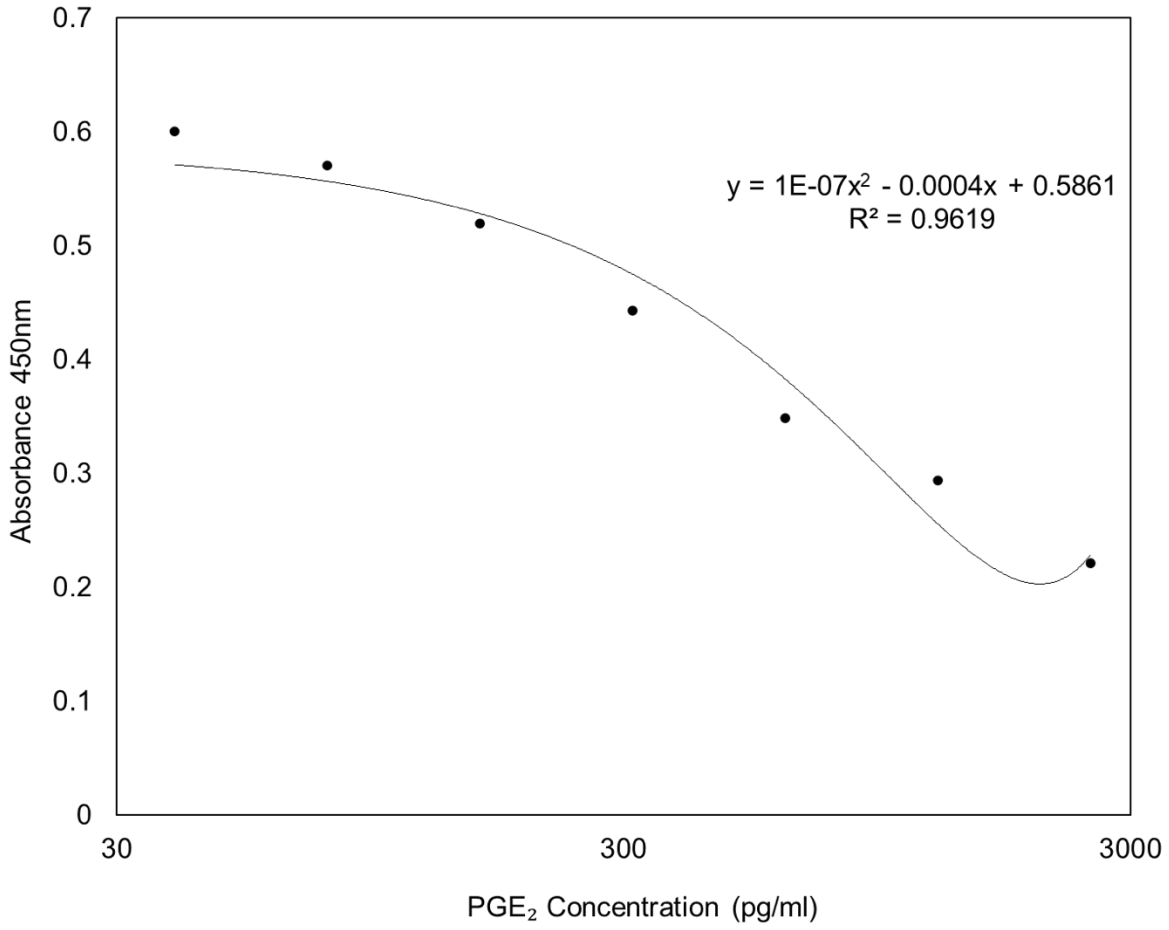

Figure 3.22: *Prostaglandin E_2 assay standard curve. There is an inverse relationship between absorbance at 450 nm and the concentration of PGE_2 standards. The equation of the line was used for calculation of sample concentrations. Image represents a typical standard curve as seen on a clear 96-well plate.*

3.7.5 Quantification of elastin concentration

Total elastin content in human AM specimens was determined using the Fastin elastin quantitative dye-binding method (Biocolor, F4000). The dye applied is 5, 10, 15, 20-tetraphenyl-21H,23H-porphine tetra-sulfonate (TPPS), a synthetic porphyrin which binds to elastin, particularly to non-polar amino acid sequences. TPPS is water soluble in the sulfonate form and contains four sulphate groups. The fastin method solubilises elastin polypeptide fragments (α-elastin, κ-elastin), after which TPPS is able to bind to insoluble cross-linked elastins, as well as soluble tropoelastins and lathyrogenic elastins, More than 98% of tissue elastin can be extracted from 50 µl of tissue sample. For analysis of soluble elastin, samples should be free of any particulate material (cell debris, insoluble extracellular matrix material). The presence of other soluble proteins or of complex carbohydrates does not interfere with the Fastin Assay. The following reagents are included within the assay kit:

1. Fastin dye reagent contains 5,10,15,20-tetraphenyl-21H,23H-porphine tetrasulfonate (TPPS) in a citrate-phosphate buffer
2. Elastin precipitating reagent contains trichloroacetic and hydrochloric acids
3. Elastin standard is a high molecular weight fraction of α-elastin prepared from bovine neck ligament elastin. The α-elastin standard is supplied as a sterile solution; concentration 1.0 mg/ml, in 0.25 M oxalic acid.
4. Dye dissociation reagent contains guanidine HCl and propan-1-ol.
5. Oxalic acid, 1.0 M. Dilute to 0.25 M for tissue samples

a) Extraction of insoluble elastin from human FM samples

Human FM samples were lyophilised and weighed so the elastin content can be expressed as µg elastin/mg dry tissue. Samples were placed in 0.25 M oxalic acid and heated for one hour to 100^{o}C on a metal heating bock. This converts hydrophobic elastin to water-soluble derivate α-elastin. Samples were removed from the heat block and allowed to cool to room temperature. Tubes were centrifuged at 10000 rpm for 10 minutes. The remaining liquid was pipetted out of

the tubes and the supernatant extract was retained in labelled containers for analysis. The residual tissue was further treated with 0.25 M oxalic acid and heated for one hour to 100ºC. During assay optimisation using new fetal membrane material, three heat extractions were completed and analysed separately for elastin to establish that elastin extraction was quantitative. The last extract contained negligible amounts of elastin. The tissue elastin in the form of α-elastin has a molecular weight range of 60 - 84 KDa. α-elastin standards were prepared in duplicate aliquots, while reagent blanks were prepared using 100 µL of test solution solvent (buffer + PBS + water + 0.25 M oxalic acid).

b) Isolation of elastin

The elastin precipitating reagent was developed by the manufacturer for elastin recovery and isolation. Elastin was precipitated using precipitating reagent pre-cooled to < 5ºC in a ratio of 1:1 by adding equal volumes of sample and reagent solutions. Following the precipitation of the elastin, the microcentrifuge tubes were centrifuged for 10,000 x g for 10 minutes, to pack the precipitated α-elastin **(Figure 3.23)**. The tubes were removed from the centrifuge, uncapped and carefully inverted to drain the supernatant into a waste beaker. On returning the tube to the upright position not more than 25 µl of fluid was found in the bottom of the tube. Recovery of the elastin-dye complex was performed by adding 1 ml dye reagent to each tube. The fastin dye reagent makes the complex insoluble by the presence of ammonium sulphate. To allow sufficient reaction between α-elastin and the dye reagent, samples then placed on a shaker at room temperature for 1.5 hours. The elastin-dye complex was separated from the remaining soluble unbound dye by centrifuging the tubes at 10,000 x g for 10 minutes. Visual inspection revealed a reddish residue within the tubes.

To release the elastin bound dye from elastin extracts, dye dissociation reagent (250 µl) was added to the solution and the tube was vortexed. The elastin content of the assayed samples is determined by the amount of bound dye released from the α-elastin. The complete 250 µl contents of the labelled microcentrifuge tubes was transferred to wells of a 96 well microplate,

(with flat-bottom wells to reduce light scatter) and ran in duplicates. The absorbance peak of TPPS in the Dye Dissociation Reagent occurs at 513 nm **(Figure 3.23)**.

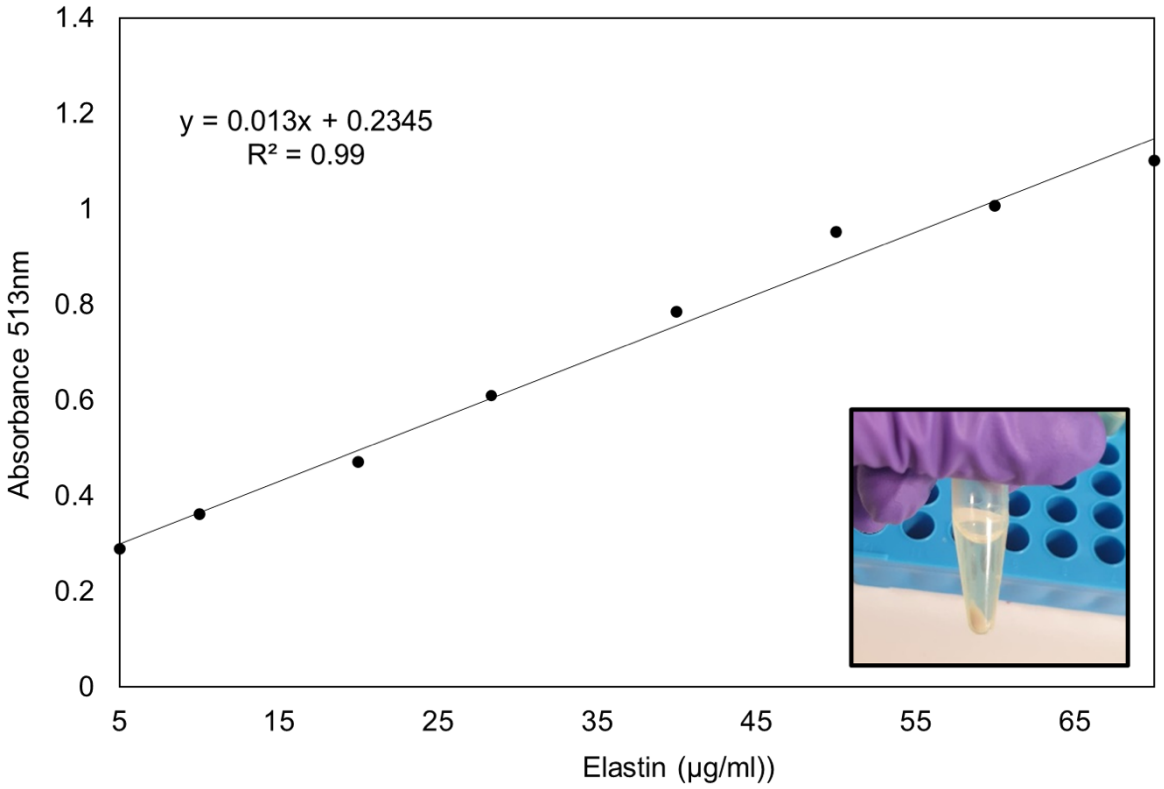

Figure 3.23: *Elastin assay standard curve. There is a direct relationship between absorbance at 513 nm and the concentration of elastin standards. The equation of the line was used for calculation of sample concentrations. The image shows extracted insoluble elastin from a 25 mg fetal membrane sample. The extract can be seen at the bottom of the tube as a light-yellow gel.*

c) *Assay optimisation*

As an initial experiment, 50 µl aliquots of test sample were tested, where the elastin concentration range was yet unknown. If the absorbance readings were found to be more than 1.0 (after subtraction of the reagent blank value) the assay was repeated using a smaller test sample aliquot or diluted. If the absorbance readings were less than 0.05 the test sample contained less than 5 µg elastin and required a larger sample aliquot or concentration before being re-assayed.

3.8 Statistical analysis

Tissue was collected from donors as detailed in **Chapters 4 to 6.** For IMF experiments, data represents the mean and SE intensity values of three replicates from three to four separate donors as indicated in figure legends in **Chapters 4 to 6**. **In Chapter 4**, statistical analysis was performed for the comparison of wound edges at days 1 and 4 of culture to controls, in either AECs or AMCs, using two-way analysis of variance (ANOVA). **In Chapter 5**, to compare the statistical differences in biochemical assays between free-swelling controls and samples after cyclic tensile strain a two-way ANOVA was also performed. All statistics were combined with a multiple *post hoc* Bonferroni test to yield corrected p-values. Values with over 95% confidence rate were considered significant ($p < 0.05$). For Real-time qPCR analysis, mean and SE values represent 6 - 9 replicates from three separate donors for PAM and CAM samples respectively as indicated in figure legends in **Chapters 4 and 5**. Significance was denoted as follows: $*p < 0.05$, $**p < 0.01$ and $***p < 0.001$.

Chapter 4

Investigating the effects of trauma on the expression of Cx43 and wound healing of term human amniotic membranes

Chapter 4: Investigating the effects of trauma on the expression of Cx43 and wound healing of term human amniotic membranes

4.1 Methods

Term human fetal membranes and patient matched AF were collected from 7 separate donors **(Table 4.1)**. Mean maternal age was 35 years (range 33 to 40 years) and mean GA 38 weeks of gestation (range 37^{+0} to 39^{+2} weeks). Women with placenta praevia, multiple pregnancies, antepartum haemorrhage, spontaneous PPROM, clinical chorioamnionitis, maternal diabetes and/or fetal complications such as fetal growth restriction were excluded. Before the incision into the uterus, some AF was sampled using a sterile syringe (15 - 1000 ml). The position of the cervix in relation to the AM was marked using a small sterile clip by the surgeon. Indications for C-sections included previous C-section, previous late miscarriage, fetal breech position and low maternal BMI. The present study utilised a well-established *in vitro* AM defect model to examine the effects of trauma, as described in **Chapter 3.**

Table 4.1: *Clinical information for patients used in the wound healing investigations for the in vitro artificial trauma model.*

Patient Sample	Maternal age	Gestational age at delivery (Weeks + Days)	Delivery indication	AF collected from patient (ml)
AMB09	34	37^{+2}	Elective C-section	15
AMB12	33	39^{+3}	Elective C-section	48
AMB13	39	37^{+0}	Elective C-section	45
AMB14	40	37^{+0}	Elective C-section	45
AMB15	34	38^{+0}	Elective C-section	40
AMB16	36	38^{+4}	Elective C-section	15
AMB20	35	39^{+1}	Elective C-section	15

4.1.1 Statistical analysis

Tissue was collected from 7 donors**.** For both immunofluorescent and qPCR analysis, data represents the mean and SE intensity values from three separate donors and *n*=3 separate tissues per donor, thus *n*=9 total replicates for controls and wounded tissue for PAM and CAM respectively, as indicated in figure legends. Statistical analysis for the comparison of wound edges at days 1 and 4 of culture to controls was performed using two-way ANOVA. All statistics were combined with a multiple *post hoc* Bonferroni test to yield corrected p-values. Values with over 95% confidence rate were considered significant ($p < 0.05$). Significance was denoted as follows: *$p < 0.05$, **$p < 0.01$ and ***$p < 0.001$.

4.2 Results

4.2.1 Differential Cx43 protein expression by cell populations in the AM defect

To investigate Cx43 protein expression levels, *n*=3 separate donors were cultured for up to 4 days. AM specimens from cervical (CAM) and placental (PAM) regions showed multiple cell populations in the wounded tissue after trauma. After day 1 and 4 of culture, qualitative analysis using IMF microscopy indicated increased Cx43 expression in PAM and CAM specimens in both the amniotic epithelial layer and the fibroblast layer containing ACEs and AMCs/MFs respectively **(Figure 4.1).** Cx43 formed distinct protein plaques within myofibroblasts of approximately 0.1 to 1 μm in size (**Figures 4.1 & 4.2**; magenta colour and arrows). Cx43 expression was evident within control regions for both cell types and in both PAM and CAM, but the presence of plaques was negligible **(Figure 4.1)**. AECs formed a thick layer of flattened cells around the edges of the wound in the epithelial layer and presented with increased Cx43 expression compared to controls **(Figure 4.1)**. Using high magnification imaging of the fibroblast layer at the wound edge, punctate staining of Cx43 expression by myofibroblasts was observed with nuclear, cytoplasmic and plasma membrane localization (**Figure 4.2**; magenta arrows) after 4 days of trauma in CAM and PAM defects. **Figure 4.2** highlights how changes in Cx43 expression within the fibroblast layer are associated with heightened αSMA intensity and elongated cell morphology of resident myofibroblasts.

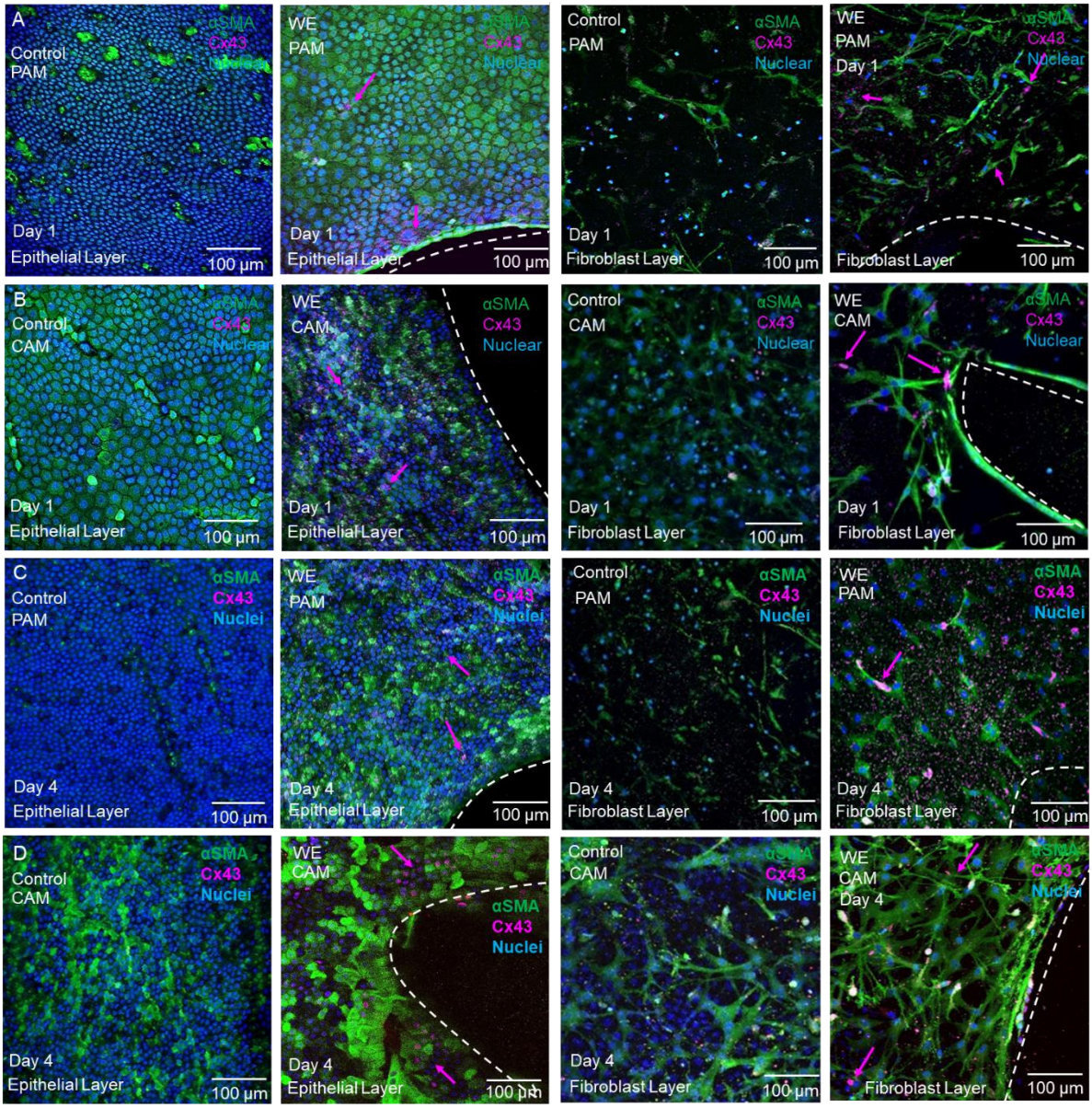

Figure 4.1: *Immunofluorescent images of human term AM showing changes in Cx43 expression across 0.8 mm wounds. After day 1 (A & B) and 4 (C & D) of culture, Cx43 protein expression was increased in PAM (A & C) and CAM (B & D) specimens in both αSMA-expressing AECs (epithelial layer) and myofibroblasts (fibroblast layer). The highest concentration of Cx43 and the creation of distinct protein plaques (approximately 0.1 to 1 μm in size) formed at the wound edge by day 4 (magenta arrows) predominantly within MFs. In both cell layers controls, the presence of Cx43 was negligible. The figure shows representative images from three separate donors and n=3 separate tissues per donor, thus n=9 total replicates for controls and wounded tissue for PAM and CAM respectively. White dotted lines show the margin of the defect. PAM = placental amniotic membrane, CAM = cervical amniotic membrane, AECs = amniotic epithelial cells, MFs = myofibroblasts, Cx43 = connexin 43, αSMA = alpha smooth muscle actin. Scale bars = 100 μm*

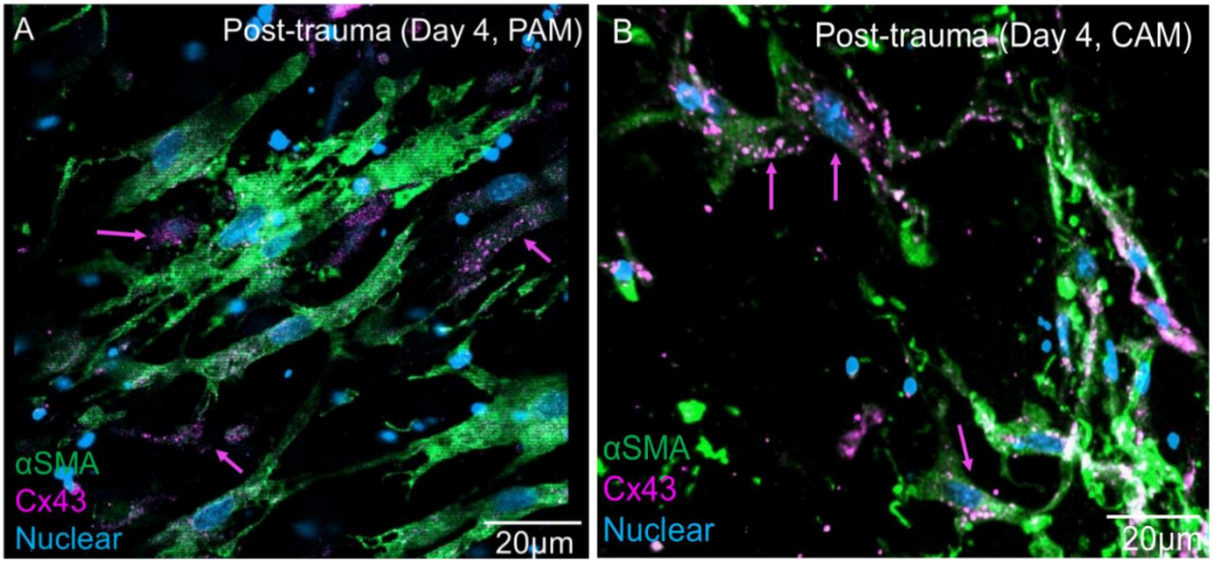

Figure 4.2: *High resolution imaging of PAM (A) and CAM (B) myofibroblasts at the wound edge. Punctate staining of Cx43 expression (magenta arrows) by myofibroblasts was observed with nuclear and cytoplasmic localization after four days of trauma. The figure shows representative images from three separate donors and n=3 separate tissues per donor, thus n=9 total replicates for controls and wounded tissue for PAM and CAM respectively. PAM = placental amniotic membrane, CAM = cervical amniotic membrane, Cx43 = connexin 43, αSMA = alpha smooth muscle actin. Scale bars = 20 μm.*

The quantification of Cx43 protein expression was calculated by pixels per area (per 500 μm^2 tissue area) and per cell nuclei. In control AM, Cx43 expression levels were low with values ranging from 205.5 to 397.8 pixels per area in the epithelial layer and 441.2 to 698.7 pixels per area in the fibroblast layer **(Figure 4.3A).** After trauma, the levels of Cx43 protein expression significantly increased in wounded AM with maximal values after four days of trauma in the fibroblast layer for CAM (10,086.3 pixels per area) and PAM specimens (10,821.1 pixels per area) when compared to the wounded epithelial layer (< 2500 pixels per area) or control (< 250 pixels per area) AM specimens (**Figure 4.3B**; all $p < 0.001$). In wounded AM, Cx43 pixel distribution was dependent on the cell type with lowest values found for AECs (0.62 - 0.74 pixels) in contrast to myofibroblasts (47.3 - 49.9 pixels) in CAM and PAM specimens (all $p < 0.001$, **Figure 4.3**). In contrast, values for Cx43 protein expression in controls were very low (< 0.2 pixels) when cultured for the same time period. Statistical comparison between AECs and AMCs cells showed significantly higher Cx43 levels in the latter ($^{+++}p < 0.005$). Cx43 distribution in vimentin-expressing AMCs was also quantified and those can be seen in **Table 4.2** in the **Appendix**. Despite increased Cx43 expression in AMCs, Cx43 expression was most prominent in myofibroblasts.

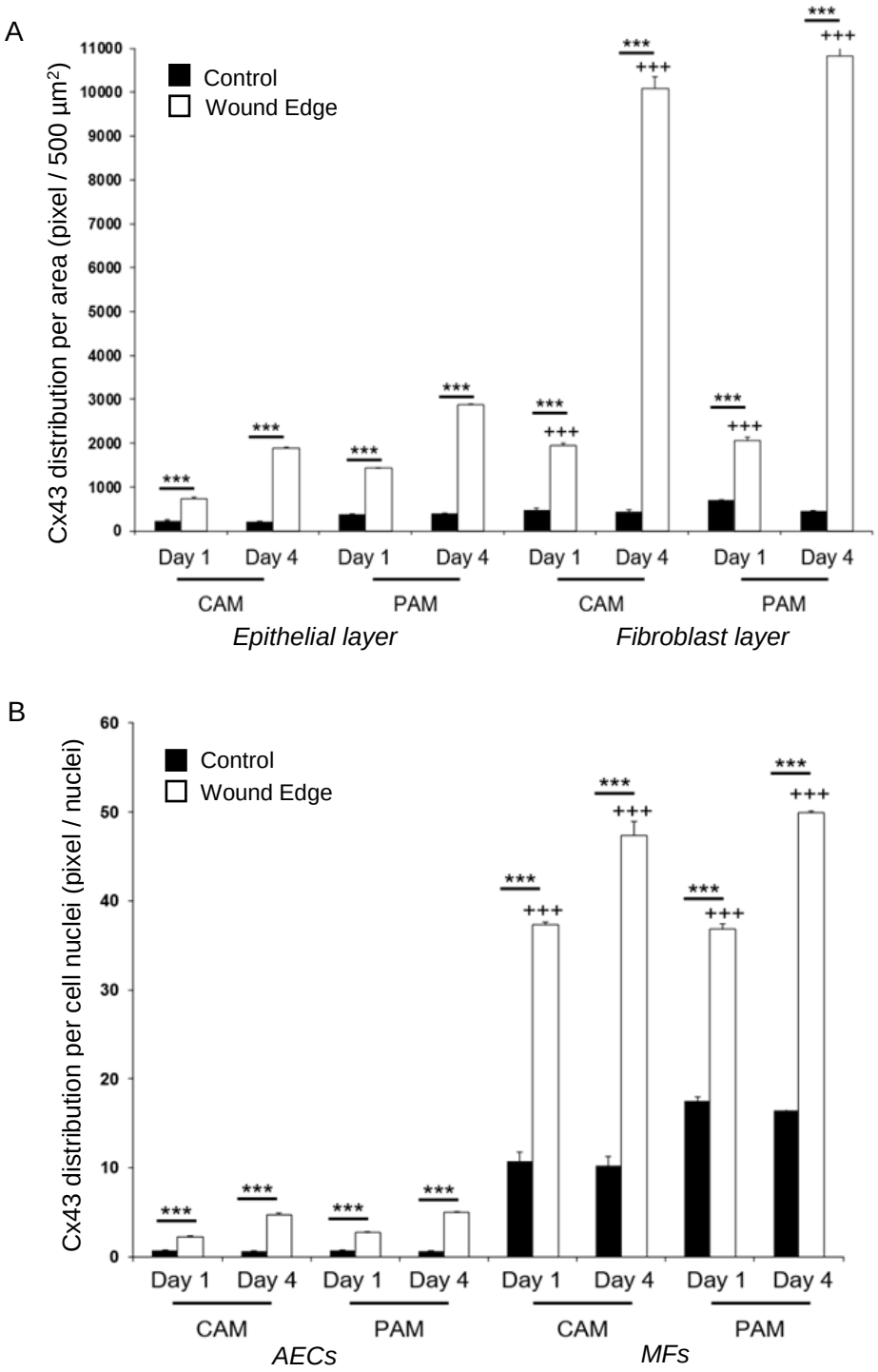

Figure 4.3: *Quantification of the distribution of Cx43 protein in PAM and CAM. The distribution of Cx43 was analysed per unit tissue area (A) for comparisons between epithelial and fibroblast layer and per AEC or myofibroblast cell nuclei (B) in control and wound edge specimens. In all cases, error bars represent the mean and SEM values for n=9 replicates, where membranes were taken from three donors. Significant differences between day 1 and 4 were found as indicated by ***p < 0.001. Comparisons between epithelial and fibroblast layer are indicated by $^{+++}p < 0.001$. All other comparisons were not statistically significant (not indicated). CAM = cervical amniotic membrane, PAM = placental amniotic membrane, AECs = amniotic epithelial cells, MFs = Myofibroblasts.*

4.2.2 Changes in expression of αSMA protein by cell populations in the AM defect

Images after 1 and 4 days of culture were collected after tissue fixation and immunostaining. Vimentin-expressing AMCs are undifferentiated cells present in the fibroblast layer [47,77]. In controls, these cells were abundant and exhibited more rounded morphologies and non-deformed nuclei **(Figure 4.4;** green vimentin staining**).** At the wound edge, they had a flattened morphology, elongated nuclei, and cytoplasmic extensions **(Figure 4.4)**. Additionally, collagen fibrils were highly aligned in parallel to both nuclei and the wound edge in contrast to more disorganised fibres seen in controls **(Figures 4.4 & 4.5).** Following trauma and 1 day of culture, migrating differentiated myofibroblasts polarised and congregated at the edge of the wound, changed in morphology, and expressed αSMA **(Figure 4.4;** green αSMA staining**).** Striking differences in myofibroblast cell morphology were seen at both timelines **(Figure 4.4)**. In controls, αSMA-expressing myofibroblasts had shorter, less defined cytoplasmic projections with more rounded nuclei **(Figures 4.4 & 4.5).** In contrast, at the wound edge, αSMA-expressing myofibroblasts had long interconnected cytoplasmic extensions stretching across the wound edges. A layer of flattened, cuboidal AECs was observed in the epithelial layer and minimal protein expression of αSMA in AECs in contrast to high expression in contractile myofibroblasts **(Figure 4.5).**

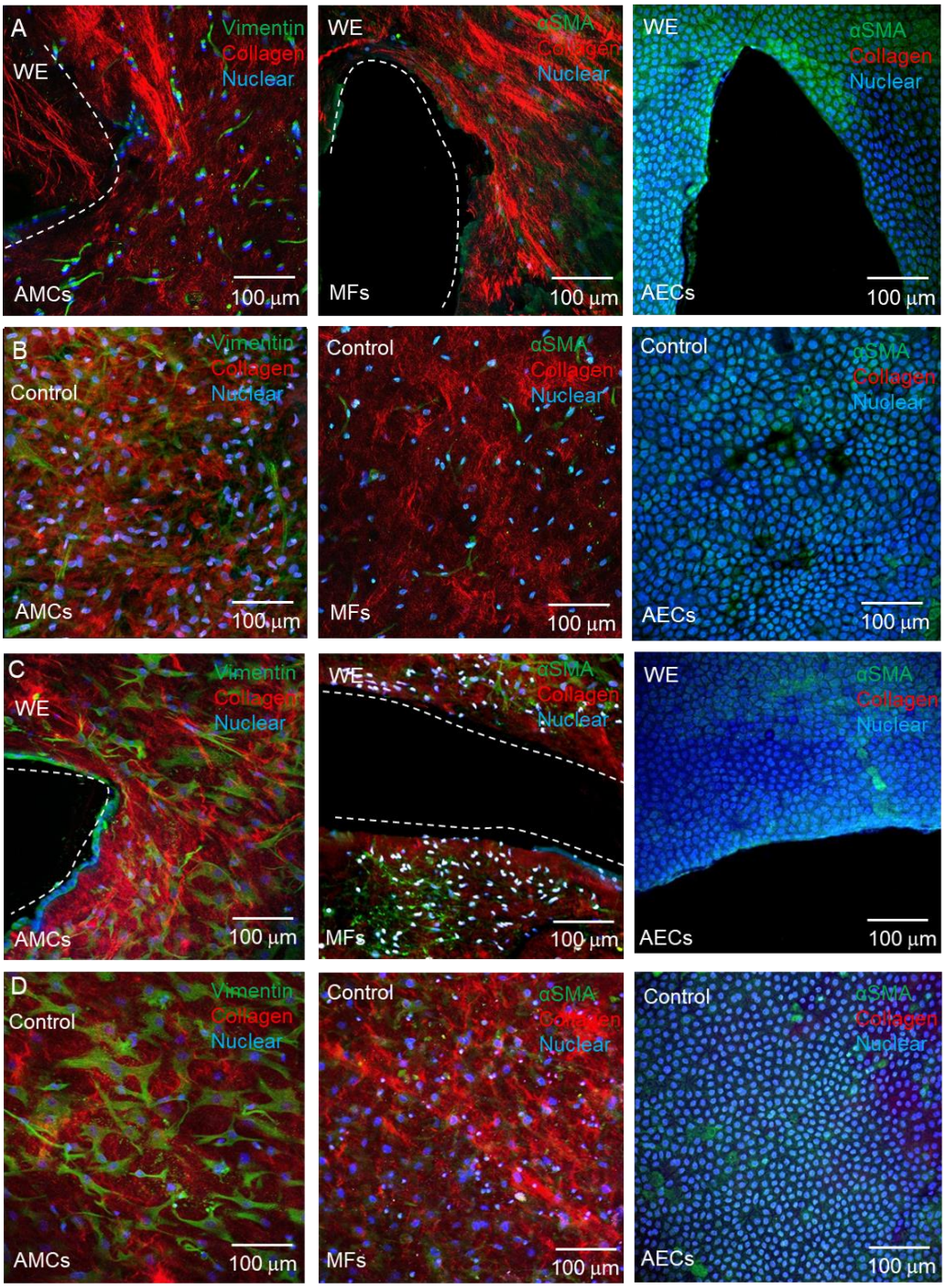

Figure 4.4: *Immunofluorescent images of human AM after 1 day of culture in AF. Changes in AMCs morphology, migration potential and αSMA expression across wounds in PAM (A & B) and CAM (C & D) regions are seen. (A & C) After 1 day, both vimentin-expressing AMCs and αSMA-expressing myofibroblasts begun to migrate toward the wound edge. Both cell types changed morphology showing elongated cytoplasmic extensions, while myofibroblasts expressed higher levels of αSMA than those seen in controls (B & D). The figure shows representative images from three separate donors for controls and wounded tissue. White dotted lines show the margins of the defect. AF = amniotic fluid, AECs = amniotic epithelial cells, AMCs = amniotic mesenchymal cells, PAM = placental amniotic membrane, CAM = cervical amniotic membrane, WE = wound edge, MFs = myofibroblasts, Cx43 = connexin 43, αSMA = alpha smooth muscle actin. Scale bar = 100 µm.*

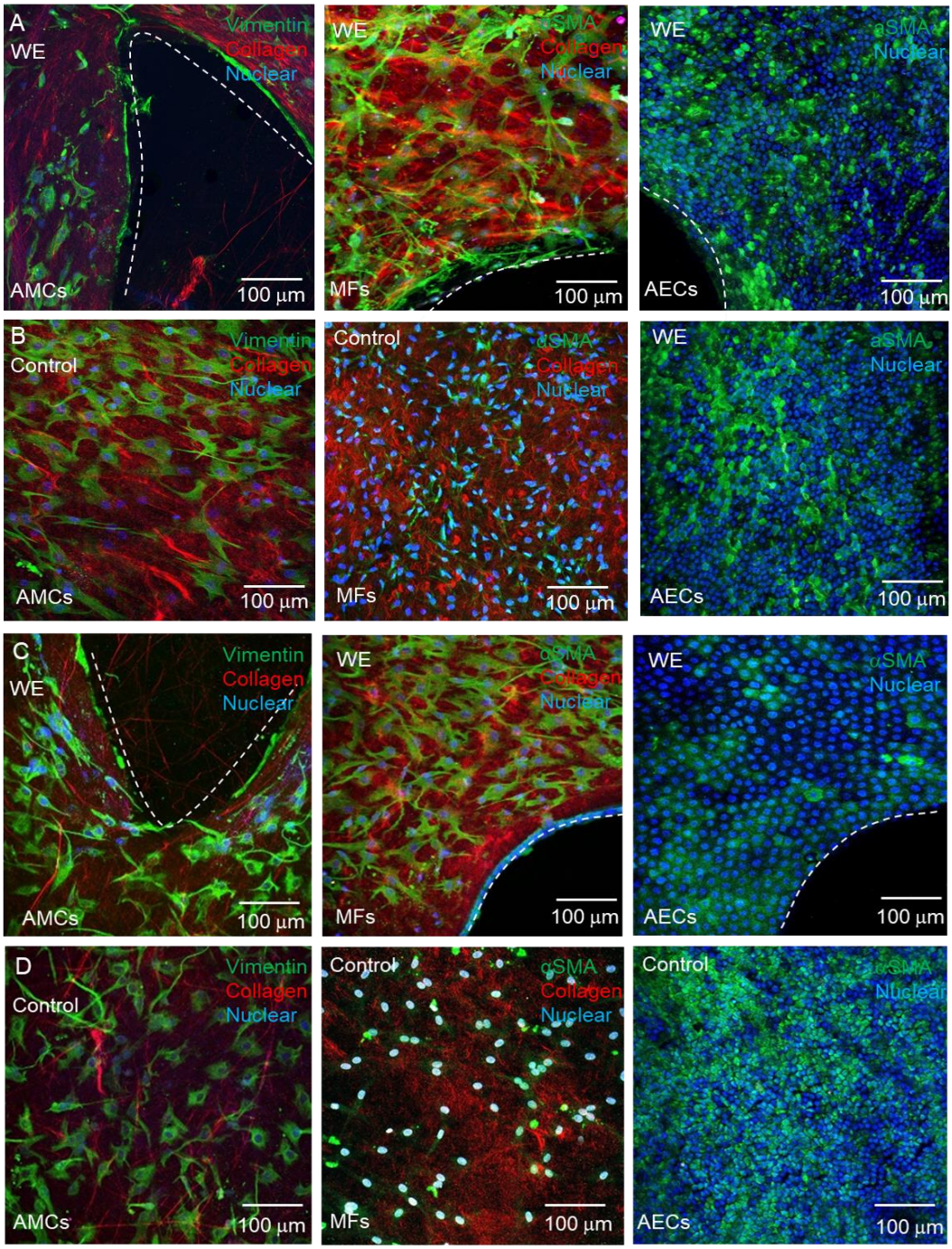

Figure 4.5: *Immunofluorescent images of human AM after 4 days of culture in AF. Changes in AMC morphology, migration potential and αSMA expression across wounds in PAM (A & B) and CAM (C & D) regions are seen. After 4 days, AMCs and myofibroblast concentration at the WE increased, cells became polarised around the wound and cytoplasmic cell projections stretched out along the edges compared to controls (B & D). New collagen fibres (SHG signal) were evident across the wound edge. The figure shows representative images from three separate donors for controls and wounded tissue. White dotted lines show the margins of the defect. AF = amniotic fluid, AECs = amniotic epithelial cells, AMCs = amniotic mesenchymal cells, PAM = placental amniotic membrane, CAM = cervical amniotic membrane, WE = wound edge, MFs = myofibroblasts, Cx43 = connexin 43, αSMA = alpha smooth muscle actin. Scale bar = 100 µm.*

To investigate cell morphology changes, the volume of αSMA-positive cells was measured using the 'Volume' and 'Surface' commands in Imaris 9.5, whereby individual cells were identified and segmented within a 3D structure of the AM **(Figure 4.6).** In CAM, the volume of myofibroblasts at the WE were 46 μm^3 ± 3.4 at day 1 and 95.6 μm^3 ± 3.2 at day 4, a marked increase of 150% and 134% respectively (**Figure 4.6A**, ***$p < 0.001$). As with αSMA intensity quantifications, PAM presented with significantly higher % increase in cell volume of 161% and 171% at day 1 and 4 respectively. αSMA distribution per cell nuclei was measured throughout the whole of the tissue (**Figure 4.6B**, ***$p < 0.001$). At day 1 and 4 in CAM specimens, there was a significant increase by 27% and 38% respectively of αSMA intensity at the WE compared to controls (**Figure 4.6B**, ***$p < 0.001$). In PAM samples, αSMA intensity was significantly higher than in CAM, with an increase of 44% and 57% at the wound edge at day 1 and day 4 respectively (**Figure 4.6B**, $^{***}p < 0.001$). However, when measuring the volume of αSMA-positive cells, CAM has significantly higher increase in volume than PAM (**Figure 4.6B**, $^{+++}p < 0.001$). No notable morphological changes were seen in the amniotic epithelial layers, with αSMA being expressed at the cell membrane to form tile-like shapes in both controls and at the wound edge (**Appendix; Table 4.3**).

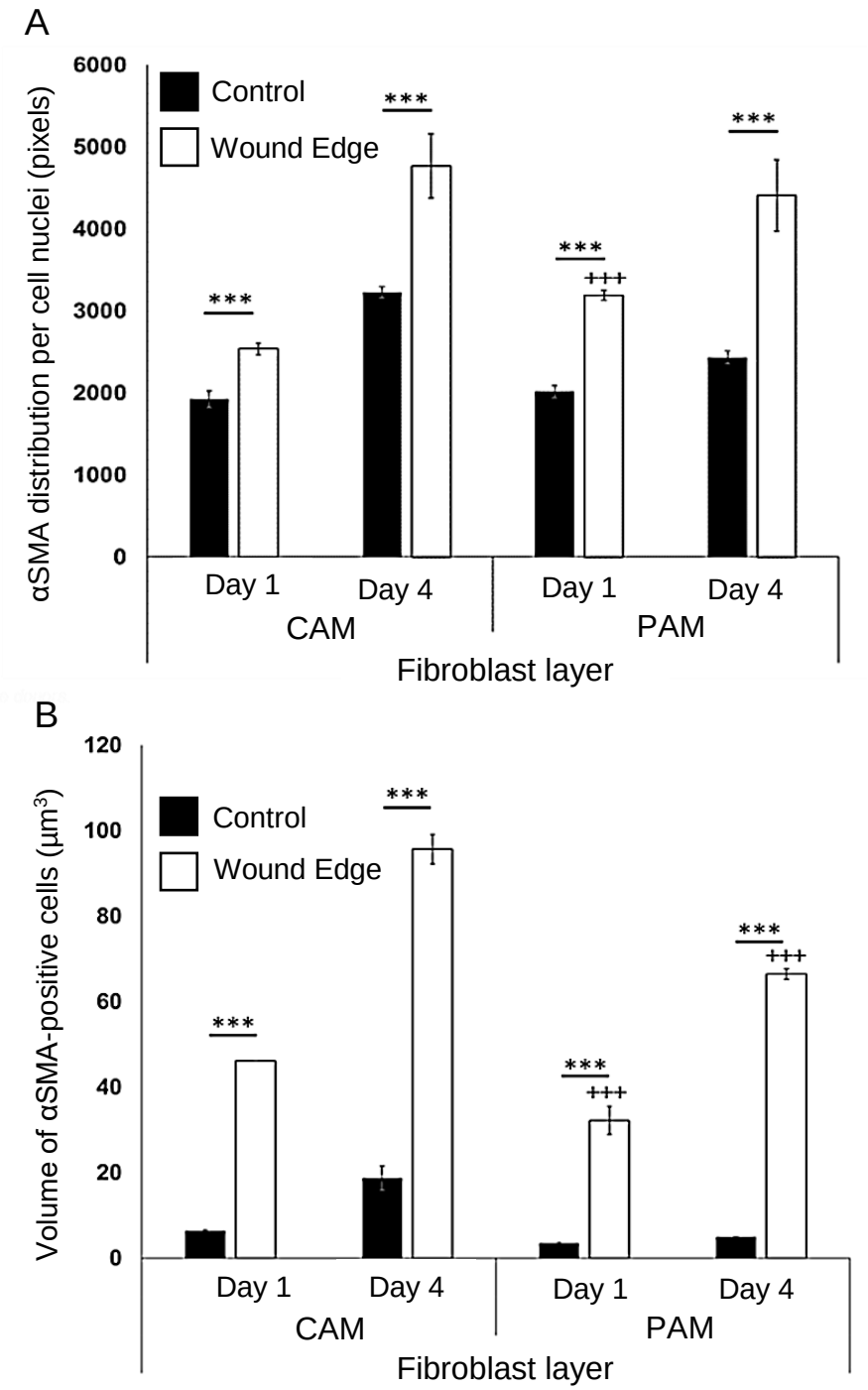

Figure 4.6: *Measurement of αSMA intensity and αSMA-positive cell volume at the wound edge. The volume of individual AMCs was measured in 3D (μm³) throughout the whole structure. Distribution of αSMA analysed (A) per volume of tissue area in the fibroblast layer and per (B) myofibroblast cell nuclei between control and wound edge specimens. In all cases, error bars represent the mean and SEM values for n=9 replicates, where membranes were taken from three donors. Significant differences are indicated by ***p < 0.001. Comparisons between CAM and PAM specimens in fibroblast layer are indicated by $^{+++}p < 0.001$. All other comparisons were not significant (not indicated). AMCs = amniotic mesenchymal cells, PAM = placental amniotic membrane, CAM = cervical amniotic membrane, αSMA = alpha smooth muscle actin.*

4.2.3 Quantification of nuclei polarisation of cell population at the AM wound edge

In the fibroblast layer of the amniotic membrane, both AMCs and MFs nuclei polarised tangentially to the edges of the wound, indicating potential increased cell deformation after trauma **(Figure 4.7A, B & C).** As shown in **Figure 4.7,** nuclei at the wound edge of both regions had circularity of less than 0.5, indicating their elongated shape, while control nuclei had circularity of 0.8 - 1 **(Figure 4.7D)**. Nuclei alignment and deformation **(Figure 4.7D, F & G)** tended to correlate with collagen fibril alignment and cytoplasmic elongation as quantified by αSMA intensity at the wound edge **(Figures 4.4 – 4.6)**.

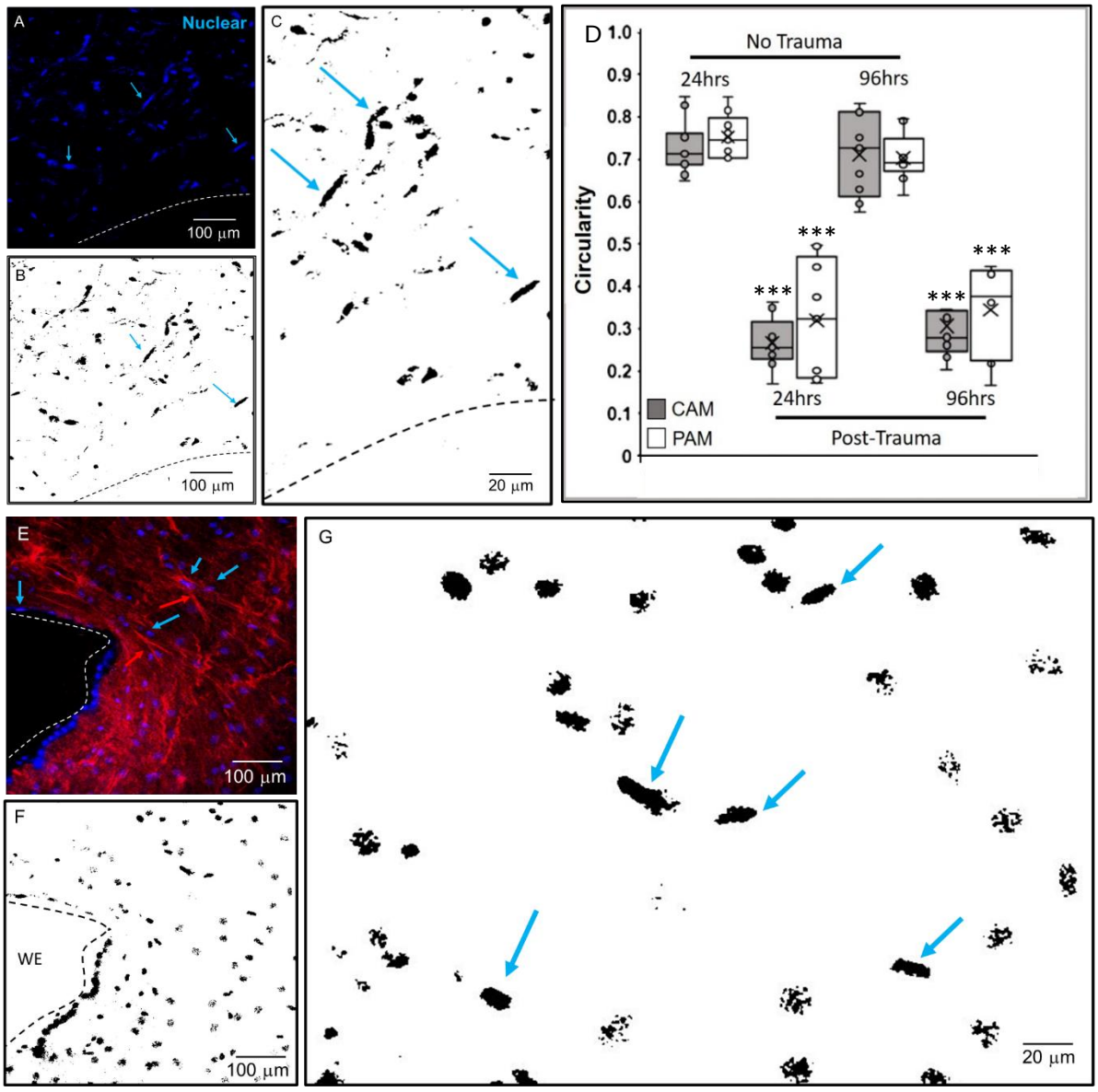

Figure 4.7: *The effects of trauma on AMC and MF nuclei morphology. (A) At the defect site, there were deformed nuclei aligned tangentially to the wound edge. (B & C) Binary conversion of RGB image shows clear nuclei deformation (Blue arrows). (D) Box and whisker representation of nuclei circularity for PAM and CAM specimens at day 1 and 4 of culture. As the value approaches 0.0, it indicates an increasingly elongated shape, while a value of 1 represents a perfect circle. Mean and SEM values represent 9 replicates from three separate donors for controls and wounded tissue for PAM and CAM respectively. Significant differences between controls and WE were found as indicated by ***p < 0.001. (E - G) Nuclei alignment and deformation (blue arrows) tended to correlate with collagen fibril alignment (red arrows) at the wound edge. AMCs = amniotic mesenchymal cells, PAM = placental amniotic membrane, CAM = cervical amniotic membrane, MFs = myofibroblasts. WE = wound edge. Scale bars = 100 µm and 20 µm.*

4.2.4 Collagen organisation in the AM after trauma

As previously indicated, collagen fibrils aligned tangentially to the wound edge by day 4 of culture similarly to the polarised alignment of the AMCs nuclei, in contrast to the more disorganised fibres seen in controls in both PAM and CAM specimens **(Figure 4.8A).** To determine preferred collagen fibre alignment, an orientation distribution analysis using the Directionality ImageJ plug-in (v2) was performed **(Figure 4.8B). Figure 4.8** shows that by day 4, collagen remained highly polarised, but there was evidence of new fibril formation across the wound in both PAM and CAM **(Figure 4.8A**, white arrows). Control regions showed more typical disorganised and "basket-shaped" fibre orientation that is interwoven throughout the basement, intermediate and spongy layers of the AM in a random fashion **(Figure 4.8A)**.

Upon examination of the newly formed collagen fibrils, there was evident changes in their shape and organisation. This was further investigated using surface intensity plots, whereby there was a significant increase in SHG intensity at the trauma site relative to controls throughout the whole of the tissue **(Figure 4.8C).** The plots further assert to the formation of a denser, highly aligned collagen ring at the wound margin that could be seen around the perimeter of the wound edge. Overall, there was a four-fold SHG signal intensity increase in fibroblast layers (approximately 100 – 350 microns thick) of wound edge regions compared to patient matched controls (**Figure 4.8**, *n*=3 patients).

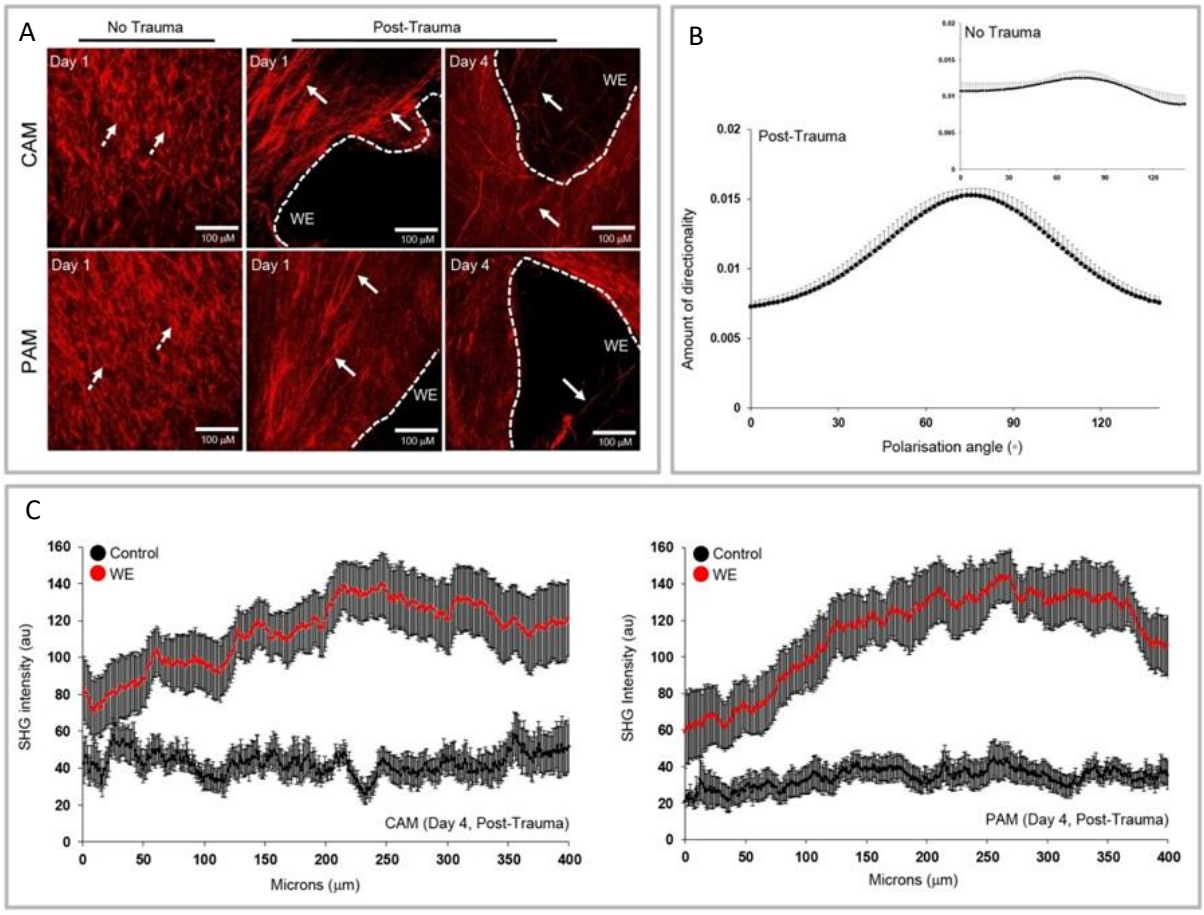

Figure 4.8: *Collagen fibre organization in AM defects after trauma. (A) SHG imaging of collagen (red) showed dense collagen fibre alignment tangential to the wound edge in CAM and PAM specimens but not in control specimens. After trauma, there was a region of highly polarized collagen fibres aligned in the direction at around 90^{o}C in wounded specimens. This intense organization was absent in control specimens. (B) Quantification of collagen fibre orientation showed a preferred polarisation angle in wounded samples relative to no trauma. (C) Quantification of collagen fibres revealed a significant increase in the SHG intensity values for wound edge specimens than controls (Bottom panel). The figure shows representative images and data from three separate donors for controls and wounded tissue. White dotted lines show the margins of the defect. AM = amniotic membrane, PAM = placental amniotic membrane, CAM = cervical amniotic membrane, SHG = second harmonic generation, WE = wound edge. Scale bar = 100 µm.*

4.2.5 Cell phenotype and collagen changes in human AM defects after trauma using 3D imaging software

To investigate the amniotic membrane wound healing process in 3D, an area of tissue (500 μm^3) was imaged. **Figure 4.9** shows a 3D image of a PAM control specimen after 1 day of culture. At the top view, the epithelial layer formed a blanket comprised of single cells that are directly in contact with amniotic fluid *in vivo* **(Figure 4.9A).** The cross section indicates the fibroblast layer under the epithelial layer interspersed with collagen fibres **(Figure 4.9B).** AMCs nuclei appeared further away from each other relative to AECs which are packed close together **(Figure 4.9B)**. 3D images of control tissues show the uniform distribution of both cell types and collagen fibres throughout the whole of the AM tissue **(Figure 4.9A & B).**

Figures 4.9C & D and **4.10** display the 3D images of traumatised CAM and PAM specimens after 4 days of culture. In contrast to controls, there was evidence of new collagen fibre deposition across the wound edge, followed by the formation of αSMA-expressing myofibroblast cytoplasmic extensions at the edge of the wound and Cx43 plaque expression **(Figure 4.9C & D).** In CAM specimens after 4 days of culture, AMCs were seen migrating from the wound edge and crossing through it, presumably to repopulate the damaged area followed by new collagen fibre secretion **(Figure 4.9D & 4.10)**. At the top view of a traumatised PAM sample, AECs within the epithelial layer formed a cluster of cells around the wound edge and did not appear to migrate through the wound **(Figure 4.9D & 4.10).** In contrast, AMCs within the fibroblast layer under the epithelial layer, have migrated and crossed the defect while simultaneously producing new collagen fibres and Cx43 plaques **(Figure 4.10)**. Increased Cx43 plaque formation was seen in both PAM and CAM specimens the longer the tissue was maintained in culture **(Figure 4.10)**.

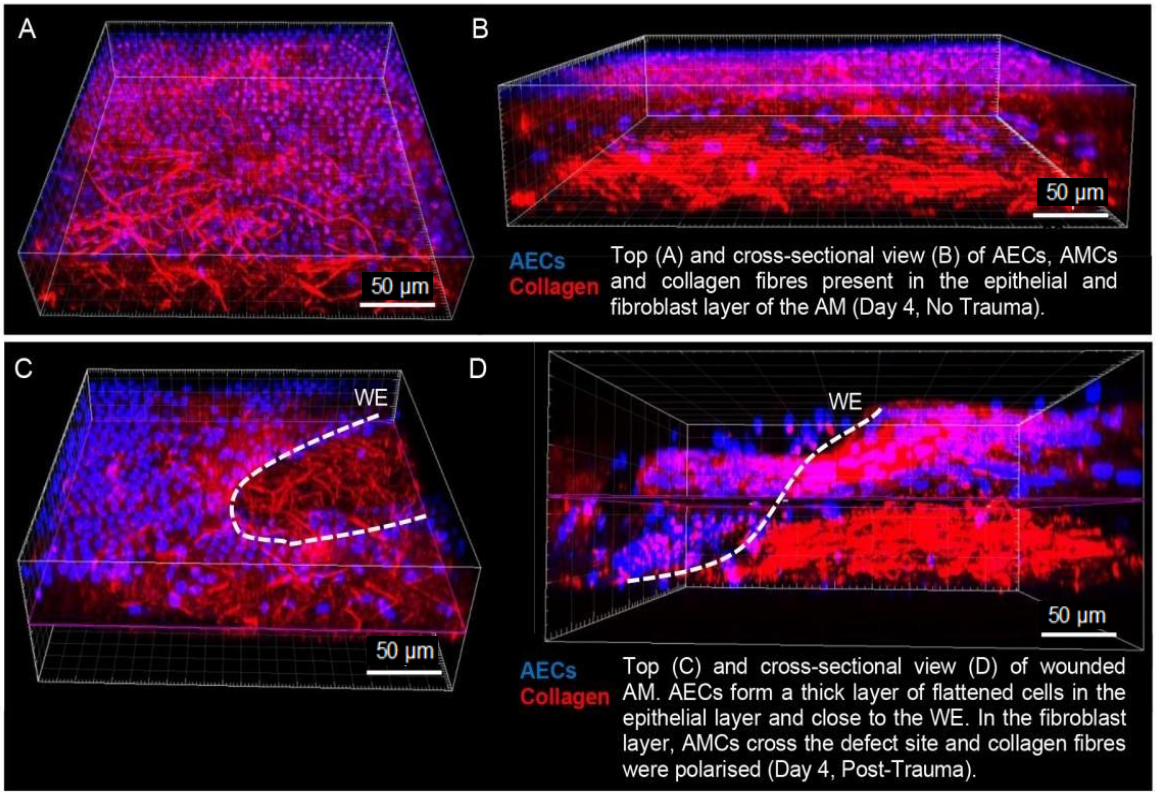

Figure 4.9: *Morphological changes in human AM defects after trauma. (A & B) In control AM specimens cultured for up to 4 days, we observed a layer of flattened AECs in the epithelial layer and a dense region of collagen fibres in the fibroblast layer by IMF confocal microscopy and SHG imaging. (C) After creation of a defect in the AM specimen and culture for up to 4 days, cells migrated to the wound edge with evidence of a greater intensity of the SHG signal close to the wound edge and polarization of collagen fibres. (D) Cells were seen migrating to repopulate the wound. The figure shows representative images from n=3 separate donors for controls and wounded tissue. White dotted lines show the margins of the defect. AM = amniotic membrane, AECs = amniotic epithelial cells, SHG = second harmonic generation, WE = wound edge. Scale bar = 50 µm.*

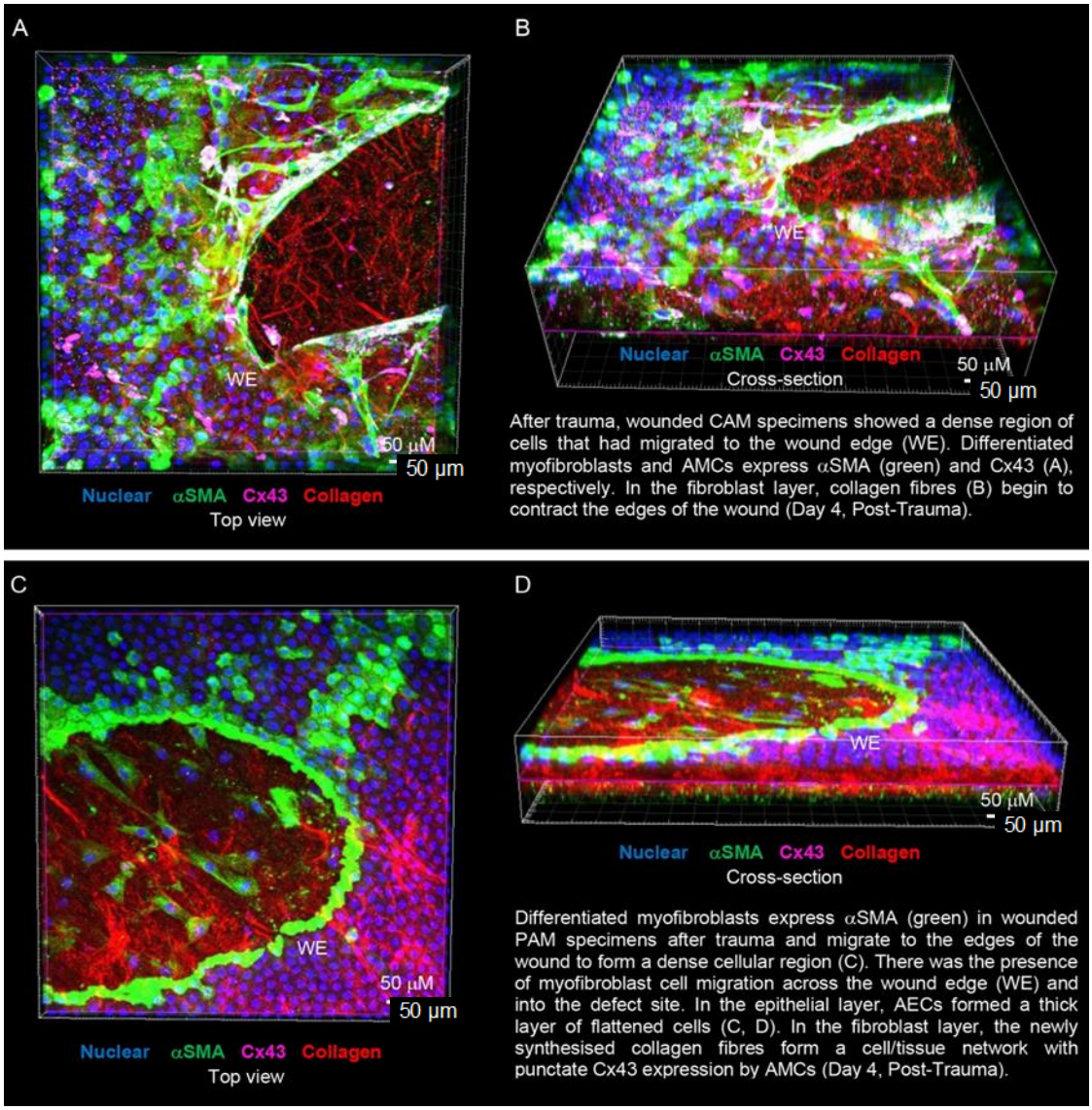

Figure 4.10: *Examination of the AM after trauma using 3D modelling software. (A) 3D imaging of a traumatised CAM specimen after 4 days of culture. There was evidence of new collagen fibre deposition across the wound edge, followed by AMCs cytoplasmic extensions at the edge of the wound and Cx43 plaque expression. (B) The same CAM sample as cross. (C) 3D image of a traumatised PAM specimen after 4 days of culture. At the top view, the epithelial layer formed a cluster of cells around the wound edge and did not appear to migrate through the wound. AMCs under the epithelial layer, have migrated and crossed the trauma while simultaneously producing new collagen fibres and Cx43 plaques (D) Cross section of the same PAM specimen. The figure shows representative images from n=3 separate donors for controls and wounded tissue. AM = amniotic membrane, PAM = placental amniotic membrane, CAM = cervical amniotic membrane, AMCs = amniotic mesenchymal cells, Cx43 = connexin 43, SHG = second harmonic generation, WE = wound edge. Scale bar = 50 µm.*

4.2.6 The expressions of Connexin 43 and TGFβ1 are increased in the AM after trauma

Figure 4.11 examines the effects of trauma on Cx43 and TGFβ1 gene expression. At day 1, the expression of Cx43 was found to be increased at the wound edge without any significant differences between CAM and PAM specimens (**Figure 4.11A**, ***$p < 0.001$) After day 4 of culture, trauma increased Cx43 gene expression in both PAM and CAM, presenting with 116% and 166% significant increase respectively relative to day 1. In PAM samples, there was a three-fold increase in Cx43 expression in comparison to CAM (***$p < 0.001$). TGFβ1 gene expression increased in CAM following trauma compared to controls at both timelines (**Figure 4.11B**, ***$p < 0.001$). Of importance, TGFβ1 gene expression was significantly higher in PAM regions than CAM (% difference between PAM and CAM 186% and 166% at day 1 and day 4 respectively).

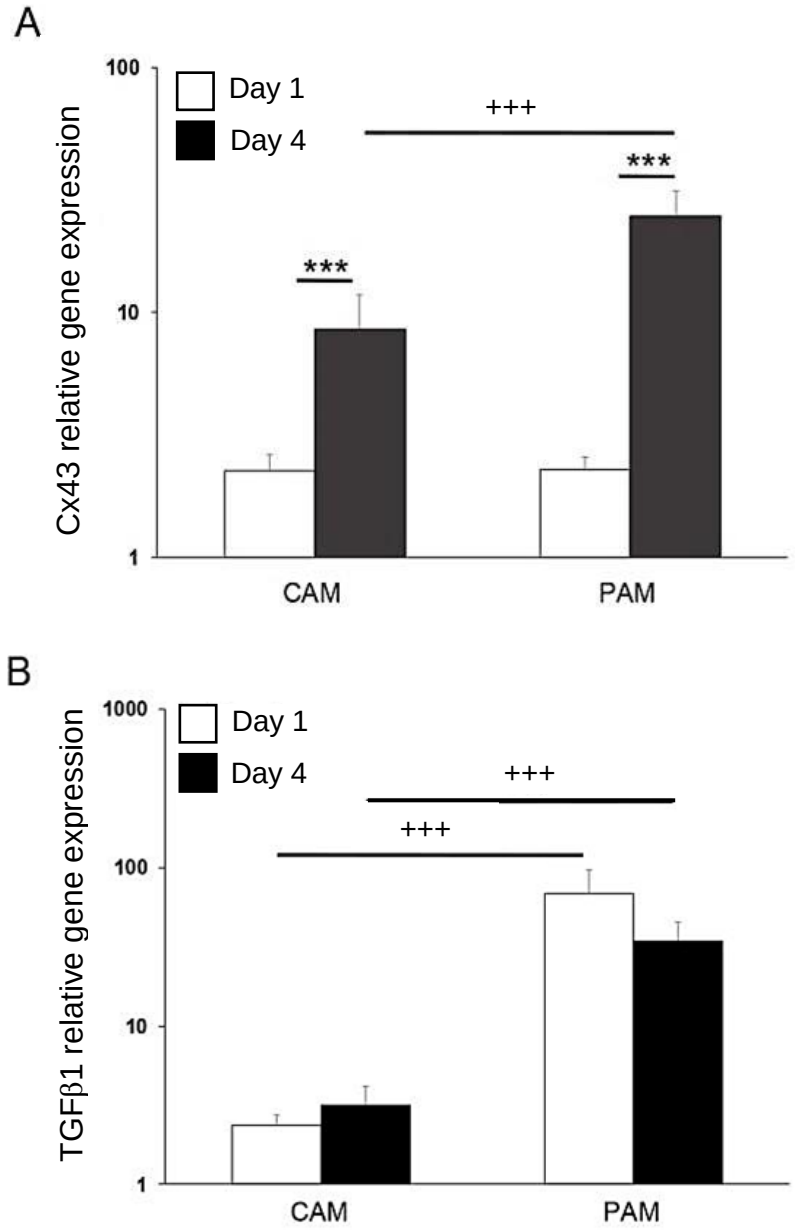

Figure 4.11: *Relative gene expression changes for Cx43 and TGFβ1 day 1 and day 4 of culture. The expression of Cx43 and TGFβ1 was increased at the wound edge when normalised to controls. To calculate relative quantification of candidate genes, the comparative Ct (ΔΔCT) Michael-Pfaffl method was used. Ct values were normalised to the target reference gene (GADPH) and the calibrator samples (controls) and expressed on a logarithmic scale. Mean and SEM values represent 9 replicates from three separate donors for controls and wounded tissue for PAM and CAM respectively. Significant differences are indicated by ***p < 0.001. Comparisons between CAM or PAM specimens in fibroblast layer are indicated by $^{+++}$p < 0.001. CAM = cervical amniotic membrane PAM = placental amniotic membrane, WE = wound edge.*

4.3 Key Findings

- Increased Cx43 protein expression (per nuclei and per tissue area) at the wound edge of the AM was quantified at 1 and 4 days after trauma in both the fibroblast and epithelial layers.
- Cx43 plaques within αSMA-expressing myofibroblasts and AECs localised in both the cytoplasm, nucleus and cell membrane.
- Vimentin-expressing AMCs with elongated lamellipodia were observed at the defect site 1 and 4 days after trauma.
- αSMA-expressing myofibroblasts significantly increased in density and volume at the wound edge 4 days after trauma, with profound differences compared to controls.
- AMC and myofibroblast nuclei within the AM fibroblast layer polarised at the wound edge 1 and 4 days after trauma.
- SHG imaging demonstrated an increase in collagen intensity and polarised orientation in PAM and CAM at 1 and 4 days after trauma.
- 3D imaging of specimens 4 days after trauma showed collagen fibres deposited within the defect concurrent with locomotive myofibroblast migration dependent on Cx43 localisation. New collagen fibres at day 4 after trauma within the defect appear shorter but still defined relative to longer fibres at the edges of the wound at day 1.
- The expressions of Cx43 and TGFβ1 genes were found to be increased in the AM after trauma over 1 and 4 days of culture compared to controls.

4.4 Discussion

Previous studies by our group have shown that Cx43 expression was altered in both the amniotic epithelial and fibroblast layers of the AM in large (> 3 mm) and small wounds (0.8 mm) [17,104]. In **Chapter 2**, it was hypothesised that trauma influences the expressions of Cx43, TGFβ1 and the morphologies of resident cell populations along with collagen content in term fetal membranes. The present study utilised an *in vitro* FM trauma model to characterize the morphological differences of AM cell populations after trauma. Focus was placed on the amniotic membrane due to its unique cellular and ECM composition as characterised by our group and others [17,49,104,201,203,205].

The mobility dynamics of Cx43 delivery to the cell membrane and the activity of gap junctions regulates the acceleration of wound healing dependent on elevating pro-inflammatory factors and cytokines via gap junction communication or hemichannel cluster formation to form large Cx43 plaques [104,250,251,291,295]. Cx43 channel function and activity participates in all stages of skin wound healing, including induction of inflammation, cell-cell communication and migration, wound contraction and formation of granulation tissue and scar remodelling [291-299]. Cx43 was found to be upregulated in fibroblasts in the deep dermis immediately after trauma, promoting granulation and scar formation, while inhibition of Cx43 disrupted calcium oscillations and the migratory potential of fascia fibroblasts leading to incomplete scar formation at the epidermis [281]. In contrast, epidermal overexpression of Cx43 leads to reduced migration, apoptosis, and loss of wound re-epithelialisation [250,281,294,295].

In previous studies, our research group showed that Cx43 localisation within the fibroblast layer was abundant but did not differentiate between AMCs and differentiated MFs [104]. Using double immunostaining confocal imaging techniques to detect αSMA-expressing myofibroblasts, Cx43 was found to localize abundantly in myofibroblast long cytoplasmic cellular processes and between cell-to-cell contacts in the fibroblast layer close to the wound edge. High resolution imaging of both PAM and CAM showed Cx43 plaques also concentrated within MF nuclei at the wound edge after 4 days of culture. Whilst the present study did not quantify the rate of cell

migration into the defect site using 2D monolayer models after cell expansion, incomplete or poor healing mechanisms have previously been attributed to the abundance of Cx43 at the cell-to-cell contacts [291-299]. In chronic diabetic and venous leg ulcers and cutaneous skin injuries the increased expression of Cx43 in the cell membrane of resident cells has been correlated with poor wound healing closure, and phenotypic changes in fibroblasts and keratinocytes that mediate sustained inflammation [250,291,294]. In epidermal mouse injuries, Becker's group used Cx43asODN to decrease the expression of Cx43 at the wound edge, leading to wound healing acceleration concurrent with a decrease in neutrophil infiltration and inflammation [273]. In corneal endothelial injuries, Cx43 expression initially increases, leading to the activation of pro-inflammatory pathways allowing the transformation of resident fibroblasts to a contractile phenotype, while knockdown of Cx43 prevents αSMA-myofibroblast activation [296,297].

Furthermore, the sub-cellular dynamic localization of Cx43 in the cytoplasm, nucleus or cell membrane was shown to have a differential effect on Cx43 transcriptional activity and influence the efficiency of adhesion or cell migration [250,268-272]. In fetal membranes, Cx43 localisation and concentration may potentially mediate differential effects on cell populations that could hinder complete closure of the wound. Menon's group showed that damage caused by cigarette exposure of AM explants or in AM cell populations increased expressions of vimentin and N-cadherin leading to a greater transition between cell states triggered by TGFβ [77,180,186]. Cx43 has also been shown to act as a direct transcriptional regulator of N-cadherin via translocation to the nucleus and binding to the N-cadherin promoter, controlling migration of neural crest cells and enhancing cellular morphological changes [266] and to modify N-cadherin levels at the cell membrane and influence migration [263].

Taking the findings of this chapter into consideration, the literature will be further compared. Becker's group demonstrated that Cx43, N-cadherin and the N-cadherin-associated protein ZO-1 were upregulated in skin punch biopsies in the dermis of human venous leg ulcers [295]. Cx43 expression in fibroblasts was concurrent with upregulation of N-cadherin and changes in β-catenin cellular localisation, both of which influenced cell migration at the wound edge [295]. In embryo fibroblast cell lines, N-cadherin cell surface expression was shown to require the

presence of Cx43 on the cell membrane, suggesting that Cx43 and N-cadherin are co-assembled in a multiprotein complex containing various N-cadherin-associated proteins [263]. In mouse brain homogenates, the association of Cx43 localisation with cytoskeletal proteins has also been shown, identifying the F-actin binding protein Drebrin as a binding partner of the C-tail of Cx43 [265]. These studies highlight how the localization of Cx43 influences different cellular behaviours, and direct correlations to the present study can only be made after targeting Cx43 with a pharmacological agent, something that has not been done here and is essential for future work. Inflammation induced by trauma will differentially influence cell behaviour in a sub-population dependent manner and further highlights the need for better human models to understand wound healing in the fetal membranes.

To understand whether Cx43 upregulation by AMCs at the WE participated in their differentiation to myofibroblasts and activation of pro-inflammatory TGFβ1, the evidence will be further evaluated**.** Using 3D-imaging of wounded AM, αSMA-expressing myofibroblasts were observed within the defect site of both AM regions. Through SEM imaging, macrophages were seen localised near the defect site and may have been recruited from the amniotic fluid during culture (**Appendix; Figure 4.13A**). In a mouse fetal membrane model, M2-macrophages from the amniotic fluid were shown to stimulate AMC differentiation into myofibroblasts after IL-1β and TNF activation, but not following TGF induction [66]. TGFβ1 has been proposed to act as both a pro- and anti-inflammatory factor, depending on species, cell, and tissue types. In Cx43asODN-treated mouse wounds, TGFβ1 mRNA was elevated on day 2 within elongated fibroblast-like cells at the wound edge compared to controls, concurrent with increased collagen type 1α deposition [250]. The expression of TGFβ1 was lowest at days 1 and 7 after injury, suggesting a time-depended activation of TGFβ1 in relation to Cx43, however other factors could also be influencing the wound healing process [250]. In vascularised tissue, TGFβ isoforms are known to promote myofibroblast differentiation [242]. In vascular endothelial cells after trauma, Cx43 expression was shown to rapidly increase, leading to a cascade of pro-inflammatory pathways to be activated, including TGFβ1 [272]. In the first few hours of trauma, this allowed for increase in vasodilation and neutrophil infiltration, promoting the transformation of resident fibroblasts to a contractile phenotype to initiate migration and re-epithelialisation at the wound [272]. However,

sustained overexpression of Cx43 led to increased inflammation and damage caused by neutrophil and macrophage infiltration [250,272].

The relationship between Cx43 and αSMA expression was investigated by the same group [250]. Using Cx43asODN knockout in mouse skin wounds, it was shown that at day 7 post-injury, αSMA staining was significantly higher in Cx43asODN-treated wounds, concurrent with increased proliferation rates and re-epithelialization. In contrast, by day 10, controls exhibited significantly higher αSMA than those treated with Cx43asODN [250]. The authors concluded that Cx43 is essential in activating myofibroblast differentiation at the first stages of skin wound healing, but following the granulation stage, Cx43 loss of function hinders myofibroblast differentiation [250].

In the current study, increased expression of TGFβ1 gene at the wound edge after 1 and 4 days of culture correlated with increased Cx43 expression and the volume of αSMA-expressing myofibroblasts in both AM regions, highlighting the discrepancies between animal and human-derived models [250,272]. Using Becker's models as examples, it is possible that as Cx43 plaque formation in AMCs increased during culture time, Cx43 expression hindered further myofibroblast differentiation and thus the complete closure of the wound. This mechanism will be dependent on the model system, including 2D primary cultures and different animal models. In addition, mechanical stimulation models will have differential effects on wound healing and gene expression changes, particularly in preterm AM. Importantly, targeting Cx43 with pharmacological agents would be the first step to determine whether this hypothesis applies to human FM defects, and not just in skin wounds. Increased Cx43 was correlated with increased TGFβ1 gene expression in this study, however pharmacological knockdown of TGFβ1 must also be investigated in the future to elucidate the influence of TGFβ1 on Cx43 expression and on resident cell populations, including αSMA-expressing myofibroblasts.

Collagen distribution and polarization at the wound edge of AM defects has been previously described [104-106]. Using SHG imaging, the present study demonstrates collagen fibres highly polarised within the fibroblast layers after trauma, compared to disorganized fibres in controls. New collagen fibril deposition and increase in SHG signal after trauma was observed, concurrent

with MF migration within the defect and significant increase in the volume of αSMA-positive cells. The number of myofibroblasts are known to be directly correlated with the concentration of sub-epithelial collagens in other models, including skin [244], suggesting similarities with the current model. New collagen fibres at day 4 within the defect appeared shorter and had less ordered orientation than long defined fibres at the edges of the wound, suggesting they were newly synthesised or released [317]. The mechanical properties of the AM have been characterized by several research groups, with collagen playing a key role in maintaining mechanical integrity of the tissue [105,106,129,212]. Loss of collagen deposition and changes in alignment after mechanical stimulation alters elastin and collagen release, influencing downstream pro-inflammatory signalling pathways, including COX-2 and MMP expressions, and PGE_2 release [105,106]. Despite observed collagen alignment changes, collagen was not quantified with other techniques and thus it is not known whether the expressions of specific collagen types were altered after trauma. **Section 4.4.1** will discuss potential future studies that can focus on the relationship between Cx43 signalling, collagen and MMP expressions following trauma.

In epidermal mouse skin models, Mori *et al*., 2006 showed that following Cx43 inhibition with Cx43asODN, collagen mRNA expression and protein deposition was significantly higher at 2 and 7 days of injury compared to untreated controls [250]. In contrast, Cogliati *et al*., 2015 used Cx43 knockout ($Cx43^{+/-}$) mice and showed that despite increased mRNA expression of collagen types I and III at defect sites, collagen protein deposition remained unchanged between wild type and $Cx43^{+/-}$ mice [280]. These studies highlight two conflicting points: Firstly, pharmacological knockdown and functional knockouts in the same species result in contrasting effects on collagen deposition at the defect side. Secondly, they exemplify how comparisons between mouse skin models and human fetal membrane explants cannot be made directly due to species and tissue differences.

In embryonic wound healing, the purse-string contraction mechanism is activated during trauma [245,246]. In embryonic and skin wound healing models, fibroblasts and myofibroblast are well known to have distinct phenotypical characteristics [245,246]. Fibroblasts are spindle-shaped, express vimentin, but not αSMA [245,246]. Myofibroblasts express αSMA and have elongated

cytoplasmic structures distinctive from fibroblasts, including extensive actin stress fibres, cell–matrix adhesions, abundant intercellular adherens and Cx43 [245,246,294,313]. Cell traction forces by myofibroblasts are generated through actomyosin filament sliding, allowing migrating cells to move through the ECM via focal adhesions [244-246,312,316]. αSMA expression increased contractility of myofibroblasts by modifying myosin stress fibres, particularly when treated with TGFβ1 [312,313]. This mechanism could be occurring in small fetal AM defects, as exemplified by myofibroblast nuclei deformation and elongation at the wound edge, concurrent with morphological changes. Nuclei elongation suggests myofibroblasts may be undergoing morphological alterations, however further studies are required to elucidate if they are migrating and promoting purse-string contraction, which will be discussed in **Section 4.4.1**. The observational findings from the current study parallel the increase in density of αSMA-expressing myofibroblasts with elongated cytoplasmic extension in the fibroblast and reticular layers of the fetal membranes taken from patients undergoing different labour inductions [76]. McParland and colleagues showed that enhanced cellular activities by AMCs and myofibroblast cell populations contributed to an increase in tissue thickness after fetal membrane rupture and PPROM [76]. The authors hypothesised that amniotic fluid-derived macrophages contributed to the differentiation of AMCs to MFs via TGFβ1 expression, while MFs increased their production of MMPs and enhanced ECM matrix degradation in response to parturition [76].

In the present study, vimentin-positive AMCs and AECs were both shown to express Cx43 at the wound edge, but myofibroblasts expressed markedly higher Cx43 concentrations than both cell types (**Appendix; Table 4.2**). Thus, more studies must be conducted to determine whether changes in Cx43 expression in all three cell types (AECs, AMCs and MFs) mediate their migratory potential, particularly through N-cadherin expression. AMCs have fibroblast characteristics and the role of locomotive fibroblasts should not be dismissed when investigating wound healing in any model, as they can generate traction forces like myofibroblasts [244]. In fact, some studies suggest that myofibroblasts are present toward the end of the proliferation stage of classical wound healing, contributing to, rather than initiating, the cell contraction process, and this mechanism could be activated in FM wound healing as well, thus warranting further investigation [314,315].

AMC differentiation and activation of pro-inflammatory signalling during fetal membrane rupture and/or pathogen exposure is known to promote tissue remodelling [77,103]. In small mouse AM defects, AECs underwent EMT, lost cell to cell adhesion and apical-basal polarity and differentiated to AMCs [66]. These AMCs expressed high levels of vimentin and moved from the epithelial layer across the defect site to repopulate small 0.47 mm wounds, while the fibroblast layer remained compromised [66]. Injection of collagen type I into the defect enhanced the migration of amniotic mesenchymal cells through myosin contractions to repopulate the wound [82]. The reversible transition of AECs and vimentin-expressing AMCs during pregnancy and labour was further shown in human fetal membrane explants, highlighting the capabilities of amniotic cell populations under stress [66,76,77]. Furthermore, spontaneous labour was associated with AM EMT in both humans and mice, mediated by TGFβ from the amniotic fluid in both species, concentrations of which were higher near term [77]. Menon's group demonstrated that microfractures within the FM caused by cellular shedding exhibit degradation of basement membrane and matrix collagen, generating localised inflammation and EMT to increase AEC migratory capacity to repopulate these gaps [181]. Despite TGFβ1 gene expression increasing at defect sites in the present study, it cannot be concluded that TGFβ1 was actively involved in AMC differentiation without further studies, which will be discussed in **Section 4.2.2**.

In the present study, AECs were seen to accumulate at the edges of the wound by day 4, expressing low levels of αSMA and Cx43 relative to myofibroblasts and mostly retained their cuboidal structures. In larger defects (1.3 to 2.4 mm) AECs were seen expressing more αSMA than in 0.8 mm defects, with extended cytoplasm, while AECs in 3 mm defects had completely unique elongated morphologies, suggesting they could be undergoing differentiation to locomotive myofibroblasts (**Appendix; Figure 4.14**). In mouse FM studies, the healing rate was dependent on the size of the defect created by the needle (20 or 26 gauge), with 100% closure in small wounds (0.47 mm) relative to 40% in large diameter (0.91 mm) wounds [66]. As purse-string contraction is limited to the proximity of the defect edges, this is expected to be the same in human fetal membrane wounds. The role of AECs transition and the purse-string contraction hypothesis at the wound edge of small AM defects warrants further investigation in the future using scratch-wound assays and/or EMT-specific markers, particularly E-cadherin. In addition,

defects sizes larger than 0.8 mm were only investigated qualitatively with only one patient donor, and thus more clinical samples and protein quantifications must be performed.

4.4.1 Study limitations and future work

The present study relies heavily on correlation and not causation evidence. One of the biggest limitations is the fact that neither Cx43 nor TGFβ1 were pharmacologically inhibited and thus all data is very observational. Importantly, the concentrations of Cx43 protein in all AM sub-populations (AECs, AMCs and myofibroblasts) was investigated (**Appendix; Table 4.2**). Myofibroblasts presented with significantly higher Cx43 pixels per nuclei and pixels per area than both AMCs and AECs, correlating with increased cytoplasmic volume. This poses an interesting correlation between Cx43 and myofibroblast differentiation, however this is merely a correlation and not a causation and further work is required to determine the role of Cx43 in FM healing.

As explored in **Chapter 2**, Cx43 hemichannels are able to co-localise with other connexins and/or form heteromeric gap junctions with multiple connexin isoforms [260-266]. The antibody used for Cx43 immunofluorescence recognizes Cx43 when the protein is un-phosphorylated at serine 368 (S^{368}) position, however it can recognize Cx43 if it is phosphorylated at other sites. The manufacturer states that in some cell types, cross-reactivity with a ~70 kDa protein of unknown identity was observed, likely of another connexin epitope. To circumvent this, more connexin subtypes should be investigated, particularly those whose expressions were altered in other wound healing models (e.g. Cx26 and Cx30 in skin). Co-immunostaining of more subtypes may also determine whether Cx43 is the only connexin overexpressed at the wound edge of FM defects, and if these isoforms also form complexes with Cx43 throughout the cell and on the plasma membrane. Combining this with western blots and qPCR analysis would enhance the validity of the data.

Post-transcriptional modifications of Cx43 such as phosphorylation or S-nitrosylation influences protein function [282,283,286,308]. In the myometrium, Cx43 was found to be S-nitrosylated by NO, concurrent with increased Cx43 phosphorylation at S^{368} which promoted hemichannel open states [308]. Furthermore, phosphorylation of S^{364}/S^{365} residues controls trafficking of the

hemichannel to the cell membrane and can cause gain-of-function phenotypes associated with skin diseases [282,283,286]. Investigating phosphorylation and S-nitrosylation states of Cx43 in small FM defects would be of interest to determine which Cx43 activities are present during different culture periods in traumatised tissue. Western immunoblotting of FM protein extracts can determine whether Cx43 is phosphorylated and/or nitrosylated at different culture periods. Despite having performed qPCR quantification of Cx43 mRNA, western blots would confirm whether the mRNA was further transcribed into the functional Cx43 protein and how this compares between controls and defects. Additionally, exploring the activity of Cx43 hemichannels on the plasma membrane using florescent dyes would be of interest, to determine whether trauma influence the open/closed states of the channel through post-translational modifications. In skin explants, Cx43 inhibition was found to influence calcium oscillation and fascia fibroblast migration [281]. Thus, the effect of trauma in calcium oscillations using a calcium indicator dye could be investigated, and its relationship to myofibroblast migration within the AM. IMF confocal microscopy has the advantage of determining which cell populations expressed Cx43 at the defect site, however the limitations associated with the Cx43 antibody can be addressed by other techniques to confirm expression patterns.

Another issue with the Cx43 antibody is that I did not perform more thorough assay optimisation, as this antibody was previously used and optimised by a different member in the lab before I joined. Thus, the specificity of the antibody should have been tested against a known positive control tissue or cell type (e.g. a human skin fibroblast cell line) that has abundant Cx43 and compared to Cx43 within the AM. Additionally, other fibroblast (e.g. CD34) and myofibroblast markers (e.g. collagen type I/III, β-actin, TGFβ1) could have been used, particularly differentiation markers to determine whether AMCs and/or AECs were differentiating at the wound edge throughout culture. To determine whether all three identified cell populations are differentiating and are locomotive, live-imaging could be used in the future, starting from the first moment of trauma and maintained for a few days in culture. This would require a powerful microscope capable of live imaging and ideally co-staining of multiple proteins to visualise if cell differentiation and migration is taking place. Despite fixation of the tissue with 4% PFA while it was still within the insert, the cells and collagen seen with IMF microscopy within the defects

could have been a result of poor tissue handling and do not provide conclusive evidence of wound healing. Live-imaging of the AM during culture would help elucidate this finding as well.

As the most ubiquitous connexin, Cx43 functionality goes beyond gap-junction channel activity. As discussed in Section 4.5, Cx43 can be a transcriptional activator or form associations with other cell membrane proteins to influence migration, morphology and hemichannel function [260-266]. Future work could focus on determining Cx43 binding partners, such as N-cadherin, ZO-1 and β-catenin via co-immunoprecipitation assays, IMF microscopy and/or western blotting.

The chorionic membrane was not investigated in this study. The CM is composed of essential ECM components and immune cell populations (e.g. Hoffbauer macrophages) that contribute to tissue structural integrity and influence inflammation [50,51,88]. The AM was chosen to remain consistent with previous studies by the group [17,104-106] and for its unique cellular composition as exemplified by many others [49,201,203,205]. However, the influence of the CM should not be ignored, and future studies could focus on the effect of trauma on the fetal membrane as a whole and how this influences the expressions of Cx43, TGFβ1 and changes in resident cell morphologies.

Heterogeneity of human tissue is an important limitation to consider, especially when classifying fetal membranes based on gestational age, labour induction and contractions, whether membranes have ruptured before delivery, or whether delivery occurred with intact membranes. Added to that, there are potential molecular and mechanical differences between FM taken from women who have started contractions and those who have not via C-sections due to the activation of the maternal systemic inflammatory response, leading to increased thrombin expression and decidual cell secretion of MMP-1 and MMP-3 that degrade FM ECM [12]. Myometrial and uterine contractions are further activated by thrombin which may lead to preterm labour with or without rupture of the FM [12]. In the present study, all term deliveries were selective C-sections, but there was no way to know whether some women had initiated labour before the surgery or if they experienced contractions as this is not always obvious. Additionally, the cutting and further manipulation of the FM during C-section and in the lab may influence the biochemistry of the tissue and its response to trauma.

Furthermore, tissue explants are limited by the lack of physiological conditions present *in vivo*. However, animal models used to study PPROM suffer from significant species variability, particularly those whose membranes have the capacity to spontaneously heal [15,66]. Sheep have been used extensively to study fetal membrane healing and for the development of biomaterials to seal PPROM defects [46]. Ideally, sheep would be used as an alternative to our study, however that is limited by resources provided. Better models to represent the *in utero* environment were suggested in **Chapter 1 Section 1.8**, including the use of bioreactors to apply strain to explants, a technique used in **Chapter 5**.

Distinct differences in PAM and CAM specimens were most evident when examining gene expression changes. In both samples, increased Cx43 expression at the wound edge had a direct relationship to TGFβ1 expression. However, significantly higher relative gene expression was seen in PAM specimens. Term FM samples collected for this study were non-laboured elective Caesarean sections, however cervical amniotic membrane is known to contain the ZAM [120-142]. During separation of PAM and CAM tissue, it is possible some of the ZAM was collected and investigated as part of CAM sampling. Despite the membranes being unlaboured, it is expected that the presence of the ZAM will affect CAM biochemical changes following trauma and thus this limitation could not be avoided. However, the collection of > 7 term AM with ample replicates and patient-matched AF were performed to minimise inter-patient variability.

This study utilised a well-described tissue culture model using sterile CellCrown™ inserts to study AM wound healing. All protocols for tissue collection and analysis have been extensively optimised by previous lab members and myself to ensure experimental accuracy [104-106]. A strength of this study was the use of patient matched AF in all experiments to best represent wound healing *in utero*. To guarantee AF was collected by the surgeon after patient consent, I had to attend early morning meetings with the consultant on call and midwives that would perform the C-sections. I then scrubbed into the theatre and observed the elective C-sections, to ensure AF was taken with a syringe to avoid blood contamination. This was challenging as consultants are incredibly busy and I had to be assertive and insistent when faced with frequent rejections due to tight scheduling. Ideally, more samples can be collected in the future to best

understand AM wound healing across multiple maternal ages, ethnicities, races, and indications for electing C-sectioning.

Myofibroblasts express a plethora of other matrix proteins, including MMPs, TIMPs and PGE_2 [47-57,66,76,77,244]. MMP-9 has been previously reported to be overexpressed in preterm FMs, correlating with programmed biochemical events leading to labour [129,188]. The signalling pathways leading to the upregulation of MMP-9 are not very well defined, but the pro-inflammatory cytokines IL-1β and TNFα acting as paracrine or autocrine modulators have been found to influence MMP-9 deregulation in premature membranes [310]. In a previous study, our group showed that inhibition of Cx43 and Akt signalling resulted in significantly decreased weakening mechanisms, including decreased PGE_2 release and MMP activity [105]. Future investigations could focus on MMP-9 activity and gene expression correlating TGFβ1 or other cytokine-induced MF activation and collagen remodelling in small AM wounds.

The present study relies heavily on the assumption that AF-resident immune populations (e.g. macrophages) are activating AMC differentiation (**Appendix; Figure 4.13**). Thus, the concentration of different immune cells within AF could be investigated, as well as their capability to express TGFβ1 proposed to influence differentiation of AMCs to MFs *in vitro*. The amniotic fluid contains a population on MSCs also capable of differentiation and regeneration, as well as production of ECM remodelling factors (MMPs, TMP-1, VEGF) and cytokines (IL-6, 1α, β and 10) which influence fetal membrane integrity and promote rupture [94,98,99]. Proteomic analysis of amniotic fluid during different culture periods would be of interest to elucidate what factors are being released to the AF after artificial trauma.

αSMA plays a role in not just migration and contraction of myofibroblasts through stress-fibres, but also interacts with signalling components and/or transcription factors. Researches have shown that αSMA facilitates nuclear translocation of transcription factors and compartmentalization and/or localization of signalling components [318]. In a rat myofibroblast cell line, p38 kinase activation induced by mechanical stress required the presence of αSMA, and the interaction between these components facilitated access to p38 substrates [318]. p38 substrates have also been found to mediate TGFβ signalling [318]. Moore and colleagues showed

p38MAPK activation controls FM senescence via β-galactosidase activity, concurrent with laminin B loss, enlargement of mitochondria and DNA fragmentation [186-188]. Exposure to CSE-oxidative stress increased the release of TGFβ by AECs, while antioxidant treatment reduced p38MAPK signalling, suggesting TGFβ-mediated signalling via TAB1 controlled p38MAPK activation [77]. p38MAPK is a complex signalling pathway which may be activated by a plethora of signals, but as an initial study p38MAPK inhibitors could be used in term AM samples to determine if there are any changes in TGFβ expression and αSMA. In addition, to investigate stress-fibre contraction and migration of resident AM populations, scratch wound assays of primary AM cells could be performed. Using markers for contraction/migration (e.g. laminin, vimentin, E-cadherin) and myofibroblast differentiation (e.g. αSMA), it could be determined whether Cx43 and/or TGFβ1 inhibition influences the rate of wound closure.

In summary, the current study shows evidence of potentially differentiated AM cell populations after trauma with Cx43 cellular localisation and increased TGFβ1 gene expression. Whilst AMCs expressed Cx43 plaques, we observed the presence of myofibroblasts in the defect site with Cx43 localised in the cytoplasm, nucleus and plasma membranes. Despite study limitations, this work is published in Scientific Reports [319]. Although Cx43 expression changes were observed, this is not the only factor affecting incomplete wound healing of fetal membranes. Preterm birth is not initiated via one isolated mechanism, and it important to keep that in mind when investigating future hypotheses. Successful repair of the membranes could promote tissue remodelling mechanisms that restore biomechanical function, reduce the risk of tissue contraction, chorionic membrane separation, amniotic fluid leakage, subsequent uterine infection, and preterm birth.

4.5 Appendix

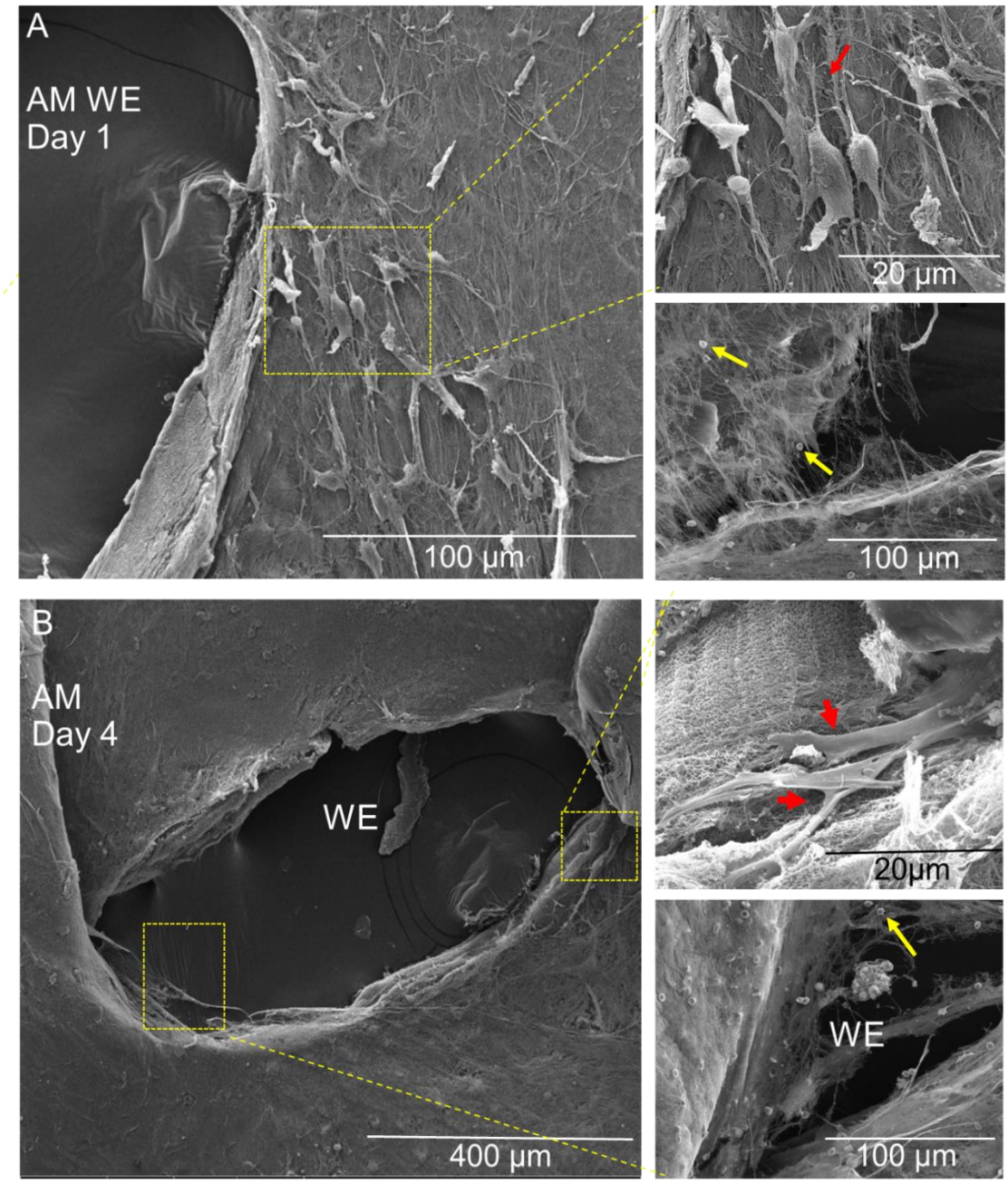

Figure 4.12: *Scanning electron microscopy showing evidence of cell contraction and macrophage migration at the wound edge of term AM. Following a 0.8 mm trauma, cells at the wound edge of the AM appear to contract and have elongated cell bodies with long cytoplasmic extension (red arrows). At day 1 (A) and 4 (B) of culture there is evidence of macrophage accumulation at the wound edge (yellow arrows). Images are representative of one PAM donor. AM = amniotic membrane, WE = wound edge. Scale bars = 20 µm, 100 µm, 400 µm.*

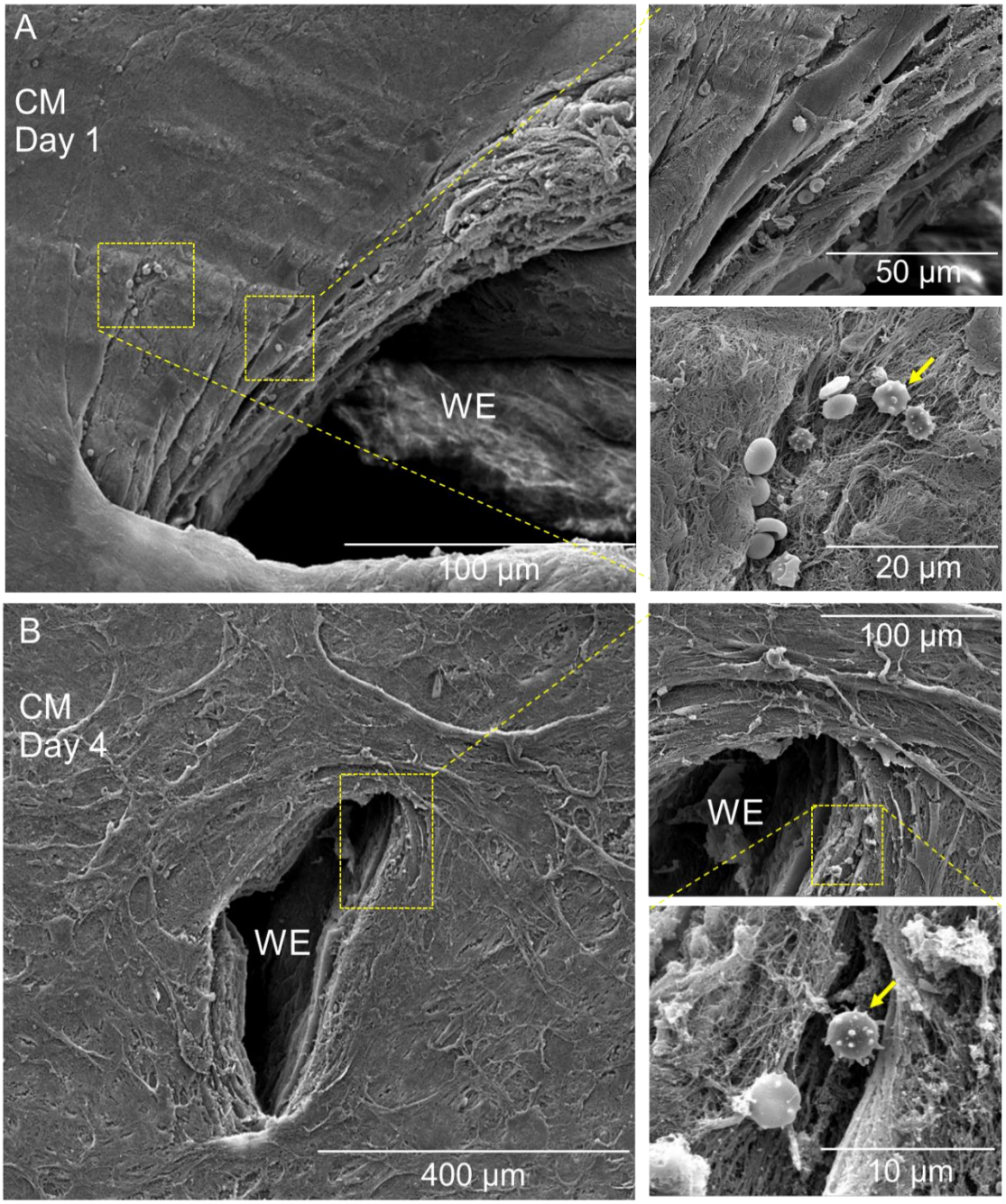

Figure 4.13: *Scanning electron microscopy showing evidence of cell contraction and macrophage migration at the wound edge of term CM. Following a 0.8 mm trauma, at day 1 (A) and 4 (B) of culture there is evidence of macrophage accumulation at the wound edge (yellow arrows). Images are representative of one PAM donor CM = chorionic membrane, WE = wound edge. Scale bars = 10 µm, 20 µm, 50 µm, 100 µm, 400 µm.*

Table 4.2: *Analysis of Cx43 protein plaques in human cell sub-populations present in the AM. Data was normalised per cell nuclei (pixels) and per area (500 μm^2). Mean and SEM values represent 9 replicates from three separate donors for controls and wounded tissue for PAM and CAM respectively. P values represent comparisons between control and wound edge, as described in Section 4.4.1. AECs = amniotic epithelial cells, AMCs = amniotic mesenchymal cells, MFs = myofibroblasts, WE = wound edge.*

Cx43 protein distribution per cell type (pixels per cell nuclei)							
		CAM			PAM		
		AECs	AMCs	MFs	AECs	AMCs	MFs
Day 1	Control	0.7 (±0.09)	4.6 (±1.67)	10.7 (±1.03)	0.7 (±0.02)	8.9 (±1.57)	17.5 (±0.42)
	WE	2.2 (±0.27, p<0.001)	17.8 (±1.45, p<0.001)	37.3 (±0.28, p<0.001)	2.7 (±0.07, p<0.001)	9.5 (±1.3)	36.8 (±0.65, p<0.001)
Day 4	Control	0.6 (±0.05)	13.1 (±1.52)	10.3 (±1.01)	0.7 (±0.03)	15.4 (±1.96)	16.9 (±0.32)
	WE	4.7 (±0.15, p<0.001)	20.8 (±1.46, p<0.001)	47.4 (±1.59, p<0.001)	5.0 (±0.08, p<0.001)	28.6 (±1.69, p<0.001)	49.9 (±0.24, p<0.001)
Cx43 protein distribution per area (pixels per 500 μm^2)							
		CAM			PAM		
		AECs	AMCs	MFs	AECs	AMCs	MFs
Day 1	Control	232.7 (±21.92)	148.5 (±17.00)	480.6 (±42.66)	374.2 (±8.67)	61.7 (±9.39)	698.8 (±19.38)
	WE	737.2 (±38.59, p<0.001)	2162.8 (±467.11, p<0.001)	1952.5 (±50.94, p<0.001)	1427.3 (±13.79, p<0.001)	1934.3 (±542.90, p<0.001)	2053.8 (±77.65, p<0.001)
Day 4	Control	205.6 (±14.55)	646.3 (±71.59)	441.0 (±47.82)	397.9 (±4.96)	195.4 (±29.88)	452.5 (±14.08)
	WE	1880.1 (±28.14, p<0.001)	4812.7 (±542.40, p<0.001)	10086.3 (±263.62, p<0.001)	2871.5 (±26.16, p<0.001)	1074.2 (±168.16, p<0.001)	10821.1 (±184.38, p<0.001)

Table 4.3: *Analysis of cell volume differences in AMCs and MFs at the wound edge. Data was normalised per tissue area (μm^3). Mean and SEM values represent 9 replicates from three separate donors for controls and wounded tissue for PAM and CAM respectively. P values represent comparisons between control and wound edge, as described in Section 4.4.1. AECs = amniotic epithelial cells, AMCs = amniotic mesenchymal cells, MFs = myofibroblasts, WE = wound edge.*

Cell volume differences in AMCs and MFs. Volume per cell tissue area (μm^3). AMCs = vimentin positive; MFs = αSMA positive					
		CAM		PAM	
		AMCs	MFs	AMCs	MFs
Day 1	Control	14.2 (±2.1)	6.5 (±0.2)	11.7 (±2.3)	3.45 (±0.2)
	WE	20.2 (±2.4)	46.1 (±3.4, p<0.001)	18.7 (±0.8, p<0.001)	32.2 (±1.3, p<0.001)
Day 4	Control	19.8 (±2.6)	18.7 (±2.7)	20.1 (±2.5)	5.0 (±0.1)
	WE	35.3 (±6.7, p<0.001)	95.6 (±3.2, p<0.001)	43.6 (±1.3, p<0.001)	66.4 (±3.4, p<0.001)

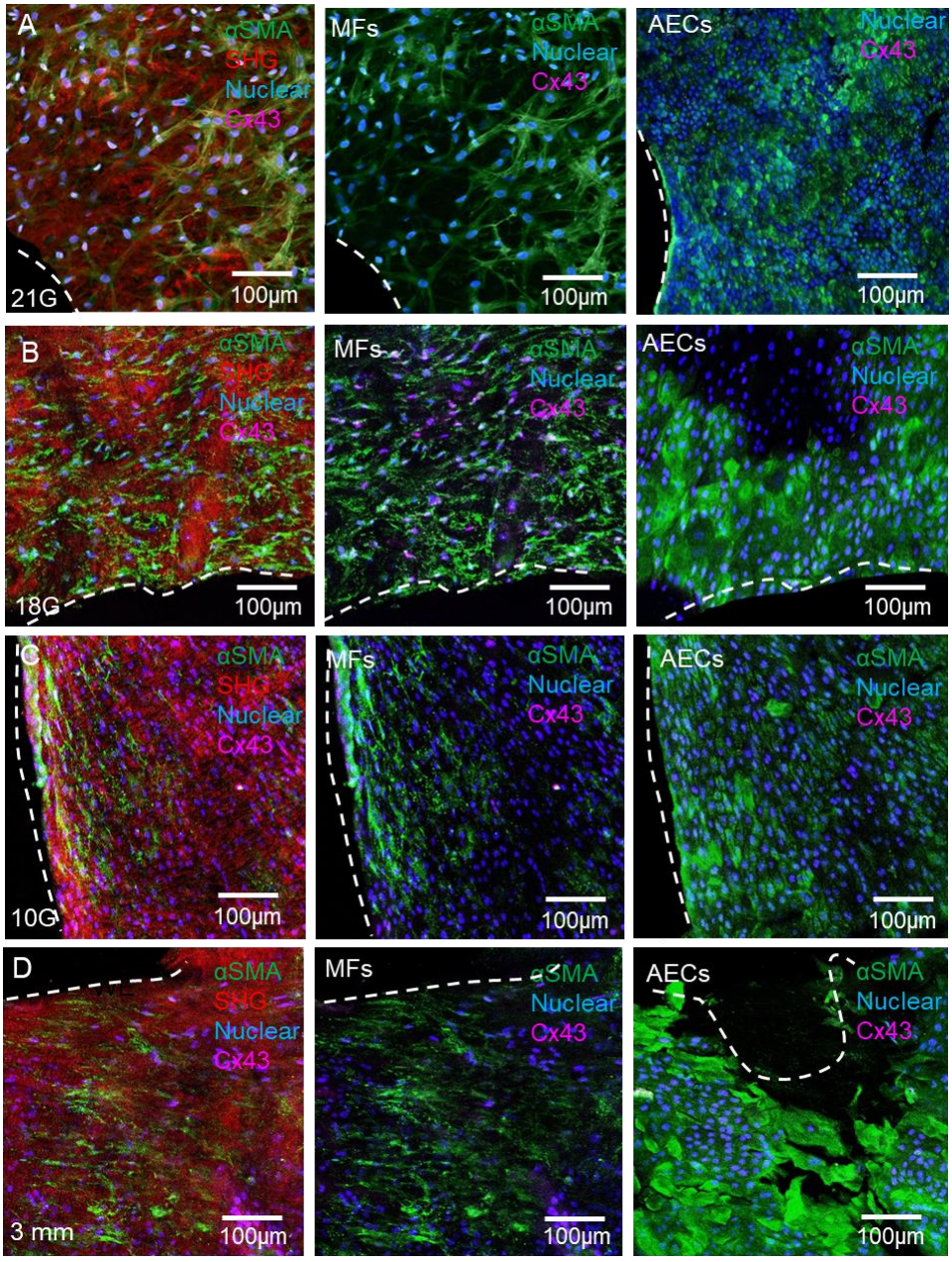

Figure 4.14: *Qualitative examination of wound edges after IMF confocal microscopy following different trauma sizes. (A) AM subjected to 0.8 mm (A), 1.3 mm (B), 2.4 mm (C) and 3 mm (D) trauma showed elongated cytoplasmic extension in αSMA-expressing myofibroblasts, with collagen fibrils evident at the edges of the wound. AECs formed cuboidal morphologies at the wound edge. AM traumatised with a 3 mm punch showed a loss of myofibroblast morphologies. AECs had more defined stretched elongated morphologies and expressed more αSMA than seen in smaller defects and controls. Cx43 was abundant within MF nuclei and lamellipodia in all defect sizes. White dotted lines indicate the edges of the wound. AECs = amniotic mesenchymal cells, AM = amniotic membrane, MFs = myofibroblasts, αSMA = alpha smooth muscle actin. Scale bars = 100 μm.*

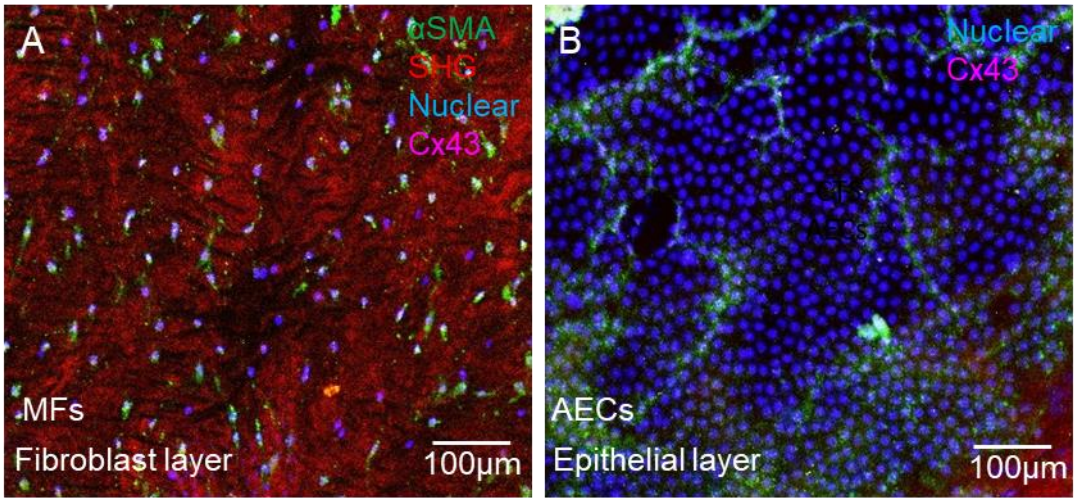

Figure 4.15: *Immunofluorescent imaging of control, non-traumatised PAM cultured for 1 day in AF. (A) Within the fibroblast layer, minimal αSMA-expressing myofibroblasts, rounded nuclei and collagen fibrils interwoven in a random fashion within the fibroblast layer. (B) AECs within the epithelial layer formed cuboidal structures with minimal αSMA expression. Cx43 plaques are negligible in both the fibroblast and epithelial layers. AECs = amniotic mesenchymal cells, AM = amniotic membrane, MFs = myofibroblasts, αSMA = alpha smooth muscle actin. Scale bars = 100 μm.*

Chapter 5

Mechanotransduction mechanisms in preterm amniotic membrane

Chapter 5: Mechanotransduction mechanisms in preterm amniotic membrane

5.1 Introduction

In the search for optimal PPROM management strategies, the biomechanics of the fetal membrane and how biochemical changes lead to its tensile failure must be better understood. Mechanotransduction refers to the ability of cells to biochemically respond to physical forces. These reactions propagate signalling pathways that affect cell structure through changes in cellular cytoskeleton, transcriptional events, integrin receptor expression and ECM alterations that lead to cell adhesion. Stretch-induced expression of growth factors influence cell shape and cause proliferation or apoptosis depending on the severity of stress. Fetal membrane weakening and rupture depend on signalling triggered by mechanotransduction, with some studies showing differential expression of integrins, cytokines and interleukins in different FM cell populations [218,219]. Weakening mechanisms underlying the ZAM have been thoroughly discussed in **Chapter 1.** In summary activation of pro-inflammatory factors, pro-apoptotic signals (TNFα), MMP expression (MMP-9, 2), cytokines, Interleukin-1 β (IL-1β), collagenases, and COX1/2-activated prostaglandins all work in harmony to trigger FM for rupture [218-221].

5.1.1 Classification of preterm fetal membranes depending on clinical aetiology

Importantly, gestational age, inflammation and labour decrease the viscoelastic properties, strength and ultimately weakening mechanisms of the FM [193,194]. Predisposition to preterm birth is increased due to uterine overdistention, with several studies characterising different aetiologies including FGR, twins, cervical weakness, and uterine structural abnormalities (e.g. unicornuate) [320]. A decade's long study in Sweden compared uterine overdistention to pregnancy duration and preterm birth in singletons versus twin pregnancies [320]. The effect of maternal height and uterine distention was further correlated with 1.4% odds ratio in small for gestational age (SGA) singletons [320]. Interestingly, when both risk factors were present within a twin pregnancy, the odds of preterm birth significantly increased, an important outcome to consider in this chapter [320]. By the same team, another paper identified an increase in risk of C-

sections in twin pregnancies versus singletons after labour initiation with oxytocin, further highlighting the sensitive nature of multiple pregnancies [321].

In another study, the author's determined that short cervixes were lengthened in patients with multiple pregnancies and polyhydramnios after amniotic fluid drainage and improved preterm birth rates [322]. In a non-human primate, uterine overdistention was associated with preterm labour mediated by pro-inflammatory factors (e.g. IL-1β, 6, 8, TNFα, CCL2 and PGE_2 and $F_{2\alpha}$) [322]. Monochorionic twin pregnancies further suffer from twin-to-twin transfusion (TTTS) syndrome in up to 20% of all cases, while FGR occurs in 10 to 15%, associated with a plethora of other risk factors such as cardiac complications, hydrops, and circulatory overload [323]. In cases where one twin dies, the other fetus is at high risk of perinatal death due to vascular anastomoses and requires frequent monitoring [323].

In investigating the mechanotransduction processes in donors with PPROM, we first must consider that PPROM occurrence throughout different gestational ages will influence pregnancy outcome and the mechanobiology of the FM after stress. Mid-trimester PPROM (14 to 26 weeks gestation) is known to be followed by chorioamnionitis, sepsis, pulmonary hypoplasia and increase neonatal morbidity, while authors reported average latency periods between rupture and delivery at 13 to 14 days [5,323]. Importantly, neonatal survival was found to be associated with gestational age at delivery rather than when rupture occurred [5]. In contrast, patients with PPROM in the third trimester (27 to 31 weeks gestation) have more favourable infant survival rates, with latency periods over 14 days having increased neonate morbidity [324]. Neonatal and maternal outcomes after third trimester PPROM were further characterised in a recent study [325]. The authors split the patients into subgroups of early PPROM (28 to 31^{+6} weeks GA) and late PPROM (32 to 36^{+6} weeks GA) and correlated significantly longer latency periods with lower gestational age [325]. This is a significant point to consider, as latency period increases the possibility of infection and thus influences FM mechanics and cellular composition.

Taking these risk factors of preterm birth into consideration, during donor collection, patients were classified by (a) clinical outcome (FGR, PPROM, open fetal surgery-induced iatrogenic PPROM) then (b) early third trimester (≤32 weeks GA) versus late third trimester PPROM (≥32

weeks GA) (**Table 5.1**). The decision to separate each group into sub-groups arose from the heterogeneity of aetiologies and their potential effects on mechanotransduction mechanisms after applied CTS.

5.2 Methods

To quantify migration and cell morphology changes, immunofluorescent imaging of preterm AMs was performed after CTS and/or trauma using αSMA and Cx43 antibodies. SHG was used to visualise collagen microstructure and measure the collagen fibre orientation in non-wounded controls and at the wound edge after CTS. Mechanotransduction changes in response to CTS were assessed by biochemical assays for collagen (hydroxyproline), elastin, sulphated glycosaminoglycan (sGAGs) content and PGE_2 release as described in **Chapter 3**. Real-Time qPCR was used to examine relative gene expression changes after CTS for both Cx43 and inflammatory marker TGFβ1. Application of Cx43 antisense oligonucleotides was used to pharmacologically knockdown Cx43 to investigate changes in pro-inflammatory and weakening mechanisms after CTS. Cx43 antisense gene expression results were compared to untreated samples, however we also determined gene expression levels in samples treated with Cx43 sense oligonucleotide as reference to ensure Cx43 was knocked down.

5.2.1 Patient recruitment

Pre-term human fetal placentas were collected (*n*=17, mean GA = 32 weeks; mean maternal age = 35 years) with informed consent from women undergoing delivery by caesarean section at UCLH as described in **Chapter 3**. Women were grouped according to whether they had emergency delivery following spontaneous PPROM associated with preterm labour, ("PPROM group"), they underwent a planned delivery due to fetal growth restriction and/or pre-eclampsia ("FGR" group) associated with placental insufficiency or a fetal anomaly, or had an emergency delivery following PPROM associated with spina bifida open fetal surgery ("open fetal surgery" group). Women delivering vaginally were excluded from this study. A comprehensive list of all donors collected with their clinical details is included in **Table 5.1**.

Table 5.1: *Clinical information for patients collected for preterm studies. All deliveries were performed via emergency C-sections.*

Patient ID	Maternal Age	GA (weeks)	Complications during pregnancy	Complications to Delivery	Membrane rupture site/hole	Final classification
Patient 1	34	35^{+5}	FGR	None	Not applicable	FGR
Patient 2	39	35^{+6}	FGR	None	Not applicable	FGR
Patient 3	38	34^{+0}	FGR	None	Not applicable	FGR
Patient 4	30	29^{+0}	Placental insufficiency and FGR	Emergency C section	None identified	FGR and PPROM ≤32 weeks
Patient 5	40	33^{+0}	FGR	Dizygotic twins both with FGR	Not applicable	FGR
Patient 6	32	34^{+6}	FGR	MCMA twins, both with FGR	Not applicable	FGR
Patient 7	42	33^{+0}	FGR One twin died at 30 weeks GA due to severe FGR	Dizygotic twins: both with FGR	Not applicable	FGR
Patient 8	32	27^{+0}	Recurrent vaginal bleeding	PPROM. Emergency C section	None identified	PPROM ≤32 weeks
Patient 9	27	29^{+1}	PPROM occurred 24-36 hours before delivery	Emergency C section due to abnormal fetal heart rate	FM rupture hole= 1.5 x 2 cm near placenta.	PPROM ≤32 weeks
Patient 10	32	35^{+6}	PPROM at 32 weeks Placental insufficiency	Delivery 4 weeks after PPROM	FM rupture hole= 3 x 2.5 cm starting from the placenta	PPROM ≥32 weeks
Patient 11	39	35^{+5}	PPROM at 35 weeks Placental insufficiency	Delivery 5 days after PPROM	None identified	PPROM ≥32 weeks
Patient 12	30	33^{+6}	Bleeding due to placenta previa	PPROM 24 hours before delivery	None identified	PPROM ≥32 weeks
Patient 13	31	34^{+6}	No infection present after surgery	Delivery 10 weeks after fetal surgery.	FM hole=3.5 x 4 cm	Open Fetal Surgery
Patient 14	25	35^{+0}	No infection present after surgery	Delivery 10 weeks after fetal surgery.	FM hole=7.5 x 6 cm	Open Fetal Surgery
Patient 15	26	34^{+0}	No infection present after surgery	Delivery 10 weeks after fetal surgery	FM hole=7 x 5 cm	Open Fetal Surgery

Patient 16	30	35^{+0}	No infection present after surgery	Delivery 11 weeks after fetal surgery.	FM hole = 5.5 x 6 cm	Open Fetal Surgery
Patient 17	31	33^{+0}	Fetal teratoma leading to FGR; normal fetal karyotype	Planned preterm delivery due to teratoma size	Not applicable	FGR

5.2.3 Statistical analysis

For immunofluorescent and qPCR experiments for PAM and CAM respectively, data represents the mean and SE values of 6 replicates from three separate donors, as indicated in figure legends. To compare Cx43 plaque intensity and nuclei directionality between **free-swelling controls (No CTS)** and samples after **CTS (+ CTS)**, a student's T-test was performed. To compare the statistical differences in biochemical assays (sGAG, collagen, elastin, PGE_2) between No CTS and + CTS samples a two-way ANOVA was performed. All statistics were combined with a multiple *post hoc* Bonferroni test to yield corrected p-values. Values with over 95% confidence rate were considered significant. Significance was denoted as follows: *$p < 0.05$, **$p < 0.01$ and ***$p < 0.001$.

Previous published work in our lab utilised 16 replicates from *n*=4 separate term donors for all biochemical assays (GAG, collage, elastin and PGE_2 assays) [105]. For qPCR analysis, 9 replicates from 3 separate donors were used in the same study [105]. Using this information, a power calculation was performed to determine the number of samples - or in this case donors - required for 95% confidence. To perform the power calculation, the G*Power software for Windows was used. The average and SEM for CAM and PAM specimens was used from previous research [105] and the following parameters were employed: Group 1 and 2 average and SEM, in this case Group 1 = Unstrained samples, and Group 1 = Samples after CTS. Enrolment ratio was set as 1, thus the same number of donors was used for both groups. The alpha number was set to 0.05 and this represents the probability of a type-I error. Most medical literature uses an alpha cut-off of 5% (0.05). The beta number and thus the probability of type II error, or 'power', was set at 80%, as medical literature also suggests power to be between 80 and 90%. Beta is

directly related to study power (Power = 1 - β) and other medical literature uses a beta cut-off of 20%, indicating a 20% chance that a significant difference is missed.

For biochemical assays, the sample number required for sGAG, collagen, elastin and PGE_2 assays is minimum *n*=3 donors. For qPCR, the minimum sample size is also *n*=3 donors. As this calculation was performed after the completion of the experimental phase of this PhD, some data will not be presented as it did not meet the minimum number of donors required. This includes any data on dizygotic twin AM and data where a defect was introduced. For IMF analysis, donor samples needed for collagen and Cx43 quantification were met for samples with and without a trauma (*n*=3 donors) and thus those will be presented throughout this chapter.

***Table 5.2**: Terminology of preterm AM samples and corresponding tissue manipulation.*

Terminology	**Tissue manipulation**
Non-wounded / non-traumatized controls	AM samples without any trauma
Wounded / traumatised	AM samples with 0.8 mm defect
Free-swelling controls (No CTS)	AM samples cultured in 12-well plates for 4 or 24 hours
Cyclic tensile strain (+ CTS)	AM samples cultured within the BOSE bioreactor and exposed to CTS for 4 or 24 hours
Cx43sODNs / sense oligonucleotide	AM samples cultured with Cx43 sense oligonucleotide
Cx43asODNs / antisense oligonucleotide	AM samples cultured with Cx43 antisense oligonucleotide

5.3 Results

5.3.1 Examination of collagen fibril alignment in preterm AM after CTS and/or trauma

Collagen fibril alignment was examined using SHG imaging for PAM and CAM specimens following 24 hours of CTS and/or trauma **(Figure 5.1).** SHG imaging of collagen showed dense collagen fibre alignment in the direction of applied strain in both PAM and CAM specimens wound edges **(Figures 5.1A & C).** At the wound edge in free-swelling controls, collagen fibrils were polarised tangential to the defect site compared to disorganised and shorter collagen fibres in control AM samples taken away from the WE **(Figures 5.1A & C).** After CTS, collagen fibrils were further aligned at the wound edge in the direction of applied strain. Graphs are representative images indicating the amount of collagen aligned at a specific polarisation angle for PAM and CAM samples respectively after CTS and/or trauma **(Figures 5.1B & D)**. Collagen fibre alignment appears to be higher after CTS over 24 hours (+ CTS) and/or trauma, indicated by a peak at approximately 100° angle. Control alignment graphs showed collagen fibres remaining unchanged for both PAM and CAM after CTS and/or trauma **(Figures 5.1B & D).**

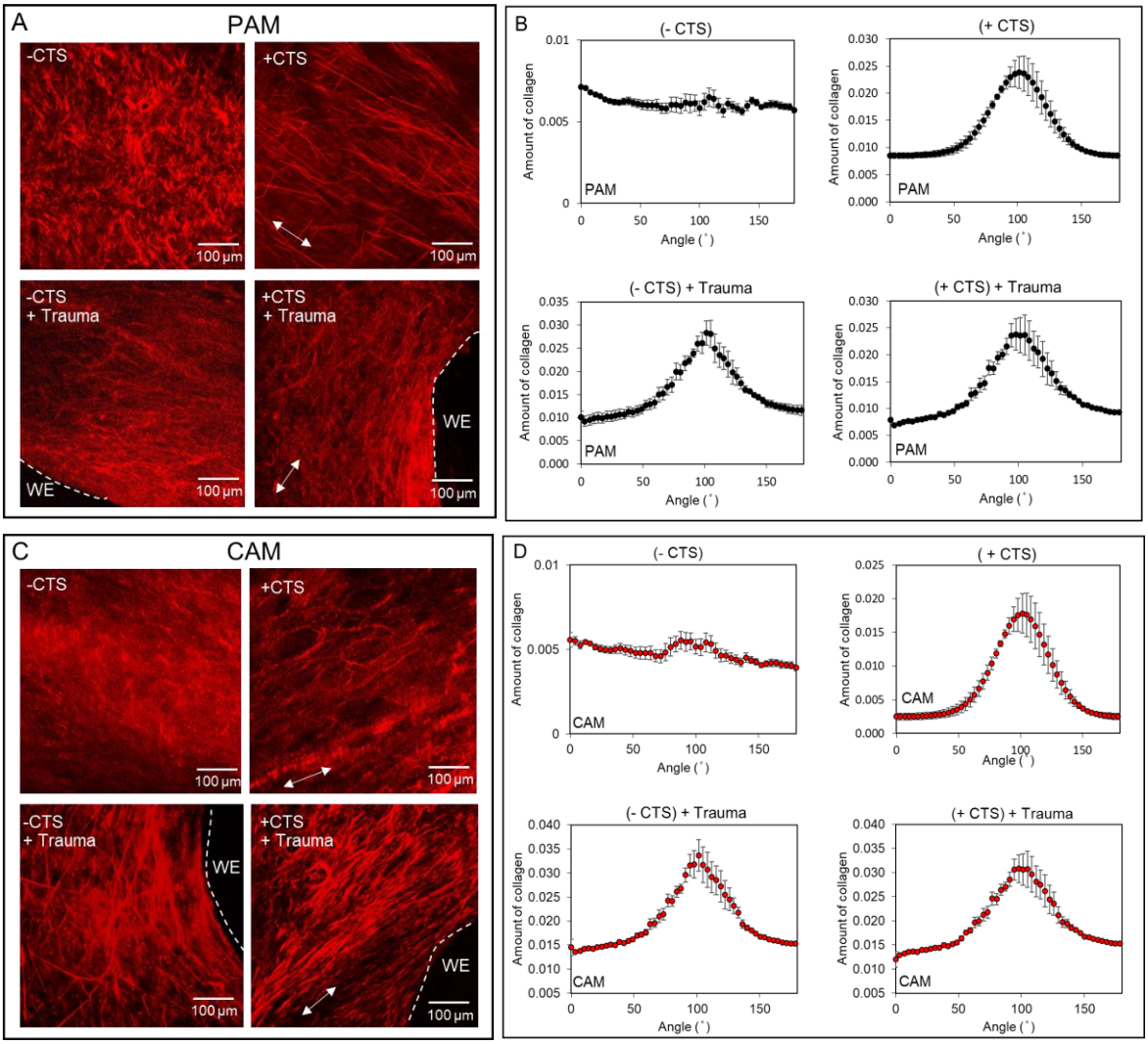

Figure 5.1: *Examination of SHG collagen fibril alignment in the AM after CTS and/or trauma. SHG imaging of collagen (red) showed dense collagen fibre alignment in the direction of strain (white arrows) in both (A) PAM and (C) CAM specimens. In free-swelling controls (-CTS), collagen fibrils aligned tangential to the wound edge (WE) compared to disorganised and shorter collagen fibres in control AM samples taken away from the WE. Collagen fibrils were further aligned at the wound edge after CTS in the direction of strain. (B) and (D) show collagen fibre alignment graphs as representative images indicating the amount of collagen aligned between 0° and 180° for PAM and CAM samples respectively after CTS and/or Trauma. Mean and SEM values represent 6 replicates from three separate FGR donors (33-35^{+5} weeks GA) for controls and wounded tissue for PAM and CAM respectively. White dotted lines show the location of the defect. PAM = placental amniotic membrane, CAM = cervical amniotic membrane, CTS = cyclic tensile strain, FGR = fetal growth restriction, WE = wound edge. Scale bar = 100 µm.*

5.3.2 Examination of nuclei deformation after CTS and/or trauma

Using representative PAM samples from three different preterm FGR donors, AMCs, MFs and AECs nuclei deformation was examined **(Figure 5.2)**. AMCs and MFs were grouped together as both subpopulations are present within the fibroblast layer of the AM, and AECs were counted separately as they are present within the epithelial layer. After application of CTS and trauma for 24 hours, AMCs and MFs in PAM specimens had elongated morphologies and were aligned in the direction of applied strain. **(Figures 5.2A-F)**. To calculate nuclei elongation, box and whisker plots were generated representing nuclei circularity after CTS and/or trauma in all cell types in the AM **(Figure 5.2G)**. AMCs and MFs were grouped together within the fibroblast layer, while AECs were quantified separately. Nuclei values following CTS had circularities of 0.388 ± 0.013 for AECs and 0.548 ± 0.012 for AMCs/MFs, indicating an increasingly elongated shape in comparison to control values (0.761 ± 0.015 and 0.881 ± 0.002 circularity for AMCs/MFs and AECs respectively), presumably due to changes in cell morphology and contraction **(Figure 5.2G)**. In traumatised samples in free swelling controls (No CTS), nuclei circularity values were 0.649 ± 0.023 and 0.531 ± 0.003 in AMCs/MFs and AECs respectively, while application of CTS significantly decreased circularity values at the WE (0.444 ± 0.023 and 0.474 ± 0.010 circularity in AMCs/MFs and AECs respectively compared to controls. Significant differences between No CTS and + CTS were found as indicated by ***$p < 0.001$.

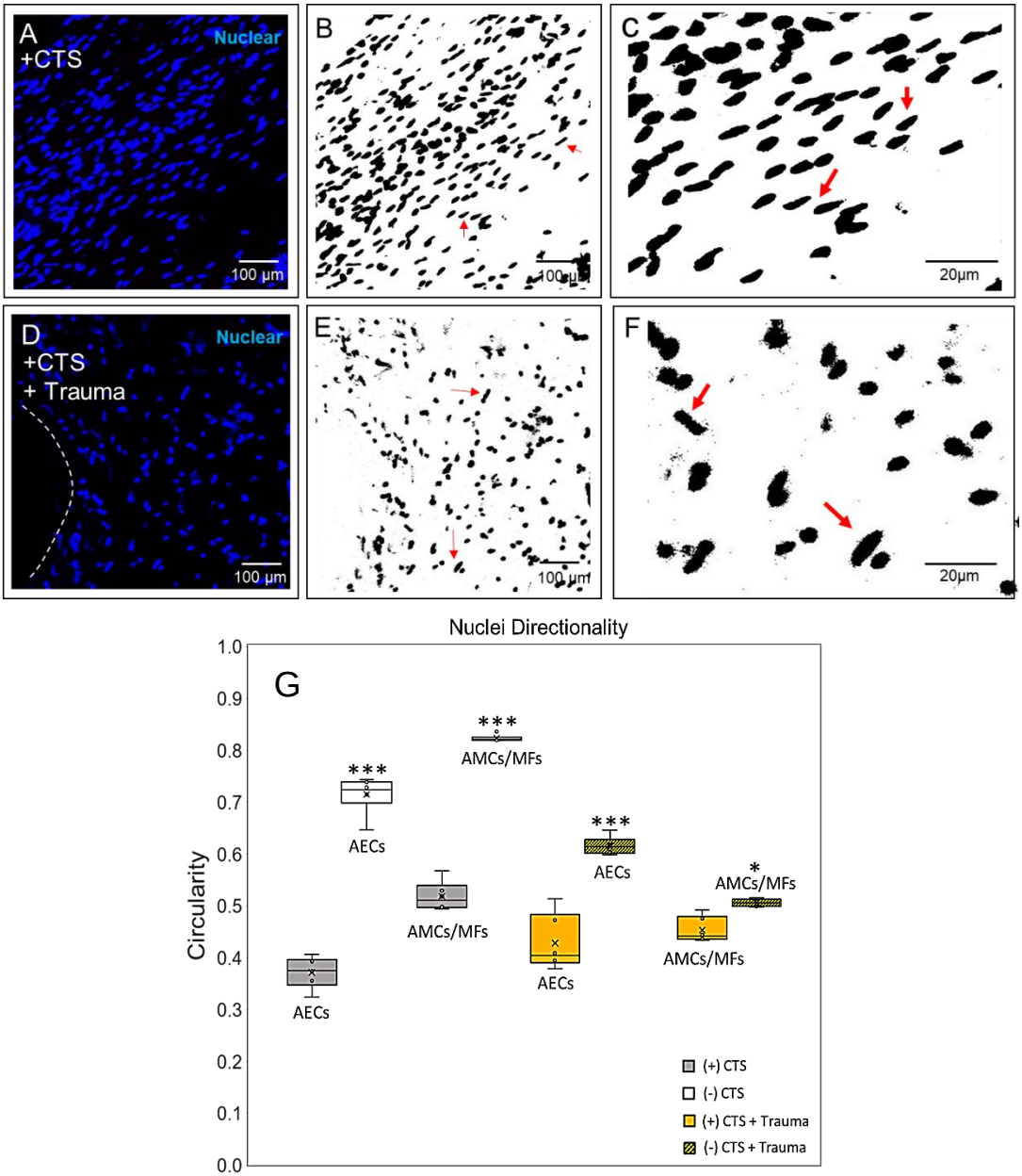

Figure 5.2: *Effect of CTS and/or trauma on AM nuclei morphology. (A) After application of CTS for 24 hours, AMCs and MFs nuclei elongated and aligned in the direction of strain (red arrows). (B) & (C) show binary conversion images with clear elongated nuclei (red arrows) in the direction of strain. (D) After CTS and trauma, the presence of deformed nuclei aligned tangentially to the WE were observed. (E) & (F) Binary conversion of RGB image shows nuclei deformation (red arrows). (G) Box and whisker representation of nuclei circularity after CTS and/or trauma in AMCs/MFs and AECs populations. Mean and SEM values represent 6 replicates from three separate FGR donors (33-35^{+5} weeks GA) for controls and wounded tissue. Significant differences between (-) CTS and (+) CTS were found as indicated by ***p < 0.001. AMCs = amniotic mesenchymal cells, MFs = myofibroblasts, AECs = amniotic epithelial cells, CTS = cyclic tensile strain, WE = wound edge. Scale bars = 100 µm and 20 µm.*

5.3.3 Inhibition of Cx43 in preterm AM after CTS and/or trauma

To quantify the inhibition of Cx43 in free-swelling controls and samples after CTS, IMF confocal microscopy was used to image treated specimens with Cx43sODNs sense oligonucleotide and Cx43asODNs antisense oligonucleotide. In both AM fibroblast and epithelial layers, Cx43 expression was clearly seen as pink plaques, while Cx43 knockdown with antisense oligonucleotide successfully decreased Cx43 protein expression after 24 hours **(Figure 5.3A)**. Quantitative expression of Cx43 distribution per area in pixels per 500 μm^2 showed Cx43 decreased in both MFs and AECs in CAM and PAM specimens in free-swelling controls (No CTS) and after CTS (+ CTS) **(Figure 5.3B).** Cx43 was significantly reduced in both non-traumatised and traumatised samples with 0.8 mm wounds (***$p < 0.001$). The highest Cx43 protein expression changes were seen in CAM myofibroblasts after CTS and trauma (2530.4 ± 601.3 pixels per area versus 470.1 ± 44.3 pixels per area in free-swelling controls). Cx43 protein expression significantly increased after CTS in all cases, except for myofibroblasts in PAM samples after treatment with Cx43 sense oligonucleotide ($^{+++}p < 0.001$; **Figure 5.3B**).

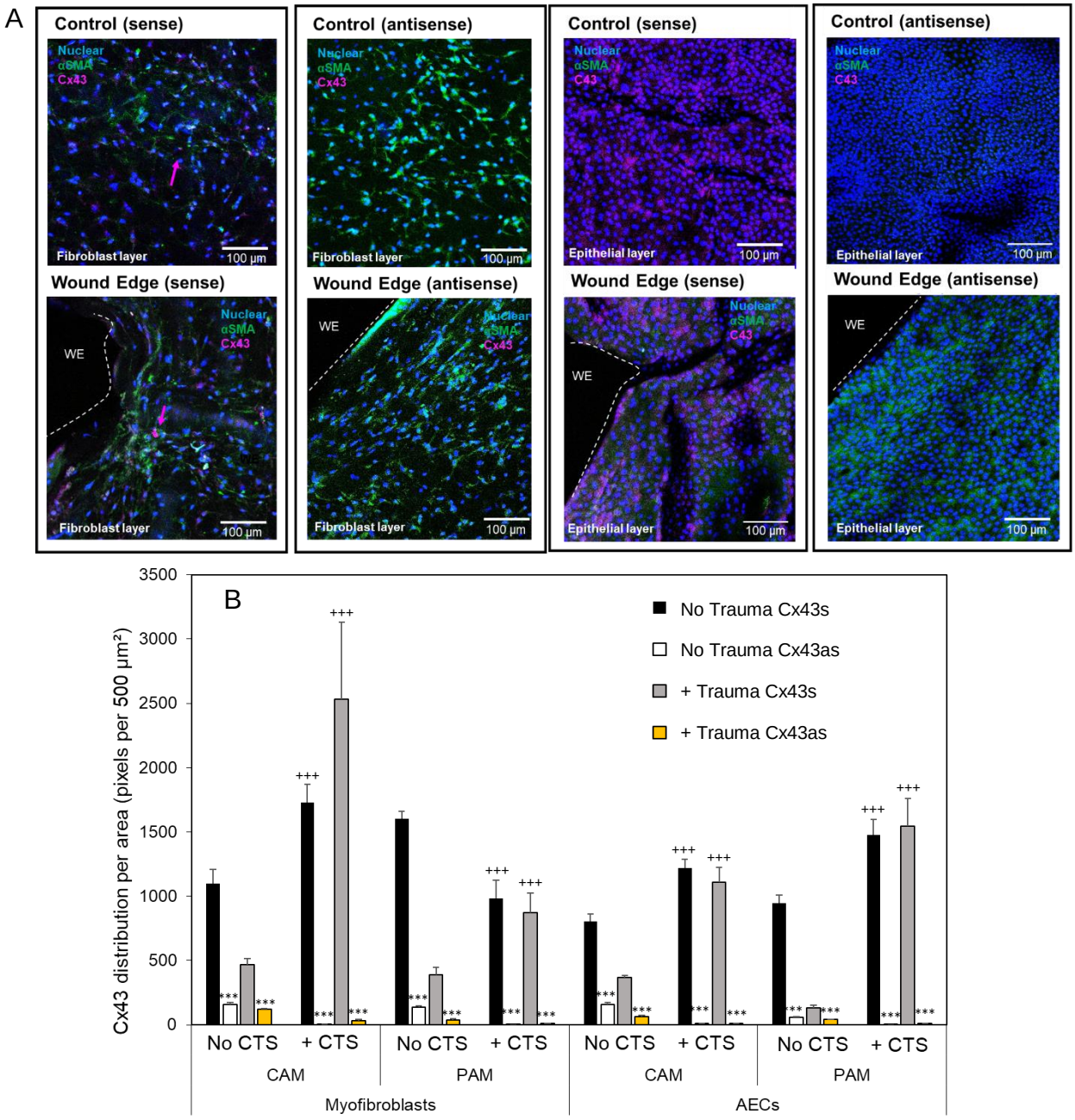

Figure 5.3: *Quantification of Cx43 knockdown using Cx43asODNs antisense. (A) IMF imaging of AM samples treated with Cx43sODNs sense oligonucleotide and Cx43asODNs antisense oligonucleotide in 2 mL media. In both AM fibroblast and epithelial layers, Cx43 knockdown with antisense successfully decreased Cx43 protein expression after 24 hours. (B) Quantitative expression of Cx43 distribution per area in pixels per 500 µm^2 showed decrease Cx43 expression in both MFs and AECs in CAM and PAM specimens in free-swelling controls (No CTS) and after CTS (+CTS). Data represents the mean and ± SEM of n=6 replicates from three separate preterm donors (33-35^{+5} weeks GA). Significant differences between Cx43s and Cx43as were found as indicated by ***p < 0.001, while $^{+++}$p < 0.001 indicates comparisons between No CTS and (+) CTS. White dotted lines represent the margins of the defect. AECs = amniotic epithelial cells, PAM = placental amniotic membrane, CAM = cervical amniotic membrane, CTS = cyclic tensile strain, Cx43as = Cx43 antisense, Cx43s = Cx43 sense. Scale bars = 100 µm.*

5.3.4 The effect of CTS and Cx43 inhibition on mechanotransduction processes in AM delivered electively preterm due to fetal growth restriction

AM taken from donors electively delivered preterm due to fetal growth restriction were exposed to cycles of 1 minute strain and 9 minutes rest for up to 24 hours at a frequency of 1 Hz. Free-swelling controls were not subjected to CTS and are labelled No CTS in all figures. In FGR-derived AM, sGAG content significantly increased while collagen concentration decreased after the application of CTS in both PAM and CAM **(Figure 5.4A & B)**. Significant changes were present between CAM and PAM specimens, with the latter generally presenting with higher sGAG content and lower collagen expression after CTS **(Figure 5.4A & B).** Following inhibition of Cx43, samples in both regions without and without CTS significantly decreased sGAG content (**Figure 5.4A;** % change range -58.95 to -231.50%, ***$p < 0.001$). After Cx43 inhibition, collagen concentration significantly decreased in CAM after CTS and in both free-swelling controls and samples following CTS in PAM (**Figure 5.4B;** % change range +35.10 to +90.00%, ***$p < 0.001$).

Following CTS, elastin content was significantly elevated in FGR AM in both CAM and PAM specimens (% change range of +70.09 to +299.10%, $^{+++}p < 0.001$; **Figure 5.5A)**. Following Cx43 inhibition, elastin concentration significantly increased in both AM regions. Following CTS, PGE_2 release did not significantly change in CAM nor PAM regions **(Figure 5.5B)**. In both CAM and PAM, PGE_2 release was significantly reduced after Cx43 inhibition, except for free swelling controls in CAM specimens (*$p < 0.05$ and ***$p < 0.001$; **Figure 5.5B)**.

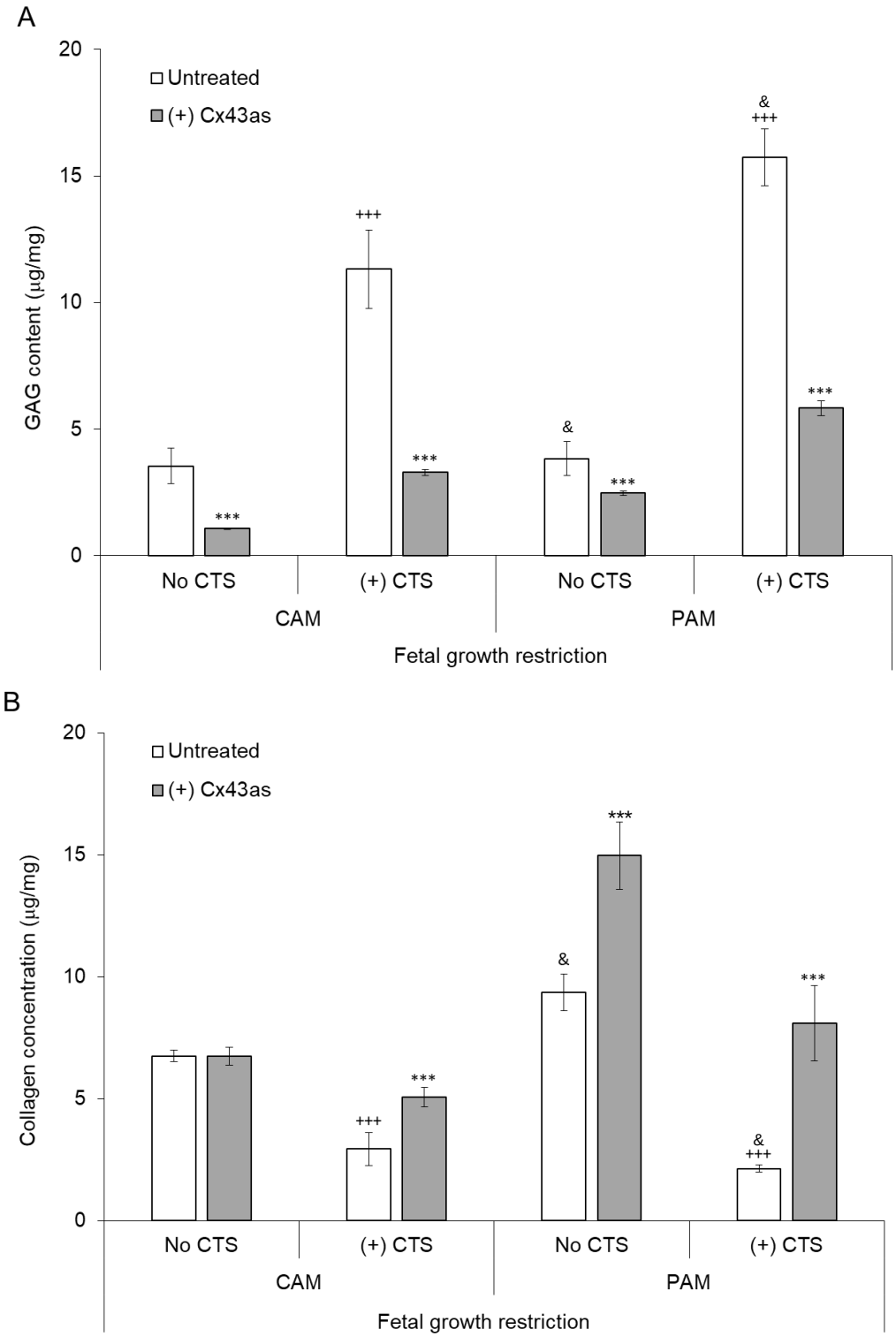

Figure 5.4: *The effect of CTS and Cx43as on preterm FGR CAM and PAM (A) sGAG and (B) collagen concentration. AM were exposed to cycles of 1 minute strain and 9 minutes rest for up to 24 hours at a frequency of 1 Hz. Free-swelling controls were not subjected to CTS (No CTS). Error bars represent mean ± SEM from n=12 replicates for sGAG and n=8 replicates for collagen from n=4 separate donors, where $^{+++}p < 0.001$ indicates comparisons between No CTS and (+) CTS, ***$p < 0.001$ indicates comparisons between untreated samples and those treated with Cx43 antisense and $^{\&\&\&}p < 0.001$ comparisons between CAM and PAM. CAM = cervical amniotic membrane, PAM = placental amniotic membrane, CTS = cyclic tensile strain, Cx43as = Cx43 antisense. FGR = fetal growth restriction.*

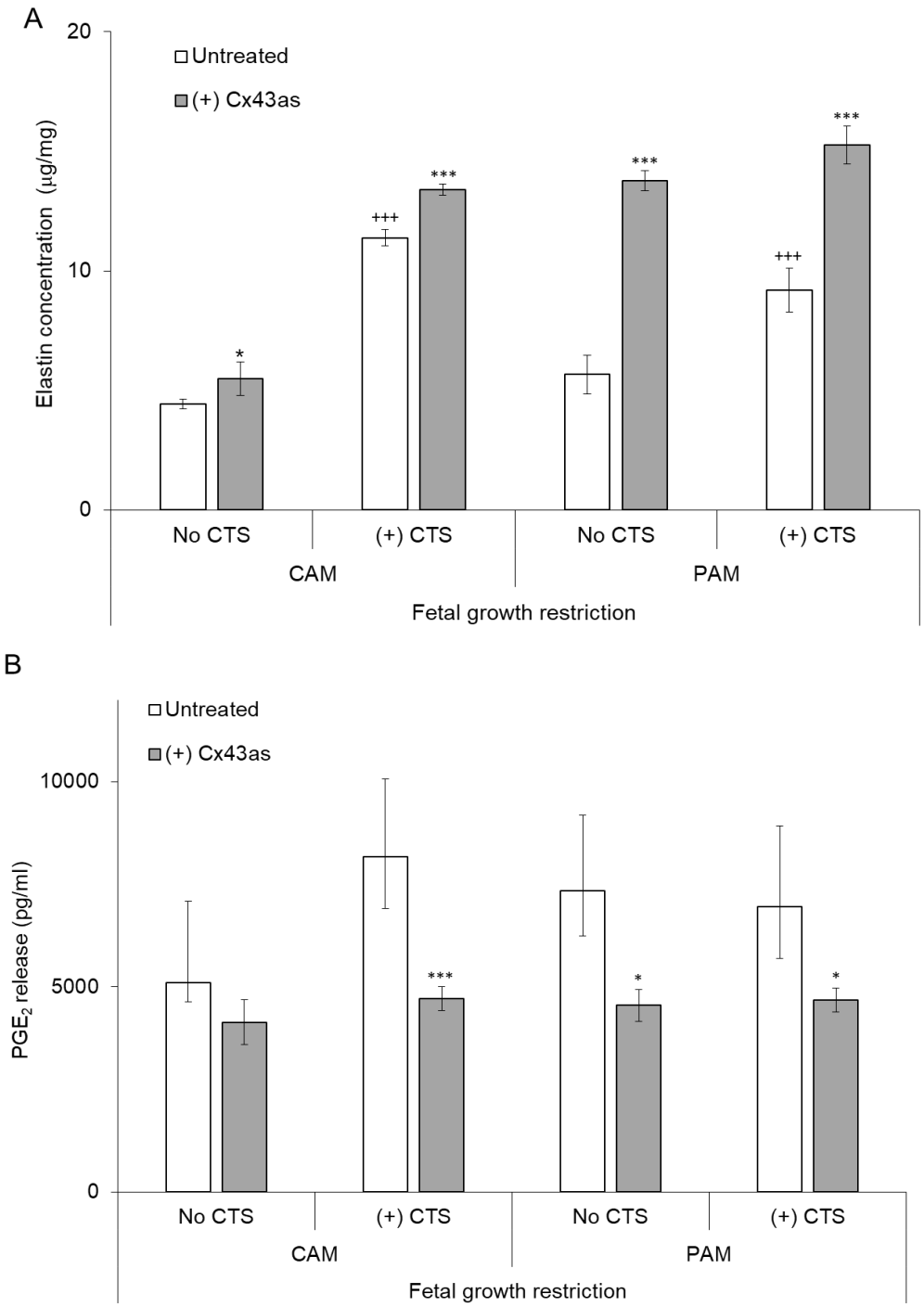

Figure 5.5: *The effect of CTS and Cx43as on preterm CAM and PAM (A) elastin content and (B) PGE_2 release taken from donors electively delivered preterm due to fetal growth restriction. AM were exposed to cycles of 1 minute strain and 9 minutes rest for up to 24 hours at a frequency of 1 Hz. Free-swelling controls were not subjected to CTS (No CTS). Error bars represent mean ± SEM from n=8 replicates for elastin and n=6 for PGE_2 taken from n=4 separate donors, where +++p < 0.001 indicates comparisons between No CTS and (+) CTS, ***p < 0.001 indicates comparisons between untreated samples and those treated with Cx43 antisense and $^{\&\&\&}p < 0.001$ comparisons between CAM and PAM. CAM = cervical amniotic membrane, PAM = placental amniotic membrane, CTS = cyclic tensile strain, Cx43as = Cx43 antisense. FGR = fetal growth restriction.*

5.3.5 The effect of CTS and Cx43 inhibition on Cx43 and TGFβ1 gene expression in fetal growth restricted AM

Following 4 hours of CTS, Cx43 gene expression was significantly increased in both CAM and PAM specimens ($^{+}$p values < 0.05, $^{++}$p values < 0.01) **(Figure 5.6)** and remained elevated after 24 hours of CTS (Data not shown; **Appendix; Figure 5.28**). Following 4 hours of Cx43 inhibition, Cx43 significantly decreased in both AM regions in specimens undergoing CTS (***p values < 0.001; **Figure 5.6**), and remained significantly decreased in both free swelling controls and specimens after CTS 24 hours (***p values < 0.001, **Appendix; Figure 5.28**).

Next, the effect of CTS and Cx43 inhibition on TGFβ1 gene expression in AM from donors delivered preterm due to fetal growth restriction was investigated. After 4 hours of CTS, TGFβ1 expression remained unchanged in both AM regions **(Figures 5.7A & 5.8A)**. At 24 hours, TGFβ1 expression increased significantly in PAM samples ($^{+++}$p values < 0.001**; Figure 5.8B**), with no changes in CAM **(Figure 5.7B)**. Following 4 hours of Cx43 inhibition, TGFβ1 gene expression significantly increased CAM specimens after CTS and in PAM free-swelling control specimens (***p values < 0.001; **Figures 5.7A & 5.8A**). TGFβ1 gene expression significantly decreased in both AM regions after 24 hours of Cx43 inhibition in both free-swelling controls and samples that underwent CTS (***p values < 0.001; **Figures 5.7B & 5.8B).**

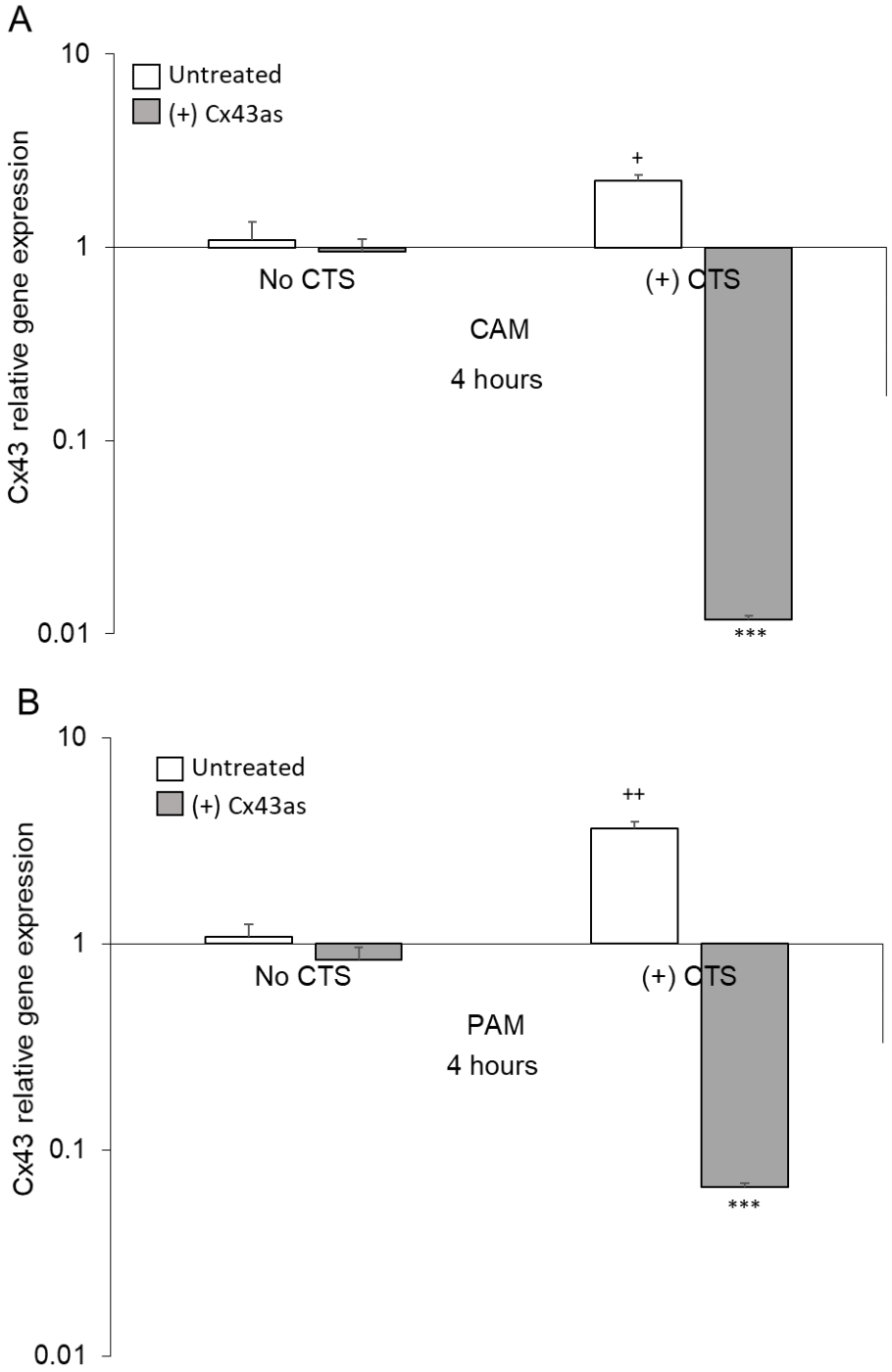

Figure 5.6: *The effect of CTS and Cx43as on Cx43 gene expression in preterm CAM and PAM taken from donors delivered preterm due to fetal growth restriction. AM were exposed to cycles of 1 minute strain and 9 minutes rest for 4 hours at a frequency of 1 Hz. Gene expression of CX43 were presented as ration values on a logarithmic scale and normalised to housekeeping gene GAPDH. In all cases, error bars represent and the mean and ± SEM values of n=6 replicates from n=3 separate donors where $^{+++}p < 0.001$ indicates comparisons between No CTS and (+) CTS while $^{***+}p < 0.001$ indicates comparisons between untreated samples and those treated with Cx43 antisense. CAM = cervical amniotic membrane, PAM = placental amniotic membrane, CTS = cyclic tensile strain, Cx43as = Cx43 antisense.*

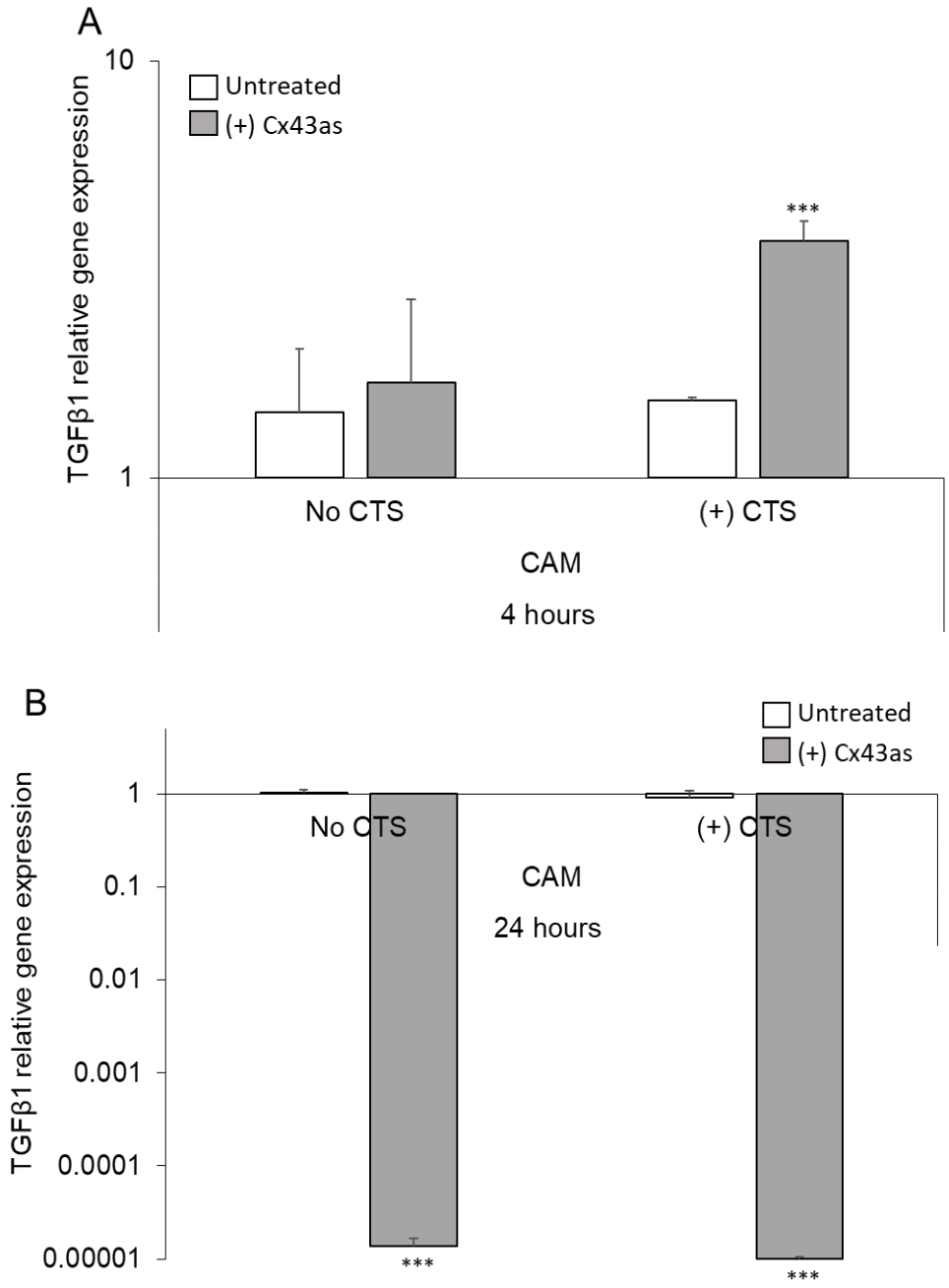

Figure 5.7: *The effect of CTS and Cx43as on TGFβ1 gene expression in preterm CAM taken from donors delivered preterm due to fetal growth restriction. AM were exposed to cycles of 1 minute strain and 9 minutes rest for 4 and 24 hours at a frequency of 1 Hz. Gene expression of CX43 were presented as ration values on a logarithmic scale and normalised to housekeeping gene GAPDH. In all cases, error bars represent and the mean and ± SEM values of n=6 replicates from n=3 separate donors where $^{+++}p < 0.001$ indicates comparisons between No CTS and (+) CTS while $^{***+}p < 0.001$ indicates comparisons between untreated samples and those treated with Cx43 antisense. CAM = cervical amniotic membrane, CTS = cyclic tensile strain, Cx43as = Cx43 antisense.*

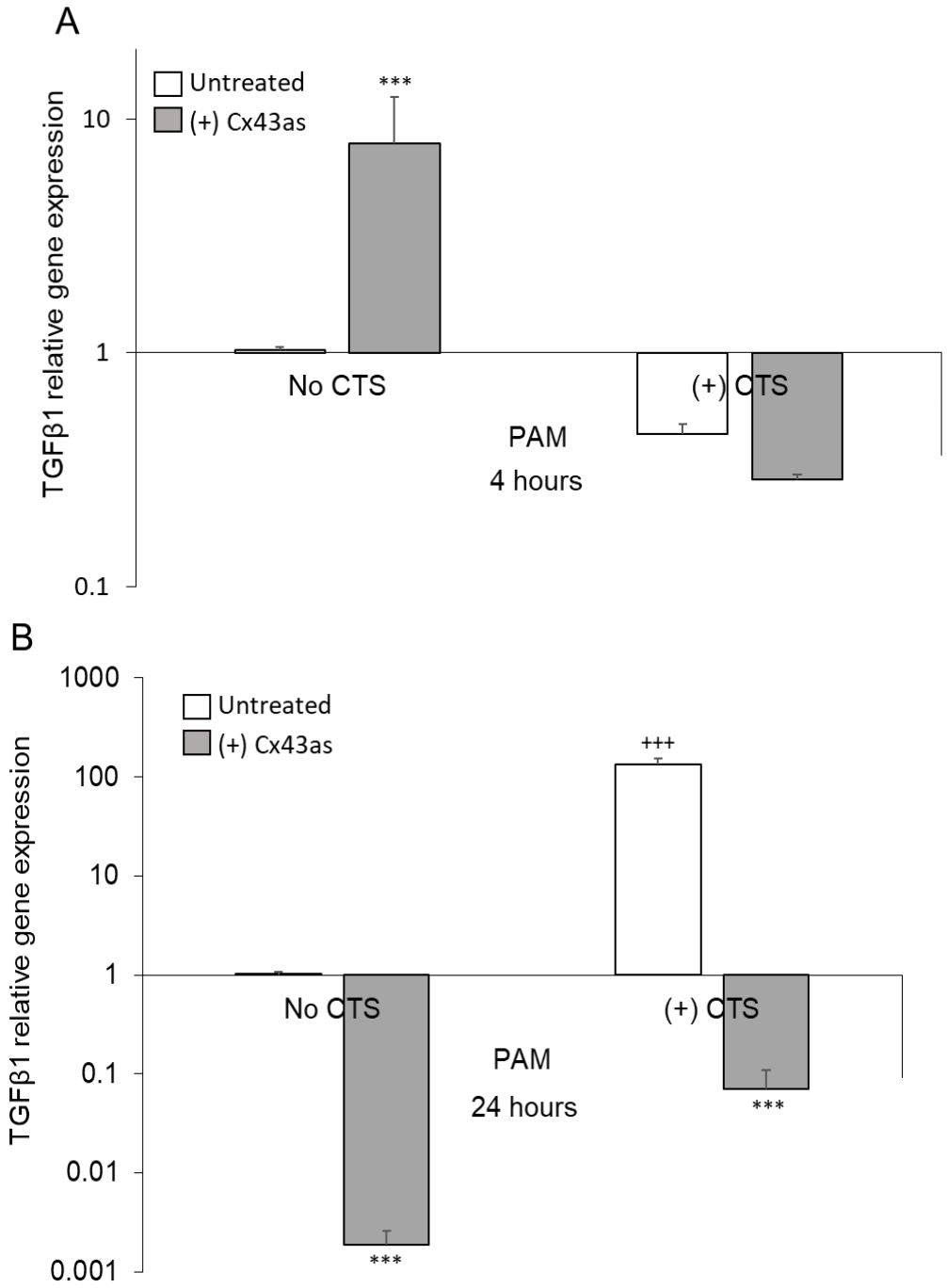

Figure 5.8: *The effect of CTS and Cx43as on TGFβ1 gene expression in preterm PAM taken from donors delivered preterm due to fetal growth restriction. AM were exposed to cycles of 1 minute strain and 9 minutes rest for 4 and 24 hours at a frequency of 1 Hz. Gene expression of Cx43 were presented as ration values on a logarithmic scale and normalised to housekeeping gene GAPDH. In all cases, error bars represent and the mean and ± SEM values of n=6 replicates from n=3 separate donors where $^{+++}p < 0.001$ indicates comparisons between No CTS and (+) CTS while $^{***+}p < 0.001$ indicates comparisons between untreated samples and those treated with Cx43 antisense. PAM = placental amniotic membrane, CTS = cyclic tensile strain, Cx43as = Cx43 antisense.*

5.3.6 The effect of CTS and Cx43 inhibition on mechanotransduction processes in preterm AM following PPROM and delivery before 32 weeks of gestation

The effect of CTS on mechanotransduction mechanisms in preterm AM taken from donors following spontaneous PPROM and delivery before 32 weeks gestation was investigated. sGAG concentration significantly increased following CTS in both PAM and CAM (% change range +21.09 to +173.27%, $^{+++}$p values < 0.001; **Figure 5.9A).** sGAG content was significantly less in PAM regions compared to CAM in untreated controls with and without CTS ($^{\&\&\&}$p values < 0.001; **Figure 5.9A**). After Cx43 inhibition, sGAG content decreased in both AM regions with and without CTS application (***p values < 0.001; **Figure 5.9A**). In CAM samples, collagen concentration significantly decreased after CTS, while in PAM the effect of CTS was reversed ($^{+++}$p values < 0.001; **Figure 5.9B)**. Collagen concentration was significantly less in PAM regions compared to CAM in untreated free-swelling controls **(Figure 5.9B).** Following Cx43 inhibition, collagen concentration significantly increased in all samples with and without CTS application ($^{+++}$p values < 0.001; **Figure 5.9B).**

Elastin concentrations did not significantly change after CTS in either AM region **(Figure 5.10A)**. Cx43 inhibition led to significantly increased elastin concentrations in all samples with and without CTS application (% change range +124.07 to +66.23%, $^{+++}$p values < 0.001; **Figure 5.10A**). PAM samples exhibited significantly higher elastin than CAM ($^{\&\&}$p values < 0.01; **Figure 5.10A**). PGE_2 release remained unchanged after CTS, and no significant differences between CAM and PAM specimens in both AM regions **(Figure 5.10B).** Cx43 inhibition significantly decreased PGE_2 release only in CAM samples after CTS and in PAM free-swelling controls ($^{+++}$p values < 0.001; **Figure 5.10B**).

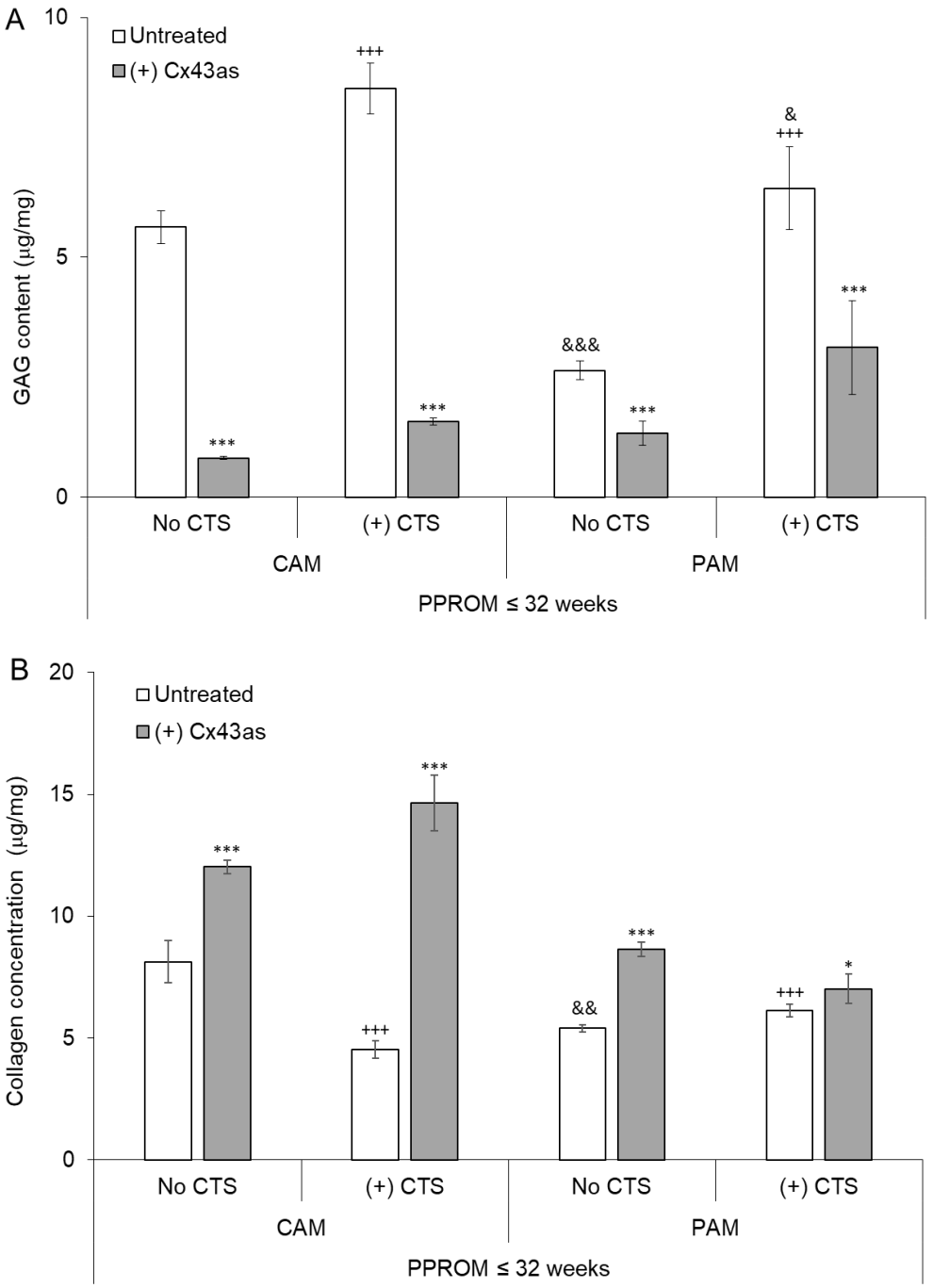

Figure 5.9: *The effect of CTS and Cx43as on preterm CAM and PAM (A) sGAG and (B) collagen content taken from donors following sPPROM at ≤32 weeks GA. AM were exposed to cycles of 1 minute strain and 9 minutes rest for up to 24 hours at a frequency of 1 Hz. Free-swelling controls were not subjected to CTS (No CTS). Error bars represent mean ± SEM from n=12 replicates for sGAG and n=8 replicates for collagen taken from n=3 patients, +++p < 0.001 indicates comparisons between No CTS and (+) CTS, ***p < 0.001 indicates comparisons between untreated samples and those treated with Cx43 antisense and* $^{\&\&\&}p <$ *0.001 comparisons between CAM and PAM. CAM = cervical amniotic membrane, PAM = placental amniotic membrane, CTS = cyclic tensile strain, Cx43as = Cx43 antisense.*

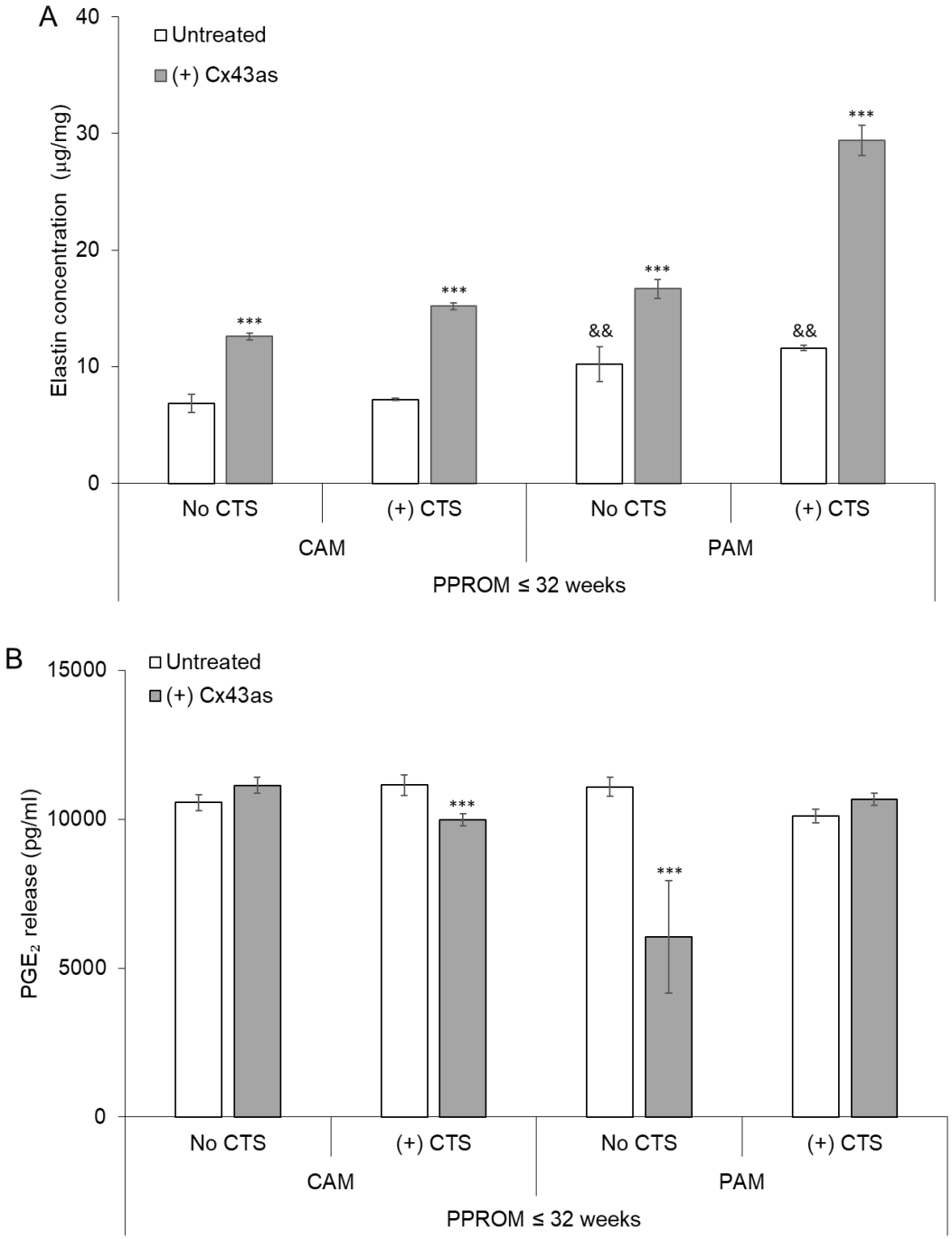

Figure 5.10: *The effect of CTS and Cx43as on preterm CAM and PAM (A) elastin content and (B) PGE_2 release taken from donors following sPPROM at ≤32 weeks GA. AM were exposed to cycles of 1 minute strain and 9 minutes rest for up to 24 hours at a frequency of 1 Hz. Free-swelling controls were not subjected to CTS (No CTS). Error bars represent mean ± SEM from n=8 replicates for elastin and n=6 for PGE_2 taken from n=3 patients, where $^{+++}p < 0.001$ indicates comparisons between No CTS and (+) CTS, ***$p < 0.001$ indicates comparisons between untreated samples and those treated with Cx43 antisense and $^{\&\&\&}p < 0.001$ comparisons between CAM and PAM. CAM = cervical amniotic membrane, PAM = placental amniotic membrane, CTS = cyclic tensile strain, Cx43as = Cx43 antisense.*

5.3.7 The effect of CTS and Cx43as on Cx43 and TGFβ1 gene expression in preterm AM following PPROM and delivery before 32 weeks of gestation

Following 4 hours of CTS, Cx43 gene expression was significantly increased in both CAM and PAM regions, ($^{++}$p values < 0.01 and $^{+++}$p values < 0.001; **Figure 5.11**), but returned to near baseline values after 24 hours of CTS (Data not shown, **Appendix; Figure 5.29**). Following Cx43 inhibition at hours, Cx43 gene expression significantly decreased compared to untreated controls in both AM regions and with and without CTS application (***p values < 0.001**; Figure 5.11**) and remained decreased at 24 hours (Data not shown, **Appendix; Figure 5.29**).

Following CTS, TGFβ1 gene expression significantly decreased only in PAM specimens after 24 hours of intermittent strain **(Figures 5.12 & 5.13).** All other comparisons were not statistically significant. After Cx43 inhibition, TGFβ1 gene expression significantly decreased in both CAM and PAM with and without strain, with the exception of CAM specimens, where TGFβ1 was significantly increased (***p value < 0.001; **Figure 5.12**).

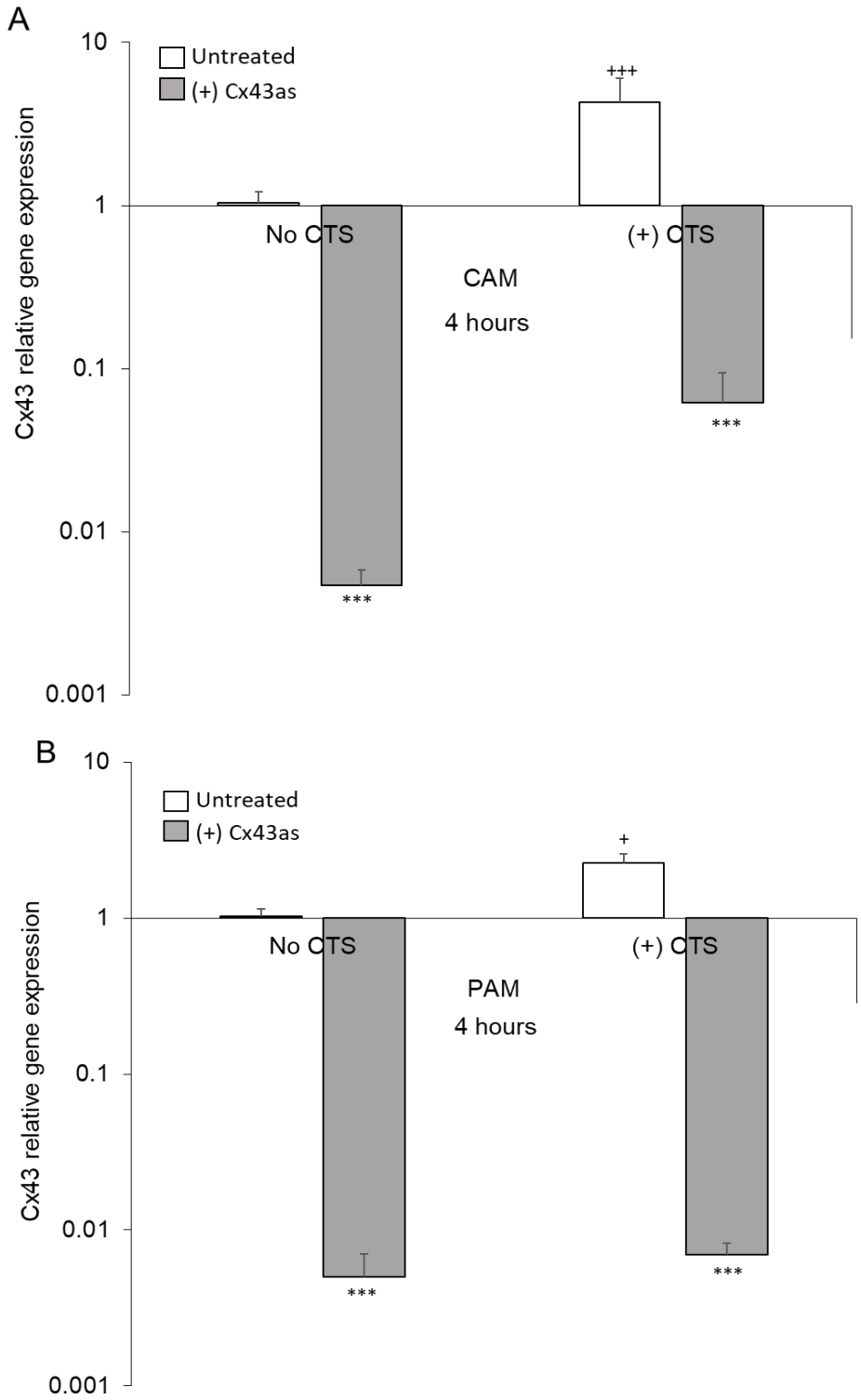

Figure 5.11: *The effect of CTS and Cx43as on Cx43 gene expression in preterm CAM and PAM taken from donors following sPPROM at ≤32 weeks GA. AM were exposed to cycles of 1 minute strain and 9 minutes rest for 4 hours at a frequency of 1 Hz. Gene expression of CX43 were presented as ration values on a logarithmic scale and normalised to housekeeping gene GAPDH. In all cases, error bars represent and the mean and ± SEM values of n=6 replicates from n=3 separate donors where $^{+++}p < 0.001$ indicates comparisons between No CTS and (+) CTS while ***$p < 0.001$ indicates comparisons between untreated samples and those treated with Cx43 antisense. CAM = cervical amniotic membrane, PAM = placental amniotic membrane, CTS = cyclic tensile strain, Cx43as = Cx43 antisense.*

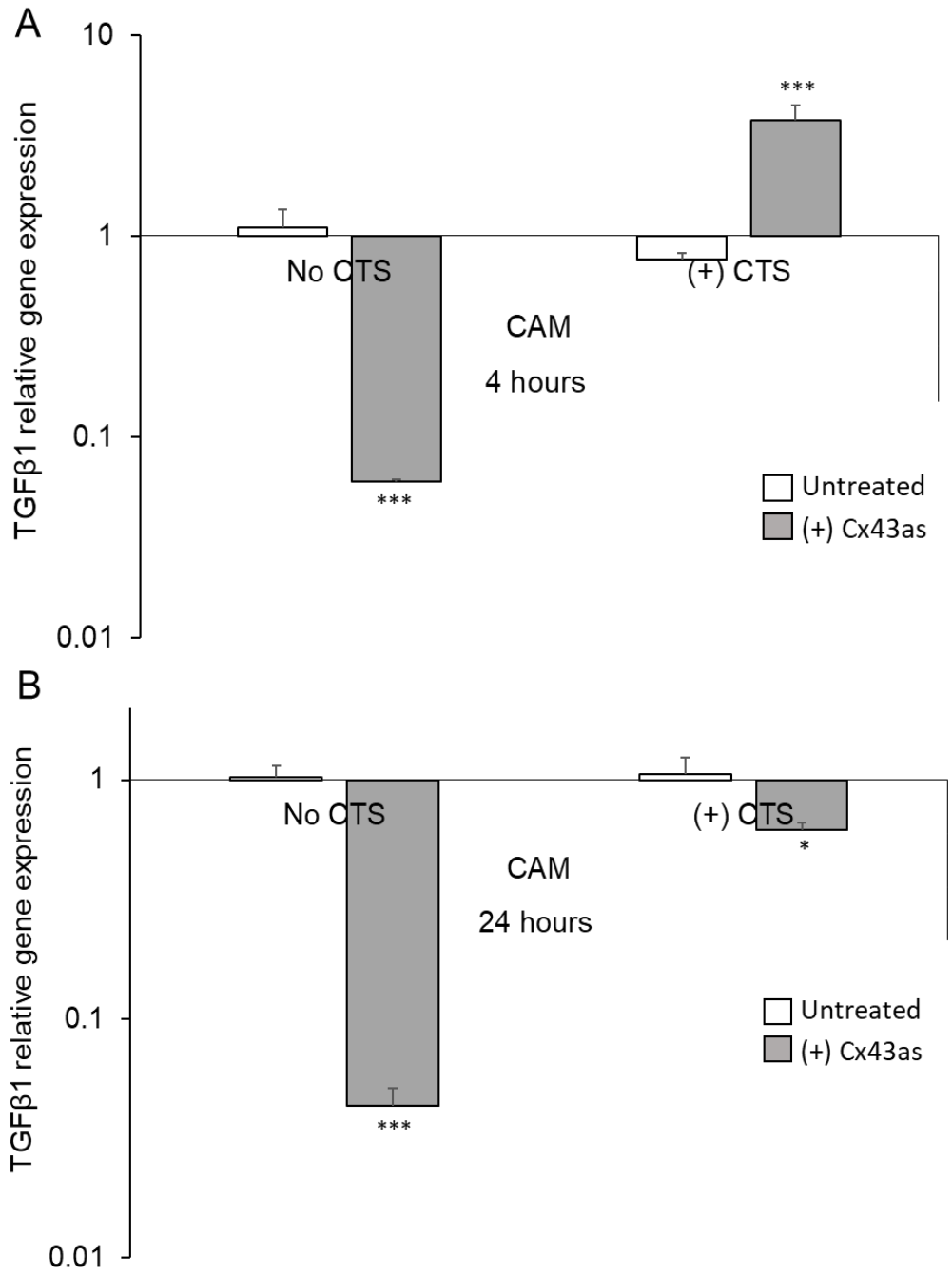

Figure 5.12: *The effect of CTS and Cx43as on TGFβ1 gene expression in preterm CAM taken from donors following sPPROM at ≤32 weeks GA. AM were exposed to cycles of 1 minute strain and 9 minutes rest for 4 and 24 hours at a frequency of 1 Hz. Gene expression of CX43 were presented as ration values on a logarithmic scale and normalised to housekeeping gene GAPDH. In all cases, error bars represent and the mean and ± SEM values of n=6 replicates from n=3 separate donors where $^{+++}p < 0.001$ indicates comparisons between No CTS and (+) CTS while $***^{+}p < 0.001$ indicates comparisons between untreated samples and those treated with Cx43 antisense. CAM = cervical amniotic membrane, CTS = cyclic tensile strain, Cx43as = Cx43 antisense.*

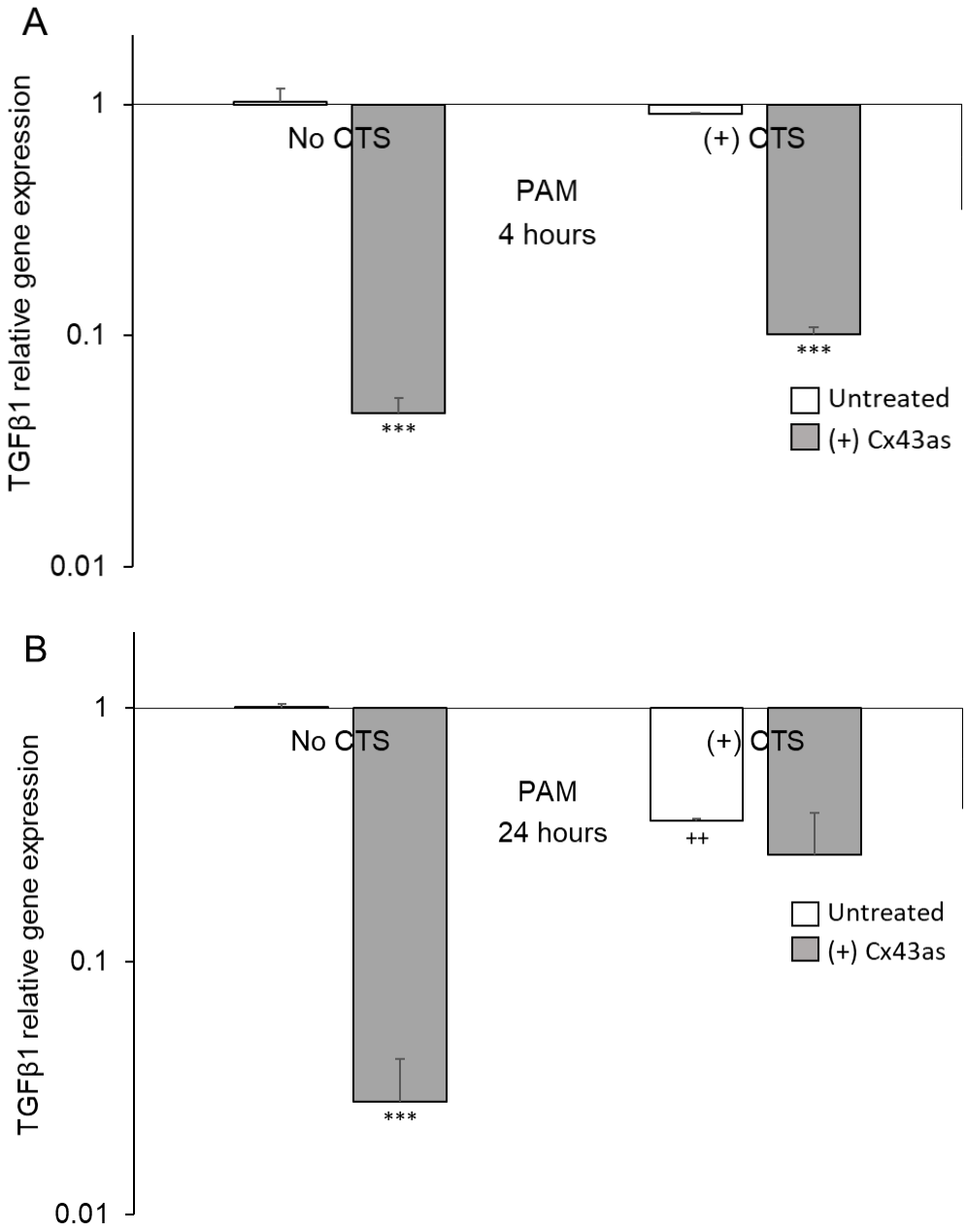

Figure 5.13: *The effect of CTS and Cx43as on TGFβ1 gene expression in preterm PAM taken from donors following sPPROM at ≤32 weeks GA. AM were exposed to cycles of 1 minute strain and 9 minutes rest for 4 and 24 hours at a frequency of 1 Hz. Gene expression of CX43 were presented as ration values on a logarithmic scale and normalised to housekeeping gene GAPDH. In all cases, error bars represent and the mean and ± SEM values of n=6 replicates from n=3 separate donors where $^{+++}p < 0.001$ indicates comparisons between No CTS and (+) CTS while $^{***+}p < 0.001$ indicates comparisons between untreated samples and those treated with Cx43 antisense. PAM = placental amniotic membrane, CTS = cyclic tensile strain, Cx43as = Cx43 antisense.*

5.3.8 The effect of CTS on mechanotransduction processes in preterm AM following PPROM and delivery after 32 weeks of gestation

Following 24 hours of intermittent CTS, GAG content significantly increased in AM from donors delivering after 32 weeks of gestation ($^{++}$p values < 0.01 and $^{+++}$p values < 0.001; **Figure 5.14A**). PAM specimens after CTS had significantly higher sGAG content than CAM ($^{\&\&}$p values < 0.01, **Figure 5.14A**). Cx43 inhibition resulted in significantly decreased sGAG content in samples with and without strain and in both AM regions (***p values < 0.001; **Figure 5.14A**). In contrast, collagen concentration significantly decreased after CTS in only CAM specimens, with no statistical differences in PAM **(Figure 5.14B)**. Collagen concentration was statistically less in PAM unstrained samples (no CTS) versus CAM ($^{\&\&}$p values < 0.01, **Figure 5.14B)**. After Cx43 inhibition, collagen concentration statistically increased in all samples, except for PAM specimens after CTS **(Figure 5.14B)**.

Elastin concentration statistically increased after CTS only in PAM specimens, while elastin concentration was higher in PAM samples with and without CTS compared to CAM ($^{\&}$p values < 0.05 and ($^{\&\&}$p values < 0.01; **Figure 5.15A**). Following Cx43 inhibition, elastin concentration significantly increased in CAM samples after strain and in unstrained PAM samples (***p values < 0.001; **Figure 5.15A**). All other comparisons were not statistically significant. There were no statistical differences in PGE_2 release in samples after strain in both AM regions, and no differences between CAM and PAM **(Figure 5.15B)**. However, Cx43 inhibition resulted in statistically decreased PGE_2 release in all samples with and without strain (***p values < 0.001; **Figure 5.14B**).

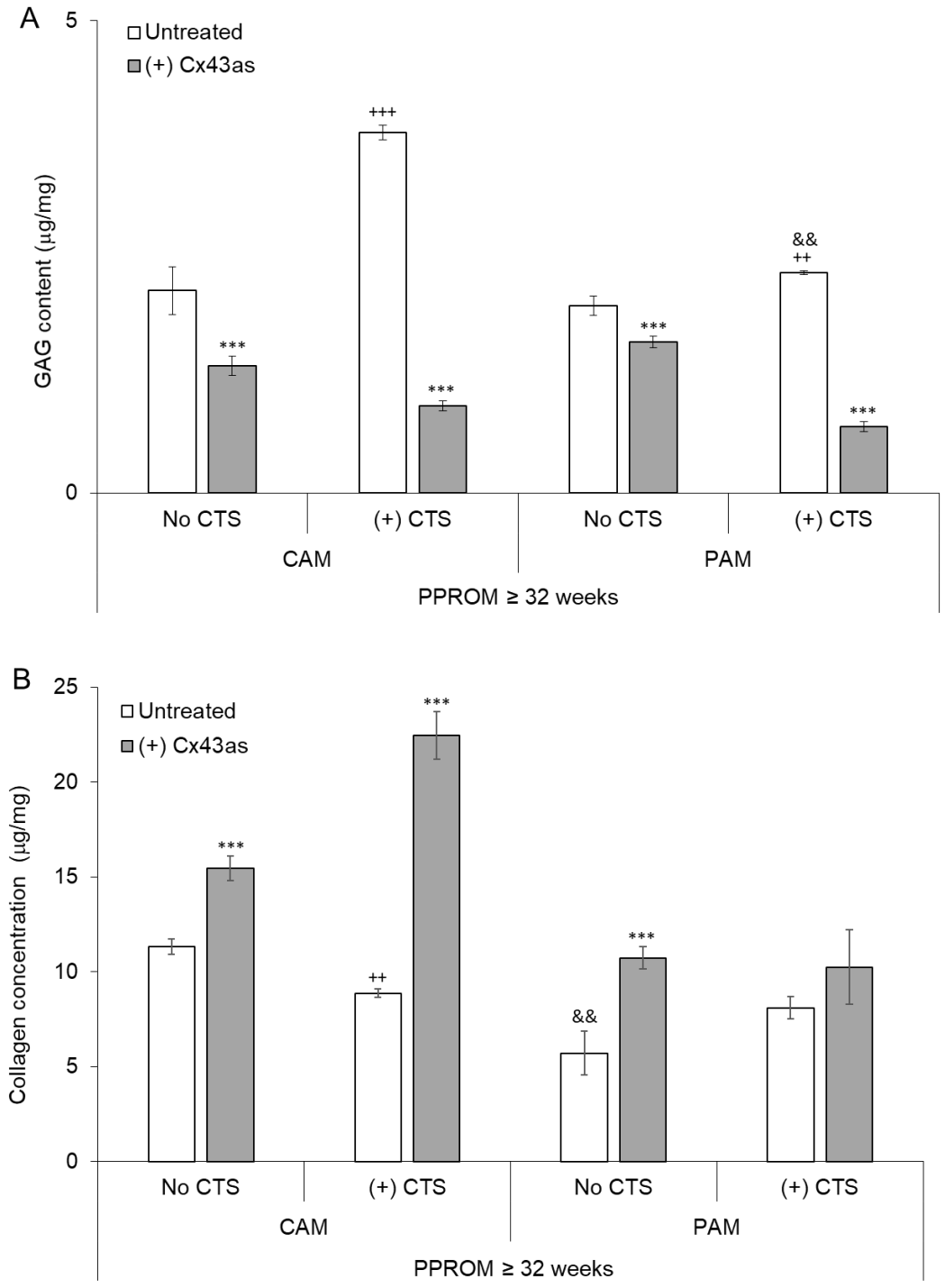

Figure 5.14: *The effect of CTS and Cx43as on preterm CAM and PAM (A) sGAG and (B) collagen content taken from donors following sPPROM at ≥32 weeks GA. AM were exposed to cycles of 1 minute strain and 9 minutes rest for up to 24 hours at a frequency of 1 Hz. Free-swelling controls were not subjected to CTS (No CTS). Error bars represent mean ± SEM from n=12 replicates for sGAG and n=8 replicates for collagen taken from n=3 patients, where +++$p < 0.001$ indicates comparisons between No CTS and (+) CTS, ***$p < 0.001$ indicates comparisons between untreated samples and those treated with Cx43 antisense and $^{\&\&\&}p < 0.001$ comparisons between CAM and PAM. CAM = cervical amniotic membrane, PAM = placental amniotic membrane, CTS = cyclic tensile strain, Cx43as = Cx43 antisense.*

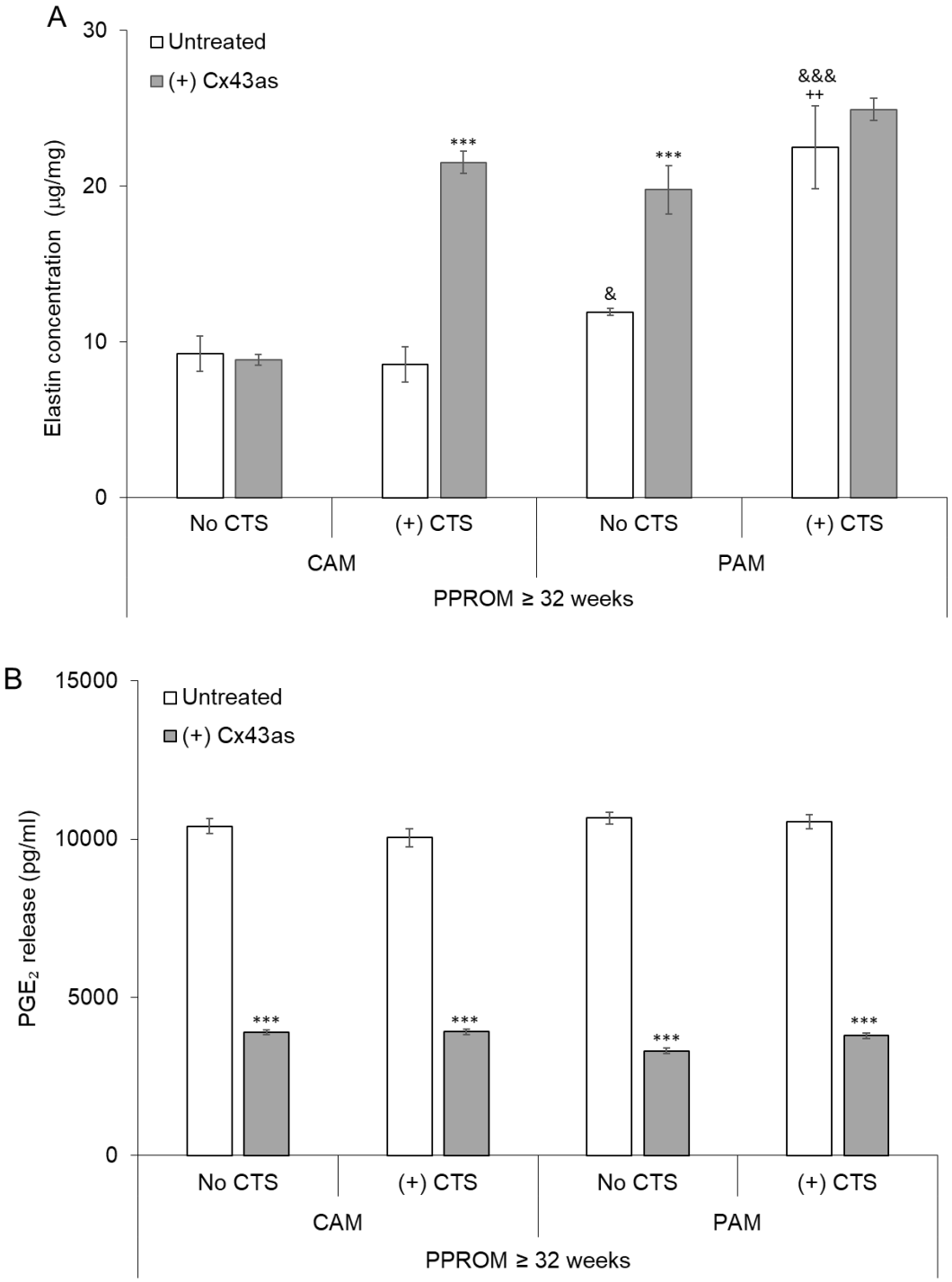

Figure 5.15: *The effect of CTS and Cx43as on preterm CAM and PAM (A) elastin content and (B) PGE_2 release taken from donors following sPPROM at ≥32 weeks GA. AM were exposed to cycles of 1 minute strain and 9 minutes rest for up to 24 hours at a frequency of 1 Hz. Free-swelling controls were not subjected to CTS (No CTS). Error bars represent mean ± SEM from n=8 replicates for elastin and n=6 for PGE_2 taken from n=3 patients, where $^{+++}p < 0.001$ indicates comparisons between No CTS and (+) CTS, $***p < 0.001$ indicates comparisons between untreated samples and those treated with Cx43 antisense and $^{\&\&\&}p < 0.001$ comparisons between CAM and PAM. CAM = cervical amniotic membrane, PAM = placental amniotic membrane, CTS = cyclic tensile strain, Cx43as = Cx43 antisense.*

5.3.9 The effect of CTS on Cx43 and TGFβ1 gene expression in preterm AM following PPROM and delivery after 32 weeks of gestation

Application of CTS on preterm AM specimens resulted in no statistical changes in Cx43 gene expression in CAM samples after 4 hours of strain, however Cx43 was significantly decreased after 24 hours ($^{+++}$p values < 0.001, **Appendix; Figure 5.30**). In PAM samples, Cx43 gene expression significantly increased after 4 hours of CTS and remained significantly increased even after 24 hours of intermittent strain ($^{++}$p value < 0.01 and $^{+++}$p value; **Figure 5.16B** and **Appendix; Figure 5.30** respectively). Cx43 inhibition at 4 hours of CTS resulted in significantly decreased Cx43 gene expression in all samples with and without CTS and in both AM regions and Cx43 remained low even after 24 hours of strain (***p values < 0.001, **Figure 5.16** and **Appendix Figure 5.30**).

In CAM specimens after 4 hours of CTS, TGFβ1 gene expression significantly decreased and remained low at 24 hours after intermittent strain ($^{+++}$p value < 0.001 and $^{+}$p value < 0.05 for 4 and 24 hours respectively; **Figure 5.17**). Following Cx43 inhibition, TGFβ1 gene expression significantly decreased at 4 hours in unstrained samples (No CTS) and in those after 24 hours of strain only (***p values < 0.001; **Figure 5.17**). All other comparisons for CAM were not significant. TGFβ1 gene expression significantly increased following 4 hours of CTS in PAM ($^{+++}$p value < 0.001, **Figure 5.18A**). Cx43 inhibition led to significant decrease in TGFβ1 gene expression at 4 hours in samples after CTS and in both samples with and without CTS after 24 hours (***p values < 0.001, **Figures 5.17 & 5.18**). All other comparisons were not significant.

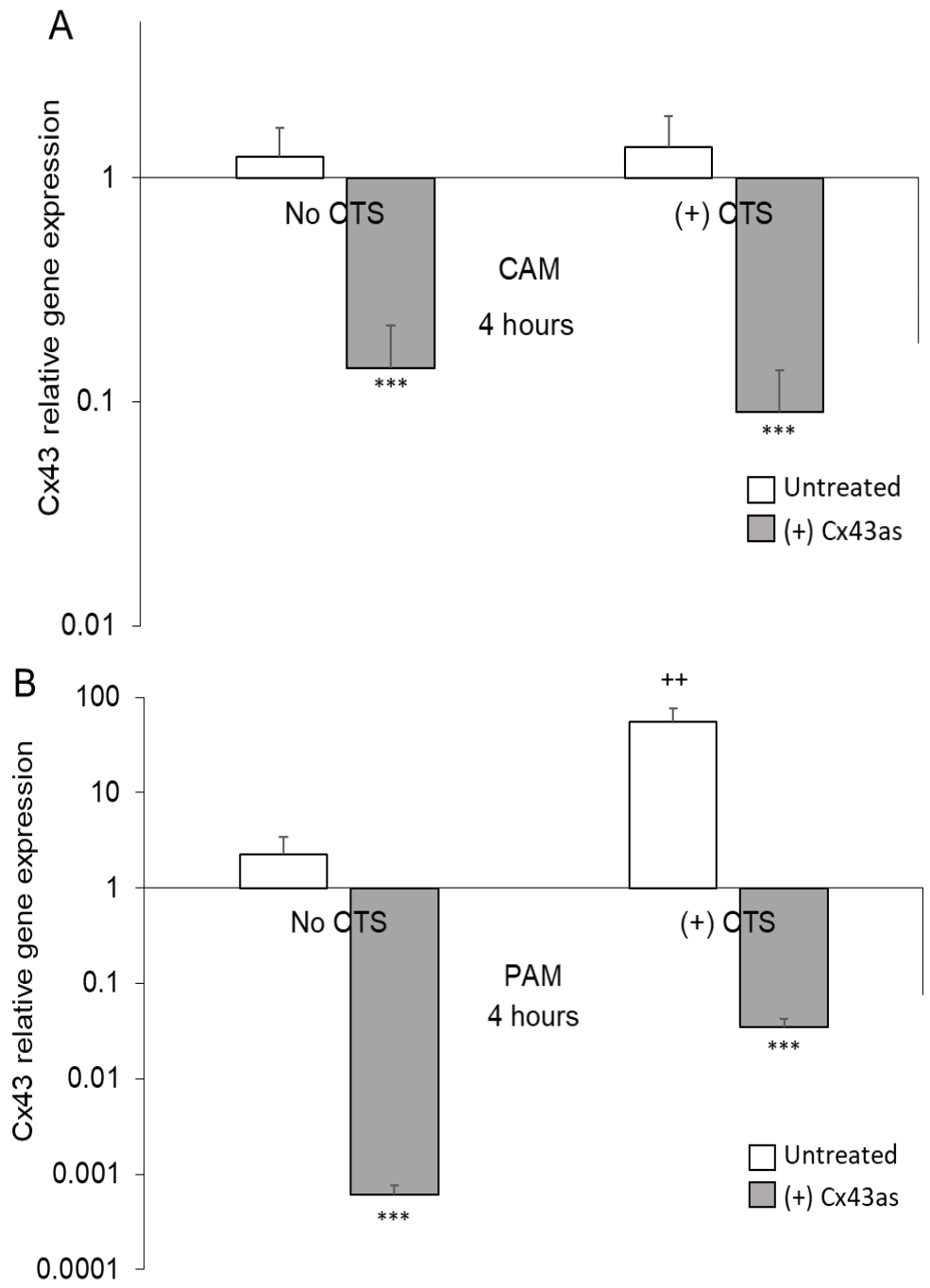

Figure 5.16: *The effect of CTS and Cx43as on Cx43 gene expression in preterm CAM and PAM taken from donors following sPPROM at ≥32 weeks GA. AM were exposed to cycles of 1 minute strain and 9 minutes rest for 4 and 24 hours at a frequency of 1 Hz. Gene expression of CX43 were presented as ration values on a logarithmic scale and normalised to housekeeping gene GAPDH. In all cases, error bars represent and the mean and ± SEM values of n=6 replicates from n=3 separate donors where $^{+++}p < 0.001$ indicates comparisons between No CTS and (+) CTS while $^{***+}p < 0.001$ indicates comparisons between untreated samples and those treated with Cx43 antisense. CAM = cervical amniotic membrane, PAM = placental amniotic membrane, CTS = cyclic tensile strain, Cx43as = Cx43 antisense.*

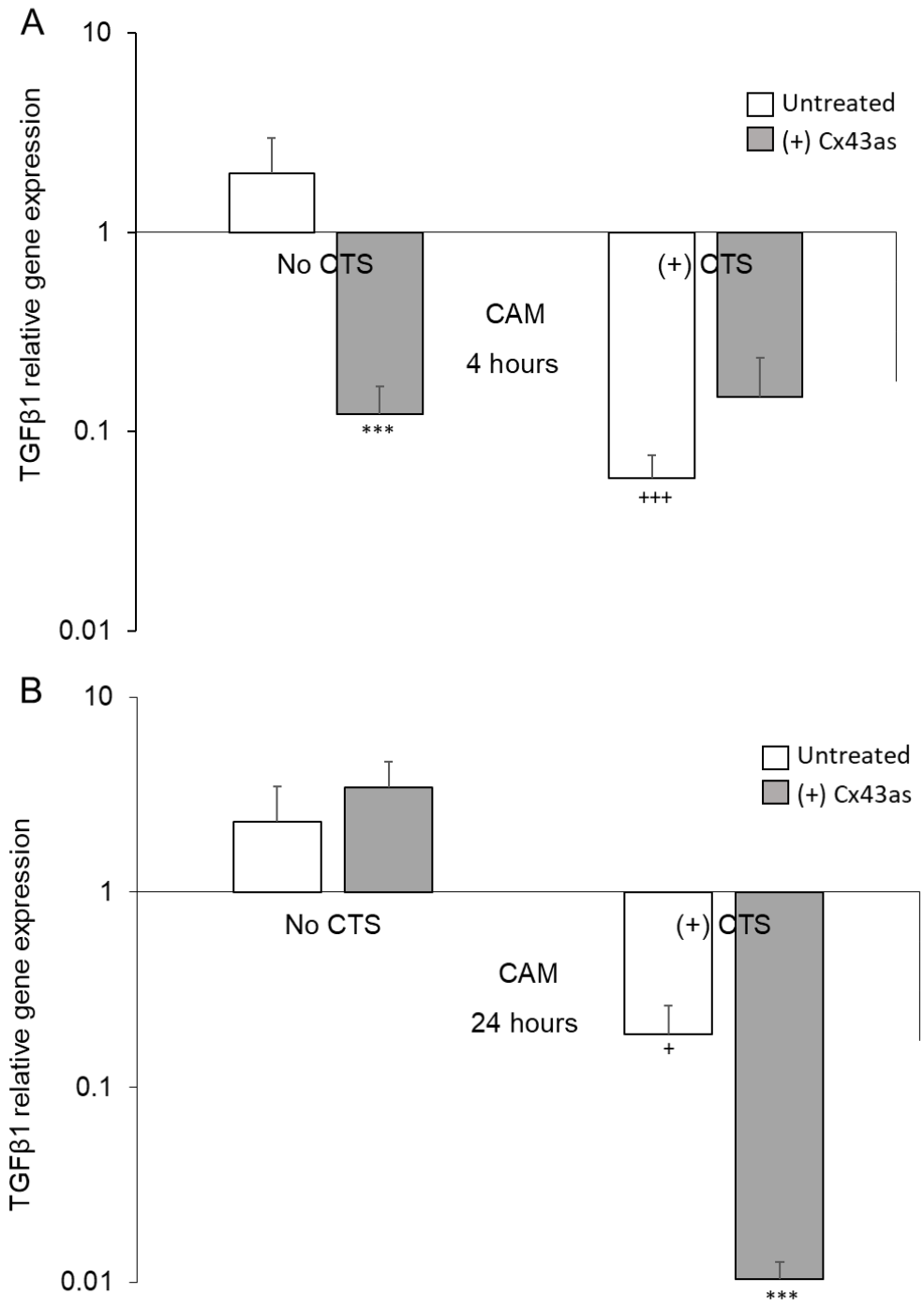

Figure 5.17: *The effect of CTS and Cx43as on TGFβ1 gene expression in preterm CAM taken from donors following sPPROM at ≥32 weeks GA. AM were exposed to cycles of 1 minute strain and 9 minutes rest for 4 and 24 hours at a frequency of 1 Hz. Gene expression of CX43 were presented as ration values on a logarithmic scale and normalised to housekeeping gene GAPDH. In all cases, error bars represent and the mean and ± SEM values of n=6 replicates from n=3 separate donors where $^{+++}p < 0.001$ indicates comparisons between No CTS and (+) CTS while $^{***+}p < 0.001$ indicates comparisons between untreated samples and those treated with Cx43 antisense. CAM = cervical amniotic membrane, CTS = cyclic tensile strain, Cx43as = Cx43 antisense.*

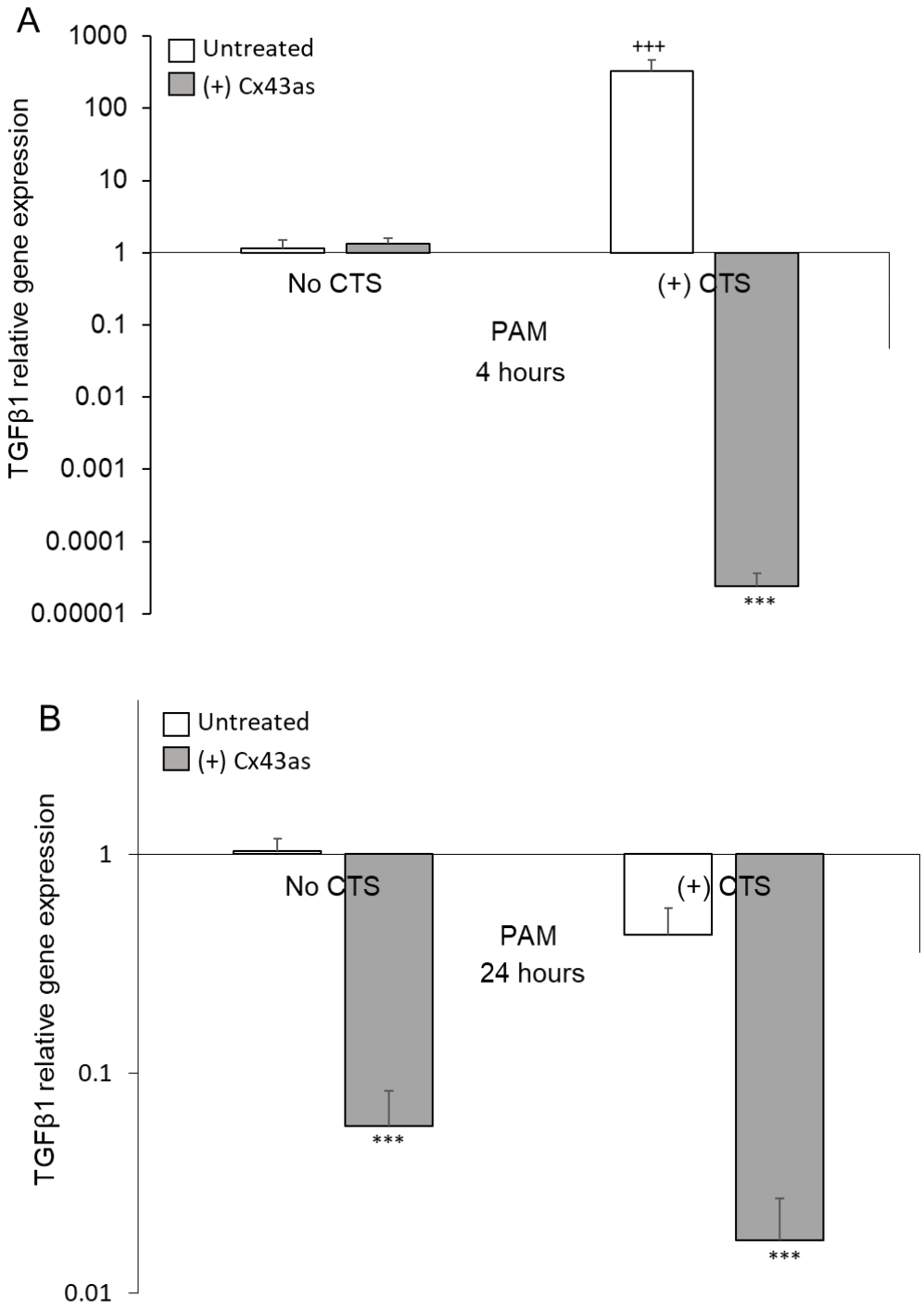

Figure 5.18: *The effect of CTS and Cx43as on TGFβ1 gene expression in preterm PAM taken from donors following sPPROM at ≥32 weeks GA. AM were exposed to cycles of 1 minute strain and 9 minutes rest for 4 and 24 hours at a frequency of 1 Hz. Gene expression of CX43 were presented as ration values on a logarithmic scale and normalised to housekeeping gene GAPDH. In all cases, error bars represent and the mean and ± SEM values of n=6 replicates from n=3 separate donors where $^{+++}p < 0.001$ indicates comparisons between No CTS and (+) CTS while $^{***+}p < 0.001$ indicates comparisons between untreated samples and those treated with Cx43 antisense. PAM = placental amniotic membrane, CTS = cyclic tensile strain, Cx43as = Cx43 antisense.*

5.3.10 The effect of CTS on mechanotransduction processes in donor AM following fetal surgery and subsequent PPROM.

The effect of CTS on mechanotransduction mechanisms in preterm AM taken from donors who delivered preterm following iatrogenic PPROM associated with open fetal surgery was investigated. In CAM specimens, sGAG content and collagen content had an inverse relationship: after 24 of CTS, sGAG significantly decreased while collagen content increased ($^{+++}$p values < 0.001; **Figure 5.19).** In PAM samples, sGAG content significantly increased after CTS and collagen concentration also increased, like in CAM. ($^{+++}$p values < 0.001; **Figure 5.19).** PAM exhibited significantly lower sGAG values than CAM in both strained and unstrained samples ($^{+++}$p values < 0.001; **Figure 5.19A)**. All other comparisons for sGAG content and collagen concentration were not significant.

In response to CTS, both CAM and PAM samples significantly elevated elastin concentration (% change range +62.79 and 115.88% for CAM and PAM respectively, $^{+++}$p values < 0.001; **Figure 5.20A).** Following Cx43 inhibition, elastin concentration was significantly increased in all specimens except for free-swelling control CAM samples (No CTS) (**p values < 0.01 and ***p values < 0.001; **Figure 5.20A**).There were no statistical differences in PGE_2 release in CAM nor PAM specimens after CTS **(Figure 5.20B)**. Following Cx43 inhibition and 24 hours of strain, PGE_2 release significantly increased in CAM and PAM specimens (*p values < 0.05; **Figure 5.20B**). All other comparison were not significant.

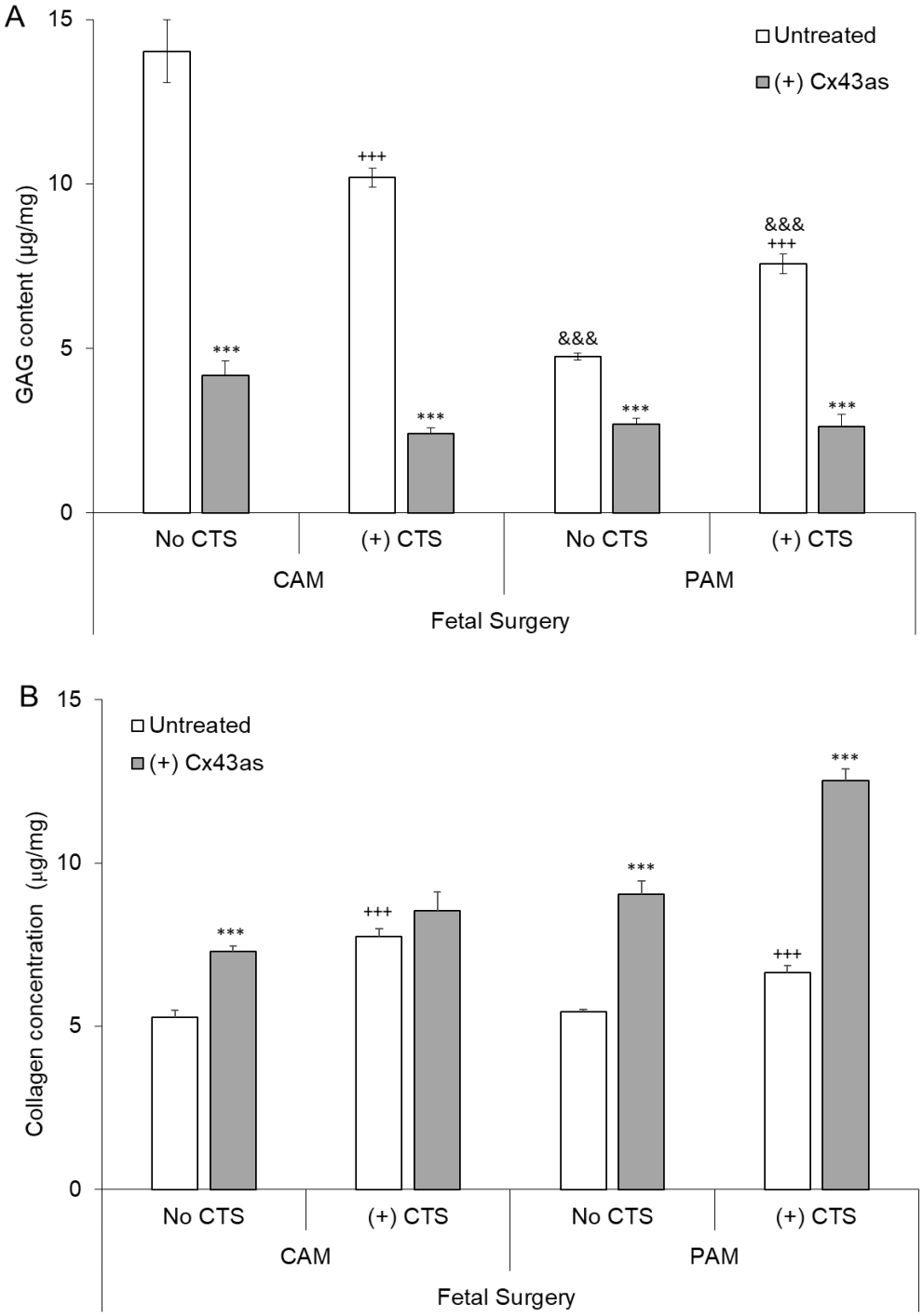

Figure 5.19: *The effect of CTS and Cx43as on preterm CAM and PAM (A) sGAG and (B) collagen content taken from donors following iPPROM associated with open fetal surgery. AM were exposed to cycles of 1 minute strain and 9 minutes rest for up to 24 hours at a frequency of 1 Hz. Free-swelling controls were not subjected to CTS (No CTS). Error bars represent mean ± SEM from n=12 replicates for sGAG and n=8 replicates for collagen taken from n=3 patients, where +++p < 0.001 indicates comparisons between No CTS and (+) CTS, ***p < 0.001 indicates comparisons between untreated samples and those treated with Cx43 antisense and* $^{\&\&\&}$*p < 0.001 comparisons between CAM and PAM. CAM = cervical amniotic membrane, PAM = placental amniotic membrane, CTS = cyclic tensile strain, Cx43as = Cx43 antisense.*

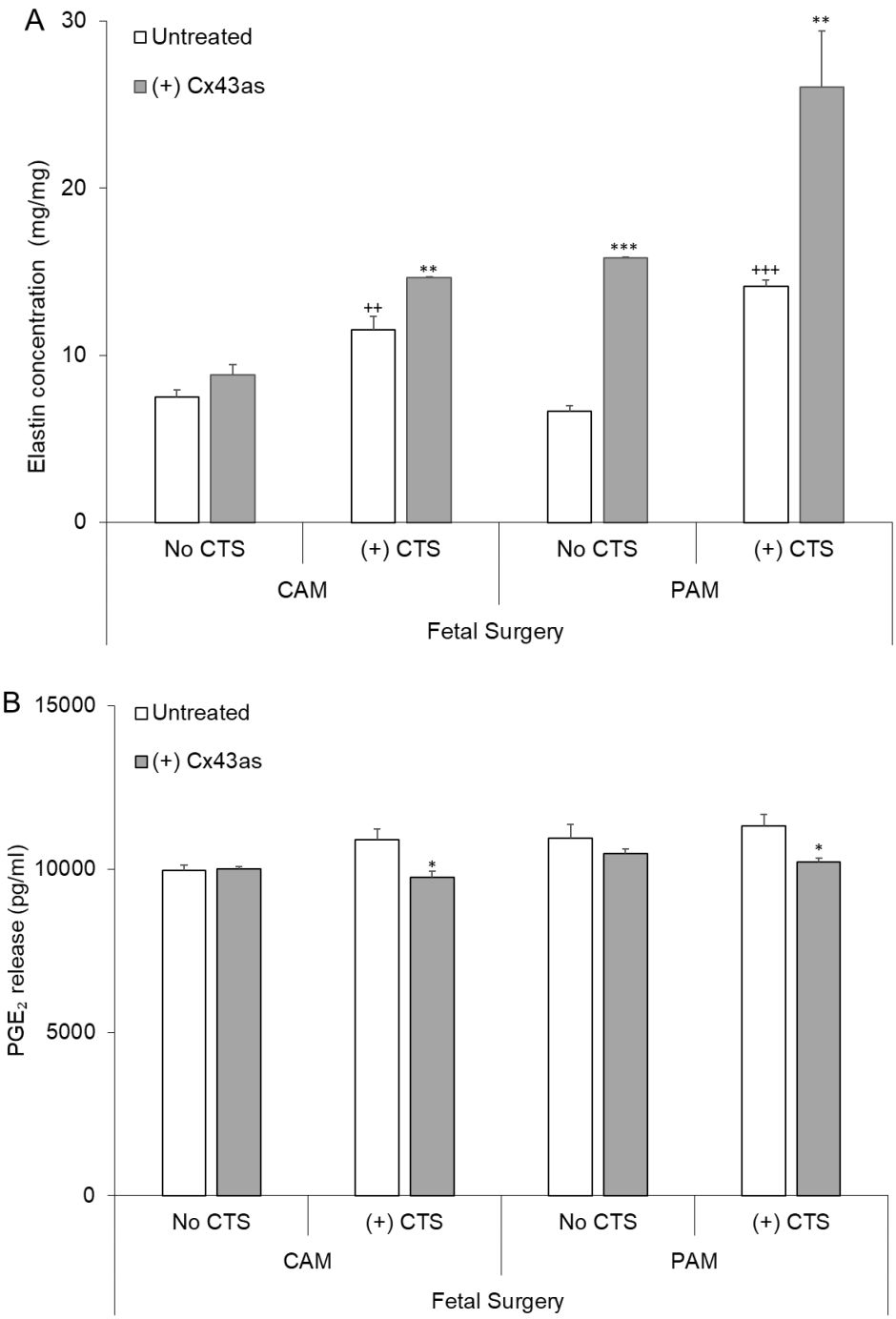

Figure 5.20: *The effect of CTS and Cx43as on preterm CAM and PAM (A) elastin content and (B) PGE_2 release taken from donors following iPPROM associated with open fetal surgery. AM were exposed to cycles of 1 minute strain and 9 minutes rest for up to 24 hours at a frequency of 1 Hz. Free-swelling controls were not subjected to CTS (No CTS). Error bars represent mean ± SEM from n=8 replicates for elastin and n=6 for PGE_2 taken from n=3 patients, where $^{+++}p < 0.001$ indicates comparisons between No CTS and (+) CTS, $***p < 0.001$ indicates comparisons between untreated samples and those treated with Cx43 antisense and $^{\&\&\&}p < 0.001$ comparisons between CAM and PAM. CAM = cervical amniotic membrane, PAM = placental amniotic membrane, CTS = cyclic tensile strain, Cx43as = Cx43 antisense.*

5.3.11 The effect of CTS on Cx43 and TGFβ1 gene expression in donor AM following fetal surgery and subsequent PPROM

Following 4 hours of CTS, Cx43 gene expression was significantly increased in CAM specimens and this remained high after 24 hours of intermittent strain ($^{++}$p values < 0.01; **Figure 5.21A** and **Appendix; Figure 5.31**). PAM samples also showed significantly increased Cx43 expression after 4 hours of strain, while at 24 hours Cx43 was downregulated ($^{+++}$p values < 0.001; **Figure 5.21B** and **Appendix**). After Cx43 inhibition and 4 hours of CTS, Cx43 gene expression was significantly decreased in both AM regions and this decrease remained after 24 hours of intermittent strain (*p values < 0.05 and ***p values < 0.001; **Figure 5.21** and **Appendix; Figure 5.31**).

In response to 24 hours of CTS, TGFβ1 gene expression was significantly decreased in CAM samples ($^{+++}$p value < 0.001; **Figure 5.22B**). Cx43 inhibition resulted in significantly increased TGFβ1 gene expression after 4 hours in samples with and without strain (*p values < 0.05; **Figure 5.22A**). In unstrained CAM samples, TGFβ1 gene expression significantly decreased after 24 hours of Cx43 inhibition (***p values < 0.001; **Figure 5.22A**). All other comparisons in CAM were not significant. In contrast to CAM, PAM samples did not exhibit significant differences after 4 and 24 hours of CTS **(Figure 5.23)**. At 4 hours following Cx43 inhibition, Cx43 gene expression significantly decreased in samples with no strain and increased in those after CTS ($^{+}$p value < 0.05 and $^{+++}$p value < 0.001 respectively; **Figure 5.23**). All other comparisons were not significant.

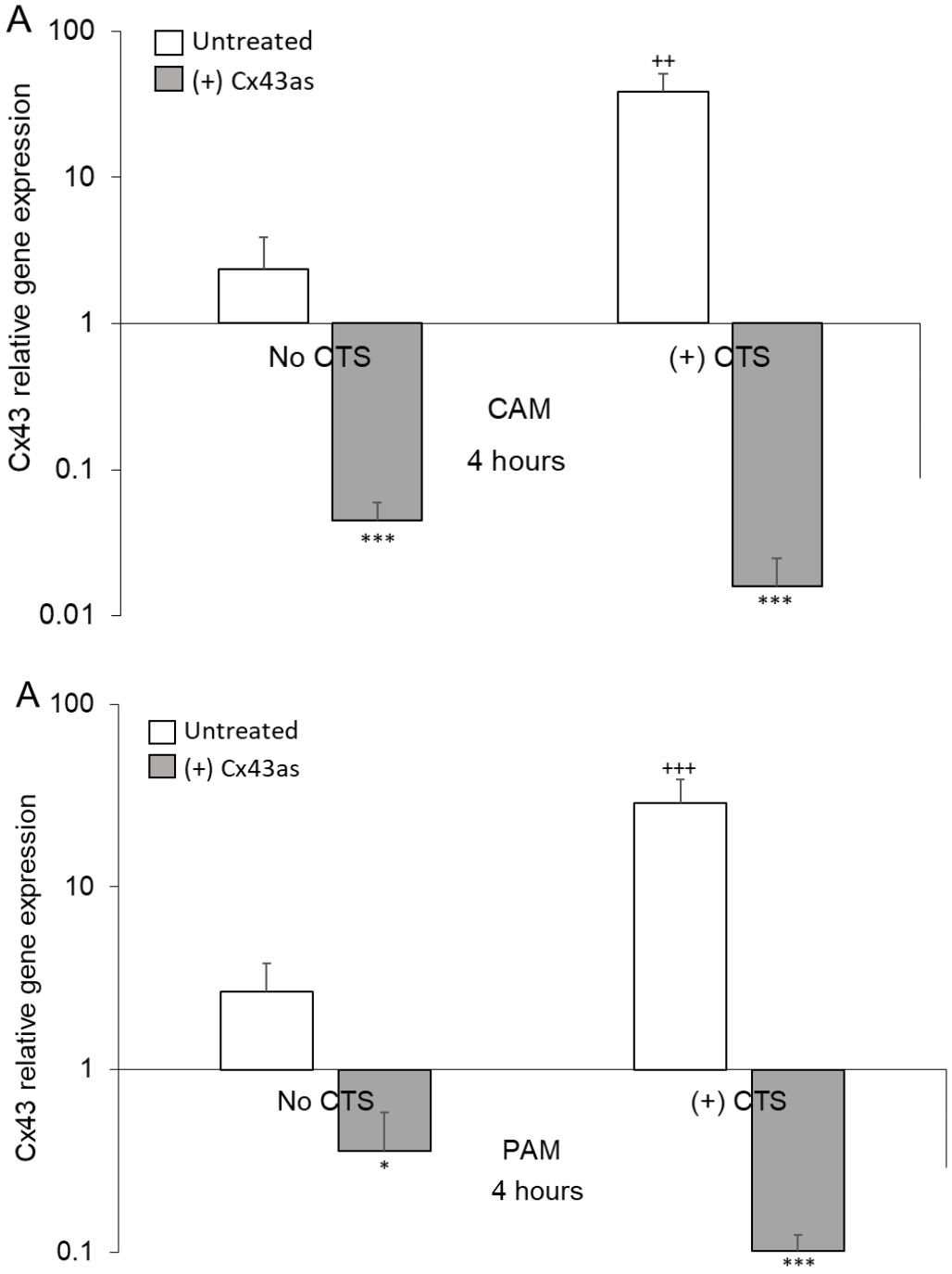

Figure 5.21: *The effect of CTS and Cx43as on Cx43 gene expression in preterm CAM and PAM taken from donors following iPPROM associated with open fetal surgery. AM were exposed to cycles of 1 minute strain and 9 minutes rest for 4 hours at a frequency of 1 Hz. Gene expression of CX43 were presented as ration values on a logarithmic scale and normalised to housekeeping gene GAPDH. In all cases, error bars represent and the mean and ± SEM values of n=6 replicates from n=3 separate donors where $^{+++}p < 0.001$ indicates comparisons between No CTS and (+) CTS while $^{***+}p < 0.001$ indicates comparisons between untreated samples and those treated with Cx43 antisense. CAM = cervical amniotic membrane, PAM = placental amniotic membrane, CTS = cyclic tensile strain, Cx43as = Cx43 antisense.*

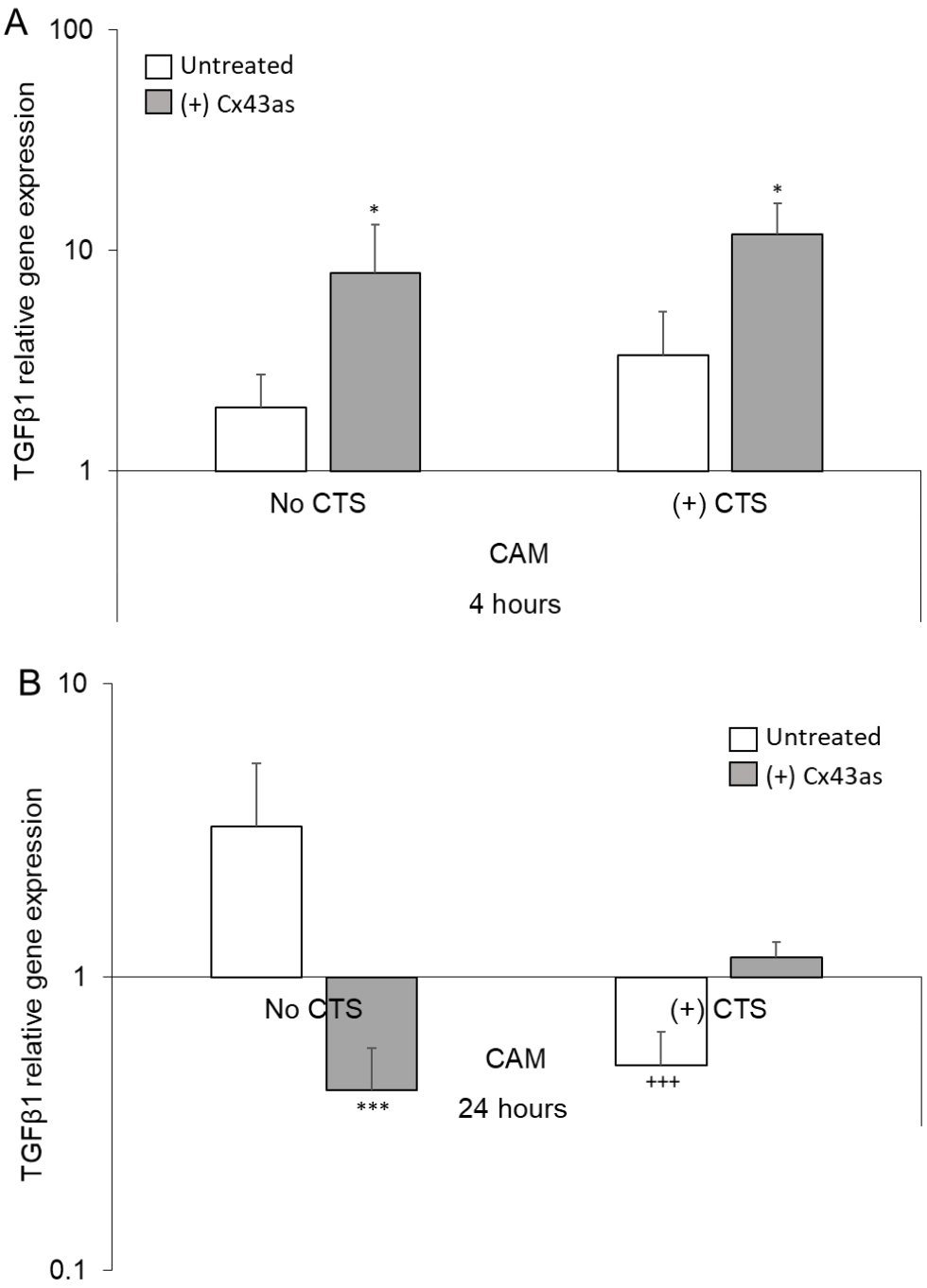

Figure 5.22: *The effect of CTS and Cx43as on TGFβ1 gene expression in preterm CAM taken from donors following iPPROM associated with open fetal surgery. AM were exposed to cycles of 1 minute strain and 9 minutes rest for 4 and 24 hours at a frequency of 1 Hz. Gene expression of CX43 were presented as ration values on a logarithmic scale and normalised to housekeeping gene GAPDH. In all cases, error bars represent and the mean and ± SEM values of n=6 replicates from n=3 separate donors where $^{+++}p < 0.001$ indicates comparisons between No CTS and (+) CTS while $^{***+}p < 0.001$ indicates comparisons between untreated samples and those treated with Cx43 antisense. CAM = cervical amniotic membrane, CTS = cyclic tensile strain, Cx43as = Cx43 antisense.*

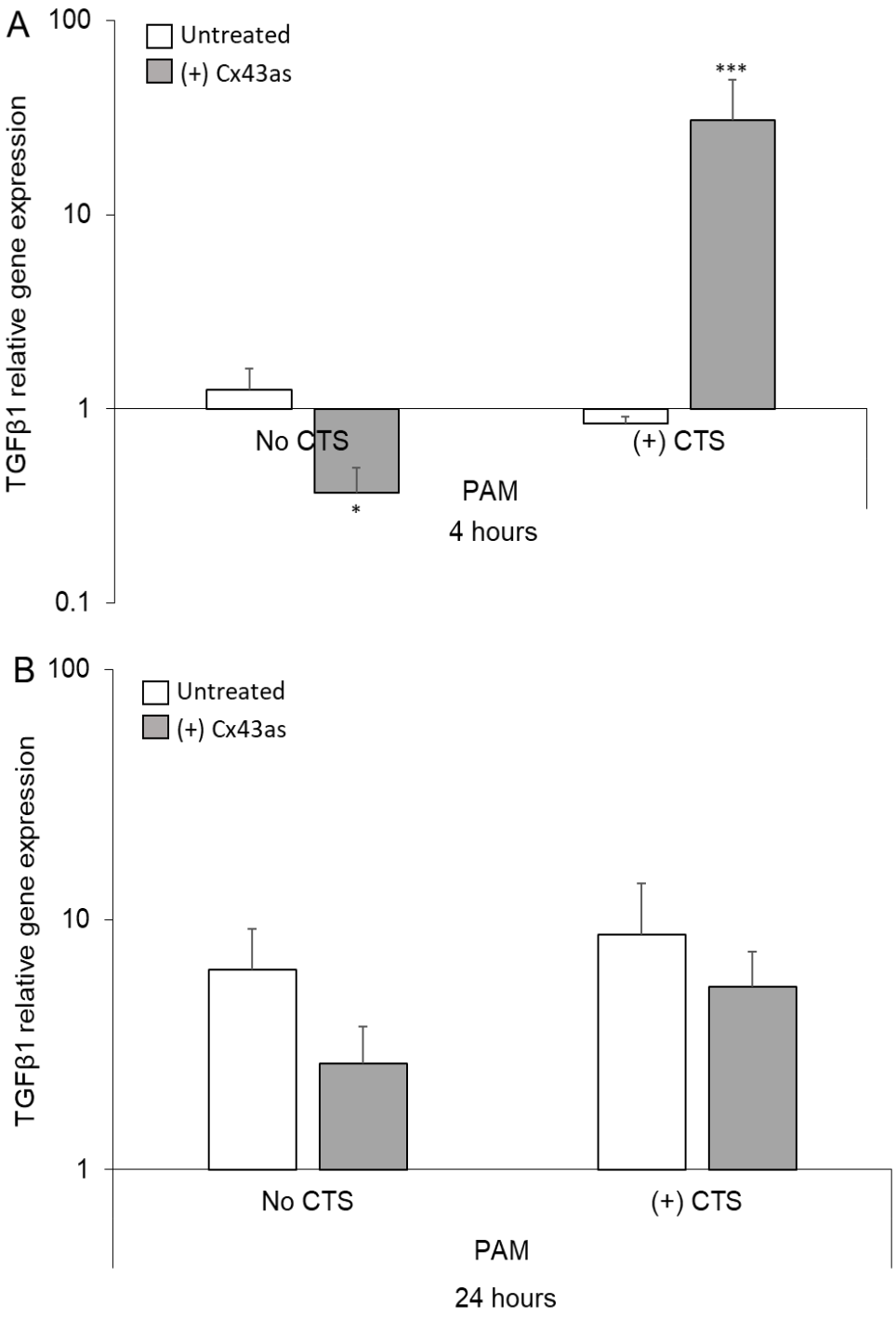

Figure 5.23: *The effect of CTS and Cx43as on TGFβ1 gene expression in preterm PAM taken from donors following iPPROM associated with open fetal surgery. AM were exposed to cycles of 1 minute strain and 9 minutes rest for 4 and 24 hours at a frequency of 1 Hz. Gene expression of CX43 were presented as ration values on a logarithmic scale and normalised to housekeeping gene GAPDH. In all cases, error bars represent and the mean and ± SEM values of n=6 replicates from n=3 separate donors where $^{+++}p < 0.001$ indicates comparisons between No CTS and (+) CTS while $***^{+}p < 0.001$ indicates comparisons between untreated samples and those treated with Cx43 antisense. PAM = placental amniotic membrane, CTS = cyclic tensile strain, Cx43as = Cx43 antisense.*

5.4 Key Findings

- SHG imaging of collagen showed dense collagen fibre alignment in the direction of applied strain in both PAM and CAM specimens. In both free-swelling controls and samples subjected to CTS, collagen fibrils aligned tangentially to the wound edge after 24 hours of trauma.
- AEC, AMC and myofibroblast nuclei aligned in the direction of applied strain.
- Following C43asODNs incubation, Cx43 plaques were qualitatively and quantitively reduced in AECs and myofibroblasts in CAM and PAM. After trauma and/or CTS, Cx43 plaques increased at the wound edge after Cx43sODN incubation.
- The effect of CTS had differential effects on mechanotransduction processes in sGAG, elastin, collagen content and PGE_2 release depending on clinical aetiology of preterm AM (iatrogenic preterm delivery due to fetal growth restriction, sPPROM and iPPROM associated with fetal surgery) and tissue type (PAM and CAM).
- Following Cx43 inhibition, AM weakening mechanotransduction mechanisms were decreased resulting in a reduction of sGAG content and PGE_2 release, and an increase of collagen and elastin concentration.
- Cx43 and TGFβ1 were differentially expressed following CTS in a tissue-dependent manner in all donor groups (iatrogenic preterm delivery due to fetal growth restriction, sPPROM and iPPROM associated with fetal surgery) after 4 and 24 hours.
- Cx43 inhibition consistently downregulated Cx43 gene expression in all donor groups.
- Cx43 inhibition led to differential expression of TGFβ1 following CTS in a tissue-dependent manner in all donor groups.

5.5 Discussion

Fetal membrane weakening and rupture depend on signalling triggered by mechanotransduction. Physiologically, the activation of pro-inflammatory factors, pro-apoptotic signals (TNFα, Bcl-2), MMP expression (MMP-9, 2), cytokines (IL-1β), collagenases (TIMPs) and COX1/2-activated prostaglandins all work in harmony to prepare the fetal membrane for parturition [151-153,160-168] . Other research groups have focused on the application of *in vitro* loading techniques including uniaxial, biaxial, inflation and/or puncture testing on human and animal FM explants and cell extracts to determine how repetitive stretching influences mechanotransduction signals that lead to membrane failure [218-225,230-234]. Importantly, researchers have primarily focused on term human FM, with limited work being done on preterm membranes [111].

In utero and *in vitro* experiments have shown FM respond to mechanical stimuli and stretching by activating COX-1/2 enzymes that synthesise prostaglandins and activate upstream transcriptional regulators AP-1 and NF-κB [219], secrete pro-inflammatory cytokines (e.g. IL-6, IL-8) and collagenases for ECM breakdown that prepare the membrane for rupture [218-221]. There is a lack of understanding of mechanotransduction mechanisms following fetal growth restriction diagnosis and spontaneous and iatrogenic PPROM from premature deliveries, thus this study aimed to further our knowledge into preterm AM weakening and trauma response.

In the present study, preterm AM was recruited from donors delivering before 36^{+6} weeks gestation and classified by (a) clinical outcome (FGR, PPROM, open fetal surgery-induced iatrogenic PPROM) and (b) delivery in early third trimester (≤32 weeks GA) versus late third trimester PPROM (≥32 weeks GA). The focus was placed on AM as it has been consistently found to be significantly more susceptible to mechanical and chemical changes during gestation and delivery [9,17,104-106,201,203,205]. The following sections will discuss the results in a gestational-age and aetiology-depended manner, while suggesting future prospects that can strengthen the current findings. Comparisons between results obtained from different preterm FM will be made where relevant. This will be followed by an analysis of the study strengths and limitations.

5.5.1 Changes in collagen fibre alignment and Cx43 expression following CTS and Cx43 inhibition

SHG imaging of collagen showed dense collagen fibre alignment in the direction of applied strain in both PAM and CAM specimens. Furthermore, in both free-swelling controls and samples subjected to CTS, collagen fibrils aligned tangentially to the wound edge after 24 hours of trauma. These results are similar to those seen in **Chapter 4** and in previous studies in term AM showing collagen alignment after 2% CTS and nuclei stretch at the wound edge, potentially due to myofibroblast differentiation and increase in surface tension [105,106]. It has been established, using uniaxial and multiaxial *ex vivo* models, that AM specimen geometry and direction of strain influences collagen alignment and content, particularly in the compact and fibroblast layers of the amnion [206]. Mazza's team used uniaxial and biaxial loading systems to characterise the mechanical response of human term AM after strain [206]. The authors determined that after application of strain, collagen fibres within the AM straightened and distended, concurrent with nuclei elongation of resident cell populations (including AECs) [206]. The collagen and subsequently hydration content of the membrane directly influenced its mechanical properties (measured as tension and creep), as collagenous fibres move in a viscous hydrated matrix [206]. A reduction in AM volume was measured microscopically by imaging the different layers and cell sub-populations [206]. SHG imaging showed that in the first 20 seconds of strain, the AM undergoes significant volume reduction but as stress time increases, collagen fibre alignment prevents permanent deformation and thus low creep, which is a measurement the tendency of a material to deform permanently under stress [206].

The elongated nuclei seen in the present study are in agreement with the aforementioned studies, as well as the ability of the AM to induce mechanotransduction changes and Cx43 protein expression after 24 hours of CTS. Nevertheless, the cell viability of the tissue was not measured in this study and thus we cannot know the direct effects on individual cell populations from imaging alone. In **Chapter 4**, I discussed the potential relationship between collagen, Cx43 and αSMA-expressing myofibroblasts. Following CTS, as seen in the **Appendix**, imaging of preterm AM tissue showed that AECs and AMCs in controls and traumatised samples were both

expressing amplified αSMA within cytoplasmic extensions and their nuclei aligned in the direction of applied strain. The mechanism by which resident cell populations are differentiating, and expressing αSMA is presumably different to the model used in **Chapter 4**, due to the applied strain and the fact that the present study utilised preterm AM.

Drawing parallels to our group's previous research and other reports in non-human primates [236], it can be concluded that repetitive stretching in preterm AM produced collagen fibre deformation [105, 236]. However, unlike Mazza's study [206], whether this deformation is non-recoverable has not been analysed. Changes in tissue thickness before and after application of strain and in free-swelling controls were not quantified either. Future work could focus on the determining the ability of collagen fibrils to return to random interwoven morphologies after repetitive stretching using not only SHG imaging but also more advanced imaging such as small-angle X-ray scattering.

In our previous studies, loss of collagen deposition and changes in alignment after mechanical stimulation altered elastin and collagen release, influencing downstream pro-inflammatory signalling pathways, including COX-2 and MMP expressions, and PGE_2 release [105,106]. Despite observed collagen alignment changes in preterm AM, collagen was not quantified with other techniques and thus it is not known whether the expressions of specific collagen types were altered after CTS. During pathological rupture, cytokines IL-1β and NF-κB were shown to enhance the secretion of MMP-9 and PGE_2 in the amniotic fluid of patients with chorioamnionitis and PPROM [129,163]. The consecutive actions of these proteins disrupt collagen fibril expression and elastin content in the AM, subsequently leading to tissue ripening and rupture [129]. Future studies could focus on the effect of strain on the expressions of collagen modifying enzymes (e.g. MMP-2, MMP-9) and collagen subtypes (e.g. collagen type IV) that are known to be activated during pathological rupture in preterm samples collected after PPROM [14,174,129,163].

Application of CTS led to elongated myofibroblast and AECs morphologies, particularly in samples treated with sense oligonucleotide in both PAM and CAM samples. The ability of AECs to undergo EMT to a migratory population was shown in small mouse defects and labour initiation in term human fetal membrane explants and scratch wound assays using primary AECs

[66,67,77,103,180]. As extensively described in **Chapter 4**, the ability of preterm AM explants to undergo EMT with defects and/or applied strain should be investigated in further studies. In the present study, the pixel intensity of αSMA and the volume of individual cells was not quantified, unlike in **Chapter 4**. This would be the first step in determining if there are any quantifiable changes in cell morphologies, followed by future work on the role of AEC transition and the purse-string contraction hypothesis in preterm AM defects using scratch-wound assays and/or MET-specific markers (such as E-cadherin).

Importantly, term AM studies determined that effects on mechanotransduction processes were strikingly different between PAM and CAM, with the latter having a weakened and less organised collagen orientation possibly owing to the presence of the ZAM in the cervical area [59,126,151-153]. In contrast, in the current preterm AM study, there were no significant changes in collagen orientation in PAM and CAM after CTS, suggesting that the preterm AM position has limited impact on how it behaves. The AM decreases in thickness and strength near term, thus differences between PAM and CAM collagen organisation may be less evident [193,194]. Additionally, the position of the cervical membrane in preterm AM is significantly trickier to determine than in term membranes, especially since preterm rupture can occur at any position of the tissue. This can influence the mechanobiology of the tissue regardless of whether the AM would have had a chance to rupture physiologically. The position of the ZAM is impossible to determine just by looking at the fetal membrane and the assumption that it is present within the CAM region collected would be incorrect without investigating it further with microscopy techniques and protein and gene expression assays, as it has been done by others [120-142].

Following C43asODNs incubation, Cx43 plaques were qualitatively and quantitively reduced in AECs and MFs in CAM and PAM. After trauma and/or CTS, Cx43 plaques increased at the wound edge after Cx43sODN incubation. Interestingly, in free-swelling controls, quantification of Cx43 protein per area showed Cx43 was upregulated to a larger extent in non-wounded tissue, a contrast to term AM studies which showed increased Cx43 expression at the wound edge, using the same model **(Chapter 4)**. As discussed in **Chapter 4**, the sub-cellular dynamic localization of Cx43 in the cytoplasm, nucleus or cell membrane was shown to have a differential

effect on Cx43 transcriptional activity and influence the efficiency of adhesion or cell migration [250,268-272]. As a contractile associated protein, Cx43 is upregulated during physiological and pathological rupture in the myometrium, resulting in accumulation of gap junctions to establish ionic coupling between myometrial smooth muscle cells for synchronization of their contractions [136,137,302]. Animal and human studies have shown that oestrogen, progesterone and prostaglandin isoforms are involved in the regulation of Cx43 expression and transport to the cell membrane during pregnancy and labour [302,307]. Cx43 was found to increase in early gestation and remain steady throughout pregnancy in both human myometrial tissues taken from term labour and spontaneous preterm labour, and in the guinea pig compared to non-pregnant animals [308]. Using an *ex vivo* organ bath by to expose the tissue to oxytocin followed by nitrous oxide, it was shown that Cx43 was S-nitrosylated by NO, correlating to increased Cx43 phosphorylation at S^{368} and promoted hemichannel open states [308]. These findings highlight the essential role of Cx43 gap junction function in regulating myometrial contractions and how interruption of Cx43 dynamics can influence preterm labour [307,308].

Despite evidence throughout the current study that Cx43 is a stretch-sensitive protein, there is insufficient evidence presented here and in the literature to suggest Cx43 is directly involved in the weakening mechanisms activated during FM pathological rupture. The following section (**Section 5.5.2**) will discuss the mechanotransduction changes in preterm AM after strain depending on clinical aetiology and to assess whether Cx43 pharmacological knockout influences the results.

5.5.2 The effect of CTS and Cx43asODNs on mechanotransduction processes in preterm delivered AM

FGR is a complicated disorder, and research surrounding its aetiology has focused mainly on placental abnormalities and genetic markers. Altered functional and structural vascular adaptations in the placenta can lead to preeclampsia, a major risk factor for FGR, small for gestational age babies, FGR and/or other complications such as preterm birth [326]. To date, there appear to be no studies on the mechanotransduction mechanisms of FGR-associated electively delivered preterm AM. There is evidence that women with pregnancies complicated by small fetal size and FGR are more likely to deliver spontaneously preterm, thus placental insufficiency may compromise the structure and function of AM and the fetal membrane as a whole [326].

The results in the current study for increased sGAG and decreased collagen concentrations agree with those seen in term AM studies following CTS [105]. In contrast, elastin concentration increased after CTS in both PAM and CAM regions, which is the opposite of the effects seen in term AM [105]. Conrad *et al*., 2022 performed a proteomic analysis on the umbilical cord (UC) of babies with FGR or FGR with preeclampsia [327]. The ECM of the umbilical cord is abundant in collagen, GAGs and elastin [327]. Following premature delivery due to FGR (mean gestational age 35.1 ± 3.3 weeks), proteins involved with extracellular matrix formation including procollagen, collagen alpha-1 chain, and matrillin were all downregulated in the UC [327]. Another study investigated the effect of insulin growth factor (IGF) and its binding proteins in regulating collagen type 1 turnover in cord plasma of small for gestational age babies with or without maternal preeclampsia (mean gestational age 28.7 ± 0.2 weeks) [328]. The authors found that cord plasma concentrations of serum markers of type I collagen synthesis and degradation were related to fetal growth, the levels being lower in small for gestational age infants and decreased with increasing gestational age [328]. The concentrations of these factors (as determined via ELISA assays) were showed to relate to IGF-I and type I collagen turnover [328]. As gestational age increases, there is considerable turnover of type I collagen during fetal growth [328]. Of interest to the current study, type I collagen is also synthesized in the placenta and in multiple layers of

the fetal membrane, suggesting that placental collagen turnover may contribute to the cord plasma markers for collagen I turnover [328].

Furthermore, significantly increased apoptosis of fetal membrane sub-populations were seen in FM taken from donors with FGR (gestational age range 30 - 37 weeks) [329]. Apoptotic cells were predominantly localized to the chorio-decidual layer of the chorionic membrane and thus there were less viable trophoblasts [329]. Increased apoptosis of FM cells during critical fetal development stages may impair molecular functions of the FM that are involved in fetal growth and could be a contributing factor to FGR etiology [329]. Nevertheless, this would require further study and, not my knowledge, has not been currently investigated in the literature [329].

In FGR samples, PGE_2 release remained statistically unchanged following CTS. This could be due to multiple factors: Firstly, PGE_2 in both groups is elevated compared to term studies, with or without CTS (maximum PGE_2 release 2500 pg/mL in term versus 12000 pg/mL in preterm FGR) [105]. High PGE_2 release indicates activation of uterine contraction phenotype that contributes to cervical ripening followed by increase in chondroitin sulphate synthesis [330,331]. Furthermore, PGE_2 release has been associated with inflammation and preterm labour in intact membranes [332]. Interestingly, in a rat FGR model, the overexpression of COX-2 and PGE_2 receptor in the placenta aggravated uterine-induced ischemia associated with PGE_2-induced vasoconstriction [333]. Further studies will need to be performed to elucidate the role of PGE_2 in the tissue weakening mechanisms of FGR membranes, particularly its role in angiogenesis and vasoconstriction that may influence fetal growth.

Inhibition of Cx43 with Cx43ODNs samples in all conditions significantly decreased the tissue wakening effects of CTS for sGAG, collagen and elastin content. There are no current studies that have investigated Cx43 expression and inhibition in the fetal membranes, with the exception of the research from our group [105,106]. However, studies in the placenta have shown that expression of a dominant negative form Cx43 increases the expression of angiogenic factor VEGFA, which alters decidua angiogenesis [334]. This leads to disorganised and abnormally dilated maternal blood spaces, decreasing the surface area available for blood exchange and affecting the growth of the fetus [334]. In **Chapter 7 Section 7.2**, I will explore future experiments

that may provide insight into the mechanism by which Cx43 influences preterm AM weakening mechanisms, including those with FGR aetiologies.

Pathological changes that lead to spontaneous PPROM are broad [129]. Favourable neonatal outcomes can be related to GA, maternal factors and the latency between PPROM and delivery [320-326]. In both ≤ and ≥32 weeks GA, sGAG content significantly increased following CTS in both PAM and CAM. In CAM tissue, collagen content decreased after CTS in both donor groups, while in PAM the effect of CTS was reversed in ≤32 weeks GA samples. Studies in amniotic fluid have indicated that during pathological rupture associated with PPROM and chorioamnionitis, ECM components were irreversibly affected by cytokine (e.g. IL-1β and NF-κB) secretion, which in turn enhanced the release of MMP-9 and PGE_2 [129,163]. The consecutive actions of these proteins disrupted collagen fibril expression and elastin content in the AM, contributing to tissue ripening and rupture [129]. MMP-9 enzymatically breaks down type IV and V collagens and is mainly expressed by AECs, chorion leave trophoblasts, decidua parietalis, and placental syncytiotrophoblasts [76,154,126,164]. The expression levels of MMP-9 was increased in the FM of preterm and term donors that experienced labour as compared to non-laboured samples [335]. Additionally, fetuses delivered after PPROM had higher concentrations of MMP-9 than those with preterm labour with intact membranes, indicating potential pathogenic role of MMP-9 during a PPROM [336].

In a previous study by our group, the total activity of MMPs was increased following 2% CTS of term human AM, and was significantly decreased after Cx43 and Akt signalling pharmacological inhibition [105]. MMPs were not investigated in the current study, and thus we cannot conclude that enzymatic activity was enhanced after strain in preterm AM. Moreover, the mechanism by which this occurs remains to be elucidated. Moore's group used primary human AM explants to induce a PPROM phenotype followed by thrombin incubation [174]. Thrombin was shown to activate MMP-2, leading to a decrease in the mechanical properties of the AM after puncture testing [174]. Using FRET, one study showed that thrombin activity was higher in rupture sites of term AM compared to lower activity in preterm AM, including those with PPROM aetiologies [14]. In primary AMCs and in mice, thrombin injections were found to increase COX-2 mRNA, PGE_2

synthesis and MMP-1, 2 and 9 concentrations [14]. By using a selective PAR-1 inhibitor in primary AMCs, it was shown that the upregulation of MMP-9 was mediated by PAR-1 signalling [14]. The role of thrombin in the pathological mechanisms leading to rupture warrant further investigation in preterm FM following strain.

In human fetal membrane explants following preterm labour, cervical AM showed hyaluronic acid, a non-sulphated GAG, accumulated in between AM and CM in cervical FM concurrent with swelling in intermediate layers concurrent with twofold elevation in biglycan concentration, 30% decrease in collagen and 50% decrease in biglycan [337]. The increase of GAGs in response to CTS may indicate a breakdown of collagen-GAG intermolecular bonds but also to production of new GAGs to resist strain or promote wound repair that was ultimately unsuccessful due to repetitive strain. Where collagen and sGAG increased in PAM samples in donors delivering before 32 weeks GA, it may be due to an imbalance in the rate of collagen production and the rate of collagen breakdown, releasing sGAGs into the media. GAGs are also core components of proteoglycans and their presence could further indicate proteoglycan remodelling and/or breakdown. Free GAGs and proteoglycans directly bind to collagen, laminin and fibronectin to promote cell-to-cell and cell-to-ECM adhesion [115]. As there was a clear observed expression of αSMA in different subpopulations of preterm AM in the current study (**Appendix; Figures 5.24-5.27**), it would be of interest to determine if changes in GAGs following strain influence the differentiation and migration capacity of myofibroblasts. The influence of strain and trauma on proteoglycan, GAGs and collagen function, structure and concentration warrants further investigation, and it will be revisited in **Section 7.2** of **Chapter 7**.

Elastin concentrations did not significantly change after CTS in either PPROM cohort, with the exception of PAM samples which increased elastin content in ≥32 weeks GA samples. Elastin fibres in the fetal membranes and the AM have been visualised by Mauri *et al*., 2013 [112], but others have failed to consistently quantify elastin in term and preterm tissues [53,110,111]. Using a uniaxial tensile strain device (0 to 20% strain), Mazza's group correlated the stress-strain response of term human FM to a set of biochemical parameters, including collagen and elastin content [111]. Following 20% strain, collagen and elastin concentrations were found to decrease

and increase respectively [111]. Of interest to the current study, Mazza and colleagues reported that after uniaxial tensile strain (20% strain) was applied to an 'early delivery' preterm membrane (31 weeks GA), elastin values increased, while collagen content decreased concurrent with high stress-strain resistance [111]. Direct comparisons to this and the PPROM samples collected in the current study cannot be made, as there is no information presented in the paper on the reasons for preterm delivery of that FM [111]. ECM components, including elastin, increase in concentration as gestational age increases, and only begin to decrease close to term and/or parturition due to the biochemical changes that lead to the initiation of labour [193,194]. When comparing the current study with our previous mechanotransduction study in term AM [105], elastin concentrations was generally higher in preterm AM. However, the response to strain, as exemplified throughout this study, will be influenced by the aetiology and/or multiple complications leading to preterm birth, as well as whether delivery was vaginal, women had intact and ruptured membranes, and whether they experienced labour contractions if they did deliver via C-sections. The role of elastin in PPROM samples versus term FM should be further investigated and correlated to the mechanical properties (e.g. Fmax, stiffness etc) of membranes delivered after pathological and physiological rupture.

Mechanisms of iPPROM after open fetal surgery are multifactorial, thus this study aimed to elucidate mechanotransduction processes that could lead to weakening and rupture in AM derived from iPPROM donors. In contrast to sPPROM samples, after CTS, sGAG significantly decreased while collagen content increased in CAM, while in PAM sGAG decreased. As explored throughout this discussion, perhaps the rate of sGAG release and collagen turnover was significantly altered by both the trauma inflicted by the fetal surgery itself and later by the repetitive strain within the bioreactor. This is exemplified by the fact that sGAG concentrations were markedly higher in free-swelling controls taken from fetal surgeries versus those from sPPROM samples (mean 14.04 ± 3.29 μg/mg for fetal surgery, 5.63 ± 1.18 μg/mg for ≤32 weeks GA PPROM and 2.14 ± 0.87 μg/mg; **Appendix; Table 5.3**).

In response to CTS, both CAM and PAM samples presented with significantly elevated elastin content, with PAM specimens showing significantly higher % change in elastin content relative to those seen in CAM. This clear distinction between PAM and CAM could be due to the positioning of the trauma inflicted during open fetal surgery that was further away from the placenta. Nevertheless, there was no way to know where exactly the position entry of the surgical instruments were as these women delivered via C-section and subsequent trauma during that procedure influenced the mechanical properties of the FM.

Mechanotransduction mechanisms of AM taken after fetal surgery and subjected to strain have not been investigated in the past and thus our comparisons can only be made to studies of FM fetoscopic and surgical defects after delivery. Studies have investigated the effect of trauma by fetoscopic practices on the integrity of the fetal membrane. Researches have shown that at point of fetoscopic port insertion, cell apoptosis and damage in both the amniotic and chorionic cellular layers occurred [17,254]. Studies *in vitro* and in animal models have determined that prolonged exposure to CO_2 during gaseous distention for visualisation increased the likelihood of FM dehydration and iPPROM [172,207]. Within the stromal layers of the FM, collagen was shown to become brittle and damage to the amniotic epithelium triggered the release of MMPs, promoting pathological rupture relating to iPPROM [172,207,254]. Additionally, the gradual replacement of amniotic fluid with Ringer's lactate after fetoscopy has initiated apoptosis of AECs in the amniotic epithelial layer, further enhancing pathological mechanisms and increases the risk of iPPROM [207,254].

Postoperative choriomembrane separation (CMS) occurs in 20 - 40% of fetoscopic procedures, leading to collagen disruption, MMP release and rupture initiation [255,256.] Cell apoptosis and damage has been recorded in both the amniotic and chorionic cellular layers at the point of fetoscopic port insertion [17,254]. Carvalho's group showed an increase in collagen deposition at sutured defect sites concurrent with site-dependent gene expression alterations of MMP-1, 9 and TIMP-1, 2 in SBA open fetal surgery defects, suggesting a complex membrane remodelling process is occurring in response to trauma [18,259]. As in PPROM, MMP activity warrants further investigation in AM collected after open fetal surgery.

In PPROM samples and in AM taken following open fetal surgery, PGE_2 release remained unchanged after CTS, with limited differences between CAM and PAM specimens in both donor cohorts. However, in donors delivering after 32 weeks GA, Cx43 inhibition led to significant reduction of PGE_2 release in all conditions. PGE_2 overexpression is a marker of preterm birth and PPROM initiation [14,129,163]. *In vitro* and *in vivo* mouse studies have shown the release of fibronectin binding to AMCs via its extra domain and Toll-like receptor 4 instigated the activation of MMP-1 and 9 to act on collagen fibrils, increasing COX-2-mediated PGE_2 synthesis and NF-κB and ERK1/2 signalling [156]. The increased expression and activity of COX-2 and subsequent prostaglandin synthesis plays an essential role in the onset and progress of labour [226]. In the myometrium, the expression and activity of COX-2 has been shown to increase at term and with the onset of labour [226]. Furthermore, stretch experiments of sheep uterus resulted in increased COX-2 mRNA expression [227] while inflation of the human uterus with a balloon in postpartum women led to increased prostaglandin synthesis [228]. The lack of PGE_2 changes from free-swelling controls to CTS samples maybe due to irreversible damage from sustained trauma and strain during pathological rupture or surgical intervention. This is exemplified by the fact that PGE_2 release was higher in PPROM and fetal surgery samples compared to those at term [105] (maximum PGE_2 release 2500 pg/mL in term and maximum 11330 pg/mL in preterm).

Nevertheless, as in FGR samples, there is no clear connection between Cx43 and collagen, sGAG, elastin and PGE_2 expression in PPROM and iPPROM-derived AM. Despite a clear effect of Cx43 inhibition in some of the samples, the mechanisms by which Cx43 influences the mechanotransduction mechanisms in preterm AM remain to be elucidated. The results of this study are thus largely observational, and the response of Cx43 inhibition merely correlates with changes in ECM components (collagen, sGAG, elastin) and inflammatory mediators (PGE_2 and TGFβ1).

Our group previously determined that repetitive CTS and pharmacological knockdown of Cx43, AKT/PI3K and COX-2/PGE_2 signalling influenced the ECM composition of term AM [105]. In agreement with the present study, studies have showed that Cx43 is a stretch-sensitive protein in the AM and the myometrium in response to mechanical stimulation [105,306]**.** In osteocytes, Cx43

possesses a SER-373 substrate binding cite for AKT which following mechanical stimulation, activated Cx43 phosphorylation and enhanced Cx43 gap junction stability and α5 integrin cellular interaction [338,339]. Cx43 hemichannels facilitated PGE_2 release in osteocytes in response to mechanical strain, which could be a key event occurring during CTS of preterm AM [340]. The increased expression of Cx43 in chronic wounds (venous leg, diabetic or pressure ulcers) has been correlated with severe inflammation, MMP activity and subsequent collagen and elastin reduction [341,342]. Taking these findings into consideration as well as our previous work, future studies could focus on the influence of downstream AKT/PI3K, MEK and COX-2 signalling on preterm AM ECM composition and inflammatory factors (e.g. PGE_2, IL-6, MMP activity) in comparison to term AM.

Others have showed that in response to mechanical stimulation, IL-8 and PBEF expressions were significantly increased in preterm membranes delivered via C-sections [221]. PBEF is an anti-apoptotic cytokine involved in both early- and late-stage apoptosis and correlates with the reduction in caspase 8 and 3 activation [221], both of which have been shown to increase in expression in term non-laboured human AM, concurrent with Fas and Fas ligand expression and Bcl-2 activation [152,153]. In human FM with chorioamnionitis, PBEF expression was correlated with increased levels pro-inflammatory cytokines TNF-α, IL-1β, and IL-6 and LPS [223]. In primary AECs and WISH cells following treatment with NF-κB and AP-1 inhibitors, static stretch was found to increase the expressions of PBEF and IL-8 [222,225]. These results support the observation that PBEF is up-regulated in vivo during labour and provide an insight into the mechanism by which NF-κB, AP-1 and IL-1β control the up-regulation of PBEF [222-225].

In addition, application of 16% stretch in primary myocytes for 6 hours correlated with increased COX-2 protein levels, prostaglandin I2 metabolite and PGE_2 concentrations in the media [229]. In cells subjected to stretch, there was increased nuclear protein DNA binding activity of AP-1 but not of NF-κB, suggesting that human myocytes stretch results in increased COX-2 activity through activation of the AP-1 mechanism [229]. The same group investigated the effects of uniaxial mechanical stretch of primary AECs taken from term elective C-sections, showing that 11% stretch for 1 and 6 hours resulted in increased expression of COX-2 and PGE_2 production [219]. This was

concurrent with increased expressions of AP-1 and NF-κB and IL-1β, suggesting the involvement of both transcriptional regulators in AEC mechanotransduction mechanisms [219]. NF-κB and AP-1 have been shown by multiple research groups to influence the pathological mechanisms that lead to rupture, and warrant further investigation in preterm AM.

CAM and PAM specimens demonstrated differential responses to CTS, in agreement with previous studies showing distinct structural and mechanical differences between placental and rupture sites [59,154,155,201,203]. In all donor cohorts, Cx43 and TGFβ1 expression was expressed in a gestational-age, site-specific manner. At specific timelines (4 or 24 hours) Cx43 and TGFβ1 expression tended to be up- or down-regulated together (with exceptions), suggesting a synergy in inducing the weakening response.

This is further evidenced when looking at IMF imaging of Cx43 protein expression after CTS concurrent with αSMA-expressing MFs which are hypothesised to differentiate in response to Cx43 and TGFβ1 signalling. Treatment with Cx43 antisense significantly decreased Cx43 gene expression and led to tissue-specific (CAM or PAM) changes in TGFβ1 expression. PAM samples tended to have the most significant changes in Cx43 and TGFβ1 (with some exceptions in a GA-dependent manner), possibly owing to less inflammatory response near the placenta relative to the cervix, which contains the ZAM. However, this can only be assumed as the position of the AM in preterm donors may not necessarily possess a ZAM and instead inflammation is present throughout the whole AM and changes are site-specific due to surgical intervention (C-section, open fetal surgery) and/or poor oxidation due to FGR.

In FGR samples, there was no changes in TGFβ1 expression after CTS, except for statistically significant increase of TGFβ1 in PAM samples after 24 hours. This change also correlated to significantly increased Cx43 expression after 24 hours of intermittent CTS in PAM. After 4 hours of Cx43 inhibition, TGFβ1 significantly increased in strained samples and free-swelling controls in CAM and PAM respectively, while sustained Cx43 inhibition led to significant TGFβ1 significantly decrease across both treatments. TGFβ1 is a critical regulator of trophoblast invasion during placenta and fetal growth. In cord blood samples [343] and maternal serum [344] taken from IUGR donors, plasma TGFβ1 concentrations were significantly higher than in term

samples. In blood cord samples taken from vaginal deliveries, TGFβ1 was higher than those delivering via C-section, potentially owing to increased cytokine expression during physiological rupture [343]. The authors hypothesised that cord blood TGFβ1 concentrations in IUGRs could be attributed to the abnormal blood flow in IUGR fetal blood vessels which in turn increase shear stress [343].

Of interest to the present study, one group showed that TGFβ1 stimulated αSMA expression in primary placental chorionic villi cultured *in vitro* [345]. The authors observed that TGFβ1 levels (mRNA and protein) were significantly higher in samples taken from pre-eclamptic placentas versus healthy GA-matched controls, suggesting a paracrine action on villous stroma myofibroblasts expressing TGFβ1 receptors and activating TGFβ1 signalling via the activator phospho-Smad2 [345]. However, there are a few limitations to this study, namely that the chorionic villi were extracted and cultured *in vitro* which may influence their ability to regulate αSMA via TGFβ1 signalling and could be different to what is occurring *in vivo*. Further work in animal models and/or human explants are required to elucidate the relationship between TGFβ1 signalling, αSMA and placental/FM abnormalities leading to FGR phenotypes.

The role of TGFβ1 in PPROM and FM wound healing has been extensively discussed throughout this thesis. Using mouse models, human AECs *in vitro* and FM explants exposed to CSE to induce PPROM mechanisms, Menon's group released a series of studies showing p32MAPK can be activated via TGFβ1 and is concurrent with p53-mediated senescence [132,186-188]. In a mouse model, biglycan and decorin signalling depended on TGFβ1 expression in a gestational-dependent manner to control MMP-8, 9 activity and collagen IVα1 degradation [168]. These studies create a link between TGFβ1 and FM weakening in PPROM activation and thus warrant further investigation into TGFβ1 signalling, which will be explored further in **Section 7.2** of **Chapter 7**.

Cx43 inhibition had a clear down-regulatory effect on TGFβ1 in growth restricted AM and sPPROM samples, with notable exceptions in FGR and ≥32 weeks GA sample particularly in PAM after CTS. In contrast, TGFβ1 tended to be upregulated after Cx43 inhibition in fetal surgery-derived CAM and PAM after CTS. The inflammatory pathways that lead to initiation of

rupture are presumably different than those activated due to surgical intervention and trauma. Using term AM and primary AM cell lines, researchers have elucidated that in the ZAM, pro-apoptotic factors (FOXO4, caspase-3 and 8), cytokines (IL-1β, 6 and 8, TNFα) and ROS work in synergy to activate MMPs (2, 9 and 13) and COX-2 mediated expression of PGE_2 [120,151,153,159,163,164,]. These molecules induce collagen degradation and loss of AM structural integrity, leading to rupture. In contrast, surgical intervention will cause accumulation of blood, immediate cell apoptosis and collagen degradation at the site of incision [17,236]. Thus, harnessing the differential effects of Cx43 inhibition in a gestational-age and clinical indication matter must be considered in future investigations. The implications of these findings will be further discussed in **Chapter 7.**

5.5.3 Study strengths and limitations

For this study, preterm FM was collected in a systematic way, and we were specific about the clinical indications and diagnosis used for experiments. Thus, we rejected some preterm deliveries that were not in the scope of the study despite the limitations associated with collecting preterm FM as described below. Initially, all preterm donors were grouped together, and the first biochemical experiments were performed without separating them into the distinct groups. As patient number increased, significant variability between donors arose and thus I, with the guidance of my supervisors and clinicians, decided to split the donors into three separate cohorts. The BOSE bioreactor methodology was extensively optimised by previous members in our lab group in the past. The choice to use 2% CTS strain for 1 minute strain and 9 minutes rest was to best represent labour contractions, however as contractions increase with time, more CTS conditions could be investigated in the future. In the current study, AF taken from the same donor was not used as those in **Chapter 4**. To obtain patient-matched AF from preterm donors would be extremely challenging, however future work could focus on using AF taken from fetoscopies or drainage instead of media. Biochemical assays, qPCR and IMF/SHG quantifications were further optimised by previous lab members and by me to ensure accurate experimentation protocols.

Preterm donors were recruited before delivery depending on when they underwent emergency C-section relative to their diagnosis. Thus, it was extremely challenging for different healthcare professionals, midwives, doctors on call and consultants to be aware that placentas needed to be preserved for scientific research if delivery times were outside working hours regardless of whether a patient had agreed to participate in the study. There were major challenges faced with discussing research with women at risk of preterm birth who are anxious, and who may have other personal reasons for not participating in research.

To overcome these challenges, I actively communicated with research midwives daily, and they would inform me when there were preterm deliveries occurring. I further liaised with the fetal surgery coordinators and Prof Jan Deprest who informed me when there would be fetal surgeries and deliveries associated with fetal surgeries that I could attend. I also spent a significant amount

of time on the labour ward waiting for preterm deliveries to occur after I consented patients. To best approach patients with FGR clinical indication, I spent many weeks at the preterm clinic shadowing consultants and observing routine ultrasounds to identify the mums who were at risk of delivering FGR babies preterm and consented them in advance of delivery. Furthermore, the identification of CAM and PAM areas in preterm FM was challenging, as I had to ensure the surgeon performing the C-section was aware to place a sterile clip near the cervical FM. This frequently required me to be present in the surgical theatre during deliveries.

As in **Chapter 4**, the present study relies heavily on correlation and not causation evidence. Despite pharmacological knockdown of Cx43, the mechanisms by which that influenced the mechanotransduction processes in preterm AM have not been elucidated. Cx43 antisense targets the mRNA of Cx43 inducing mRNA cleavage, and thus both gene expression and protein analysis is required to determine if Cx43 expression has been successfully decreased. Despite using IMF confocal microscopy to quantify Cx43, other protein analysis methods should have also been used, including Western blots. In **Chapter 4** discussion, the limitations associated with the Cx43 antibody and potential cross-reactivity were discussed, and future studies should focus on replacing the protein analysis from IMF microscopy to Western blots.

Cx43 expression was not found to be consistently downregulated at both timelines in all patent cohorts, suggesting the antisense may have degraded and the effects of the mRNA inhibition was diminished at an undetermined time point. It's essential to determine at which time point Cx43asODN degrades and is no longer effective, as this would undoubtedly influence the biochemical changes observed throughout this study. Despite using 4 and 24 hour time points, a comprehensive timeline of Cx43 inhibition must be performed by investigating the gene and protein expression changes of Cx43, especially in the first few hours of inhibition. Cx43asODN was placed within the media which fully submerged the AM, and the movement of the tissue within the bioreactor presumably aided in the distribution of the antisense throughout the sample. However, topical application of Cx43asODN may be favourable to ensure Cx43 is inhibited in a specific area of the tissue.

Previous research in our lab utilised a peptide amphiphile plug enriched with Cx43asODN to close 0.8 defects in term AM explants, leading to increased collagen levels and fibril expression across the defect [43]. However, the limitations with using plugs as vectors are associated with poor adhesion, integration, biocompatibility and decrease in resident cell population viability [43]. Lastly, antisense oligonucleotides are prone to binding to other single-stranded motifs or negatively charged proteins, resulting in off target effects that may affect mechanotransduction mechanisms in preterm AM [346].

The changes in expression of TGFβ1 in all preterm cohorts were correlated to changes in ECM components and PGE_2 release, however there are a myriad of other cytokines, growth factors and hormones alike that could be influencing the weakening mechanisms observed in this study. Targeting TGFβ1 may be the next step to determine whether it plays a role in the observed biochemical alterations. As described in **Chapter 4**, TGFβ1 is thought to play a role in the differentiation of AECs and AMCs in αSMA-expressing myofibroblasts, which in turn may influence the expression of ECM components seen throughout the current chapter. Pharmacological inhibition TGFβ1 will further elucidate its effects on myofibroblast populations as quantified by IMF confocal microscopy and appropriate imaging analysis. The current study did not quantify the changes in αSMA intensity and volume as in **Chapter 4**, rather only measured the nuclei elongation of all three cell subpopulations within the AM (AECs, AMCs, myofibroblasts). Nuclei changes are not indicative of differentiation and thus correct imaging analysis of αSMA and a combination of myofibroblast differentiation markers is required.

Inter-patient variability is another critical limitation in this study. Despite splitting donors into clinical indications, variability arose in all groups. Replicate numbers per donor ranged from n=6 to n=12 depending on the biochemical assay or qPCR performed, with each group having minimum n=3 separate donors per experiment. Inter-patient variability resulted in some cases where the average result changed relative to CTS but with no statistical differences were observed. Ensuring replicate values were high was important in minimising variability, but a larger cohort could be studied in the future to best characterise individual patients depending on their clinical indications. This will determine the most accurate donor grouping to best personalise potential PPROM

treatments. Lastly, controls in this study were samples cultured in 12-well plates. This led to the terminology of ‘free-swelling’ controls, as there was no applied strain for the duration of culture. In the future, controls could be placed in the bioreactor instead without applied strain to more accurately compare changes in samples with and without strain.

In conclusion, this chapter provided evidence that a combination of mechanical and inflammatory factors disrupts mechanotransduction mechanisms in preterm AM. Future directions for mechanotransduction studies and identifying potential targets for inhibition will be addressed in **Chapter 7.** Further optimisation of CTS conditions, pharmacological agents and donor availability must be addressed to characterise how the perturbation of pro-inflammatory and stretch-sensitive pathways translate to develop optimal FM sealing strategies.

5.6 Appendix

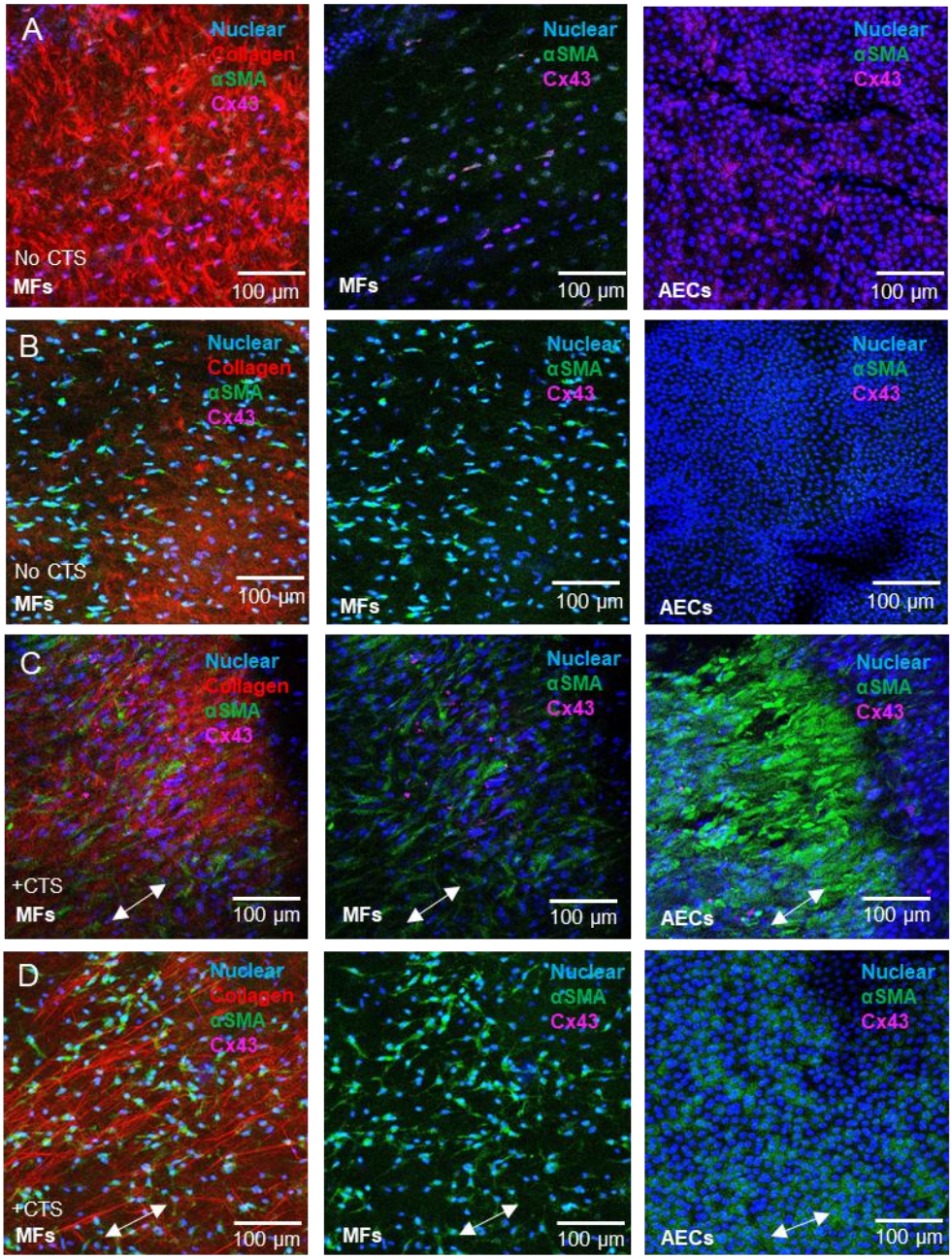

Figure 5.24: *Examination of immunofluorescent images of PAM specimens after CTS in the presence of Cx43sODNs and Cx43asODNs. (A & B) represent free-swelling controls after (A) Cx43s and (B) Cx43as incubation. (C & D) samples represent samples after CTS following (C) Cx43s and (D) Cx43as incubation. Following C43asODNs incubation, Cx43 plaques were reduced in all samples and αSMA expression increased, particularly in MFs. Application of CTS led to polarisation of collagen fibrils and nuclei in the direction of strain (white arrows) and an increase in Cx43 plaques after Cx43sODN incubation. CTS enhanced the expression of αSMA in both MFs and AECs, both of which formed elongated morphologies. White dotted lines show the location of the defect. MFs = myofibroblasts, AECs = amniotic epithelial cells, Sense = C43sODNs, Cx43as = C43asODNs, WE = wound edge. Scale bars = 100 µm.*

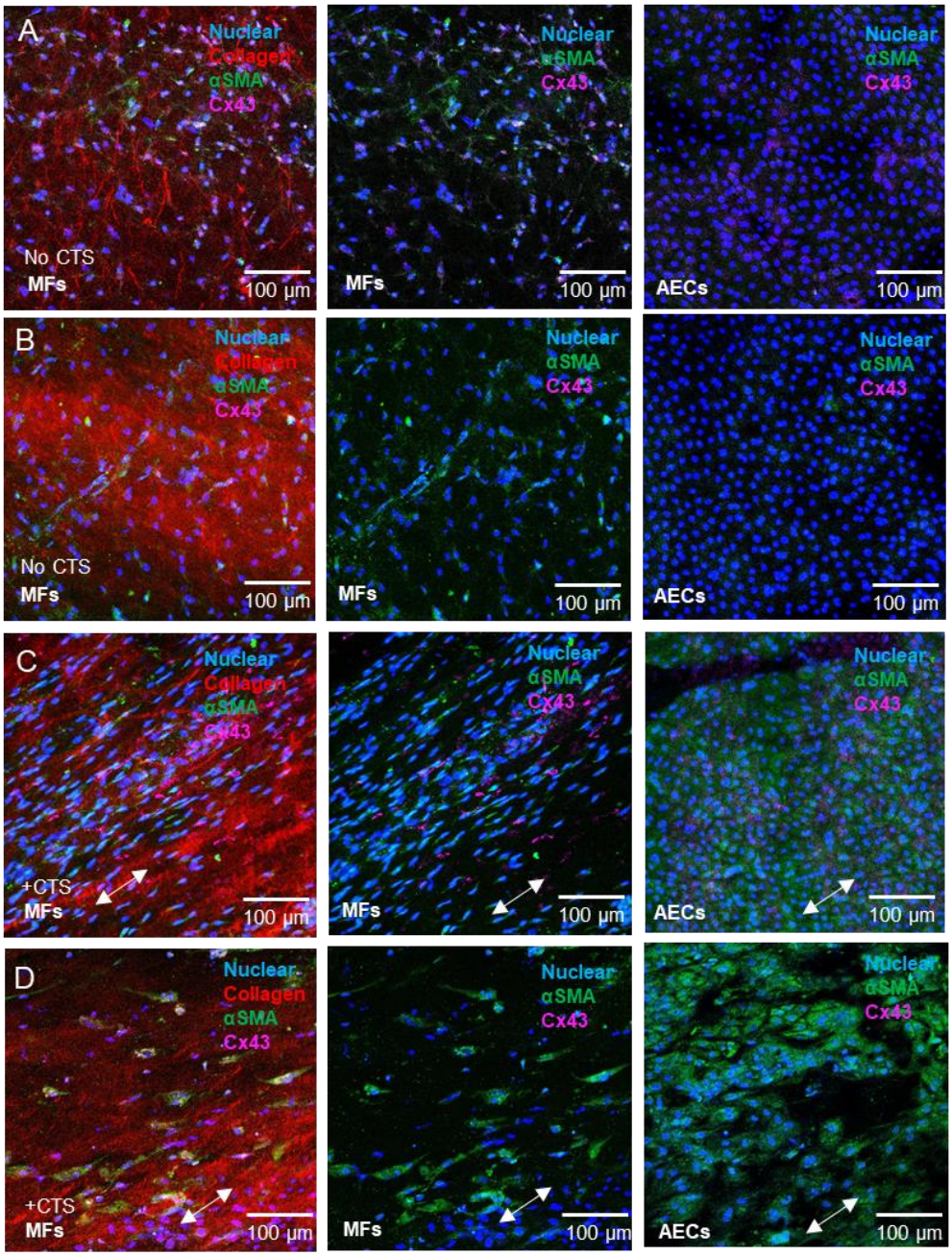

Figure 5.25: *Examination of immunofluorescent images of CAM samples after CTS in the presence of Cx43sODNs and Cx43asODNs. (A & B) represent free-swelling controls after (A) Cx43s and (B) Cx43as incubation. (C & D) samples represent samples after CTS following (C) Cx43s and (D) Cx43as incubation. Following C43asODNs incubation, Cx43 plaques were reduced in all samples and αSMA expression increased, particularly in MFs. Application of CTS led to polarisation of collagen fibrils and nuclei in the direction of strain (white arrows) and an increase in Cx43 plaques after Cx43sODN incubation. CTS enhanced the expression of αSMA in both MFs and AECs, both of which formed elongated morphologies. White dotted lines show the location of the defect. MFs = myofibroblasts, AECs = amniotic epithelial cells, Sense = C43sODNs, Cx43as = C43asODNs, WE = wound edge. Scale bars = 100 µm.*

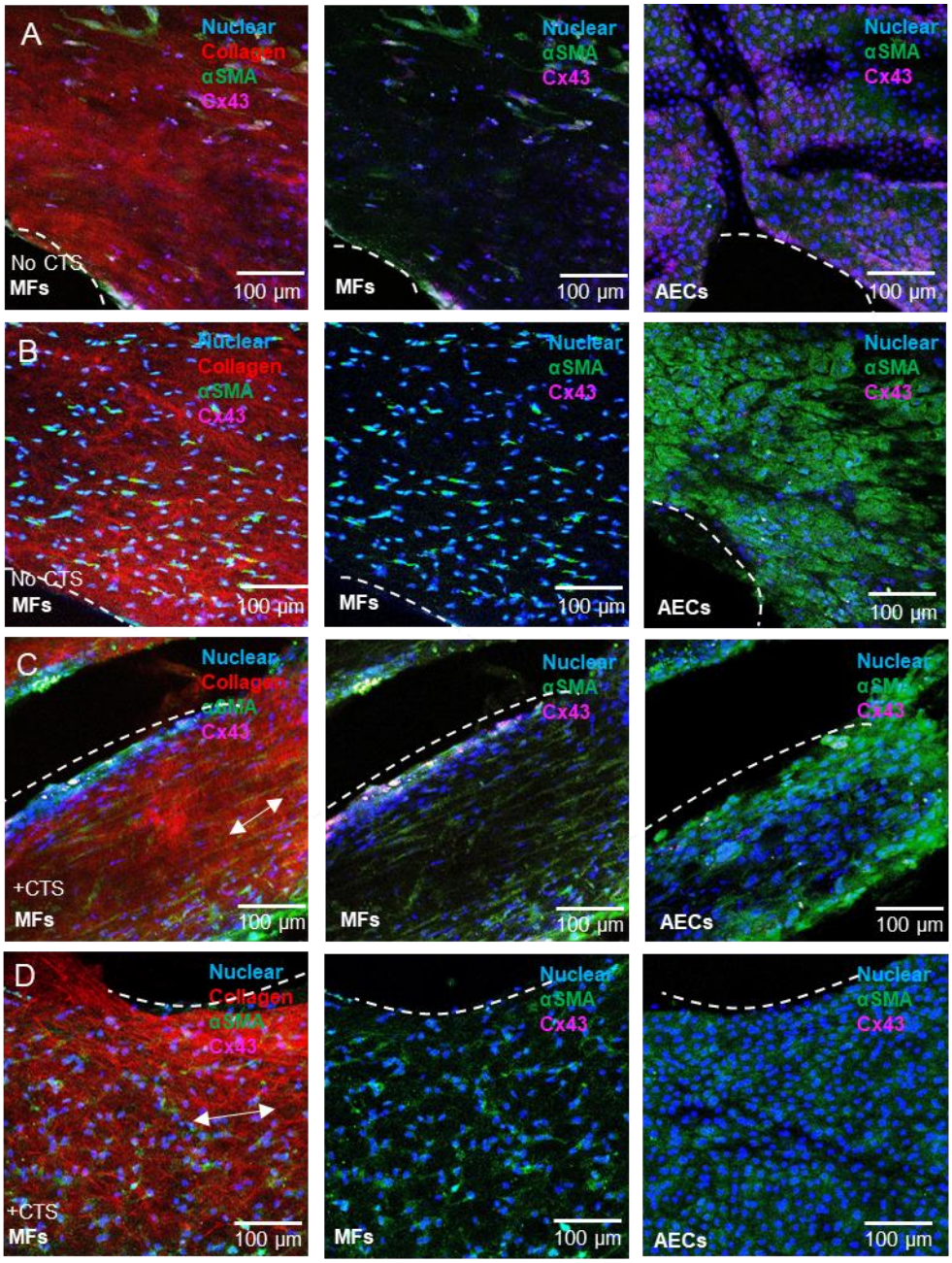

Figure 5.26: *Examination of immunofluorescent images of PAM specimens after CTS and trauma in the presence of Cx43sODNs and Cx43asODNs. (A & B) represent free-swelling controls after (A) Cx43s and (B) Cx43as incubation. (C & D) samples represent samples after CTS following (C) Cx43s and (D) Cx43as incubation. SHG collagen fibrils aligned tangentially to the WE after trauma. Application of CTS led to polarisation of collagen fibrils in the direction of strain (white arrows) and an increase in Cx43 plaques at the WE after Cx43sODN incubation. Following C43asODNs incubation, Cx43 plaques were reduced in both cell types, while αSMA expression increased, particularly in MFs. White dotted lines show the location of the defect. MFs = myofibroblasts, AECs = amniotic epithelial cells, Sense = C43sODNs, Cx43as = C43asODNs, WE = wound edge. Scale bars = 100 µm.*

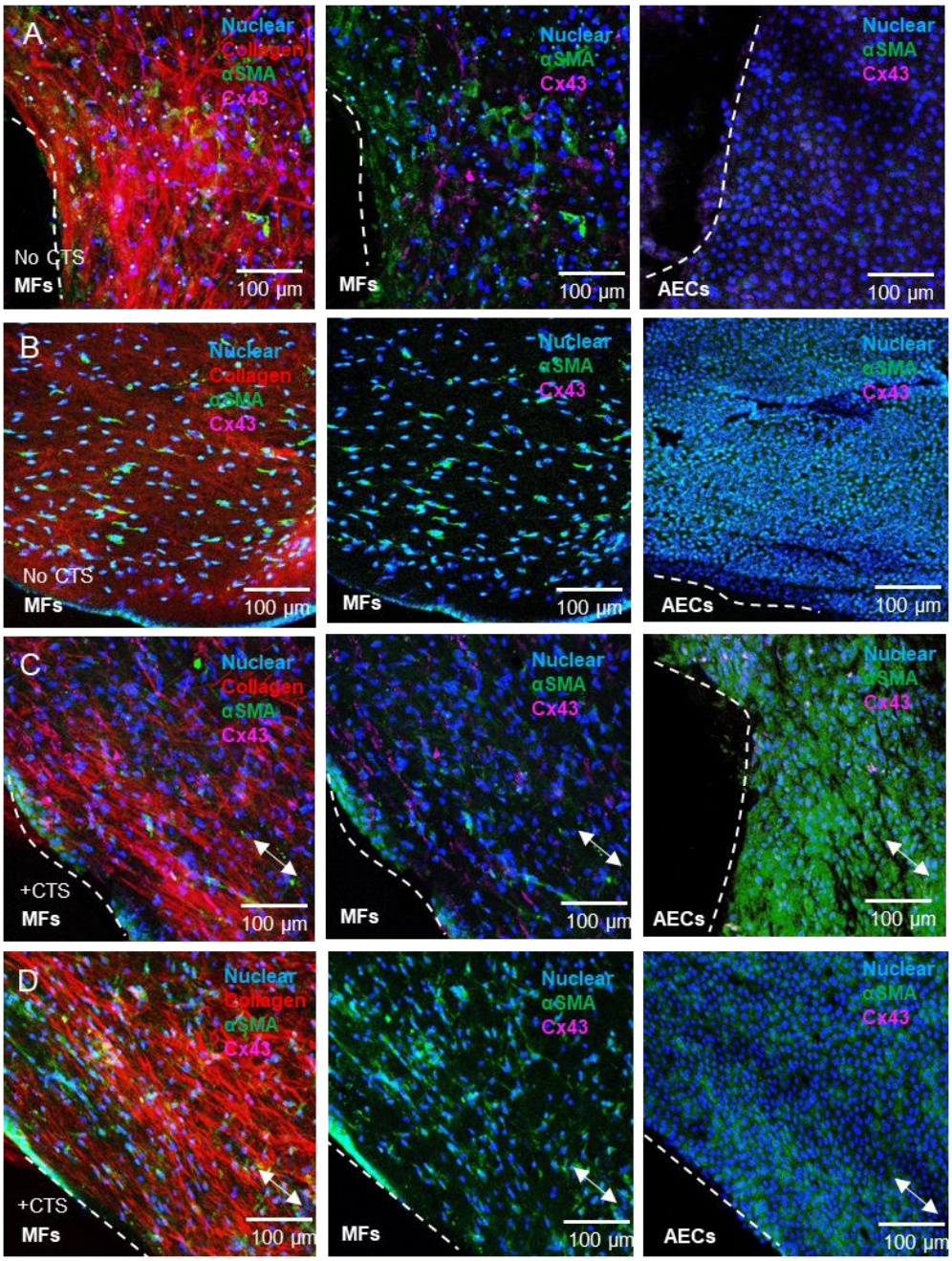

Figure 5.27: *Examination of immunofluorescent images of CAM samples after CTS and/or trauma in the presence of Cx43sODNs and Cx43asODNs. (A & B) represent free-swelling controls after (A) Cx43s and (B) Cx43as incubation. (C & D) samples represent samples after CTS following (C) Cx43s and (D) Cx43as incubation. Following CTS, Cx43 plaques were evident in pink staining at the WE in MFs and AECs after treatment with Cx43sODNs. SHG collagen fibrils aligned tangentially to the WE after trauma. Application of CTS led to collagen and fibril alignment in the direction of strain (white arrows) and an increase in Cx43 plaques at the WE after Cx43sODN incubation. CTS enhanced the expression of αSMA in both MFs and AECs. White dotted lines show the location of the defect. MFs = myofibroblasts, AECs = amniotic epithelial cells, Sense = C43sODNs, Cx43as = C43asODNs, WE = wound edge. Scale bars = 100 µm.*

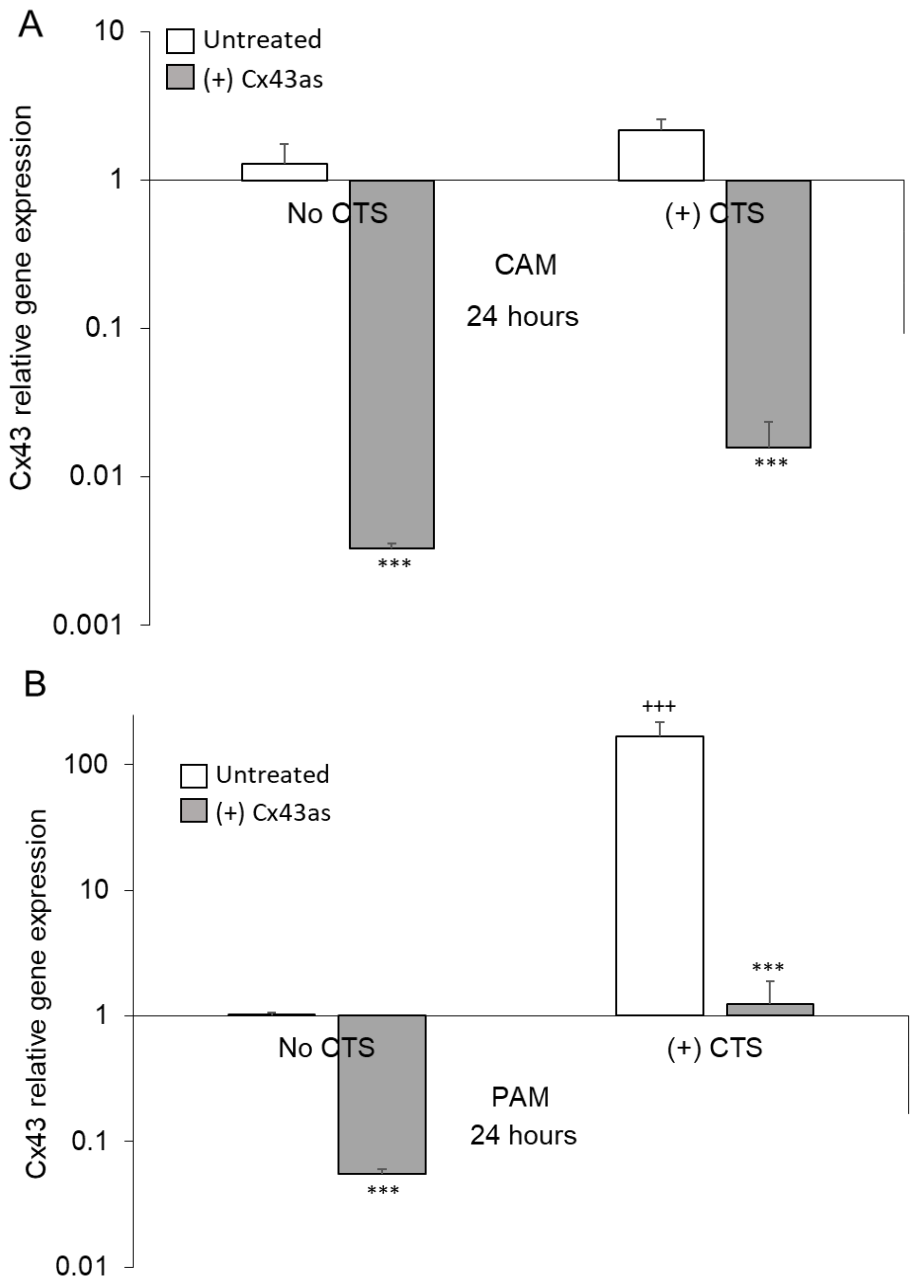

Figure 5.28: *The effect of CTS and Cx43as on Cx43 gene expression in preterm CAM and PAM taken from donors with FGR. AM were exposed to cycles of 1 minute strain and 9 minutes rest for 24 hours at a frequency of 1 Hz. Gene expression of CX43 were presented as ration values on a logarithmic scale and normalised to housekeeping gene GAPDH. In all cases, error bars represent and the mean and ± SEM values of n=6 replicates from n=3 separate donors where $^{+++}p < 0.001$ indicates comparisons between No CTS and (+) CTS while $^{***+}p < 0.001$ indicates comparisons between untreated samples and those treated with Cx43 antisense. CAM = cervical amniotic membrane, PAM = placental amniotic membrane, CTS = cyclic tensile strain, Cx43as = Cx43 antisense, FGR = fetal growth restriction.*

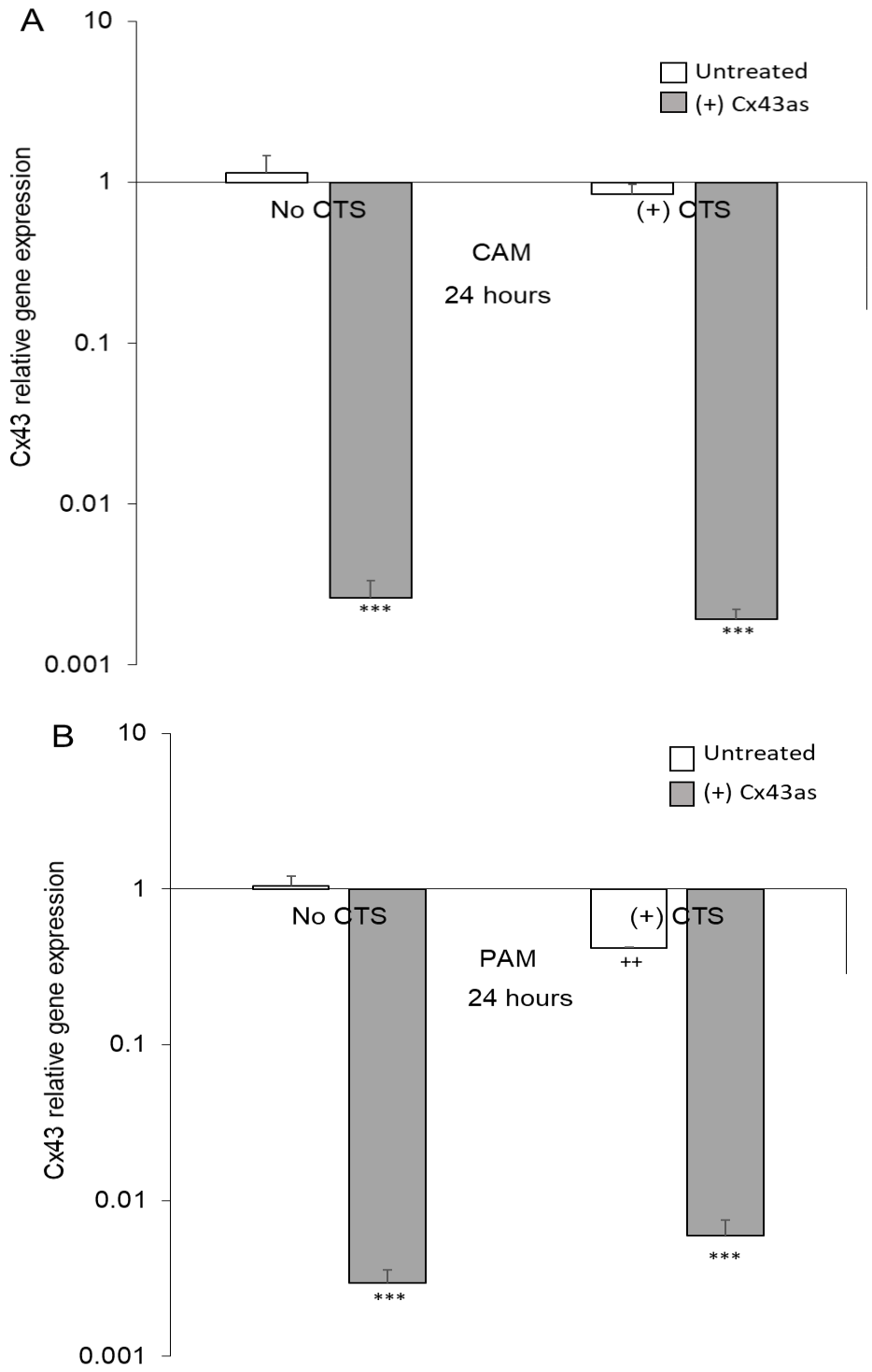

Figure 5.29: *The effect of CTS and Cx43as on Cx43 gene expression in preterm CAM and PAM taken from donors following sPPROM at ≤32 weeks GA. AM were exposed to cycles of 1 minute strain and 9 minutes rest for 24 hours at a frequency of 1 Hz. Gene expression of CX43 were presented as ration values on a logarithmic scale and normalised to housekeeping gene GAPDH. In all cases, error bars represent and the mean and ± SEM values of n=6 replicates from n=3 separate donors where $^{+++}p < 0.001$ indicates comparisons between No CTS and (+) CTS while ***$p < 0.001$ indicates comparisons between untreated samples and those treated with Cx43 antisense. CAM = cervical amniotic membrane, PAM = placental amniotic membrane, CTS = cyclic tensile strain, Cx43as = Cx43 antisense.*

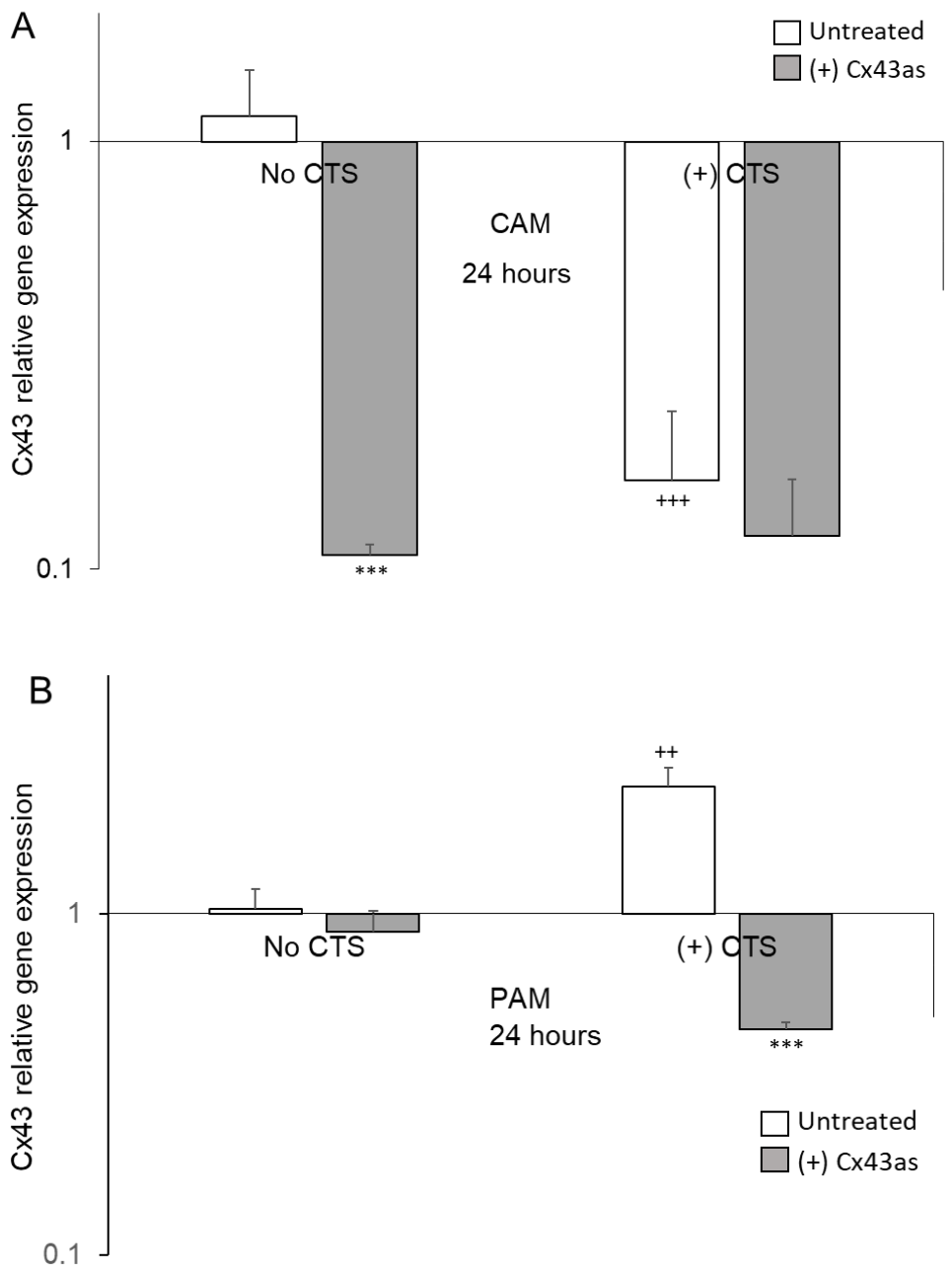

Figure 5.30: *The effect of CTS and Cx43as on Cx43 gene expression in preterm CAM and PAM taken from donors following sPPROM at ≥32 weeks GA. AM were exposed to cycles of 1 minute strain and 9 minutes rest for 24 hours at a frequency of 1 Hz. Gene expression of CX43 were presented as ration values on a logarithmic scale and normalised to housekeeping gene GAPDH. In all cases, error bars represent and the mean and ± SEM values of n=6 replicates from n=3 separate donors where $^{+++}p < 0.001$ indicates comparisons between No CTS and (+) CTS while ***$p < 0.001$ indicates comparisons between untreated samples and those treated with Cx43 antisense. CAM = cervical amniotic membrane, PAM = placental amniotic membrane, CTS = cyclic tensile strain, Cx43as = Cx43 antisense.*

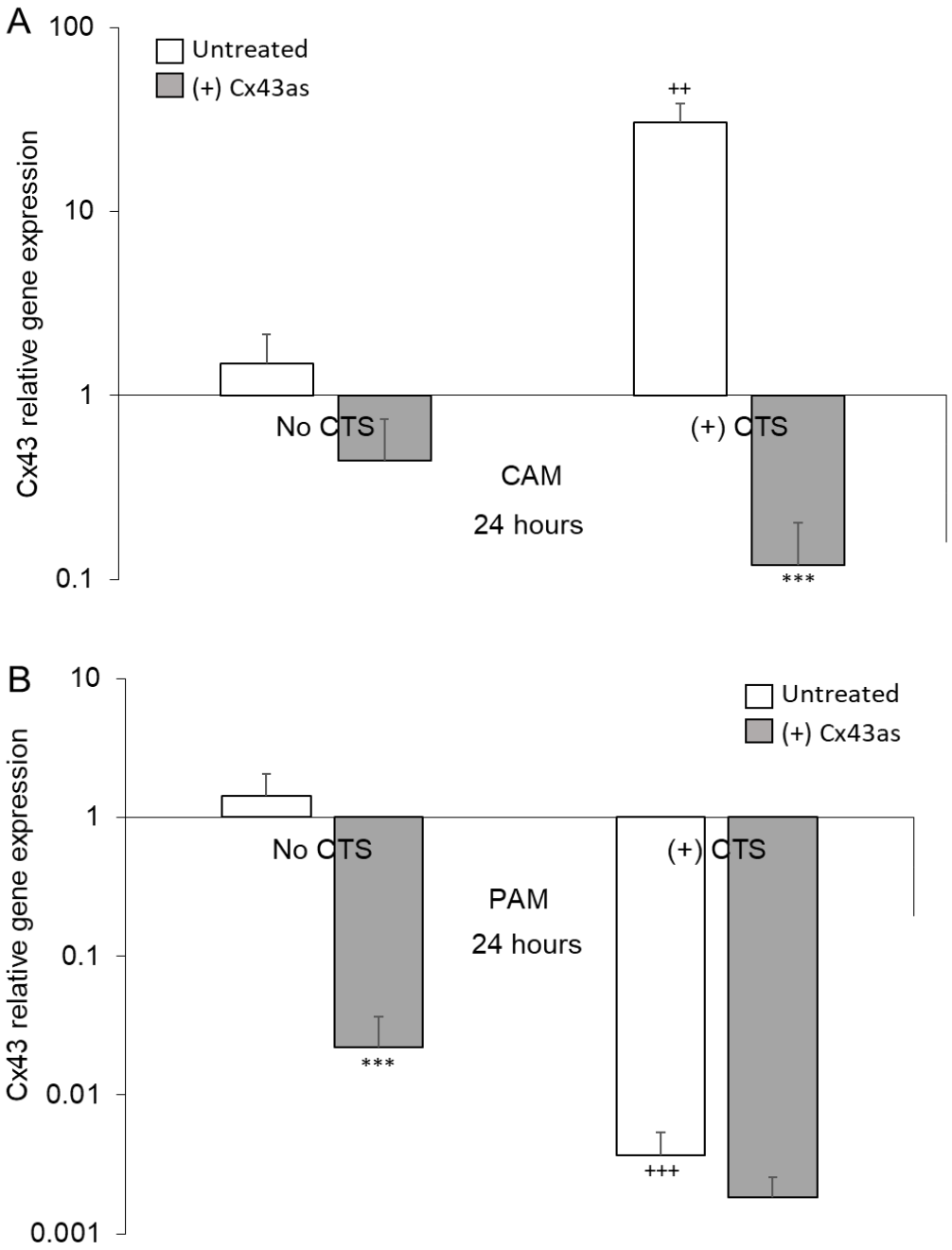

Figure 5.31: *The effect of CTS and Cx43as on Cx43 gene expression in preterm CAM and PAM taken from donors following iPPROM associated with open fetal surgery. AM were exposed to cycles of 1 minute strain and 9 minutes rest for 4 hours at a frequency of 1 Hz. Gene expression of CX43 were presented as ration values on a logarithmic scale and normalised to housekeeping gene GAPDH. In all cases, error bars represent and the mean and ± SEM values of n=6 replicates from n=3 separate donors where $^{+++}p < 0.001$ indicates comparisons between No CTS and (+) CTS while $^{***+}p < 0.001$ indicates comparisons between untreated samples and those treated with Cx43 antisense. CAM = cervical amniotic membrane, PAM = placental amniotic membrane, CTS = cyclic tensile strain, Cx43as = Cx43 antisense.*

Table 5.3: Average concentration of sGAG, collagen elastin and PGE_2 in preterm AM following CTS and Cx43 inhibition.

	Fetal growth restriction			
	GAG concentration (µg/mg)			
	CAM		**PAM**	
	No CTS	**(+) CTS**	**No CTS**	**(+) CTS**
Untreated	3.54	11.32	3.83	15.73
± SEM	0.69	1.54	0.66	1.13
(+) Cx43as	1.07	3.29	2.47	5.83
± SEM	0.03	0.12	0.09	0.29
	Collagen concentration (µg/mg)			
Untreated	6.76	2.95	9.36	2.14
± SEM	0.24	0.68	0.74	0.15
(+) Cx43as	6.76	5.08	14.97	8.12
± SEM	0.37	0.39	1.37	1.54
	Elastin concentration (µg/mg)			
Untreated	4.43	11.38	5.67	9.19
± SEM	0.21	0.34	0.80	0.91
(+) Cx43as	5.48	13.39	13.77	15.27
± SEM	0.70	0.24	0.42	0.80
	PGE_2 release (pg/ml)			
Untreated	5099.04	8172.16	7344.88	6958.97
± SEM	469.60	1264.95	1101.08	1262.43
(+) Cx43as	4142.81	4717.49	4556.23	4682.97
± SEM	544.80	291.86	386.13	289.77

	≤32 weeks GA PPROM			
	GAG concentration (µg/mg)			
	CAM		**PAM**	
	No CTS	**(+) CTS**	**No CTS**	**(+) CTS**
Untreated	5.63	8.52	2.64	6.44
± SEM	0.34	0.53	0.19	0.86
(+) Cx43as	0.82	1.58	1.33	3.12
± SEM	0.03	0.07	0.25	0.98
	Collagen concentration (µg/mg)			
Untreated	8.13	4.52	5.40	6.14
± SEM	0.86	0.35	0.15	0.26
(+) Cx43as	12.02	14.65	8.63	7.01
± SEM	0.28	1.14	0.30	0.60
	Elastin concentration (µg/mg)			
Untreated	6.86	7.21	10.23	11.61
± SEM	0.76	0.11	1.49	0.22
(+) Cx43as	12.61	15.21	16.70	29.41
± SEM	0.28	0.29	0.81	1.30
	PGE_2 release (pg/ml)			
Untreated	10555.56	11143.05	11081.83	10102.26
± SEM	262.40	344.89	317.94	223.91
(+) Cx43as	11139.51	9977.34	6036.99	10674.39
± SEM	278.21	206.58	1888.04	207.65

	≥32 weeks GA PPROM			
	GAG concentration (µg/mg)			
	CAM		PAM	
	No CTS	(+) CTS	No CTS	(+) CTS
Untreated	2.14	3.82	1.98	2.33
± SEM	0.25	0.08	0.10	0.02
(+) Cx43as	1.35	0.92	1.60	0.70
± SEM	0.10	0.06	0.06	0.05
	Collagen concentration (µg/mg)			
Untreated	11.32	8.87	5.70	8.09
± SEM	0.41	0.23	1.15	0.59
(+) Cx43as	15.46	22.47	10.74	10.24
± SEM	0.65	1.26	0.57	1.95
	Elastin concentration (µg/mg)			
Untreated	9.24	8.55	11.92	22.50
± SEM	1.13	1.13	0.23	2.67
(+) Cx43as	8.86	21.54	19.78	24.93
± SEM	0.33	0.73	1.55	0.71
	PGE_2 release (pg/ml)			
Untreated	10414.97	10044.27	10671.10	10552.38
± SEM	227.18	285.46	183.15	220.38
(+) Cx43as	3894.44	3913.14	3307.61	3792.99
± SEM	75.39	91.91	86.61	84.66

	Fetal Surgery			
	GAG concentration (µg/mg)			
	CAM		PAM	
	No CTS	(+) CTS	No CTS	(+) CTS
Untreated	14.04	10.20	4.75	7.57
± SEM	0.95	0.29	0.12	0.29
(+) Cx43as	4.17	2.40	2.69	2.63
± SEM	0.45	0.20	0.18	0.37
	Collagen concentration (µg/mg)			
Untreated	5.27	7.74	5.44	6.65
± SEM	0.21	0.25	0.08	0.20
(+) Cx43as	7.30	8.54	9.05	12.53
± SEM	0.17	0.57	0.41	0.36
	Elastin concentration (µg/mg)			
Untreated	7.48	11.52	6.67	14.15
± SEM	0.43	0.79	0.32	0.37
(+) Cx43as	8.85	14.63	15.81	26.07
± SEM	0.61	0.06	0.04	3.35
	PGE_2 release (pg/ml)			
Untreated	9969.52	10911.63	10951.26	11330.11
± SEM	152.73	312.82	413.15	357.51
(+) Cx43as	10001.86	9759.15	10482.24	10229.91
± SEM	73.57	184.45	141.36	99.39

Chapter 6

Cell morphology and collagen structural changes in large diameter FM defects

Chapter 6: Cell morphology and collagen structural changes in large diameter FM defects

6.1 Introduction

In this study, the morphological changes of the AM after spontaneous PPROM (sPPROM) and iatrogenic PPROM (iPPROM) following open fetal surgery were investigated. Patients with spontaneous PPROM delivering before 35 weeks of gestation presented with large rupture sites (1.5 to 4 cm) in the FM. Patients who underwent open fetal surgery for open spina bifida had rupture site sizes ranging from 3.5 to 7.5 cm in diameter. The differential effects of trauma on AECs, MFs and AECs cell population, as well as Cx43 protein expression and collagen fibril alignment of spontaneous rupture versus iatrogenic rupture was explored using IMF confocal microscopy and 3D imaging. **Chapters 1** and **2** describe in detail the differences between spontaneous and iatrogenic PPROM.

6.2 Methods

6.2.1 Patient recruitment

Pre-term human placentas were collected (*n*=3 sPPROM*,* average defect size 2.5 cm*, n*=4 iPPROM, open fetal surgery, average defect size 6 cm) **(Table 6.1)** with informed consent from women undergoing delivery by elective caesarean section at University College London Hospitals. Women with preterm premature ruptured membranes, open fetal surgery for open spina bifida and/or fetal growth restriction were included. Women with multiple pregnancies were excluded from this study. A comprehensive list of all donors collected with their clinical details is included in **Table 6.1**.

6.2.2 Image analysis and Quantification

Chapter 3 describes in detail the protocols for tissue fixing with PFA and immunofluorescence techniques. Using IMF confocal microscopy and SHG imaging, we visualised (a) spontaneous PPROM rupture sites and (b) open fetal surgery defect sites **(Figure 6.1).** Amniotic membranes were separated from chorionic membranes via gentle traction and analysed. Quantification of Cx43 plaque distribution, collagen fibrillar alignment and nuclei deformation was performed for each patient group (*n*=3 patients sPPROM and *n*=4 patients open fetal surgery) as described in **Chapter 3**.

6.2.3 Statistical analysis

Tissue was collected from 7 donors as detailed in **Table 6.1.** For immunofluorescent experiments, data represents the mean and SE values of 6 replicates from three separate donors, as indicated in figure legends. To compare Cx43 plaque intensity and nuclei directionality between defect sites and controls, a student's T-test was performed. All statistics were combined with a multiple *post hoc* Bonferroni test to yield corrected p-values. Values with over 95% confidence rate were considered significant ($p < 0.05$). Significance was denoted as follows: *$p < 0.05$, **$p < 0.01$ and *** $p < 0.001$.

Table 6.1: *Clinical information for patients collected for preterm studies for Chapter 6. All patients delivered preterm (before 37 weeks GA). Patients with sPPROM at delivery where rupture defects were evident are indicated. Patients who underwent open fetal surgery and had evident defects are also indicated. All deliveries were performed via emergency Caesarean section.*

Patient ID	Maternal Age	GA at delivery (weeks)	Surgical Intervention	Complications during pregnancy	Complications & findings at delivery	Clinical Indication
Patient 4	30	29^{+0}	None	Placental insufficiency and FGR	Rupture hole = 4 x 4 cm	FGR and PPROM <32 weeks
Patient 9	27	29^{+1}	None	PPROM occurred 24-36 hours before delivery	Rupture hole= 1.5 x 2 cm near placenta. Emergency C section due to abnormal fetal heart rate	sPPROM <32 weeks
Patient 10	32	35^{+6}	None	PPROM at 32 weeks Placental insufficiency	Delivery 4 weeks after sPPROM. Rupture hole= 3 x 2.5 cm starting from the placenta	sPPROM >32 weeks
Patient 13	31	34^{+6}	Spina bifida repair at 24+0 weeks	No infection present after surgery.	Delivery 10 weeks after surgery. Hole=3.5 x 4 cm	Spina bifida surgery
Patient 14	25	35^{+0}	Spina bifida repair at 25+0 weeks	No infection present after surgery.	Delivery 10 weeks after surgery. Hole=7.5 x 6 cm	Spina bifida surgery
Patient 15	26	34^{+0}	Spina bifida repair at 24+0 weeks	No infection present after surgery.	Delivery 10 weeks after surgery. Hole=7 x 5 cm	Spina bifida surgery
Patient 16	30	35^{+0}	Spina bifida repair at 24+0 weeks	No infection present after surgery.	Delivery 11 weeks after surgery. Hole=5.5 x 6 cm	Spina bifida surgery

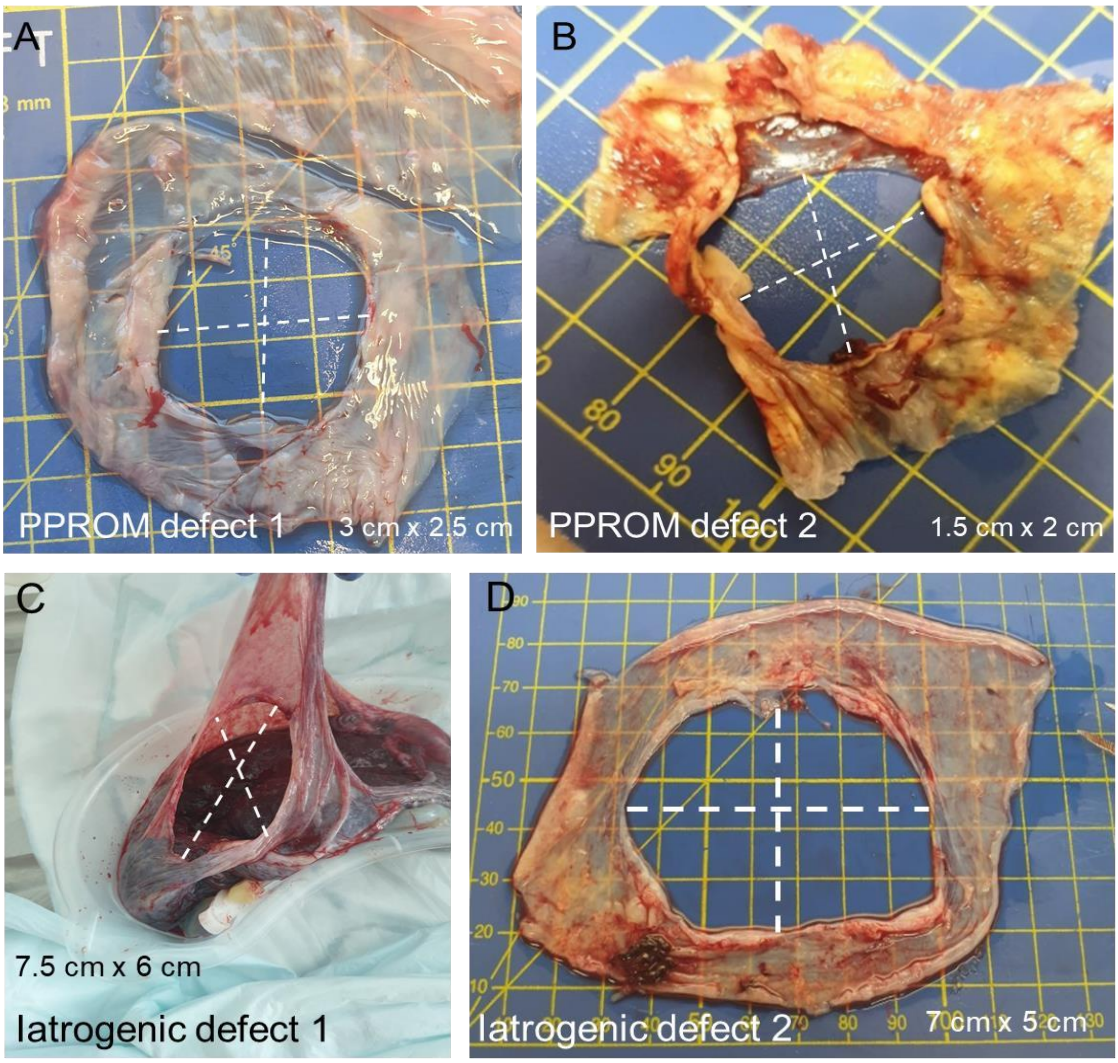

***Figure 6.1**: Representative images of defects after spontaneous PPROM and preterm birth following open fetal surgery. (A) PPROM defect from a patient delivering at 29^{+1} weeks GA after sPPROM at 24 hours before delivery and abnormal fetal heart rate. (B) sPPROM defect from a patient delivering at 35^{+6} weeks gestation following sPPROM at 32 weeks and placental insufficiency. Both defects were found to be close to the placenta. (C) Iatrogenic defect from a patient delivering at 35 weeks gestation after spontaneous preterm birth following open fetal surgery at 25 weeks. (D) Iatrogenic defect from a patient delivering at 34 weeks after spontaneous preterm birth following open fetal surgery. Defect sizes are indicated on each image. GA = gestational age, sPPROM = spontaneous PPROM, iPPROM = iatrogenic PPROM.*

6.3 Results

This section analyses IMF images taken from defect sites of AM from women that delivered preterm due to sPPROM or iPPROM associated with open fetal surgery.

6.3.1 Morphological changes and changes in Cx43 expression at the defect site after spontaneous PPROM

Representative images of one sPPROM defect site are shown in this section. Using pair-wise stitching, 15 individual images take at 25x magnification were stitched together to display immunofluorescent imaging of a representative AM sPPROM defect site after delivery following 24 hours of rupture **(Figure 6.2).** At the defect edge, myofibroblasts changed morphologies and expressed αSMA relative to controls and produced long extended cytoplasmic extensions aligned along the wound **(Figure 6.2B, C & F).** Collagen fibres were polarised tangentially to the wound and had elongated morphologies relative to controls **(Figure 6.2D & E).** AECs migrated at the edges of the wound and formed cellular clusters in comparison to uniform epithelial layer in controls **(Figures 6.2D & G-H).**

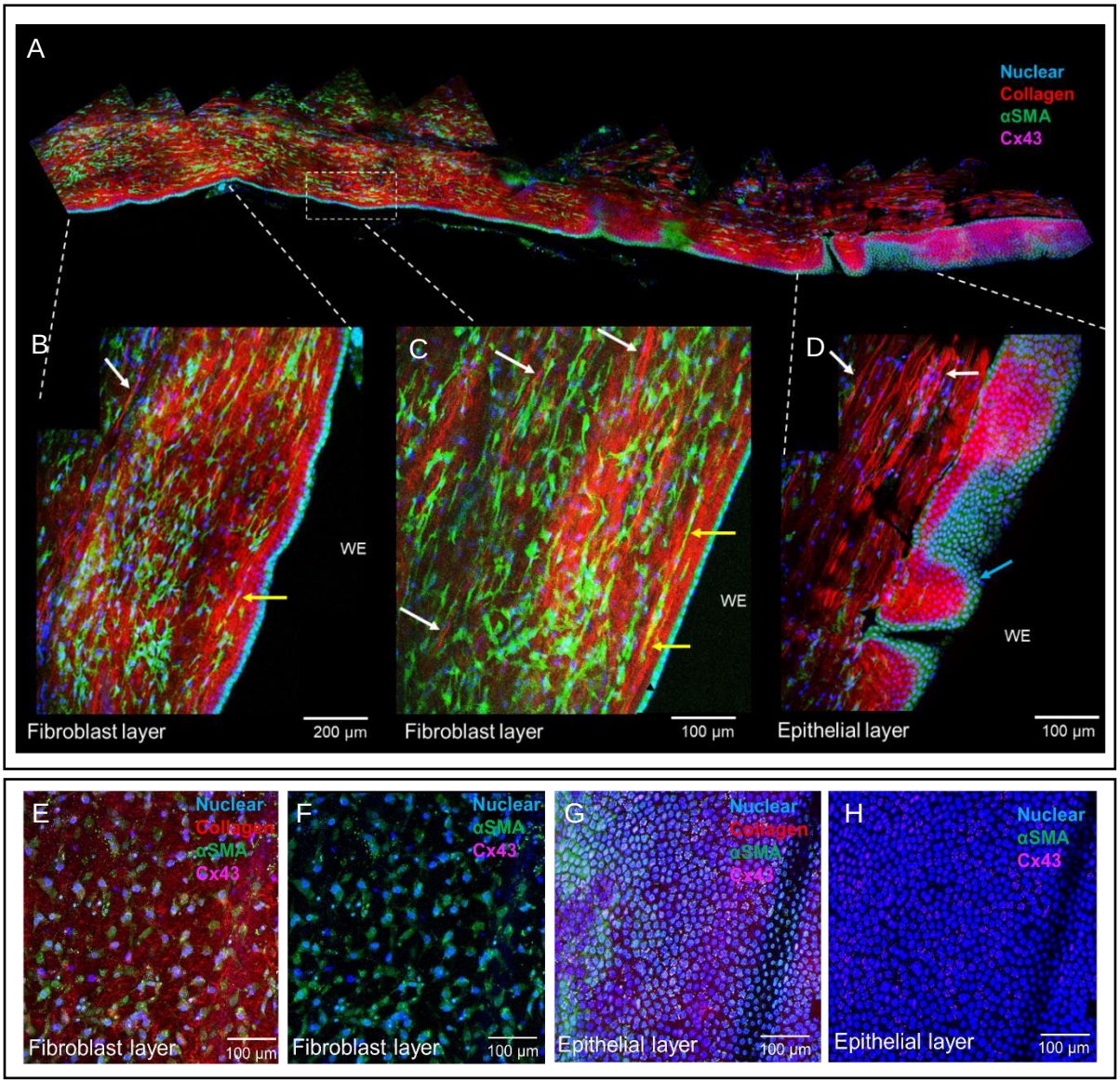

Figure 6.2: *Immunofluorescent imaging of an AM sPPROM defect site after 24 hours of rupture. The figure shows representative images from one donor (total donors n=3). (A) Pair-wise stitching of 15 individual images taken at 25x magnification. (B) Pair-wise stitching of two images, while (C) is one image taken at 25x magnification. Changes in myofibroblast morphology and αSMA expression across the defect is evident relative to controls (E, F). MF concentration at the defect increased, cells became polarised around the wound and cytoplasmic cell projections stretched out along the edges (yellow arrows showing cytoplasmic extensions). Collagen fibres were aligned tangentially to the wound (white arrows, B-D) and had long elongated morphologies relative to controls. (D) Epithelial cells have migrated at the edges of the wound and formed cellular clusters (blue arrow) in comparison to uniform epithelial layer in controls expressing minimal αSMA (G, H). Cx43 plaques are evident in both the defect site and controls. AM = amniotic membrane, Cx43 = connexin 43, αSMA = alpha smooth muscle actin, sPPROM = spontaneous PPROM, MFs = myofibroblasts, WE = wound edge.* Dotted white lines indicate the margin of the defect. *Scale bars = 500 µm, 200 µm, 100 µm.*

Immunofluorescent images further indicated Cx43 plaques and nuclei deformation at the AM sPPROM defect site. Cx43 expression was increased at the defect site in both the epithelial and fibroblast layers **(Figures 6.2 & 6.3).** The highest concentration of Cx43 and the creation of distinct protein plaques (0.1 - 1 μm in size) formed within both the nuclei and cytoplasmic lamellipodia of αSMA-stained myofibroblasts **(Figure 6.2).** This is further evidenced after 3D slicing of the defect site showing individual frames of 1.5 microns in thickness and tracing individual elongated myofibroblasts following the direction of collagen fibril alignment **(Figure 6.4A & B).** In the fibroblast layer, myofibroblasts expressed significantly higher Cx43 plaque numbers (355.7 ± 36.3 pixels) relative to controls (209.7 ± 5 pixels), as evidenced by pixel analysis of Cx43 distribution per myofibroblast cell nuclei (**Figure 6.4D**, p value < 0.001) In the epithelial layer, Cx43 distribution in AECs at the rupture site was significantly higher than controls, but not as high as in myofibroblasts (**Figure 6.4D**, p value < 0.001). It's worth noting Cx43 expression in controls in both cell types was higher (106.3 pixels per nuclei in AECs and 355.3 pixels per nuclei in MFs) than those seen in artificially induced 0.8 mm defects (**Chapter 4,** 0.62 - 0.74 pixels for AECs and 47.3 - 49.9 pixels for MFs).

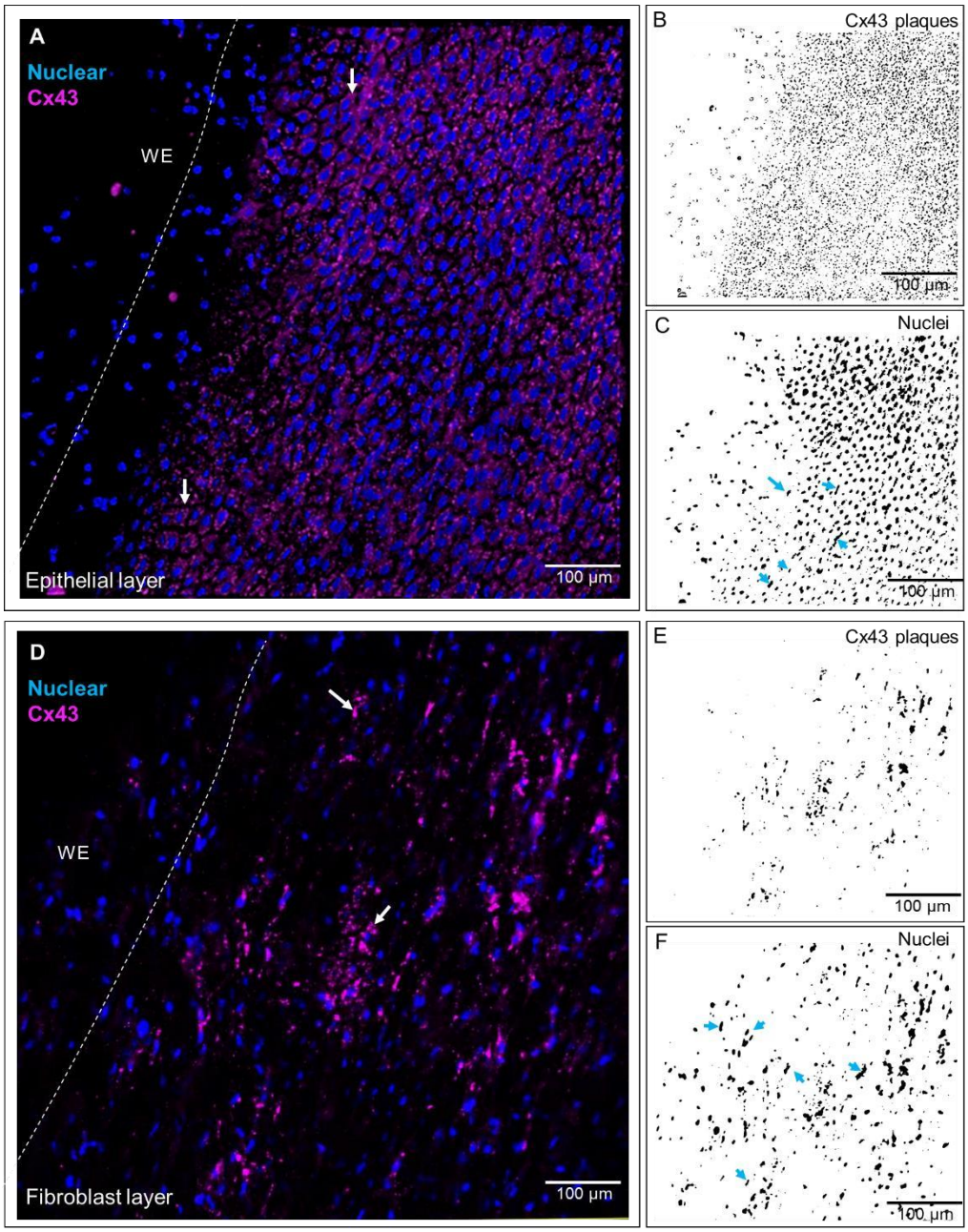

Figure 6.3: *Immunofluorescent images of Cx43 plaques and nuclei deformation at the AM sPPROM defect site. The figure shows representative images from one donor (total donors n=3). Cx43 expression increased at the defect site in both the epithelial (A) and fibroblast layers (D) (white arrows). (B), (C), (E) and (F) shows binary images of Cx43 plaques in AECs and AMCs. The highest concentration of Cx43 and the creation of distinct protein plaques (approximately 0.1-1um in size) formed within both the nuclei and cytoplasmic extensions of AMCs and myofibroblasts (D; white arrows). Blue arrows indicate elongated nuclei at the defect site. White dotted lines show the margin of the defect. AM = amniotic membrane, AECs = amniotic epithelial cells, AMCs = amniotic mesenchymal cells, Cx43 = connexin 43, sPPROM = spontaneous PPROM, WE = wound edge. Scale bars = 100 µm.*

6.3.2 Nuclei deformation and collagen fibril alignment at the spontaneous PPROM defect site

Nuclear stretching and elongated deformation at the margin of the wound was clear after binary conversion **(Figure 6.3).** Circularity values for AECs in the epithelial layer and AMCs/MFs in the fibroblast layer at the sPPROM rupture site demonstrated cell roundness in controls was closer to 1, representing a more circular shape **(Figure 6.4C)**. In contrast, values from nuclei at the rupture site were closer to 0 and represent an elongated shape (0.593 ± 0.009 and 0.573 ± 0.027 circularity for epithelial layer and fibroblast layer respectively; **Figure 6.4C**). 3D imaging of the rupture site showed a layer of cuboidal AECs expressing αSMA curving under the wound edge and formed a barrier preventing AMCs and collagen from crossing into the WE and initiating repair **(Figure 6.5C).** In contrast, within control specimens, AECs expressed minimal αSMA **(Figure 6.2H).**

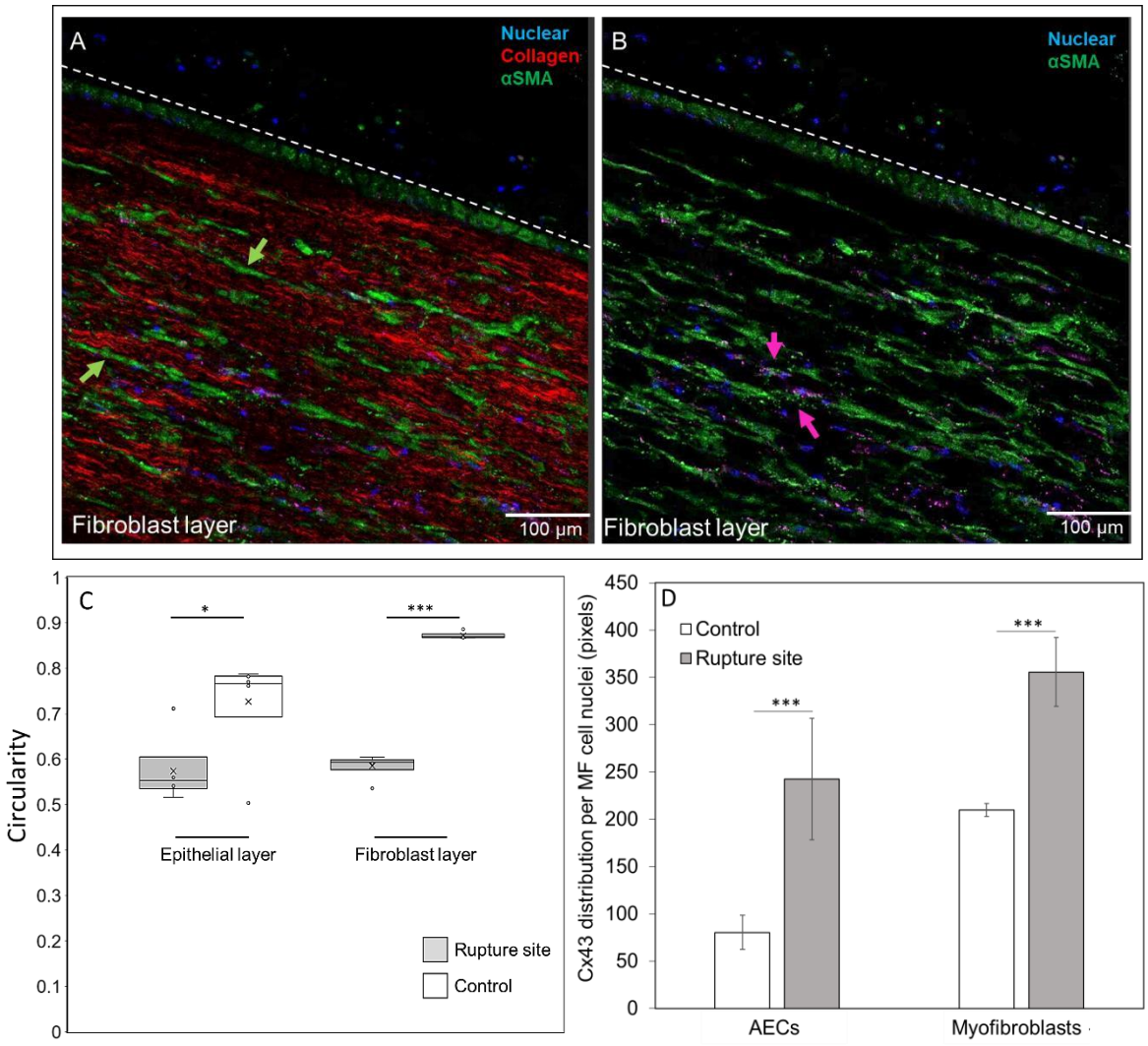

Figure 6.4: *Quantification of nuclei deformation and Cx43 intensity at the sPPROM defect site. The figure shows representative images from one donor (total donors n=3). (A) 3D slicing of the sPPROM defect site showing the fibroblast layer and elongated myofibroblasts following the direction of collagen fibril alignment (green arrows). (B) Cx43 plaque expression within both the nuclei and cytoplasmic extension are evident (pink . staining, pink arrow). (C) Circularity values for AMCs and MFs at the PPROM rupture site. Cells in controls in both cell types were closer to 1, representing a more circular shape, while values from nuclei at the rupture site are closer to 0 and represent an elongated shape. (D) Chart shows the Cx43 distribution per MF nuclei (in pixels) at the rupture site relative to controls. In the fibroblast layer, MFs expressed higher Cx43 plaque numbers relative to controls. Cx43 was evident in controls in both cell types. Data represents 6 replicates from three separate donors. Significant differences were found as indicated by ***p<0.001. AM = amniotic membrane, AECs = amniotic epithelial cells, AMCs = amniotic mesenchymal cells, Cx43 = connexin 43, αSMA = alpha smooth muscle actin, sPPROM = spontaneous PPROM, MFs = myofibroblasts, WE = wound edge. Scale bars = 100 µm, dotted white lines indicate the margin of the defect.*

Second-harmonic generation imaging of collagen at the sPPROM defect site showed dense collagen fibre alignment tangential to the defect site in the fibroblast layer of the AM **(Figure 6.2D, 6.4A & 6.6A).** The collagen fibre alignment graphs in **Figure 6.5** are representative images that indicate the amount of collagen distributed between 0° and 180° at a specific polarisation angle. Collagen fibre alignment at the defect site appeared to be higher, concurrent with IMF imaging **(Figure 6.5D).** Control fibre alignment had a random orientation, with collagen interwoven within the AM matrix to form 'basket-like-structures', as seen via IMF imaging **(Figure 6.5E).**

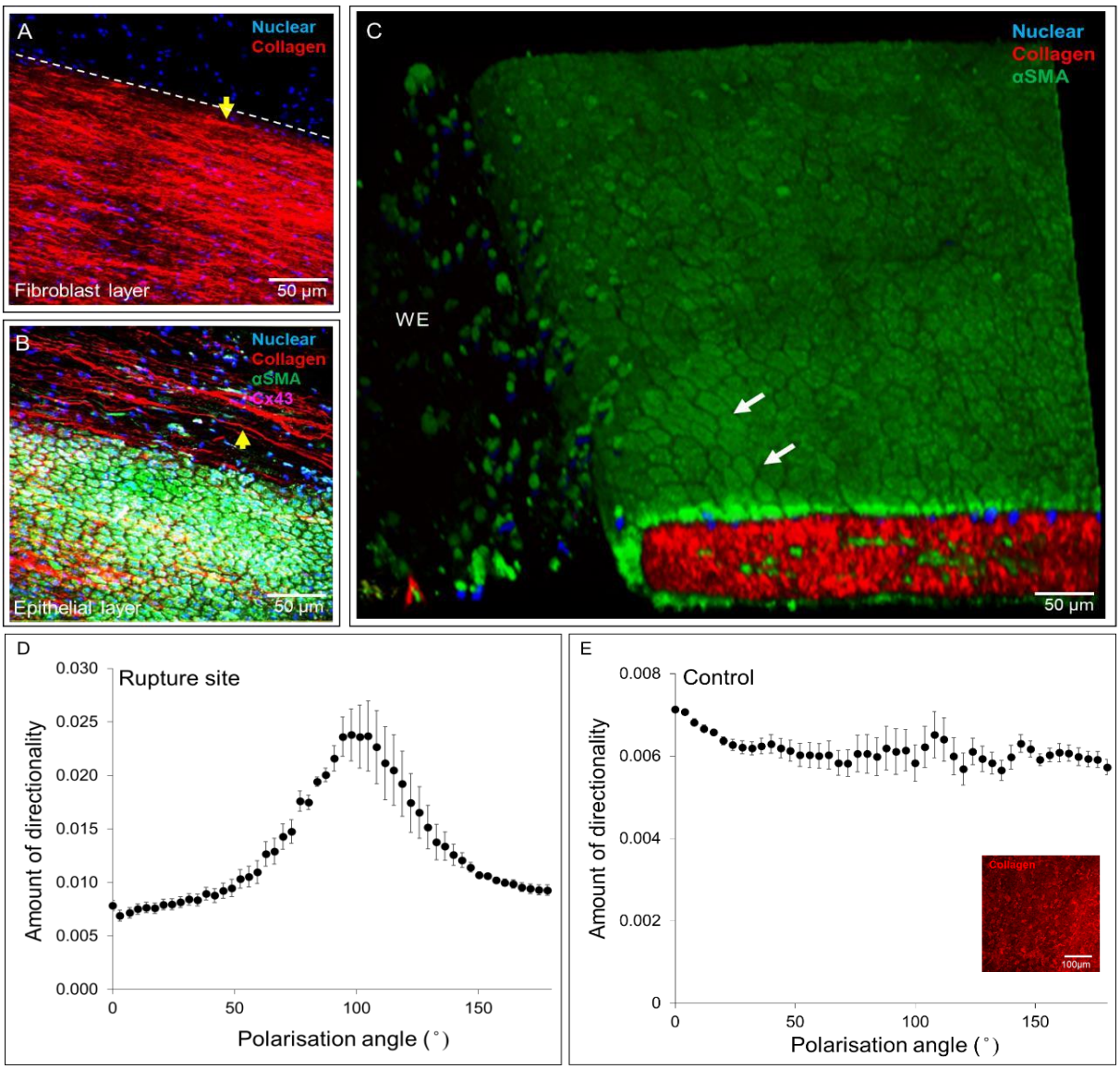

Figure 6.5: *Immunofluorescent images and quantification of collagen fibre alignment at the AM sPPROM defect site. The figure shows representative images from one donor (total donors n=3). (A) SHG imaging of collagen (yellow arrows) showed dense collagen fibre alignment tangential to the defect site in the fibroblast layer of the AM. (B) Shows the epithelial layer at the defect site, with collagen fibres visible below the cells highly aligned at the wound edge. (C) 3D imaging at the defect site indicated cuboidal AECs (white arrows) curve under the wound edge and form a barrier preventing MFs and collagen from crossing into the WE and initiating repair. (D-E) The collagen fibre alignment graphs are representative images and indicate the amount of collagen aligned at a specific polarisation angle. Collagen fibre alignment at the defect site (D) appeared to be higher, while control fibre alignment (E) had a random orientation. Mean and SEM values represent 6 replicates from three separate donors for controls and defect sites. Dotted white lined indicate the margin of the defect. AM = amniotic membrane, AECs = amniotic epithelial cells, AMCs = amniotic mesenchymal cells, Cx43 = connexin 43, αSMA = alpha smooth muscle actin, sPPROM = spontaneous PPROM, MFs = myofibroblasts, WE = wound edge. Scale bars = 100 µm, 50 µm.*

6.3.3 Morphological changes and changes in Cx43 expression at the iatrogenic defect site after open fetal surgery for open spina bifida

Representative images of one iatrogenic fetal surgery defect site are shown in this section. Using pair-wise stitching, 6 individual images were taken at 25x magnification and stitched together to display immunofluorescent imaging of the AM iatrogenic defect site at least 10 weeks following open fetal surgery **(Figure 6.6A).** At the defect site, the epithelial layer with αSMA staining showed a loss of the cuboidal structure frequently seen in AECs, when compared to control areas **(Figures 6.6B & G).**

Myofibroblasts produced elongated cytoplasmic extensions and αSMA expression across the defect, compared to more rounded morphologies in controls **(Figures 6.6A & E).** Cx43 expression was increased at the defect site in both AECs and myofibroblasts, with distinct protein plaques localising within both the cytoplasm and nucleus **(Figure 6.6D)**.

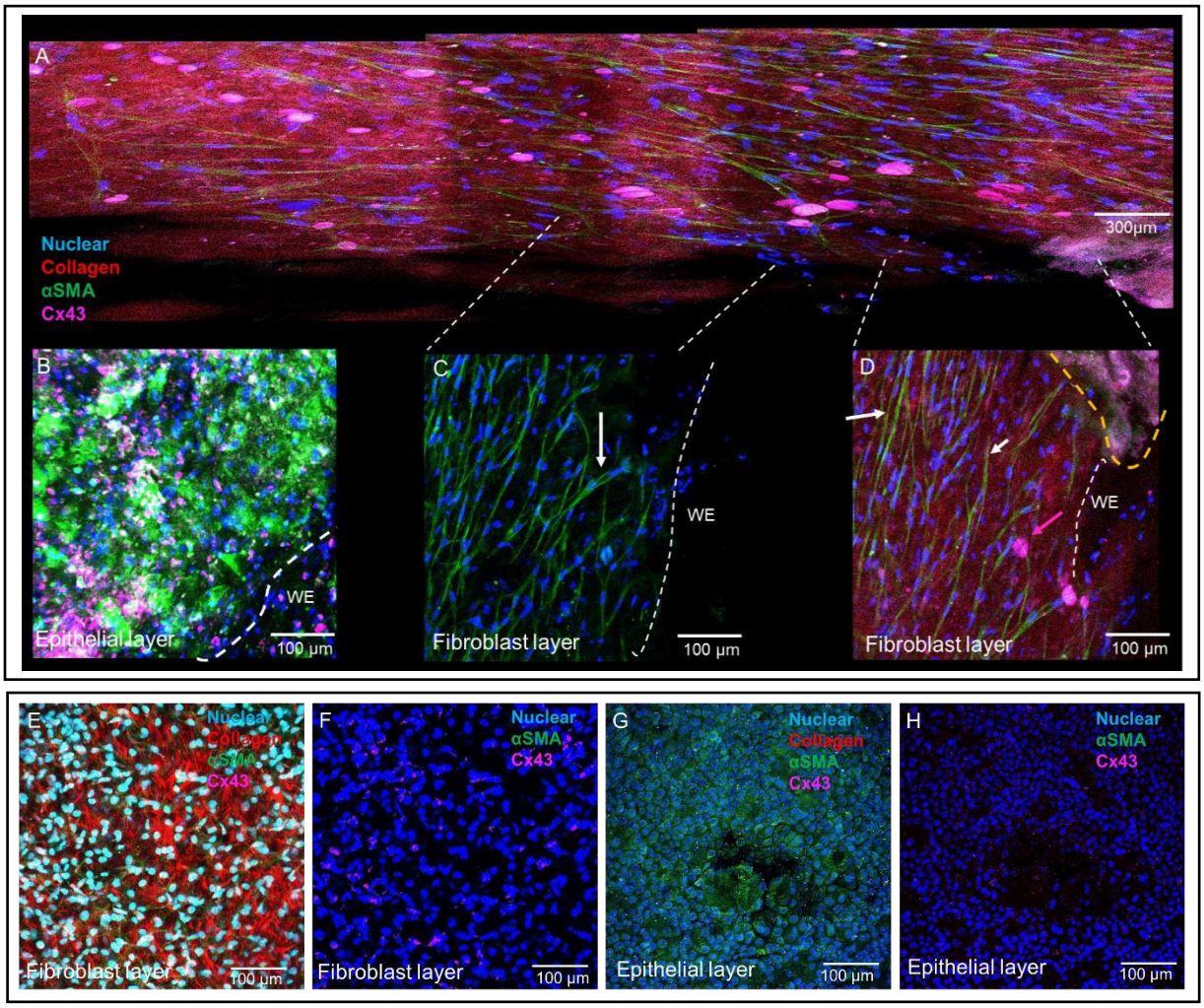

Figure 6.6: *Immunofluorescent imaging of an AM defect site following open fetal surgery for spina bifida repair. (A) Shows a pair-wise stitching of 6 individual images taken at 25x magnification at the fibroblast layer. (B) Shows the epithelial layer, with αSMA staining showing a loss of the cuboidal structure usually seen in AECs, when compared to control areas (G). Cx43 plaques are abundant within the AECs (pink). (C) In the fibroblast layer, MFs produced elongated cytoplasmic extensions and αSMA expression across the defect is relative to less prominent morphologies in controls (white arrows showing cytoplasmic extensions (D) Some collagen fibres were aligned at the wound edge, while some fibres appear to have broken down. Cx43 plaques were large and evident within cells. (E) Controls show the fibroblast layer with collagen fibres forming 'basket-like' morphologies with clear fibrillar formation. (F) Cx43 was expressed in controls. (G-H) Epithelial layer showing AECs in controls expressing minimal αSMA and low levels of Cx43. Dotted white lines indicate the margin of the defect. Dotted yellow lines indicate degraded tissue auto-fluorescing. AECs = amniotic epithelial cells, AMCs = amniotic mesenchymal cells, AM = amniotic membrane, Cx43 = connexin 43, αSMA = alpha smooth muscle actin, MFs = myofibroblasts, WE = wound edge. Scale bars = 300 µm, 100 µm.*

Plaque localisation is more evident after maximum projection of an area near the defect site showing individual elongated myofibroblasts within the cells **(Figure 6.7A & D).** Quantification of Cx43 distribution showed a significant increase of Cx43 intensity at the rupture site relative to controls in AECs (73.7 ± 8.7 pixels), while Cx43 plaques doubled in myofibroblasts (89.2 ± 12.2 pixels) **(Figure 6.8D)**. Like in sPPROM specimens, Cx43 expression was higher in controls compared to artificially induced wounds **(Chapter 4).**

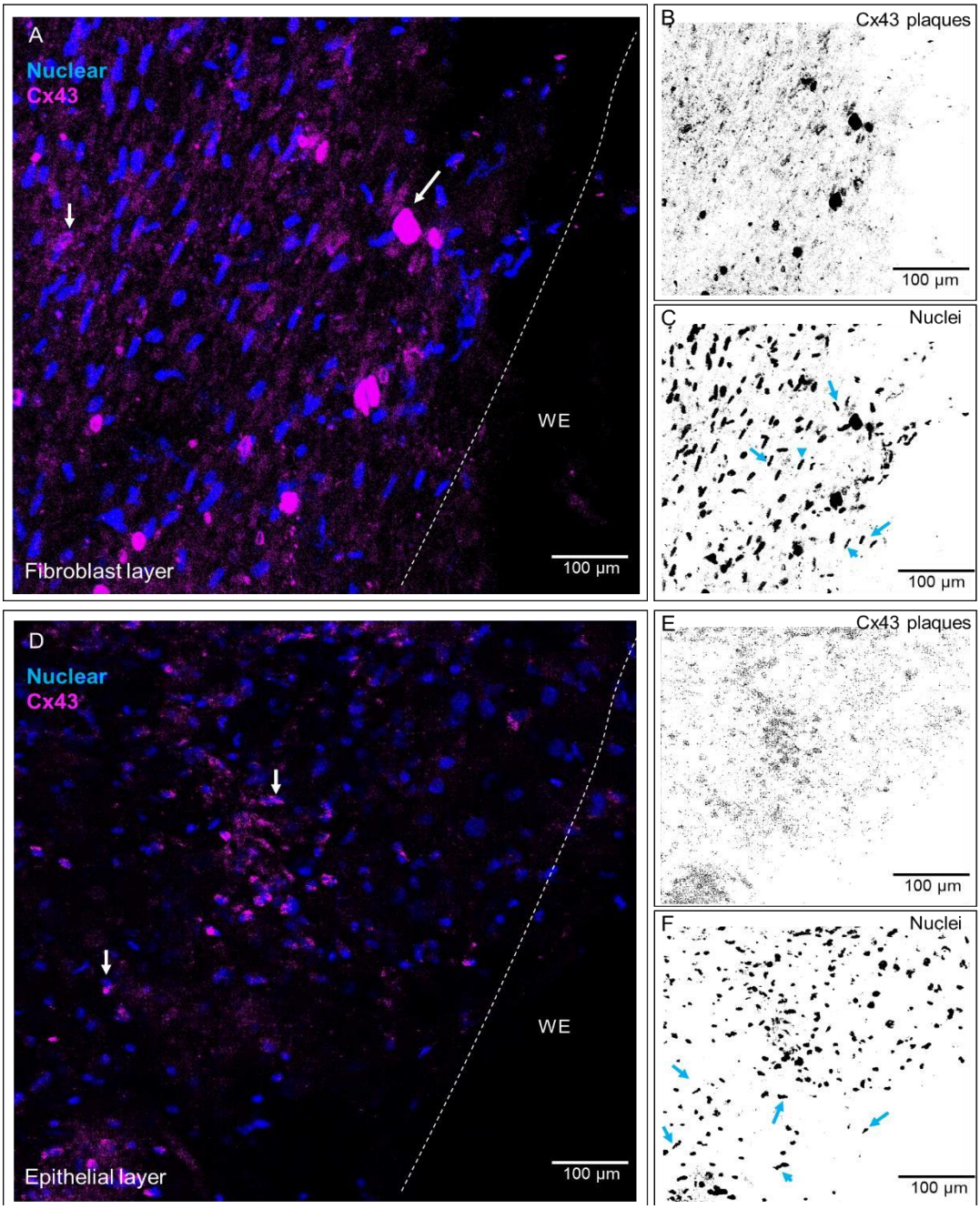

Figure 6.7: *Immunofluorescent images of Cx43 plaques and nuclei deformation at the AM defect site following open fetal surgery. Cx43 expression increased at the defect site in both the epithelial (A) and fibroblast layers (D) (white arrows). (B), (C), (E) and (F) shows binary images of Cx43 plaques in AECs and AMCs. The highest concentration of Cx43 and the creation of distinct protein plaques (approximately 0.1-1um in size) formed within both the nuclei and cytoplasmic extensions of AMCs and myofibroblasts (D; white arrows). Blue arrows indicate elongated nuclei at the defect site. White dotted lines show the margin of the defect. AM = amniotic membrane, AECs = amniotic epithelial cells, AMCs = amniotic mesenchymal cells, Cx43 = connexin 43, WE = wound edge. Scale bars = 100 µm.*

6.3.4 Nuclei deformation and collagen fibril alignment at the iatrogenic fetal surgery defect site

Images were converted to 8-bit binary to best visualise nuclear stretching and deformation **(Figure 6.7C & E).** Circularity values for AECs within the epithelial layer and AMCs/MFs in the fibroblast at the iatrogenic fetal surgery defect site indicated cell roundness in controls was closer to 1, representing a more circular shape. In contrast, values from nuclei at the rupture site were closer to 0 and represent an elongated shape, particularly in myofibroblasts (**Figure 6.8C**, circularities are 0.605 ± 0.006 for the epithelial layer and 0.567 ± 0.005 for the fibroblast layer). 3D imaging of the defect site indicated the epithelial layer is not clearly visible at the edges of the wound, a contrast to the cuboidal AECs in sPPROM defects **(Figure 6.9B & C)**. The epithelial layer is visible only on some tile areas of the defect **(Figure 6.6B)**, suggesting AECs have either differentiated into locomotive AMCs/MFs or AECs have disintegrated due to sustained trauma and inflammation.

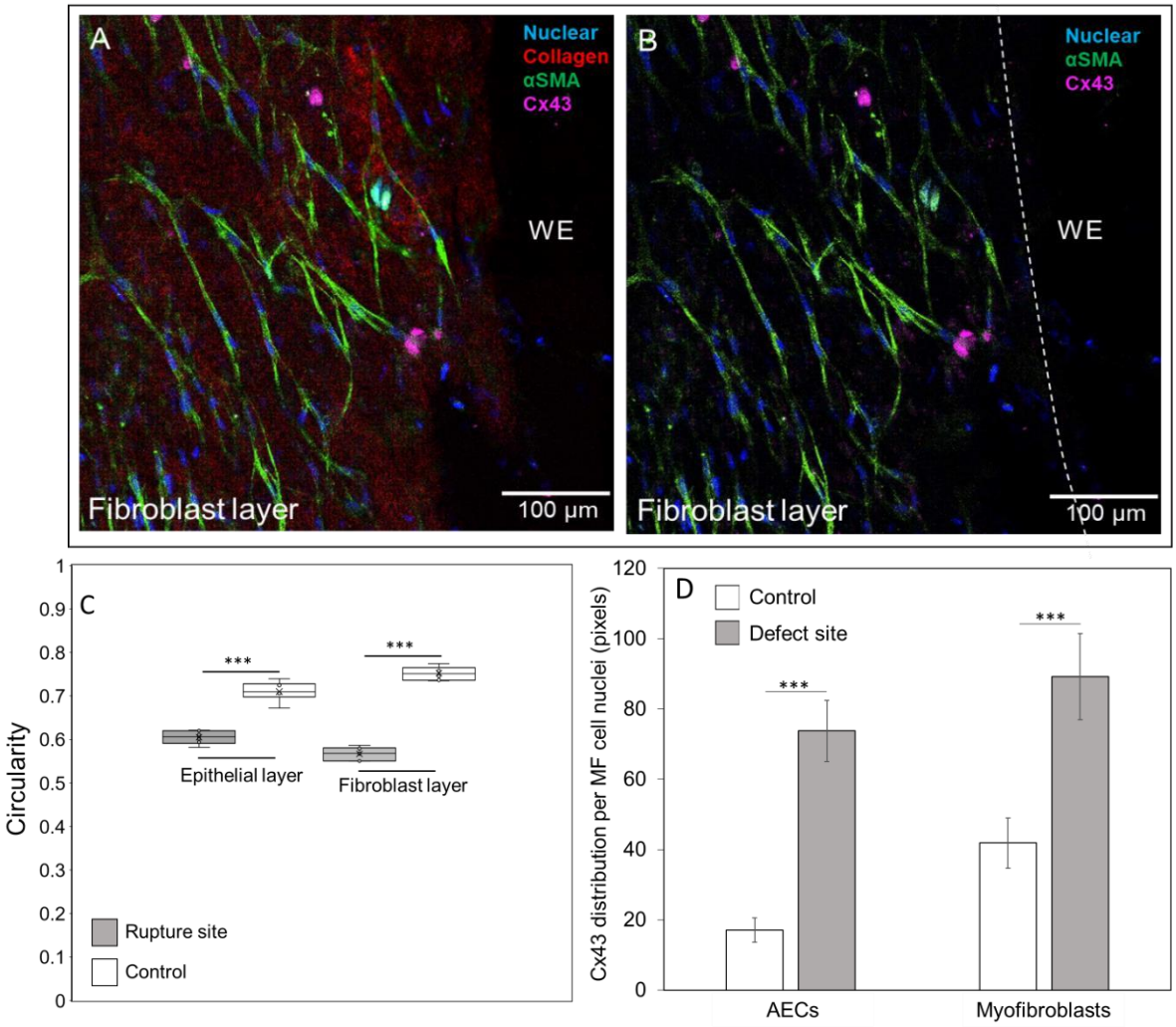

Figure 6.8: *Quantification of nuclei deformation and Cx43 intensity of the AM defect site following open fetal surgery for spina bifida repair. (A) 3D slicing of the defect site showing the fibroblast layer and elongated MFs aligned tangentially to the wound. Collagen fibres were not clearly visible. (B) Cx43 plaque expression within both the nuclei and cytoplasmic extension was evident (pink staining). (C) Circularity values for AECs and MFs at the PPROM defect site. Cells in controls in both cell types were closer to 1, representing a more circular shape, while values from nuclei at the rupture site are closer to 0 and represent an elongated shape. (D) Chart shows the Cx43 distribution per MF cell nuclei (in pixels) at the defect site relative to controls. In both cell layers, myofibroblasts expressed higher Cx43 plaque numbers relative to controls. Data represents 6 replicates from three separate donors. Significant differences were found as indicated by ***p<0.001. Dotted white lines indicate the margin of the defect. AM = amniotic membrane, AECs = amniotic epithelial cells, AMCs = amniotic mesenchymal cells, Cx43 = connexin 43, αSMA = alpha smooth muscle actin, WE = wound edge, Scale bars = 100 µm.*

Second-harmonic generation imaging showed some collagen fibre alignment tangential to the defect site in the fibroblast layer of the AM **(Figure 6.9A).** However, using 3D analysis of the defect site, collagen fibres were also seen to form clusters, indicating potential collagen breakdown is taking place **(Figure 6.9C).** This is further evident by the collagen fibre alignment graphs which indicate the amount of collagen aligned at a specific polarisation angle **(Figure 6.9D, E).** Representative alignment graphs showed the distribution of collagen morphologies between 0˚and 180˚had a preferential polarisation angle only between 88˚and 99˚, while most fibres were polarised randomly throughout the defect site **(Figure 6.9D).** This random alignment resembled those seen in control tissues where fibres had a random orientation with 'basket-like' morphologies with clear fibrillar formation **(Figure 6.6E).**

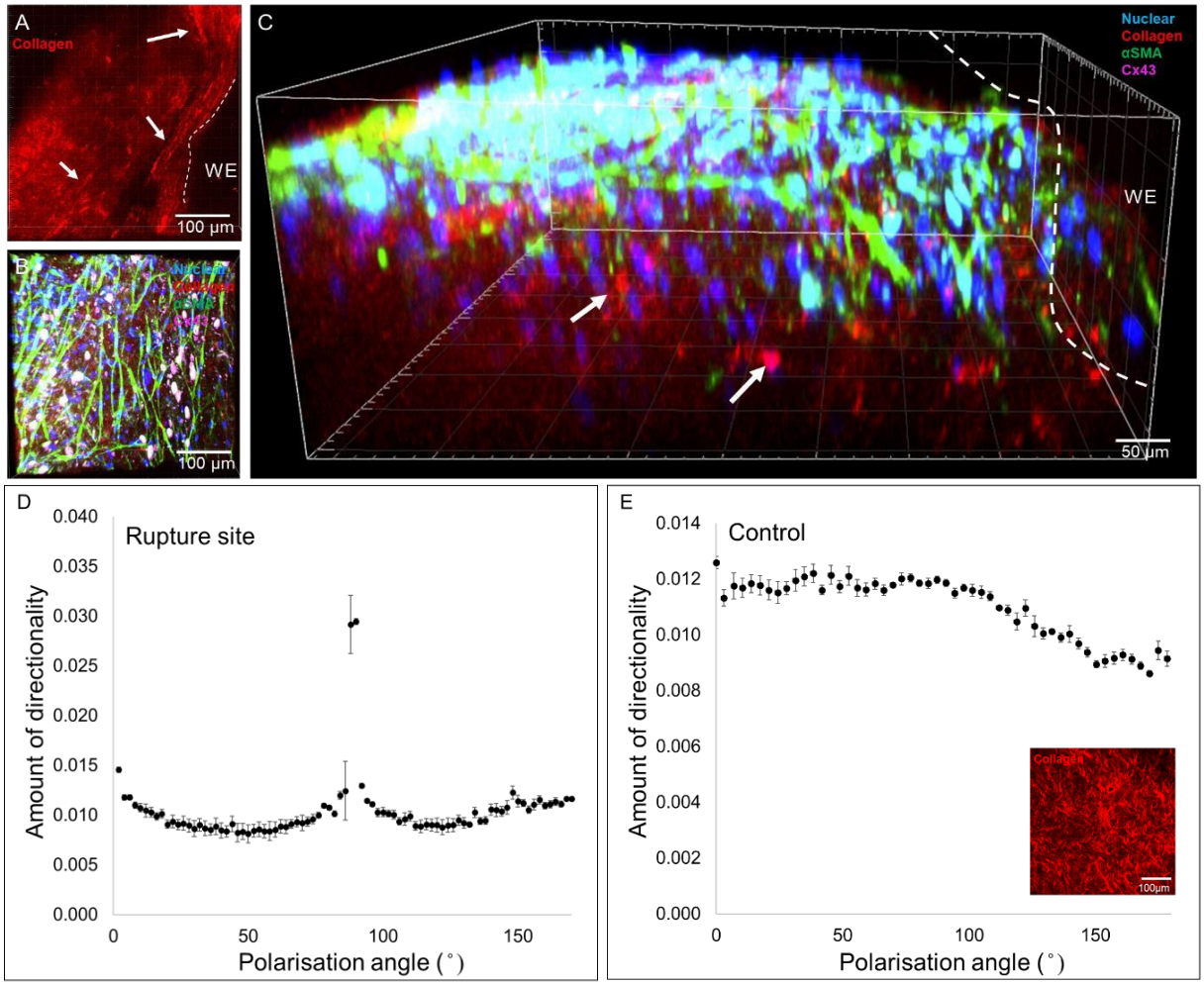

Figure 6.9: *Immunofluorescent images and quantification of collagen fibre alignment at the AM iatrogenic defect site following open fetal surgery. (A) SHG imaging of collagen (white arrows) showed some collagen fibre alignment tangential to the defect site in the fibroblast layer of the AM. (B) Maximum projection of the whole imaged tissue on the fibroblast layer side at the defect site, with Cx43 plaques visible. (C) 3D imaging at the defect site indicated AECs have disintegrated and are not obviously visible at the wound edge. Collagen fibres are also seen to form clusters, indicating potential collagen breakdown is taking place. The collagen fibre alignment graphs are representative images and indicate the amount of collagen aligned at a specific polarisation angle. (D) Some collagen fibres were aligned at the wound edge, while some fibres seem to have broken down. (E) Control fibre alignment had a random orientation with clear fibrillar formation. Mean and SEM values represent 6 replicates from three separate experiments for controls and defect sites. Dotted white lined indicate the margin of the defect. AM = amniotic membrane, AECs = amniotic epithelial cells, AMCs = amniotic mesenchymal cells, Cx43 = connexin 43, αSMA = alpha smooth muscle actin, WE = wound edge. Scale bars = 100 µm, 50 µm.*

6.4 Key Findings

- In the fibroblast layers of sPPROM defects, αSMA-expressing myofibroblasts changed morphologies relative to controls and produced elongated cytoplasmic extensions aligned along the wound.
- Using SHG imaging and orientation analysis, collagen fibres were seen polarised tangentially to the sPPROM defect site and had elongated morphologies relative to random fibre alignment in controls.
- In sPPROM AM, AECs formed a layer of cuboidal cells expressing αSMA that migrated at the edges of the wound and formed cellular clusters that curved under the wound edge to form a barrier preventing AMCs and collagen from crossing into the WE and initiating repair.
- Cx43 protein increased in expression (per nuclei) at the sPPROM defect site was quantified in both the fibroblast and epithelial layers, with significant differences compared to controls.
- In sPPROM AM, Cx43 plaques within αSMA-expressing myofibroblasts and AECs localised in both the cytoplasm and nucleus.
- AMC and myofibroblast nuclei within the AM fibroblast layer polarised tangentially to the sPPROM defect site.
- 3D imaging of sPPROM defect sites showed collagen fibres aligned concurrently with myofibroblast nuclei and lamellipodia.
- In the fibroblast layers of iatrogenic fetal surgery defects, αSMA-expressing myofibroblasts changed morphologies relative to controls and produced elongated cytoplasmic extensions aligned along the wound edge.
- SHG imaging and orientation analysis showed some collagen fibre alignment tangential to the iatrogenic fetal surgery defect site in the fibroblast layer of the AM, with evidence of collagen breakdown.
- At the iatrogenic fetal surgery defect site, the epithelial layer with αSMA staining showed a loss of the cuboidal structures and AECs had unique elongated morphologies, when compared to controls.

- Cx43 protein increased in expression (per nuclei) at the iatrogenic fetal surgery defect site was quantified in both the fibroblast and epithelial layers, with significant differences compared to controls.
- In iatrogenic fetal surgery defect sites, Cx43 plaques within αSMA-expressing myofibroblasts and AECs localised in both the cytoplasm and nucleus.
- AMCs and myofibroblast nuclei within the AM fibroblast layer polarised tangentially to the iatrogenic fetal surgery defect site, with minimal alignment concurrent with collagen fibres.

6.5 Discussion

Comparing and contrasting morphological changes following spontaneous PPROM and in iatrogenic fetal surgery defect sites could provide insight to the development of potential therapeutic interventions. The latency period from rupture to delivery, presence of infections (e.g. chorioamnionitis) and the size of the defect all play a role into the FM wound healing capabilities *in utero* [6,7]. Using IMF confocal microscopy and SHG imaging, the present study showed that at the defect site of sPPROM specimens, myofibroblasts changed morphologies and expressed αSMA relative to controls and produced long extended cytoplasmic extensions aligned along the wound**.** Collagen fibres were polarised tangentially to the wound and had elongated morphologies relative to controls. Similarly, in iatrogenic fetal surgery defects, myofibroblasts showed the same elongated morphologies as in sPPROM, however collagen fibrils were unclear and appeared to form clusters at the wound edge. In both groups, Cx43 was abundantly expressed in MFs and AECs.

Researchers have shown the FM does not heal after fetoscopic surgeries and there is no proliferation present after trauma or a change in defect size suggesting no significant wound healing [47,102]. In patients undergoing amniocentesis with a small diameter needle, perinatal survival in amniocentesis related PPROM pregnancies was 82% higher than those complicated by spontaneous rupture, suggesting that the size of the tear on the membrane following sPPROM may be larger, which may influence fetal mortality outcomes [21]. Our research group has previously shown that absence of healing in term AM was concurrent with collagen fibril alignment tangential to the defect site [17]. Papanna and colleagues showed collagen deposition at the defect site after fetoscopy for TTTS was abundant with a loss of normal fibril pattern and an increased number of distorted 'whorl-like' fibrils creating thickened wound edges [254]. Collagen fibril degradation using SHG imaging has been visualised in other studies of wound healing and inflammation, manifested by poor SHG signal, loss of collagen content measurements and/or fibril density and abnormal orientation [347,348]. These studies of collagen degradation agree with our observations of collagen 'clusters' in iatrogenic fetal surgery defect

samples. In contrast, in sPPROM specimens, the collagen signal remained strong, coupled with myofibroblast differentiation.

To date, there have been no critical analysis studies of sPPROM defects, rather focus has been placed on iatrogenic fetal surgery defects in both animal models and human explants [8,18,66]. In one study of TTTS fetoscopy defects, myofibroblast differentiation was absent, coupled with increased apoptosis in all FM layers, indicating complete loss of wound healing abilities [254]. Importantly, gestation to delivery in these samples was on average 79 days, and delivery occurred at 31 ± 4 weeks GA [254]. In our study, average latency between deliveries was 70 days, however delivery occurred after 34 weeks GA. The open fetal surgical intervention for fetal spina bifida repair creates a larger defect size (7.5 - 6 cm), which is significantly more invasive that TTTS fetoscopy which in a previous study has been found to create a defect size area of up to 14.7 mm^2 [102]. This could influence the healing abilities of the FM and thus the differentiation capability of AMCs and AECs.

Another study investigated the healing capabilities of the myometrium and FM following open fetal surgery for SBA [349]. The authors reported avital areas of both the myometrium and FM, coupled with CD68+ macrophage infiltration and no correlation between surgery and delivery interval, and healing markers [349]. In contrast, in our study both AM from sPPROM and fetal surgery showed abundant myofibroblast concentration concurrent with nuclei deformation and lamellipodia alignment in the direction of collagen fibril polarisation within the fibroblast layer of the AM. Collagen alignment and nuclei polarisation parallel a previous study by our group in smaller fetoscopy defects [17]. Carvalho and colleagues showed FMs undergo collagen redeposition at suture sites following SBA open fetal surgery, in contrast to non-suture sites [18,259]. The authors reported an increase in collagen concentration at the defect site concurrent with site-dependent gene expression alterations of MMP-1/9 and TIMP-1/2 in surgical areas, suggesting membrane remodelling processes were activated [18,259]. Thus, the discrepancies in whether whole FM and AM possess vital areas capable of wound healing are evident. In the current study, vitality assays were not performed and in the future this must be done to elucidate whether cell populations are alive and thus capable to promote healing.

Complications associated with PPROM are multifactorial, but commonly depend on whether a patient has undergone surgical intervention, or the presence of infection. Variability in outcomes and latency period depend on the type of surgery or fetoscopy while for sPPROM differences are influenced by timing of rupture relative to gestational age. Thus, morphological differences in iPPROM and sPPROM AM specimens cannot be directly compared, rather contrasted, and discussed as independent disorders that could be managed with different sealing strategies and interventions.

Novel inflammatory processes that lead to PPROM initiation have been proposed. Moore's group showed GM-CSF induced progesterone P4 concurrent with MMP-2 induction to remodel ECM, initiating inflammation and PPROM induction [176]. Senescence has been proposed to play a role in FM weakening and aging, and telomere shortening occurs in a gestational age-dependent manner [176,180-182]. In FM collected from PPROM patients, DNA telomere lengths and antioxidant enzyme activity were reduced, as measured by the decrease in superoxide dismutase 1 and elevation of AF F2-Isoprostane, a marker for oxidative stress [183]. Lappa's group released a series of papers elucidating the role of abnormal ROS activation in FM explants. The authors showed that, to rescue weakening and PPROM phenotypes, treatment with antioxidant N-Acetyl-cysteine resulted in inhibition of pro-inflammatory factors PGE_2, IL8, TNFα and MMP-9 activity concurrent with NF-κB DNA binding activity [184].

In PPROM-derived FM treated with CSE, they further showed the LOX gene was overexpressed, which can remodel ECM components such as elastin and induce cellular senescence under oxidative stress [184]. Using p38MAPK inhibitors in mouse models, AECs and FM explants, Moore and colleagues showed p38MAPK activation controls FM senescence through β-galactosidase activity and can be activated by TGFβ1 concurrent with p53mediated senescence and associated with laminin B loss, mitochondria enlargement and DNA fragmentation [132,186-188]. DAMPs release in FM during inflammation has been proposed to initiate cellular injury and tissue damage, including the HMGB1 protein responsible for inflammasome activation [132]. In the amniotic fluid of mice, HMGB1 was found to accumulate and stimulate oxidative stress, p38MAPK activation and senescence, triggering PPROM-

associated rupture. [185,187]. These novel studies highlight the multifactorial biochemical mechanisms that lead to PPROM, thus investigating the morphological changes at the defect site is not enough to elucidate the mechanisms by which rupture is initiated.

Bacterial infections further initiate inflammatory pathways in the FM, causing host immune activation and accumulation of macrophages and cytokine release as the peripheral tissue attempts to fight off the infection, resulting in irreversible damage that predisposes the FM to PPROM [177,178]. Activation of Toll-like receptors by pathogen-associated molecular patterns (PAMPs) activates transcription factor NF-κB by B-cells resulting in p65 translocation and secretion of pro-inflammatory IL-4, 6, 8 and GM-CSF commonly found in bacterial infections [58,179]. In the current study none of the donors investigated had an infection detected at delivery. Future studies could focus on donors delivering after PPROM and proven infection to elucidate the influence of bacterial populations on cellular behaviour.

Additionally, cytokine secretion (eg. IL-1β and NF-κB) enhanced the release of MMP-9 and PGE_2 in the amniotic fluid of patients with chorioamnionitis and PPROM [129,163]. Furthermore, natural amicrobial factors in cervicovaginal fluid have been investigated as markers for prediction of spontaneous preterm birth in at risk patients [350]. Trapin/elafin (or peptise inhibitor 3) overexpression has been shown in the FM of donors after PPROM [350]. Elafin inhibits human neutrophil elastase (HNE), a pro-inflammatory factor that can induce FM inflammation and breakdown, and thus elevated HNE concentrations were seen in cervicovaginal fluid of women with cervical shortening and delivered preterm [350]. The synergistic actions of these factors disrupt collagen and elastin expression in the AM, subsequently leading to tissue ripening and rupture [129].

PPROM initiation can also occur through excessive vaginal bleeding. Patients participating in the current study did not have evidence of bleeding, however increase in maternal systemic inflammatory response due to vaginal bleeding has shown to activate the extrinsic pathway of coagulation through monocyte release of tissue factor and correlated with PPROM initiation [12]. This results in thrombin overexpression, concurrent with decidual cell secretion of MMP-1 and

3 that degrade FM collagens [12]. Thrombin further activates myometrial and uterine contractions which may lead to preterm labour [12]. Others have shown that following placental abruption and subsequent PPROM, neutrophil infiltration in the FM and placenta was markedly increased, concurrent with fibrin deposition [351]. The authors determined that the neutrophil chemoattractant IL-8 was elevated after incubation of primary term decidual cells with thrombin, further highlighting the role of thrombin in the pathogenesis of PPROM [351]. **Chapter 7** will discuss in more detail on how we can harness the inflammatory environment of PPROM defects to potentially promote healing using novel sealing strategies.

Mechanisms that lead to iPPROM during fetoscopy and open fetal surgery are not the same as those in sPPROM imitation, although the accumulation of inflammatory and potential infection could arise with latency time and defect size [172]. During open fetal surgery, the FM undergoes severe manipulations including cutting, stretching and dehydration that are not comparable to sPPROM defects and will undoubtedly influence the integrity of FM cell populations. Postoperative choriomembrane separation (CMS) has been recorded in 20-40% of fetoscopic procedures, leading to collagen disruption and initiating rupture [252,253]. This results in amniotic fluid accumulation in the myometrium, formation of amniotic bands, umbilical cord strangulation and increased fetal morbidity [237]. Other fetoscopic practises frequently require the use of liquid or gaseous distention of the FM, resulting in an increased insufflation pressures in membranes with iPPROM [24,253]. Using *in vitro* and in animal models, researchers have shown sustained exposure to CO_2 increases the likelihood of FM dehydration [172,207]. Collagen within the stromal layers of the FM become brittle while damage to the amniotic epithelium triggers the release of MMPs and promotes rupture [172,254].

The gradual replacement of amniotic fluid with Ringer's lactate and antibiotics after fetoscopy was shown to initiate apoptosis in the AM epithelium, further enhancing pathological mechanisms and increasing the risk of iPPROM [207,254]. To mimic fetoscopic procedures whereby CO_2 dehydration of the AM is expected, Bircher *et al.,* 2020 characterised the effects of osmolarity and hydration on the tear resistance of term AM using mode I fracture tests [207].

To mimic Ringer's lactate, the authors used physiological saline on FM under deformation and determined that treatment with physiological saline resulted in higher membrane tearing energy (Γ_a; average 0.032 J/m) than FM treated with distilled water (average 0.014 J/m) [207]. Thus, it is clear that the use Ringer's lactate may contribute to iPPROM after open fetal surgery [207,254].

Retrospective studies have attempted to characterise risk factors associated with PPROM following laser fetoscopy for TTTS correction and open fetal surgery for spina bifida correction. In a multicentre study using 487 patients, Papanna *et al.,* 2014 determined that latency period from TTTS laser treatment to delivery was average 10 weeks + 4 days (mean GA at fetoscopy 145.6 ± 15.7 days and mean GA of delivery 31.2 ± 4.9 weeks) with 51% of patients delivering before 32 weeks GA [19]. 28% of patients experienced PPROM, and favourable outcomes correlated with the size of cannula used (9 Fr, 10 Fr or 12 Fr) and the use of collagen plug after the procedure [19]. Lower GA at delivery was correlated with younger maternal age, history of previous prematurity, shorter cervical length and the use of 12 Fr cannula and thus a larger defect size [19]. Another multicentre study evaluated 847 pregnancies after TTTS laser correction whereby un-favourable outcomes correlated with history of prior amnioreduction, cervical cerclage and increased GA at diagnosis [352]. They similarly determined that average latency to delivery was 10.11 ± 4.8 weeks and mean GA at delivery was 30.7 ± 4.5 weeks with 17.1% of patients experiencing PPROM [352]. In open fetal surgeries for spina bifida, studies have reported the mean GA at surgery was 26.09 ± 0.3 weeks and at delivery 33.81 ± 0.82 weeks, while favourable outcomes including increased collagen deposition correlated with the presence of sutures on the defects [18,259]. In evaluating the success of mini-hysterotomy for SBA correction, whereby a smaller incision (< 4 cm) is made, Botelho *et al*., 2016 determined latency period to delivery was 11 weeks, 23.1% of patients developed PPROM at a median of 34.1 weeks GA [353].

Nevertheless, despite different initiation mechanisms and risk factors leading to preterm birth, iPPROM defects can be affected by chorioamnionitis and sustained inflammation like in those in sPPROM. Researchers have characterised risk factors influencing latency periods in

sPPROM [5,354]. Mid-trimester sPPROM (14-26 weeks gestation) is known to be followed by chorioamnionitis, sepsis, pulmonary hypoplasia and increased neonatal morbidity, while authors report average latency periods between rupture and delivery at 13 - 14 days [5,354]. Neonatal survival was found to be associated with GA at delivery rather than when rupture occurred [5.] In contrast, patients with sPPROM in the third trimester (27 - 31 weeks gestation) had more favourable infant survival rates, with latency periods over 14 days having higher neonate morbidity [324]. This is a significant point to consider, as a longer latency period might increase the possibility of infection and thus influence FM mechanics and cellular composition. On the other hand, if infection is present after sPPROM, spontaneous preterm birth may be more likely to ensue

The role of Cx43 in regulation of distinctive wound healing mechanisms in AM defects has been discussed in previous chapters [104,250,251,291,295]. In the current study we showed Cx43 increased in expression in both AECs and MFs in sPPROM and iPPROM defects. Overall, spontaneous PPROM defects had higher average Cx43 pixel intensity per nuclei than those in iPPROM in both cell types (355.7 ± 36.3 pixels and 89.2 ± 12.2 pixels in MFs respectively). It's worth noting Cx43 expression in controls in both groups was higher than those seen in artificially induced 0.8 mm defects (See **Chapter 4**). Cx43 upregulation may indicate the activation of the wound healing mechanism. When comparing these observations to small artificial defects and fetoscopy defects, it becomes evident that the size of the wound coupled with the overexpression of Cx43, hinders FM wound healing [104].

In **Chapter 4**, it was hypothesised that healing may be influenced by the spatial-temporal dynamics and localization of Cx43 leading to differential effects on cell populations that could hinder complete closure of the wound. This is further evidenced in this study, whereby following Cx43 expression, the concentration of myofibroblasts and nuclei stretching was abundant in both iatrogenic fetal surgery defects and sPPROM studies, indicating cell contraction and migration. This further supports the hypothesis that Cx43 may participate in myofibroblast differentiation, presumably through pro-inflammatory macrophage-activated TGFβ1 signalling,

N-cadherin gene expression to aid migration and subsequent αSMA filament sliding. Nevertheless, these larger defects cannot undergo purse-string wound contraction that is seen in embryonic wound healing [245,246] and as is hypothesised to occur in small artificial defects, due to the sheer size and potential lack of proximity of the wound edges even when sutured. Further studies could focus on elucidating the presence of pro-inflammatory immune cells in both AF and FM taken from PPROM patients, followed by gene expression analysis of TGFβ1 at the defect site. This could be followed with N-cadherin immunofluorescence staining to determine its overexpression in MFs and thus potentially correlate it with Cx43 expression at the wound edge.

In the **Appendix, Figure 6.10** highlights the differences in AEC morphologies seen in sPPROM and iPPORM defects. In iatrogenic fetal surgery defects, AECs were seen to lose their characteristic cuboidal structures, expressed αSMA and had unique elongated morphologies, concurrent with nuclei deformation **(Appendix; Figure 10.6A)**. In contrast, AECs in sPPROM defects formed a layer of cuboidal cells expressing αSMA that migrated at the edges of the wound and formed cellular clusters that curved under the wound edge to form a barrier, preventing AMCs and collagen from crossing into the WE and initiating repair **(Appendix; Figure 10.6B)**. It remains to be elucidated if AECs are undergoing EMT or have the capacity to do so in large FM defects, however others have shown that cyclic EMT-MET is responsible to FM integrity maintenance throughout gestation, while favourable EMT differentiation increases towards term and preterm inflammation [77]. In primary human AMCs, the same authors showed that progesterone P4 incubation stimulated MET via through progesterone receptor membrane component 2 (PGRMC2) and c-MYC [77].

The same group suggested that FM senescence and EMT inflammation may promote parturition through extracellular vesicles carrying inflammatory factors such as MMPs from gestational tissues (e.g. myometrium) to the FM and initiate ECM breakdown [77,191]. Mechanisms of EMT using microfractures in human FM explants are proposed to be due to TGFβ release from ACS after exposure to oxidative stress [77,181]. The authors showed that increased microfracture density in the FM of PPROM patients (4.6-fold) compared to non-

laboured preterm birth membranes, as measured by collagen degradation via SHG imaging [181]. The mechanism by which TGFβ influences EMT was elucidated by inhibiting TGFβ-activated kinase 1 binding protein 1 (TAB1), which suppressed EMT transcription factors and maintained epithelial cell morphological characteristics [77].

In their physiological morphologies, AECs express αSMA minimally and do not have lamellipodia. Cx43 distribution appears to be mostly nuclear in iatrogenic fetal surgery defect specimens versus cytoplasmic localisation in sPPROM defects. Thus, these observations could be from either (a) AECs cytoplasmic disintegration due to trauma and sustained inflammation because of iatrogenic trauma or (b) AECs expressing αSMA and undergoing EMT in response to sustained inflammation to aid potential wound healing mechanisms. This is further evidenced by 3D imaging of the defect site showing AECs were not clearly visible at the wound edge in contrast to sPPROM defects. Taking the key findings of this study into consideration, we could hypothesise that AECs undergo EMT in large defects, particularly when the latency period between rupture and delivery occurs increases. However, it is important to stress that these are merely observations and further studies must be performed to test this hypothesis. The role of AEC transition and the purse-string contraction hypothesis at the wound edge of large AM defects warrants further investigation in the future using scratch-wound assays and/or MET-specific markers, particularly E-cadherin.

6.5.1 Study Limitations

Like in **Chapters 4** and **5**, the present study presents semi-quantitative data that rely heavily on correlation and not causation evidence. The volume of myofibroblasts and the intensity of αSMA was not quantified via imaging analysis in contrast to **Chapter 4**, thus changes in cellular morphologies are purely observational. To conclusively determine AMCs and/or AECs have differentiated into myofibroblasts proper quantification must be performed in the future. Additionally, despite clear increase of Cx43 protein expression at defect sites compared to sites away from the wound, there is no evidence to suggest Cx43 plays a role in preventing wound healing of large AM defects. In fact, compared to small artificial defects in **Chapter 4**, the lack of healing is presumably due to the size of these defects and the repeated mechanical and biochemical stresses the FM was exposed to during pathological or surgical trauma. In addition, as previously stated, the Cx43 antibody used throughout this thesis was not properly optimised and other techniques should be used in the future to elucidate the expression of Cx43, such as western immunoblotting and qPCR.

Furthermore, like in **Chapter 4**, other fibroblast (e.g. CD34) and myofibroblast markers (e.g. collagen type I/III, β-actin, TGFβ1) need to be used in the future, particularly differentiation markers to determine whether AMCs and/or AECs were differentiating at the wound edge throughout culture. To determine whether all three identified cell populations are differentiating and are locomotive, live-imaging could be used in the future. This would require a powerful microscope capable of live imaging and ideally co-staining of multiple proteins to visualise if cell differentiation and migration is taking place. This would be particularly useful to determine the differences observed in AEC morphologies between sPPROM and iPPROM defects.

The concentrations of other pro-inflammatory factors such as TGFβ1 was not determined in this chapter. Future studies could compare the expressions of both Cx43 and TGFβ1 in large fetal membrane defects taken from sPPROM and iPPROM donors to small artificial defects in term and preterm samples. Furthermore, there were no assays performed to determine the levels of viable cells at the defect sites. To best design biomaterials for fetal membrane healing,

we must first understand whether the wound edges have the ability to heal. Despite evidence of cell morphological changes through the expression of αSMA, a live/dead assay should be performed as changes in cell morphology are not enough to determine if a cell is viable.

The patient replicates for this study were *n*=3 for sPPROM and *n*=4 for iatrogenic fetal surgery defects, and a larger cohort should be used to examine the effect of latency, GA and maternal factors on AM morphology. Furthermore, the focus was only on the AM, while changes in CM morphology were not investigated. Further studies could characterise whole FM changes at defects site using both IMF confocal microscopy and histology to directly compare results with other histological studies.

Using SHG imaging, it became clear that in iPPROM defects collagen fibrils were deformed and did not align tangentially to the wound like in sPPROM wounds. Despite observed collagen alignment changes, collagen was not quantified with other techniques and thus it is not known whether the expressions of specific collagen types were altered after trauma. Collagen remodelling and breakdown could be elucidated further by examining MPPs, particularly MMP-9, 2 and 13, and TIMPs activity and expression at the defect site. Collagen types known to influence fetal membrane pathological rupture could be also investigated, particularly types 1, III and IV.

In summary, the present study shows that large iatrogenic fetal surgery AM defects and sPPROM defects do not heal after AM rupture, and AECs, AMCs and MFs have increased Cx43 expression at the wound edge. The presence of elongated MFs and AECs expressing αSMA are promising and indicate that despite prolonged rupture, the AM retains areas that may be promoted by sealing strategies to initiate wound healing in the future. **Chapter 7** will discuss further study limitations and future work to elucidate the mechanisms behind FM healing and repair.

6.6 Appendix

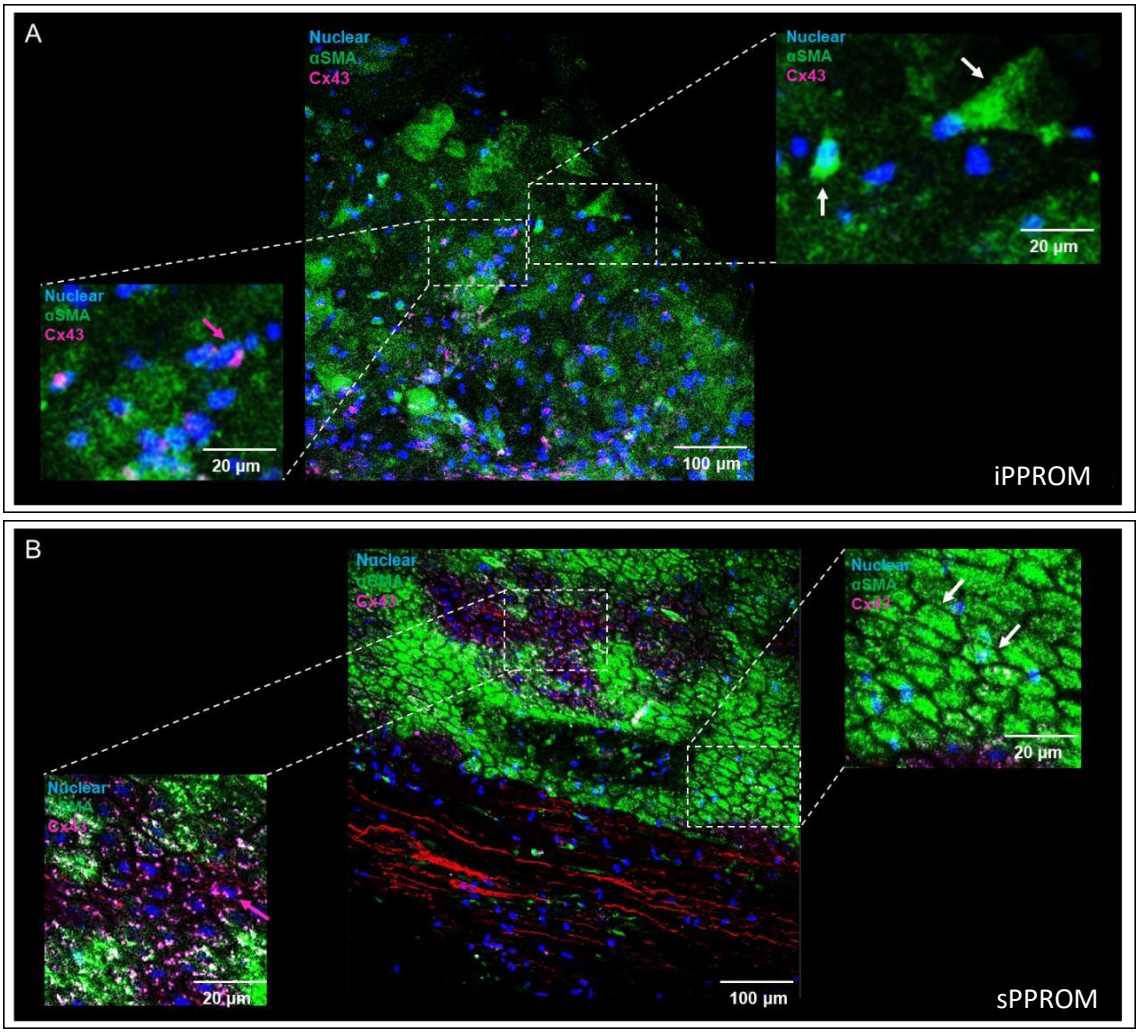

Figure 6.10: *Immunofluorescent imaging of AECs at (A) fetal surgery-induced iPPORM and (B) sPPROM defects. (A) In fetal surgery defects, AECs were visible only at some areas of the defect. (A) The epithelial layer, with αSMA staining showing a loss of the cuboidal structure usually seen in AECs. In a close-up image, AECs can be seen with elongated cytoplasmic extensions, suggesting they are changing morphologies into potential locomotive AMC/MFs. Cx43 plaques within αSMA-expressing amniotic epithelial cells localised in both the cytoplasm and nucleus (pink arrows). (B) In PPROM defects, AECs retained cuboidal morphologies with elongated nuclei tangential to the wound. Cx43 plaques were concentrated around and within the nuclei of AECs (pink arrows). AM = amniotic membrane, AECs = amniotic epithelial cells, AMCs = amniotic mesenchymal cells, Cx43 = connexin 43, αSMA = alpha smooth muscle actin. Scale bars = 100 µm, 20 µm.*

Chapter 7

Final Discussion

Chapter 7: Final Discussion and potential impact of findings

The multifactorial aetiology of PPROM has complicated research attempts to understand FM wound healing and weakening mechanisms that lead to rupture. Strategies to repair wounds in human FM defects with glues, collagen or fibrin plugs have failed to restore structural function of the FM and promote tissue regeneration to repair the wounds. The mechanisms that promote healing and closure of wounds in FM defects are unclear and influenced by the species and model system used to investigate the healing pathways. The present study investigated the mechanisms that heal human FM after spontaneous and iatrogenic rupture in term and preterm AM.

Despite some clear correlations between Cx43 and TGFβ1 expression with the increased expression of αSMA concurrent with changes in cell morphologies after trauma and/or CTS, this thesis has presented largely observational results. In **Chapter 4**, the most prominent limitation was the fact that neither Cx43 nor TGFβ1 were pharmacologically targeted, thus their actions on AM resident populations after trauma were not elucidated. In addition, the limitations associated with the Cx43 antibody, as extensively described in **Chapter 4**, makes the imaging results unreliable despite the quantification of the Cx43 gene via qPCR. Western blots should have been performed to ensure the Cx43 protein was increased in expression, and future studies should ensure this is done.

In **Chapter 5**, despite pharmacological inhibition of Cx43, TGFβ1 was not inhibited, thus if there is any synergy between the two proteins it is impossible to know until those experiments are performed. Additionally, the number of donors collected for **Chapter 5** are extremely low, resulting in some data not being used in the final thesis as it did not meet the minimum number required by the power calculations. I have addressed the challenges with collecting preterm fetal membranes and the COVID-19 pandemic made collections even more difficult. I spent hours on end on the labour ward to be rejected by doctors, midwives and patients alike and every day I was uncertain on whether I would have a donor to take to the lab. The

pandemic resulted in about five months where I could not even enter the hospital as students were not permitted to enter during the peak of the crisis. When I was able to, I found that patients were not as willing to consent to my study as the pandemic increased their hesitancy to participate in any research studies. Furthermore, although the midwives were polite and helpful, during the pandemic it became extremely difficult for them to help me with donor collections are they had other priorities. Ideally in the future, more donors will be collected for each cohort to elucidate the mechanotransduction processes in preterm FM.

Chapter 6 is merely an observational study which only aimed to investigate changes in cell morphology and collagen orientation in defects caused by spontaneous or iatrogenic PPROM. Future studies could focus on the changes in collagen types known to be altered during pathological rupture and the MMPs responsible for their breakdown. The influence of Cx43 on cell viability, morphology and healing can be investigated after Cx43 pharmacological knockdown at the wound edge. Please refer to the discussions for all results chapters for more detailed study limitations and future experiment recommendations.

To further the work presented in this thesis, the following research priorities will be considered: a) Investigating the Cx43 and TGFβ wound healing mechanisms in a larger patient cohort with a broader indication for PPROM and preterm birth to develop a better understanding of healing and tissue weakening under CTS; b) To identify novel therapeutic targets for pharmacological intervention and harness the wound healing capabilities of the AM that this thesis, as well as others, have elucidated and; c) To develop novel sealing technologies with bioactive materials to promote the vital areas of the FM as described by this study and others, in a gestational-age, defect size and clinical indication manner. Each research priority will be explored in more detail in this chapter.

7.1 Further investigating Cx43, TGFβ and mechanotransduction mechanisms in term and preterm AM

Future studies could be performed to elucidate the role of Cx43 in AM wound healing and repair. To do so, we must first consider the role of Cx43 in wound healing in other tissue types, which was briefly touched on in **Chapter 2**. In skin wounds, Prof David Becker's group has extensively shown how Cx43 regulates the wound healing mechanism [250-252,294,299]. The spatial-temporal effects of Cx43 observed in AM healing throughout this study are further highlighted when looking at dermal versus epidermal wound healing [250,251]. Initially, Cx43 was downregulated within 24 hours in cutaneous skin injuries in the epidermis, followed by keratinocyte migration and fibroblast migration across defects [250,251]. However, sustained Cx43 upregulation hindered cell migration and fibroblast differentiation during the granulation stage of wound healing [272]. In contrast, Cx43 was overexpressed in fibroblasts in deep dermis immediately after trauma, promoting granulation and scar formation [272]. The mechanism by which this occurs in the deep dermis involves the intracellular transfer of calcium among fascia fibroblasts and signal transduction mediated by Cx43 intracellular communication [272]. This results in fascia fibroblasts migration to the wound centre, leading to synthesis and deposition of collagen type I in defect sites [272].

Similarly, in the defect site of buccal mucosal and gingival tissues, Cx43 was initially downregulated to allow for quick healing response [298,299]. In vascular endothelial cells, Cx43 expression rapidly increases, leading to a cascade of pro-inflammatory pathways to be activated, resulting in enhanced vasodilation and neutrophil infiltration, which promotes the differentiation of fibroblasts to a contractile phenotype to initiate migration and reepithelialisation at the wound [272]. Sustained overexpression of Cx43 leads to increased inflammation and damage caused by neutrophil and macrophage action [250,272]. Thus, the findings in the current thesis may imply that Cx43 is essential for the initiation of wound healing mechanisms but its effects on cell migration and ECM synthesis become counteractive depending on time, defect size and tissue type.

The differential effects of Cx43 in highly vascularised tissue versus those seen in the avascular AM are presumably due to the lack of angiogenic growth factors (e.g. VEGF) that promote tissue granulation [244]. Despite this, we can assume that sustained Cx43 upregulation in the AM also promotes immune cells accumulation, as high AF concentrations of CD4+, CD8+ T cells and monocytes/macrophages concurrent with IL-6 increase have been shown in PPROM patients between two days of rupture [355]. The downregulation of regulatory T cells (T regs) in maternal peripheral blood has also been associated with pre-eclampsia and increased risk of preterm birth [356]. Thus, the upregulation of Cx43 and immune cell activation warrants further investigation to best correlate the inflammatory response in the AM and FM to other tissue types.

Poor healing mechanisms have previously been attributed to the overexpression of Cx43 at cell-to-cell contacts [249-251]. The focus of the study in **Chapter 4** was on Cx43 and TGFβ1 expression at the wound edge after 4 days of trauma, thus the next natural step would be to complement this work with experiments that investigate Cx43 signalling in more detail. Different research groups have shown AECs undergo EMT to locomotive cell types, thus the role of AEC transition and the purse-string contraction hypothesis at the wound edge of term AM defects warrants further investigation in the future [49,66,77]. Using term human FM, defects from iatrogenic fetal surgery or sPPROM patients and/or scratch-wound assays of primary AECs and AMCs, MET-specific markers (such as E-cadherin) and Cx43 expression could be correlated to cell migration and collagen expression.

In **Chapter 6**, the expression of TGFβ-mediated EMT was discussed, with emphasis how this can activate pathological inflammation in patients at risk of PPROM and preterm birth [77,183]. In other wound healing models, such as corneal endothelial healing, growth factors (EGF, TGF, PDGF), interleukins (IL-1, 6 and 10) and TNFα are released by corneal cells after trauma [357]. TGFβ isoforms (1, 2 and 3) are abundantly expressed by the corneal epithelium and stromal keratocytes. TGFβ types can act as both anti-inflammatory (e.g. by inhibiting EGF-induced proliferation) and pro-inflammatory stimulants [357]. TGFβ2 enhances corneal

epithelial wound healing via integrin β1, mediating p38MAPK signalling through the TGFβ Smad signalling pathway and promoting EMT to a migratory population [357]. Keratocytes are differentiated to fibroblasts and myofibroblasts, mediated by TGFβ and other growth factors (e.g. FGF) and secrete tenacin-C, collagen type III and promote actin filament sliding to generate contractile forces [357]. Crosstalk of signalling pathways through ERK, MAPK, PI3K/Akt and NF-κB between these epithelial cells promotes cell migration and proliferation [357]. This is further followed by IL-1-activated keratinocyte apoptosis through Fas/Fas ligand activation [357]. These signalling pathways are activated in FM, particularly in the ZAM, during labour initiation and *in vitro* strain [105,152,161]. The differential effects of TGFβ subtypes should thus be investigated in the context of fetal membranes.

In **Chapter 5**, TGFβ gene expression was found to be gestational-age and site dependent and importantly down regulated after Cx43 inhibition in preterm growth restricted and PPROM AM. In contrast, in FM taken from fetal surgeries, TGFβ tended to be upregulated after Cx43as treatment, highlighting the differences between pathological rupture, mechanisms of growth restriction and iatrogenic PPROM. Damage caused by cigarette exposure of AM explants or AM cell populations increased expression of vimentin and N-cadherin leading to a greater transition between cell states triggered by TGFβ [77,180]. Cx43 has also been shown to act as a direct transcriptional regulator of N-cadherin via translocation to the nucleus and binding to the N-cadherin promoter, controlling migration of neural crest cell and enhancing cellular morphological changes [266]. In **Chapter 6**, senescence and oxidative stress-induced inflammatory pathways were discussed in context to large sPPROM and fetal surgery-derived defects [184,185]. Decidua activation through DAMPs secretion and p38MAPK activation in the FM have also been shown to influence FM inflammation [186-188]. Thus, the differential effects of trauma on Cx43 transcriptional activity could be investigated in context to novel pathways of FM aging, senescence and TGFβ release. To do so, the expression of N-cadherin, ROS and/or TGF-mediated p38MAPK signalling could be correlated with Cx43 nuclear localisation in our *in vitro* trauma model or in large sPPROM and iatrogenic fetal surgery defects.

The expression of MMPs by myofibroblasts has not been investigated in this thesis. MMP-9 was overexpressed in whole preterm FMs, correlating with programmed biochemical events leading to parturition [129]. The pro-inflammatory cytokines IL-1β and TNFα acting as paracrine or autocrine modulators have been shown to influence MMP-9 deregulation in premature membranes and thus investigating their expression after trauma could elucidate signalling pathways upstream of MMP-9 [310]. The activity and expression of MMP-9 could be correlated in future investigations to TGFβ1 or other cytokine-induced MF activation and collagen remodelling. To determine a more accurate timing of Cx43 activation and TGFβ1 expression correlating with MF differentiation and collagen deposition at the WE, studies could investigate shorter time intervals between day 1 and day 4 of culture. Additionally, the concentration of macrophages within AF and their expression of TGFβ1 proposed to influence differentiation of AMCs to MFs could be investigated *in vitro*.

Future investigations of mechanotransduction mechanisms in preterm AM could be studied in more detail. We showed that Cx43 and TGFβ1 are stretch-sensitive proteins with significant differences in expression in a gestational age-dependent manner. However, in **Chapter 5** the distinct signalling effects of Cx43 and TGFβ1 expressions on biochemical changes in preterm AM were not investigated. TGFβ1 was found to influence proteoglycan production by increasing the synthesis of chondroitin sulphate, dermatan sulphate and sulphated hyaluronan in *in vitro* models of other tissue types [358,359]. PGE_2 release in cervical biopsies was markedly elevated after spontaneous term vaginal deliveries and found to increase the accumulation of labelled sulphated proteoglycans such as chondroitin sulphate and biglycan and to decrease decorin compared to unlaboured term cervices [330,331]. In preterm cervical fibroblast cultures, the concentrations of heparan sulphate were elevated compared to non-laboured donors [360]. In dental pulp cells, TGFβ1 enhanced collagen content and MMP-1 expression through the MEK/ERK signalling pathway [361]. TGFβ1 is also a key regulator of myofibroblast differentiation, and this is concurrent in our studies showing abundance of αSMA-expressing MFs in preterm AM after CTS and trauma [76]. The relationship of TGFβ1,

PGE_2, proteoglycan and sGAG release warrants further investigation with TGFβ1 and PGE_2/COX-specific knockout studies in preterm AM.

In term AM, our group previously determined that repetitive CTS and pharmacological knockdown of Cx43, AKT/PI3K and COX-2/PGE_2 signalling influenced the ECM composition [105]. In osteocytes, Cx43 has a SER-373 substrate binding site for AKT which following mechanical stimulation, activated Cx43 phosphorylation and enhanced Cx43 gap junction stability and interaction with α5 integrin [328,339]. In response to mechanical strain, Cx43 hemichannels facilitated PGE_2 release in osteocytes, which could be a key event occurring during CTS in preterm AM [340]. The overexpression of Cx43 in chronic wounds has been correlated with severe inflammation, MMP activity and subsequent collagen and elastin reduction [341,342]. Taking these findings, future work could focus on the influence of downstream AKT/PI3K, MEK and COX-2 signalling on preterm AM ECM composition and inflammatory factors (e.g. PGE_2, IL-6, MMP activity) in comparison to term AM. In term AM studies, a potential synergistic relationship of AKT and Cx43 in weakening AM mechanotransduction was suggested [105]. Functional pharmacological studies could focus on whether in preterm AM, AKT phosphorylates Cx43 in SER-373, which could provide a new therapeutic area for development to prevent AM weakening and rupture.

The importance of MPP expression should be further investigated. Mogami's group has shown that incubation of human primary AMCs, but not AECs, with thrombin resulted in MMP-1 and MMP-9 gene expression and activity, concurrent with COX-2 expression and PGE_2 release [14]. In AMCs and fetoscopy samples, PAR-1 induced thrombin-mediated regulation of MMP9 [14,362], while TLR4 induced thrombin-mediated regulation of MMP-1 and COX-2 [14]. The regulation of MMPs by thrombin, a marker for blood coagulation and wound healing, could be investigated in preterm AM in response to CTS and trauma.

In **Chapter 5**, it was hypothesised that extensive ECM remodelling was occurring due to mechanical stimuli and/or inflammation in preterm AM after comparisons to CTS response in term AM [105]. The increase of sGAGs in response to trauma could indicate a breakdown of

collagen fibril connections but also to production of new GAGs for wound repair that was ultimately unsuccessful due to repetitive strain. Where collagen and sGAG increased in the same sample, it may be due to an imbalance in the rate of collagen production and the rate of collagen breakdown, releasing sGAGs into the media. GAGs are also core components of proteoglycans and their presence could further indicate proteoglycan remodelling and/or breakdown. This response to CTS frequency correlated with elastin content elevation, particularly in traumatised PAM samples in all preterm patient groups, with variation between clinical indications. The concentrations of proteoglycan biglycan and decorin, which are essential components of the AM during development and parturition, could be further investigated in preterm AM after CTS and trauma. Where Cx43 antisense did not rescue weakening mechanisms, it could be because the tissue was significantly damaged or biochemically altered due to preterm birth or because higher Cx43 antisense concentrations are needed depending on the clinical indication, to influence the mechanotransduction response.

In this study, SHG imaging was used to visualise collagen fibrils. Whilst a powerful technique, SHG does not differentiate between different collagen types and whether fibres are newly synthesised. To provide more collagen structural information, future studies could use other imaging techniques such as polarised Raman spectroscopy and small-angle X-ray scattering (SAXS) diffraction to derive information on collagen fibril orientation and AM mineral composition. The AM has an abundant organisation of different collagen types, some of which, such as the degradation of collagen type IV, are key markers in preterm AM [129,310]. Correlating MMP-9 and 13 with changes in different collagens expressions could provide insight into the role of trauma and inflammation relative to non-traumatised tissue. Previous efforts to visualise elastin by SHG imaging have been unsuccessful by our group and thus alternatively the fastin-elastin assay kit could be used to determine changes in elastin content after *in vitro* trauma in term AM.

Patient variability due to the multifactorial nature of PPROM was observed throughout the mechanotransduction studies in **Chapter 5,** which should be studied in a larger patient cohort. Thus, it would be critical to develop an extensive tissue sample database whereby Cx43, TGFβ1 expression and structural composition of the AM can be compared depending on patient information. Patient details could include maternal age, previous preterm birth history, maternal and placental complications, race/ethnicity, exposure to pollution and more that could influence FM weakening to identify patients with greater risk of PPROM. Vaginal deliveries were excluded in this study and thus it would be of interest to investigate mechanotransduction mechanisms in FM after natural labour in term and preterm donors.

The mechanical properties of preterm AM are poorly understood and thus to complement these studies, mechanical strength testing will determine whether biochemical alterations induced by CTS, trauma and inhibition of therapeutic targets correlate to changes in mechanical strength. The BOSE bioreactor system is capable of measuring strain to failure (rupture strength (N)), tangent modulus and ultimate tensile stress over time. Comparing changes in mechanical properties of preterm samples from sPPROM patients to iPPROM and term AM will provide further insight into the effects of CTS and inhibition of stress sensitive proteins on membrane integrity.

Whilst the present study attempted to quantify ECM disruption, MF differentiation and wound healing markers in preterm AM, repetitive stretch may not mimic the *in-utero* environment. To best mimic FM weakening mechanisms *in utero*, more accurate bio-reactor models must be developed to represent repetitive strain that could lead to PPROM. Inflation mechanical testing could provide an alternative to mimic how pressure from amniotic fluid influences the mechanical and biochemical properties of preterm AM. Novel models to study AM cell populations using FM organ-on-a-chip (FM-OO-C) methods have been recently developed [362,363]. The authors used primary AECs in a 2-chamber FM-OO-C with a semi-permeable membrane treated with CSE [362,363]. These studies highlights the use of FM-OO-Cs for detailed molecular investigations into FM weakening mechanisms by subverting animal models [362,363].

7.2 Identifying novel therapeutic targets in the FM for pharmacological intervention

Using FM explants, researchers have attempted to mimic pro-inflammatory pathways by incubating tissues with TNF and IL-1β, ROS and other factors to recapitulate biochemical changes that lead to weakening [183]. Moore *et al.,* 2021 showed GM-CSF induced progesterone P4 concurrent with MMP-2 induction to remodel ECM, suggesting this pathway could propagate inflammation and PPROM induction [176]. Using P4 inhibitors, the authors showed progesterone then acts in a paracrine fashion to inhibit GM-CSF-induced weakening in FM explants and thus if progesterone activity is altered, GM-CSF-mediated inflammation will cause MMP-2 overexpression and ECM degradation [176]. Progesterone administration in women at risk of preterm birth is routinely used, however targeting novel pathways that influence progesterone activity such as GM-CSF could further perturb pathological inflammation and rupture [364].

Lipopolysaccharide is an endotoxin of gram-negative bacteria which can invade the feto-maternal environment, placenta, and FM and has been implicated as a triggering factor in preterm birth [365.] LPS-induced inflammation has been associated with elevated IL-1β, 10, 6, and TNF in the placenta of pregnant mice, leading to fetal ilea injury and preterm birth and death [366,367]. Lappas and colleagues have utilised the bio-active plant component polyphenol to decrease the FM weakening response [368]. Resveratrol has been shown to activate the antiinflammatory sirtuin 1 (SIRT1) leading to a decrease in lipopolysaccharide (LPS)-induced cytokine gene expression (IL-1β, 6 ,8 and TNF) in FM explants after term spontaneous onset, concurrent with a decrease in PGE_2 release [368].

Furthermore, the use of flavonoids has been shown to reduce LPS and IL-1β induced expression of IL-6 and 8, COX-2 mediated PGE_2 secretion and MMP-9 activity in FM explants and primary AM cells [183,369]. Notably, the flavonoids nobiletin and sibilin downregulated cytokine release and MMP-9 activity in FM explants from spontaneous preterm deliveries [183,369,370]. Chemokine expression by gestational tissues (cervix, myometrium, FM) during pathological labour has been explored, with researchers showing the CX3CL1-CX3CR1 axis

controls intrauterine recruitment of macrophages and neutrophils and thus accumulation of macrophage-induced inflammatory mediators such as COX-2. This causes PGE_2 release and propagates FM rupture in a mouse model [371].

In FM taken from preterm deliveries, Lappas' group showed the overexpression of the endoplasmic reticulum proteins GRP78, IRE1 and spliced XBP1 [372]. After treatment with LPS endotoxin, the authors further showed increased expression of ER stress proteins and IL-1β induced-MMP-9 release in primary AM cells [372]. Using the FDA-approved chemical chaperones 4-phenylbutyric acid (4-PBA) and tauroursodeoxycholic acid (TUDCA) led to the decrease in inflammatory IL-1β-induced MMP-9 response [372]. Despite human use approval, clinical studies for the use of these drugs in pregnant women have yet to be performed. Other studies have found that glycogen synthase kinase 3 (GSK3) activity was elevated in the FM following term and preterm labour [373]. The authors stimulated FM using three known TLR ligands: *E. coli* derived-LPS, synthetic FSL1 and flagellin to simulate bacterial infections and initiate AM cell inflammatory response [373]. Using the GSK3 inhibitor CHIR99021, they determined that GSK3 activity decreased TLR-mediated IL1β, TNFα and PGE_2, indicating GSK3 as a potential target for pharmacological intervention [373].

PPROM-derived FM also exhibits a decrease in AMP-activated kinase (AMPK) activity compared to term FM. Treatment with AMPK activators (AICAR, phenformin and A769662) in PPROM FM and primary AM cells decreased LPS, flagellin, and viral dsDNA analogue poly(I:C)-mediated IL-6 and 8 and MMP-9 release [374]. Metformin, an AMPK activator has been indicated to be safe to use in pregnancy and thus warrants further investigation as a potential therapeutic [374]. The pro-viral integration site for Moloney murine leukemic virus 1 (PIM1) kinase has been significantly overexpressed in FM following spontaneous term labour and preterm chorioamnionitis [375]. The SMI-4a and AZD1208 inhibitors for PIM1 caused significant downregulation of LPS or flagellin-mediated IL-8 and $PGF_{2\alpha}$ expression. Some PIM1 inhibitors are currently in clinical trials for various cancers and thus could pave the way for clinical and preclinical testing for decreasing inflammation in preterm birth [375].

7.3 Novel sealing strategies for fetal membrane repair

This thesis identified the presence of elongated MFs and AECs expressing αSMA at the defect sites of both term and preterm FM after trauma, surgery and/or CTS. This is promising and indicates that despite prolonged rupture, the AM retains vital areas that could be promoted to initiate wound healing by future sealing strategies. To investigate novel sealing strategies to repair FM wounds, we must first consider the limitations of those that have failed to promote successful tissue repair and regeneration. **Chapter 2** briefly touched on the challenges and setbacks of using collagen, fibrin, and synthetic polymers in FM wound healing. Despite some promising results in animal models, researchers have failed to develop successful sealants that adhere to the FM over long periods of time [26-35]. This section will discuss the implications of this study that contribute to our knowledge on how to harness the native wound healing properties of the AM in a gestational-age and clinical indication manner.

Let's first consider sealing strategies in skin wounds, which have been extensively researched and suggest properties that could be used in the FM. Sealants in skin wounds include the use of biomimetic hydrogel scaffolds, such as proteins (collagen, gelatine), polysaccharides (chitosan, heparin, destran), synthetic polymers (PEG, poly(lactic-*co*glycolic acid) (PLGA)) and stem cell based therapies [376]. Importantly, bioactive functionalisation of hydrogels is essential to promote tissue regeneration, particularly in the context of FM healing where weakening factors can be specifically targeted. In mouse diabetic ulcers, the use of heparan sulphate hydrogel enhanced granulation, vascularisation, and reduced inflammation by scavenging pro-inflammatory chemokines, presumably by increasing cross-linking of ECM proteins to negatively charged heparin [377]. In fetal membranes, heparan sulphate and other GAGs are abundant throughout, and particularly in the spongy layer, creating a viscous environment that sustains the FM's mechanical properties [113,114]. In **Chapter 5**, the release of sGAGs after CTS and/or trauma in preterm AM could be a consequence of the loss of covalent bonds between GAGs and proteoglycans and other ECM components that are

essential in maintaining FM structure. Thus, replacing GAGs in a carefully dosed manner as to avoid increased oedema in the AM could be a beneficial approach to promoting FM healing.

In skin wounds, the abilities of different hydrogel sealing plugs have been used to harvest fibroblast and myofibroblast healing capabilities. In a skin mouse study, Chen *et al* used peptide-modified PEG-chitosan hydrogels to accelerate fibroblast proliferation, TGFβ1 expression and collagen secretion, all of which could be activated in FM defects [378]. Combining myofibroblast-favouring hydrogels with Cx43 antisense technology could further enhance the wound healing response in AM defects, potentially through the purse string contraction mechanism.

Exploring clinically approved products in other tissue types and the FM such as PEG and collagen scaffolds in combination with Cx43 or TGFβ are another potential option. Using gene transfer of TGFβ1 or 3 in cartilage tissue engineering, researchers have used bone marrow derived MSCs within polyglycolic hydrogels and PEG/hyaluronic acid hydrogels in mice [379,380]. The authors showed controlled release of growth factors resulted in increased neocartilage formation higher GAG production and collagen type II [379,380]. In venous leg ulcer modelled in rats, collagen scaffolds coated with Cx43 antisense resulted in reduced inflammation, increased wound re-epithelialisation, and sustained Cx43 release over 7 days [381]. Exploiting the presence of MFs and Cx43 in the AM at different gestational ages to harness healing with growth factors is an area of research that can be explored to target natural AM healing mechanisms.

Human amniotic membranes have been used in clinical and preclinical trials to heal different tissue wounds, including human burns and corneal defects [48]. Decellularized AM (DAMs) are used as a scaffold material to promote tissue remodelling owing to its biological properties such as anti-inflammatory effects due to HA production, antibacterial factors such as elafin and β-defences, anti-fibrotic properties due to generally low TGFβ expression and importantly, low antigenicity [48]. AECs have been shown to secrete immunomodulatory factors that prevent maternal-derived immune cell infiltration [48]. DAMs have been used a native AM,

allogenic grafts and as a tissue engineering approach by combining DAMs with collagen or HA hydrogels and /or electrospun with umbilical cord MSCs [48]. In corneal treatments, regenerated epithelium grows over the DAMs and the membranes is almost fully incorporated into the defect [48]. In FM defects in rabbits, DAMs displayed better sealing capacity and reepithelization of the defects compared to synthetic polyester-urethane scaffold (DegraPol), with minimal inflammation [33]. However, as with other sealing techniques, adhesion to the FM is minimal and thus warrants further investigation into incorporating adhesive properties.

Furthermore, we must consider if it is beneficial to seal ruptured FM defects if there is a detected infection. This could result in sealing the infected part of the FM and unwillingly creating an environment in which microbial colonies can thrive, furthering the risk of preterm birth and maternal and fetal sepsis. **Chapter 6** discussed the implications of pathogen-activated inflammatory pathways and their influence on FM weakening and rupture. Here, we will discuss novel targets that can be pharmacologically inhibited in combination with sealants to decrease inflammatory pathways in FM that lead to PPROM [60].

There are studies emerging that suggest antibiotic treatment may be able to target intra-amniotic infection. Maternal intravenous antibiotic administration (regimen of ceftriaxone, clarithromycin, and metronidazole) between 16^{+0} to 29^{+6} weeks GA in a small patient group (*n*=22) was found to be effective in resolving intra-amniotic infections in 75% of patients with singleton pregnancies and cervical insufficiency following bacterial detection using amniocentesis [382]. Infection status was measured by a decreased in amniotic fluid-derived IL-6 and MMP-8 [382.] Intrauterine inflammation was also minimised after anti-inflammatory drug incubation in human FM explants taken from women delivering spontaneously preterm between 30 to 34 weeks GA [383]. Intravenous administration of antibiotic regiments in PPROM patients between 24^{+0} to 33^{+6} weeks GA reduced the intensity of both intra-amniotic inflammation and infection as measured by IL-6 concentrations in amniotic fluid [384].

Optimisation of sealant biomimetic properties is an essential consideration, as plugs must be able to mimic tissue stiffness, mechanical properties, adhesiveness, and porosity to decipher

biochemical cues at the defect site. In the context of FM healing, we could consider infusing antibiotic and/or anti-inflammatory drugs in future sealing strategies to promote FM healing after PPROM, prevent infections and tackle existing ones. Reducing ROS activation and excessive chemokine release would be desirable. Cleverly designed PEG and GAG derivative hydrogels were able to scavenge the inflammatory chemokines monocyte chemoattractant protein 1, IL-8 and macrophage inflammatory proteins (MIP)-1α and 1β, reducing inflammation in diabetic mice [376,385]. The addition of the anti-inflammatory SEW2871 compound to gum-chitosan hydrogels gels led to M2 macrophage recruitment and reduced oxidative stress in diabetic wound healing [376,386]. Zhao *et al* developed a ROS scavenging hydrogel composed of polyvinyl alcohol (PVA) cross-linked by a ROS-responsive linker [376,387]. After treatment of mouse dermal wounds, the authors determined there was a decrease in ROS-induced inflammatory response and M2 macrophage migration to the defect site promoting integrin α3 and collagen deposition, followed by a downregulation of pro-inflammatory cytokines (IL-6, TNFα) [387]. The authors further showed that their hydrogel could be loaded with antibiotics and growth factors, suggesting they can be used to delivery drugs to damages tissue [387]. This would be a particular interest in FM healing, as drug-loading hydrogels can be used to delivery pharmacological agents to specifically target FM weakening factors, such as Cx43.

Sealing strategies for PPROM patients must further account for the presence of antimicrobial colonies that could interact with the plug composition. Resident macrophage populations within the amniotic fluid are presumably activated to M2 macrophage phenotypes in response to infection. In a mouse model, Mogami's group showed that collagen type 1 injection led to improved closure rates in 0.8 mm defects concurrent with M2-macrophage accumulation, activating collagen receptor domain DDR2 and inducing AMC migration [82]. Despite success in animals, AF pro-inflammatory cell populations, particularly in the presence of infection, are likely to act on these plugs and degrade them. The concentration of immune cells (T cells, B cells, NK cells, monocytes/macrophages, and neutrophils) were elevated in the amniotic fluid of women with intra-amniotic infection and inflammation concurrent with IL-6 overexpression

compared to those without infections, which can affect sealant hydrolysis and instability by activating phagocytosis [97,99,100].

Collagen plug degradation can occur by resident AF and FM cells. In the dermis, dermal fibroblasts and M2-macrophages internalise collagen fibres in lysosomes and then degrade them by lysosomal cysteine protease [388]. Elastin, as well as collagen, also suffers from increased enzymatic and non-enzymatic degradation and calcification before and after implantation into animal models [389]. Biomimetic hydrogels, collagen fibril plug and DAMs mimic ECM components and presumably promote cell migration and collagen deposition at the wound site. This is particularly important in FM defects, where the lack of vasculature prevents common wound healing mechanisms of being activated and thus a favourable environment that FM cell populations can harness to repair the defect. We must thus consider how to stabilise sealants while promoting resident ECM remodelling and synthesis. The use of tannic acid cross-linking with aortic elastin prevented enzymatic degradation by elastase and collagenases, as opposed to the traditional glutaraldehyde-based tissue treatments in cardiovascular implants [389]. Tannic acid's phenol groups can bond to elastin's proline-rich hydrophobic regions, further enhancing the toughness of the hydrogel and could be a promising approach to hydrogel stabilisation and tissue regeneration [389].

Despite the negative effects of a host reaction discussed, chemoattraction of AF macrophage and stem cell populations is still a desirable aim when designing novel sealing strategies, as these can promote MF differentiation and wound healing mechanisms. In **Chapter 4**, the role of myofibroblast differentiation was shown; thus, after considering studies where macrophage infiltration led to AM cell population differentiation, AMC transformation was hypothesised to be triggered, in part, by resident AF immune cell populations. To subvert the host-immune cell activation by AF cells and promote favourable AF cell accumulation, collagen plugs have been developed enriched with amniotic fluid cells to seal iatrogenic FM defects in rabbits, which led to accumulation of heterologous AF cells fibroblast and epithelial cells in the centre

of the plug [45]. Despite these promising results, the plug has poor adhesive properties and has not been investigated in humans [45].

Novel adhesives have since been used in preclinical models of other tissue types. Tough gel adhesives (TA) are composed of calcium ion cross-linked alginate mixed with a polyacrylamide (Alg-PAAm) covalent network with a strong adhesive surface made up of chitosan [390]. The biocompatibility and strong adhesive properties of TA were demonstrated after implantation of TA into a rat model for 2 weeks and through an *in vitro* viability assessment of human dermal fibroblasts in a 24-hour culture [390]. Histological results from the rat model showed lower inflammation levels than those of the commercial adhesive cyanoacrylate [390]. Recently, the same team showed the reparation of Achilles tendons in live rats with TA sustainably released the corticosteroid triamcinolone acetonide and strongly adhered to the rupture site [390]. The adherent TA reduced inflammation, chemokine-induced tendon stem and progenitor cell accumulation and M2-macrophage infiltration [390].

In iPPROM defects, FM sealants would further interact with bleeding around the fetoscopic hole caused by fetoscopic or surgical trauma. The same can be presumed in sPPROM patients where vaginal bleeding is present. As discussed in **Chapter 6**, increase in maternal systemic inflammatory response due to vaginal bleeding has shown to activate the extrinsic pathway of coagulation through monocyte release of TF, thrombin-activated myometrial contractions, and neutrophil accumulation cell secretion of MMP-1 and 3 that degrade FM collagens [12,351]. These factors could influence sealants' ability to adhere to the defect site and enzymatic activation from blood components can lead to hydrolysis of plugs, particularly if they are composed of collagen or other natural ECM components that can be targeted for degradation.

Testing novel sealing strategies in tissue surrounding the unborn fetus and in particular knockdown technologies such as Cx43 antisense or growth factor gene delivery, pose a significant challenge due to ethical implications. Approving drugs or plugs for pregnant mothers and fetuses in the womb is challenging. First there is a need for extensive

reproductive toxicology data and choosing the right animal model in which to test the technique out is complex, although likely to be the rabbit which has been used previously to develop collagen plugs [34,45]. The first-in-human safety/efficacy study would need strict inclusion/exclusion criteria with review of adverse events after each patient which will take time and be costly. Targeting defect sites in sPPROM patients is difficult as plugs would need to be inserted through the cervix and be designed to specifically target the defect site as binding to other parts of the FM could trigger more harmful side effects for the mother and the baby. In iPPROM patients, a plug could be inserted after fetoscopy, or open fetal surgery and targeted to the defect site using ultrasound in the former or by observation during surgery in the latter.

7.4 Final thoughts

This thesis has presented new evidence into the wound healing capabilities of term and preterm AM after trauma, CTS, and open fetal surgery. Harnessing the natural healing properties of the AM and the FM is an essential aim in designing novel sealant technologies to combat rupture. Pharmacologically targeting weakening pathways, such as Cx43, is an avenue that warrants further investigation to determine if this is beneficial in *in vitro* models. Better models are needed to mimic the FM environment *in utero*, including the activation of contraction-associated molecules that lead to FM strain and deformation during labour. In conclusion, the present study provides an improved understanding of the wound healing mechanisms and mechanotransduction processes of term and preterm AM that could lead to premature rupture and delivery.

Publications:

Costa E, Okesola B, Thrasivoulou C, Becker D, Deprest J, David A and TT Chowdhury. Cx43 mediates changes in myofibroblast contraction and collagen release in human amniotic membrane defects after trauma. Scientific Reports. 2021;11(1).

Barrett D, Okesola B, Costa E, Thrasivoulou C, Becker D, Mata A, Deprest J, David A and TT Chowdhury. Potential sealing and repair of human FM defects after trauma with peptide amphiphiles and Cx43 antisense. Prenatal Diagnosis. 2020;41(1):89-99.

To be submitted:

Costa C, Thrasivoulou C, Becker DL, Deprest J, David AL, Chowdhury TT. Mechanotransduction Mechanims in preterm fetal membranes following trauma. *To be submitted to Scientific Reports.*

Oral Presentations at National and International conference contributions

1. **Costa E**, Thrasivoulou C, Becker D, Deprest J, David A and TT Chowdhury. *Trauma induced overexpression of Cx43 and potential healing mechanisms in small fetal membrane defects*. 23rd International Conference on Prenatal Diagnosis and Therapy, Singapore (https://www.ispdhome.org/ISPD2019).

Date: 9th to 11th September 2019

2. **Costa E**, Thrasivoulou C, Becker D, Deprest J, David A and TT Chowdhury. *Trauma induced overexpression of Cx43 and potential healing mechanisms in small fetal membrane defects* Preterm Birth Conference 2020. Online Event. (https://pretermconference.com/)

Date: 2nd to 3rd November 2020

3. **Costa E**, Thrasivoulou C, Becker D, Deprest J, David A and TT Chowdhury. *Mechanotransduction mechanisms in human preterm fetal membranes after trauma.* Preterm Birth Conference 2021. Online Event. (https://pretermconference.com/)

Date: 15th to 16th November 2021

4. **Fetal membrane Repair Network** Recurring event. Organised and presented FMR NT twice a year and held every April and November (2019 to 2022).
5. **Russell Binions PhD Symposium**. *Trauma induced overexpression of Cx43 and potential healing mechanisms in small fetal membrane defects.* Queen Mary University of London, School of Engineering and Materials Science Online Event.

Date: 19th of May 2020

6. **SEMS Research Showcase conference.** . *Trauma induced overexpression of Cx43 and potential healing mechanisms in small fetal membrane defects.* Queen Mary University of London, School of Engineering and Materials Science Online Event.

Date: 21st of January 2021

Poster presentations:

1. **Costa E,** Thrasivoulou C, Becker D, Deprest J, David A and TT Chowdhury. *Trauma induced overexpression of Cx43 and potential healing mechanisms in small fetal membrane defects*. 23rd International Conference on Prenatal Diagnosis and Therapy, Singapore (https://www.ispdhome.org/ISPD2019).

Date: 9th to 11th September 2019

2. **Costa E,** Thrasivoulou C, Becker D, Deprest J, David A and TT Chowdhury. *Trauma induced overexpression of Cx43 and potential healing mechanisms in small fetal membrane defects*. Biomaterials for Fetal and Child Health special symposium, 11th World Biomaterials Congress. Online event. (https://wbc2020.org/registration/)

Date: 11th to 15th December 2020

3. **Costa E,** Thrasivoulou C, Becker D, Deprest J, David A and TT Chowdhury. *Cx43 mediates myofibroblast contraction, migration and collagen release in human amniotic membrane defects after trauma*. Dynamic Cell IV. Royal Society of Biochemistry. Online event. (https://biochemistry.org/events/dynamic-cell-iv/)

Date: 14th to 9th of March 2021

4. **Costa E,** Thrasivoulou C, Becker D, Deprest J, David A and TT Chowdhury. *Mechanotransduction mechanisms in human preterm fetal membranes after trauma.* 25th International Conference on Prenatal Diagnosis and Therapy. (https://www.ispdhome.org/ISPD2021/Register)

Date: 6th to 8th of June 2021

5. The Industrial Liaison Forum. *Mechanotransduction mechanisms in human preterm fetal membranes after trauma.* Queen Mary University of London, School of Engineering and Materials Science. **Date:** 11th of November 2021,

Awards

Best Oral Presentation

Winner of Best Oral Presentation after presenting '*Mechanotransduction mechanisms in human preterm fetal membranes after trauma'* at the Preterm Birth Conference 2021 held on the 15th to 16th November 2021. Award Received on the 23rd of November 2021.

European Society for Biomaterials Poster Winner

Winner of Best Poster Award after presenting '*Trauma induced overexpression of Cx43 and potential healing mechanisms in small fetal membrane defects'.* The award was issued by European Society for Biomaterials during the 11th World Biomaterials Congress held on the 11th to 15th December 2020. Awad Received on the 20th of December 2020.

SEMS PhD Research Showcase Winner

Winner of Best PhD Oral Research Showcase Award after presenting '*Trauma induced overexpression of Cx43 and potential healing mechanisms in small fetal membrane defects'* at the PhD Research Showcase held by the QMUL Industrial Liaison Forum on the 21st of January 2021. The award was received on the 30th of January 2021.

Russell Binions Research Symposium Winner

Winner of the Best Oral Representation Award after presenting *Trauma induced overexpression of Cx43 and potential healing mechanisms in small fetal membrane defects'* at the Russell Binions Research Symposium held by QMUL on the 19th of May 2020. The award was received on the 25th of May 2020.

Funding Awards

Winner of the *Postgraduate Research Foundation Award* in June 2020 for the amount of £525 for conference expenses toward the 11th World Biomaterials Congress.

Training

Visited Prof David Becker and his team in Singapore at the Lee Kong Chian School of Medicine in NTU and discussed collaborative ideas for healing and repairing FM defects with biomaterials.

Fundraising and public engagement activities

1. Royal Academy of Engineering public engangement events with the Ideas Foundation (May 2019) and the Science Museum (Nov 2019).
2. The Bioengineering Experience events held in May 2019, September 2019 and September 2021.
3. Summer Science School with Prof Brian Cox.

Other Activities

Completion of “Introduction to good clinical practice” e-learning course.

Completed April 10th 2019

Completion of 210 hours of researcher development activities for the Queen Mary Diploma of Researcher Development (Q-Dip) award.

September 2021

References

1. Birth characteristics in England and Wales - Office for National Statistics [Internet]. Ons.gov.uk. 2022 [cited 7 February 2022]. Available from: https://www.ons.gov.uk/peoplepopulationandcommunity/birthsdeathsandmarriages/livebirths/bulletins/birthcharacteristicsinenglandandwales/2019

2. Overview | Preterm labour and birth | Guidance | NICE [Internet]. Nice.org.uk. 2022 [cited 7 February 2022]. Available from: https://www.nice.org.uk/guidance/ng25

3. Mehrotra D, Mishra D. Assessment of outcome of premature rupture of membrane. International Journal of Clinical Obstetrics and Gynaecology. 2021;5(3):394-396.

4. Medina TM, Hill DA. Preterm premature rupture of membranes: diagnosis and management. Am Fam Physician. 2006;15;73(4):659-64.

5. Al-Riyami N, Al-Shezawi F, Al-Ruheili I, Al-Dughaishi T, Al-Khabori M. Perinatal outcome in pregnancies with extreme preterm premature rupture of membranes (Mid-Trimester PROM). Sultan Qaboos University Medical Journal. 2013;13(1):51-56.

6. Boskabadi H, Zakerihamidi M. Evaluation of Maternal Risk Factors, Delivery, and Neonatal Outcomes of Premature Rupture of Membrane: A Systematic Review Study. Journal of Pediatrics Review. 2018;:77-88.

7. Doyle R, Alber D, Jones H, Harris K, Fitzgerald F, Peebles D et al. Term and preterm labour are associated with distinct microbial community structures in placental membranes which are independent of mode of delivery. Placenta. 2014;35(12):1099-1101.

8. Devlieger R, Millar L, Bryant-Greenwood G, Lewi L, Deprest J. Fetal membrane healing after spontaneous and iatrogenic membrane rupture: A review of current evidence. American Journal of Obstetrics and Gynecology. 2006;195(6):1512-1520.

9. Sivarajasingam SP, Imami N, Johnson MR. Myometrial cytokines and their role in the onset of labour. J Endocrinol. 2016;231(3):R101-R119

10. Menon R, Moore J. Fetal Membranes, Not a Mere Appendage of the Placenta, but a Critical Part of the Fetal-Maternal Interface Controlling Parturition. Obstetrics and Gynecology Clinics of North America. 2020;47(1):147-162.

11. Sinkey RG, Guzeloglu-Kayisli O, Arlier S, Semerci N, Moore R, Ozmen A, et al. Thrombin-induced decidual colony-stimulating factor-2 promotes abruption-related preterm birth by weakening fetal membranes. The American journal of pathology. 2020;190(2):388-399.

12. Erez O, Espinoza J, Chaiworapongsa T, Gotsch F, Kusanovic J, Than N et al. A link between a hemostatic disorder and preterm PROM: a role for tissue factor and tissue factor pathway inhibitor. The Journal of Maternal-Fetal & Neonatal Medicine. 2008;21(10):732-744.

13. Puthiyachirakkal M, Lemerand K, Kumar D, Moore R, Philipson E, Mercer B et al. Thrombin weakens the amnion extracellular matrix (ECM) directly rather than through protease activated receptors. Placenta. 2013;34(10):924-931.

14. Mogami H, Keller P, Shi H, Word R. Effect of thrombin on human amnion mesenchymal cells, mouse fetal membranes, and preterm birth. Journal of Biological Chemistry. 2014;289(19):13295-13307.

15. Papanna R, Mann LK, Tseng SC, et al. Cryopreserved human amniotic membrane and a bioinspired underwater adhesive to seal and promote healing of iatrogenic fetal membrane defect sites. Placenta. 2015; 36: 888–94

16. Tabor A, Philip J, Madsen M, Bang J, Obel EB, Norgaard-Pedersen B. Randomised controlled trial of genetic amniocentesis in 4606 low risk women. Lancet 1986;1:1287-93

17. Barrett D, David A, Thrasivoulou C, Mata A, Becker D, Engels A et al. Connexin 43 is overexpressed in human fetal membrane defects after fetoscopic surgery. Prenatal Diagnosis. 2016;36(10):942-952.

18. Carvalho N, Moron A, Menon R, Cavalheiro S, Barbosa M, Milani H et al. Histological evidence of reparative activity in chorioamniotic membrane following open fetal surgery for myelomeningocele. Experimental and Therapeutic Medicine. 2017;14(4):3732-3736.

19. Papanna R, Block-Abraham D, Mann L, Buhimschi I, Bebbington M, Garcia E et al. Risk factors associated with preterm delivery after fetoscopic laser ablation for twin-twin transfusion syndrome. Ultrasound in Obstetrics & Gynecology. 2014;43(1):48-53.

20. Harrison M, Keller R, Hawgood S, Kitterman J, Sandberg P, Farmer D et al. A randomized trial of fetal endoscopic tracheal occlusion for severe fetal congenital diaphragmatic hernia. New England Journal of Medicine. 2003;349(20):1916-1924.

21. Borgida A, Mills A, Feldman D, Rodis J, Egan J. Outcome of pregnancies complicated by ruptured membranes after genetic amniocentesis. American Journal of Obstetrics and Gynecology. 2000;183(4):937-939.

22. Sival D, Guerra M, den Dunnen W, Bátiz L, Alvial G, Castañeyra-Perdomo A et al. Neuroependymal denudation is in progress in full-term human foetal spina bifida aperta. brain pathology. 2011;21(2):163-179.

23. Mitchell L, Adzick N, Melchionne J, Pasquariello P, Sutton L, Whitehead A. Spina bifida. The Lancet. 2004;364(9448):1885-1895.

24. Adzick N, Thom E, Spong C, Brock J, Burrows P, Johnson M et al. A randomized trial of prenatal versus postnatal repair of myelomeningocele. New England Journal of Medicine. 2011;364(11):993-1004.

25. Adzick N. Fetal surgery for myelomeningocele: trials and tribulations. Journal of Pediatric Surgery. 2012;47(2):273-281

26. Chowdhury, T., Barrett, D., & David, A. Strategies to repair defects in the fetal membrane. In M. Kilby, A. Johnson, & D. Oepkes. Fetal Therapy: Scientific Basis and Critical Appraisal of Clinical Benefits. Cambridge: Cambridge University Press. Chapter 5. 2020;520-531.

27. Deprest J, Papadopulos N, Decaluwé H, Yamamoto H, Lerut T, Gratacós E. Closure techniques for fetoscopic access sites in the rabbit at mid-gestation. Human Reproduction. 1999;14(7):1730-1734.

28. Bilic G, Brubaker C, Messersmith PB, et al. Injectable candidate sealants for fetal membrane repair: bonding and toxicity in vitro. Am J Obstet Gynecol. 2010; 202: 85. e1–9.

29. Haller CM, Buerzle W, Brubaker CE, et al. Mussel-mimetic tissue adhesive for fetal membrane repair: a standardized ex vivo evaluation using elastomeric membranes. Prenat Diagn. 2011; 31: 654–60.

30. Mann LK, Papanna R, Moise KJ, Jr., et al. Fetal membrane patch and biomimetic adhesive coacervates as a sealant for fetoscopic defects. Acta Biomater. 2012; 8: 2160–5.

31. Kivelio A, Dekoninck P, Perrini M, et al. Mussel mimetic tissue adhesive for fetal membrane repair: initial in vivo investigation in rabbits. Eur J Obstet Gynecol Reprod Med. 2013; 171: 240–5

32. Papanna R. The problem of preterm delivery after laser surgery. Am J Perinatol. 2014;31(Suppl 1):S47–50.

33. Ochsenbein-Kolble N, Jani J, Lewi L, et al. Enhancing sealing of fetal membrane defects using tissue engineered native amniotic scaffolds in the rabbit model. Am J Obstet Gynecol. 2007; 196: 263. e1–7.

34. Engels AC, Joyeux L, Van der Merwe J, Jimenez J, Prapanus S, Barrett DW, et al. Tissuepatch is biocompatible and seals iatrogenic membrane defects in a rabbit model. Prenat Diagn. 2018; 38: 99–105.

35. Quintero RA, Morales WJ, Bornick PW, Allen M, Garabelis N. Surgical treatment of spontaneous rupture of membranes: the amniograft —first experience. Am J Obstet Gynecol. 2002; 186: 155–7.

36. Sung JH, Kuk JY, Cha HH, et al. Amniopatch treatment for preterm premature rupture of membranes before 23 weeks' gestation and factors associated with its success. Taiwan J Obstet Gynecol. 2017; 56: 599–605.

37. Engels AC, Van Calster B, Richter J, et al. Collagen plug sealing of iatrogenic fetal membrane defects after fetoscopic surgery for congenital diaphragmatic hernia. Ultrasound Obstet Gynecol. 2014; 43: 54–9.

38. Papanna R, Molina S, Moise KY, Moise KJ Jr., Johnson A. Chorioamnion plugging and the risk of preterm premature rupture of membranes after laser surgery in twin-twin transfusion syndrome. Ultrasound Obstet Gynecol. 2010; 35: 337–43.

39. Engels AC, Hoylaerts MF, Endo M, et al. In vitro sealing of iatrogenic fetal membrane defects by a collagen plug imbued with fifibrinogen and plasma. Prenat Diagn. 2013: 33: 162–7.

40. Mendoza GA, Acuna E, Allen M, Arroyo J, Quintero RA. In vitro laser welding of amniotic membranes. Lasers in surgery and medicine 1999;24:315-8Pathak B, Khan A, Assaf SA, Miller DA, Chmait RH. Amniopatch as a treatment for rupture of membranes following laser surgery for twin-twin transfusion syndrome. Fetal diagnosis and therapy 2010;27:134-7.

41. Pathak B, Khan A, Assaf SA, Miller DA, Chmait RH. Amniopatch as a treatment for rupture of membranes following laser surgery for twin-twin transfusion syndrome. Fetal diagnosis and therapy 2010;27:134-7.#

42. Chmait RH, Kontopoulos EV, Chon AH, Korst LM, Llanes A, Quintero RA. Amniopatch treatment of iatrogenic preterm premature rupture of membranes (iPPROM) after fetoscopic laser surgery for twin-twin transfusion syndrome. The journal of maternal-fetal & neonatal medicine the official journal of the European Association of Perinatal Medicine, the Federation of Asia and Oceania Perinatal Societies, the International Society of Perinatal Obstet 2017;30:1349-54

43. Barrett D, Okesola B, Costa E, Thrasivoulou C, Becker D, Mata A et al. Potential sealing and repair of human FM defects after trauma with peptide amphiphiles and Cx43 antisense. Prenatal Diagnosis. 2020;41(1):89-99.

44. Mallik A, Fichter M, Rieder S, Bilic G, Stergioula S, Henke J et al. Fetoscopic closure of punctured fetal membranes with acellular human amnion plugs in a rabbit model. Obstetrics & Gynecology. 2007;110(5):1121-1129.

45. Liekens D, Lewi L, Jani J, et al. Enrichment of collagen plugs with platelets and amniotic fluid cells increases cell proliferation in sealed iatrogenic membrane defects in the foetal rabbit model. Prenatal diagnosis 2008;28:503-7.

46. Devlieger R, Riley S, Verbist L, Leask R, Pijnenborg R, Deprest J. Matrix metalloproteinases-2 and -9 and their endogenous tissue inhibitors in tissue remodelling after sealing of the fetal membranes in a sheep model of fetoscopic surgery. Journal of the Society for Gynecologic Investigation. 2002;9(3):137-145.

47. McLaren J. Structural characteristics of term human fetal membranes prior to labour: identification of an area of altered morphology overlying the cervix. Human Reproduction. 1999;14(1):237-241.

48. Leal-Marin S, Kern T, Hofmann N et al. Human Amniotic Membrane: a review on tissue engineering, application, and storage. journal of biomedical materials research part b: Applied Biomaterials. 2020;109(8):1198-1215.

49. Richardson L, Menon R. Proliferative, migratory, and transition properties reveal metastate of human amnion cells. Am J Pathol. 2018;188(9):2004-2015.
50. Jacobs S, Sheller-Miller S, Richardson L, Urrabaz-Garza R, Radnaa E, Menon R. Characterizing the immune cell population in the human fetal membrane. American Journal of Reproductive Immunology. 2020;85(5).
51. Strauss, J. Extracellular matrix dynamics and fetal membrane rupture. Reproductive Sciences. 2012;20(2):140-153.
52. Weidinger A, Poženel L, Wolbank S, Banerjee A. sub-regional differences of the human amniotic membrane and their potential impact on tissue regeneration application. Front Bioeng Biotechnol. 2021;8.
53. Hieber A, Corcino D, Motosue J et al. Detection of elastin in the human fetal membranes: Proposed molecular basis for elasticity. Placenta. 1997;18(4):301-312.
54. Koo B, Park I, Kim J et al. Isolation and characterization of chorionic mesenchymal stromal cells from human full term placenta. J Korean Med Sci. 2012;27(8):857.
55. Parry S, Strauss J. Premature Rupture of the Fetal Membranes. New England Journal of Medicine. 1998;338(10):663-670.
56. Menon R, Radnaa E, Behnia F, Urrabaz-Garza R. Isolation and characterization human chorion membrane trophoblast and mesenchymal cells. Placenta. 2020;101:139-146.
57. Gupta A, Kedige SD, Jain K. Amnion and chorion membranes: potential stem cell reservoir with wide applications in periodontics. International journal of biomaterials 2015;2015:274082.
58. Martin L, Richardson L, Menon R. Characteristics, properties, and functionality of fetal membranes: an overlooked area in the field of parturition. Encyclopedia of Reproduction. 2018:387-398.
59. Malak T, Bell S. Distribution of fibrillin-containing microfibrils and elastin in human fetal membranes: A novel molecular basis for membrane elasticity. Am J Obstet Gynecol. 1994;171(1):195-205.
60. Menon R, Richardson LS, Lappas M. Fetal membrane architecture, aging and inflammation in pregnancy and parturition. Placenta. 2019;79:40-45.
61. Insausti C, Blanquer M, García A, Castellanos G, Moraleda J. Amniotic membrane-derived stem cells: immunomodulatory properties and potential clinical application. Stem Cells and Cloning: Advances and Applications. 2014:53.
62. Li J, Koike-Soko C, Sugimoto J, Yoshida T, Okabe M, Nikaido T. Human amnion-derived stem cells have immunosuppressive properties on nk cells and monocytes. Cell Transplant. 2015;24(10):2065-2076.

63. Tseng S, Li D, Ma X. Suppression of transforming growth factor-beta isoforms, TGF receptor type II, and myofibroblast differentiation in cultured human corneal and limbal fibroblasts by amniotic membrane matrix. J Cell Physiol. 1999;179(3):325-335.

64. Kim J, Kim J, N B, Jeong J, Song C. Amniotic membrane patching promotes healing and inhibits proteinase activity on wound healing following acute corneal alkali burn. Exp Eye Res. 2000;70(3):329-337.

65. King A, Paltoo A, Kelly R, Sallenave J, Bocking A, Challis J. Expression of natural antimicrobials by human placenta and fetal membranes. Placenta. 2007;28(2-3):161-169. doi:10.1016/j.placenta.2006.01.006

66. Mogami H, Hari Kishore A, Akgul Y, Word R. Healing of preterm ruptured fetal membranes. Sci Rep. 2017;7(1).

67. de Castro Silva M, Richardson L, Kechichian T, Urrabaz-Garza R, da Silva M, Menon R. Inflammation, but not infection, induces EMT in human amnion epithelial cells. Reproduction. 2020;160(4):627-638.

68. Centurione L, Passaretta F, Centurione M et al. Mapping of the human placenta. Cell Transplant. 2018;27(1):12-22.

69. Gibbons G. Grafix®, a Cryopreserved placental membrane, for the treatment of chronic/stalled wounds. Adv Wound Care (New Rochelle). 2015;4(9):534-544.

70. Lavery L, Fulmer J, Shebetka K et al. The efficacy and safety of Grafix ® for the treatment of chronic diabetic foot ulcers: results of a multi-centre, controlled, randomised, blinded, clinical trial. Int Wound J. 2014;11(5):554-560.

71. Battula V, Bareiss P, Treml S et al. Human placenta and bone marrow derived MSC cultured in serum-free, b-FGF-containing medium express cell surface frizzled-9 and SSEA-4 and give rise to multilineage differentiation. Differentiation. 2007;75(4):279-291.

72. Antoniadou E, David A. Placental stem cells. Best Practice & Research Clinical Obstetrics & Gynaecology. 2016;31:13-29.

73. Soncini M, Vertua E, Gibelli L et al. Isolation and characterization of mesenchymal cells from human fetal membranes. J Tissue Eng Regen Med. 2007;1(4):296-305.

74. Jones B, Li C, Park M et al. Comprehensive comparison of amnion stromal cells and chorion stromal cells by RNA-Seq. Int J Mol Sci. 2021;22(4):1901.

75. Giannoulias D, Haluska G, Gravett M, Sadowsky D, Challis J, Novy M. Localization of prostaglandin H synthase, prostaglandin dehydrogenase, corticotropin releasing hormone and glucocorticoid receptor in rhesus monkey fetal membranes with labor and in the presence of infection. Placenta. 2005;26(4):289-297.

76. McParland P, Taylor D, Bell S. Myofibroblast differentiation in the connective tissues of the amnion and chorion of term human fetal membranes—implications for fetal membrane rupture and labour. Placenta. 2000;21(1):44-53.

77. Richardson L, Taylor R, Menon R. Reversible EMT and MET mediate amnion remodelling during pregnancy and labor. Sci Signal. 2020;13(618).

78. Baum J, Duffy H. Fibroblasts and myofibroblasts: what are we talking about?. J Cardiovasc Pharmacol. 2011;57(4):376-379.

79. Petrov V, Fagard R, Lijnen P. Stimulation of collagen production by transforming growth factor-β 1 during differentiation of cardiac fibroblasts to myofibroblasts. Hypertension. 2002;39(2):258-263.

80. Gomez-Lopez N, StLouis D, Lehr M, Sanchez-Rodriguez E, Arenas-Hernandez M. Immune cells in term and preterm labor. Cell Mol Immunol. 2014;11(6):571-581.

81. Kanayama N, Terao T, Kawashima Y, Horiuchi K, Fujimoto D. Collagen types in normal and prematurely ruptured amniotic membranes. Am J Obstet Gynecol. 1985;153(8):899-903.

82. Mogami H, Kishore A, Word R. Collagen type 1 accelerates healing of ruptured fetal membranes. Sci Rep. 2018;8(1).

83. Le Blanc K, Davies L. Mesenchymal stromal cells and the innate immune response. Immunol Lett. 2015;168(2):140-146.

84. Magatti M, Vertua E, Cargnoni A, Silini A, Parolini O. The Immunomodulatory properties of amniotic cells. Cell Transplant. 2018;27(1):31-44.

85. Tolar J, Le Blanc K, Keating A, Blazar B. Concise Review: hitting the right spot with mesenchymal stromal cells. Stem Cells. 2010;28(8):1446-1455.

86. Pianta S, Bonassi Signoroni P, Muradore I et al. Amniotic membrane mesenchymal cells-derived factors skew t cell polarization toward treg and downregulate Th1 and Th17 cells subsets. Stem Cell Rev Rep. 2014;11(3):394-407.

87. Magatti M, Pianta S, Silini A, Parolini O. Isolation, culture, and phenotypic characterization of mesenchymal stromal cells from the amniotic membrane of the human term placenta. Mesenchymal Stem Cells. 2016:233-244.

88. Reyes L, Golos T. Hofbauer Cells: their role in healthy and complicated pregnancy. Front Immunol. 2018;9.

89. Ingman K, Cookson V, Jones C, Aplin J. Characterisation of Hofbauer cells in first and second trimester placenta: incidence, phenotype, survival in vitro and motility. Placenta. 2010;31(6):535-544.

90. Joerink M, Rindsjö E, van Riel B, Alm J, Papadogiannakis N. Placental macrophage (Hofbauer cell) polarization is independent of maternal allergen-sensitization and presence of chorioamnionitis. Placenta. 2011;32(5):380-385.

91. Brown M, von Chamier M, Allam A, Reyes L. M1/M2 Macrophage polarity in normal and complicated pregnancy. Front Immunol. 2014;5.

92. Davydova D, Vorotelyak E, Smirnova Y et al. Cell phenotypes in human amniotic fluid. Acta Naturae. 2009;1(2):98-103.

93. Moraghebi R, Kirkeby A, Chaves P et al. Term amniotic fluid: an unexploited reserve of mesenchymal stromal cells for reprogramming and potential cell therapy applications. Stem Cell Res Ther. 2017;8(1). 6

94. Roubelakis M, Trohatou O, Anagnou N. Amniotic fluid and amniotic membrane stem cells: marker discovery. Stem Cells Int. 2012;2012:1-9.

95. De Coppi P, Bartsch G, Siddiqui M et al. Isolation of amniotic stem cell lines with potential for therapy. Nat Biotechnol. 2007;25(1):100-106.

96. Zagoura D, Roubelakis M, Bitsika V et al. Therapeutic potential of a distinct population of human amniotic fluid mesenchymal stem cells and their secreted molecules in mice with acute hepatic failure. Gut. 2011;61(6):894-906.

97. Gomez-Lopez N, Romero R, Xu Y et al. The immunophenotype of amniotic fluid leukocytes in normal and complicated pregnancies. American Journal of Reproductive Immunology. 2018;79(4):e12827.

98. Romero R, Chaiworapongsa T, Alpay Savasan Z et al. Damage-associated molecular patterns (DAMPs) in preterm labor with intact membranes and preterm PROM: a study of the alarmin HMGB1. The Journal of Maternal-Fetal & Neonatal Medicine. 2011;24(12):1444-1455.

99. Gomez-Lopez N, Romero R, Leng Y et al. The origin of amniotic fluid monocytes/macrophages in women with intra-amniotic inflammation or infection. J Perinat Med. 2019;47(8):822-840.

100. Gomez-Lopez N, Romero R, Galaz J et al. Cellular immune responses in amniotic fluid of women with preterm labor and intra-amniotic infection or intra-amniotic inflammation. American Journal of Reproductive Immunology. 2019;82(5).

101. Silini A, Di Pietro R, Lang-Olip I et al. Perinatal Derivatives: Where do we stand? a roadmap of the human placenta and consensus for tissue and cell nomenclature. Front Bioeng Biotechnol. 2020;8.

102. Gratacós E, Sanin-Blair J, Lewi L et al. A histological study of fetoscopic membrane defects to document membrane healing. Placenta. 2006;27(4-5):452-456.

103. Janzen C, Sen S, Lei M, Gagliardi de Assumpcao M, Challis J, Chaudhuri G. The role of epithelial to mesenchymal transition in human amniotic membrane rupture. The Journal of Clinical Endocrinology & Metabolism. 2016:jc.2016-3150.

104. Barrett D, Kethees A, Thrasivoulou C et al. Trauma induces overexpression of Cx43 in human fetal membrane defects. Prenat Diagn. 2017;37(9):899-906.

105. Barrett D, John R, Thrasivoulou C et al. Targeting mechanotransduction mechanisms and tissue weakening signals in the human amniotic membrane. Sci Rep. 2019;9(1).

106. Chowdhury B, David A, Thrasivoulou C, Becker D, Bader D, Chowdhury T. Tensile strain increased COX-2 expression and PGE2 release leading to weakening of the human amniotic membrane. Placenta. 2014;35(12):1057-1064.

107. Liu M, Yin Y, Yu H, Zhou R. Laminins regulate placentation and pre-eclampsia: focus on trophoblasts and endothelial cells. Front Cell Dev Biol. 2020;8.

108. Roediger M, Miosge N, Gersdorff N. Tissue distribution of the laminin β1 and β2 chain during embryonic and fetal human development. J Mol Histol. 2010;41(2-3):177-184.

109. Okamura Y, Watari M, Jerud E et al. The extra domain a of fibronectin activates toll-like receptor 4. Journal of Biological Chemistry. 2001;276(13):10229-10233.

110. Wilshaw S, Kearney J, Fisher J, Ingham E. Production of an acellular amniotic membrane matrix for use in tissue engineering. Tissue Eng. 2006;12(8):2117-29

111. Jabareen M, Mallik A, Bilic G, Zisch A, Mazza E. Relation between mechanical properties and microstructure of human fetal membranes: An attempt towards a quantitative analysis. European Journal of Obstetrics & Gynecology and Reproductive Biology. 2009;144:S134-S141.

112. Mauri A, Perrini M, Mateos J et al. Second harmonic generation microscopy of fetal membranes under deformation: Normal and altered morphology. Placenta. 2013;34(11):1020-1026.

113. Ramuta T, Kreft M. Human amniotic membrane and amniotic membrane–derived cells. Cell Transplant. 2018;27(1):77-92.

114. Niknejad H, Peirovi H, Jorjani M, Ahmadiani A, Ghanavi J, Seifalian A. Properties of the amniotic membrane for potential use in tissue engineering. European Cells and Materials. 2008;7:88-99.

115. Han W, Jang Y, García A. The extracellular matrix and cell–biomaterial interactions. Biomater Sci. 2020:701-715.

116. Dadkhah Tehrani F, Firouzeh A, Shabani I, Shabani A. A review on modifications of amniotic membrane for biomedical applications. Front Bioeng Biotechnol. 2021;8.

117. Hortensius R, Ebens J, Harley B. Immunomodulatory effects of amniotic membrane matrix incorporated into collagen scaffolds. Journal of Biomedical Materials Research Part A. 2016;104(6):1332-1342.

118. Taghiabadi E, Nasri S, Shafieyan S, Jalili Firoozinezhad S, Aghdami N. Fabrication and characterization of spongy denuded amniotic membrane-based scaffold for tissue engineering. Cell J. 2015 Winter;16(4):476-87.

119. Lei J, Priddy L, Lim J, Massee M, Koob T. Identification of extracellular matrix components and biological factors in micronized dehydrated human amnion/chorion membrane. Advances in Wound Care. 2017;6(2):43-53

120. Osman I, Young A, Jordan F, Greer I, Norman J. Leukocyte density and proinflammatory mediator expression in regional human fetal membranes and decidua before and during labot at term. Journal of the Society for Gynecologic Investigation. 2006;13(2):97-103

121. Keelan J. Intrauterine inflammatory activation, functional progesterone withdrawal, and the timing of term and preterm birth. Journal of Reproductive Immunology. 2018;125:89-99.

122. Thomson A. Leukocytes infiltrate the myometrium during human parturition: further evidence that labour is an inflammatory process. Human Reproduction. 1999;14(1):229-236.

123. Gomez-Lopez N, Tanaka S, Zaeem Z, Metz G, Olson D. Maternal circulating leukocytes display early chemotactic responsiveness during late gestation. BMC Pregnancy and Childbirth. 2013;13(S1).

124. Zhang J, Shynlova O, Sabra S, Bang A, Briollais L, Lye S. Immunophenotyping and activation status of maternal peripheral blood leukocytes during pregnancy and labour, both term and preterm. Journal of Cellular and Molecular Medicine. 2017;21(10):2386-2402.

125. Menon R, Mesiano S, Taylor R. Programmed fetal membrane senescence and exosome-mediated signaling: a mechanism associated with timing of human parturition. Frontiers in Endocrinology. 2017;8.

126. McLaren J, Taylor D, Bell S. Increased concentration of pro–matrix metalloproteinase 9 in term fetal membranes overlying the cervix before labor: Implications for membrane remodeling and rupture. American Journal of Obstetrics and Gynecology. 2000;182(2):409-416.

127. Shynlova O, Lee Y, Srikhajon K, Lye S. Physiologic Uterine inflammation, and labor onset. Reproductive Sciences. 2012;20(2):154-167.

128. Shynlova O, Nedd-Roderique T, Li Y, Dorogin A, Nguyen T, Lye S. Infiltration of myeloid cells into decidua is a critical early event in the labour cascade and post-partum uterine remodelling. Journal of Cellular and Molecular Medicine. 2013;17(2):311-324.

129. Kumar D, Moore R, Mercer B, Mansour J, Redline R, Moore J. The physiology of fetal membrane weakening and rupture: Insights gained from the determination of physical properties revisited. Placenta. 2016;42:59-73

130. Hamilton S, Oomomian Y, Stephen G, Shynlova O, Tower C, Garrod A et al. Macrophages infiltrate the human and rat decidua during term and preterm labor: evidence that decidual inflammation precedes labor. Biology of Reproduction. 2012;86(2).

131. Hamilton S, Tower C, Jones R. Identification of chemokines associated with the recruitment of decidual leukocytes in human labour: potential novel targets for preterm labour. PLoS ONE. 2013;8(2):e56946.

132. Menon R, Bonney E, Condon J, Mesiano S, Taylor R. Novel concepts on pregnancy clocks and alarms: redundancy and synergy in human parturition. Human Reproduction Update. 2016;22(5):535-560.

133. Zhao Y, Koga K, Osuga Y, Izumi G, Takamura M, Harada M et al. Cyclic Stretch Augments Production of Neutrophil Chemokines and Matrix Metalloproteinases-1 (MMP-1) from

Human Decidual Cells, and the Production was Reduced by Progesterone. American Journal of Reproductive Immunology. 2013;69(5):454-462.

134. Makino S, Zaragoza D, Mitchell B, Robertson S, Olson D. Prostaglandin F2α and Its Receptor as Activators of Human Decidua. Seminars in Reproductive Medicine. 2007;25(1):060-068.

135. Mitchell M, Edwin S, Romero R. Prostaglandin biosynthesis by human decidual cells: Effects of inflammatory mediators. Prostaglandins, Leukotrienes and Essential Fatty Acids. 1990;41(1):35-38.

136. Shynlova O, Tsui P, Jaffer S, Lye S. Integration of endocrine and mechanical signals in the regulation of myometrial functions during pregnancy and labour. European Journal of Obstetrics & Gynecology and Reproductive Biology. 2009;144:S2-S10.

137. Shynlova O, Nadeem L, Zhang J, Dunk C, Lye S. Myometrial activation: Novel concepts underlying labor. Placenta. 2020;92:28-36.

138. Pomini F. Interleukin-10 Modifies the Effects of Interleukin-1 and Tumor Necrosis Factor- on the Activity and Expression of Prostaglandin H Synthase-2 and the NAD+-Dependent 15-Hydroxyprostaglandin Dehydrogenase in Cultured Term Human Villous Trophoblast and Chorion Trophoblast Cells. Journal of Clinical Endocrinology & Metabolism. 1999;84(12):4645-4651.

139. Tattersall M, Engineer N, Khanjani S, Sooranna S, Roberts V, Grigsby P et al. Pro-labour myometrial gene expression: are preterm labour and term labour the same?. Reproduction. 2008;135(4):569-579.

140. Lye S. Initiation of parturition. Animal Reproduction Science. 1996;42(1-4):495-503.

141. Fuchs A, Fuchs F, Husslein P, Soloff M. Oxytocin receptors in the human uterus during pregnancy and parturition. American Journal of Obstetrics and Gynecology. 1984;150(6):734-741.

142. Slater D, Dennes W, Campa J, Poston L, Bennett P. Expression of cyclo-oxygenase types-1 and -2 in human myometrium throughout pregnancy. MHR: Basic science of reproductive medicine. 1999;5(9):880-884.

143. Döring B, Shynlova O, Tsui P, Eckardt D, Janssen-Bienhold U, Hofmann F et al. Ablation of connexin43 in uterine smooth muscle cells of the mouse causes delayed parturition. Journal of Cell Science. 2006;119(9):1715-1722.

144. Vink J, Mourad M. The pathophysiology of human premature cervical remodelling resulting in spontaneous preterm birth: Where are we now?.Seminars in Perinatology. 2017;41(7):427-437

145. Akins M, Luby-Phelps K, Bank R, Mahendroo M. Cervical softening during pregnancy: regulated changes in collagen cross-linking and composition of matricellular proteins in the mouse. Biology of Reproduction. 2011;84(5):1053-1062

146. House M, Kaplan DL, Socrate S. Relationships between mechanical properties and extracellular matrix constituents of the cervical stroma during pregnancy. Semin Perinatol.2009;33(5):300–307

147. Nallasamy S, Mahendroo M. Distinct roles of cervical epithelia and stroma in pregnancy and parturition. Semin ReprodMed. 2017;35(2):190–200.49.

148. Poellmann M, Chien E, McFarlin B, Wagoner Johnson A. Mechanical and structural changes of the rat cervix in late-stage pregnancy. Journal of the Mechanical Behavior of Biomedical Materials. 2013;17:66-75.

149. Gonzalez JM, Franzke CW, Yang F, Romero R, Girardi G. Complement activation triggers metalloproteinases release inducing cervical remodelling and preterm birth in mice.AmJ Pathol. 2011;179(2):838–849.53

150. Stygar D, Wang H, Vladic YS, Ekman G, Eriksson H, Sahlin L. Increased level of matrix metalloproteinases 2 and 9 in the ripening process of the human cervix. Biol Reprod. 2002;67(3):889–89

151. Lei H, Kalluri R, Furth E, Baker A, Strauss J. Rat amnion type iv collagen composition and metabolism: implications for membrane breakdown. Biology of Reproduction. 1999;60(1):176-182.

152. Kumagai K, Otsuki Y, Ito Y, Shibata M, Abe H, Ueki M. Apoptosis in the normal human amnion at term, independent of Bcl-2 regulation and onset of labour. MHR: Basic science of reproductive medicine. 2001;7(7):681-689.

153. Reti N, Lappas M, Riley C, Wlodek M, Permezel M, Walker S et al. Why do membranes rupture at term? Evidence of increased cellular apoptosis in the supracervical fetal membranes. American Journal of Obstetrics and Gynecology. 2007;196(5):484.e1-484.e10.

154. El Khwad M, Stetzer B, Moore R, Kumar D, Mercer B, Arikat S et al. Term human fetal membranes have a weak zone overlying the lower uterine pole and cervix before onset of labor. Biology of Reproduction. 2005;72(3):720-726.

155. Tchirikov M, Schlabritz-Loutsevitch N, Maher J, Buchmann J, Naberezhnev Y. Mid-trimester preterm premature rupture of membranes (PPROM): etiology, diagnosis, classification, international recommendations of treatment options and outcome. Journal of Perinatal Medicine. 2017;46(5):465-488.

156. Mogami H, Kishore A, Shi H, Keller P, Akgul Y, Word R. Fetal fibronectin signaling induces matrix metalloproteases and cyclooxygenase-2 (cox-2) in amnion cells and preterm birth in mice. Journal of Biological Chemistry. 2013;288(3):1953-1966.

157. Oh K, Romero R, Park J, Kang J, Hong J, Yoon B. A high concentration of fetal fibronectin in cervical secretions increases the risk of intra-amniotic infection and inflammation in patients with preterm labor and intact membranes. Journal of Perinatal Medicine. 2019;47(3):288-303.

158. Ferrand P. A polymorphism in the matrix metalloproteinase-9 promoter is associated with increased risk of preterm premature rupture of membranes in African Americans. Molecular Human Reproduction. 2002;8(5):494-501.

159. McParland P, Taylor D, Bell S. Mapping of zones of altered morphology and chorionic connective tissue cellular phenotype in human fetal membranes (amniochorion and decidua) overlying the lower uterine pole and cervix before labor at term. American Journal of Obstetrics and Gynecology. 2003;189(5):1481-1488.

160. Lappas M, Odumetse T, Riley C, Reti N, Holdsworth-Carson S, Rice G et al. Pre-labour fetal membranes overlying the cervix display alterations in inflammation and NF-κB Signalling Pathways. Placenta. 2008;29(12):995-1002.

161. Lappas M, Riley C, Lim R, Barker G, Rice G, Menon R et al. MAPK and AP-1 proteins are increased in term pre-labour fetal membranes overlying the cervix: Regulation of enzymes involved in the degradation of fetal membranes. Placenta. 2011;32(12):1016-1025.

162. Lappas M, Lim R, Riley C, Menon R, Permezel M. Expression and localisation of FoxO3 and FoxO4 in human placenta and fetal membranes. Placenta. 2010;31(12):1043-1050.

163. Lappas M, Permezel M, Georgiou H, Rice G. Nuclear factor kappa b regulation of proinflammatory cytokines in human gestational tissues in vitro. Biology of Reproduction. 2002;67(2):668-673.

164. Chai M, Barker G, Menon R, Lappas M. Increased oxidative stress in human fetal membranes overlying the cervix from term non-labouring and post labour deliveries. Placenta. 2012;33:604-10

165. Fortunato S, LaFleur B, Menon R. Collagenase-3 (MMP-13) in fetal membranes and amniotic fluid during pregnancy*. American Journal of Reproductive Immunology. 2003;49(2):120-125.

166. Meinert M, Malmström A, Tufvesson E, Westergren-Thorsson G, Petersen A, Laurent C et al. Labour induces increased concentrations of biglycan and hyaluronan in human fetal membranes. Placenta. 2007;28(5-6):482-486.

167. de Miranda de Araujo L, Horgan C, Aron A, Iozzo R, Lechner B. Compensatory fetal membrane mechanisms between biglycan and decorin in inflammation. Molecular Reproduction and Development. 2015;82(5):387-396.

168. Wu Z, Horgan C, Carr O, Owens R, Iozzo R, Lechner B. Biglycan and decorin differentially regulate signalling in the fetal membranes. Matrix Biology. 2014;35:266-275.

169. Malak TM, Bell SC. Structural characteristics of term human fetal membranes: a novel zone of extreme morphological alteration within the rupture site. Br J Obstet Gynaecol. 1994;101(5):375-86

170. McParland P, Bell S, Pringle J, Taylor D. Regional and cellular localization of osteonectin/SPARC expression in connective tissue and cytotrophoblastic layers of human fetal membranes at term. Molecular Human Reproduction. 2001;7(5):463-474.

171. Marcellin L, Schmitz T, Messaoudene M, Chader D, Parizot C, Jacques S et al. Immune modifications in fetal membranes overlying the cervix precede parturition in humans. The Journal of Immunology. 2016;198(3):1345-1356.

172. Amberg B, Hodges R, Rodgers K, Crossley K, Hooper S, DeKoninck P. Why do the fetal membranes rupture early after fetoscopy? ZA review. Fetal Diagnosis and Therapy. 2021;48(7):493-503.

173. Lee J, Lee S, Oh K, Park C, Jun J, Yoon B. Fragmented forms of insulin-like growth factor binding protein-1 in amniotic fluid of patients with preterm labor and intact membranes. Reproductive Sciences. 2011;18(9):842-849.

174. Puthiyachirakkal M, Lemerand K, Kumar D, Moore R, Philipson E, Mercer B et al. Thrombin weakens the amnion extracellular matrix (ECM) directly rather than through protease activated receptors. Placenta. 2013;34(10):924-931.

175. Chaiworapongsa T., Espinoza J., Yoshimatsu J., Kim Y. M., Bujold E., Edwin S et al. Activation of coagulation system in preterm labor and preterm premature rupture of membranes. J. Matern. Fetal Neonatal Med. 2002;11, 368–373.

176. Moore R, Kumar D, Mansour J, Mercer B, Mesiano S, Moore J. Effect of inflammatory signals on progesterone production at the maternal-fetal interface. Medical Research Archives. 2021;9(11).

177. Ravanos K, Dagklis T, Petousis S, Margioula-Siarkou C, Prapas Y, Prapas N. Factors implicated in the initiation of human parturition in term and preterm labor: a review. Gynecological Endocrinology. 2015;31(9):679-683.

178. Menon R, Moore J. Fetal Membranes, not a mere appendage of the placenta, but a critical part of the fetal-maternal interface controlling parturition. Obstetrics and Gynecology Clinics of North America. 2020;47(1):147-162.

179. Sato B, Collier E, Vermudez S, Junker A, Kendal-Wright C. Human amnion mesenchymal cells are pro-inflammatory when activated by the Toll-like receptor 2/6 ligand, macrophage-activating lipoprotein-2. Placenta. 2016;44:69-79.

180. Richardson L, Radnaa E, Urrabaz-Garza R, Lavu N, Menon R. Stretch, scratch, and stress: Suppressors and supporters of senescence in human fetal membranes. Placenta. 2020;99:27-34.

181. Richardson L, Vargas G, Brown T, Ochoa L, Sheller-Miller S, Saade G et al. Discovery and characterization of human amniochorionic membrane microfractures. The American Journal of Pathology. 2017;187(12):2821-2830.

182. Longini M, Perrone S, Vezzosi P, Marzocchi B, Kenanidis A, Centini G et al. Association between oxidative stress in pregnancy and preterm premature rupture of membranes. Clinical Biochemistry. 2007;40(11):793-797.

183. Menon R, Behnia F, Polettini J, Richardson L. Novel pathways of inflammation in human fetal membranes associated with preterm birth and preterm pre-labor rupture of the membranes. Seminars in Immunopathology. 2020;42(4):431-450.

184. Lappas M, Permezel M, Rice G. N-Acetyl-Cysteine inhibits phospholipid metabolism, proinflammatory cytokine release, protease activity, and Nuclear Factor-κB deoxyribonucleic acid-binding activity in human fetal membranes in vitro. The Journal of Clinical Endocrinology & Metabolism. 2003;88(4):1723-1729.

185. Polettini J, Silva M, Kacerovsky M, Syed T, Saade G, Menon R. Screening of lysyl oxidase (LOX) and lysyl oxidase like (LOXL) enzyme expression and activity in preterm prelabor rupture of fetal membranes. Journal of Perinatal Medicine. 2015;0(0).

186. Richardson L, Dixon C, Aguilera-Aguirre L, Menon R. Oxidative stress-induced TGF-beta/TAB1-mediated p38MAPK activation in human amnion epithelial cells. Biology of Reproduction. 2018;99(5):1100-1112.

187. Menon R, Behnia F, Polettini J, Saade G, Campisi J, Velarde M. Placental membrane aging and HMGB1 signalling associated with human parturition. Aging. 2016;8(2):216-230.

188. Menon R, Boldogh I, Hawkins H, Woodson M, Polettini J, Syed T et al. Histological evidence of oxidative stress and premature senescence in preterm premature rupture of the human fetal membranes recapitulated in vitro. The American Journal of Pathology. 2014;184(6):1740-1751.

189. Girard S, Heazell A, Derricott H, Allan S, Sibley C, Abrahams V et al. Circulating cytokines and alarmins associated with placental inflammation in high-risk pregnancies. American Journal of Reproductive Immunology. 2014;72(4):422-434.

190. Gomez-Lopez N, Romero R, Plazyo O, Panaitescu B, Furcron A, Miller D et al. Intra-amniotic administration of HMGB1 induces spontaneous preterm labor and birth. American Journal of Reproductive Immunology. 2015;75(1):3-7.

191. Sheller-Miller S, Trivedi J, Yellon S, Menon R. Exosomes cause preterm birth in mice: evidence for paracrine signaling in pregnancy. Scientific Reports. 2019;9(1).

192. Menon R, Mesiano S, Taylor R. Programmed fetal membrane senescence and exosome-mediated signaling: a mechanism associated with timing of human parturition. Frontiers in Endocrinology. 2017;8

193. Severi F, Bocchi C, Voltolini C, Borges L, Florio P, Petraglia F. Thickness of fetal membranes: a possible ultrasound marker for preterm delivery. Ultrasound in Obstetrics and Gynecology. 2008;32(2):205-209.

194. Avila C, Santorelli J, Mathai J, Ishkin S, Jabsky M, Willins J et al. Anatomy of the fetal membranes using optical coherence tomography: Part 1. Placenta. 2014;35(12):1065-1069.

195. Meller CH, Carducci ME, Ceriani Cernadas JM, Otaño L. Preterm premature rupture of membranes. Archivos Argentinos de Pediatria. 2018;1;116(4):575-e581

196. Fortner K, Grotegut C, Ransom C, Bentley R, Feng L, Lan L et al. Bacteria localization and chorion thinning among preterm premature rupture of membranes. PLoS ONE. 2014;9(1):83338.

197. Micili S, Valter M, Oflaz H, Ozogul C, Linder P, Föckler N et al. Optical coherence tomography: A potential tool to predict premature rupture of fetal membranes. Proceedings of the Institution of Mechanical Engineers, Part H: Journal of Engineering in Medicine. 2012;227(4):393-401.

198. Buerzle W, Mazza E. On the deformation behavior of human amnion. Journal of Biomechanics. 2013;46(11):1777-1783

199. Borazjani A, Weed B, Patnaik S, Feugang J, Christiansen D, Elder S et al. A comparative biomechanical analysis of term fetal membranes in human and domestic species. American Journal of Obstetrics and Gynecology. 2011;204(4):365.e25-365.e36

200. Pressman E, Cavanaugh J, Woods J. Physical properties of the chorioamnion throughout gestation. American Journal of Obstetrics and Gynecology. 2002;187(3):672-675.

201. Oyen M, Calvin S, Landers D. Premature rupture of the fetal membranes: Is the amnion the major determinant?. American Journal of Obstetrics and Gynecology. 2006;195(2):510-515.

202. Joyce E, Diaz P, Tamarkin S, Moore R, Strohl A, Stetzer B et al. In-vivo stretch of term human fetal membranes. Placenta. 2016;38:57-66

203. Oyen M, Cook R, Calvin S. Mechanical failure of human fetal membrane tissues. Journal of Materials Science: Materials in Medicine. 2004;15(6):651-658.

204. Arikat S, Novince R, Mercer B, Kumar D, Fox J, Mansour J et al. Separation of amnion from choriodecidua is an integral event to the rupture of normal term fetal membranes and constitutes a significant component of the work required. American Journal of Obstetrics and Gynecology. 2006;194(1):211-217.

205. Oyen M, Cook R, Stylianopoulos T, Barocas V, Calvin S, Landers D. Uniaxial and biaxial mechanical behavior of human amnion. Journal of Materials Research. 2005;20(11):2902-2909

206. Mauri A, Perrini M, Ehret A, De Focatiis D, Mazza E. Time-dependent mechanical behavior of human amnion: Macroscopic and microscopic characterization. Acta Biomaterialia. 2015;11:314-323.

207. Bircher K, Merluzzi R, Wahlsten A, Spiess D, Simões-Wüst A, Ochsenbein-Kölble N et al. Influence of osmolarity and hydration on the tear resistance of the human amniotic membrane. Journal of Biomechanics. 2020;98:109419.

208. Bircher K, Ehret A, Spiess D, Ehrbar M, Simões-Wüst A, Ochsenbein-Kölble N et al. On the defect tolerance of fetal membranes. Interface Focus. 2019;9(5):20190010.

209. Ehret A, Bircher K, Stracuzzi A, Marina V, Zündel M, Mazza E. Inverse poroelasticity as a fundamental mechanism in biomechanics and mechanobiology. Nature Communications. 2017;8(1).

210. Chua W, Oyen M. Do we know the strength of the chorioamnion?. European Journal of Obstetrics & Gynecology and Reproductive Biology. 2009;144:S128-S133.

211. Buerzle W, Haller C, Jabareen M, Egger J, Mallik A, Ochsenbein-Koelble N et al. Multiaxial mechanical behavior of human fetal membranes and its relationship to microstructure. Biomechanics and Modeling in Mechanobiology. 2012;12(4):747-762.

212. Joyce E, Moore J, Sacks M. Biomechanics of the fetal membrane prior to mechanical failure: Review and implications. European Journal of Obstetrics & Gynecology and Reproductive Biology. 2009;144:S121-S127.

213. Bürzle W, Mazza E, Moore J. About puncture testing applied for mechanical characterization of fetal membranes. Journal of Biomechanical Engineering. 2014;136(11).

214. Sumanovac A. Biomechanics of fetal membranes – relation with newborn and maternal anthropometric data. Periodicum Biologorum. 2017;119(2):119-123.

215. Verbruggen S, Oyen M, Phillips A, Nowlan N. Function and failure of the fetal membrane: Modelling the mechanics of the chorion and amnion. PLOS ONE. 2017;12(3):e0171588.

216. Koh C, Tonsomboon K, Oyen M. Fracture toughness of human amniotic membranes. Interface Focus. 2019;9(5):20190012.

217. Perrini M, Bürzle W, Haller C, Ochsenbein-Kölble N, Deprest J, Zimmermann R, Mazza E, Ehrbar M. Contractions, a risk for premature rupture of fetal membranes: a new protocol with cyclic biaxial tension. Med Eng Phys. 2013 Jun;35(6):846-51

218. El Maradny E, Kanayama N, Halim A, Maehara K, Terao T. Stretching of fetal membranes increases the concentration of interleukin-8 and collagenase activity. Am J Obstet Gynecol. 1996;174:843-849.

219. Mohan AR, Soorranna SR, Lindstrom TM, Johnson MR, Bennett PR.The effect of mechanical stretch on cyclooxygenase type 2 expression and AP-1 and NF-κB activity in human amnion cells. Endocrinology. 2007;148:1850-1857.

220. Sasamoto A, Nagino M, Kobayashi S, Naruse K, Nimura Y, Sokabe M. Mechanotransduction by integrin is essential for IL-6 secretion from endothelial cells in response to uniaxial continuous stretch. Am J Physiol Cell Physiol. 2004;288:1012-1022.

221. Nemeth E, Millar LK, Bryant-Greenwood GD. Fetal membrane distension II. Differentially expressed genes regulated by acute distension in vitro. Am J Obstet Gynecol. 2000;182:60-67.

222. Kendal CE, Bryant-Greenwood GD. Pre-B-cell colony enhancing factor (PBEF/Visfatin) gene expression is modulated by NF-κB and AP-1 in human amniotic epithelial cells. Placenta. 2007;28:305-314.

223. Ognjanovic S, Bryant-Greenwood GD. Pre-B-cell colonyenhancing factor, a novel cytokine of human fetal membranes. Am J Obstet Gynecol. 2002;187:1051-1058.

224. Marvin KW, Keelan JA, Eykholt RL, Sato TA, Mitchell MD. Use of cDNA arrays to generate differential expression profiles for inflammatory genes in human gestational membranes delivered at term and preterm. Mol Hum Reprod. 2002; 8:399-408.

225. Kendal CE, Trefz D, Ward K, Bryant-Greenwood GD. Expression of pre-B-cell colony-enhancing factor (PBEF) in primary human amniotic epithelial cells response to long-term static stretch. J Soc Gynecol Investig. 2006;13(2 suppl):245A.

226. Slater D, Allport V, Bennett P. Changes in the expression of the type-2 but not the type-1 cyclo-oxygenase enzyme in chorion-decidua with the onset of labour. Br J Obstet Gynaecol. 1998;105,745-748

227. Wu WX, Ma XH, Yoshizato T, Shinozuka N, Nathanielsz PW. Differential expression of myometrial oxytocin receptor and prostaglandin H synthase 2, but not estrogen receptor alpha and heat shock protein 90 messenger ribonucleic acid in the gravid horn and nongravid horn in sheep during betamethasone-induced labor. Endocrinology. 1999;140,5712-5718

228. Manabe Y, Manabe A, Takahashi A. Effect of indomethacin on stretch-induced uterine activity in the post-partum. Prostaglandins. 1983:25,653-659.

229. Sooranna SR, Lee Y, Kim LU, Mohan AR, Bennett PR, Johnson MR. Mechanical stretch activates type 2 cyclooxygenase via activator protein-1 transcription factor in human myometrial cells. Mol Hum Reprod. 2004;10:109-113

230. Sooranna SR, Bennet PR, Johnson MR. Effect of mechanical stretch on the expression of interleukin-1beta in human uterine myocytes. Placenta. 2005;26:A44

231. Copland IB, Post M. Stretch-activated signaling pathways responsible for early response gene expression in fetal lung epithelial cells. J Cell Physiol. 2007;210:133-143.

232. Nemeth E,Tashima LS,Yu Z, Bryant-Greenwood GD. Fetal membrane distension:I.Differentially expressed genes regulated by acute distension in amniotic epithelial cells. Am J Obstet Gynecol. 2000;182:50-59.

233. Harada M, Osuga Y, Hirota Y, et al. Mechanical stretch stimulates interleukin-8 production in endometrial stromal cells: possible implications in endometrium-related events. J Clin Endocrinol Metab. 2005;90:1144-1148.

234. Takemura M, Itoh H, Sagawa N, et al. Cyclic mechanical stretch augments both interleukin-8 and monocyte chemotactic protein-3 production in the cultured human uterine cervical fibroblast cells. Mol Hum Reprod. 2004;10:573-580

235. Fawthrop RK, Ockleford CD. Cryofracture of human term amniochorion. Cell Tissue Res. 1994;277(2):315-23

236. Adams Waldorf K, Singh N, Mohan A, Young R, Ngo L, Das A et al. Uterine overdistention induces preterm labor mediated by inflammation: observations in pregnant women and nonhuman primates. American Journal of Obstetrics and Gynecology. 2015;213(6):830.e1-830.e19.

237. Sydorak R, Hirose S, Sandberg P, Filly R, Harrison M, Farmer D et al. Chorioamniotic membrane separation following fetal surgery. Journal of Perinatology. 2002;22(5):407-410.

238. Sopher D. The response of rat fetal membranes to injury. Annals of the Royal College of Surgeons of England 1972;51:240-9.

239. Perrone E, Galganski L, Tarantal A, Olstad K, Treadwell M, Berman D et al. Fetal surgery in the primate 4.0: A New Technique 30 Years Later. Fetal Diagnosis and Therapy. 2020;48(1):43-49.

240. Gratacós E, Wu J, Yesildaglar N, Devlieger R, Pijnenborg R, Deprest J. Successful sealing of fetoscopic access sites with collagen plugs in the rabbit model. American Journal of Obstetrics and Gynecology. 2000;182(1):142-146.

241. Devlieger R, A.Deprest J, Gratacós E, Pijnenborg R, Leask R, C.Riley S. Matrix metalloproteinases -2 and -9 and their endogenous tissue inhibitors in fetal membrane repair following fetoscopy in a rabbit model. MHR: Basic science of reproductive medicine. 2000;6(5):479-485.

242. Barrientos S, Stojadinovic O, Golinko M, Brem H, Tomic-Canic M. Perspective article: Growth factors and cytokines in wound healing. Wound Repair and Regeneration. 2008;16(5):585-601.

243. Gurtner G, Werner S, Barrandon Y, Longaker M. Wound repair and regeneration. Nature. 2008;453(7193):314-321.

244. Li B, Wang J. Fibroblasts and myofibroblasts in wound healing: Force generation and measurement. Journal of Tissue Viability. 2011;20(4):108-120.

245. McCluskey J, Martin P. Analysis of the tissue movements of embryonic wound healing—dii studies in the limb bud stage mouse embryo. Developmental Biology. 1995;170(1):102-114.

246. Martin P, Lewis J. Actin cables and epidermal movement in embryonic wound healing. Nature. 1992;360(6400):179-183.

247. Bilic G, Ochsenbein-Kölble N, Hall H, Huch R, Zimmermann R. In vitro lesion repair by human amnion epithelial and mesenchymal cells. American Journal of Obstetrics and Gynecology. 2004;190(1):87-92.

248. Ochsenbein-Kölble N, Bilic G, Hall H, Huch R, Zimmermann R. Inducing proliferation of human amnion epithelial and mesenchymal cells for prospective engineering of membrane repair. Journal of Perinatal Medicine. 2003;31(4).

249. Montgomery J, Ghatnekar G, Grek C, Moyer K, Gourdie R. Connexin 43-Based Therapeutics for Dermal Wound Healing. International Journal of Molecular Sciences. 2018;19(6):1778.

250. Mori R, Power K, Wang C, Martin P, Becker D. Acute downregulation of connexin43 at wound sites leads to a reduced inflammatory response, enhanced keratinocyte proliferation and wound fibroblast migration. Journal of Cell Science. 2006;119(24):5193-5203.

251. Faniku C, O'Shaughnessy E, Lorraine C, Johnstone S, Graham A, Greenhough S et al. The Connexin Mimetic Peptide Gap27 and Cx43-Knockdown Reveal Differential Roles for Connexin43 in Wound Closure Events in Skin Model Systems. International Journal of Molecular Sciences. 2018;19(2):604.

252. Sanz Cortes M, Lapa D, Acacio G, Belfort M, Carreras E, Maiz N et al. Proceedings of the First Annual Meeting of the International Fetoscopic Myelomeningocele Repair Consortium. Ultrasound in Obstetrics & Gynecology. 2019;53(6):855-863.

253. Belfort M, Whitehead W, Shamshirsaz A, Bateni Z, Olutoye O, Olutoye O et al. Fetoscopic Open Neural Tube Defect Repair. Obstetrics & Gynecology. 2017;129(4):734-743.

254. Papanna R, Mann L, Moise K, Kyriakides T, Johnson A, Garcia E et al. Histologic changes of the fetal membranes after fetoscopic laser surgery for twin-twin transfusion syndrome. Pediatric Research. 2015;78(3):247-255.

255. Behzad F, Dickinson M, Charlton A, Aplin J. Sliding displacement of amnion and chorion following controlled laser wounding suggests a mechanism for short-term sealing of ruptured membranes. Placenta. 1994;15(7):775-778.

256. C. Johnson J, Egerman R, Moorhead J. Cases with ruptured membranes that “reseal”. American Journal of Obstetrics and Gynecology. 1990;163(3):1024-1030

257. Papanna R, Mann LK, Johnson A, Sangi-Haghpeykar H, Moise KJ, Jr. Chorioamnion separation as a risk for preterm premature rupture of membranes after laser therapy for twin-twin transfusion syndrome. Obstet Gynecol 2010;115:771– 776.

258. Papanna R, Bebbington M, Moise K. Novel findings of iatrogenic fetal membrane defect after previous fetoscopy for twin-twin transfusion syndrome. Ultrasound in Obstetrics & Gynecology. 2013;42(1):118-119.

259. Carvalho N, Moron A, Witkin S, Menon R, Cavalheiro S, Barbosa M et al. Histological response and expression of collagen, metalloproteinases MMP-1 and MMP-9 and tissue inhibitors of metalloproteinases TIMP-1 and TIMP-2 in fetal membranes following open intrauterine surgery: an experimental study. The Journal of Maternal-Fetal & Neonatal Medicine. 2020;:1-9.

260. Valiunas V, Polosina Y, Miller H, Potapova I, Valiuniene L, Doronin S et al. Connexin-specific cell-to-cell transfer of short interfering RNA by gap junctions. The Journal of Physiology. 2005;568(2):459-468.

261. Hervé J, Bourmeyster N, Sarrouilhe D, Duffy H. Gap junctional complexes: From partners to functions. Progress in Biophysics and Molecular Biology. 2007;94(1-2):29-65

262. Altevogt BM, Paul DL. Four classes of intercellular channels between glial cells in the CNS. J Neurosci. 2004;24(18):4313-23

263. Wei CJ, Francis R, Xu X, Lo CW. Connexin43 associated with an N-cadherin-containing multiprotein complex is required for gap junction formation in NIH3T3 cells. J Biol Chem. 2005;280(20):19925-36.

264. Yamane Y, Shiga H, Asou H, Haga H, Kawabata K, Abe K, Ito E. Dynamics of astrocyte adhesion as analyzed by a combination of atomic force microscopy and immuno-cytochemistry: the involvement of actin filaments and connexin 43 in the early stage of adhesion. Arch Histol Cytol. 1999;62(4):355-61

265. Butkevich E, Hülsmann S, Wenzel D, Shirao T, Duden R, Majoul I. Drebrin is a novel connexin-43 binding partner that links gap junctions to the submembrane cytoskeleton. Curr Biol. 2004;14(8):650-8.

266. Kotini M, Barriga E, Leslie J, Gentzel M, Rauschenberger V, Schambony A et al. Gap junction protein Connexin-43 is a direct transcriptional regulator of N-cadherin in vivo. Nature Communications. 2018;9(1).

267. Hawat G, Baroudi G. Connexin 43 hemichannels and pharmacotherapy of myocardial ischemia injury. Novel Strategies in Ischemic Heart Disease. 2012.

268. Rhett J, Ghatnekar G, Palatinus J, O'Quinn M, Yost M, Gourdie R. Novel therapies for scar reduction and regenerative healing of skin wounds. Trends in Biotechnology. 2008;26(4):173-180.

269. Ghatnekar G, O'Quinn M, Jourdan L, Gurjarpadhye A, Draughn R, Gourdie R. Connexin43 carboxyl-terminal peptides reduce scar progenitor and promote regenerative healing following skin wounding. Regenerative Medicine. 2009;4(2):205-223.

270. Martin P, Easton J, Hodgins M, Wright C. Connexins: Sensors of epidermal integrity that are therapeutic targets. FEBS Letters. 2014;588(8):1304-1314.

271. Churko J, Laird D. Gap junction remodeling in skin repair following wounding and disease. Physiology. 2013;28(3):190-198.

272. Coutinho P. Dynamic changes in connexin expression correlate with key events in the wound healing process. Cell Biology International. 2003;27(7):525-541.

273. Qiu C, Coutinho P, Frank S, Franke S, Law L, Martin P et al. Targeting Connexin43 expression accelerates the rate of wound repair. Current Biology. 2003;13(19):1697-1703.

274. Mutsaers SE, Bishop JE, McGrouther G, Laurent GJ. Mechanisms of tissue repair: from wound healing to fibrosis. Int J Biochem Cell Biol. 1997;(1):5-17.

275. Postlethwaite, A. E., Keski-Oja, J., Moses, H. L. and Kang, A. H. Stimulation of the chemotactic migration of human fibroblasts by transforming growth factor beta. J. Exp. Med. 1997;65:251-256.

276. Beck, L. S, Deguzman, L, Lee, W. P, Xu, Y, McFatride, L, Amento, E. P. TGF-1 accelerates wound healing: reversal of steroid-impaired healing in rats and rabbits. Growth Factors 5. 1991:295-304.

277. Chesnoy, S, Lee, P. Y, Huang, L. Intradermal injection of transforming growth factor-beta1 gene enhances wound healing in genetically diabetic mice. Pharm. Res. 2003;(20): 345-350.

278. Desmouliere, A, Geinoz, A, Gabbiani, F, Gabbiani, G. Transforming growth factor-beta 1 induces alpha-smooth muscle actin expression in granulation tissue myofibroblasts and in quiescent and growing cultured fibroblasts. J. Cell Biol.1193;(22):103-111

279. Shah, M., Foreman, D. M. and Ferguson, M. W. Neutralising antibody to TGFbeta 1,2 reduces cutaneous scarring in adult rodents. J. Cell Sci. 1994;(107):1137-1157

280. Cogliati B, Vinken M, Silva T, Araújo C, Aloia T, Chaible L et al. Connexin 43 deficiency accelerates skin wound healing and extracellular matrix remodeling in mice. Journal of Dermatological Science. 2015;79(1):50-56.

281. Wan L, Jiang D, Correa-Gallegos D, Ramesh P, Zhao J, Ye H et al. Connexin43 gap junction drives fascia mobilization and repair of deep skin wounds. Matrix Biology. 2021;97:58-71.

282. Solan, J.L, Lampe, P.D. Spatio-temporal regulation of connexin43 phosphorylation and gap junction dynamics. Biochim. Biophys. Acta Biomembr. 2018;(1860):83–90.

283. Sosinsky, G.E, Solan, J.L, Gaietta, G.M, Ngan, L, Lee, G, Mackey, M.R, Lampe, P.D. The C-terminus of connexin43 adopts different conformations in the Golgi and gap junction as detected with structure-specific antibodies. Biochem. J. 2007, 408, 375–385.

284. Li X, Guo L, Yang X, Wang J, Hou Y, Zhu S, Du J, Feng J, Xie Y, Zhuang L, He X, Liu Y. TGF-β1-induced connexin43 promotes scar formation via the Erk/MMP-1/collagen III pathway. J Oral Rehabil. 2020;Suppl:(1):99-106.

285. Cottrell GT, Lin R, Warn-Cramer BJ, Lau AF, Burt JM. Mechanism of v-Src- and mitogen-activated protein kinase-induced reduction of gap junction communication. Am J Physiol Cell Physiol. 2003;284(2):C511-20.

286. Cocozzelli AG, White TW. Connexin 43 Mutations Lead to Increased Hemichannel Functionality in Skin Disease. Int J Mol Sci. 2019;20(24):6186.

287. Dobrowolski, R. Sommershof, A. Willecke, K. Some oculodentodigital dysplasia-associated Cx43 mutations cause increased hemichannel activity in addition to deficient gap junction channels. J. Membr. Biol. 2007;(219):9-17.

288. Gong, X.Q, Shao, Q, Langlois, S, Bai, D, Laird, D.W. Differential potency of dominant negative connexin43 mutants in oculodentodigital dysplasia. J. Biol. Chem. 2007;(282):19190-19202.

289. Srinivas, M, Jannace, T.F, Cocozzelli, A.G, Leping Li, Nefeli Slavi, Caterina Sellitto, Thomas W. White. Connexin43 mutations linked to skin disease have augmented hemichannel activity. Sci Rep. 201;(9):19.

290. Wang H, Cao X, Lin Z, Lee M, Jia X, Ren Y et al. Exome sequencing reveals mutation in GJA1 as a cause of keratoderma-hypotrichosis-leukonychia totalis syndrome. Hum Mol Genet. 2015;24(1):243-50.

291. Becker D, Thrasivoulou C, Phillips A. Connexins in wound healing; perspectives in diabetic patients. Biochimica et Biophysica Acta (BBA) - Biomembranes. 2012;1818(8):2068-2075.

292. Brandner JM, Houdek P, Hüsing B, Kaiser C, Moll I. Connexins 26, 30, and 43: differences among spontaneous, chronic, and accelerated human wound healing. J Invest Dermatol. 2004;122(5):1310-20

293. Kanapathy M, Simpson R, Madden L, Thrasivoulou C, Mosahebi A, Becker D et al. Upregulation of epidermal gap junctional proteins in patients with venous disease. British Journal of Surgery. 2017;105(1):59-67.

294. Wang C, Lincoln J, Cook J, Becker D. Abnormal connexin expression underlies delayed wound healing in diabetic skin. diabetes. 2007;56(11):2809-2817.

295. Mendoza-Naranjo A, Cormie P, Serrano A, Hu R, O'Neill S, Wang C et al. Targeting Cx43 and N-cadherin, which are abnormally upregulated in venous leg ulcers, influences migration, adhesion and activation of Rho GTPases. PLoS ONE. 2012;7(5):e37374.

296. Nakano Y, Oyamada M, Dai P, Nakagami T, Kinoshita S, Takamatsu T. Connexin43 knockdown accelerates wound healing but inhibits mesenchymal transition after corneal endothelial injury in vivo. Investigative Opthalmology & Visual Science. 2008;49(1):93.

297. Elbadawy, H. M, Elshawarby, A, Raafat, M. H, Bahaa, N, Abdul, M. I, Aljuhani, N et al. Blocking connexin 43 accelerates corneal healing and improves tissue remodeling during the healing of diabetic rat corneas: A histological and immunohistochemical study. European Journal of Inflammation. 2019;(17):1-8.

298. Tarzemany R, Jiang G, Larjava H, Häkkinen L. Expression and function of connexin 43 in human gingival wound healing and fibroblasts. PLOS ONE. 2015;10(1):e0115524.

299. Davis N, Phillips A, Becker D. Connexin dynamics in the privileged wound healing of the buccal mucosa. Wound Repair and Regeneration. 2013;21(4):571-578.

300. Lye S, Ou C, Teoh T, Erb G, Stevens Y, Casper R et al. The molecular basis of labour and tocolysis. Fetal and Maternal Medicine Review. 1998;10(3):121-136.

301. Lye S, Mitchell J, Nashman N, Oldenhof A, Ou R, Shynlova O et al. Role of Mechanical Signals in the Onset of Term and Preterm Labor. Frontiers of Hormone Research. 2001;:165-178.

302. M Kidder G, Winterhager E. Physiological roles of connexins in labour and lactation. Reproduction. 2015;150(4):R129-36

303. Cook JL, Zaragoza DB, Sung DH, Olson DM. Expression of myometrial activation and stimulation genes in a mouse model of preterm labor: myometrial activation, stimulation, and preterm labor. Endocrinology. 2000;(14):1718–1728.

304. Cook JL, Shallow MC, Zaragoza DB, Anderson KI, Olson DM. Mouse placental prostaglandins are associated with uterine activation and the timing of birth. Biology of Reproduction. 2003;(68):579–587.

305. Xu C, Long A, Fang X, Wood SL, Slater DM, Ni X, Olson DM. Effects of PGF2a on the expression of uterine activation proteins in pregnant human myometrial cells from upper and lower segment. Journal of Clinical Endocrinology and Metabolism. 2013;(98):2975–2983.

306. Ou C, Orsino A, Lye S. Expression of Connexin-43 and Connexin-26 in the rat myometrium during pregnancy and labor is differentially regulated by mechanical and hormonal signals. Endocrinology. 1997;138(12):5398-5407

307. Nadeem, L, Shynlova, O, Mesiano, S, Lye S. Progesterone via its type-a receptor promotes myometrial gap junction coupling. Sci Rep. 2017;(7):13357.

308. Barnett SD, Asif H, Mitchell A, Buxton ILO. Cx43 activity and modulation in the myometrium. Journal of Pharmacology and Experimental Therapeutics. 2021;376:(3):444-453.

309. Barnett SD, Smith CR, Ulrich CC, Baker JE, Buxton ILO. S-nitrosoglutathione reductase underlies the dysfunctional relaxation to nitric oxide in preterm labor. Sci Rep. 2018;(8):5614.

310. Vadillo-Ortega F, Estrada-Gutiérrez G. Role of matrix metalloproteinases in preterm labour. BJOG: An International Journal of Obstetrics & Gynaecology. 2005;112:19-22.

311. Dammann O, Leviton A. Maternal Intrauterine Infection, Cytokines, and Brain Damage in the Preterm Newborn. Pediatric Research. 1997;42(1):1-8.

312. Hinz B, Gabbiani G. Mechanisms of force generation and transmission by myofibroblasts. Current Opinion in Biotechnology. 2003;14(5):538-546.

313. Li J, Chen J, Kirsner R. Pathophysiology of acute wound healing. Clinics in Dermatology. 2007;25(1):9-18.

314. Ehrlich H. Wound closure: evidence of cooperation between fibroblasts and collagen matrix. Eye. 1988;2(2):149-157.

315. Ehrlich H, Rajaratnam J. Cell locomotion forces versus cell contraction forces for collagen lattice contraction: An in vitro model of wound contraction. Tissue and Cell. 1990;22(4):407-417.

316. Tomasek J, Gabbiani G, Hinz B, Chaponnier C, Brown R. Myofibroblasts and mechano-regulation of connective tissue remodelling. Nature Reviews Molecular Cell Biology. 2002;3(5):349-363.

317. Williams R, Zipfel W, Webb W. Interpreting second-harmonic generation images of collagen i fibrils. Biophysical Journal. 2005;88(2):1377-1386.

318. Phan SH. Biology of fibroblasts and myofibroblasts. Proc Am Thorac Soc. 2008;5(3):334-337.

319. Costa E, Okesola BO, Thrasivoulou C, Becker, D L, Deprest, J A, David, A L et al. Cx43 mediates changes in myofibroblast contraction and collagen release in human amniotic membrane defects after trauma. Sci Rep. 2021;11(1):16975.

320. Bacelis J, Juodakis J, Adams Waldorf K, Sengpiel V, Muglia L, Zhang G et al. Uterine distention as a factor in birth timing: retrospective nationwide cohort study in Sweden. BMJ Open. 2018;8(10):e022929.

321. Jonsson M. Induction of twin pregnancy and the risk of caesarean delivery: a cohort study. BMC Pregnancy and Childbirth. 2015;15(1).

322. Engineer N, O'Donoghue K, Wimalasundera R, Fisk N. the effect of polyhydramnios on cervical length in twins: a controlled intervention study in complicated monochorionic pregnancies. PLoS ONE. 2008;3(12):e3834.

323. Santana D, Surita F, Cecatti J. Multiple Pregnancy: Epidemiology and association with maternal and perinatal morbidity. Revista Brasileira de Ginecologia e Obstetrícia / RBGO Gynecology and Obstetrics. 2018;40(09):554-562.

324. Pharande P, Mohamed A, Bajuk B, Lui K, Bolisetty S. Preterm infant outcomes in relation to the gestational age of onset and duration of prelabour rupture of membranes: a retrospective cohort study. BMJ Paediatrics Open. 2017;1(1):e000216.

325. Chandra I, Sun L. Third trimester preterm and term premature rupture of membranes: Is there any difference in maternal characteristics and pregnancy outcomes? Journal of the Chinese Medical Association. 2017;80(10):657-661.

326. Partap U, Sovio U, Smith G. Fetal growth and the risk of spontaneous preterm birth in a prospective cohort study of nulliparous women. American Journal of Epidemiology. 2016;184(2):110-119.

327. Conrad MS, Gardner ML, Miguel C, Freitas MA, Rood KM, Ma'ayeh M. Proteomic analysis of the umbilical cord in fetal growth restriction and preeclampsia. PLoS One. 2022;17(2):e0262041.

328. Kajantie E, Hytinantti T, Koistinen R, Risteli J, Rutanen EM, Seppälä M et al. Markers of type I and type III collagen turnover, insulin-like growth factors, and their binding proteins in cord plasma of small premature infants: relationships with fetal growth, gestational age, preeclampsia, and antenatal glucocorticoid treatment. Pediatr Res. 2001;49(4):481-489.

329. Murthi P, Kee MW, Gude NM, Brennecke SP, Kalionis B. Fetal growth restriction is associated with increased apoptosis in the chorionic trophoblast cells of human fetal membranes. Placenta. 2005;26(4):329-338.

330. Norman M, Ekman G, Malmström A. Prostaglandin E2-induced ripening of the human cervix involves changes in proteoglycan metabolism. Obstet Gynecol. 1993;82(6):1013-20.

331. Norman M, Ekman G, Malmström A. Changed proteoglycan metabolism in human cervix immediately after spontaneous vaginal delivery. Obstet Gynecol. 1993;81(2):217-23.

332. Park J, Romero R, Lee J, Chaemsaithong P, Chaiyasit N, Yoon B. An elevated amniotic fluid prostaglandin F2α concentration is associated with intra-amniotic inflammation/infection, and clinical and histologic chorioamnionitis, as well as impending preterm delivery in patients with preterm labor and intact membranes. The Journal of Maternal-Fetal & Neonatal Medicine. 2015;:1-10.

333. Yamazaki K, Endo T, Kitajima Y, Manase K, Nagasawa K, Honnma H et al. Elevation of both Cyclooxygenase-2 and Prostaglandin E2 Receptor EP3 expressions in rat placenta after uterine artery ischemia–reperfusion. Placenta. 2006;27(4-5):395-401.

334. Winterhager E, Gellhaus A, Blois SM, Hill LA, Barr KJ, Kidder GM. Decidual angiogenesis and placental orientation are altered in mice heterozygous for a dominant loss-of-function Gja1 (connexin43) mutation. Biol Reprod. 2013;89:111.

335. Xu P, Alfaidy N, and Challis JR. Expression of matrix metalloproteinase (MMP)-2 and MMP-9 in human placenta and fetal membranes in relation to preterm and term labor. J. Clin. Endocrinol. Metab. 2002;87;1353–1361.

336. Romero R, Chaiworapongsa T, Espinoza J, Gomez R, Yoon BH, Edwin S et al. Fetal plasma MMP-9 concentrations are elevated in preterm premature rupture of the membranes. Am. J. Obstet. Gynecol. 2022;187;1125–1130.

337. Meinert M, Malmström A, Tufvesson E, Westergren-Thorsson G, Petersen A, Laurent C et al. Labour Induces Increased Concentrations of Biglycan and Hyaluronan in Human Fetal Membranes. Placenta. 2007;28(5-6):482-486.

338. Dunn C, Su V, Lau A, Lampe P. Activation of Akt, not connexin 43 protein ubiquitination, regulates gap junction stability. Journal of Biological Chemistry. 2012;287(4):2600-2607.

339. Batra N, Riquelme M, Burra S, Kar R, Gu S, Jiang J. Direct regulation of osteocytic connexin 43 hemichannels through akt kinase activated by mechanical stimulation. Journal of Biological Chemistry. 2014;289(15):10582-10591.

340. Cherian P, Siller-Jackson A, Gu S, Wang X, Bonewald L, Sprague E et al. Mechanical strain opens connexin 43 hemichannels in osteocytes: a novel mechanism for the release of prostaglandin. Molecular biology of the cell. 2005;16(7):3100-3106.

341. Sutcliffe J, Chin K, Thrasivoulou C, Serena T, O'Neil S, Hu R et al. Abnormal connexin expression in human chronic wounds. British Journal of Dermatology. 2015;173(5):1205-1215.

342. Sutcliffe J, Thrasivoulou C, Serena T, Madden L, Richards T, Phillips A et al. Changes in the extracellular matrix surrounding human chronic wounds revealed by 2-photon imaging. International. Wound Journal. 2017;14(6):1225-1236.

343. Briana DD, Liosi S, Gourgiotis D, Boutsikou M, Marmarinos A, Baka S et al. Fetal concentrations of the growth factors TGF-α and TGF-β1 in relation to normal and restricted fetal growth at term. Cytokine. 2012;60(1):157-161.

344. Singh M, Orazulike NC, Ashmore J, Konje JC. Changes in maternal serum transforming growth factor beta-1 during pregnancy: a cross-sectional study. Biomed Res Int. 2013;2013:318464.

345. Todros T, Marzioni D, Lorenzi T, Piccoli E, Capparuccia L, Perugini V et al. Evidence for a role of TGF-beta1 in the expression and regulation of alpha-SMA in fetal growth restricted placentae. Placenta. 2007;28(11-12):1123-1132.

346. Gagnon KT, Corey DR. Guidelines for experiments using antisense oligonucleotides and double-stranded rnas. Nucleic Acid Ther. 2019;29(3):116-122.

347. Schenke-Layland K, Xie J, Angelis E, Starcher B, Wu K, Riemann I et al. Increased degradation of extracellular matrix structures of lacrimal glands implicated in the pathogenesis of Sjögren's syndrome. Matrix Biology. 2008;27(1):53-66.

348. Le T, Langohr I, Locker M, Sturek M, Cheng J. Label-free molecular imaging of atherosclerotic lesions using multimodal nonlinear optical microscopy. Journal of Biomedical Optics. 2007;12(5):054007.

349. Ochsenbein-Kölble N, Brandt S, Bode P, Krähenmann F, Hüsler M, Möhrlen U et al. Clinical and histologic evaluation of the hysterotomy site and fetal membranes after open fetal surgery for fetal spina bifida repair. Fetal Diagnosis and Therapy. 2018;45(4):248-255.

350. Hezelgrave N, Seed P, Chin-Smith E, Ridout A, Shennan A, Tribe R. Cervicovaginal natural antimicrobial expression in pregnancy and association with spontaneous preterm birth. Scientific Reports. 2020;10(1).

351. Lockwood C, Toti P, Arcuri F, Paidas M, Buchwalder L, Krikun G et al. Mechanisms of abruption-induced premature rupture of the fetal membranes. The American Journal of Pathology. 2005;167(5):1443-1449.

352. Zaretsky M, Tong S, Lagueux M, Lim F, Khalek N, Emery S et al. North American Fetal Therapy Network: timing of and indications for delivery following laser ablation for twin-twin transfusion syndrome. American Journal of Obstetrics & Gynecology MFM. 2019;1(1):74-81.

353. Botelho R, Imada V, Rodrigues da Costa K, Watanabe L, Rossi Júnior R, De Salles A et al. Fetal myelomeningocele repair through a mini-hysterotomy. Fetal Diagnosis and Therapy. 2016;42(1):28-34.

354. Linehan L, Walsh J, Morris A, Kenny L, O'Donoghue K, Dempsey E et al. Neonatal and maternal outcomes following midtrimester preterm premature rupture of the membranes: a retrospective cohort study. BMC Pregnancy and Childbirth. 2016;16(1).

355. Galaz J, Romero R, Slutsky R, Xu Y, Motomura K, Para R et al. Cellular immune responses in amniotic fluid of women with preterm prelabor rupture of membranes. Journal of Perinatal Medicine. 2020;48(3):222-233.

356. Green S, Politis M, Rallis K, Saenz de Villaverde Cortabarria A, Efthymiou A, Mureanu N et al. Regulatory T Cells in pregnancy adverse outcomes: a systematic review and meta-analysis. Frontiers in Immunology. 2021;12.

357. Ljubimov A, Saghizadeh M. Progress in corneal wound healing. Progress in Retinal and Eye Research. 2015;49:17-45.

358. Maniscalco W, Campbell M. Transforming growth factor-beta induces a chondroitin sulfate/dermatan sulfate proteoglycan in alveolar type II cells. American Journal of Physiology-Lung Cellular and Molecular Physiology. 1994;266(6):L672-L680.

359. Hintze V, Miron A, Moeller S, Schnabelrauch M, Wiesmann H, Worch H et al. Sulfated hyaluronan and chondroitin sulfate derivatives interact differently with human transforming growth factor-β1 (TGF-β1). Acta Biomaterialia. 2012;8(6):2144-2152.

360. Åkerud A, Dubicke A, Sennström M, Ekman-Ordeberg G, Malmström A. Differences in heparan sulfate production in cervical fibroblast cultures from women undergoing term and preterm delivery. Acta Obstetricia et Gynecologica Scandinavica. 2008;87(11):1220-1228.

361. Lin P, Chang H, Yeh C, Chang M, Chan C, Kuo H et al. Transforming growth factor beta 1 increases collagen content, and stimulates procollagen I and tissue inhibitor of metalloproteinase-1 production of dental pulp cells: Role of MEK/ERK and activin receptor-like kinase-5/Smad signaling. Journal of the Formosan Medical Association. 2017;116(5):351-358.

362. Richardson L, Gnecco J, Ding T, Osteen K, Rogers L, Aronoff D et al. Fetal membrane organ-on-chip: an innovative approach to study cellular interactions. reproductive sciences. 2020;27(8):1562-1569.

363. Kim S, Richardson L, Radnaa E, Chen Z, Rusyn I, Menon R et al. Molecular mechanisms of environmental toxin cadmium at the feto-maternal interface investigated using an organ-on-chip (FMi-OOC) model. Journal of Hazardous Materials. 2022;422:126759.

364. Choi S. Use of progesterone supplement therapy for prevention of preterm birth: review of literatures. Obstetrics & Gynecology Science. 2017;60(5):405.

365. Romero R, Espinoza J, Kusanovic J, Gotsch F, Hassan S, Erez O et al. The preterm parturition syndrome. BJOG: An International Journal of Obstetrics & Gynaecology. 2006;113:17-42.

366. Salminen A, Paananen R, Vuolteenaho R, Metsola J, Ojaniemi M, Autio-Harmainen H et al. Maternal endotoxin-induced preterm birth in mice: fetal responses in toll-like receptors, collectins, and cytokines. Pediatric Research. 2008;63(3):280-286.

367. Fricke E, Elgin T, Gong H, Reese J, Gibson-Corley K, Weiss R et al. Lipopolysaccharide-induced maternal inflammation induces direct placental injury without alteration in placental blood flow and induces a secondary fetal intestinal injury that persists into adulthood. American Journal of Reproductive Immunology. 2018;79(5):e12816.

368. Lappas M, Mitton A, Lim R, Barker G, Riley C, Permezel M. SIRT1 is a novel regulator of key pathways of human labor. Biology of Reproduction. 2011;84(1):167-178.

369. Morwood C, Lappas M. The citrus flavone nobiletin reduces pro-inflammatory and pro-labour mediators in fetal membranes and myometrium: implications for preterm birth. PLoS ONE. 2014;9(9):e108390.

370. Lim R, Morwood C, Barker G, Lappas M. Effect of silibinin in reducing inflammatory pathways in in vitro and in vivo models of infection-induced preterm birth. PLoS ONE. 2014;9(3):e92505.

371. Mizoguchi M, Ishida Y, Nosaka M, Kimura A, Kuninaka Y, Yahata T et al. Prevention of lipopolysaccharide-induced preterm labor by the lack of CX3CL1-CX3CR1 interaction in mice. PLOS ONE. 2018;13(11):e0207085.

372. Liong S, Lappas M. Endoplasmic Reticulum Stress Is Increased after Spontaneous Labor in Human Fetal Membranes and Myometrium Where It Regulates the Expression of Prolabor Mediators1. Biology of Reproduction. 2014;91(3).

373. Lim R, Lappas M. A novel role for GSK3 in the regulation of the processes of human labour. REPRODUCTION. 2015;149(2):189-202.

374. Lim R, Barker G, Lappas M. Activation of AMPK in human fetal membranes alleviates infection-induced expression of pro-inflammatory and pro-labour mediators. Placenta. 2015;36(4):454-462.

375. Lim R, Barker G, Lappas M. Inhibition of PIM1 kinase attenuates inflammation-induced pro-labour mediators in human foetal membranes in vitro. MHR: Basic science of reproductive medicine. 2017;23(6):428-440.

376. Fan F, Saha S, Hanjaya-Putra D. Biomimetic hydrogels to promote wound healing. Frontiers in Bioengineering and Biotechnology. 2021;9.

377. Lohmann N, Schirmer L, Atallah P, Wandel E, Ferrer R, Werner C et al. Glycosaminoglycan-based hydrogels capture inflammatory chemokines and rescue defective wound healing in mice. Science Translational Medicine. 2017;9(386).

378. Chen X, Zhang M, Chen S, Wang X, Tian Z, Chen Y et al. Peptide-modified chitosan hydrogels accelerate skin wound healing by promoting fibroblast proliferation, migration, and secretion. Cell Transplantation. 2017;26(8):1331-1340.

379. Deng Y, Sun A, Overholt K, Yu G, Fritch M, Alexander P et al. Enhancing chondrogenesis and mechanical strength retention in physiologically relevant hydrogels with incorporation of hyaluronic acid and direct loading of TGF-β. Acta Biomaterialia. 2019;83:167-176.

380. Xia W, Jin Y, Kretlow J, Liu W, Ding W, Sun H et al. Adenoviral transduction of hTGF-β1 enhances the chondrogenesis of bone marrow derived stromal cells. Biotechnology Letters. 2009;31(5):639-646.

381. Gilmartin D, Soon A, Thrasivoulou C, Phillips A, Jayasinghe S, Becker D. Sustained release of cx43 antisense oligodeoxynucleotides from coated collagen scaffolds promotes wound healing. Advanced Healthcare Materials. 2016;5(14):1786-1799.

382. Oh K, Romero R, Park J, Lee J, Conde-Agudelo A, Hong J et al. Evidence that antibiotic administration is effective in the treatment of a subset of patients with intra-amniotic infection/inflammation presenting with cervical insufficiency. American Journal of Obstetrics and Gynecology. 2019;221(2):140.e1-140.e18.

383. Ireland D, Nathan E, Li S, Charles A, Stinson L, Kemp M et al. Preclinical evaluation of drugs to block inflammation-driven preterm birth. Innate Immunity. 2016;23(1):20-33.

384. Kacerovsky M, Romero R, Stepan M, Stranik J, Maly J, Pliskova L et al. Antibiotic administration reduces the rate of intraamniotic inflammation in preterm prelabor rupture of the membranes. American Journal of Obstetrics and Gynecology. 2020;223(1):114.e1-114.e20.

385. Upadhyay A, Chattopadhyay P, Goyary D, Mitra Mazumder P, Veer V. Ixora coccinea Enhances cutaneous wound healing by upregulating the expression of collagen and basic fibroblast growth factor. ISRN Pharmacology. 2014;2014:1-9.

386. Shukla R, Kashaw S, Jain A, Lodhi S. Fabrication of Apigenin loaded gellan gum–chitosan hydrogels (GGCH-HGs) for effective diabetic wound healing. International Journal of Biological Macromolecules. 2016;91:1110-1119.

387. Zhao H, Huang J, Li Y, Lv X, Zhou H, Wang H et al. ROS-scavenging hydrogel to promote healing of bacteria infected diabetic wounds. Biomaterials. 2020;258:120286.

388. Madsen D, Leonard D, Masedunskas A, Moyer A, Jürgensen H, Peters D et al. M2-like macrophages are responsible for collagen degradation through a mannose receptor–mediated pathway. Journal of Cell Biology. 2013;202(6):951-966.

389. Isenburg J, Simionescu D, Vyavahare N. Elastin stabilization in cardiovascular implants: improved resistance to enzymatic degradation by treatment with tannic acid. Biomaterials. 2004;25(16):3293-3302.

390. Freedman B, Kuttler A, Beckmann N, Nam S, Kent D, Schuleit M et al. Enhanced tendon healing by a tough hydrogel with an adhesive side and high drug-loading capacity. Nature Biomedical Engineering. 2022;6(10):1167-1179